VOLUME I

STUDIES IN TILT-ROTOR VTOL AIRCRAFT AEROELASTICITY

by

RAYMOND GEORGE KVATERNIK

Submitted in partial fulfillment of the requirements

for the Degree of Doctor of Philosophy

Thesis Advisor: Professor Robert H. Scanlan

Department of Solid Mechanics, Structures, and Mechanical Design

CASE WESTERN RESERVE UNIVERSITY

June 1973

STUDIES IN TILT-ROTOR VTOL AIRCRAFT AEROELASTICITY

Abstract

by

RAYMOND GEORGE KVATERNIK

The results of some aeroelastic and dynamic studies which complement and extend various aspects of technology applicable to tilt-rotor VTOL aircraft are presented. Particular attention is given to proprotor/pylon whirl instability, a precession-type instability akin to propeller/nacelle whirl flutter. The blade flapping and pitch-change freedoms of a proprotor are shown to lead to a fundamentally different situation as regards the manner in which the precession-generated aerodynamic forces and moments act on the pylon and induce whirl flutter relative to that of a propeller. The implication of these forces and moments with regard to their capacity for instigating a whirl instability is examined, demonstrating, apparently for the first time, precisely why a proprotor can exhibit whirl flutter in either the backward or forward directions in contrast to a propeller which is found to always whirl in the backward direction. Analytical trend studies delineating the effect of several system design parameters on proprotor/pylon stability and response are shown. Results of experimental studies, principally those of joint NASA/Bell Helicopter Company investigations of a 0.133-scale, semispan, dynamic,

aeroelastic model in the NASA-Langley transonic dynamics tunnel, are presented and compared with theoretical results where applicable. Analytical predictions are shown to be in good agreement with the measured dynamic characteristics. Computational procedures for natural mode vibration analysis by direct and component mode synthesis techniques are described and the results of some comparative analytical and experimental studies shown. The concept of a gyroscopic finite element to approximate the dynamic effects of rotating components such as propellers or proprotors is introduced and both analyses for natural mode analysis extended to include gyroscopic coupling effects. A method for effecting a reduction of the resulting equations of motion to a form amenable to eigenvalue solution in the general case in which both the mass and stiffness matrices are singular is proposed.

ACKNOWLEDGEMENTS

The work reported herein was supported by the author's employer the National Aeronautics and Space Administration and conducted at its Langley Research Center facility. The author wishes to express his appreciation to his supervisors in the Aeroelasticity Branch, A. Gerald Rainey, Wilmer H. Reed, III, and Frank T. Abbott, Jr., for encouraging the work and making time available.

Thanks are also extended to the author's advisor, Professor Robert H. Scanlan, for his careful review of the final draft of this dissertation. It seems appropriate to mention that Professor Scanlan was instrumental in introducing the author to the fascinating field of aircraft aeroelasticity and subsequently providing guidance for the author's Master's work in this area. This dissertation essentially represents an extension of that earlier work.

In addition to the persons mentioned above, several of the author's colleagues have contributed to the successful completion of this dissertation and also deserve individual acknowledgement: Troy M. Gaffey of Bell Helicopter Company for many elucidating discussions on proprotor dynamics and for his general guidance during development of the proprotor stability and response analyses. Mr. Gaffey was in no small measure responsible for making the author a VTOL dynamics enthusiast; William C. Walton, Jr. of NASA-Langley and Earl C. Steeves of the U. S. Army

Natick Laboratories (formerly of Langley) for kindling the author's interest in the application of the stiffness matrix method to dynamic analyses based on substructuring techniques thereby providing motivation for the work on natural mode vibration analysis reported in this dissertation. Discussions held with Mr. Walton during this phase of the investigation contributed greatly to formulating the analyses; Barbara J. Durling and Robert N. Desmarais of NASA-Langley for several contributions to the computer programming. Their specific contributions are cited in the appendix containing the listing of computer programs.

The author also acknowledges the assistance provided by Bell Helicopter Company in testing of the wind-tunnel models. This dissertation would be conspicuously lacking in experimental data for correlation with the developed proprotor analyses were it not for their support.

Last but not least, the author extends heartfelt appreciation to his wife Jean for her encouragement, patience, and understanding during the course of this undertaking, particularly the period during which the final draft of this dissertation was set down in writing. It is to her that this dissertation is dedicated.

TABLE OF CONTENTS

CHAPTER 1

INTRODUCTION

A wide variety of civil and military missions requiring an aircraft which combines the high payload vertical lift capability of the helicopter with the high-speed cruise efficiency and range of a fixed-wing aircraft have been established in recent years (Refs. 1-1 to 1-5). These missions include such applications as passenger and utility inter-city transport, center-of-city to airport commuter service, utility through medium weight tactical and logistic transports, search and rescue, and reconnaissance. Several composite V/STOL concepts based on the use of rotary-wings have been proposed to meet the need for an operational aircraft having the desirable hybrid characteristics (Refs. 1-6 to 1-10). One example of this concept is the tilt-proprotor characterized by wing-tip mounted rotors which tilt forward 90^{o} from the vertical position employed for helicopter flight to a horizontal position to function as propellers for high-speed airplane flight.

The feasibility of the tilt-proprotor composite aircraft concept was established in the mid-1950's on the basis of the successful flight demonstration of the Bell XV-3 and Transcendental Model 1-G and Model 2 convertiplanes (Figs. 1-1 to 1-3). A summary of the experience pertaining to these "test bed" aircraft as well as

subsequent related work to serve in an introductory capacity are described below.

The Transcendental Model 1-G was designed and built as a private undertaking during the period 1951-1953. Although accumulating a respectable amount of flight time, the aircraft was used primarily in a funded study for the Air Force of the mechanical instability and vibrational characteristics of tilt-rotor convertiplanes during simulated conversion, the full-scale aircraft being suspended in an elastic "cradle" during these tests. Results of this work are given in Ref. 1-11. An accident, resulting from a mechanical malfunction, severely damaged the aircraft in 1955. The Transcendental Model 2, built under Air Force contract in 1956 as a successor to the Model 1-G, was of the same basic design but was slightly larger and had 50% more installed power. Helicopter flight was demonstrated in the same year but a proposed flight test program to study the stability and control characteristics in the helicopter, conversion, and airplane modes of flight was never initiated due to termination of funding. Refs. 1-12 and 1-13 provide some general descriptive information relating to both the Model 1-G and Model 2.

The Bell XV-3, built under joint Army-Air Force sponsorship, had a considerably longer research existence. Two XV-3s were built under this program. The first, during 1953-1955, had three-bladed fully-articulated proprotors (Fig. 1-4). A blade oscillation problem associated with the articulated rotor was identified

in flight and was the cause of an accident which badly damaged the aircraft in 1956. Some of the early development work related to this design is summarized in Ref. 1-14. A two-bladed semi-rigid proprotor design was incorporated in the second XV-3 and successfully eliminated the blade oscillation problem of the original design. The second XV-3, shown in Fig. 1-5, was the subject of extensive flight and full-scale wind-tunnel studies (Refs. 1-15 to 1-19). Early flight experience identified several deficiencies and problem areas, especially while operating in the airplane mode of flight with the rotors fully converted forward. In particular, transient blade flapping during longitudinal and directional maneuvering and low levels of longitudinal (short period) stability near the dive speed were unacceptable. The low levels of short period stability were found to be related to the inplane forces generated by the proprotors as a result of blade flapping associated with aircraft pitching motions (Ref. 1-18). These were in a direction to produce negative pitch damping. Prior to further flight testing, full-scale wind-tunnel tests were conducted in 1962 in the NASA Ames 40 x 80-ft tunnel to investigate proposed solutions to these deficiencies. During these tests, a heretofore unknown proprotor/pylon instability, similar to propeller whirl flutter, was experienced in which the proprotor/pylon exhibited a low frequency precessional motion in a direction opposite to the direction of rotor rotation. Clearly, in order to maintain the viability of the tilt-proprotor concept it remained to demonstrate

that neither the whirl flutter anomaly nor the major flight deficiencies were endemic to the design principle. An analytical and experimental research program having this objective was undertaken by Bell in 1962. Results of this research, which defined the instability mechanism and established several basic design solutions, were reported by Hall (Ref. 1-20). Edenborough (Ref. 1-21) presented results of subsequent full-scale tests at Ames in 1966 which verified the analytical prediction techniques, the proposed design solutions, and demonstrated stability of the XV-3 through the maximum wind tunnel speed of 195 knots. During the final run in this test program the aircraft suffered severe damage as a result of the abrupt loss of both pylons. Post-failure examination revealed that the failure was not related to the proprotor/pylon stability problem under investigation but was the result of proprotor speed operation near one-per-rev pylon whirl resonance which loosened and fatigued a main supporting member in the left pylon.

In 1965 the U. S. Army inaugurated the Composite Aircraft Program which had the goal of producing a rotary-wing research aircraft combining the hovering capabilities of the helicopter with the high-speed cruise capabilities of a fixed-wing aircraft to be used in evaluating its operational potential for future Army missions. Bell Helicopter Company, with a tilt-proprotor design proposal, was awarded one of two exploratory definition contracts in 1967. The Bell Model 266 (Fig. 1-6) was the design

resulting from their work which is documented in Ref. 1-22. The research aircraft program which was to have been initiated subsequent to the exploratory definition phase was never begun, however, primarily due to lack of funding.

Concurrent with the developments described above various VTOL concepts based on the use of propellers having hinged blades were proposed as research vehicles, several reaching flight test status. These included the Grumman proposal in the Tri-Service VTOL transport competition, the Vertol VZ-2 built for the Army, and the Kaman K-16 amphibian built for the Navy. A vigorous investigation of the whirl flutter phenomenon peculiar to conventional propellers had been initiated in 1960 as a result of the loss of two Lockheed Electra aircraft in fatal accidents. The likelihood that hinged blades could adversely affect the whirl flutter behavior of a propeller undoubtedly contributed considerable impetus to examine the whirl flutter characteristics of these unconventional propellers. Work related to these efforts may be found in Refs. 1-23 to 1-28.

The foregoing generally constitutes an overview of proprotor and proprotor-related experience through the year 1967. The work presented herein is a comprehensive account of the principal achievements of an aeroelastic proprotor research program initiated in 1968. Motivating factors leading to the work, scope and nature of the investigation, and considerations guiding the analytical development are outlined below.

A 0.133-scale semi-span dynamic and aeroelastic model of the Bell Model 266 tilt-proprotor built by Bell in support of their work pertaining to the Composite Aircraft Program was given to NASA Langley by the Army. The availability of this model and the continued interest of both government and industry in the proprotor composite V/STOL concept suggested the usefulness of continuing the experimental research initiated by Bell with this model during the Composite Aircraft Program and developing supporting analyses. The usefulness of a "fresh" approach was also suggested by the fact that the work reported in the literature has generally been of a fragmentary nature, each being directed to different aspects of tilt-rotor aeroelasticity, and sparse in correlations of theory with experiment. It was therefore judged that a somewhat broader but unified treatment emphasizing detailed analytical developments, trend studies, and correlations with experimental results would provide a useful contribution to existing knowledge.

The wide variety of technical considerations confronting the aeroelastician and structural dynamicist in the design of a proprotor V/STOL aircraft are brought into perspective in Fig. 1-7, which enumerates several design problems associated with each regime of flight in which vehicles of this type operate. Many important areas of research present themselves. In the interest of expediency, the scope of the investigation to be undertaken had to be limited in some sense. Because both the XV-3 experience and Bell studies conducted during the Composite Aircraft Program

identified certain high-risk areas associated with proprotor V/STOLs operating in the airplane flight mode, specifically proprotor/pylon stability (whirl flutter), blade flapping, and short period stability, and because operations in this mode generally dictate the major vehicle design requirements, it was judged that studies pertaining to these high-risk areas and related aspects would constitute both a prudent and contributary research effort. The specific areas to be treated herein, either explicitly or implicitly, are indicated in Fig. 1-7 by a check mark.

In the early stages of planning the lines along which the analytical development would proceed it was recognized that a mathematical formulation, ab initio, for the flutter analysis of a complete proprotor V/STOL aircraft represented a formidable task. Prudence and mathematical tractability suggested a sequential analytical development, approaching the complete problem in a coordinated manner. It was also reasoned that, from a research point of view, a more meaningful contribution could be made by emphasizing theoretical methods which provide a preliminary design analysis capability, as contrasted to the generally complex analyses employed in establishing a final design. Based on these considerations it was decided to have recourse to the generally accepted engineering practice of analyzing selected components of the aircraft as a prelude to attacking the complete aircraft. Methodologies developed during these intermediate stages of analysis would then provide a rational mathematical basis from which

to synthesize a stability analysis of the complete aircraft.

Since preliminary design analyses generally entail broad parametric studies during which controlling parameters must be quickly isolated, a linear analysis is strongly recommended. Fortunately, stability considerations associated with proprotor operation in the airplane mode of flight admit of a linear formulation, in particular a linear eigenvalue formulation. This fortuitous circumstance arises from the fact that the proprotor shaft is nominally aligned with the airstream and perturbations from this position contribute first order small quantities to the proprotor aerodynamic loading, as contrasted to operations in the helicopter or conversion modes where finite angles of the shaft relative to the airstream lead to time-dependent coefficients in the equations of motion. Also, since the proprotor does not operate in its own wake when in the airplane mode, the problem is not one of forced response, as would be the case when operating as a helicopter.

With a view toward developing the ingredients needed for the sequential analytical approach outlined above, the theoretical considerations in this dissertation are directed toward providing the analysis capability and associated computer programs related to two aspects of the overall problem. First, the flutter analysis of an idealized proprotor/pylon system supported on constraints simulating the force-deflection characteristics of the local wing attachment point. Attention to this aspect is perhaps obvious in

view of the fact that the model employed in the experimental investigation was a semi-span model and the fact that proprotor V/STOL flutter tests employing semi-span models generally precede flutter tests of complete models. However, this approach also follows the customary engineering practice of performing preliminary flutter analyses for conventional propeller-driven aircraft by assuming the propeller/nacelle system to be flexibly mounted to a rigid wing. The next logical step in this sequence would normally be a flutter analysis of the wing assuming the proprotor/pylon system to be rigidly attached to the wing. Subsonic wing flutter analysis schemes are generally available and can be adapted to this phase of the overall analysis procedure if the structural or modal information required by these various methods are available. This observation, the recognized need for modal information in related disciplines such as dynamic response analyses, and the design requirement of keeping airframe natural frequencies clear of resonances with harmonics of the proprotor speed, suggested that the second directed effort concern itself with developing computational procedures for the natural mode vibration analysis of airframe structures.

In accordance with the analytical philosophy adopted herein attention is directed to two methodologies for natural mode vibration analysis. The first consists of a direct approach based on solving the matrix eigenvalue problem resulting from a finite element representation of the complete structure as an entity.

This approach was suggested by the need for a straightforward vibration analysis scheme to provide the system modal information required for wing flutter and dynamic response analyses based on a normal mode method. For large, complex structural systems the determination of the natural modes by a direct method often leads to a problem size which exceeds the storage capacity of available computers. An alternative approach to natural mode vibration analysis in such circumstances is that of component mode synthesis. This method is based on the concept of synthesizing the vibration modes of the complete structure from modes of conveniently defined subsystems, or components, into which the structure has been divided. The expedient of reducing the system degrees of freedom, and hence the size of the eigenvalue problem, is introduced by partial modal synthesis wherein only a relatively few of the modes from each component are chosen as degrees of freedom and employed in the synthesizing procedure. In recognition of the fact that large rotating components (such as proprotors or propellers) may alter the vibratory characteristics of an airframe relative to the case in which the spin is zero, attention is also directed to extending both analyses for natural mode vibration analysis to include the effects of gyroscopic coupling forces.

The analyses for natural mode vibration analysis by direct and component mode synthesis techniques developed in this dissertation are, in principle, applicable to a structural idealization based on any type of finite element (segments of beams, plates, shells,

etc.). The computer programs based on these analyses* are, however, limited to structures which admit of a "stick" model representation in which the structure is taken to be composed of an assemblage of beams, springs, and rigid bodies. Since many structures of practical interest can be represented in this manner for dynamic analyses, particularly in the preliminary stages of design, the computer programs constitute more than an academic exercise and have a relatively wide range of engineering applicability.

The subject matter has been arranged with a view toward achieving a pedagogical presentation. A retrospective of the proprotor V/STOL concept as embodied in the tilt-proprotor — and its variant the tilt-fold proprotor — and a discussion of the mechanism of proprotor/pylon instability, particularly as it relates to "classical" propeller whirl flutter, are presented in Chapter 2. Other salient dynamic features indigenous to proprotor-type aircraft are reviewed both for completeness and as an aid to understanding subsequent discussions. A comprehensive analytical development for the flutter analysis of a mathematical model of an idealized proprotor/pylon system supported on local wing constraints is given in Chapter 3. These equations also provide the basis for formulating the equations for calculating the proprotor-generated oscillatory force and moment derivatives and the oscillatory blade

---

* Only the case of zero gyroscopic coupling has been programmed.

flapping derivatives. The details, however, are relegated to the Appendices. Using the design configuration of the Bell Model 266, Chapter 4 is devoted to relatively extensive analytical trend studies to delineate the effects of various design parameters on proprotor/pylon stability, blade flapping response, and proprotor-generated forces and moments. Chapter 5 is primarily concerned with validation of the developed proprotor analyses by demonstrating correlation with experimental results, principally those from joint NASA/Bell studies of the Model 266 in the Langley transonic dynamics tunnel. The analytical bases for the natural mode vibration analysis of complex structural systems by direct and component mode synthesis techniques are outlined in Chapter 6. A detailed illustrative example of the free-free vibration analysis of the Model 266 by the direct method as well as the results of the application of the modal synthesis scheme to two simple structural systems are given in the Appendices. Chapter 6 also introduces the concept of a gyroscopic finite element. By means of this artifice, both analyses for determining natural modes and frequencies of vibration are extended to include the case of a gyroscopically coupled elastic system.

The results reported herein are primarily aimed at advancing the technology applicable to proprotor V/STOL aircraft. Selected analytical and experimental studies and related topic discussions are presented to highlight concepts, analytical developments, and present a composite view of various aeroelastic and dynamic aspects peculiar to proprotor vehicles. The work herein generally extends

and complements selected analytical and experimental work in the literature and presents aspects and methods not presently in the literature.

A listing of all computer programs developed in conjunction with the analyses herein is included in the Appendix.

CITED REFERENCES

1-1. Burkhardt, R. B.: "V/STOLs Can Capture Short-Haul Intercity Market", Vertical World, Feb. 1967, pp. 36-39.

1-2. Armstrong, LTC M.B.: "Tactical Uses and Future Concepts for Vertical Lift Aircraft in Marine Corps Operations", presented at the AHS/US Army Symposium on Operational Characteristics and Tactical Uses of Vertical Lift Aircraft, November 1967.

1-3. Doty, L.: "V/STOL Seen as Solution to Congestion", Aviation Week and Space Technology, June 24, 1968, pp. 100-106.

1-4. Carter, J. W.: "Urban Growth Gives V/STOL Incentive", Aviation Week and Space Technology, June 24, 1968, pp. 107-111.

1-5. Anon.: "Vertical-Lift Advances Sought for Army Missions of 1990s", Aviation Week and Space Technology, June 24, 1968, pp. 152-157.

1-6. Yaffee, M. L.: "Composite Aircraft Seen Emerging as Next Basic VTOL", Aviation Week and Space Technology, May 1, 1967, pp. 60-67.

1-7. Lichten, R. L., et al.: "A Survey of Low-Disc-Loading VTOL Aircraft Designs", AIAA Paper 65-756, November 1965.

1-8. Dulberger, L. H.: "Advanced Rotary-Wing Aircraft", Space/ Aeronautics, April 1967, pp. 68-82.

1-9. Brown, E. L. and J. N. Fischer: "Comparative Projections of Helicopters, Compound Helicopters, and Tilting-Proprotor Low-Disc-Loading VTOL Aircraft for Civil Applications", AIAA Paper 67-939, October 1967.

1-10. Plattner, C. M.: "Speed Studies Spur Rotary-Wing Designs", Aviation Week and Space Technology, June 24, 1968, pp. 86-99.

1-11. Cobey, W. E.: "Tests on Transcendental Convertiplane", Transcendental Aircraft Engineering Report 1R90-17, July 18, 1955.

1-12. Cobey, W. E.: "Convertiplane Development Tests", Proceedings of the 9th Annual National Forum of the American Helicopter Society, May 1953, pp. 200-209.

1-13. Cobey, W. E.: "Transcendental Convertiplanes", American Helicopter Society Newsletter, Vol. 2, No. 11, November 1956.

1-14. Lichten, R. L. and J. R. Mertens: "Development of the XV-3 Convertiplane", Proceedings of the 12th Annual National Forum of the American Helicopter Society, May 1956.

1-15. Koenig, D. G., R. K. Greif, and M. W. Kelly: "Full-Scale Wind-Tunnel Investigation of the Longitudinal Characteristics of a Tilting-Rotor Convertiplane", NASA TN D-35, December 1959.

1-16. Deckert, W. H. and R. G. Ferry: "Limited Flight Evaluation of the XV-3 Aircraft", Air Force Flight Test Center, Report TR-60-4, May 1960.

1-17. Reeder, J. P.: "Handling Qualities Experience with Several VTOL Research Aircraft", NASA TN D-735, March 1961.

1-18. Quigley, H. C. and D. G. Koenig: "A Flight Study of the Dynamic Stability of a Tilting-Rotor Convertiplane", NASA TN D-778, April 1961.

1-19. Anon.: "Pilot Evaluation of the Bell Model XV-3 Vertical Takeoff and Landing Aircraft", U. S. Army Transportation Material Command, Report ATO-TR-62-1, February 1962.

1-20. Hall, W. E.: " Prop-Rotor Stability at High Advance Ratios", Journal of the American Helicopter Society, June 1966.

1-21. Edenborough, H. K.: "Investigation of Tilt-Rotor VTOL Aircraft Rotor-Pylon Stability," AIAA Paper 67-17, January 1967.

1-22. Exploratory Definition Final Report, Model 266 Composite Aircraft Program, Bell Helicopter Company, Report Nos. 266-099-201-223, July 1967.

1-23. Richardson, J. R., and H. F. W. Naylor: "Whirl Flutter of Propellers with Hinged Blades", Report No. 24, Engineering Research Associates, Toronto, Canada, March 1962.

1-24. Gallardo, V., Jr.: "Propeller-Nacelle Whirl Flutter Analysis of K-16B Amphibious VTOL/STOL Aircraft", Kaman Aircraft Corp., Report No. G-113-41, August 1962.

1-25. Reed, W. H., III, and R. M. Bennett: "Propeller Whirl Considerations for V/STOL Aircraft", presented at the CAL/TRECOM Symposium on Dynamic Loads Problems Associated with Helicopters and V/STOL Aircraft, June 26-27, 1963.

1-26. Reed, W. H., III.: "Propeller-Rotor Whirl Flutter: A State-of-the-Art Review", presented at the Symposium on the Noise and Loading Actions on Helicopter V/STOL Aircraft and Ground Effect Machines , Southhampton, England, Aug. 30-Sept. 3, 1965.

1-27. Reed, W. H., III: "Review of Propeller-Rotor Whirl Flutter", NASA TR R-264, July 1967.

1-28. Young, M. I., and R. T. Lytwyn: "The Influence of Blade Flapping Restraint on the Dynamic Stability of Low Disk Loading Propeller-Rotors", Proceedings of the 23rd Annual National Forum of the American Helicopter Society, May 1967.

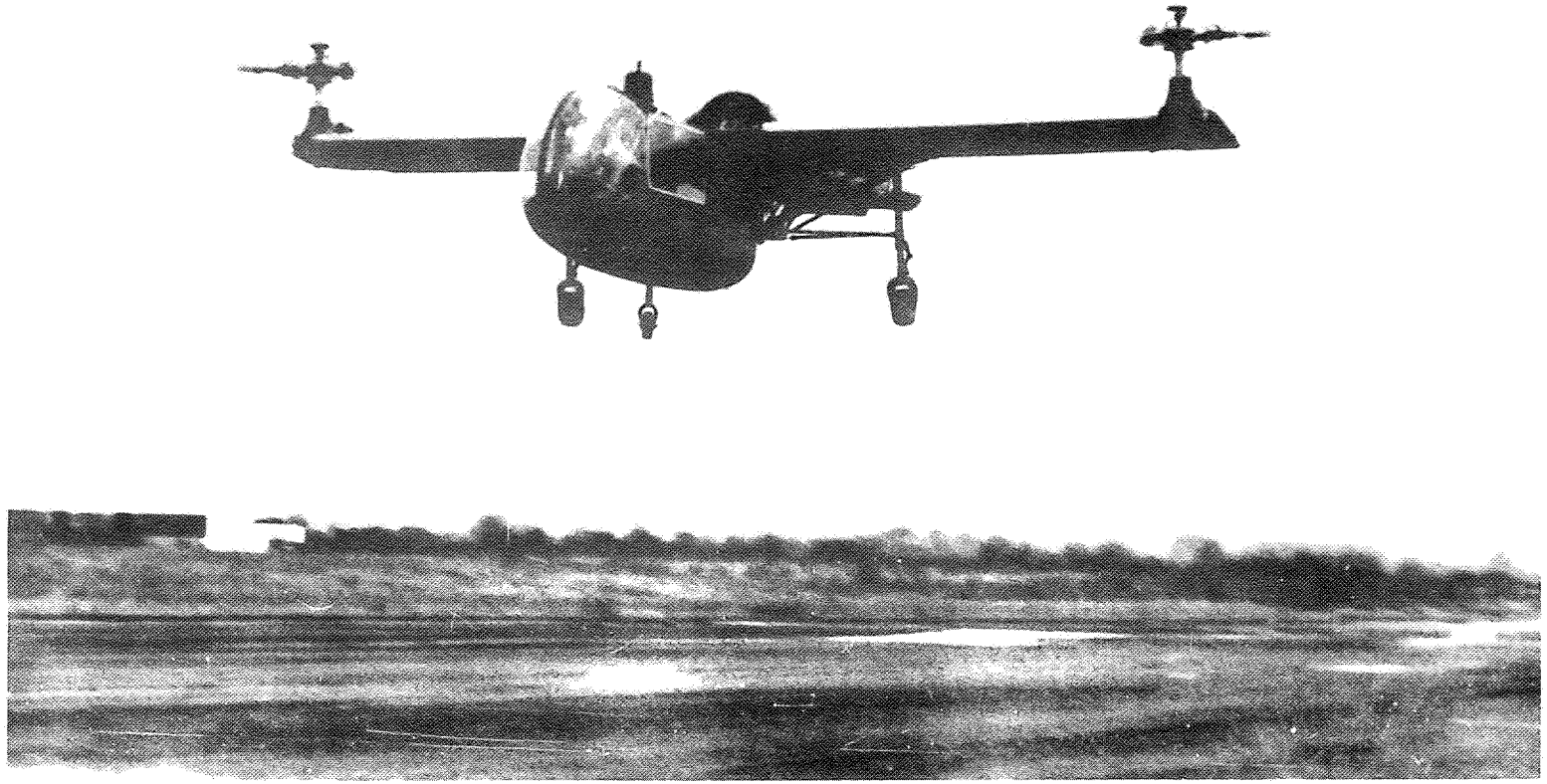

Figure 1-1.- Transcendental Model 1-G tilt-rotor convertiplane (1954).

Figure 1-2.- Bell XV-3 tilt-rotor convertiplane in hover and low-speed flight (1955).

Figure 1-3.- Transcendental Model 2 tilt-rotor convertiplane (1956).

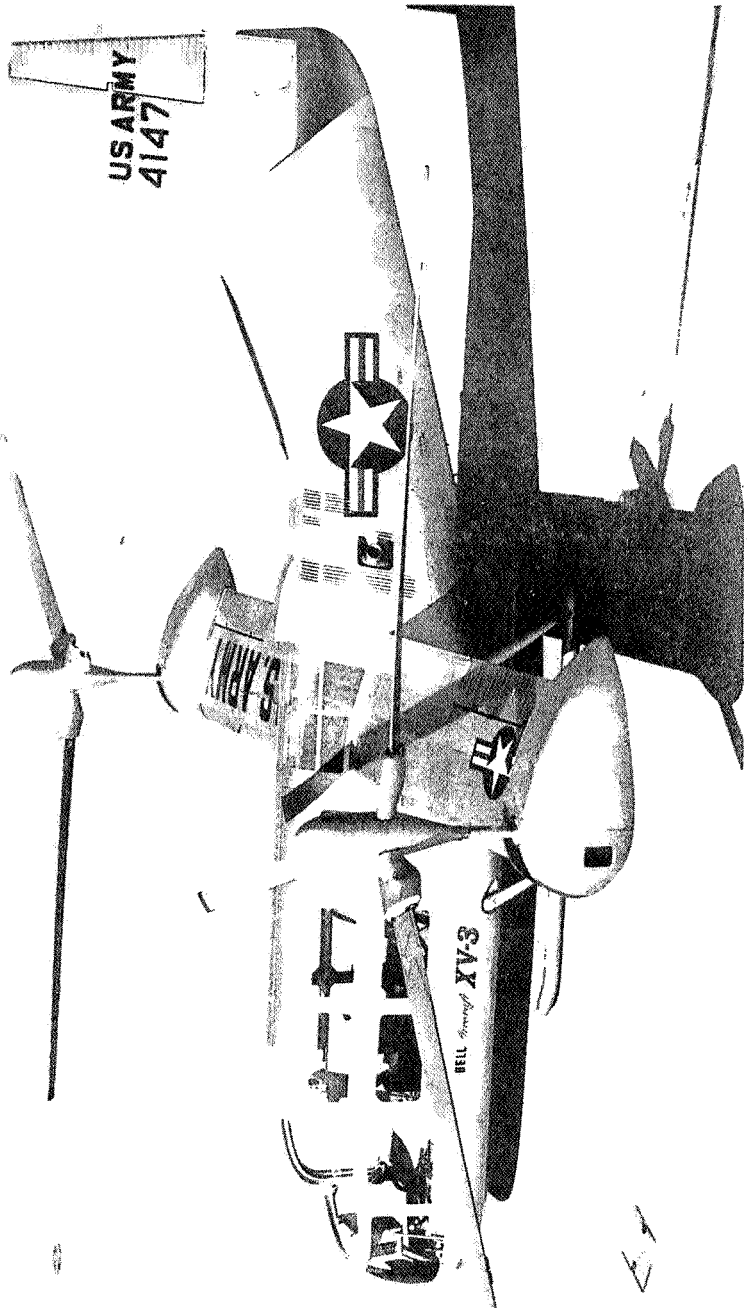

Figure 1-4.- First Bell XV-3 tilt-rotor convertiplane.

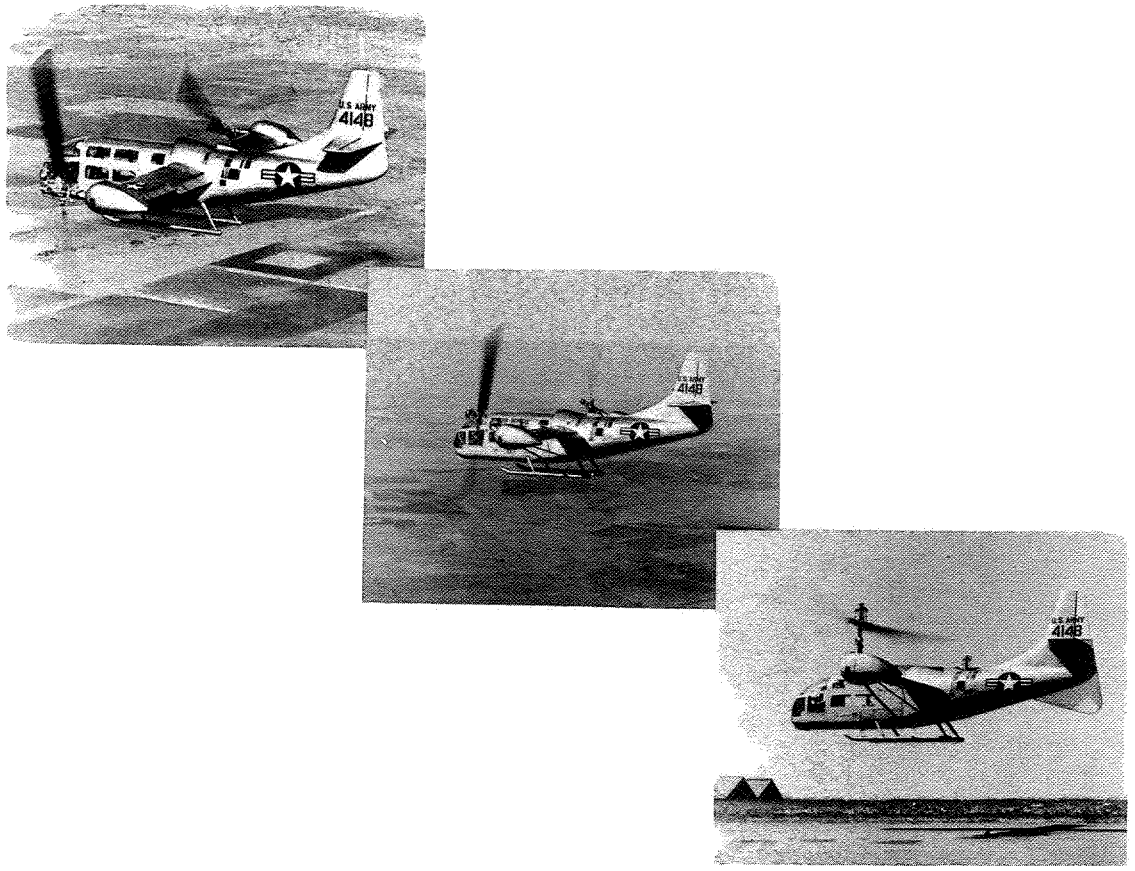

Figure 1-5.- Second Bell XV-3 tilt-rotor convertiplane in hover, conversion, and airplane modes of flight.

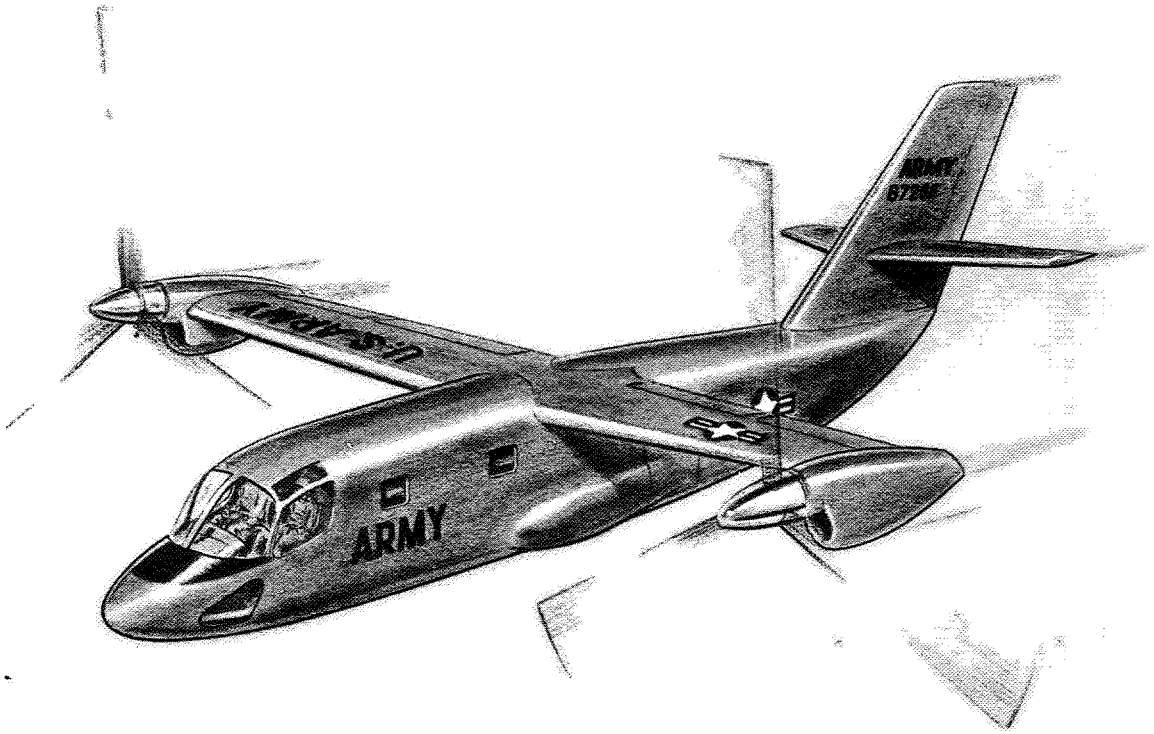

Figure 1-6.- Artist's conception of Bell Model 266 tilt-proprotor design evolved during the Army Composite Aircraft Program.

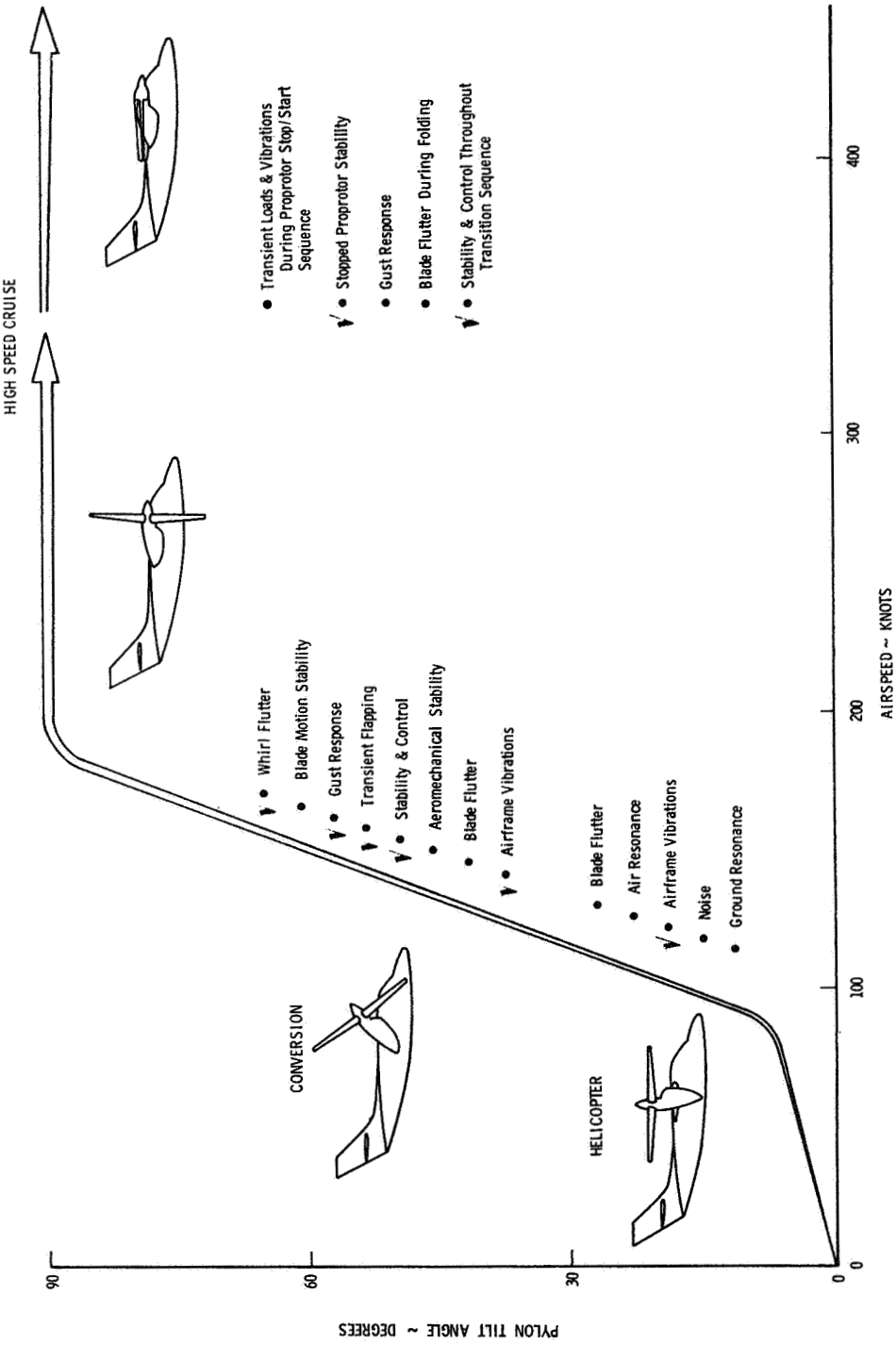

Figure 1-7.- Aeroelastic considerations affecting tilt-proprotor and folding-proprotor V/STOL aircraft design.

CHAPTER 2

A RETROSPECTIVE ON PROPELLER AND PROPROTOR WHIRL FLUTTER

Introduction

Continuing in the introductory spirit of Chapter 1, the present chapter, after briefly reviewing some of the conceptual aspects of proprotor V/STOL aircraft design, reexamines several salient features of propeller-and proprotor-related dynamics with a view toward providing insight into the mechanism of whirl flutter for both propellers and proprotors through relatively simple physical considerations. The fundamental difference in the manner in which precession-generated aerodynamic forces act on the pylon and induce whirl flutter is delineated. The source of this difference is described, providing a basis for showing why a proprotor can exhibit whirl flutter in either the backward or forward directions while a propeller whirls only in the backward direction.

The Proprotor V/STOL Aircraft Concept

The low-disc-loading helicopter has established itself as the most efficient vehicle having a vertical lift and hovering capability. The aerodynamic limitations imposed by advancing blade Mach number and retreating blade stall on high-speed helicopter performance are well-known.* Increasing demands on

*See, for example, "Extending Helicopter Speed Performance", by R.M. Carlson, R. E. Donham, R. A. Blay, and D. W. H. Godfrey, Lockheed Horizons, July 1967.

extending the forward speed capability of the helicopter have led to so-called compound helicopters which partially unload the rotor in forward flight through the use of small wings and employment of an auxiliary propulsion system to provide forward thrust, thereby delaying the aerodynamic limitations. However, at speeds approaching about 300 knots the compressibility drag rise on the advancing blades becomes excessive even on a compound configuration. Continued extension of rotary-winged vehicle speed performance depends on altering the conventional edgewise-flying rotor orientation in a manner which circumvents the aerodynamic limitations at high forward speeds. This trend has led to composite or convertible aircraft which, after take-off using the rotor system in the manner of a conventional helicopter, convert the rotor function into a fixed-wing configuration. Conceptually, there are several means available for accomplishing this metamorphosis, allowing efficient airplane-type cruise speeds with no sacrifice of vertical lift capability. Several such techniques are discussed in Refs. 2-1 and 2-2. Two particular concepts that employ proprotors will be discussed here.

(a) The Tilt-Rotor

One concept which offers an efficient cruise speed potential in the 300-350 knot range and is currently the subject of active design studies is the tilt-rotor. After lift-off as a helicopter, transition from helicopter to fixed-wing flight is made by gradually shifting lift from rotors mounted on wing tip-mounted pylons to wings as the pylons convert from the vertical or

zero degree conversion angle to the horizontal or 90° conversion angle. When fully converted the rotors act as tractive propellers (hence the acronym proprotor) and the weight of the aircraft is completely supported by conventional high aspect ratio wings. The typical conversion "corridor" is quite broad, thereby eliminating the need for precisely scheduled conversion with power or airspeed. A typical conversion would be made in the 120-150 knot speed range, the minimum airspeed for conversion being dictated by wing stall.

The helicopter mode of flight is generally taken to be that for pylon conversion angles less than 15° and the conversion mode for pylon angles between 15° and 90°. When fully converted (90°) the mode has been variously designated as the airplane, high-speed, or proprotor mode. STOL-type operational capability (under overload gross weight conditions) is made possible by converting the pylons up to 30° for rolling takeoffs and landings. An interconnecting shaft joining the two rotors provides for synchronization of rotor speeds and insures that in the event of an engine failure either engine may drive both rotors. Autorotational landings may be made from any flight mode in the event of total power failure. This feature was demonstrated by power-off reconversions of the Bell XV-3 convertiplane during its flight evaluation.

Specific considerations relating to these and other aspects of the tilt-rotor aircraft concept may be found in Refs. 2-3 to 2-6. Figs. 2-1 to 2-6 illustrate artists' concepts of several

tilt-rotor designs depicted in various civil and military roles. Fig. 2-7 is a composite photograph of a 1/5-scale model of the Bell Model 300 tilt-rotor.

(b) The Folding Tilt-Rotor

Decreasing propulsive efficiency with increasing airspeed, resulting from proprotor drag in the high speed mode, generally limits the maximum cruise speed of the tilt-rotor to about 350 knots. An approach for extending the speed range of the tilt-rotor configuration into the high subsonic/transonic Mach number regime is through the expedient of stopping and folding the blades. This variant of the tilt-rotor aircraft concept has been termed the folding proprotor. Such vehicles add a proprotor stopping, folding, and stowing sequence subsequent to the pylon conversion process. After conversion to the airplane mode of flight and the attainment of a speed which allows a smooth transfer of forward thrust the proprotor thrust is gradually reduced while jet thrust from auxiliary turbofan engines or compound engines is gradually increased to approximate the decrease in proprotor thrust. This progressively unloads the proprotors until they are in a zero shaft torque (that is, windmilling) condition. The proprotors can then be decoupled from the drive train, aerodynamically feathered to a stop, positioned, folded back along the wing tip pylons, and locked. With the blades folded, proprotor drag is significantly reduced and the aircraft can accelerate to a cruise speed limited only by the installed thrust of the jet engines.

For landing in the helicopter mode the procedure is reversed. In the folded configuration the aircraft could land as a conventional fixed-wing aircraft.

The interested reader may find a broad spectrum of considerations applicable to various design aspects of this type vehicle in Refs. 2-4 to 2-10. Artists' concepts of several folding proprotor designs are illustrated in Figs. 2-8 to 2-11.

Some Design Problems Associated with Proprotor Aircraft

As pointed out in Chapter 1, the feasibility of the tilt-rotor V/STOL aircraft concept was demonstrated by the Bell XV-3 and Transcendental convertiplanes. However, several flight deficiencies were pointed out during flight evaluation of the XV-3, particularly during operation in the airplane mode. These included longitudinal (short period) and lateral-directional (Dutch roll) stability and flapping during maneuvers.

The proprotor-generated aerodynamic forces and moments affecting aircraft rigid-body stability while operating in the high-speed cruise mode with the pylons fully converted are brought into perspective in Fig. 2-12. The aerodynamic forces and moments associated with low frequency pitch, yaw, and roll oscillations about the aircraft center of gravity (such as might be induced by a disturbance) are indicated. Since the proprotors are located ahead of the center of gravity in the proprotor mode Fig. 2-12 clearly indicates that these forces and moments will strongly influence all aspects of longitudinal and lateral-directional stability.

The shear forces H and Y will be shown to be the result of proprotor flapping required to induce the aerodynamic moments necessary to precess the proprotor in response to aircraft pitch and yaw motions. Proprotor flapping is also an important design consideration because the flapping natural frequency in the non-rotating system is close to the aircraft rigid-body frequencies and hence can couple with them.

These same shear forces can, quite independently of any rigid-body motions, destabilize the proprotor/pylon/wing system aeroelastically. This was dramatized during full-scale tests of the XV-3 in the Ames 40 x 80 ft wind-tunnel in 1962 when a limit cycle whirl instability was encountered. This instability portended a more complex variety of whirl flutter and elevated proprotor/pylon stability analyses to a place of prime importance in the design process of tilt-rotor aircraft. Because of the flapping freedom of the proprotor, several types of instability associated with the proprotor/pylon/wing system can be experienced, these being characterized by frequency, direction of pylon whirl, and the amount of flapping in space. In particular, the flapping modes can become unstable (the XV-3 instability was a flapping mode instability). Because of these added complexities a proprotor will not respond in the same rigid-body manner as a propeller. Hence, additional ingredients need be considered in assessing system stability.

The folding proprotor operates in the helicopter, conversion, and proprotor modes as does a tilt-rotor and thus has similar

dynamic problems. However, as the maximum speed in the proprotor mode is about 250 knots for the folding proprotor the design requirements are dictated by considerations other than rigid-body and proprotor/pylon stability in the proprotor mode. These considerations are primarily those of stability and control during the stopping and folding sequence of transition. In particular, the requirements imposed by the variation of the aerodynamic forces and moments shown in Fig. 2-12 as the rotor rotational speed is decreased to zero pose several interesting design problems. These include such items as the decrease in static margin as the proprotors are stopped, aircraft trim changes, and proprotor rigid-body flapping behavior as rpm is decreased to zero. These and other dynamic considerations which must be addressed with regard to the total design of a folding proprotor aircraft are discussed in depth in Refs. 2-4 to 2-10.

Because of the central role played by the proprotor-generated aerodynamic forces and moments in aircraft rigid-body stability and proprotor/pylon/wing aeroelastic stability (whirl flutter) the origin of these forces will be reviewed. For completeness, a review of the mechanism of propeller-nacelle whirl flutter will be presented first. This will also provide the opportunity to examine similarities and dissimilarities as regards the whirl flutter mechanism of propellers and proprotors.

A Review of Several Aspects of Propeller/Nacelle Whirl Flutter

A particular manifestation of the flutter phenomenon known as propeller whirl flutter came into prominence in 1960 as a result of the loss of two Lockheed Electra aircraft in fatal accidents. This instability, which can occur on flexibly mounted propeller/nacelle installations, involves a self-sustained or divergent whirling precessional motion of the propeller hub about its undeflected position. The possibility that such an instability could occur in a flexibly mounted propeller/nacelle combination was cited in a paper by Taylor and Browne as early as 1938 (Ref. 2-11). However, the large margins of safety prevalent at that time on existing configurations precluded anything more than an academic interest in this phenomenon.* Extensive wind-tunnel tests conducted by NASA at its Langley Research Center facility (Ref. 2-14) verified the possibility of whirl flutter in Electra aircraft if the engine support stiffness was sufficiently reduced. Whether or not the support stiffness was in fact so reduced in the said aircraft has never been conclusively established. Various analytical and experimental studies were subsequently undertaken to identify and study the basic governing parameters important in propeller whirl flutter. The results of several of these studies may be found in Refs. 2-15 to 2-20.

*In particular, this academic interest was exemplified by R. H. Scanlan and his group at Rensselaer Polytechnic Institute. Refs. 2-12 and 2-13 are some results of their work.

The distinguishing feature of the Electra aircraft were their engines, which were of the turboprop type. They differed from piston engines in that the propeller was connected to the engine through a remote drive arrangement rather than directly attached to the engine. This created a structural configuration in which propeller-generated aerodynamic and gyroscopic forces assumed the dominant role in establishing the dynamic behavior of the coupled propeller/nacelle/wing system. The dynamic implications of turboprop installations, and the trend to softer engine mounts, long overhung nacelles, and "unorthodox" methods for the placement of propeller/nacelle systems in some V/STOL aircraft raised propeller whirl stability analyses to a position of importance in the design process for propeller driven aircraft. This importance is reflected in amendments to the U. S. Civil Air Regulations (Ref. 2-21) which require that freedom from whirl flutter be demonstrated under failure of any single element in the mount system.

Because of the central role played by propeller-generated aerodynamic and gyroscopic forces in the dynamic behvaior of a propeller/nacelle/wing system, in particular whirl flutter, they will be discussed in somewhat more detail below. Since relatively simple physical considerations assuming quasi-steady aerodynamics and small angle-of-attack changes can aptly portray the features of interest, the discussion will be qualitative in nature and proceed along the lines of Ref. 2-22, which is an excellent non-mathematical account of propeller whirl flutter.

(a) Role of Aerodynamic Forces in the Flutter Mechanism

Perturbed motions of a propeller/nacelle combination in pitch or yaw while in forward flight disrupt the axial-flow symmetry over the propeller disc. This aerodynamic asymmetry induces cyclic angle-of-attack changes, and hence cyclic lift force changes, on blade elements of the propeller. These give rise to resultant aerodynamic forces and moments which, even in the absence of gyroscopic coupling forces, can couple the pitch and yaw degrees of freedom of the propeller to form a whirl mode. From established small vibration theory it is known that in harmonic motion (such as occurs at the critical flutter speed) the phase shift between force and displacement is directly associated with any exchange of energy between a system and the forces acting on it. Forces and displacements which are inphase or 180^{o} out-of-phase with each other are known to be associated with no net energy input in any complete cycle of oscillation. Inertial and elastic forces fall in this category. However, the perturbation aerodynamic forces and moments generally have phase angles of 90^{o} relative to the nacelle motions and hence provide a mechanism for a net energy input to the system. The origin of these forces and moments can be demonstrated by simple considerations based on blade element theory. Under quasi-steady conditions the pitching and yawing motions that constitute a whirl motion induce flows at the propeller disc which arise from pitch and yaw angles and from pitching and yawing angular velocities. Propeller blade elements

experience an increase or decrease in their angle of attack depending on whether these induced flows add to or subtract from the unperturbed inflow and rotational velocity.

Results of considerations of this type are given in Figs. 2-13 to 2-15. Thrust and drag have been neglected. Consider motion in the pitch plane only. Forces due to both pitch angle and pitch rate arise. When the propeller shaft is inclined at an angle α relative to the free-stream direction as shown in Fig. 2-13a the forward flight velocity V has a cross-flow component $V\alpha$ directed upward in the plane of the propeller disc. If azimuthal changes in blade element inflow angle, and hence angle of attack, are established as outlined in Ref. 2-22, the cross-flow component is seen to increase the angle of attack and hence lift of blade elements on the downgoing side of the propeller disc while decreasing the angle of attack, and hence lift, of blade elements on the upgoing side. This appears as an unsteady motion, the angle of attack of all blade elements varying harmonically around the azimuth. The directions of these perturbation lift changes are indicated in Fig. 2-13a for elements in laterally disposed blades where the absolute magnitude of the lift changes is a maximum. Resolving these perturbation lift forces into components parallel and normal to the propeller plane the integrated effects over one complete cycle of propeller rotation produce the resultant force and moment shown in Fig. 2-14a. When the propeller has an upward pitch rate about a pivot aft of the propeller plane the axial aerodynamic symmetry is modified by two types of

perturbation flows, a cross-flow velocity $h\dot{\alpha}$ downward in the propeller plane and an inflow distribution $r\dot{\alpha}$ normal to the propeller plane. These are illustrated in Fig. 2-13b. Since the cross-flow is in a direction opposite to that due to pitch angle the lift changes are in the directions indicated in Fig. 2-13b. The inflow $r\dot{\alpha}$ increases the angle of attack and hence lift on the upper half of the propeller disc and decreases the angle of attack and hence lift on the lower half, the maximum lift changes occurring on elements of the vertically oriented blades as indicated. The integrated effects produce the resultant forces and moments shown in Fig. 2-14b. If similar considerations of azimuthal changes in blade element angle of attack are carried out for motion in the yaw direction one can establish the existence of the static and dynamic forces and moments summarized in Fig. 2-15. In Figs. 2-13 to 2-15, the particular perturbation velocity component giving rise to a force or moment is indicated in parentheses.

The static and dynamic aerodynamic forces and moments indicated in Figs. 2-14 and 2-15 govern the stability of motion following a disturbance. Consider the implication of these forces and moments as regards the possibility of instigating a whirl instability. Assume that the propeller hub is executing a constant amplitude backward whirl precessional motion. The aerodynamic forces and moments generated by the whirling motion at the instant the hub is at its maximum nose-up pitch attitude are indicated in Fig. 2-16a. Note that the moments $N(V\alpha)$ and

$N(r\dot{\psi})$ and the force $Y(h\dot{\psi})$ are the only aerodynamic disturbances which can induce (or maintain) a whirl motion. In particular, note that the yawing moment due to pitch $N(V\alpha)$ is in the same direction as the yawing velocity for the backward whirl mode and hence constitutes negative (destabilizing) aerodynamic damping for the backward whirl mode. To maintain system stability this negative damping must be balanced by other positive damping contributions. The aerodynamic portion of this positive damping is found in $N(r\dot{\psi})$ and $Y(h\dot{\psi})$. A similar inspection of forces for the propeller hub in a nose-left yaw attitude would give a pitching moment due to yaw $M(V\psi)$ in the same direction as the whirl velocity for the backward whirl mode. Hence, a negative damping contribution is again indicated. Consequently, the cross-stiffness moments $N(V\alpha)$ and $M(V\psi)$, being in phase with the velocity in the backward whirl mode, must be the aerodynamic terms responsible for whirl flutter. Since these cross-stiffness moments are proportional to V^2 while the positive aerodynamic damping terms are proportional to V, the destabilizing moments will exceed the combined positive damping moments at some speed and precipitate a whirl instability. The nacelle spring rates in conjunction with $H(V\alpha)$, $M(h\dot{\psi})$, and $H(r\dot{\psi})$ govern the static stability of the propeller/nacelle combination in pitch. As discussed in Ref. 2-23 $H(r\dot{\psi})$ is a cross-damping force which acts as a stiffness term in the pitch plane. $H(V\alpha)$ opposes the pylon spring restoring force. The cross-damping moment $M(h\dot{\psi})$ acts as an aerodynamic cross-stiffness term since it is inphase with the pitch angle.

Now assume that the propeller hub is executing a constant amplitude whirl in the forward direction. The forces and moments acting on the hub at the maximum pitch-up attitude of its whirl motion lead to the situation shown in Fig. 2-16b. Note that a contradiction exists. Although a whirl motion in the forward direction was assumed, the only forces and moments which can induce and sustain a whirl are in the direction of the backward whirl mode. Hence, based on aerodynamic considerations, propeller whirl flutter can not occur in the forward whirl mode.

If unsteady aerodynamic effects associated with the shed vorticity are considered as in Ref. 2-16, cross-stiffness forces are induced which act in the direction of the forward whirl velocity. These contribute negative damping to the forward whirl mode and positive damping to the backward whirl mode. These terms, however, are small and can not destabilize the forward whirl mode. Since the backward whirl mode is stabilized, this suggests, as indicated in Ref. 2-22, that the use of quasi-steady aerodynamics, which neglect the effects of the oscillating wake created by the shed vorticity, is conservative.

The foregoing discussion has been conspicuous in its lack of any mention of the role played by gyroscopic forces in the whirl flutter mechanism. As a point of fact, the preceding is completely valid if in some manner the propeller rotational speed could be maintained but the gyroscopic forces taken to be identically zero. In other words, purely on the basis of aerodynamic considerations a mechanism for whirl flutter is present:

the uncoupled pitch and yaw nacelle modes can be coupled aerodynamically to yield whirl modes, one of which will become unstable at some forward speed. Flutter speeds based on the neglect of gyroscopic forces are generally well beyond normal flight speeds of propeller-driven aircraft. However, as pointed out in Ref. 2-22 the presence of gyroscopic forces provides a mechanism whereby these flutter speeds can be significantly reduced, bringing them well within speed ranges of interest. The manner in which this is brought about is outlined in the next section.

(b) Role of Gyroscopic Forces in the Whirl Flutter Mechanism

Basically, the gyroscopic coupling principle involved is this: a rotating propeller responds to a torque applied perpendicular to its spin axis by precessing, the precession vector being perpendicular to both the spin and torque axes rather than parallel to the torque axis as would be the case for a non-rotating propeller. In the absence of aerodynamic forces, a rigid non-rotating propeller mounted on a flexibly supported nacelle exhibits two modes of vibration, one in pitch and one in yaw. Each can occur independently of the other when the propeller is not rotating. However, when the propeller is rotating (still neglecting aerodynamic forces) gyroscopic forces exist which couple these modes together into two whirl modes characterized by the direction in which the propeller hub whirls or precesses about its undeflected shaft axis. As gyroscopic coupling is increased by increasing the propeller rotational speed, the whirl

mode for which the precession direction is the same as the propeller rotation has an increasing frequency while the whirl mode for which the precession is in a direction opposite to the propeller rotation has a decreasing frequency. The former is termed the forward or posigrade whirl mode and the latter the backward or retrograde whirl mode.

Pylon pitch and yaw are phased at 90^{o} to each other in the whirl mode. Since gyroscopic forces are proportional to velocity they are 90^{o} out-of-phase with pitch and yaw displacement throughout a cycle of whirl. It might thus appear that gyroscopic forces have the necessary phasing for a net energy input to the system. Gyroscopic forces are conservative however, the positive work done by the gyroscopic couple in one plane being exactly balanced by the negative work in the other plane (Ref. 2-24). Hence gyroscopic forces contribute neither positive nor negative damping to system motion but merely couple pitch and yaw together at 90^{o} to form two whirl modes. The conservative nature of gyroscopic forces can be demonstrated indirectly by solving the flutter equations for the system in a vacuum for the case of no structural damping as a function of propeller rotational speed. Inspection of the resultant complex roots and modes will show that the damping parts of the eigenvalues will be zero and the modes will all indicate a 90^{o} phase relation between pitch and yaw. The conclusion then is that gyroscopic action in itself can not precipitate a divergent whirl motion.

Although the gyroscopic forces are neither stabilizing nor destabilizing in a dynamic sense they were shown in Ref. 2-22 to contribute in effect statically to decreased dynamic stability in the backward whirl mode. Although it was not pointed out in Ref. 2-22, gyroscopic forces have a corresponding stabilizing effect on the forward whirl mode. Both these assertions can be verified with the aid of Fig. 2-17, which shows a propeller hub tracing out a whirl mode in an as yet unspecified direction. The in-vacuum equations of motion applicable at four instantaneous positions on the path are indicated. These equations are independent of the whirl direction. Now assume a constant amplitude whirl in the backward direction and consider the situation at position 1 say, as regards the sign of the gyroscopic term $2\Omega I_R \dot{\alpha}$ compared to the physical spring term $K_\psi \psi$. The table in the lower part of the figure indicates that at position 1 ψ is positive and $\dot{\alpha}$ is negative. Hence the gyroscopic term is of opposite sign compared to the spring term and thus has a "negative" spring effect, that is it tends to increase the whirl amplitude statically. The same is true at the other positions on the path. Now consider the situation at position 1 if the whirl is in the forward direction. In this case both ψ and $\dot{\alpha}$ are positive and hence the gyroscopic force has a positive spring effect, tending to reduce the amplitude of whirl statically. The same is true at any other position.

It was shown earlier that aerodynamic cross-stiffness moments $N(V\alpha)$ and $M(V\psi)$ are the driving moments for backward whirl flutter. For a fixed forward flight speed these moments increase with whirl amplitude. Now, since the gyroscopic forces have just been shown to increase the amplitude of the backward whirl mode, this has the effect of increasing the destabilizing aerodynamic cross-stiffness moments. This is the means by which gyroscopic forces can reduce the backward whirl flutter speeds to values within the operating envelopes of propeller-driven aircraft. Conversely, since gyroscopic forces reduce the whirl amplitude of the forward whirl mode they stabilize the forward whirl mode. These effects of the gyroscopic forces are clearly brought out in Fig. 2-18 which shows the variation of modal damping in both the forward and backward whirl modes with continually decreasing gyroscopic coupling. The results shown are for a non-isotropically supported nacelle at a subcritical airspeed. The gyroscopic forces were analytically reduced by multiplying the gyroscopic coupling terms in the equations of motion by numbers ranging from 1.0 to 0.0 and then solving the resulting flutter equations. This held the total pitch and yaw inertias constant. A significant reduction in the damping of the backward whirl mode with increase in the gyroscopic coupling terms is evident. The forward whirl mode is seen to be only modestly stabilized.

Summarizing: based solely on aerodynamic considerations the aerodynamic cross-stiffness moments $N(V\alpha)$ and $M(V\psi)$ provide the coupling necessary to induce an unstable whirl motion. In the

presence of gyroscopic forces the backward whirl mode is additionally destabilized while the forward whirl mode is stabilized. Propeller whirl flutter, when it occurs, invariably occurs in the backward whirl mode.

The Mechanism of Proprotor/Pylon Instability

A flapping proprotor on a flexibly supported pylon can also exhibit an instability similar in nature to propeller/nacelle whirl flutter. In fact, the fundamental cause of proprotor/pylon instability is the same as that of propeller whirl flutter, namely, the aerodynamic loads generated by precession. However, because of the additional flapping degrees of freedom of the proprotor the manner in which the precession-generated aerodynamic forces act on the pylon and hence promote whirl is significantly different. Because a propeller is rigidly attached to its shaft it is constrained to follow any nacelle motion in pitch and yaw and the aerodynamic cross-stiffness moments which drive the backward whirl mode act directly on the nacelle. In the case of a free-to-flap proprotor*, no airload moments can be transferred to the pylon. Consequently, in contradistinction to a propeller, airload moments can not be the direct cause of any proprotor/pylon whirl instability. Aerodynamic forces must then constitute the source of

*A free-to-flap proprotor is taken to be one which can not transfer any airload moments to the pylon. As such it represents the opposite extreme to a rigid fixed-blade propeller. All practical proprotor designs would fall between these two extremes, but closer to the free-to-flap situation. Such a configuration would be realized in practice by a rotor having central flapping hinges or a gimbaled hub, with zero flapping restraint.

any net energy input into a whirl mode. Some of the salient features of the means by which this is brought about will be discussed below. The methodology was motivated by the original work of Hall (Ref. 2-25).

(a) Precession of a Free-to-Flap Proprotor

As noted above, a free-to-flap proprotor is unable to transmit any moments to the pylon. Conversely, the pylon is unable to transmit any moments to the proprotor. During a precessional motion of the pylon there is no means by which the pylon can physically constrain the proprotor to follow its precessional motion. This suggests that airloads must, in some manner, constitute the necessary ingredient in the proprotor precession mechanism. Recall that in the case of a propeller airloads are a consequence of precession rather than the cause. In a vacuum the proprotor would not precess in response to pylon pitch or yaw oscillatory motions since the pylon would have no way of "telling" the proprotor that it should precess. The proprotor disc would merely oscillate edgewise in space remaining parallel to its original position. A flapping proprotor is essentially a gyroscope and requires a couple across its rotor disk 90° out of phase with any angular motion of the pylon to make it precess in response to the pylon motion. This is illustrated in Fig. 2-19. The couples required to precess the proprotors in response to the aircraft upward pitch rate follow directly from the gyroscopic rule. To generate these couples resultant force unbalances normal to the proprotor plane in the directions shown on each side are necessary.

These force unbalances can only be generated aerodynamically. The airloads necessary to precess the proprotor will be generated only if the blade angle of attack is cyclically changed, with increasing lift on one half of the disc and decreasing lift on the other half, in a manner to create the necessary couples. This is illustrated in Fig. 2-20 for the case of motion in the pitch direction. As in the helicopter rotor this cyclic blade angle of attack is introduced through affecting the angular position of the tip-path-plane with respect to the proprotor control plane (swashplate). This is because it is the control plane and not the shaft (mast) that determines the rotor behavior in space. The means by which this is accomplished is illustrated in Figs. 2-20 and 2-21. The proprotor disc lags the shaft angular rate until sufficient flapping is present to produce the necessary couple aerodynamically by increasing lift on the downgoing side of the disc and decreasing it on the upgoing side. This circumstance arises because, relative to the swashplate (control plane), the blades on the upgoing side have a forward flapping rate, with a maximum when in the horizontal position, which adds to the forward flight speed, while on the downgoing side of the disc the blades have a rearward flapping rate, with a maximum when in the horizontal position, which subtracts from the forward flight speed. The resultant perturbation lifts are shown in Fig. 2-21. The moments arising from the axial components of the perturbation lift change, ΔF_β, sum to produce the necessary moment to precess the proprotor. Note that perturbation inplane shear forces are additionally generated. These sum to produce a

resultant vertical and lateral force. Note that the vertical component ΔH acts in the direction of the upward pitch rate and thus constitutes a negative (destabilizing) damping force for pylon pitch motion. Similar results would be obtained for an assumed motion in the yaw plane. This implies that in contrast to a propeller/nacelle combination, which can not be dynamically destabilized in a single plane, a proprotor/pylon system can experience an instability with either the pylon pitch or yaw degrees of freedom locked out. In the general case of a proprotor aircraft executing longitudinal and lateral oscillations about axes through its center of gravity the resultant inplane shears would constitute negative damping in both pitch and yaw simultaneously. Depending on the excitation frequency this can destabilize either the aircraft rigid-body motion or the elastic motion of the proprotor/pylon/wing system. Since the tip-path-plane lags the swashplate a component of the thrust acts normal to the mast and opposite in phase to the destabilizing shear forces and constitutes positive damping. At low advance ratios, such as occur in low speed helicopter flight, the destabilizing shears are small and the net damping is positive (Ref. 2-26). However, at the advance ratios typical of high-speed proprotor flight the shears become sufficiently large to offset the stabilizing force produced by the tilt of the thrust vector and the resultant force is in the direction to give a negative damping moment. When this overcomes the positive damping of the system instability results.

(b) Role of Precession-Generated Shear Forces in Whirl Flutter

Although a proprotor/pylon instability is possible if either the pylon pitch or yaw degrees of freedom are rigidly restrained the general case of flexible restraints in both pylon degrees of freedom permits of a whirl flutter instability in the "classical" sense. This can be demonstrated in the same manner employed for the propeller earlier, namely, assuming a constant amplitude whirl in the forward and backward directions, determining the forces which act on the pylon during the whirl motion, and assessing whether or not they constitute a potential source of negative damping. Because of the additional degrees of freedom involved this would be quite difficult to do qualitatively. Consequently, the motion-dependent forces have been evaluated using an analytical method developed herein and embodied in computer program HFORCE1.

Assume the proprotor to be executing a low-frequency constant amplitude whirl in the backward direction. The shear forces acting on the shaft when it is at its maximum upward pitch attitude are shown in Fig. 2-22a. Although the forces are generally functions of all the degrees of freedom and their first time derivative, their primary dependency is on the coordinates enclosed in parentheses. The direct damping force $Y(\dot{\psi}, \dot{b}_1)$ is inphase with the backward whirl velocity and hence contributes negative damping to the backward whirl mode. Note that this force arises from a yaw rate and that it is resisted by $Y(\alpha, a_1)$, a cross-stiffness force which acts like a positive damping term.

Static stability is determined by the direct stiffness term $H(\alpha, a_1)$ and the cross-damping term $H(\dot{\psi}, \dot{b}_1)$ which acts as a spring term. Similar results and conclusions will be reached at any other position. A similar assessment of the conditions at the same point for the case of a forward whirl motion, as shown in Fig. 2-22b, indicates that forward whirl flutter is additionally possible. Hence, based on the forces which are induced by an assumed whirl motion, no contradiction is found to exist which would negate the possibility of whirl in either the forward or backward direction. Therefore a proprotor/pylon can exhibit whirl flutter in either the forward or backward whirl modes.

Because the lag of the proprotor tip-path-plane is a function of the pylon precessional whirl frequency, the precessional air-loads and hence the destabilizing shears are inherently frequency-dependent. Now, depending on the whirl frequency (i.e., the pylon structural spring rates) the magnitudes and/or signs of the de-stabilizing proprotor shears can change. (This will be shown in Chapter 4). With reference to Fig. 2-22, this again indicates that the proprotor/pylon whirl instability can be in either direction. In both the forward and backward whirl modes the shear forces due to flapping are phased in a direction that contributes to instability at high advance ratio. In contrast, the aerodynamic forces and moments of a propeller are independent of the frequency of nacelle motions because there is no lag of the propeller disc relative to the shaft.

If proprotor aerodynamic moments can be transferred to the pylon they would modify the foregoing results only to the extent that they would be additionally stabilizing or destabilizing, since their magnitude and sign would also be a function of the pylon whirl frequency. The aerodynamic moments associated with the shear forces in Fig. 2-22, but acting on the proprotor, are summarized in Fig. 2-23. As inspection of this figure indicates, if these moments can be transferred to the pylon (through a flapping spring say) they could have a stabilizing or destabilizing influence on whirl.

The key points of the foregoing can be summarized as follows:

(1) The basic destabilizing factors on proprotor/pylon motion are the inplane shear forces generated by the airload moments required to precess the rotor in space in response to shaft motions.

(2) In addition to a true whirl instability involving both pitch and yaw motions a proprotor/pylon system can exhibit a dynamic instability in either the pitch or yaw direction depending on the pylon support conditions.

(3) Flapping during precession and the associated forces and moments are frequency-dependent.

The destabilizing shear forces have a first order effect on both aircraft rigid-body stability and the aeroelastic stability of the proprotor/pylon/wing system. Since these shears are dependent on the frequency response of the tip-path-plane relative to the swashplate stability will be strongly sensitive to those

parameters which control the response rate as well as the pylon support conditions. Two of the more important rotor design parameters which affect the frequency response are blade flapping restraint and pitch-flap coupling. The effects of several such design parameters on proprotor/pylon stability, the frequency response characteristics of the proprotor shear forces and moments, and blade flapping will be the subject of the analytical trend studies of Chapter 4.

CITED REFERENCES

2-1. Dulberger, L. H.: "Advanced Rotary-Wing Aircraft", Space/ Aeronautics, April 1967, pp. 68-82.

2-2. Ludi, L. H.: "Composite Aircraft Design", Proceedings of the 23rd Annual National Forum of the American Helicopter Society, May 1967.

2-3. Wernicke, K. G.: "Tilt Proprotor Composite Aircraft, Design State of the Art", Proceedings of the 24th Annual National Forum of the American Helicopter Society, May 1968.

2-4. Brandt, D. E.: "Aeroelastic Problems of Flexible V/STOL Rotors", Presented at the AGARD 34th Flight Mechanics Panel Meeting on "Aeroelastic Effects from a Flight Mechanics Standpoint", Marseilles, France, April 1969.

2-5. Borst, H. V. and B. Fry: "Propeller and Rotor VTOL Concepts and Their Relative Places in the Mission Spectrum", Presented at the U. S. Air Force V/STOL Technology and Planning Conference, Las Vegas, Nevada, September 1969.

2-6. Lichten, R. L.: "Design Problems and Solutions for Five Types of Low-Disc-Loading, High-Speed VTOL Aircraft", Presented at the 7th International Congress of Aeronautical Sciences, Rome, Italy, September 1970.

2-7. DeTore, J. A. and T. M. Gaffey: "The Stopped-Rotor Variant of the Proprotor VTOL Aircraft", Presented at the AIAA/AHS VTOL Research, Design and Operations Meeting, Atlanta, Georgia, Feb. 1969.

2-8. Engle, F. V. and K. W. Sambell: "Performance Aspects of Folding-Proprotor V/STOL Aircraft", Presented at the 25th Annual National Forum of the American Helicopter Society, May 1969.

2-9. Tiller, F. E. and R. Nicholson: "Stability and Control Considerations for a Tilt-Fold-Proprotor Aircraft", Presented at the 26th Annual National Forum of the American Helicopter Society, June 1970.

2-10. DeTore, J. A.: "Lift/Propulsion System Size-Selection Considerations for Stoppable Rotor VTOL Aircraft", Presented at the U. S. Air Force V/STOL Technology and Planning Conference, Las Vegas, Nevada, September 1969.

2-11. Taylor, E. S. and K. A. Browne: "Vibration Isolation of Aircraft Power Plants", Journal of the Aeronautical Sciences, Vol. 6, Dec. 1938, pp. 43-49.

2-12. Scanlan, R. H. and J. C. Truman: "The Gyroscopic Effect of a Rigid Rotating Propeller on Engine and Wing Vibration Modes", Journal of the Aeronautical Sciences, Vol. 17, Oct. 1950, pp. 653-659, 666.

2-13. Brower, W. B. and R. H. Lassen: "The Effects of Gyroscopic Coupling of Propulsion Units on the Vibration Modes of a Dynamically Similar Model of the Lockheed Constitution Airplane", Masters Thesis, Rensselaer Polytechnic Institute, Troy, New York, June 1950.

2-14. Abbott, F. T., Jr., H. N. Kelly, and K. D. Hampton: "Investigation of 1/8-Size Dynamic-Aeroelastic Model of the Lockheed Electra Airplane in the Langley Transonic Dynamics Tunnel", NASA TM SX-456, November 1960.

2-15. Reed, W. H., III, and S. R. Bland: "An Analytical Treatment of Aircraft Propeller Precession Instability", NASA TN D-659, 1961.

2-16. Houbolt, J. C. and W. H. Reed, III: "Propeller-Nacelle Whirl Flutter", Journal Aerospace Sciences, Vol. 29, March 1962, pp. 333-346.

2-17. Zwaan, R. J. and H. Bergh: "Propeller-Nacelle Flutter of the Lockheed Electra Aircraft", Rept. F288, Natl. Lucht-en Ruimtevaartlab, Amsterdam, Feb. 1962.

2-18. Sewall, J. L.: "An Analytical Trend Study of Propeller Whirl Instability, NASA TN D-996, 1962.

2-19. Bland, S. R. and R. M. Bennett: "Wind-Tunnel Measurement of Propeller Whirl-Flutter Speeds and Static-Stability Derivatives and Comparison with Theory", NASA TN D-1807, 1963.

2-20. Bennett, R. M. and S. R. Bland: "Experimental and Analytical Investigation of Propeller Whirl Flutter of a Power Plant on a Flexible Wing," NASA TN D-2399, 1964.

2-21. Anon.: "Airplane Airworthiness; Transport Categories - Flutter , Deformation, and Vibration Requirements", Civil Air Regulations Amendment 4b-16, FAA, August 1964.

2-22. Baker, K. E., R. Smith, and K. W. Toulson: "Notes on Propeller Whirl Flutter", Canadian Aeronautics and Space Journal, Vol. 11, Oct. 1965, pp. 305-313.

2-23. Reed, W. H., III: "Review of Propeller-Rotor Whirl Flutter", NASA TR R-264, 1967.

2-24. Griffin, J. A., Jr.: "A General Approach to the Vibration and Flutter Analysis of a Gyroscopically Coupled Elastic System", Report No. 2-53450/2R50079, Chance Vought Corp., July 1962.

2-25. Hall, W. E.: "Prop-Rotor Stability at High Advance Ratios", Journal of the American Helicopter Society, June 1966.

2-26. Amer, K. A.: " Theory of Helicopter Damping in Pitch or Roll and a Comparison with Flight Measurements", NACA TN 2136, 1950.

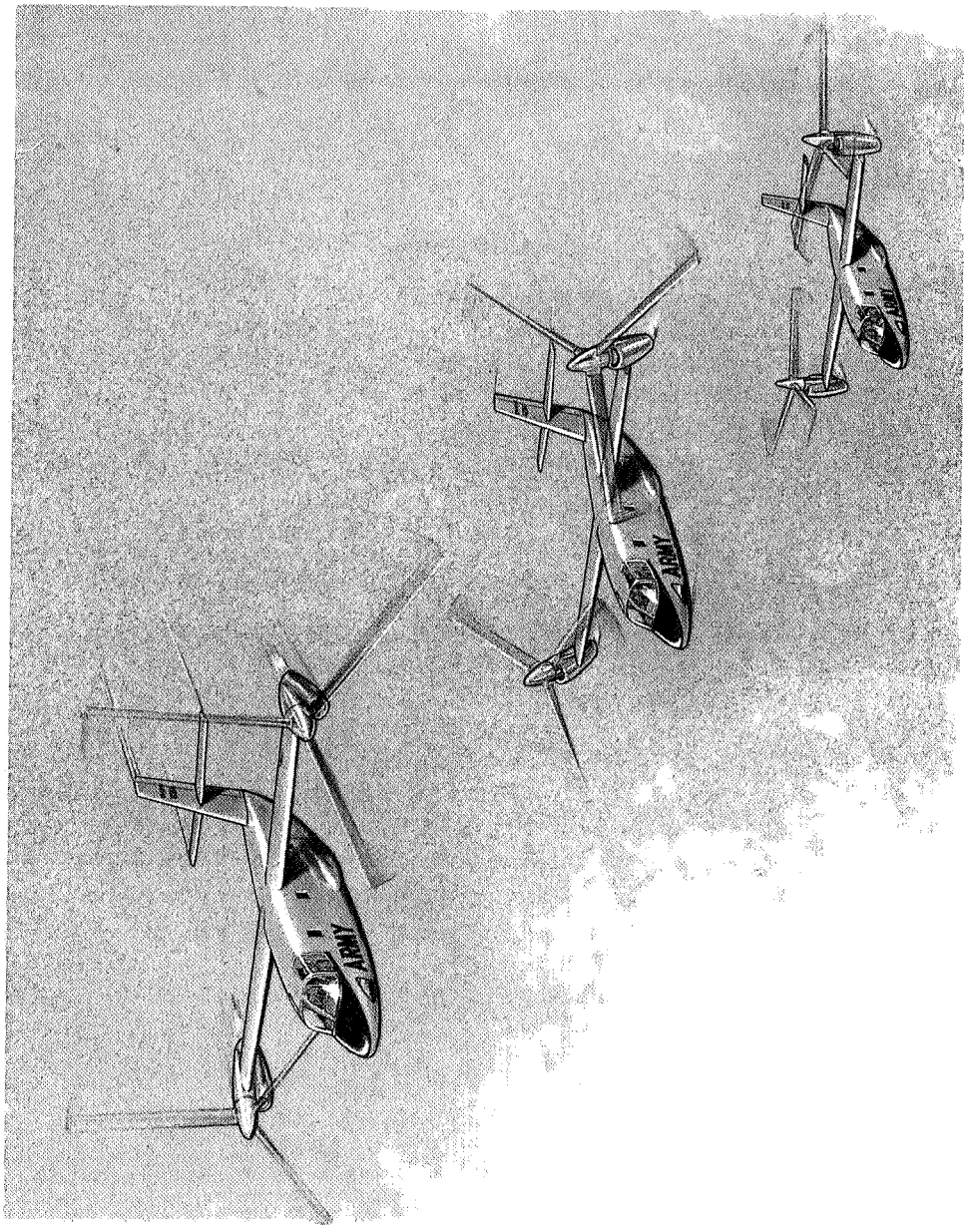

Figure 2-1.- Bell Model 266.

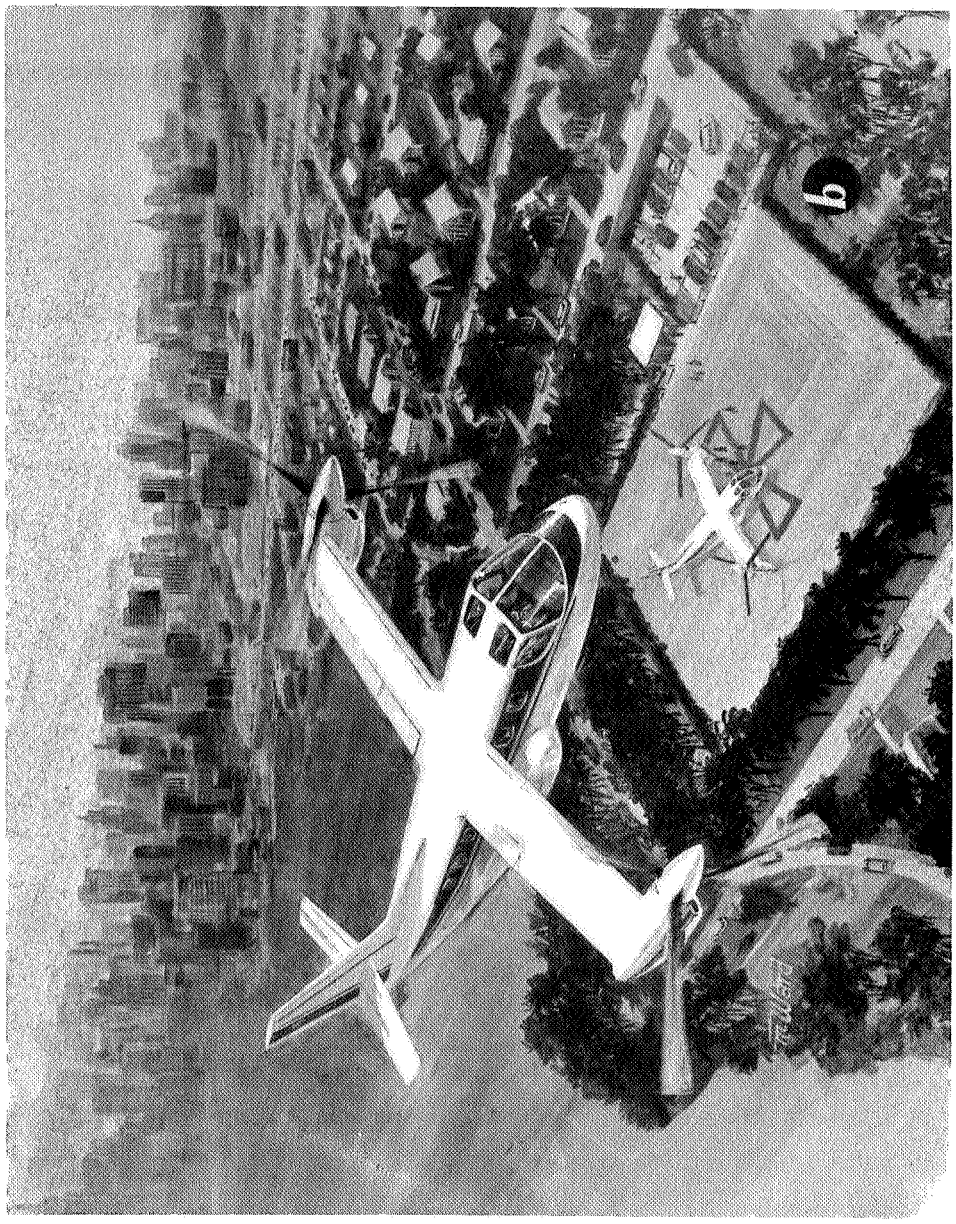

Figure 2-2.- A Bell tilt-rotor design for transportation between urban centers.

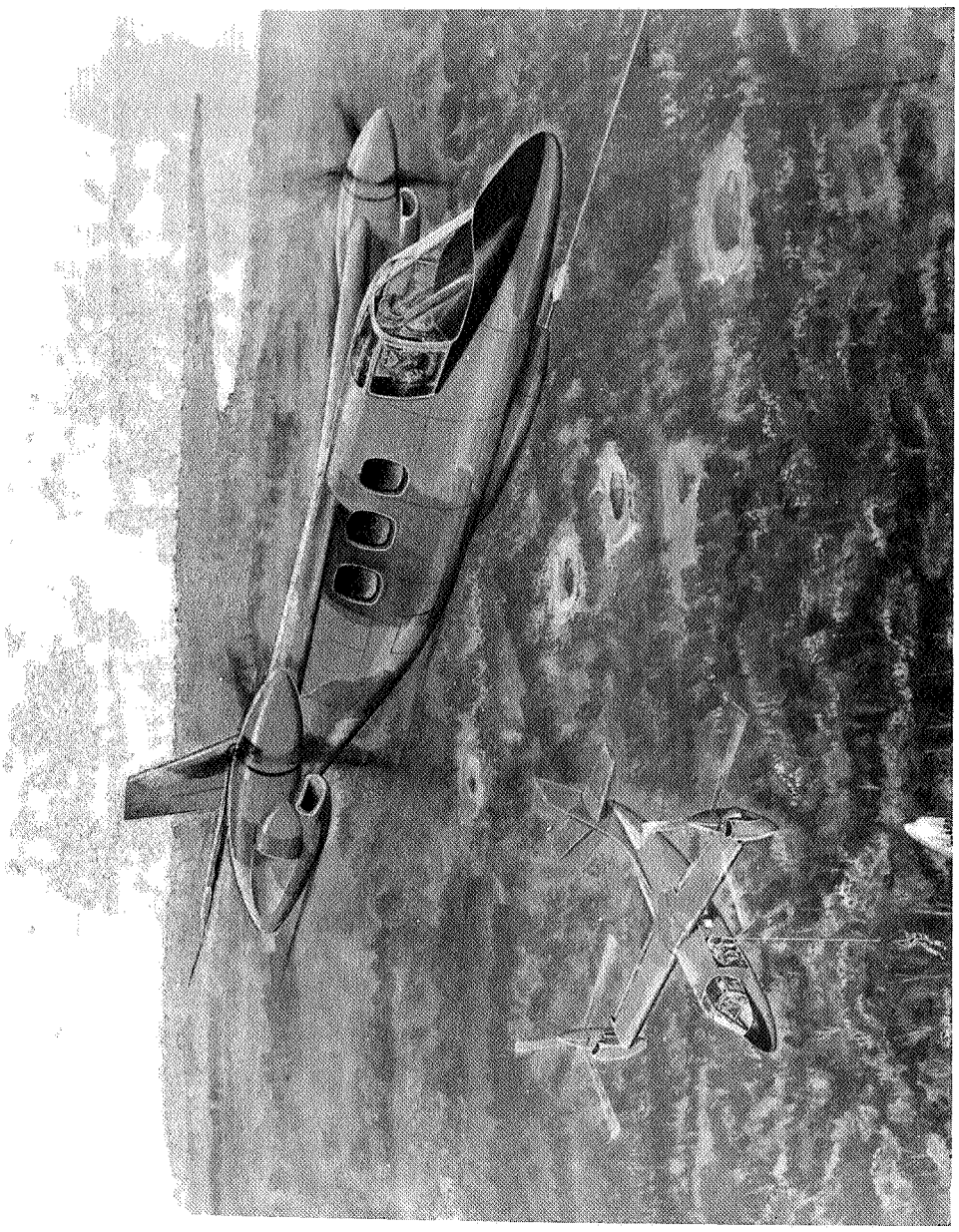

Figure 2-3.- Tilt-rotor rescue aircraft (Bell Helicopter Co.).

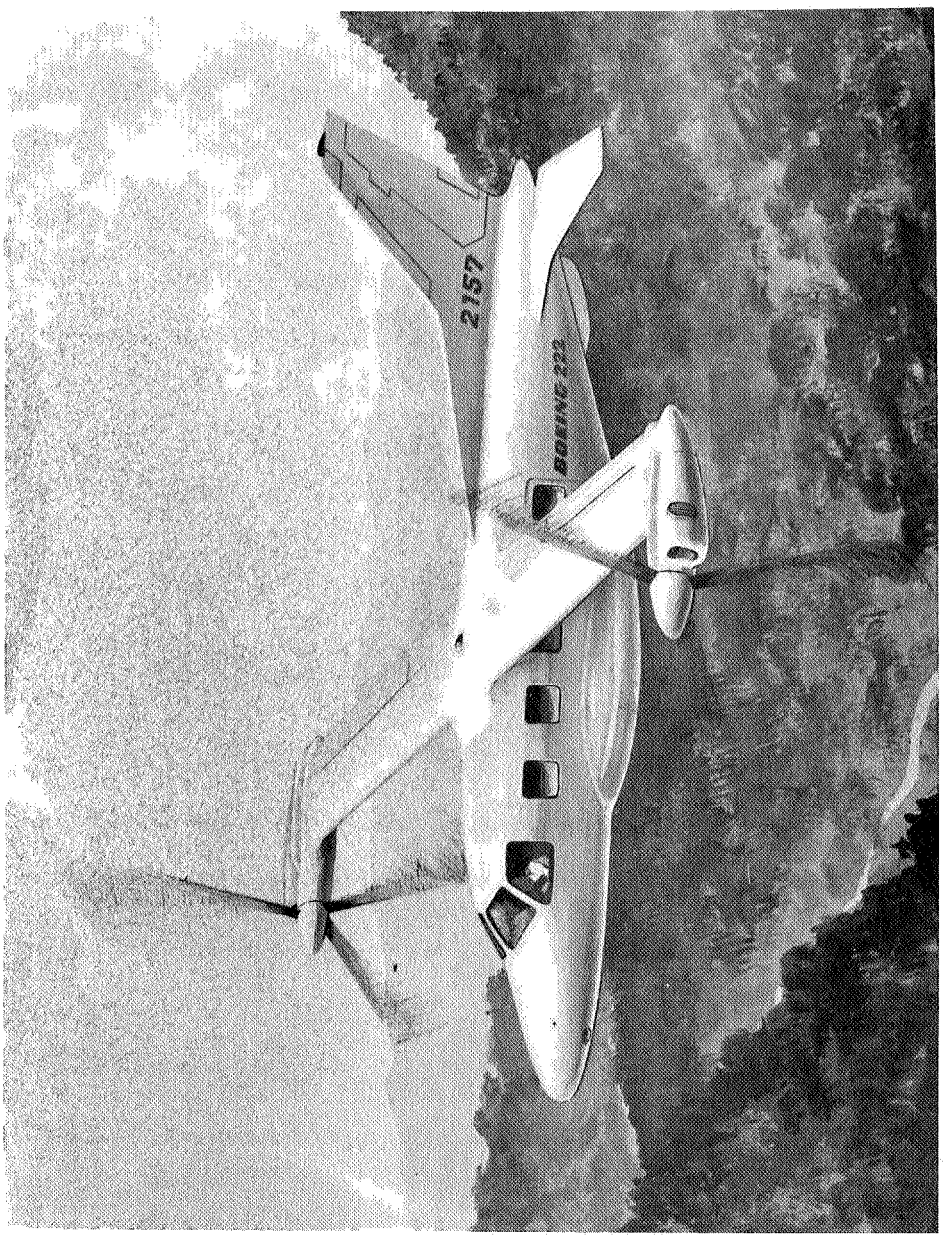

Figure 2-4.- An executive/commuter tilt-rotor (Boeing-Vertol).

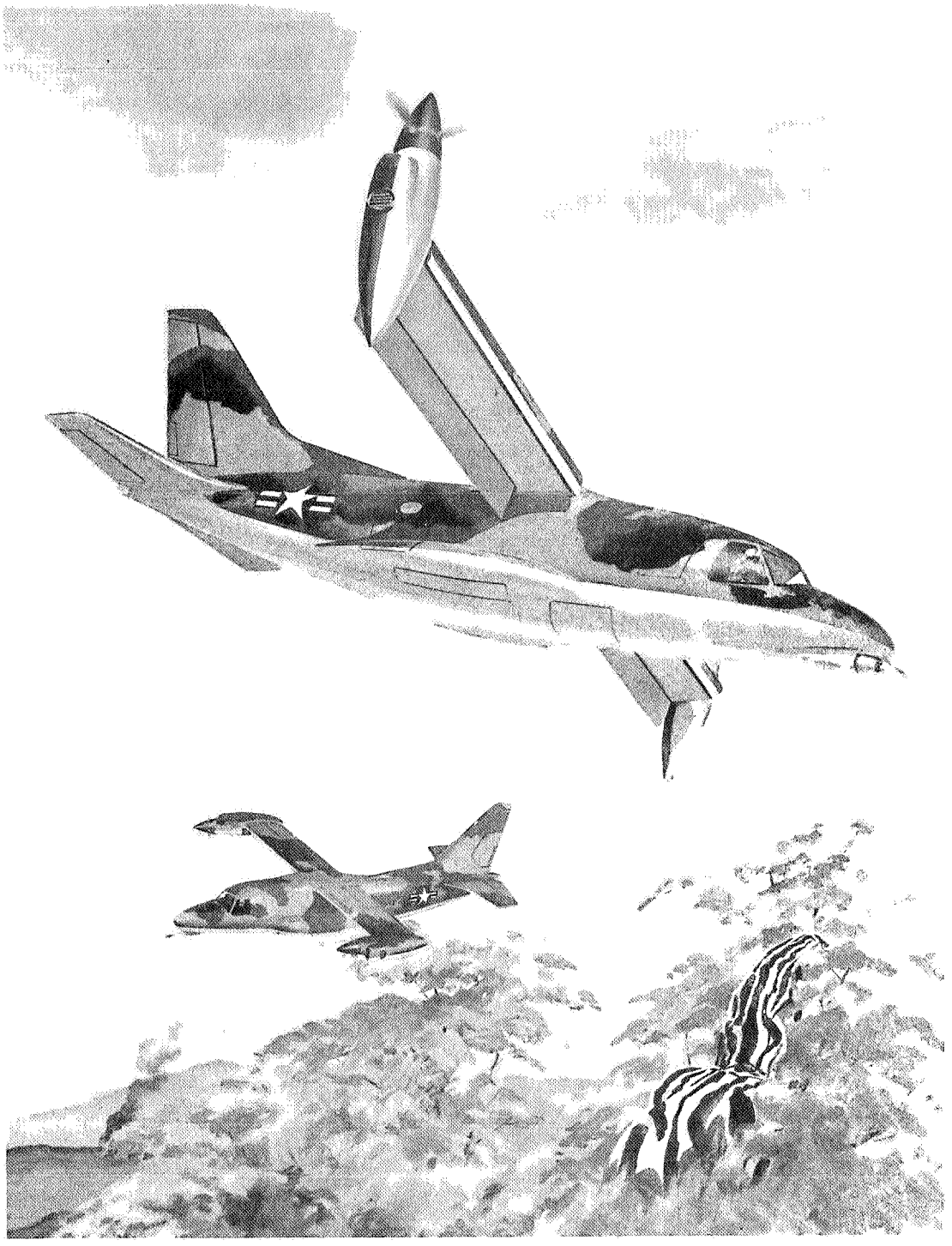

Figure 2-5.- A Boeing-Vertol tilt-rotor rescue aircraft.

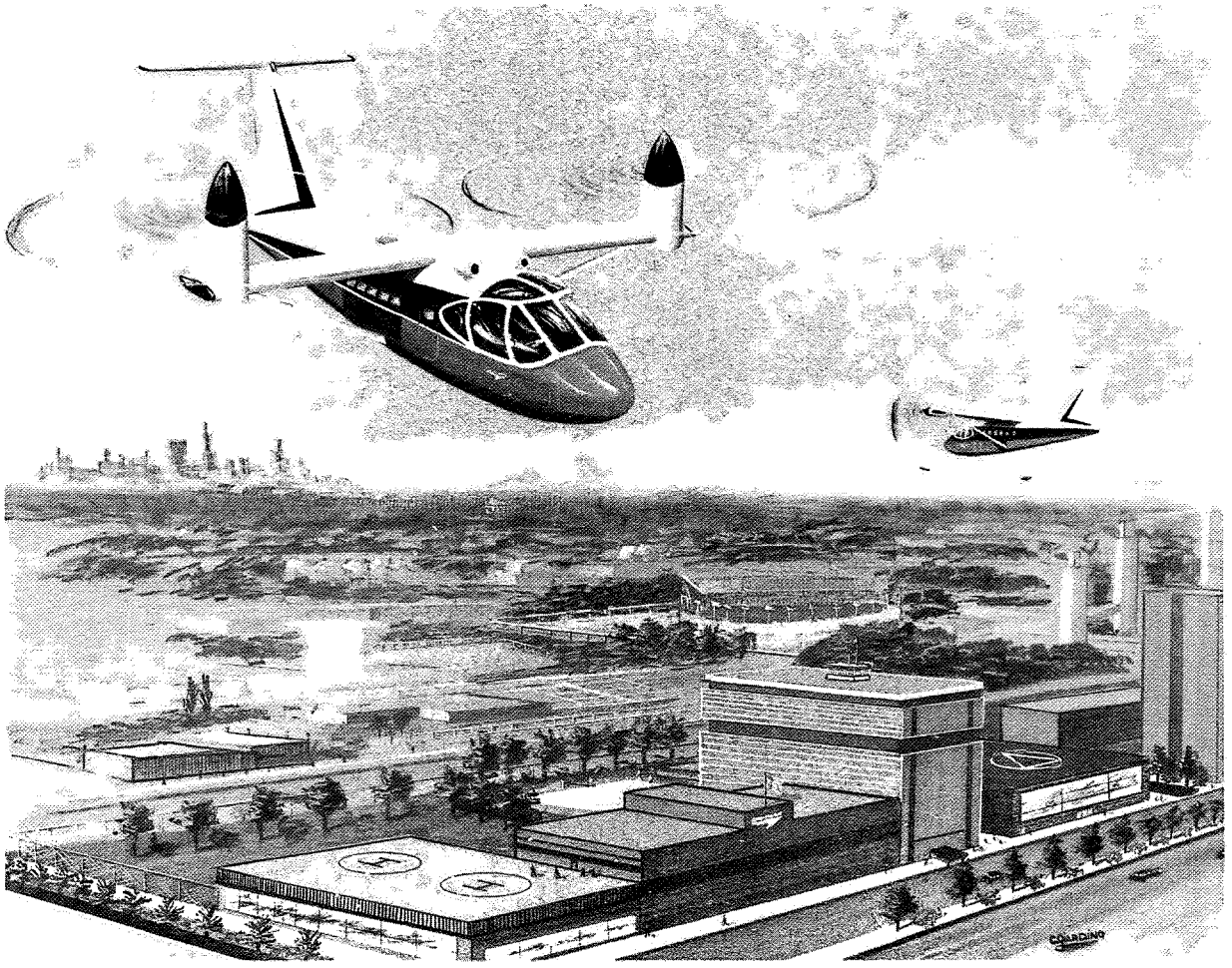

Figure 2-6.- Grumman tilt-rotor design for city center-to-city center commuter service.

Figure 2-7.- Model of Bell Model 300 in simulated helicopter, conversion, and high-speed cruise modes of flight.

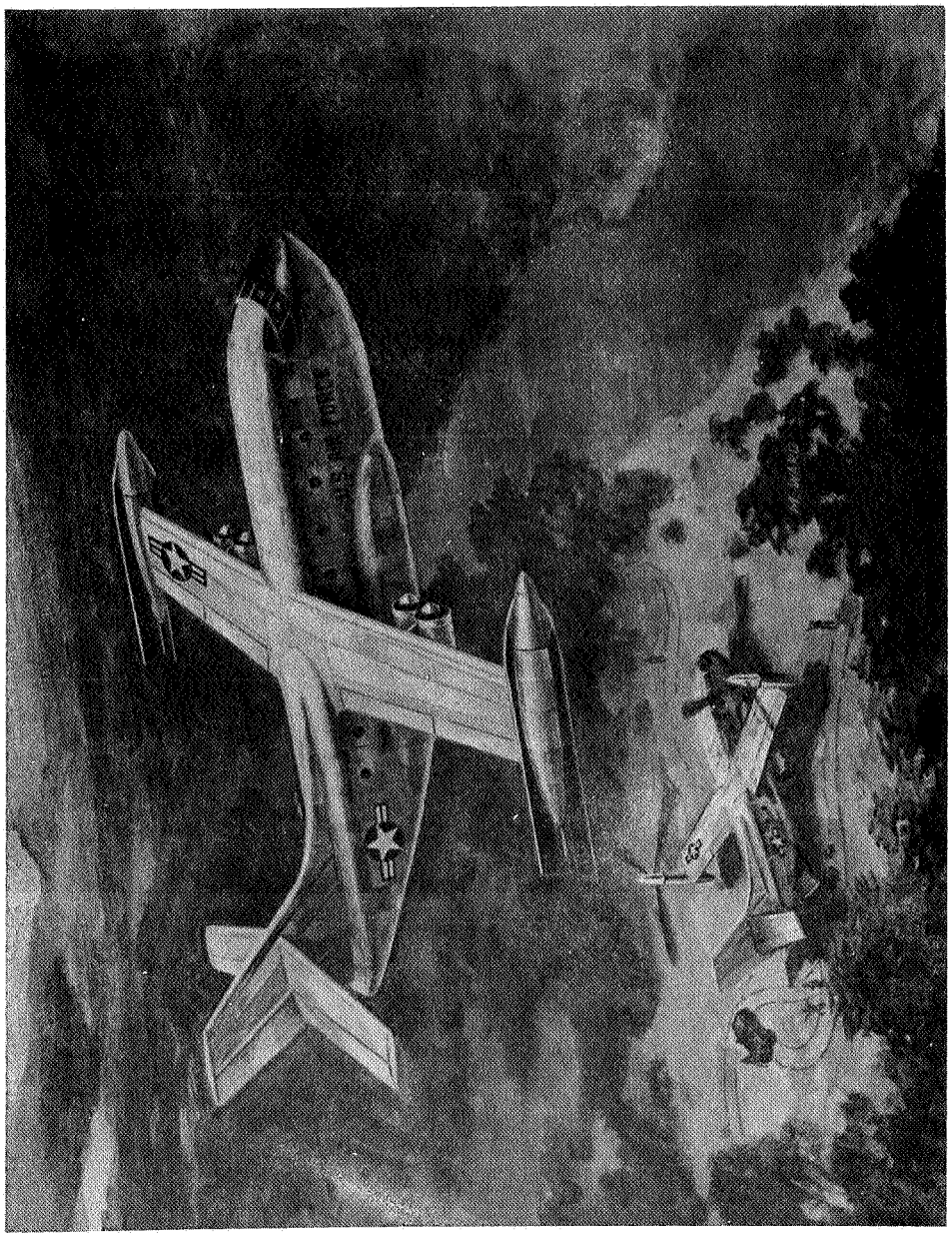

Figure 2-8.- Logistics application of a folding tilt-rotor (Bell Helicopter Co.).

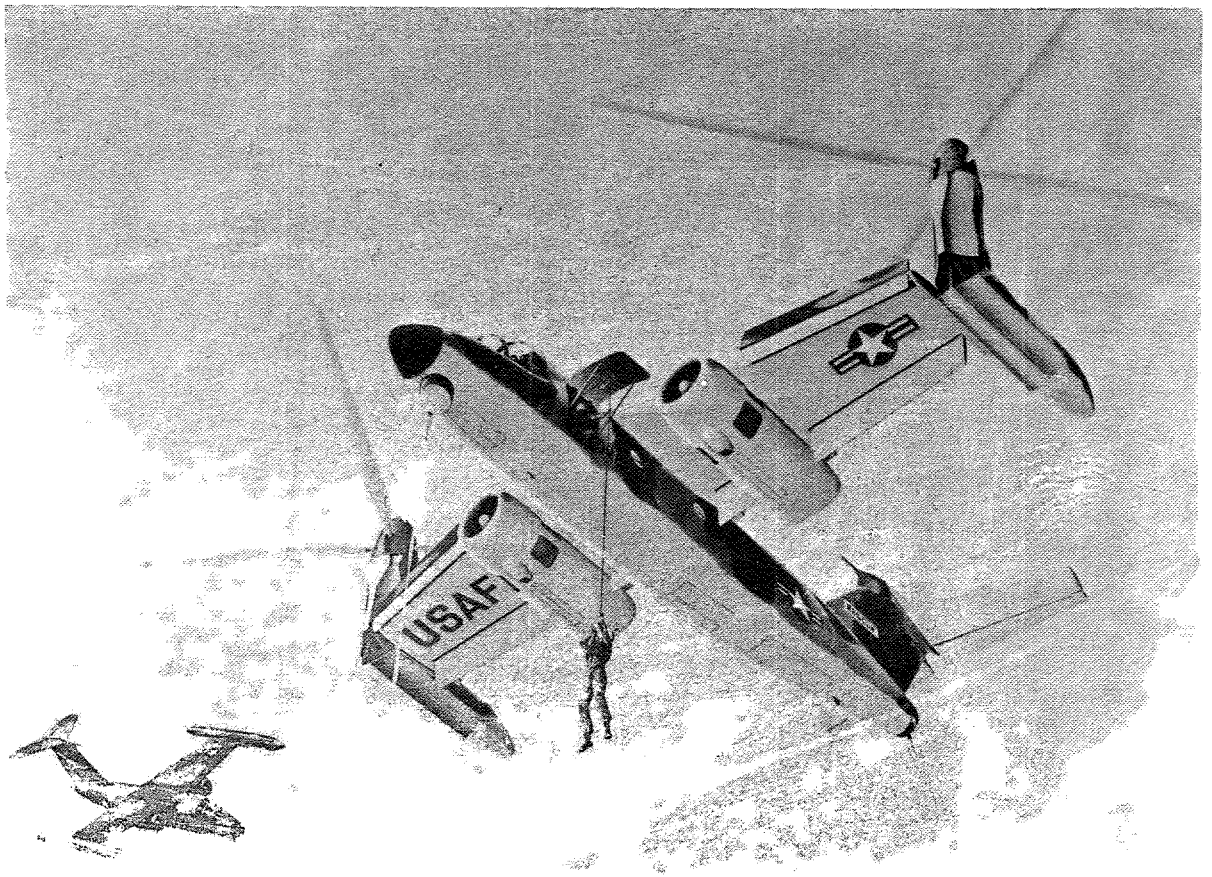

Figure 2-9.- Boeing-Vertol stowed tilt-rotor rescue aircraft.

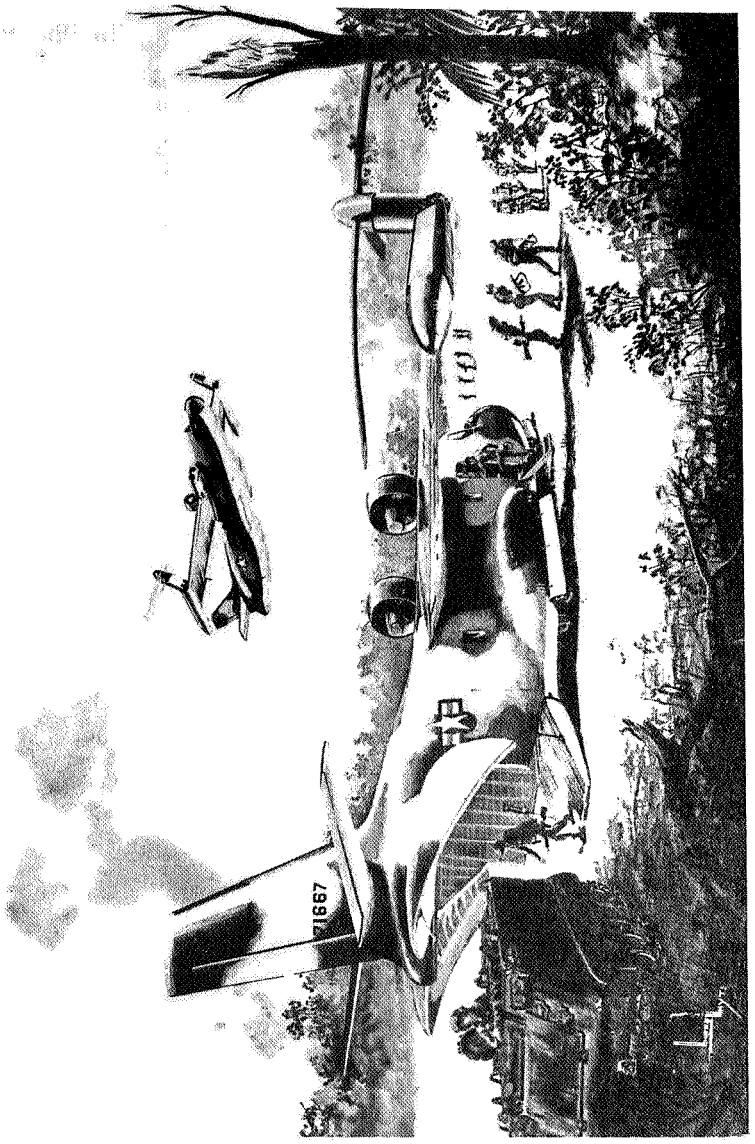

Figure 2-10.- Sikorsky concept of an intra-theater transport.

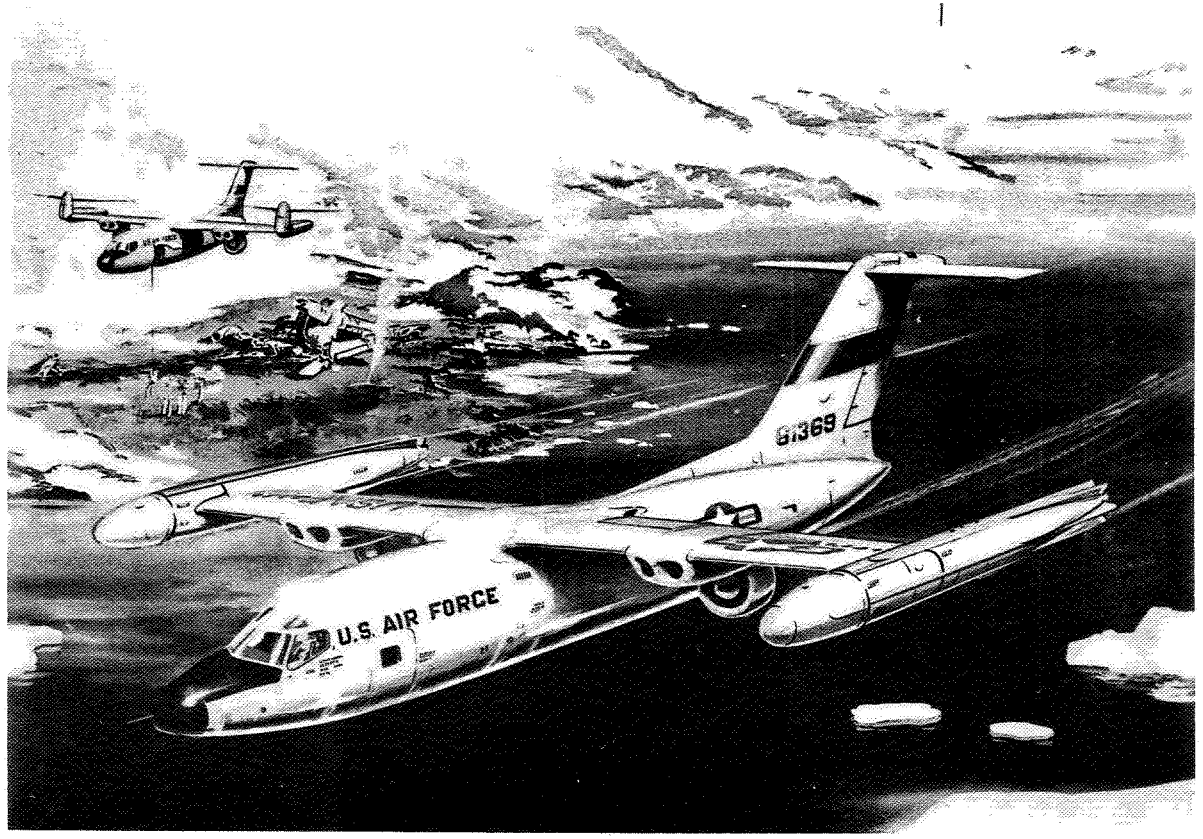

Figure 2-11.- A folding tilt-rotor search and rescue aircraft (Sikorsky Aircraft).

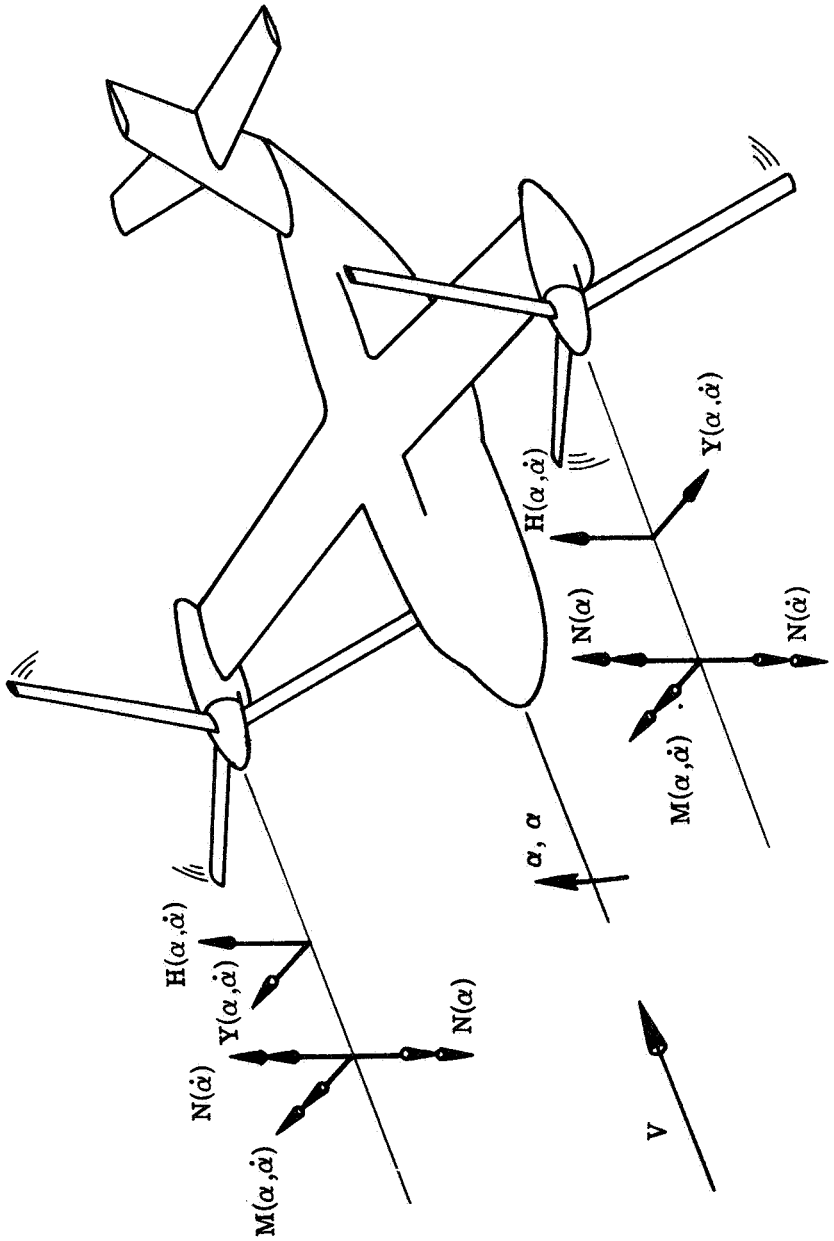

(a) Pitch

Figure 2-12.- Perturbation aerodynamic forces and moments acting on a proprotor aircraft during low-frequency rigid-body pitch, yaw, and roll oscillations. (Proprotors interconnected)

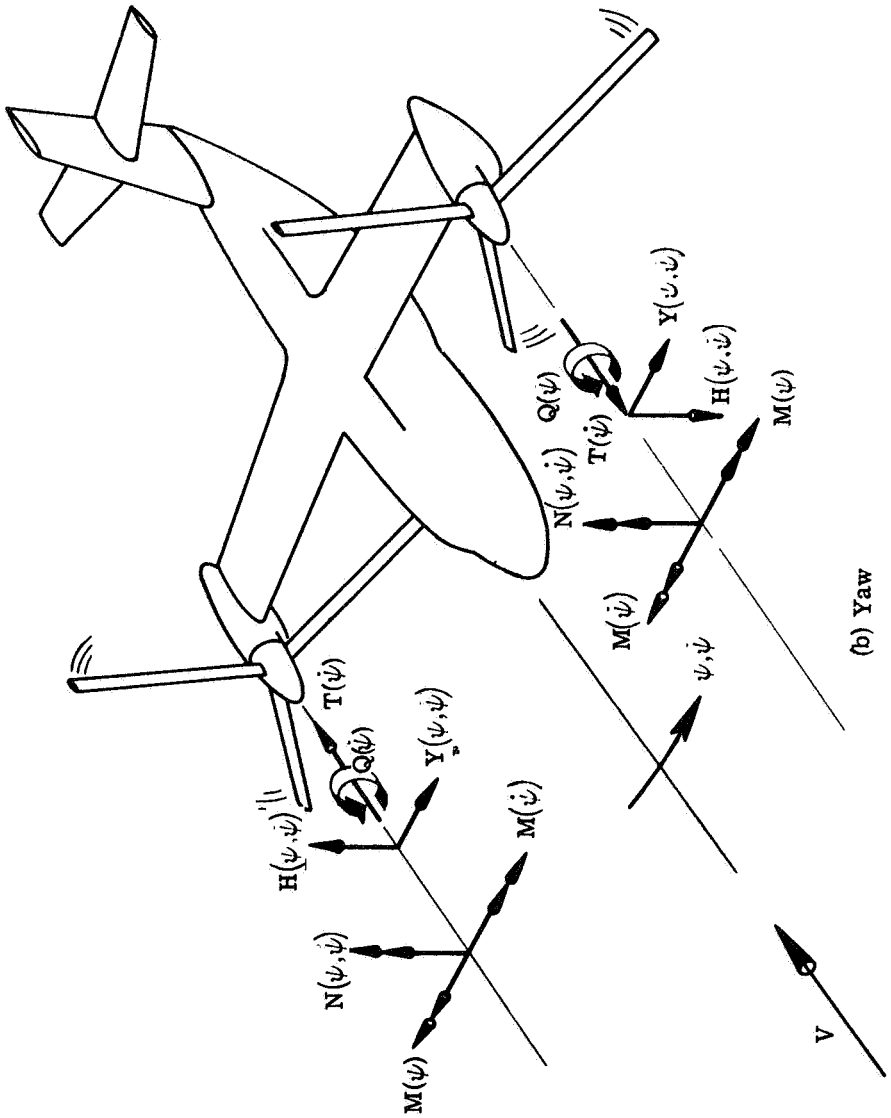

(b) Yaw

Figure 2-12.- Continued.

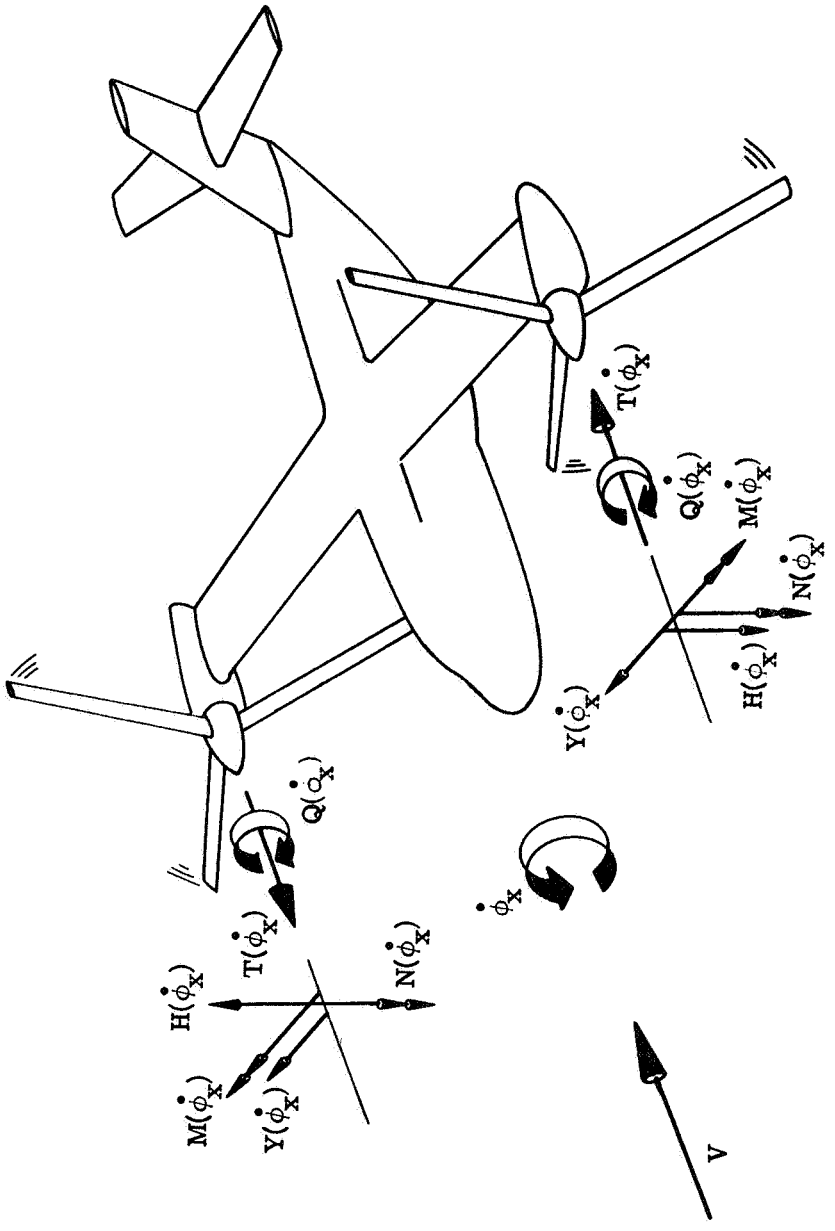

(c) Roll

Figure 2-12.- Concluded.

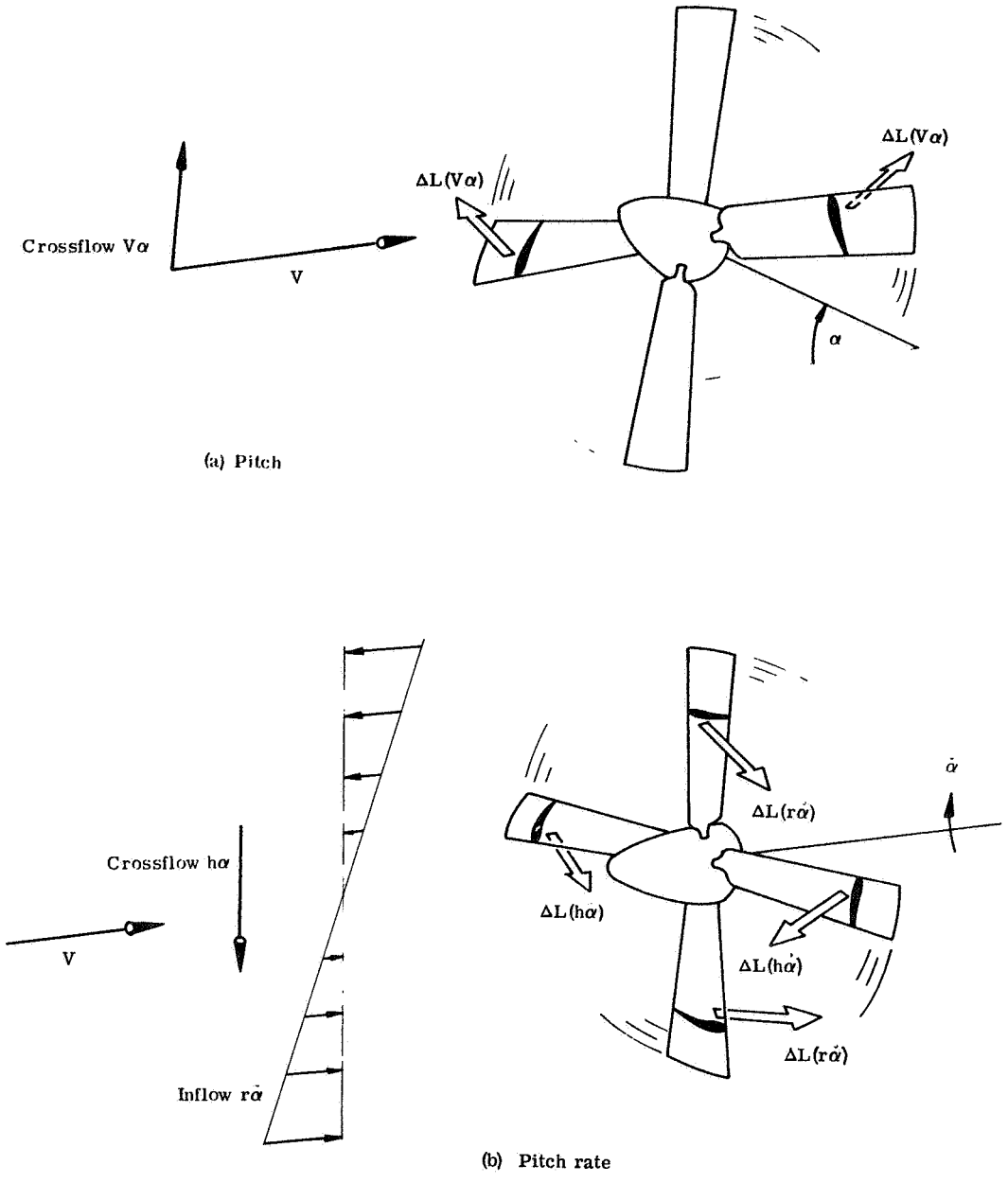

Figure 2-13.- Perturbation airflows and resultant blade element lifts induced by a pitching propeller.

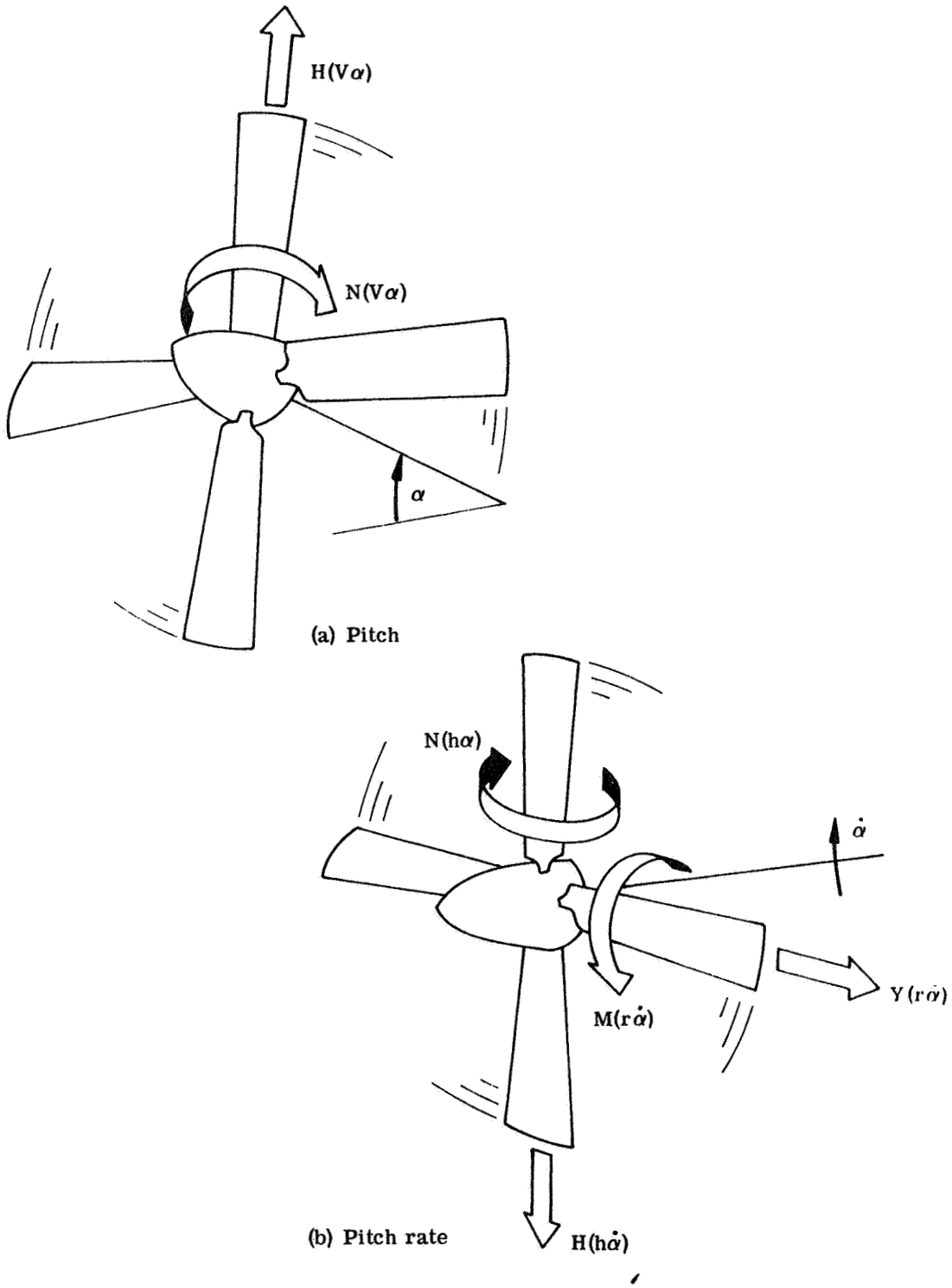

Figure 2-14.- Resultant perturbation airloads acting on a pitching propeller.

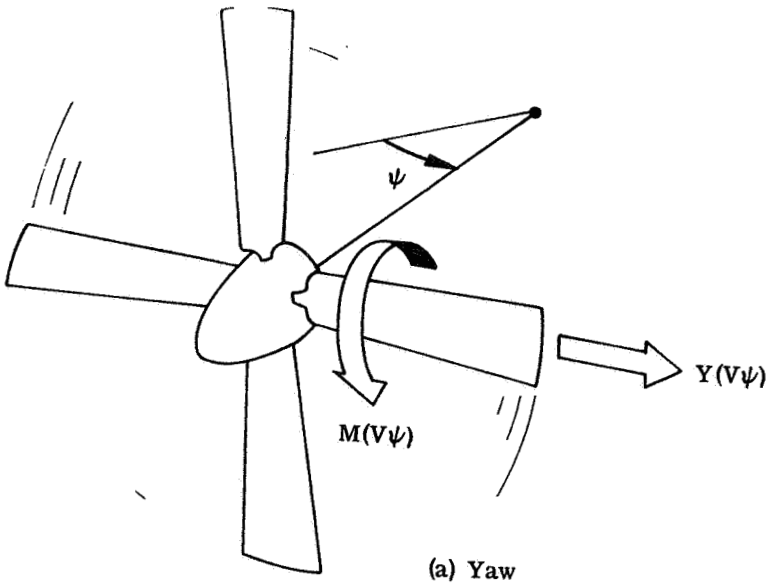

(a) Yaw

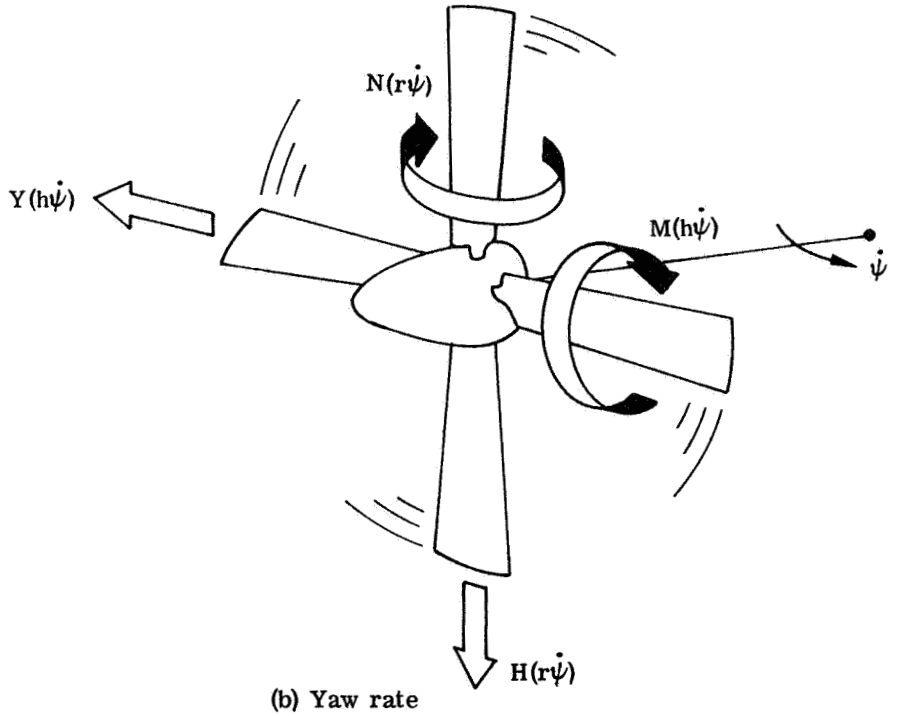

(b) Yaw rate

Figure 2-15.- Resultant perturbation airloads acting on a yawing propeller.

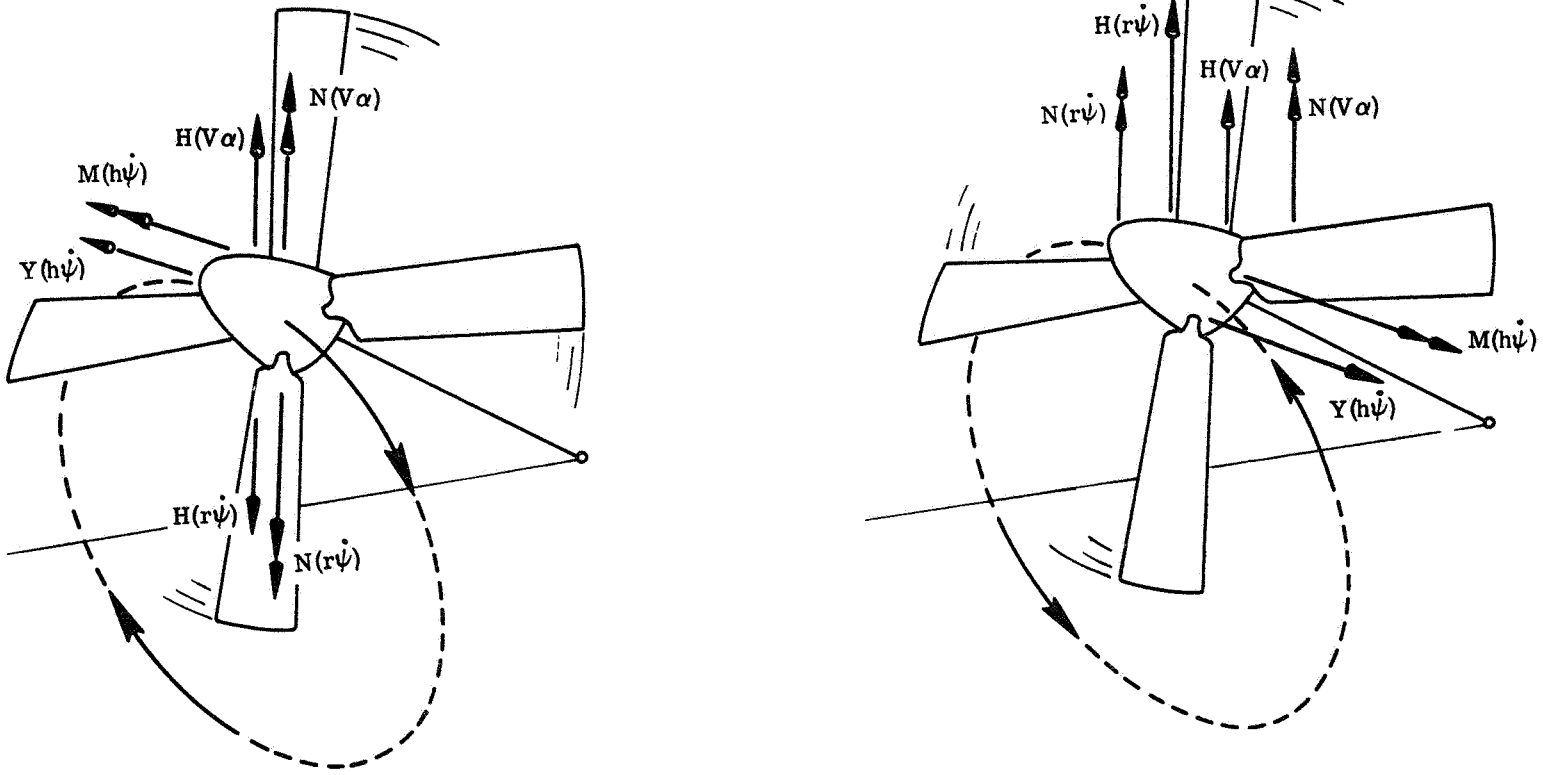

(a) Backward whirl

(b) Forward whirl

Figure 2-16.- Airloads acting on a whirling propeller (position of maximum positive pitch attitude shown).

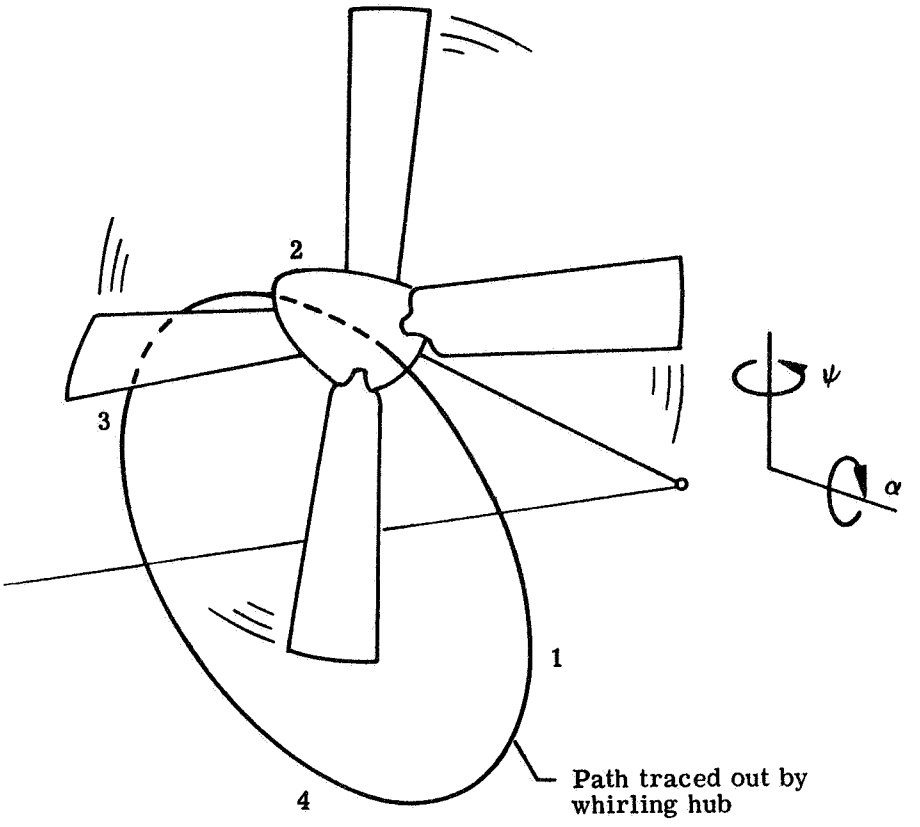

Hub Position	Instantaneous Equation of Motion
1, 3	$I_\psi\ddot{\psi} + K_\psi\psi + 2\Omega I_R\dot{\alpha} = 0$
2, 4	$I_\alpha\ddot{\alpha} + K_\alpha\alpha - 2\Omega I_R\dot{\psi} = 0$

	Backward Whirl				Forward Whirl			
	α	$\dot{\alpha}$	ψ	$\dot{\psi}$	α	$\dot{\alpha}$	ψ	$\dot{\psi}$
1	0	-	+	0	0	+	+	0
2	+	0	0	+	+	0	0	-
3	0	+	-	0	0	-	-	0
4	-	0	0	-	-	0	0	+

Figure 2-17.- Establishment of the "static" nature of the gyroscopic coupling forces.

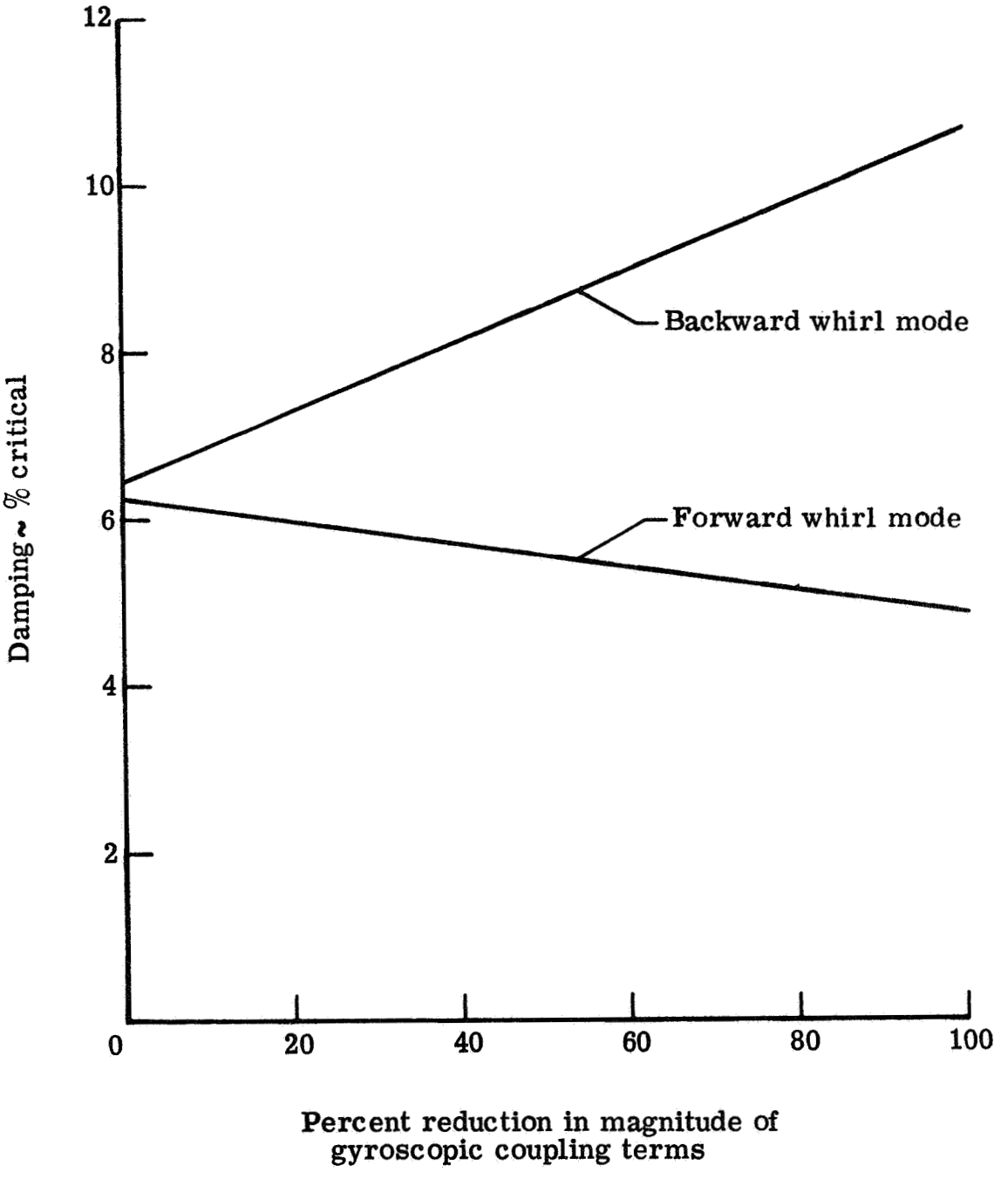

Figure 2-18.- Calculated effects of gyroscopic forces on propeller whirl mode damping.

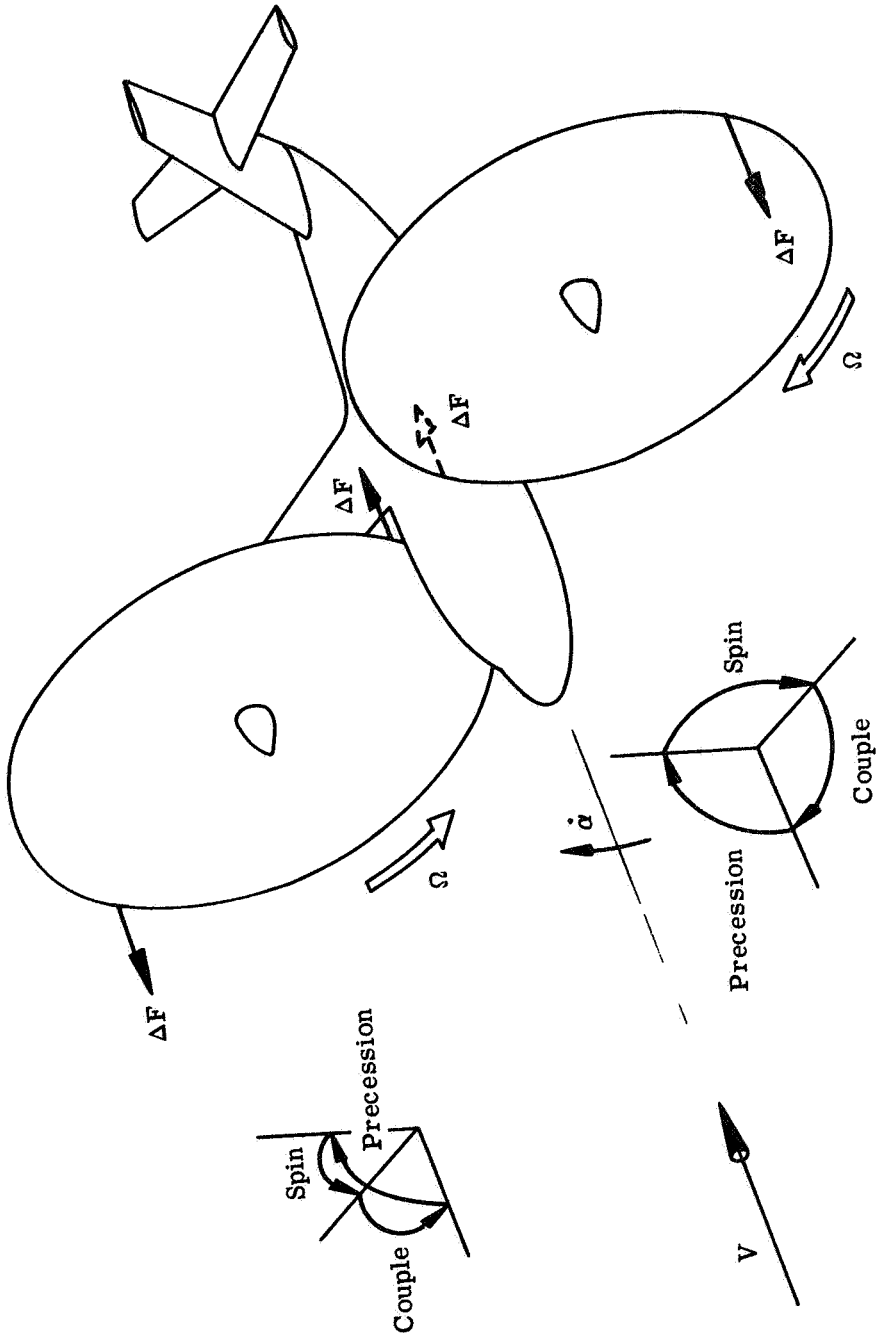

Figure 2-19.- Gyroscopic rule applied to a flapping proprotor.

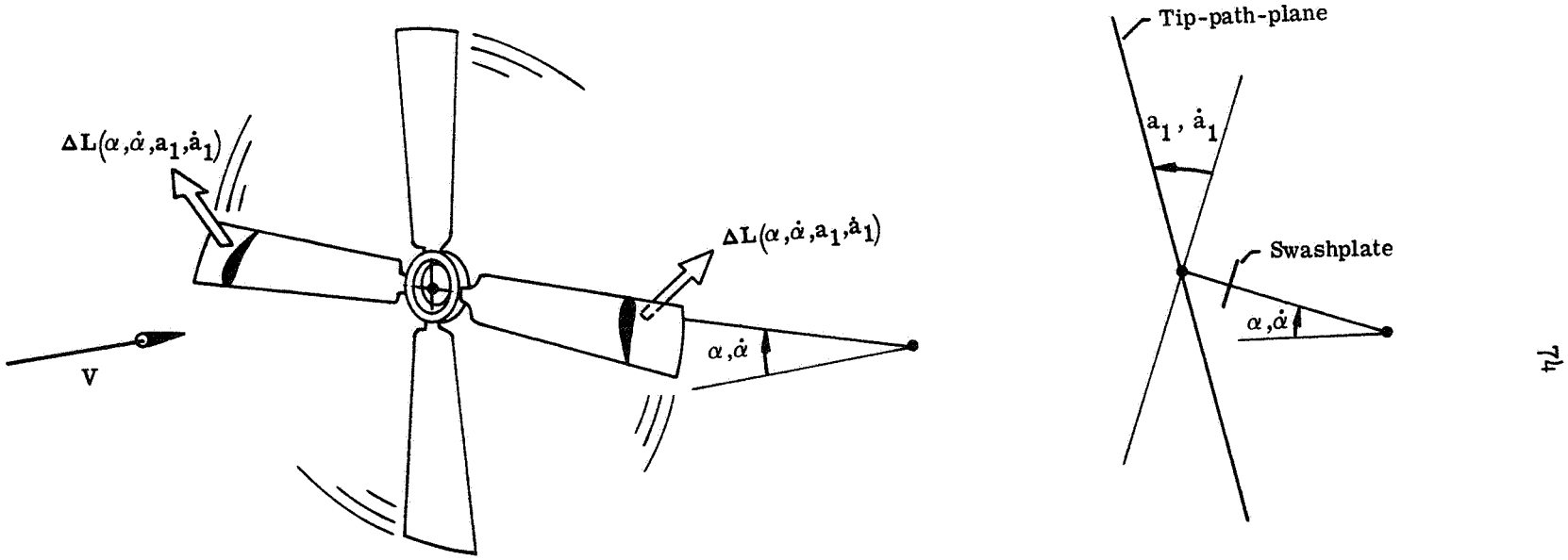

Figure 2-20.- Origin of airload moment to precess proprotor in response to shaft motion. (Blade pitch horns and pitch links not shown)

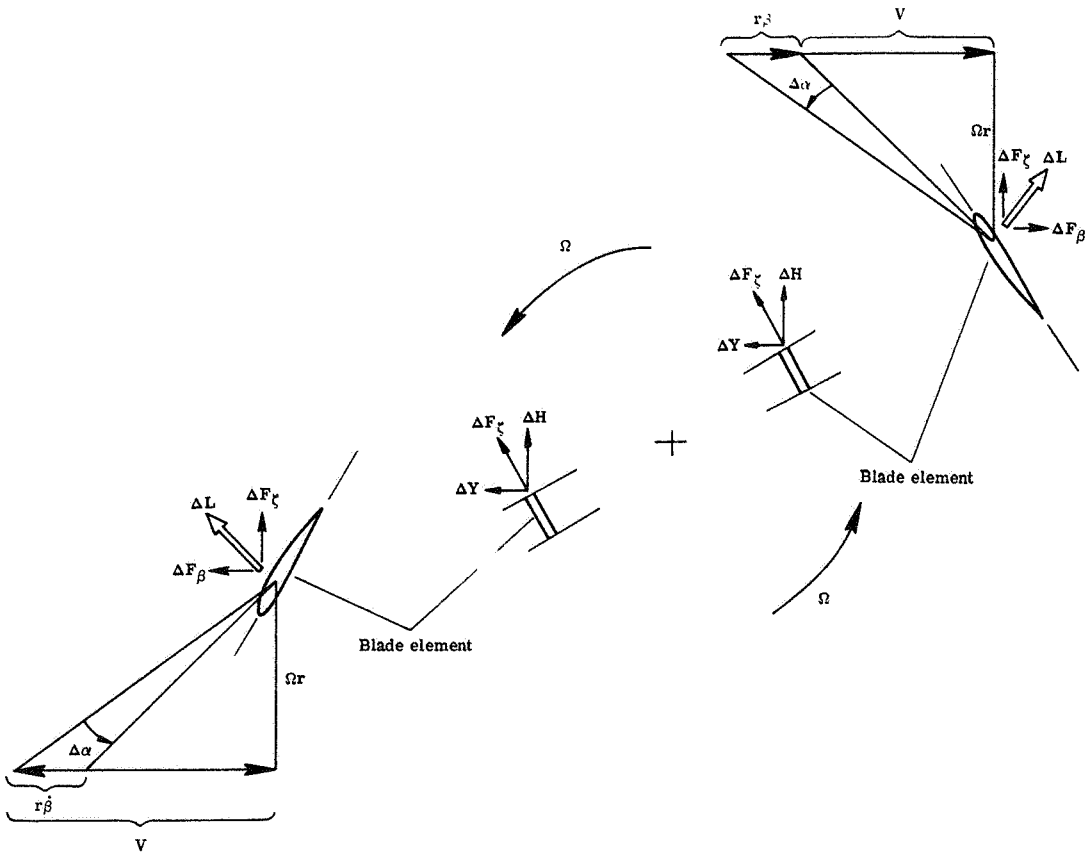

Figure 2-21.- Perturbation airload acting on the blade elements of a pitching proprotor.

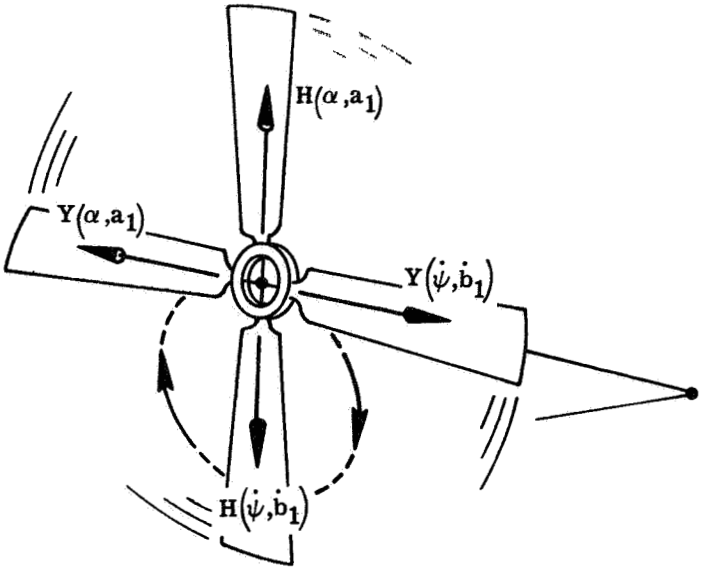

(a) Backward whirl

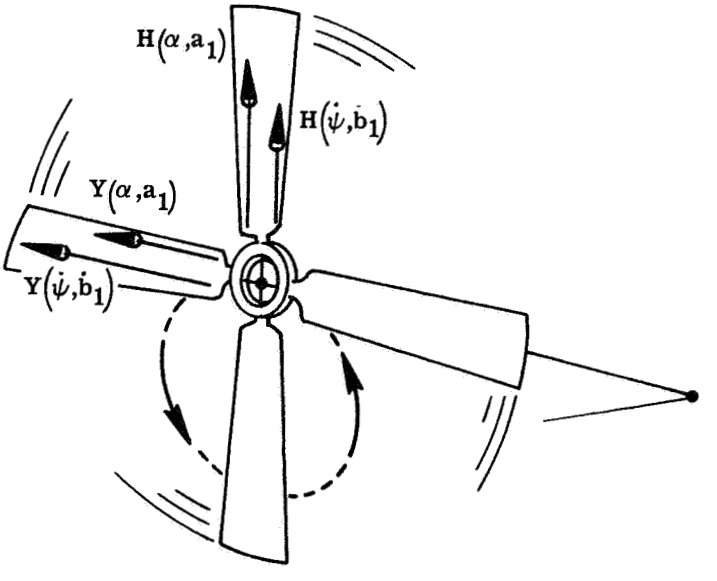

(b) Forward whirl

Figure 2-22.- Airload forces acting on a whirling proprotor (Position of maximum positive pitch attitude shown).

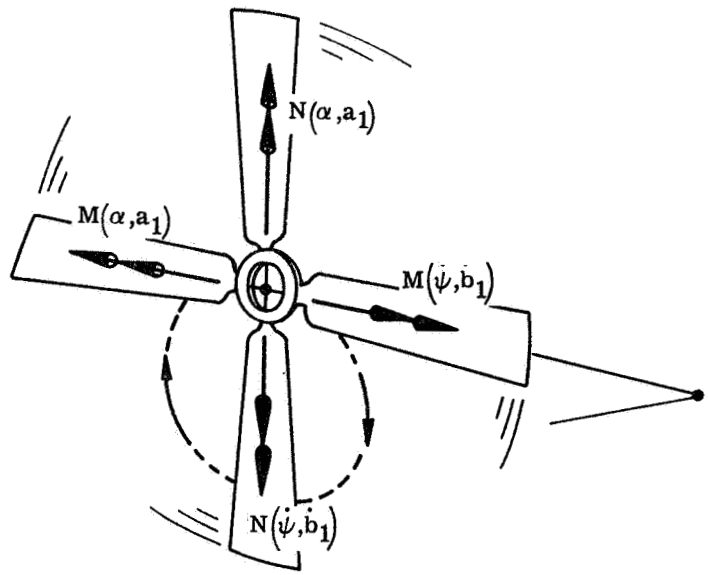

(a) Backward whirl

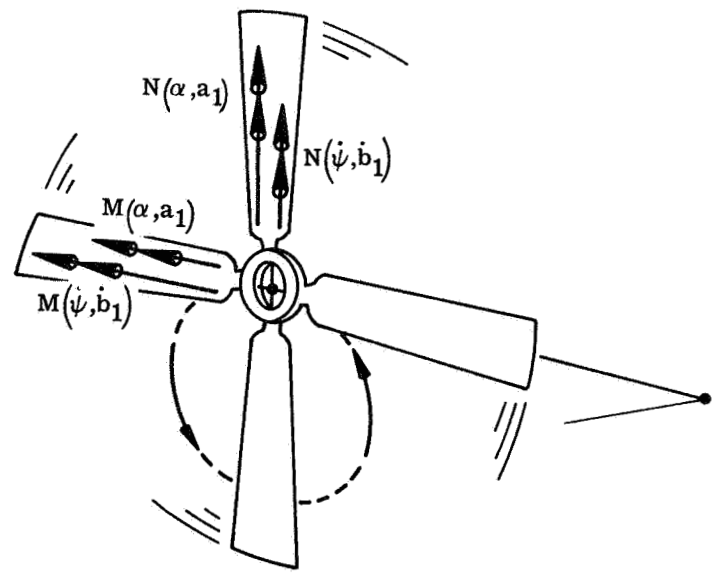

(b) Forward whirl

Figure 2-23.- Airload moments acting on a whirling proprotor (Position of maximum positive pitch attitude shown).

CHAPTER 3

MATHEMATICAL FORMULATION FOR ANALYSIS OF PROPROTOR/PYLON AEROELASTIC STABILITY

Introduction

The equations describing the perturbed motion of an idealized proprotor/pylon/wing system encastré at the wing root and the proprotor fully converted forward are developed in this chapter. In addition to providing the analytical basis from which to assess the aeroelastic stability of the system these equations furnish the basis for calculating the frequency response characteristics of the proprotor force and moment derivatives (Appendix C) and blade flapping derivatives (Appendix D). Following customary engineering practice in dealing with complicated structures recourse is had to the approximation of replacing the continuous system having an infinite number of degrees of freedom by an equivalent discrete system having a finite number of degrees of freedom. Herein, this simplification is introduced by the expedient of physical discretization or "lumping" in contrast to mathematical discretization through a normal mode approach.

The fact that flutter investigations require consideration of only small motions from a steady-state flight condition allows both a structural and aerodynamic simplification in the analytical formulation. Structurally, recourse can be directly made to well-established small vibration theory as a basis from which the

dynamic theory of flutter can proceed; aerodynamically, the incremental changes in the external forces can be taken as linear functions of the disturbance displacements, velocities, and accelerations.

The pertinent equations of motion are derived using the Lagrangian approach. Since attention is directed to the flight mode in which the proprotor is fully-converted forward the mathematical convenience of reducing the resulting equations of motion having time-dependent coefficients (dependent on blade azimuth position ψ) to those having time-independent coefficients can be realized under certain simplifying assumptions for the blade motions. This expedient is exercised herein in order to permit an eigenvalue formulation for assessing system stability, thereby obviating the need for a more involved solution of the equations of motion by numerical integration. The reader will recall that the analytical philosophy adopted in this dissertation as outlined in Chapter 1, particularly as regards the intended preliminary design nature of the analyses, recommended an eigenvalue formulation in contrast to a time history solution for each degree of freedom. An eigenvalue approach to the "solution" of the equations of motion provides a means for quickly establishing trends and isolating the effect of parameters on stability whereas considerable computer time and user judgment is generally associated with a time history solution.

Considerations influencing various aspects of the structural idealization, particularly the proprotor idealization, are discussed, and the specific assumptions employed are pointed out. Because the resulting equations of motion contain non-proportional damping a transformation of the equations into a form amenable to an eigenvalue solution necessitates adoption of a method used to uncouple the forced equations of motion in the general dynamic response problem. These methods are summarized briefly prior to applying the appropriate aspects to the present equations. The interpretation of the complex eigensolutions is discussed and a simple method for ascertaining the direction of pylon whirl shown. Some general comments concerning the solution of the stability determinant conclude the chapter.

Derivation of the Equations of Motion

Formulation of the equations of motion reduces to two fundamental problem types: (1) A structural dynamic or mechanical vibration problem in which consideration is given to the specification of the equations of motion for an elastic system under the influence of external forces and internal damping. Implicit here is the required prior determination of the inertial and elastic characteristics of the system. (2) An aerodynamic problem in which incremental changes in the aerodynamic forces due to small changes in the degrees of freedom are desired (i.e., the generalized aerodynamic forces). The dynamic portion of the total aerodynamic loading is of interest, the steady forces making no

contribution to the disturbed motion within small perturbation theory. A methodical blending of these dynamic and aerodynamic ingredients leads to a systematized statement of the general dynamic response problem, a special case being the flutter problem. Interest in this section is directed toward a detailed exposé of the dynamic and aerodynamic aspects of the subject mathematical model and the formulation of the system equations of motion.

(a) Lagrange's Equation

Lagrange's equation is a consequence of Hamilton's variational principle which, extended to include nonconservative forces, has the form (Ref. 3-1)

$$\int_{t_1}^{t_2} \delta(T - V + W)\, dt = 0 \qquad (3\text{-}1)$$

Here T is the kinetic energy of the system, V is the potential energy derivable from a potential function, and W represents the work done by all nonconservative forces. Lagrange's equation for a holonomic system, as derivable from Eq. 3-1, assumes the form

$$\frac{d}{dt}\left(\frac{\partial T}{\partial \dot{q}_r}\right) - \frac{\partial T}{\partial q_r} + \frac{\partial V}{\partial q_r} = Q_r \qquad (r = 1, 2, \ldots N) \qquad (3\text{-}2)$$

where T and V have the same definition as in Eq. 3-1, Q_r are the generalized nonconservative forces (which are related to the virtual work done by the aerodynamic forces), and q_r are the generalized coordinates.

In the form of Lagrange's equation given in Eq. 3-2 no explicit account is taken of internal damping. The complicated nature of the true damping mechanism in typical aeroelastic structures generally precludes a precise mathematical description of the observed damping characteristics. Hence, if damping must be included in the analysis it can only be accounted for in an approximate manner. Furthermore, mathematical tractability suggests that any approximate damping theory so introduced maintain the mathematical linearity of the equations of motion. Fortunately, damping is usually small in most structures and a simplified concept of damping which is easily incorporated into the equations of motion can be used to account for the actual mechanism of energy dissipation.

Two damping models are in general use for introducing a linear damping law into an already linearized structural motion: the hysteretic or structural damping model and the viscous damping model.* The hysteretic model of damping is based on the experimental observation that in simple harmonic motion many structural materials exhibit an energy dissipation per cycle which is proportional to the strain amplitude squared but independent of the frequency at which the strain is applied. Thus this model of damping is rigorously valid only for harmonic motion. The viscous

---

*An excellent account of these two types of damping, particularly in relation to their proper usage, is given by S. Neumark: "Concept of Complex Stiffness Applied to Problems of Oscillations with Viscous and Hysteretic Damping," R & M 3269, 1957.

damping model provides for an energy dissipation which is proportional to frequency. The structural damping model appears to be better suited to account for internal damping of the hysteresis type which is the predominant type of damping exhibited by aircraft structures. This led to its early adoption by fixed-wing flutter analysts, as exemplified by the work of Theodorsen and Garrick (Ref. 3-2).

For simple harmonic motion of the form $e^{i\omega t}$ the structural damping model implies that the ratio of spring force to displacement is given by the complex quantity $k(1 + ig)$ where g is the nondimensional damping coefficient; the magnitude of the damping force is proportional to the elastic force but advanced in phase by 90°. Hence, for simple harmonic motion one can write

$$F_{D_{structural}} = ig\, F_E \tag{3-3}$$

which implies (Ref. 3-3) that the corresponding generalized forces are related in the manner

$$Q_D = ig\, Q_E \tag{3-4}$$

Since

$$Q_E = -\frac{\partial V}{\partial q_r} \tag{3-5}$$

Lagrange's equation with damping assumes the form

$$\frac{d}{dt}\left(\frac{\partial T}{\partial \dot{q}_r}\right) - \frac{\partial T}{\partial q_r} + (1 + ig_{rs})\frac{\partial V}{\partial q_r} + \frac{\partial D}{\partial \dot{q}_r} = Q_r \qquad \begin{pmatrix} r = 1, 2, \ldots N \\ s = 1, 2, \ldots N \end{pmatrix} \tag{3-6}$$

where D is the Rayleigh dissipation function accounting for energy dissipation by viscous damping. For small vibrations T, V, and D are given by homogeneous quadratic expressions in the generalized velocities and displacements of the form

$$T = \frac{1}{2}\sum_{r=1}^{N}\sum_{s=1}^{N} \bar{M}_{rs}\,\dot{q}_r\dot{q}_s + \sum_{r=1}^{N}\sum_{s=1}^{N} \bar{\Gamma}_{rs}\,q_r\dot{q}_s$$

$$V = \frac{1}{2}\sum_{r=1}^{N}\sum_{s=1}^{N} \bar{K}_{rs}\,q_r q_s \qquad (3\text{-}7)$$

$$D = \frac{1}{2}\sum_{r=1}^{N}\sum_{s=1}^{N} \bar{C}_{rs}\,\dot{q}_r\dot{q}_s$$

The second term in the first of Eqs. 3-7 is included to account for the presence of gyroscopic coupling forces. Inspection of Eqs. 3-6 and 3-7 indicates that the structural damping model is introduced by simply replacing the stiffness terms $\bar{K}_{rs}$ by $(1 + ig_{rs})\bar{K}_{rs}$, thereby making the stiffness complex. $[\bar{M}_{rs}]$, $[\bar{K}_{rs}]$, and $[\bar{C}_{rs}]$ are symmetric matrices; $[\bar{\Gamma}_{rs}]$ is non-symmetric.

Because of the lack of knowledge as to the distribution of damping only the direct damping terms are generally retained in practice. That is, the off-diagonal damping terms (g_{rs}, $\bar{C}_{rs}$; $r \neq s$) accounting for damping coupling between degrees of freedom are taken to be identically zero and only the direct damping in a given

degree of freedom is retained.* This simplification will also be employed herein. However, it should be noted that this in no way restricts the dynamic development presented herein since the formulation and solution of the final equations are not dependent on the absence of damping coupling terms.

The generalized forces in Lagrange's equation take on various forms depending on whether they are motion-dependent or motion independent. Aerodynamic forces are of the former type and the complexity of the resultant terms is influenced by the particular aerodynamic theory used to calculate the loading. For quasi-steady aerodynamics the resultant equations of motion can be written in the general matrix form

$$[\bar{M}]\{\ddot{q}\} + [\Gamma]\{\dot{q}\} + [\bar{C}]\{\dot{q}\} + [\bar{K}]\{q\} = [\text{Aero}]_1 \{\dot{q}\} + [\text{Aero}]_2 \{q\} \tag{3-8}$$

where the coefficient matrices on the left hand side of Eq. 3-8 are dependent on the system parameters and the aerodynamic matrices are additionally dependent on the airspeed V and air density ρ. The specification of each of these coefficient matrices is the subject of the next two subsections.

---

*Suggested procedures for evaluating both the direct and coupling damping coefficients from experimental data are given in Refs. 3-4 and 3-5. Several useful formulas for evaluating the direct damping terms, either viscous or structural, are contained in Ref. 3-6.

(b) Dynamic Development

Proprotor: Neglecting inplane motions and assuming independently flapped blades an N-bladed rotor ($N \geq 3$)* has N modes in which each blade can oscillate as a rigid body with the same frequency and maximum amplitude as the others. This can most easily be visualized by considering a four-bladed rotor. An observer located in and moving with the rotating coordinate system would observe four possible distinct blade flapping modes. In the fixed coordinate system these flapping modes would manifest themselves as a collective or symmetric flapping mode in which all four blades flap forward or aft simultaneously, a two-per-rev flapping mode in which two oppositely disposed blades flap forward or aft while the other pair of oppositely disposed blades flap aft or forward, and two one-per-rev cyclic flapping modes wherein the path traced by the tips of the blades (the tip-path-plane) is tilted longitudinally or laterally. The coning mode produces only axial forces at the proprotor hub (neglecting coupling between flap and lag) and, as indicated in Ref. 3-7 for example, cannot couple with any pylon motions which are important in whirl. The two-per-rev flapping mode is "reactionless," producing a zero net force on the hub and thus also being a mode which cannot couple with pylon whirl motions. The cyclic pitch and yaw modes, however, can couple with pylon pitch and yaw, respectively, and thus constitute modes which

---

*For $N \geq 3$ the rotor has rotational symmetry.

are important in whirl flutter. Rotors with more than four blades will contribute additional modes of the "reactionless" type which, as pointed out above, are not important in whirl flutter. Hence, based on flapping considerations there are only two blade modes which are relevant to the whirl flutter problem: a cyclic pitch mode and a cyclic yaw mode. These appear in the fixed system as a longitudinal or lateral tilt of the tip-path-plane.

In the case of a fully-articulated rotor the inplane freedoms of an N-bladed rotationally symmetric configuration additionally lead to N independent inplane blade modes in which each blade can oscillate as a rigid body with the same frequency and maximum amplitude as the others. As in the flapping considerations above these inplane modes can be separated into modes which can couple with pylon pitch and yaw and those which cannot.* The modes which can couple with pylon whirl motions are characterized by a blade displacement pattern in which the center of gravity of the blade system is offset from the hub position. There are two such modes. In one the cg of the displaced blades whirls in the direction of rotor rotation while in the other the cg whirls in a direction opposite to the direction of rotor rotation.† The other blade inplane modes are either of the "reactionless" type or those which produce a torque about the rotor mast. Again, these latter modes

---

*See, for example, the excellent physical considerations presented by Gevarter (Ref. 3-8).

†These characteristic directions are with respect to a rotating coordinate system.

cannot couple with pylon whirl.

Hingeless proprotors, characterized by blades which are cantilevered from a fixed hub assembly, have first out-of-plane bending mode frequencies on the order of 1.1 to 1.2 cycles/rev and first in-plane bending mode frequencies on the order of .6 to .7 cycles/rev. For stability analyses, the effects of blade flexibility can often be adequately accounted for in the guise of the first out-of-plane and inplane bending modes by means of a virtual hinge dynamic representation originally suggested by Young (Ref. 3-9) for out-of-plane bending of hingeless helicopter rotors. Here both the first out-of-plane and first inplane bending modes would be approximated simultaneously by the rigid-body flapping and inplane modes of an articulated blade having non-coincident virtual flap and lag hinges. In terms of this equivalent system the proprotor would, in accordance with previous considerations, have only four blade modes of consequence in whirl flutter: two cyclic flapping modes, appearing in the fixed system as a longitudinal and lateral tilt of the tip-path-plane, and two inplane modes, appearing in the rotating system as a forward and backward whirl of the center of gravity of the displaced blades.

A gimbaled proprotor is characterized by blades which are cantilevered from a rigid hub assembly which is attached to the drive shaft by means of a gimbal housed within the hub. If the blades are taken to be rigid the proprotor freedoms are constrained to be those representing a longitudinal and lateral tilt of the

tip-path-plane relative to the shaft. Superposition of these tip-path-plane modes then gives any actual rigid-body flapping motion which the blades can perform. In the fixed system these tip-path-plane flapping modes manifest themselves as a wobbling or weaving of the tip-path-plane as a rigid disc in the forward or backward direction.* It is to be noted that these two "rigid-disc modes" are geometrically equivalent to the one-per-rev cyclic flapping modes described earlier for the articulated and hingeless proprotors. As a consequence of its gimbal mounting arrangement, the first out-of-plane blade mode of a gimbaled proprotor is the rigid-body flapping mode. Hence, if blade flexibility must be included in the analysis it can be essentially completely accounted for solely in the guise of blade first inplane bending via a virtual hinge dynamic representation in the manner given by Young (Ref. 3-9). Another procedure is described by Gaffey in Ref. 3-10.

The gimbaled proprotor on the Model 266 is of the "stiff-inplane" type so that dynamic phenomena associated with it, in particular proprotor/pylon instability, are characterized by the blades acting as rigid in flapping and coupling with the pylon/wing elastic modes, with negligible blade inplane bending. These proprotor characteristics are very similar to those of the ideal rigid-blade gimbaled proprotor described above. In the dynamic analyses developed in this dissertation it is assumed that the blades can be

---

*This is shown in Chapter 4.

taken to be rigid* and that any rigid-body flapping behavior of the blades can be described as a linear combination of the longitudinal and lateral flapping modes of the tip-path-plane taken as a rigid disc. It is the use of this tip-path-plane representation for the description of the blade flapping modes that permits the removal of the time dependency from the coefficients in the equations of motion.†

The two-degree-of-freedom proprotor (having the tip-path-plane freedoms described above) is taken to be mounted on a rigid pylon having three linear and three rotational degrees of freedom. These freedoms and the associated sign convention are indicated in Fig. 3-1. Because the wing torsional stiffness is generally significantly different from the wing fore and aft (chordwise) bending stiffness the pylon support stiffness in pitch can be quite different from that in yaw. In this instance the distance from the rotor plane to the effective pitch pivot is generally different from the corresponding distance to the effective yaw pivot. The present analysis accounts for this possible difference in the manner shown in Fig. 3-2. The dynamic contribution of the proprotor to the

---

*The control system is also taken as rigid. Blade feathering then enters only as a kinematic freedom and does not contribute to the system degrees of freedom.

†In the more general case in which blade inplane flexibility is included this time dependency can also be removed if the blade inplane motions are described in terms of the "modes" of the center of mass of the displaced blades. See, for example, R. L. Johnson and K. H. Hohenemser : "On the Dynamics of Lifting Rotors with Thrust or Tilting Moment Feedback Controls," J. Amer. Hel. Soc., Vol. 15, No. 1, January 1970.

equations of motion, as embodied in its contribution to T, V, and D for use in Lagrange's equation, is derived below.

(1) Kinetic Energy - Specification of the rotor kinetic energy requires the prior determination of the absolute velocity of a mass element on the n^{th} blade. Because the blades are rotating this involves the general problem of motion in a moving coordinate system. Vector methods, such as described in Ref. 3-11, will be used to express this velocity in terms of the specified system degrees of freedom. The pertinent vector quantities and associated coordinate systems are illustrated in Fig. 3-3. X_o, Y_o, Z_o are axes fixed in inertial space. The axis systems xyz and $\bar{x}\bar{y}\bar{z}$ are both moving coordinate systems. The xyz system moves in both translation and rotation such that its coordinate axes remain parallel to the corresponding axes of the inertial coordinates. The $\bar{x}\bar{y}\bar{z}$ system rotates about the $\bar{x}$ axis and moves such that $\bar{x}$ remains parallel to x (and hence X_o); the $\bar{y}$ axis is taken to be oriented in the spanwise direction of the n^{th} blade (but not in the plane of the blade), its angular position with respect to the y axis being given by ψ. The direction of rotor rotation in forward flight is taken to be clockwise when viewed from the rear. $\bar{R}$ is the position vector of the moving origin situated at the proprotor hub position referred to the inertial coordinate system and $\bar{\rho}$ is the position vector of an element of mass on the n^{th} blade referred to the $\bar{x}\bar{y}\bar{z}$ coordinate system. The position vector to an arbitrary point on the spanwise axis of the n^{th} blade with respect to inertial axes is

given by

$$\bar{r} = \bar{R} + \bar{\rho} \tag{3-9}$$

Differentiating the vector quantity $\bar{r}$ with respect to time yields

$$\dot{\bar{r}} = \dot{\bar{R}} + \dot{\bar{\rho}} = \dot{\bar{R}} + \bar{v} + \bar{\omega} \times \bar{\rho} \tag{3-10}$$

where $\bar{v}$ is the velocity of the mass element as seen by an observer in the $\bar{x}\bar{y}\bar{z}$ coordinate system and $\bar{\omega}$ is the angular velocity of the $\bar{x}\bar{y}\bar{z}$ coordinate system referred to the $\bar{x}\bar{y}\bar{z}$ coordinate system. Now

$$R = X\bar{i}_o + Y\bar{j}_o + Z\bar{k}_o \tag{3-11}$$

where $\bar{i}_o$, $\bar{j}_o$, $\bar{k}_o$ are unit vectors in the fixed system. With reference to Figs. 3-1, 3-3, and 3-4 $\bar{R}$ can be written in terms of the system degrees of freedom as

$$R = x\bar{i}_o + (y + h_2\phi_z)\bar{j}_o + (z - h_1\phi_y)\bar{k}_o \tag{3-12}$$

small motions being assumed throughout. For small angles we can also write

$$\bar{\omega} = \dot{\psi}\bar{i} \tag{3-13}$$

where, for an N-bladed rotor,

$$\psi = \Omega t + 2\pi \frac{n - 1}{N} + \phi_x \tag{3-14}$$

and $\bar{i}$ is a unit vector along the $\bar{x}$ axis. The rotor rotational speed Ω is taken to be constant.

The flapping angle β between the spanwise axis of the n^{th} blade and a plane normal to the rotor mast will vary periodically

with the aximuth angle ψ. The flapwise angular position of the n^{th} blade relative to the $\bar{y}$ axis can be written in terms of the tip-path-plane freedoms a_1 and b_1 and rotor precone β_o in the form

$$\beta' \equiv \beta + \beta_o = a_1 \sin \psi - b_1 \cos \psi + \beta_o \tag{3-15}$$

The contribution of the pylon pitch and yaw angular displacement to the tip-path-plane angular displacement is

$$\gamma' = \phi_y \sin \psi - \phi_z \cos \psi \tag{3-16}$$

The angular position of the n^{th} blade in space is then given by

$$\eta' = \beta' + \gamma' = (a_1 + \phi_y) \sin \psi - (b_1 + \phi_z) \cos \psi + \beta_o \tag{3-17}$$

Now $\bar{\rho}$ can be expressed as

$$\bar{\rho} = r \cos \eta' \, \bar{j} + r \sin \eta' \, \bar{i} \tag{3-18}$$

from which

$$\bar{v} = - r \dot{\eta}' \sin \eta' \, \bar{j} + r \dot{\eta}' \cos \eta' \, \bar{i} \tag{3-19}$$

Substituting Eqs. 3-12, 3-13, 3-18, and 3-19 into Eq. 3-10 yields

$$\begin{aligned} \dot{\bar{r}} = {} & \dot{x} \, \bar{i}_o + (\dot{y} + h_2 \dot{\phi}_z) \bar{j}_o + (\dot{z} - h_1 \dot{\phi}_y) \bar{k}_o \\ & - r \dot{\eta}' \sin \eta' \, \bar{j} + r \dot{\eta}' \cos \eta' \, \bar{i} + r \dot{\psi} \cos \eta' \, \bar{k} \end{aligned} \tag{3-20}$$

From the geometry of Fig. 3-4 the unit vectors in the $\bar{x}\bar{y}\bar{z}$ and $X_o Y_o Z_o$ coordinate systems are related as

$$\bar{i} = \bar{i}_o$$

$$\bar{j} = \bar{j}_o \cos \psi + \bar{k}_o \sin \psi \tag{3-21}$$

$$\bar{k} = -\bar{j}_o \sin \psi + \bar{k}_o \cos \psi$$

Using Eqs. 3-21 in Eq. 3-20 there results

$$\begin{aligned}\dot{\bar{r}} = {} & \bar{i}_o[\dot{x} + r\dot{\eta}' \cos \eta'] + \bar{j}_o[\dot{y} + h_2\dot{\phi}_z \\ & - r\dot{\eta}' \sin \eta' \cos \psi - r\dot{\psi} \cos \eta' \sin \psi] \\ & + \bar{k}_o[\dot{z} - h_1\dot{\phi}_y - r\dot{\eta}' \sin \eta' \sin \psi \\ & + r\dot{\psi} \cos \eta' \cos \psi]\end{aligned} \tag{3-22}$$

The kinetic energy of the n^{th} blade is given by

$$T_B = \frac{1}{2}\int_0^R m(r)\, \dot{\bar{r}} \cdot \dot{\bar{r}}\, dr \tag{3-23}$$

Substituting Eq. 3-22 into Eq. 3-23 gives

$$\begin{aligned}T_B = \frac{1}{2}\int_0^R m(r)\Big[& \dot{x}^2 + 2\dot{x}r\dot{\eta}' \cos \eta' + r^2\dot{\eta}'^2 \cos^2 \eta' \\ & + \dot{y}^2 + 2\dot{y}h_2\dot{\phi}_z - 2\dot{y}r\dot{\eta}' \sin \eta' \cos \psi \\ & - 2\dot{y}r\dot{\psi} \cos \eta' \sin \psi + h_2^2\dot{\phi}_z^2 - 2h_2\dot{\phi}_z r\dot{\eta}' \sin \eta' \cos \psi \\ & - 2h_2\dot{\phi}_z r\dot{\psi} \cos \eta' \sin \psi + r^2\dot{\eta}'^2 \sin^2 \eta' \cos^2 \psi \\ & + 2\dot{\psi}r^2\dot{\eta}' \sin \eta' \cos \eta' \sin \psi \cos \psi + r^2\dot{\psi}^2 \cos^2 \eta' \sin^2 \psi \\ & + \dot{z}^2 - 2\dot{z}h_1\dot{\phi}_y - 2\dot{z}r\dot{\eta}' \sin \eta' \sin \psi \\ & + 2\dot{z}\dot{\psi}r \cos \eta' \cos \psi + h_1^2\dot{\phi}_y^2 + 2h_1\dot{\phi}_y r\dot{\eta}' \sin \eta' \sin \psi\end{aligned} \tag{3-24}$$

$$- 2h_1\dot{\phi}_y\dot{\psi}r\cos\eta'\cos\psi + r^2\dot{\eta}'^2\sin^2\eta'\sin^2\psi$$

$$- 2\dot{\psi}r^2\dot{\eta}'\sin\eta'\cos\eta'\sin\psi\cos\psi + \dot{\psi}^2r^2\cos^2\eta'\cos^2\psi\Big]\,dr$$

Expanding $\sin\eta'$ and $\cos\eta'$ and making the customary small angle assumption for the perturbation quantities the trigonometric terms involving η' in Eq. 3-24 can be approximated as

$$\begin{aligned}
\sin\eta' &\approx (\beta+\gamma')\cos\beta_o + \left[1-\tfrac{1}{2}(\beta+\gamma')^2\right]\sin\beta_o \\
\cos\eta' &\approx \left[1-\tfrac{1}{2}(\beta+\gamma')^2\right]\cos\beta_o - (\beta+\gamma')\sin\beta_o \\
\sin^2\eta' &\approx (\beta+\gamma')^2\cos^2\beta_o + \left[1-\tfrac{1}{2}(\beta+\gamma')^2\right]^2\sin^2\beta_o \\
&\quad + 2(\beta+\gamma')\left[1-\tfrac{1}{2}(\beta+\gamma')^2\right]\sin\beta_o\cos\beta_o \\
\cos^2\eta' &\approx \left[1-\tfrac{1}{2}(\beta+\gamma')^2\right]^2\cos^2\beta_o + (\beta+\gamma')^2\sin^2\beta_o \\
&\quad - 2(\beta+\gamma')\left[1-\tfrac{1}{2}(\beta+\gamma')^2\right]\sin\beta_o\cos\beta_o \\
\sin\eta'\cos\eta' &\approx (\beta+\gamma')\left[1-\tfrac{1}{2}(\beta+\gamma')^2\right]\cos^2\beta_o \\
&\quad - (\beta+\gamma')^2\sin\beta_o\cos\beta_o \\
&\quad + \left[1-\tfrac{1}{2}(\beta+\gamma')^2\right]^2\sin\beta_o\cos\beta_o \\
&\quad - (\beta+\gamma')\left[1-\tfrac{1}{2}(\beta+\gamma')^2\right]\sin^2\beta_o
\end{aligned} \tag{3-25}$$

Substituting the approximations of Eq. 3-25 into Eq. 3-24 the blade kinetic energy can be written as

$$T_B = \frac{1}{2}\int_0^R m(r)\Big[\dot{x}^2 + 2\dot{x}r(\dot{\beta}+\dot{\gamma}')\Big\{\Big[1-\tfrac{1}{2}(\beta+\gamma')^2\Big]\cos\beta_o - (\beta+\gamma')\sin\beta_o\Big\} + r^2(\dot{\beta}+\dot{\gamma}')^2\Big\{\Big[1-\tfrac{1}{2}(\beta+\gamma')^2\Big]^2\cos^2\beta_o + (\beta+\gamma')^2\sin^2\beta_o - 2(\beta+\gamma')\Big[1-\tfrac{1}{2}(\beta+\gamma')^2\Big]\sin\beta_o\cos\beta_o\Big\} + \dot{y}^2 + 2\dot{y}h_2\dot{\phi}_z - 2\dot{y}r\cos\psi\,(\dot{\beta}+\dot{\gamma}')\Big\{(\beta+\gamma')\cos\beta_o + \Big[1-\tfrac{1}{2}(\beta+\gamma')^2\Big]\sin\beta_o\Big\} - 2\dot{y}r\dot{\psi}\sin\psi\Big\{\Big[1-\tfrac{1}{2}(\beta+\gamma')^2\Big]\cdot\cos\beta_o - (\beta+\gamma')\sin\beta_o\Big\} + h_2^2\dot{\phi}_z^2 - 2h_2\dot{\phi}_z r\cos\psi(\dot{\beta}+\dot{\gamma}')\Big\{(\beta+\gamma')\cdot\cos\beta_o + \Big[1-\tfrac{1}{2}(\beta+\gamma')^2\Big]\sin\beta_o\Big\} - 2h_2\dot{\phi}_z r\dot{\psi}\sin\psi\Big\{\Big[1-\tfrac{1}{2}(\beta+\gamma')^2\Big]\cdot\cos\beta_o - (\beta+\gamma')\sin\beta_o\Big\} + r^2\cos^2\psi\,(\dot{\beta}+\dot{\gamma}')^2\Big\{(\beta+\gamma')^2\cos^2\beta_o + \Big[1-\tfrac{1}{2}(\beta+\gamma')^2\Big]^2\sin^2\beta_o + 2(\beta+\gamma')\Big[1-\tfrac{1}{2}(\beta+\gamma')^2\Big]\cdot\sin\beta_o\cos\beta_o\Big\} + 2\dot{\psi}r^2\sin\psi\cos\psi\,(\dot{\beta}+\dot{\gamma}')\Big\{(\beta+\gamma')\Big[1-\tfrac{1}{2}(\beta+\gamma')^2\Big]\cos^2\beta_o - (\beta+\gamma')^2\sin\beta_o\cos\beta_o + \Big[1-\tfrac{1}{2}(\beta+\gamma')^2\Big]^2\sin\beta_o\cos\beta_o - (\beta+\gamma')\Big[1-\tfrac{1}{2}(\beta+\gamma')^2\Big]\sin^2\beta_o\Big\} + \dot{z}^2 + r^2\dot{\psi}^2\sin^2\psi\Big\{\Big[1-\tfrac{1}{2}(\beta+\gamma')^2\Big]^2\cos^2\beta_o + (\beta+\gamma')^2\sin^2\beta_o$$

$$- 2(\beta + \gamma')\left[1 - \tfrac{1}{2}(\beta + \gamma')^2\right] \sin \beta_o \cos \beta_o \Big\} - 2\dot{z}h_1\dot{\phi}_y$$

$$- 2\dot{z}r \sin \psi(\dot{\beta} + \dot{\gamma}')\Big\{(\beta + \gamma') \cos \beta_o + \left[1 - \tfrac{1}{2}(\beta + \gamma')^2\right] \sin \beta_o\Big\}$$

$$+ 2\dot{z}r\dot{\psi} \cos \psi\Big\{\left[1 - \tfrac{1}{2}(\beta + \gamma')^2\right] \cos \beta_o - (\beta + \gamma') \sin \beta_o\Big\}$$

$$+ h_1^2 \dot{\phi}_y^2 + 2h_1\dot{\phi}_y r \sin \psi(\dot{\beta} + \dot{\gamma}')\Big\{(\beta + \gamma') \cos \beta_o$$

$$+ \left[1 - \tfrac{1}{2}(\beta + \gamma')^2\right] \sin \beta_o\Big\} - 2h_1\dot{\phi}_y r\dot{\psi} \cos \psi\Big\{\left[1 - \tfrac{1}{2}(\beta + \gamma')^2\right] \cdot$$

$$\cos \beta_o$$

$$- (\beta + \gamma') \sin \beta_o\Big\} + r^2 \sin^2\psi\ (\dot{\beta} + \dot{\gamma}')^2\ \Big\{(\beta + \gamma')^2 \cos^2\beta_o$$

$$+ \left[1 - \tfrac{1}{2}(\beta + \gamma')^2\right]^2 \sin^2\beta_o + 2(\beta + \gamma')\left[1 - \tfrac{1}{2}(\beta + \gamma')^2\right] \cdot$$

$$\sin \beta_o \cos \beta_o\Big\}$$

$$- 2r^2\dot{\psi} \sin \psi \cos \psi(\dot{\beta} + \dot{\gamma}')\Big\{(\beta + \gamma')\left[1 - \tfrac{1}{2}(\beta + \gamma')^2\right] \cos^2\beta_o$$

$$- (\beta + \gamma')^2 \sin \beta_o \cos \beta_o + \left[1 - \tfrac{1}{2}(\beta + \gamma')^2\right]^2 \sin \beta_o \cos \beta_o$$

$$- (\beta + \gamma')\left[1 - \tfrac{1}{2}(\beta + \gamma')^2\right] \sin^2\beta_o\Big\} + r^2\dot{\psi}^2 \cos^2\psi\ \Big\{\left[1 - \tfrac{1}{2}(\beta +\right.$$

$$\left.\gamma')^2\right]^2 \cos^2\beta_o + (\beta + \gamma')^2 \sin^2\beta_o$$

$$- 2(\beta + \gamma')\left[1 - \tfrac{1}{2}(\beta + \gamma')^2\right] \sin \beta_o \cos \beta_o\Big\}\Big] dr \qquad (3\text{-}26)$$

Noting that β_o is in practice small (a few degrees) the small angle approximation is also valid for the trigonometric terms involving β_o. Making these additional approximations in Eq. 3-26, expanding, and retaining terms up to second order in the dependent coordinates and first order in β_o leads to

$$T_B = \frac{1}{2}\int_0^R m(r)\Big[\dot{x}^2 + 2\dot{x}r(\dot{\beta} + \dot{\gamma}') + r^2(\dot{\beta} + \dot{\gamma}')^2$$

$$+ \dot{y}^2 + 2\dot{y}h_2\dot{\phi}_z - 2\dot{y}r\cos\psi(\dot{\beta} + \dot{\gamma}')\,\beta_o$$

$$- 2\dot{y}r\dot{\psi}\sin\psi\Big\{1 - (\beta + \gamma')\,\beta_o\Big\} + h_2^2\,\dot{\phi}_z^2$$

$$- 2h_2\dot{\phi}_z r\cos\psi(\dot{\beta} + \dot{\gamma}')\,\beta_o - 2h_2\dot{\phi}_z r\dot{\psi}\sin\psi\Big\{1 - (\beta + \gamma')\beta_o\Big\}$$

$$+ \dot{z}^2 + r^2\dot{\psi}^2\sin^2\psi\Big\{1 - (\beta + \gamma')^2$$

$$- 2\,(\beta + \gamma')\beta_o\Big\} - 2\dot{z}\,h_1\,\dot{\phi}_y \qquad (3\text{-}27)$$

$$- 2\dot{z}r\sin\psi(\dot{\beta} + \dot{\gamma}')\,\beta_o + 2\dot{z}r\dot{\psi}\cos\psi\Big\{1 - (\beta + \gamma')\beta_o\Big\}$$

$$+ h_1^2\,\dot{\phi}_y^2 + 2h_1\dot{\phi}_y r\sin\psi(\dot{\beta} + \dot{\gamma}')\,\beta_o - 2h_1\dot{\phi}_y r\dot{\psi}\cos\psi\Big\{1 -$$

$$(\beta + \gamma')\beta_o\Big\} + r^2\dot{\psi}^2\cos^2\psi\Big\{1 - (\beta + \gamma')^2 - 2(\beta + \gamma')\,\beta_o\Big\}\Big]\,dr$$

Substituting the expressions for β and γ' from Eqs. 3-15 and 3-16 into Eq. 3-27

$$T_B = \frac{1}{2}\int_0^R m(r)\Big[\dot{x}^2 + 2\dot{x}r\Big\{\textcircled{1}\cos\psi + \textcircled{2}\sin\psi\Big\}$$

$$+ r^2\Big\{\textcircled{1}^2\cos^2\psi + 2\textcircled{1}\,\textcircled{2}\sin\psi\cos\psi + \textcircled{2}^2\sin^2\psi\Big\}$$

$$+ \dot{y}^2 + 2\dot{y}\,h_2\,\dot{\phi}_z - 2\dot{y}r\cos\psi\,\beta_o\Big\{\textcircled{1}\cos\psi + \textcircled{2}\sin\psi\Big\}$$

$$- 2\dot{y}r\dot{\psi}\sin\psi\Big\{1 - \beta_o A\sin\psi + \beta_o B\cos\psi\Big\} + h_2^2\,\dot{\phi}_z^2$$

$$- 2h_2\dot{\phi}_z r\,\beta_o\cos\psi\Big\{\textcircled{1}\cos\psi + \textcircled{2}\sin\psi\Big\} \qquad (3\text{-}28)$$

$$- 2h_2\dot{\phi}_z r\,\dot{\psi}\sin\psi\Big\{1 - \beta_o\,A\sin\psi + \beta_o B\cos\psi\Big\} + \dot{z}^2$$

$$+ r^2\dot{\psi}^2\Big\{1 - A^2 \sin^2\psi + 2AB \sin\psi \cos\psi - B^2 \cos^2\psi$$

$$- 2\beta_o A \sin\psi + 2\beta_o B \cos\psi\Big\}$$

$$- 2\dot{z}h_1\dot{\phi}_y - 2\dot{z}r\beta_o \sin\psi\Big\{① \cos\psi + ② \sin\psi\Big\}$$

$$+ 2\dot{z}r\dot{\psi} \cos\psi\Big\{1 - \beta_o A \sin\psi + \beta_o B \cos\psi\Big\} + h_1^2 \dot{\phi}_y^2$$

$$+ 2h_1\dot{\phi}_y r\beta_o \sin\psi\Big\{① \cos\psi + ② \sin\psi\Big\}$$

$$- 2h_1\dot{\phi}_y r\dot{\psi} \cos\psi\Big\{1 - \beta_o A \sin\psi + \beta_o B \cos\psi\Big\}\Big] \, dr$$

where the following definitions have been made:

$$① = \dot{\psi}\, a_1 - \dot{b}_1 + \dot{\psi}\, \phi_y - \dot{\phi}_z$$

$$② = \dot{a}_1 + b_1\dot{\psi} + \dot{\phi}_y + \dot{\psi}\, \phi_z \qquad (3\text{-}29)$$

$$A = a_1 + \phi_y \qquad B = b_1 + \phi_z$$

The rotor contribution to the kinetic energy is obtained from Eq. 3-28 by summing over the number of blades using the relationships

$$\sum_{n=1}^{N} \cos^2\psi = \sum_{n=1}^{N} \sin^2\psi = \frac{N}{2}$$

$$\sum_{n=1}^{N} \sin\psi \cos\psi = \sum_{n=1}^{N} \sin\psi = \sum_{n=1}^{N} \cos\psi = 0 \qquad (3\text{-}30)$$

This results in

$$T_R = \frac{1}{2}\int_0^R m(r)\Bigg[N\dot{x}^2 + \frac{N}{2} r^2\Big(\Omega^2 a_1^2 - 2\Omega\, a_1\dot{b}_1 + 2\Omega^2 a_1\phi_y - 2\Omega\, a_1\dot{\phi}_z$$

$$+ \dot{b}_1^2 - 2\Omega\, \dot{b}_1\phi_y + 2\dot{b}_1\dot{\phi}_z + \Omega^2\phi_y^2 - 2\Omega\, \phi_y\dot{\phi}_z + \dot{\phi}_z^2 + \dot{a}_1^2$$

$$+ 2\Omega\, \dot{a}_1 b_1 + 2\dot{a}_1\dot{\phi}_y + 2\Omega\, \dot{a}_1\phi_z + \Omega^2 b_1^2 + 2\Omega\, b_1\dot{\phi}_y + 2\Omega^2 b_1\phi_z$$

$$+ \dot{\phi}_y^2 + 2\Omega\, \dot{\phi}_y\phi_z + \Omega^2\phi_z^2\Big) + N\dot{y}^2 + 2N\dot{y}h_2\dot{\phi}_z - 2\dot{y}r\beta_o \frac{N}{2}\Big\{\Omega a_1$$

$$- \dot{b}_1 + \Omega\phi_y - \dot{\phi}_z\Big\} + 2\dot{y}r\Omega \frac{N}{2}\beta_o\Big\{a_1 + \phi_y\Big\} + Nh_2^2\,\dot{\phi}_z^2$$

$$- 2h_2\dot{\phi}_z r\beta_o \frac{N}{2}\Big\{\Omega a_1 - \dot{b}_1 + \Omega\phi_y - \dot{\phi}_z\Big\} + 2h_2\dot{\phi}_z r\,\Omega\beta_o \frac{N}{2}\Big\{a_1 + \phi_y\Big\}$$

$$+ N\dot{z}^2 + Nr^2\Big(\Omega + \dot{\phi}_x\Big)^2 - \frac{N}{2} r^2\Omega^2\Big\{a_1^2 + 2a_1\phi_y + \phi_y^2 + b_1^2 + 2b_1\phi_z + \phi_z^2\Big\}$$

$$- 2N\dot{z}h_1\dot{\phi}_y - 2\dot{z}r\beta_o \frac{N}{2}\Big\{\dot{a}_1 + b_1\Omega + \dot{\phi}_y + \Omega\phi_z\Big\} + 2\dot{z}r\Omega\beta_o \frac{N}{2}\Big\{b_1 + \phi_z\Big\}$$

$$+ Nh_1^2\,\dot{\phi}_y^2 + 2h_1\dot{\phi}_y r\beta_o \frac{N}{2}\Big\{\dot{a}_1 + \Omega b_1 + \dot{\phi}_y + \Omega\phi_z\Big\}$$

$$- 2h_1\dot{\phi}_y r\Omega\beta_o \frac{N}{2}\Big\{b_1 + \phi_z\Big\}\Bigg]\, dr \qquad (3\text{-}31)$$

Introducing the definitions

$$N\int_0^R m(r)\,dr \quad M_R$$

$$\frac{N}{2}\int_0^R r^2 m(r)\,dr = \frac{N}{2} I_B \equiv I_R \tag{3-32}$$

$$\frac{N}{2}\int_0^R rm(r)\,dr = \frac{N}{2} S_B \equiv S_R$$

the kinetic energy of the proprotor assumes the final form

$$\begin{aligned} T_R = \frac{1}{2}\Big[& M_R\left(\dot{x}^2 + \dot{y}^2 + \dot{z}^2\right) + I_R\left(\Omega^2 a_1^2 - 2\Omega\, a_1\dot{b}_1 + 2\Omega^2 a_1\phi_y - 2\Omega\, a_1\dot{\phi}_z\right. \\ & + \dot{b}_1^2 - 2\Omega\,\dot{b}_1\phi_y + 2\dot{b}_1\dot{\phi}_z + \Omega^2\phi_y^2 - 2\Omega\,\dot{\phi}_y\dot{\phi}_z + \dot{\phi}_z^2 + \dot{a}_1^2 \\ & + 2\Omega\,\dot{a}_1 b_1 + 2\dot{a}_1\dot{\phi}_y + 2\Omega\,\dot{a}_1\phi_z + \Omega^2 b_1^2 + 2\Omega\, b_1\dot{\phi}_y + 2\Omega^2 b_1\phi_z \\ & \left. + \dot{\phi}_y^2 + 2\Omega\,\dot{\phi}_y\phi_z + \Omega^2\phi_z^2\right) + M_R\left(2\dot{y}h_2\dot{\phi}_z + h_2^2\,\dot{\phi}_z^2 - 2\dot{z}h_1\dot{\phi}_y + h_1^2\,\dot{\phi}_y^2\right) \\ & + NI_B\left(\Omega + \dot{\phi}_x\right)^2 - \Omega^2 I_R\left(a_1^2 + 2a_1\phi_y + \phi_y^2 + b_1^2 + 2b_1\phi_z + \phi_z^2\right) \\ & + S_R\beta_o\Big\{2y\left(\dot{b}_1 + \dot{\phi}_z\right) + 2h_2\dot{\phi}_z\left(\dot{b}_1 + \dot{\phi}_z\right) - 2\dot{z}\left(\dot{a}_1 + \dot{\phi}_y\right) \\ & + 2h_1\dot{\phi}_y\left(\dot{a}_1 + \dot{\phi}_y\right)\Big\}\Big] \end{aligned} \tag{3-33}$$

(2) Potential Energy - The proprotor contribution to the system potential energy arises from the deflection of the hub flapping springs. For the n^{th} blade this energy, in the rotating coordinate system, can be written as

$$V_B = \frac{1}{2} K_\beta \beta^2 \tag{3-34}$$

where K_β is the blade flapping restraint and β is defined in terms of tip-path-plane coordinates as

$$\beta = a_1 \sin \psi - b_1 \cos \psi \tag{3-35}$$

For K_β a constant (that is, independent of ψ) the substitution of Eq. 3-35 into Eq. 3-34 and a summation over N blades results in

$$V_R = \frac{1}{2} K_\beta \frac{N}{2}\left[a_1^2 + b_1^2\right] \tag{3-36}$$

from which the following definition is made

$$K_H \equiv \frac{N}{2} K_\beta \tag{3-37}$$

Eq. 3-37 establishes the "equivalence" between the blade flapping restraint K_β and the symmetric hub flapping restraint K_H. In the general case of a non-symmetric hub restraint Eq. 3-36 is replaced by

$$V_R = \frac{1}{2}\left[K_{a_1} a_1^2 + K_{b_1} b_1^2\right] \tag{3-38}$$

(3) Damping - A viscous damping model is employed to account for energy dissipation at the hub gimbal. The Rayleigh dissipation function for the case of nonsymmetric hub damping is given by

$$D_R = \frac{1}{2} C_{a_1}\left[\dot{a}_1^2 + 2\Omega \dot{a}_1 b_1 + \Omega^2 a_1^2\right] + \frac{1}{2} C_{b_1}\left[\dot{b}_1^2 - 2\Omega \dot{b}_1 a_1 + \Omega^2 b_1^2\right] \tag{3-39}$$

where the damping coefficients are given by

$$C_{a_1} = \zeta_{a_1}\left(2\sqrt{I_R K_{a_1}}\right)$$
$$C_{b_1} = \zeta_{b_1}\left(2\sqrt{I_R K_{b_1}}\right) \qquad (3\text{-}40)$$

Eqs. 3-40 are based on the definition of the critical viscous damping coefficient for motion in one degree of freedom.

Pylon/Wing: Motion of the proprotor/pylon/wing system is influenced mainly by the proprotor/pylon combination because of its large concentrated mass in comparison to the smaller distributed mass of the wing. This suggests that the contribution of the wing elastic degrees of freedom to the proprotor/pylon motion can be fairly well accounted for by considering only wing tip deflections in the wing modes of importance. Since the proprotor couples with one of the fundamental wing modes (wing vertical bending, wing fore and aft bending or wing torsion) it is necessary to consider only the wing tip deflections in these fundamental modes of motion. This permits the use of equivalent concentrated wing tip spring rates to represent the deflection characteristics of the wing tip in the fundamental wing modes. Since the pylon centerline is offset laterally from the wing tip these wing tip spring rates are referenced to the appropriate pylon pitch or yaw effective pivot as depicted in Fig. 3-5.* An energy dissipation device, either structural or viscous, is associated with each of the support

*Stiffness coupling is neglected.

springs shown. The wing distributed mass and inertia are replaced by generalized masses and inertias based on the fundamental mode shapes and referenced to the appropriate location on the pylon centerline. The distributed mass of the pylon (less rotor) is replaced by an equivalent rigid body mass-inertia matrix referenced to axes fixed at the pylon center of mass. To allow for non-coincident effective pitch and yaw pivot locations, $\bar{h}_1 \neq \bar{h}_2$ (see Fig. 3-2). Summarizing, the basic pylon/wing assumptions are:

1. Rigid pylon having three translational and three rotational degrees of freedom
2. Pylon constrained in translation and rotation by linear springs and dampers
3. Wing distributed mass, stiffness, and damping replaced by equivalent concentrated masses, springs, and dampers referenced to the centerline of the pylon

(1) Kinetic Energy - Assuming that the body axes fixed at the pylon center of mass are principal axes the kinetic energy of the pylon with respect to those axes can be immediately written in the matrix form

$$T_{P_c} = \frac{1}{2} \{\dot{x}\}_c^T \begin{bmatrix} M_P & 0 & 0 & 0 & 0 & 0 \\ 0 & M_P & 0 & 0 & 0 & 0 \\ 0 & 0 & M_P & 0 & 0 & 0 \\ 0 & 0 & 0 & I_{P_{xx}} & 0 & 0 \\ 0 & 0 & 0 & 0 & I_{P_{yy}} & 0 \\ 0 & 0 & 0 & 0 & 0 & I_{P_{zz}} \end{bmatrix} \{\dot{x}\}_c \qquad (3\text{-}41)$$

This energy must be expressed in terms of the pylon degrees of freedom which are defined at the effective pylon pitch and yaw pivots. The necessary transformation is effected in the manner outlined in Appendix A, the required transformation matrix $[\theta]$ being obtained from Eq. A-13 by making the following substitutions: $\ell_{rs} = 0$ for $r \neq s$, $a = \bar{h}_1$ or $\bar{h}_2$ depending on whether pitch or yaw, $b = 0$, $c = -\bar{c}$, $\alpha_o = \phi_x$, $\beta_o = \phi_y$, $\gamma_o = \phi_z$, $x_o = x$, $y_o = y$, and $z_o = z$. The final result is

$$T_P = \frac{1}{2} \begin{Bmatrix} x \\ y \\ z \\ \phi_x \\ \phi_y \\ \phi_z \end{Bmatrix}^T \left[\begin{array}{ccc:ccc} M_P & 0 & 0 & 0 & -M_P\bar{c} & 0 \\ 0 & M_P & 0 & M_P\bar{c} & 0 & M_P\bar{h}_2 \\ 0 & 0 & M_P & 0 & -M_P\bar{h}_1 & 0 \\ \hdashline 0 & M_P\bar{c} & 0 & I_{P_{xx}}+M_P\bar{c}^2 & 0 & M_P\bar{c}\bar{h}_2 \\ -M_P\bar{c} & 0 & -M_P\bar{h}_1 & 0 & I_{P_{yy}}+M_P\bar{c}^2+M_P\bar{h}_1^2 & 0 \\ 0 & M_P\bar{h}_2 & 0 & M_P\bar{c}\bar{h}_2 & 0 & I_{P_{zz}}+M_P\bar{h}_2^2 \end{array}\right] \begin{Bmatrix} \dot{x} \\ \dot{y} \\ \dot{z} \\ \dot{\phi}_x \\ \dot{\phi}_y \\ \dot{\phi}_z \end{Bmatrix} \tag{3-42}$$

(2) Potential Energy - Based on the equivalent linear springs shown in Fig. 3-5 the potential energy contributed by the pylon can be written as

$$V_P = \frac{1}{2} K_x x^2 + \frac{1}{2} K_y y^2 + \frac{1}{2} K_z z^2 + \frac{1}{2} K_{\phi_x} \phi_x^2 + \frac{1}{2} K_{\phi_y} \phi_y^2 + \frac{1}{2} K_{\phi_z} \phi_z^2 \tag{3-43}$$

(3) Damping - The Rayleigh dissipation function to account for viscous damping is given by

$$D_P = \frac{1}{2} C_x \dot{x}^2 + \frac{1}{2} C_y \dot{y}^2 + \frac{1}{2} C_z \dot{z}^2 + \frac{1}{2} C_{\phi_x} \dot{\phi}_x^2 + \frac{1}{2} C_{\phi_y} \dot{\phi}_y^2 + \frac{1}{2} C_{\phi_z} \dot{\phi}_z^2 \tag{3-44}$$

Substituting Eqs. 3-33, 3-38, 3-39, 3-42, 3-43, and 3-44 into the left hand side of Lagrange's equation (Eq. 3-6) and performing the indicated differentiations establishes the dynamic matrices in Eq. 3-8. These are given in Eqs. 3-45 through 3-48 below.

$$[\bar{M}] =$$

x	y	z	a_1	b_1	ϕ_x	ϕ_y	ϕ_z	
$M_R+M_P+W_x$	0	0	[illegible]	[illegible]	0	$-M_P\bar{c}$	0	x
0	$M_R+M_P+W_y$	0	[illegible]	$S_R\beta_o$	$M_P\bar{c}$	0	$M_Rh_2+S_R\beta_o+M_P\bar{h}_2$	y
0	0	$M_R+M_P+W_z$	$-S_R\beta_o$	0	$-M_P\bar{h}_1$	$-M_Rh_1-S_R\beta_o-M_P\bar{h}_1$	0	z
0	0	$-S_R\beta_o$	I_R	0	0	$I_R+S_R\beta_oh_1$	0	a_1
0	$S_R\beta_o$	0	0	I_R	0	0	$I_R+S_R\beta_oh_2$	b_1
0	$M_P\bar{c}$	0	0	0	$NI_B+I_{P_{xx}}+M_P\bar{c}^2+W_{I_{xx}}$	0	$M_P\bar{c}\bar{h}_2$	ϕ_x
$-M_P\bar{c}$	0	$-M_Rh_1-S_R\beta_o-M_P\bar{h}_1$	[illegible]	0	0	$M_P\bar{c}^2+M_P\bar{h}_1^2+I_R+M_Rh_1^2$ $+2S_R\beta_oh_1+I_{P_{yy}}+W_{I_{yy}}$	0	ϕ_y
0	$M_Rh_2+S_R\beta_o+M_P\bar{h}_2$	0	[illegible]	[illegible]	$M_P\bar{c}\bar{h}_2$	0	$M_P\bar{h}_2^2+I_{P_{zz}}+I_R$ $+M_Rh_2^2+2S_R\beta_oh_2+W_{I_{zz}}$	ϕ_z

(3-45)

$$[\Gamma] = \Omega \begin{bmatrix} 0 & 0 & 0 & 0 & 0 & 0 & 0 & 0 \\ 0 & 0 & 0 & 0 & 0 & 0 & 0 & 0 \\ 0 & 0 & 0 & 0 & 0 & 0 & 0 & 0 \\ 0 & 0 & 0 & 0 & 2I_R & 0 & 0 & 2I_R \\ 0 & 0 & 0 & -2I_R & 0 & 0 & -2I_R & 0 \\ 0 & 0 & 0 & 0 & 0 & 0 & 0 & 0 \\ 0 & 0 & 0 & 0 & 2I_R & 0 & 0 & 2I_R \\ 0 & 0 & 0 & -2I_R & 0 & 0 & -2I_R & 0 \end{bmatrix} \tag{3-46}$$

$$[\bar{C}] = \begin{bmatrix} C_x & & & & & & & \\ & C_y & & & & & & \\ & & C_z & & & \text{Null} & & \\ & & & C_{a_1} & & & & \\ & & & & C_{b_1} & & & \\ & & \text{Null} & & & C_{\phi_x} & & \\ & & & & & & C_{\phi_y} & \\ & & & & & & & C_{\phi_z} \end{bmatrix} \tag{3-47}$$

$$[\bar{K}] = \begin{bmatrix} (1 + ig_x)K_x & & & & & & & \\ & (1 + ig_y)K_y & & & & & & \\ & & (1 + ig_z)K_z & & & & & \\ & & & K_{a_1} & \Omega C_{a_1} & & & \\ & & & -\Omega C_{b_1} & K_{b_1} & & & \\ & & & & & (1 + ig_{\phi_x})K_{\phi_x} & & \\ & & & & & & (1 + ig_{\phi_y})K_{\phi_y} & \\ & & & & & & & (1 + ig_{\phi_z})K_{\phi_z} \end{bmatrix} \tag{3-48}$$

(c) Aerodynamic Development

General Considerations: Historically, propeller/nacelle whirl flutter analyses have not required inclusion of unsteady aerodynamic effects arising from the wake, mainly because the vorticity shed by the blades is carried away from the propeller plane at a much faster rate than the corresponding wake associated with a helicopter in forward flight. The same appears to be true for a proprotor in axial flight so that for flight operations at high advance ratios, such as in the airplane cruise mode of flight, wake effects can be taken to be of secondary importance. Consequently a first-order linear approximation to the non-steady aerodynamic

forces and moments acting on a proprotor performing transient motions can be established via a quasi-steady aerodynamic theory. Characteristic features of a quasi-steady approximation are the neglect of the effects of the oscillatory wake (i.e., aerodynamic phase lags), the airloads being taken to adjust themselves instantaneously to the motions producing them,* and the neglect of the (generally) small aerodynamic acceleration terms (i.e., the noncirculatory lift terms).

In addition to the explicit assumptions associated with the use of a quasi-steady aerodynamic theory several simplifying assumptions are associated with the aerodynamic development herein. The majority of these are "classical" in nature, being of the type which are customarily made when employing a quasi-steady aerodynamic theory in a linear formulation for propeller and proprotor whirl flutter stability analyses. Thrust and blade profile drag are initially included in the formulation to indicate the manner in which they might be incorporated in the analysis, but they are eventually dropped. The principal additional aerodynamic assumptions are:

1. Axial flow through proprotor
2. Aerodynamic loading is applied stripwise along the blade

---

*Mathematically, quasi-steady aerodynamic theory is obtained from a general unsteady theory by setting the reduced frequency, which is a measure of the wake unsteadiness, to zero.

3. Lift coefficient is linear with angle of attack; profile drag coefficient is a quadratic function of angle of attack

4. Perturbation velocity components acting on the blade sections only contribute to changes in the inflow angle and have negligible effect on the resultant section velocity

5. Induced velocity due to thrust is negligible

6. The aerodynamic forces acting on the pylon and spinner are zero

7. No wing aerodynamics

8. No rotor/wing aerodynamic interference

9. The precone angle is small

10. Negligible blade section pitching moment

11. Blade chord is constant along span

The first assumption restricts consideration to the airplane mode of flight with the proprotor fully converted forward. Assumption 2 means that the blade is treated as a rotating airfoil with each blade element following a helical path and treated as a segment of an infinite aspect ratio (i.e., two-dimensional) wing with no spanwise aerodynamic interference between elements. Corrections for finite span are introduced separately. Blade stall effects are precluded by assumption 3. Assumption 4 restricts applicability to determining the stability of small oscillations about a steady-state trim flight condition. Assumption 5 implies that the disc loading under thrusting conditions is "small." This requirement is met in the airplane cruise mode of flight where the proprotor thrust (or lift) coefficient is on the order of 1/10th that in

hover. This low lift coefficient in combination with high aspect ratio blades minimizes the induced drag, which can then be neglected relative to the blade profile drag. The assumption of no wing aerodynamic loading is a consequence of the simplified mathematical model selected to represent the pylon/wing system. Although this assumption may appear to be a severely limiting one, limited results (to be shown in Chapter 5) indicate that the neglect of wing aerodynamics in proprotor/pylon whirl stability analyses is conservative. On the basis of assumption 9 precone can be taken to have no effect on the inflow geometry and perturbation flow velocities. Control system loading considerations dictate the use of rotor blade airfoil sections that minimize the sectional pitching moments. Also, for blades which are stiff in torsion, the contribution of the section pitching velocity to the local inflow velocity is considerably smaller than the contribution from the blade flapping velocity. The blade section pitching moment contribution to the generalized aerodynamic forces important in whirl flutter is thus generally small and can be neglected. The assumption of constant chord blades is not really restrictive since proprotor blades are characteristically very nearly of constant chord, at least over the major portion of their span.

Although the aforementioned aerodynamic assumptions and those employed earlier in the dynamic development are quite extensive the reduction of the stability formulation in this way to its rudiments will, hopefully, permit a better insight into proprotor-related

dynamic phenomena, which should more than compensate for any lack of mathematical elegance.

The matrices constituting the dynamic portion of Eq. 3-8 have been established above. There now remains the task of determining the aerodynamic matrices indicated in Eq. 3-8. Considerations relating to the definition of these quantities are presented below.

Perturbation Forces Acting on an Elemental Blade Section: The pertinent aerodynamic forces and associated inflow geometry applicable to a typical blade section of a proprotor in axial flight are shown in Fig. 3-6. Steady-state values of lift and drag, blade geometric pitch angle, inflow angle, and angle of attack are denoted by L, D, θ, ϕ, and α_o respectively. Corresponding changes in these quantities as a consequence of perturbations from the steady-state condition are given by ΔL, ΔD, $\Delta\theta$, $\Delta\phi$, and $\Delta\alpha$. Resolving the blade element lift and drag vectors into components parallel and normal to the freestream direction*

$$(F + \Delta F)_\beta = (L + \Delta L)\cos(\phi + \Delta\phi) - (D + \Delta D)\sin(\phi + \Delta\phi)$$
$$(F + \Delta F)_\zeta = (L + \Delta L)\sin(\phi + \Delta\phi) + (D + \Delta D)\cos(\phi + \Delta\phi) \qquad (3\text{-}49)$$

where the subscripts β and ζ denote components in the axial and normal directions, respectively. Expanding and retaining terms up to first order in the perturbation quantities Eqs. 3-49 reduce to

---

*The aerodynamics herein are developed with respect to a wind-axis system.

$$(F + \Delta F)_\beta = L \cos \phi - L\Delta\phi \sin \phi + \Delta L \cos \phi - D \sin \phi - D\Delta\phi \cos \phi - \Delta D \sin \phi \quad (3\text{-}50a)$$

$$(F + \Delta F)_\zeta = L \sin \phi + L\Delta\phi \cos \phi + \Delta L \sin \phi + D \cos \phi - D\Delta\phi \sin \phi - \Delta D \cos \phi \quad (3\text{-}50b)$$

where recourse has been made to the small angle approximation for $\Delta\phi$. Equating terms of like order in Eqs. 3-50 yields

$$F_\beta = L \cos \phi - D \sin \phi \quad (3\text{-}51a)$$

$$F_\zeta = L \sin \phi + D \cos \phi \quad (3\text{-}51b)$$

as the zero order terms, i.e., those independent of the perturbation quantities and thus describing the steady-state forces, and

$$\Delta F_\beta = \Delta L \cos \phi - \underline{L\Delta\phi \sin \phi} - \Delta D \sin \phi - D\Delta\phi \cos \phi \quad (3\text{-}52a)$$

$$\Delta F_\zeta = \Delta L \sin \phi + \underline{L\Delta\phi \cos \phi} - \Delta D \cos \phi - D\Delta\phi \sin \phi \quad (3\text{-}52b)$$

as the contribution of the first order perturbation terms to the blade section force components.* Eqs. 3-51, describing the steady-state trim condition, are not of concern here. Eqs. 3-52 are the desired expressions for the perturbation forces acting on the blade element. Examination of these equations indicates that the steady-state quantities L, D, and ϕ and the perturbation quantities ΔL, ΔD, and $\Delta\phi$ require definition.

---

*The significance of the underlined terms will be pointed out later.

The quasi-steady steady-state lift and drag acting on a blade element of width dr and chord c are given by

$$L = \frac{1}{2} \rho C_{L_o} c U_o^2 dr \tag{3-53a}$$

$$D = \frac{1}{2} \rho C_{D_o} c U_o^2 dr \tag{3-53b}$$

where C_{L_o} and C_{D_o} are the elemental lift and drag coefficients, U_o is the resultant steady velocity seen by the blade element (Fig. 3-6), and ρ is the freestream density. To account for perturbation motions Eqs. 3-53 can be generalized to

$$L + \Delta L = \frac{1}{2} \rho c \left(C_{L_o} + \Delta C_L\right)\left(U_o + \Delta U\right)^2 dr \tag{3-54a}$$

$$D + \Delta D = \frac{1}{2} \rho c \left(C_{D_o} + \Delta C_D\right)\left(U_o + \Delta U\right)^2 dr \tag{3-54b}$$

so that the perturbation lift and drag, to first order in the perturbation quantities, are given by

$$\Delta L = \frac{1}{2} \rho c \left(U_o^2 \Delta C_L + 2 U_o C_{L_o} \Delta U\right) dr \tag{3-55a}$$

$$\Delta D = \frac{1}{2} \rho c \left(U_o^2 \Delta C_D + 2 U_o C_{D_o} \Delta U\right) dr \tag{3-55b}$$

Assuming a linear variation of blade section lift coefficient with angle of attack

$$C_L = a_o \alpha \tag{3-56}$$

and a quadratic variation of blade section profile drag with angle

of attack (Ref. 3-12)

$$C_D = d_o + d_1\alpha + d_2\alpha^2 \tag{3-57}$$

the steady-state and perturbation lift and drag coefficients appearing in Eqs. 3-55 can be written as

$$C_{L_o} = a_o\alpha_o \tag{3-58a}$$

$$C_{D_o} = d_o + d_1\alpha_o + d_2\alpha_o^2 \tag{3-58b}$$

and

$$\Delta C_L = a_o\,\Delta\alpha \tag{3-59a}$$

$$\Delta C_D = d_1\,\Delta\alpha + 2d_2\alpha_o\,\Delta\alpha \tag{3-59b}$$

where a_o is the two-dimensional blade section lift curve slope and d_o, d_1, and d_2 are constants* chosen to fit the series 3-58b as closely as possible to the experimental curve of drag coefficient versus angle of attack over the appropriate angle of attack range. The steady-state angle of attack α_o is a function of blade radius and must be evaluated for each flight condition to be analyzed. Using the results of Eqs. 3-58 and 3-59 in Eqs. 3-55, the expressions for the perturbation lift and drag assume the form

---

*The coefficients are constants only below the critical Mach number and for angles of attack below stall.

$$\Delta L = \frac{1}{2} \rho\, a_o c \left[U_o^2\, \Delta\alpha + 2U_o \alpha_o\, \Delta U \right] dr \tag{3-60a}$$

$$\Delta D = \frac{1}{2} \rho c \Big[U_o^2 (d_1 \Delta\alpha + 2d_2 \alpha_o\, \Delta\alpha) + 2U_o (d_o + d_1 \alpha_o + d_2 \alpha_o^2)\, \Delta U \Big] dr \tag{3-60b}$$

Substituting Eqs. 3-53, 3-58, and 3-60 into Eqs. 3-52, the elemental perturbation aerodynamic forces acting parallel and normal to the freestream direction are given by

$$\Delta F_\beta = \frac{1}{2} \rho c \Big[(a_o U_o^2\, \Delta\alpha + 2U_o a_o \alpha_o\, \Delta U) \cos\phi - a_o \alpha_o U_o^2\, \Delta\phi \sin\phi - \Big\{ U_o^2 (d_1\, \Delta\alpha + 2d_2 \alpha_o\, \Delta\alpha) + 2U_o (d_o + d_1 \alpha_o + d_2 \alpha_o^2)\, \Delta U \Big\} \sin\phi - \Big\{ U_o^2 (d_o + d_1 \alpha_o + d_2 \alpha_o^2)\, \Delta\phi \cos\phi \Big\} \Big] dr \tag{3-61a}$$

and

$$\Delta F_\zeta = \frac{1}{2} \rho c \Big[(a_o U_o^2\, \Delta\alpha + 2U_o a_o \alpha_o\, \Delta U) \sin\phi + a_o \alpha_o U_o^2\, \Delta\phi \cos\phi - \Big\{ U_o^2 (d_1\, \Delta\alpha_1 + 2d_2 \alpha_o\, \Delta\alpha) + 2U_o (d_o + d_1 \alpha_o + d_2 \alpha_o^2)\, \Delta U \Big\} \cos\phi - \Big\{ U_o^2 (d_o + d_1 \alpha_o + d_2 \alpha_o^2)\, \Delta\phi \sin\phi \Big\} \Big] dr \tag{3-61b}$$

Neglecting all profile drag terms, Eqs. 3-61 reduce to

$$\Delta F_\beta = \frac{1}{2} \rho\, a_o c \Big[(U_o^2\, \Delta\alpha + 2U_o \alpha_o\, \Delta U) \cos\phi - \alpha_o U_o^2\, \Delta\phi \sin\phi \Big] dr \tag{3-62a}$$

$$\Delta F_\zeta = \frac{1}{2}\rho\, a_o c\Big[(U_o^2\,\Delta\alpha + 2U_o\alpha_o\,\Delta U)\sin\phi + \alpha_o U_o^2\,\Delta\phi\cos\phi\Big]\,dr \tag{3-62b}$$

Eqs. 3-62 represent the elemental perturbation lift force components acting on a thrusting proprotor with zero profile drag. The subsequent development neglects drag and proceeds from Eqs. 3-62.

From the inflow geometry of Fig. 3-6 the quantities required in Eqs. 3-62 follow as

$$U_o^2 = (\Omega r)^2 + V^2 = \left[\frac{\Omega r}{\cos\phi}\right]^2 \tag{3-63}$$

$$\Delta U \approx U_e - U_o = \Delta U_T \cos(\phi + \Delta\phi) + \Delta U_N \sin(\phi + \Delta\phi) \tag{3-64}$$

or, to first order in the perturbation quantities,

$$\Delta U = \Delta U_T \cos\phi + \Delta U_N \sin\phi \tag{3-65}$$

and

$$\Delta\alpha = \Delta\theta - \Delta\phi \tag{3-66}$$

The perturbation blade pitch and inflow angle changes and the perturbation velocities appearing in Eqs. 3-65 and 3-66 must now be evaluated in terms of the perturbation motions.

Perturbation Change in Blade Element Geometric Pitch: A general expression for the geometric pitch change $\Delta\theta$ experienced by an element of a rigid blade is given by

$$\Delta\theta = \Delta\theta_{collective} + \Delta\theta_{cyclic} \tag{3-67}$$

The first term on the right hand side of Eq. 3-67 represents all

pitch changes of a collective type wherein the angle of attack of all similarly situated blade elements is changed simultaneously in the same direction and by the same amount. Changes of this type are associated with pitch-cone coupling and collective control inputs for example. The second term represents pitch changes of a cyclic nature such as those resulting from the use of pitch-flap coupling or cyclic control inputs. Incorporation of blade pitch control feedback systems for augmenting proprotor/pylon stability or providing gust alleviation would also contribute to collective and cyclic changes in blade pitch. Although collective pitch changes are not considered herein inflow velocity changes which are uniform over the rotor disc (such as that arising from an axial perturbation in velocity for example) are of a collective nature. Terms of this latter type arise naturally during the blade aerodynamic force summation process and will thus be deferred till later. Cyclic blade pitch changes due to pitch-flap coupling and to one type of control feedback will be considered below.

(1) Pitch-Flap Coupling - The kinematic action known as pitch-flap coupling acts to couple the blade flapping motions with respect to the mast and the blade geometric pitch and has the effect of reducing both steady-state flapping and flapping in maneuvers. This arrangement is realized physically by establishing a virtual flapping hinge by having the end of the blade pitch horn offset from the physical flapping axis of the blade so that when the blade flaps up the blade pitch increases or decreases depending on the sign of the pitch-flap coupling ratio. Let a line be drawn between the end of the pitch horn and the point of intersection of the

feathering axis with the physical flapping axis of the blade. The acute angle made by this line with the physical flapping axis is taken to be the pitch-flap coupling angle δ_3.

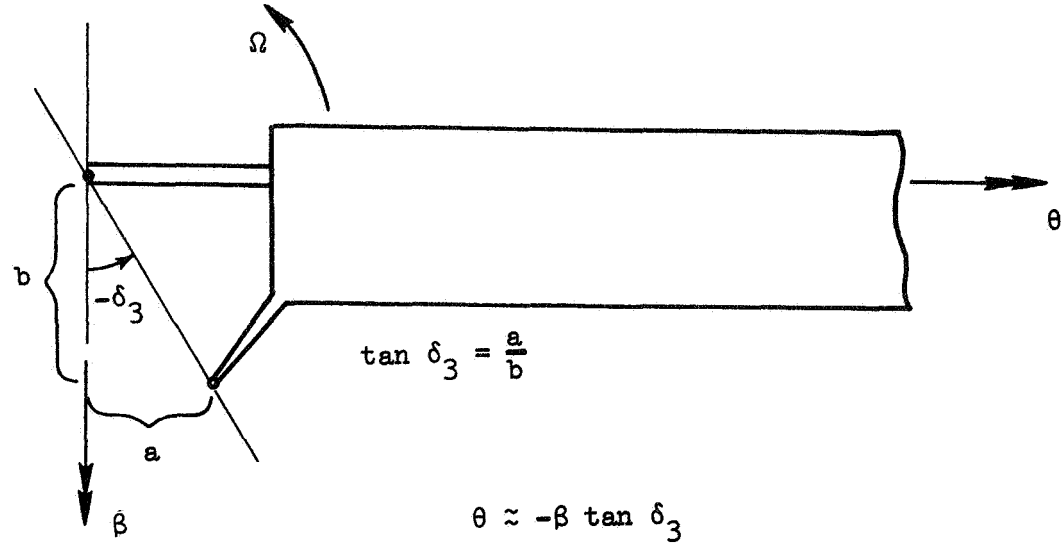

The pitch-flap coupling is defined to be positive and associated with a negative δ_3 angle if the blade pitch increases when the blade flaps up (the situation depicted in the sketch) and negative and associated with a positive δ_3 angle if the blade pitch decreases when the blade flaps up. The perturbation pitch change relative to the shaft normal plane due to pitch-flap coupling is given by

$$\Delta\theta = -\beta \tan \delta_3 = -(a_1 \sin \psi - b_1 \cos \psi) \tan \delta_3 \quad (3\text{-}68)$$

Now in the wind axis system the shaft normal plane has been pitched (ϕ_y) and yawed (ϕ_z) so that, relative to wind axes, the perturbation pitch change is

$$\Delta\theta = (-a_1 \tan \delta_3 + \phi_z) \sin \psi + (b_1 \tan \delta_3 + \phi_y) \cos \psi \tag{3-69}$$

(2) Swashplate/Pylon Coupling - A displacement feedback arrangement which mechanically couples the angular displacement of the pylon and the angular deflection of the swashplate relative to the pylon has been termed swashplate/pylon coupling (Ref. 3-13). By appropriately choosing the coupling ratios, the angular motion of the rotor control axis (swashplate) in space can be divorced from the angular motions of the pylon thereby effecting a significant reduction in the magnitude of the destabilizing shear forces generated by rotor precession. With respect to the wind axis system the blade perturbation pitch change in the presence of this type of blade pitch control feedback is given by

$$\Delta\theta = -K_1\phi_y \cos \psi - K_2\phi_z \sin \psi \tag{3-70}$$

where K_1 and K_2 are the longitudinal and lateral feedback gains. If K_1 and K_2 are positive a swashplate motion which is out of phase with the pylon angular motion results, the amount being a function of the gains. For the particular case in which K_1 and K_2 are both equal to +1.0, the swashplate will be exactly 180° out-of-phase with the pylon, i.e.,

$$K_1 = +1.0 \longrightarrow a_1 = -\phi_y \qquad K_2 = +1.0 \longrightarrow b_1 = -\phi_z \tag{3-71}$$

The situation in the pitch plane is illustrated in the sketch below.

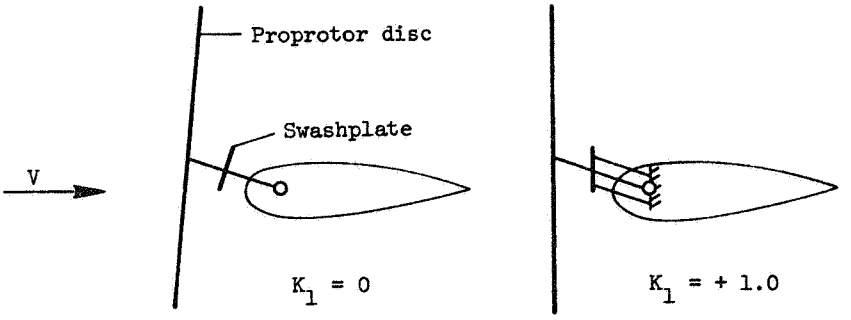

(3) Control Phasing - The signal which the swashplate transmits to the blades through the pitch links is generally phased relative to the blade azimuthal position such that control inputs to the blades appear on the rotor at an azimuth position more advanced (if $\omega_\beta < \Omega$) or retarded (if $\omega_\beta > \Omega$) than the swashplate tilt which is the source of the control deflections. This control phasing is introduced analytically by replacing ψ with $\psi - \varepsilon$ in Eq. 3-70, which gives

$$\Delta\theta = - K_1\phi_y \cos(\psi - \varepsilon) - K_2\phi_z \sin(\psi - \varepsilon) \qquad (3\text{-}72)$$

The phasing angle ε is defined in the sketch below.

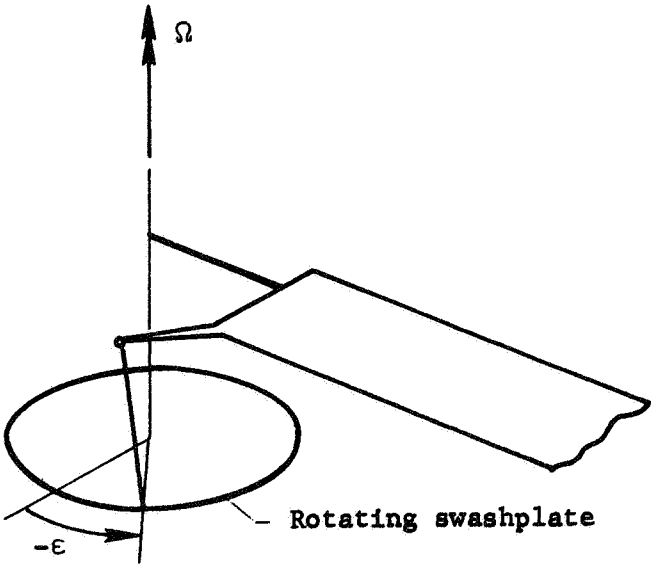

Combining the above individual contributions and denoting the collective changes by $\Delta\theta_c$ the total perturbation pitch change assumes the form

$$\begin{aligned}\Delta\theta = \Delta\theta_c &+ \cos\psi\left[-K_1\phi_y \cos\varepsilon + K_2\phi_z \sin\varepsilon\right. \\ &\left. + b_1 \tan\delta_3 + \phi_y\right] + \sin\psi\left[-K_1\phi_y \sin\varepsilon\right. \\ &\left. - K_2\phi_z \cos\varepsilon - a_1 \tan\delta_3 + \phi_z\right]\end{aligned} \tag{3-73}$$

Perturbation Change in Blade Element Inflow Angle: With reference to Fig. 3-6 the quantity $U_e\,\Delta\phi$ is approximately given by

$$U_e\,\Delta\phi = \Delta U_N \cos(\phi + \Delta\phi) - \Delta U_T \tan\phi \cos(\phi + \Delta\phi) \tag{3-74}$$

Now, from Eq. 3-64,

$$U_e = U_o + \Delta U = U_o + \Delta U_T \cos(\phi + \Delta\phi) + \Delta U_N \sin(\phi + \Delta\phi) \tag{3-75}$$

Substituting Eq. 3-75 into Eq. 3-74, expanding, and retaining terms up to first order in the perturbation quantities gives

$$U_o \Delta\phi = \Delta U_N \cos\phi - \Delta U_T \sin\phi \tag{3-76}$$

Since

$$U_o = \Omega r/\cos\phi \tag{3-77}$$

the perturbation inflow angle follows from Eq. 3-76 as

$$\Delta\phi = \frac{\cos^2\phi}{\Omega r}\left[\Delta U_N - \Delta U_T \tan\phi\right] \tag{3-78}$$

Blade Element Perturbation Velocities: The perturbation velocity component parallel to the freestream direction can be written as

$$\Delta U_N = r\dot{\eta}' + \dot{x} \tag{3-79}$$

Using Eq. 3-17 the above equation becomes

$$\begin{aligned}\Delta U_N = r\Big[&-\left\{(\dot{\phi}_z + \dot{b}_1) - \Omega(\phi_y + a_1)\right\}\cos\psi \\ &+ \left\{(\dot{\phi}_y + \dot{a}_1) + \Omega(\phi_z + b_1)\right\}\sin\psi\Big] + \dot{x}\end{aligned} \tag{3-80}$$

From Fig. 3-7 the perturbation velocity normal to the blade span is

$$\Delta U_T = \dot{Z}\cos\psi - \dot{Y}\sin\psi + r\dot{\phi}_x \tag{3-81}$$

Now from Fig. 3-4 we have

$$\begin{aligned}\dot{Z} &= \dot{z} - h_1\dot{\phi}_y \\ \dot{Y} &= \dot{y} + h_2\dot{\phi}_z\end{aligned} \tag{3-82}$$

so that Eq. 3-81 becomes

$$\Delta U_T = (\dot{z} - h_1\dot{\phi}_y)\cos\psi - (\dot{y} + h_2\dot{\phi}_z)\sin\psi + r\dot{\phi}_x \qquad (3\text{-}83)$$

For a wing encastré at its root the contribution of $\dot{\phi}_x$ (here, the time rate of change of wing tip bending slope) to ΔU_T will be small relative to the other terms and is thus neglected.

Proprotor Forces and Moments:

(1) Blade Perturbation Forces and Moments - The drag component of the lift force acting on the n^{th} blade is given by

$$F_\zeta = \int_{r_1}^{r_2} \Delta F_\zeta \, dr \qquad (3\text{-}84)$$

which, using Eq. 3-62b and the result

$$2U_o\alpha_o \, \Delta U = 2a_o(\Omega r \, \Delta U_T + V \, \Delta U_N) \qquad (3\text{-}85)$$

can be written as

$$F_\zeta = \frac{1}{2}\rho\left[\int_{r_1}^{r_2} a_o c\left\{U_o^2 \, \Delta\alpha + 2\Omega r \, \Delta U_T\alpha_o + 2V \, \Delta U_N\alpha_o\right\}\sin\phi \, dr + \int_{r_1}^{r_2} a_o c \, \Delta\phi U_o^2 \, \alpha_o \cos\phi \, dr\right] \qquad (3\text{-}86)$$

Assuming that a_o and c are constant along the blade and using Eq. 3-66, Eq. 3-86 becomes

$$F_\zeta = \frac{1}{2}\rho\, a_o c\left[\int_{r_1}^{r_2} U_o^2(\Delta\theta - \Delta\phi)\sin\phi\, dr + \int_{r_1}^{r_2}\left\{(2\Omega r\,\Delta U_T + 2V\,\Delta U_N)\,\alpha_o \sin\phi + U_o^2\,\alpha_o\,\Delta\phi\cos\phi\right\}dr\right] \tag{3-87}$$

Now $\Delta\theta$, given by Eq. 3-73, is not a function of r. Hence, using Eq. 3-78, Eq. 3-87 can be rewritten in the form

$$F_\zeta = \frac{1}{2}\rho\, a_o c\left[\int_{r_1}^{r_2}(V^2 + \Omega^2 r^2)\sin\phi\left\{\Delta\theta - \frac{\cos^2\phi}{\Omega r}(\Delta U_N - \Delta U_T\tan\phi)\right\}dr + \int_{r_1}^{r_2}\left\{2\alpha_o(\Omega r\,\Delta U_T + V\,\Delta U_N)\sin\phi + \Omega r\,\alpha_o\cos\phi(\Delta U_N - \Delta U_T\tan\phi)\right\}dr\right] \tag{3-88}$$

Introducing the nondimensional quantities

$$\eta \equiv r/R \qquad \lambda \equiv V/\Omega R = J/\pi \tag{3-89}$$

the resultant steady velocity becomes

$$U_o^2 = V^2 + (\Omega r)^2 = (\Omega R)^2\,[\eta^2 + \lambda^2] \tag{3-90a}$$

or

$$U_o^2 = (\Omega R)^2\, W^2 \tag{3-90b}$$

where

$$W^2 \equiv \eta^2 + \lambda^2 \tag{3-91}$$

Additionally,

$$\sin \phi = \lambda/W, \cos \phi = \eta/W, \tan \phi = \lambda/\eta \tag{3-92}$$

Introducing the above notation into Eq. 3-88 yields

$$F_\zeta = \frac{1}{2} \rho a_o c \, \Omega^2 R^3 \lambda \int_{\eta_1}^{\eta_2} W \left\{ \Delta\theta - \frac{\eta}{\Omega R W^2} \left(\Delta U_N - \Delta U_T \frac{\lambda}{\eta} \right) \right\} d\eta$$

$$+ \frac{1}{2} \rho a_o c \left[2R^2 \lambda \left\{ \Omega \, \Delta U_T \int_{\eta_1}^{\eta_2} \alpha_o \frac{\eta}{W} \, d\eta + V \, \Delta\hat{U}_N \int_{\eta_1}^{\eta_2} \alpha_o \frac{\eta}{W} \, d\eta \right\} \right.$$

$$\left. + \Omega R^3 \, \Delta\hat{U}_N \int_{\eta_1}^{\eta_2} \alpha_o \frac{\eta^3}{W} \, d\eta - \Omega R^2 \lambda \, \Delta U_T \int_{\eta_1}^{\eta_2} \alpha_o \frac{\eta}{W} \, d\eta \right] \tag{3-93}$$

where

$$\Delta U_N \equiv r \, \Delta\hat{U}_N \tag{3-94}$$

The flapping moment induced by the axial component of the blade perturbation lift is given by

$$M_\beta = \int_{r_1}^{r_2} r \, \Delta F_\beta \, dr \tag{3-95}$$

or, using Eqs. 3-62a and 3-85,

$$M_\beta = \frac{1}{2} \rho \left[\int_{r_1}^{r_2} r \left\{ a_o c (U_o^2 \, \Delta\alpha + 2\Omega r \, \Delta U_T \alpha_o \right. \right.$$

$$\left. \left. + 2V \, \Delta U_N \alpha_o) \right\} \cos \phi \, dr - \int_{r_1}^{r_2} a_o c r \, \Delta\phi U_o^2 \alpha_o \sin \phi \, dr \right] \tag{3-96}$$

Proceeding as for F_ζ there finally results

$$M_\beta = \frac{1}{2}\rho a_o c\,\Omega^2 R^4 \int_{\eta_1}^{\eta_2} \eta^2 W\left\{\Delta\theta - \frac{\eta}{\Omega R W^2}\left(\Delta U_N - \Delta U_T \frac{\lambda}{\eta}\right)\right\} d\eta$$

$$+ \frac{1}{2}\rho a_o c\left[2R^3\left\{\Omega\,\Delta U_T \int_{\eta_1}^{\eta_2} \alpha_o \frac{\eta^3}{W}\,d\eta + V\,\Delta\hat{U}_N \int_{\eta_1}^{\eta_2} \alpha_o \frac{\eta^3}{W}\,d\eta\right\}\right. \tag{3-97}$$

$$\left. - \Omega R^4\,\Delta\hat{U}_N \lambda \int_{\eta_1}^{\eta_2} \alpha_o \frac{\eta^3}{W}\,d\eta + \Omega R^3 \lambda^2\,\Delta U_T \int_{\eta_1}^{\eta_2} \alpha_o \frac{\eta}{W}\,d\eta\right]$$

Although the coning angle β_o was assumed to have a negligible effect on the inflow geometry a first-order contribution to the flapping moment does arise as a consequence of the fact that the drag component of lift, ΔF_ζ, is offset axially from the hub plane. The elemental moment due to precone is

$$\Delta M_{\beta_o} = \Delta F_\zeta r \sin\beta_o \approx \Delta F_\zeta r\,\beta_o \tag{3-98}$$

so that

$$M_{\beta_o} = \int_{r_1}^{r_2} \Delta F_\zeta r \beta_o\,dr \tag{3-99}$$

Proceeding as above for F_ζ and M_β:

$$M_{\beta_o} = \frac{1}{2}\rho a_o c\,\Omega^2 R^4 \lambda \int_{\eta_1}^{\eta_2} \eta W \left\{ \Delta\theta - \frac{\eta}{\Omega R W^2}\left(\Delta U_N - \Delta U_T \frac{\lambda}{\eta}\right)\right\} d\eta + \frac{1}{2}\rho a_o c \left[2R^3\lambda \left\{ \Omega\, \Delta U_T \int_{\eta_1}^{\eta_2} \alpha_o \frac{\eta^2}{W}\, d\eta + V\, \Delta\hat{U}_N \int_{\eta_1}^{\eta_2} \alpha_o \frac{\eta^2}{W}\, d\eta \right\} + \Omega R^4\, \Delta\hat{U}_N \int_{\eta_1}^{\eta_2} \alpha_o \frac{\eta^4}{W}\, d\eta - \Omega R^3 \lambda\, \Delta U_T \int_{\eta_1}^{\eta_2} \alpha_o \frac{\eta^2}{W}\, d\eta \right] \tag{3-100}$$

The aerodynamically induced collective pitch changes alluded to earlier lead to perturbation thrust and torque terms. These arise from the $\dot{x}$ and $r\dot{\phi}_x$ terms in ΔU_N and ΔU_T. It will be recalled that $r\dot{\phi}_x$ due to wing elastic bending was neglected. For a tilt-rotor aircraft in free flight a rigid-body rolling angular velocity also contributes to ΔU_T via a term of this form (with $\dot{\phi}_x$ = aircraft roll rate)* and could <u>not</u> be neglected in an aircraft dynamic stability analysis. This term is included here in that sense. The blade perturbation thrust is

$$\Delta T = \Delta F_{\beta_c} \tag{3-101}$$

where the subscript c is used here and below to denote terms in the quantities indicated which are of the collective type. Using Eqs. 3-62a and 3-85

*The cross flow over the rotors leads to the longitudinal and lateral forces and moments shown in Fig. 2-12c.

$$\Delta T = \frac{1}{2}\rho a_o c\left[\left\{U_o^2\,\Delta\alpha_c + 2\alpha_o \Omega r\,\Delta U_{T_c} + 2V\,\Delta U_{N_c}\,\alpha_o\right\}\cos\phi - U_o^2\,\alpha_o \sin\phi\,\Delta\phi_c\right] dr \tag{3-102}$$

Now

$$\Delta\alpha_c = \Delta\theta_c - \Delta\phi_c \tag{3-103}$$

where

$$\Delta\phi_c = \frac{\cos^2\phi}{\Omega r}\left[\Delta U_{N_c} - \Delta U_{T_c}\tan\phi\right] \tag{3-104}$$

and the collective type perturbation velocities are given by

$$\begin{aligned}\Delta U_{N_c} &= \dot{x}\\ \Delta U_{T_c} &= r\dot{\phi}_x\end{aligned} \tag{3-105}$$

Substituting Eqs. 3-103 through 3-105 into Eq. 3-102, nondimensionalizing, and integrating over the blade span leads to

$$\begin{aligned}T = \frac{1}{2}\rho a_o cR\Bigg[&\Omega^2R^2\int_{\eta_1}^{\eta_2}\eta W\,\Delta\theta_c\,d\eta - \Omega R\dot{x}\int_{\eta_1}^{\eta_2}\frac{\eta^2}{W}\,d\eta\\ &+ \dot{\phi}_x\Omega R^2\lambda\int_{\eta_1}^{\eta_2}\frac{\eta^2}{W}\,d\eta + 2V\dot{x}\int_{\eta_1}^{\eta_2}\alpha_o\frac{\eta}{W}\,d\eta\\ &+ 2\Omega\dot{\phi}_x R^2\int_{\eta_1}^{\eta_2}\alpha_o\frac{\eta^3}{W}\,d\eta - \Omega R\lambda\dot{x}\int_{\eta_1}^{\eta_2}\alpha_o\frac{\eta}{W}\,d\eta\\ &+ \Omega R^2\dot{\phi}_x\lambda^2\int_{\eta_1}^{\eta_2}\alpha_o\frac{\eta}{W}\,d\eta\Bigg]\end{aligned} \tag{3-106}$$

With reference to Fig. 3-8 the blade perturbation torque is

$$\Delta Q = - r \, \Delta F_{\zeta_c} \tag{3-107}$$

which leads to

$$\begin{aligned} Q = - \frac{1}{2} \rho a_o c R^2 \Bigg[& \lambda \Omega^2 R^2 \int_{\eta_1}^{\eta_2} \eta W \, \Delta\theta_c \, d\eta - \lambda \Omega R \dot{x} \int_{\eta_1}^{\eta_2} \frac{\eta^2}{W} \, d\eta \\ & + \dot{\phi}_x \Omega R^2 \lambda^2 \int_{\eta_1}^{\eta_2} \frac{\eta^2}{W} \, d\eta + 2V\lambda\dot{x} \int_{\eta_1}^{\eta_2} \alpha_o \frac{\eta}{W} \, d\eta \\ & + \Omega R \dot{\phi}_x \int_{\eta_1}^{\eta_2} \alpha_o \frac{\eta^3}{W} \, d\eta + \dot{x} \, \Omega R \int_{\eta_1}^{\eta_2} \alpha_o \frac{\eta^3}{W} \, d\eta \\ & - R^2 \Omega \dot{\phi}_x \lambda \int_{\eta_1}^{\eta_2} \alpha_o \frac{\eta^3}{W} \, d\eta \Bigg] \end{aligned} \tag{3-108}$$

The aerodynamic development beyond this point will neglect thrust (i.e., all terms containing α_o).

(2) Decomposition of Blade Forces and Moments into Longitudinal and Lateral Components and Summation Over the Number of Blades - With the forces and moments defined as positive in the same direction as the corresponding displacements shown in Fig. 3-1 the vertical and lateral components of the shear force F_ζ (Fig. 3-8) are given by

$$H = - F_\zeta \cos \psi \tag{3-109a}$$

$$Y = F_\zeta \sin \psi \tag{3-109b}$$

and the longitudinal and lateral components of the moments (Fig. 3-8) by

$$M = M_\beta \sin\psi + M_{\beta_o} \cos\psi \tag{3-110a}$$

$$N = -M_\beta \cos\psi + M_{\beta_o} \sin\psi \tag{3-110b}$$

Substituting the known expressions for F_ζ, M_β, and M_{β_o} into Eqs. 3-109 and 3-110 and summing over the number of blades (using the relations in Eq. 3-30) leads to

$$H = -\frac{1}{2}\gamma\Omega^2 I_R \frac{\lambda}{R}\int_{\eta_1}^{\eta_2}\left[W(b_1 \tan\delta_3 - K_1\phi_y\cos\varepsilon + K_2\phi_z \sin\varepsilon) + \frac{\lambda^2}{W}\phi_y + \frac{\eta^2}{\Omega W}(\dot{\phi}_z + \dot{b}_1) - \frac{\eta^2}{W}a_1 + \frac{\lambda}{\Omega R W}(\dot{z} - h_1\dot{\phi}_y)\right]d\eta \tag{3-111}$$

and

$$Y = \frac{1}{2}\gamma\Omega^2 I_R \frac{\lambda}{R}\int_{\eta_1}^{\eta_2}\left[W(-a_1 \tan\delta_3 - K_1\phi_y\sin\varepsilon - K_2\phi_z\cos\varepsilon) + \frac{\lambda^2}{W}\phi_z - \frac{\eta^2}{\Omega W}(\dot{\phi}_y + \dot{a}_1) - \frac{\eta^2}{W}b_1 - \frac{\lambda}{\Omega R W}(\dot{y} + h_2\dot{\phi}_z)\right]d\eta \tag{3-112}$$

for the normal and side force shear components and

$$M = \frac{1}{2}\gamma\Omega^2 I_R \int_{\eta_1}^{\eta_2} \left[\eta^2 W(-a_1 \tan\delta_3 - K_1\phi_y \sin\varepsilon - K_2\phi_z \cos\varepsilon) + \frac{\eta^2\lambda^2}{W}\phi_z - \frac{\eta^4}{\Omega W}(\dot{\phi}_y + \dot{a}_1) - \frac{\eta^4}{W} b_1 - \frac{\eta^2\lambda}{\Omega R W}(\dot{y} + h_2\dot{\phi}_z) \right] d\eta + \frac{1}{2}\gamma\Omega^2\lambda I_R\beta_o \int_{\eta_1}^{\eta_2} \left[\eta W(b_1 \tan\delta_3 - K_1\phi_y \cos\varepsilon + K_2\phi_z \sin\varepsilon) + \frac{\lambda^2\eta}{W}\phi_y + \frac{\eta^3}{\Omega W}(\dot{\phi}_z + \dot{b}_1) - \frac{\eta^3}{W} a_1 + \frac{\eta\lambda}{\Omega R W}(\dot{z} - h_1\dot{\phi}_y) \right] d\eta \tag{3-113}$$

and

$$N = -\frac{1}{2}\gamma\Omega^2 I_R \int_{\eta_1}^{\eta_2} \left[\eta^2 W(b_1 \tan\delta_3 - K_1\phi_y \cos\varepsilon + K_2\phi_z \sin\varepsilon) + \frac{\eta^2\lambda^2}{W}\phi_y + \frac{\eta^4}{\Omega W}(\dot{\phi}_z + \dot{b}_1) - \frac{\eta^4}{W} a_1 + \frac{\eta^2\lambda}{\Omega R W}(\dot{z} - h_1\dot{\phi}_y) \right] d\eta + \frac{1}{2}\gamma\Omega^2\lambda I_R\beta_o \int_{\eta_1}^{\eta_2} \left[\eta W(-a_1 \tan\delta_3 - K_1\phi_y \sin\varepsilon - K_2\phi_z \cos\varepsilon) + \frac{\lambda^2\eta}{W}\phi_z - \frac{\eta^3}{\Omega W}(\dot{\phi}_y + \dot{a}_1) - \frac{\eta^3}{W} b_1 - \frac{\eta\lambda}{\Omega R W}(\dot{y} + h_2\dot{\phi}_z) \right] d\eta \tag{3-114}$$

for the longitudinal and lateral flapping moment components. The thrust and torque become

$$T = -\frac{\gamma I_R \Omega}{R^2}\dot{x}\int_{\eta_1}^{\eta_2}\frac{\eta^2}{W}\,d\eta + \frac{\gamma I_R \Omega\lambda}{R}\dot{\phi}_x\int_{\eta_1}^{\eta_2}\frac{\eta^2}{W}\,d\eta \qquad (3\text{-}115)$$

$$Q = \frac{\gamma I_R \Omega\lambda}{R}\dot{x}\int_{\eta_1}^{\eta_2}\frac{\eta^2}{W}\,d\eta - \gamma I_R \Omega\lambda^2\dot{\phi}_x\int_{\eta_1}^{\eta_2}\frac{\eta^2}{W}\,d\eta \qquad (3\text{-}116)$$

In each of the above γ is the blade Lock number defined by

$$\gamma = \frac{\rho a_o c R^4}{I_B} \qquad (3\text{-}117)$$

and the terms containing $\Delta\theta_c$ have been dropped since there are no blade collective pitch changes through the control system. The forces and moments in Eqs. 3-111 through 3-116 were previously shown schematically in Fig. 2-12 of Chapter 2.

(3) Corrections for Mach Number and Aspect Ratio - Compressibility and the effects of finite aspect ratio blades are taken into account approximately by modifying the two-dimensional incompressible lift curve slope a_o in the same manner as in fixed-wing theory along the lines suggested in Ref. 3-14. Actually, two corrections are applied to a_o, the Prandtl-Glauert factor

$$\frac{1}{\sqrt{1 - M_{hel}^2}} \qquad (3\text{-}118)$$

to account for the increase in aerodynamic forces as Mach number increases in the subsonic Mach number range and a compressible flow aspect-ratio correction given by

$$\frac{AR_{comp}}{AR_{comp} + 2} = \frac{AR_{incomp}\sqrt{1 - M_{hel}^2}}{AR_{incomp}\sqrt{1 - M_{hel}^2} + 2} \qquad (3\text{-}119)$$

The overall correction is given by the product of these two factors and takes the form

$$a_o(3\text{-}D,M) = \frac{AR_{incomp}}{2 + AR_{incomp}\sqrt{1 - M_{hel}^2}}\, a_o(2\text{-}D,\ M=0) \qquad (3\text{-}120)$$

where the helical Mach number M_{hel} can be expressed in terms of the nondimensional quantities introduced earlier as

$$M_{hel}^2 = M^2W^2/\lambda^2 \qquad (3\text{-}121)$$

M being the flight Mach number. Eq. 3-120 can be viewed as one form of the Göthert rule for three-dimensional compressible flow.

(4) Inclusion of Theodorsen Unsteady Aerodynamics - Vortex shedding from the proprotor blades results in a lag of the blade local lift from its quasi-steady value based merely on the instantaneous angle of attack. For high aspect ratio blades operating at high advance ratios the wake effect can be approximately accounted for by multiplying the quasi-steady results by Theodorsen's circulation function C(k). This effectively reduces the magnitude of the quasi-steady lift and induces a lag so that the true (unsteady) lift lags the quasi-steady lift.

Theodorsen's circulation function (Ref. 3-1) is a mathematically complex function of reduced frequency which can be written in

the form

$$C(k) = F(k) + iG(k) \tag{3-122}$$

where F and G are defined in terms of Bessel functions of the first and second kind. The reduced frequency appropriate to Eq. 3-122 is given by

$$k = \frac{\omega c}{2V_{hel}} = \frac{\omega c\lambda}{2VW} \tag{3-123}$$

where V_{hel} is the helical velocity at the blade section and ω is the wake frequency.

The factor to be inserted into the integrands of all the aerodynamic terms which approximately accounts for both three-dimensional compressible flow and the shed vorticity is

$$\bar{A}(k, M) \equiv \frac{C(k)\, AR_{incomp}}{2 + AR_{incomp}\sqrt{1 - M_{hel}^2}} \tag{3-124}$$

Close inspection of the equations defining the aerodynamic forces and moments indicates that the integrals are of two general forms and can be defined as follows:

$$A_n \equiv \int_{\eta_1}^{\eta_2} \bar{A}\, \frac{\eta^{n-1}}{W}\, d\eta \qquad n = 1,2,3,4,5 \tag{3-125}$$

$$B_n \equiv \int_{\eta_1}^{\eta_2} \bar{A}W\, \eta^{n-1}\, d\eta \qquad n = 1,2,3 \tag{3-126}$$

If $M = k = 0$, these integrals are real and have closed form solutions, otherwise they must be evaluated numerically and are complex

if $k \neq 0$. Using the definitions of Eqs. 3-125 and 3-126 the final expressions for the forces and moments then follow from Eqs. 3-111 through 3-116 as

$$H = -\frac{1}{2}\gamma\Omega^2 I_R \frac{\lambda}{R}\left[B_1(b_1 \tan\delta_3 - K_1\phi_y \cos\varepsilon + K_2\phi_z \sin\varepsilon) + A_1\lambda^2\phi_y + \frac{A_3}{\Omega}(\dot{\phi}_z + \dot{b}_1) - A_3 a_1 + \frac{A_1\lambda}{\Omega R}(\dot{z} - h_1\dot{\phi}_y)\right] \tag{3-127}$$

$$Y = \frac{1}{2}\gamma\Omega^2 I_R \frac{\lambda}{R}\left[-B_1(a_1 \tan\delta_3 + K_1\phi_y \sin\varepsilon + K_2\phi_z \cos\varepsilon) + A_1\lambda^2\phi_z - \frac{A_3}{\Omega}(\dot{\phi}_y + \dot{a}_1) - A_3 b_1 - \frac{A_1\lambda}{\Omega R}(\dot{y} + h_2\dot{\phi}_z)\right] \tag{3-128}$$

$$\begin{aligned} M = {} & \frac{1}{2}\gamma\Omega^2 I_R\left[-B_3(a_1 \tan\delta_3 + K_1\phi_y \sin\varepsilon + K_2\phi_z \cos\varepsilon) + A_3\lambda^2\phi_z - \frac{A_5}{\Omega}(\dot{\phi}_y + \dot{a}_1) - A_5 b_1 - \frac{A_3\lambda}{\Omega R}(\dot{y} + h_2\dot{\phi}_z)\right] \\ & + \frac{1}{2}\gamma\Omega^2\lambda I_R\beta_o\left[B_2(b_1 \tan\delta_3 - K_1\phi_y \cos\varepsilon + K_2\phi_z \sin\varepsilon) + A_2\lambda^2\phi_y + \frac{A_4}{\Omega}(\dot{\phi}_z + \dot{b}_1) - A_4 a_1 + \frac{A_2\lambda}{\Omega R}(\dot{z} - h_1\dot{\phi}_y)\right] \end{aligned} \tag{3-129}$$

$$\begin{aligned} N = {} & -\frac{1}{2}\gamma\Omega^2 I_R\left[B_3(b_1 \tan\delta_3 - K_1\phi_y \cos\varepsilon + K_2\phi_z \sin\varepsilon) + A_3\lambda^2\phi_y + \frac{A_5}{\Omega}(\dot{\phi}_z + \dot{b}_1) - A_5 a_1 + \frac{A_3\lambda}{\Omega R}(\dot{z} - h_1\dot{\phi}_y)\right] \\ & + \frac{1}{2}\gamma\Omega^2\lambda I_R\beta_o\left[-B_2(a_1 \tan\delta_3 + K_1\phi_y \sin\varepsilon + K_2\phi_z \cos\varepsilon) + A_2\lambda^2\phi_z - \frac{A_4}{\Omega}(\dot{\phi}_y + \dot{a}_1) - A_4 b_1 - \frac{A_2\lambda}{\Omega R}(\dot{y} + h_2\dot{\phi}_z)\right] \end{aligned} \tag{3-130}$$

$$T = \frac{-\gamma I_R \Omega A_3}{R^2} \dot{x} + \frac{\gamma I_R \Omega\lambda A_3}{R} \dot{\phi}_x \tag{3-131}$$

$$Q = \frac{\gamma I_R \Omega\lambda A_3}{R} \dot{x} - \gamma I_R \Omega\lambda^2 A_3 \dot{\phi}_x \tag{3-132}$$

Eqs. 3-127 through 3-132 constitute the definition of the aerodynamic forces and moments acting on the proprotor. There now remains the task of determining the generalized forces to be used in Lagrange's equation.

Generalized Aerodynamic Forces: The virtual work done by an applied force $\bar{F}$ and moment $\bar{M}$ on a translating and rotating rigid body (i.e., the proprotor) can be written as (Ref. 3-15)

$$\delta W = \bar{F} \cdot \delta\bar{R} + \bar{M} \cdot \delta\bar{\Theta} \tag{3-133}$$

where $\bar{F}$ is the resultant force acting on the proprotor, $\bar{M}$ the resultant moment, $\bar{R}$ (Fig. 3-3) the position vector of the hub, and $\bar{\theta}$ the rotation of the hub in space. The quantities in Eq. 3-133 are given by

$$\bar{F} = T\bar{i}_o + Y\bar{j}_o + H\bar{k}_o \tag{3-134a}$$

$$\bar{R} = x\bar{i}_o + (y + h_2\phi_z)\bar{j}_o + (z - h_1\phi_y)\bar{k}_o \tag{3-134b}$$

$$\bar{M} = Q\bar{i}_o + M\bar{j}_o + N\bar{k}_o \tag{3-134c}$$

$$\bar{\Theta} = \phi_x\bar{i}_o + (\phi_y + a_1)\bar{j}_o + (\phi_z + b_1)\bar{k}_o \tag{3-134d}$$

The virtual work can also be expressed in terms of the generalized forces Q_r and displacements q_r as

$$\delta W = \sum_{r=1}^{N} Q_r \, \delta q_r \tag{3-135}$$

Substituting Eqs. 3-134 into Eq. 3-133 and equating the resulting expression for virtual work to that given in Eq. 3-135 yields the generalized force matrix

$$\begin{Bmatrix} Q_x \\ Q_y \\ Q_z \\ Q_{a_1} \\ Q_{b_1} \\ Q_{\phi_x} \\ Q_{\phi_y} \\ Q_{\phi_z} \end{Bmatrix} = \begin{Bmatrix} T \\ Y \\ H \\ M \\ N \\ Q \\ M - Hh_1 \\ N + Yh_2 \end{Bmatrix} \tag{3-136}$$

The aerodynamic matrices in Eq. 3-8 follow from Eq. 3-136 by substituting the expressions for the forces and moments given in Eqs. 3-127 to 3-132 and grouping terms according to whether they are proportional to the perturbation velocities or the perturbation displacements.

Defining

$$\kappa \equiv \frac{1}{2} \gamma \Omega^2 I_R$$

the aerodynamic matrices assume the form given in Eqs. 3-137 and 3-138.

$$[\text{AERO}]_1 = K$$

$\dot{x}$	$\dot{y}$	$\dot{z}$	$\dot{a}_1$	$\dot{b}_1$	$\dot{\phi}_x$	$\dot{\phi}_y$	ϕ_z	
$-\frac{2A_3}{\Omega R^2}$	0	0	0	0	$\frac{2A_3\lambda}{\Omega R}$	0	0	$\dot{x}$
0	$-\frac{A_1\lambda^2}{\Omega R^2}$	0	$-\frac{A_3\lambda}{\Omega R}$	0	0	$\frac{A_3\lambda}{\Omega R}$	$-\frac{A_1\lambda^2 h_2}{\Omega R^2}$	$\dot{y}$
0	0	$-\frac{A_1\lambda^2}{\Omega R^2}$	0	$-\frac{A_3\lambda}{\Omega R}$	0	$\frac{A_1\lambda^2 h_1}{\Omega R^2}$	$-\frac{A_3\lambda}{\Omega R}$	$\dot{z}$
0	$-\frac{A_3\lambda}{\Omega R}$	$\frac{A_2\lambda^2\beta_o}{\Omega R}$	$-\frac{A_5}{\Omega}$	$\frac{A_4\lambda\beta_o}{\Omega}$	0	$-A_5/\Omega$ $-A_2\lambda^2 h_1\beta_o/\Omega R$	$-A_3\lambda h_2/\Omega R$ $+A_4\lambda\beta_o/\Omega$	$\dot{a}_1$
0	$-\frac{A_2\lambda^2\beta_o}{\Omega R}$	$-\frac{A_3\lambda}{\Omega R}$	$-\frac{A_4\lambda\delta_o}{\Omega}$	$-\frac{A_5}{\Omega}$	0	$A_3\lambda h_1/\Omega R$ $-A_4\lambda\beta_o/\Omega$	$-A_5/\Omega$ $-A_2\lambda^2 h_2\beta_o/\Omega R$	$\dot{b}_1$
$\frac{2A_3\lambda}{\Omega R}$	0	0	0	0	$-\frac{2\lambda^2 A_3}{\Omega}$	0	0	$\dot{\phi}_x$
0	$-\frac{A_3\lambda}{\Omega R}$	$A_2\lambda^2\beta_o/\Omega R$ $+A_1\lambda^2 h_1/\Omega R^2$	$-\frac{A_5}{\Omega}$	$A_4\lambda\beta_o/\Omega$ $+A_3 h_1\lambda/\Omega R$	0	$-A_5/\Omega$ $A_2\lambda^2 h_1\beta_o/\Omega R$ $-A_1\lambda^2 h_1^2/\Omega R^2$	$-A_3\lambda h_2/\Omega R$ $+A_4\lambda\beta_o/\Omega$ $+A_3 h_1\lambda/\Omega R$	ϕ_y
0	$-A_2\lambda^2\beta_o/\Omega R$ $-A_1\lambda^2 h_2/\Omega R^2$	$-\frac{A_3\lambda}{\Omega R}$	$A_4\lambda\beta_o/\Omega$ $-A_3 h_2\lambda/\Omega R$	$-\frac{A_5}{\Omega}$	0	$A_3\lambda h_1/\Omega R$ $-A_4\lambda\beta_o/\Omega$ $-A_3 h_2\lambda/\Omega R$	A_5/Ω $-A_2\lambda^2 h_2\beta_o/\Omega R$ $-A_1\lambda^2 h_2^2/\Omega R^2$	ϕ_z

(3-137)

$$[AERO]_2 = K$$

x	y		a_1	b_1	ϕ_x	ϕ_y	ϕ_z	
0	0	0	$-(\lambda/R)B_1 \tan\delta_3$	$A_3\lambda/R$	0	$(\lambda/R)B_1K_1 \sin\varepsilon$	$-(\lambda/R)B_1K_2 \cos\varepsilon + A_1\lambda^3/R$	x
0	0	0	$A_3\lambda/R$	$-(\lambda/R)B_1 \tan\delta_3$	0	$(\lambda/R)B_1K_1 \cos\varepsilon - A_1\lambda^3/R$	$-(\lambda/R)B_1K_2 \sin\varepsilon$	y
0	0	0	$B_3 \tan\delta_3 - A_4\lambda\beta_o$	$-A_5 + \lambda\beta_oB_2 \tan\delta_3$	0	$B_3K_1 \sin\varepsilon - \lambda\beta_oB_2K_1 \cos\varepsilon + A_2\lambda^3\beta_o$	$B_3K_2 \cos\varepsilon + A_3\lambda^2 + \lambda\beta_oB_2K_2 \sin\varepsilon$	z
0	0	0	$+A_5 - \lambda\beta_oB_2 \tan\delta_3$	$B_3 \tan\delta_3 - \lambda\beta_oA_4$	0	$B_3K_1 \cos\varepsilon - A_3\lambda^2 - \lambda\beta_oB_2K_1 \sin\varepsilon$	$A_2\lambda^3\beta_o - B_3K_2 \sin\varepsilon - \lambda\beta_oB_2K_2 \cos\varepsilon$	a_1
0	0	0	0	0	0	0	0	b_1
0	0	0	$-B_3 \tan\delta_3 - \lambda\beta_oA_4 - A_3h_1\lambda/R$	$\lambda\beta_o B_2 \tan\delta_3 - A_5 - (\lambda/R)B_1h_1 \tan\delta_3$	0	$A_2\lambda^3\beta_o + A_1\lambda^3h_1/R - B_3K_1 \sin\varepsilon - \lambda\beta_oB_2K_1 \cos\varepsilon - (\lambda/R)B_1K_1h_1 \cos\varepsilon$	$A_3\lambda^2 + B_3K_2 \cos\varepsilon + \lambda\beta_oB_2K_2 \sin\varepsilon + (\lambda/R)B_1K_2h_1 \sin\varepsilon$	ϕ_y
0	0	0	$A_5 - \lambda\beta_oB_2 \tan\delta_3 - (\lambda/R)B_1h_2 \tan\delta_3$	$B_3 \tan\delta_3 - \lambda\beta_oA_4 - A_3h_2\lambda/R$	0	$B_3K_1 \cos\varepsilon - A_3\lambda^2 - \lambda\beta_oB_2K_1 \sin\varepsilon - (\lambda/R)B_1K_1h_2 \sin\varepsilon$	$A_2\lambda^3\beta_o + A_1\lambda^3h_2/R - B_3K_2 \sin\varepsilon - \lambda\beta_oB_2K_2 \cos\varepsilon - (\lambda/R)B_1K_2h_2 \cos\varepsilon$	ϕ_z

(3-138)

Effects of Thrust on Propeller Stability Derivatives: Experimental and analytical studies have generally demonstrated that the assumption of a windmilling (non-thrusting) propeller or proprotor is conservative in whirl flutter analyses. The work of Ravera (Ref. 3-16) constitutes, to the author's best knowledge, the only published analytical derivation explicitly delineating the effects of thrust on the stability derivatives required for the whirl flutter analysis of a two degree of freedom propeller system. In the course of the present work the results of Ref. 3-16 were compared to those resulting from the results herein reduced to the two degree of freedom case considered by Ravera. This comparison identified an apparent error in Ravera's derivation and final results for the thrusting derivatives. Since his work is generally cited as a justification for neglecting thrust in propeller whirl flutter analyses it seems appropriate to comment on the discrepancy, particularly as it relates to his conclusion on the effects of thrust.

Making the appropriate changes for notation differences there is agreement between Ref. 3-16 and the present work for $L + \Delta L$.* In resolving this total lift into components parallel and normal to the freestream direction Ravera indicates (page 19 of Ref. 3-16) that $(L + \Delta L)$ is to be multiplied by $\cos \phi$ and $\sin \phi$ respectively. As shown in Eqs. 3-49 of the present work, the correct factors are $\cos(\phi + \Delta\phi)$ and $\sin(\phi + \Delta\phi)$. As a consequence of

---

*Ref. 3-16 does not consider drag.

this incorrect resolution the terms shown underlined in Eqs. 3-52, 3-93, and 3-97 are absent from Ravera's comparable expressions. To ascertain the effect of these omitted terms on the thrust correction to the windmilling derivatives presented by Ravera in Ref. 3-16 the numerical information therein was used to evaluate the additional terms and the stability derivatives including thrust recalculated for the 35,000 foot cruise flight condition shown in Table 3 of that reference. Results of this comparison are summarized below for the four derivatives specifically considered by Ravera. The notation is that of Ref. 3-16, with a positive sign denoting a non-thrusting

	Percent Deviation from the Zero-Thrust Derivatives	
Derivative	Ravera (Ref. 3-16)	Present Analysis
C_{m_ψ}	+7.31	+3.65
C_{y_ψ}	+3.10	+6.93
C_{m_q}	-4.40	-2.22
C_{y_q}	-3.10	-6.77

derivative larger in magnitude than the corresponding derivative including thrust and a negative sign denoting that the thrusting derivative is larger. It is seen that the only derivative which has increased due to the presence of the additional terms is C_{y_q}. However, as pointed out in Chapter 2, the cross-stiffness moment C_{m_ψ} is the driving moment for propeller whirl flutter and this derivative has been decreased. The other derivatives are of lesser

importance.* Although the present analysis shows that the inclusion of thrust is somewhat less stabilizing than shown in Ref. 3-16, Ravera's conclusion that thrust is generally not a significant factor in propeller whirl flutter analyses remains valid.

Representative Section Aerodynamic Theory: An intermediate effort during the analytical effort, for the purpose of providing a quick check on the aerodynamic formulation, was the use of a representative section aerodynamic theory for the blade loading. In this simplification the aerodynamic loading is lumped at some "representative" blade spanwise station, akin to the typical section approximation of a finite-span wing employed in early fixed-wing flutter analyses. To introduce this aerodynamic simplification it is assumed that all quantities which are a function of blade radius may be held constant during the integration if they are evaluated at the representative section, say the 3/4 blade radius. The details concerning this formulation are not presented here. However, since some analytical results employing this aerodynamic representation are presented in Chapters 4 and 5 it was deemed appropriate to at least mention the basis of the theory.

Solution of the Equations of Motion

(a) Formulation of the Matrix Eigenvalue Problem

Transferring the aerodynamic matrices in Eq. 3-8 to the left hand side and combining matrices the resultant equations of motion

---

*This will be numerically demonstrated in Chapter 4.

can be written in the form

$$[M]\{\ddot{X}\} + [C]\{\dot{X}\} + [K]\{X\} = \{0\} \tag{3-139}$$

where

$$\begin{aligned} [M] &= [\bar{M}] \\ [C] &= [\Gamma] - [\text{Aero}]_1 + [\bar{C}] \\ [K] &= [\bar{K}] - [\text{Aero}]_2 \\ \{X\} &= \{q\} \end{aligned} \tag{3-140}$$

[M] is symmetric and positive definite; [C] and [K] are non-symmetric*, [K] being complex-valued. Eigenvalue routines that are available in computer libraries generally require that the equations be in the standard eigenvalue form

$$[A]\{X\} = \lambda\{X\} \tag{3-141}$$

If [C] is zero Eqs. 3-139 can easily be reduced to this form by the well-known method of multiplying through by the inverse of [M]. In the more general case in which [C] is not zero this approach will not work. It is possible, however, to reduce Eqs. 3-139 to the required form using methods developed for uncoupling the forced equations of motion for systems containing non-proportional damping. A brief review of these techniques is included here for completeness.

---

*Mathematically, this lack of symmetry characterizes flutter as a nonself-adjoint eigenvalue problem.

Review of Methods for Uncoupling Systems of Equations with Damping: In a lumped parameter analysis of a linearly damped dynamic system the equations of motion resulting from an application of Lagrange's equation can be written in the matrix form

$$[M]\{\ddot{X}\} + [C]\{\dot{X}\} + [K]\{X\} = \{f(t)\} \qquad (3\text{-}142)$$

If [M], [C], and [K] are symmetric the classical approach to the solution of these equations is to find the eigenvectors of the reduced problem

$$[M]\{\ddot{X}\} + [K]\{X\} = \{0\} \qquad (3\text{-}143)$$

and use them to obtain the normal coordinates which will eliminate the inertial and elastic coupling in Eqs. 3-142. However, as first shown by Rayleigh (Ref. 3-17), unless [C] is linearly proportional to either the mass or stiffness matrices (or to a linear combination of them) velocity coupling will still exist. If [C] fulfills the proportionality conditions stated above* the transformation matrix composed of the eigenvectors of Eq. 3-143 will simultaneously diagonalize [M], [C], and [K] so that the left hand side of Eqs. 3-142 are completely uncoupled. The system is said to be solvable in N-space, where N is the number of degrees of freedom.

If [C] does not satisfy the proportionality conditions the classical uncoupling approach does not work because the natural modes are complex, indicating that both amplitude and phase

---

*Caughey (Ref. 3-18) showed that the damped system can be completely diagonalized under somewhat less restrictive conditions on [C] than that given by Rayleigh.

distinguish the components in each vector. In contrast, the real vector corresponding to a mode of an undamped or proportionally damped system has components which are distinguished from other components of the same vector by amplitude only, the phase being zero or 180° as determined by the sign. 2N equations are thus required to determine all components of a mode for an N degree of freedom system with non-proportional damping. Hence to the N equations of motion must be added another N equations. The auxiliary equations are generally taken to be those given in Ref. 3-19. This in effect transforms the problem to 2N-space, the transformation being such that the N equations of second order are replaced by an equivalent set of 2N first order equations. If $[M]^{-1}$ exists this method will always work. Since [M] is symmetric and and positive definite,* two distinct cases present themselves in 2N-space: (1) [C] and [K] are symmetric and [C] is non-proportional; (2) [C] and/or [K] is not symmetric. In the first case the eigenvectors obtained from the solution of the homogeneous form of the 2N equations of motion serve as a suitable transformation matrix to uncouple the 2N forced equations of motion. If the matrices are not symmetric the system of equations is said to be nonself-adjoint. The preceding manipulations in 2N space must then be augmented by corresponding manipulations on the set of equations adjoint to the 2N equations. The matrix of eigenvectors

*[M] could, in general, be positive semi-definite. Here it is assumed that [M] is positive definite.

of the equations adjoint to the 2N equations are used in conjunction with the set of eigenvectors of the original 2N equations to diagonalize the original 2N non-homogeneous equations. This leads to a set of uncoupled equations in what are sometimes termed bi-normal coordinates. The details concerning these procedures are lengthy and will not be dealt with here.* The particular aspect of these procedures of interest here is the means for effecting the transformation to 2N-space. This will be dealt with in detail below.

Transformation of the Proprotor Equations of Motion into Eigenvalue Form: Multiplying Eq. 3-139 through by $[M]^{-1}$

$$[I]\{\ddot{X}\} + [M]^{-1}[C]\{\dot{X}\} + [M]^{-1}[K]\{X\} = \{0\} \qquad (3\text{-}144)$$

and introducing the N generalized velocities as auxiliary variables by means of the matrix identity

$$\{\dot{X}\} - \{\dot{X}\} = \{0\} \qquad (3\text{-}145)$$

Eqs. 3-144 and 3-145 can be combined to yield

$$\begin{Bmatrix} \{\dot{X}\} \\ \hline \{\ddot{X}\} \end{Bmatrix} = \left[\begin{array}{c|c} 0 & [I] \\ \hline -[M]^{-1}[K] & -[M]^{-1}[C] \end{array}\right] \begin{Bmatrix} \{X\} \\ \hline \{\dot{X}\} \end{Bmatrix} \qquad (3\text{-}146)$$

*The interested reader is referred to the discussions in Refs. 3-20 through 3-23 for treatment of these various aspects.

Defining

$$\{W\} = \left\{\begin{array}{c}\{X\} \\ \hline \{\dot{X}\}\end{array}\right\} \tag{3-147}$$

Eq. 3-146 can be written in the compact form

$$\{\dot{W}\} = [A]\{W\} \tag{3-148}$$

where the definition of [A] is obvious. Assuming a solution of the form

$$\{W\} = \{W_o\}\, e^{\lambda t} \tag{3-149}$$

Eq. 3-148 reduces to

$$[A]\{W_o\} = \lambda\{W_o\} \tag{3-150}$$

which is in the desired eigenvalue form. Writing Eq. 3-150 in the form

$$\Big[[A] - \lambda[I]\Big]\{W_o\} = \{0\} \tag{3-151}$$

the equations are seen to constitute a homogeneous set of complex algebraic equations. Requiring that this set of equations have more than just the trivial solution corresponding to a state of rest implies that the determinant of coefficients in Eq. 3-151 vanish. This is the classical characteristic-value or eigenvalue problem in which it is required to determine the λ for which non-trivial solutions to the homogeneous equations 3-151 exist.

(b) Interpretation of Results

Eigensolutions: Solution of Eq. 3-151 leads to $2N$ complex

eigenvalues λ_p and eigenvectors $W^{(p)}$. If [A] is real (i.e., if [M], [C], and [K] are real) the eigenvalues and eigenvectors occur in N complex conjugate pairs; if [A] is complex the 2N eigenvalues and eigenvectors are distinct. Experience has shown that for flutter solutions only roots having positive imaginary part (i.e., positive frequency) have any physical significance as far as the actual system behavior is concerned. Discarding the negative frequency roots (and their associated eigenvectors) the p^{th} eigenvalue has the general form

$$\lambda_p = \alpha_p + i\beta_p \tag{3-152a}$$

and can be interpreted as

$$\lambda_p = -\zeta_p\omega_p + i\omega_p\sqrt{1-\zeta_p^2} \tag{3-152b}$$

where ζ_p is the damping as a fraction of critical damping and ω_p is the undamped coupled frequency. For $\omega_p \neq 0$, if $\zeta_p\omega_p > 0$ the motion is exponentially convergent while for $\zeta_p\omega_p < 0$ the motion is exponentially divergent. Plotting (ζ_p,ω_p) as a function of velocity in the complex plane a concise picture of the variation of system stability with airspeed can be established. Extensive use will be made of these "root loci" in Chapters 4 and 5.

The complex vector associated with the eigenvalue λ_p can be written in the form

$$\{W^{(p)}\} = \begin{Bmatrix} \{w^{(p)}\} \\ \hline \lambda_p\{w^{(p)}\} \end{Bmatrix} \tag{3-153}$$

The upper N elements $\{w^{(p)}\}$ in each modal vector of 2N elements define the mode shape. Since these elements are complex, phase differences exist between the harmonic motions at different points of the system in a given mode of motion. The relative amplitude and phasing existing in a given mode could be ascertained by converting the complex elements of the mode to polar form and then normalizing on one of them.

Whirl Direction: The pylon whirl direction in any given mode can be established by plotting the elements of the vector corresponding to pylon pitch and yaw in the complex plane and interpreting the phasing from the rotating vector components.* After doing this manually several times it became evident that a specific orientation of the pylon pitch and yaw vectors on the complex plane was associated with the forward and backward whirl directions, as indicated in Fig. 3-9. This suggests a numerical procedure to ascertain the whirl direction. Let

$$\begin{aligned} \bar{\phi}_y &= a + ib = a\bar{i} + b\bar{j} \\ \bar{\phi}_z &= c + id = c\bar{i} + d\bar{j} \end{aligned} \tag{3-154}$$

be the complex elements corresponding to pylon pitch and yaw in any eigenvector. Forming the vector cross product $\bar{\phi}_z * \bar{\phi}_y$ gives

$$\begin{aligned} \bar{\phi}_z \times \bar{\phi}_y &= (c\bar{i} + d\bar{j}) \times (a\bar{i} + b\bar{j}) \\ &= (bc - ad)\bar{k} \end{aligned} \tag{3-155}$$

*All complex components in a given mode have the same frequency and decay rate; only the phase is different.

Eq. 3-155, in conjunction with the commentary in Fig. 3-10, indicates that for

$$\begin{aligned} \text{Forward whirl} &\longrightarrow bc - ad > 0 \\ \text{Backward whirl} &\longrightarrow bc - ad < 0 \end{aligned} \tag{3-156}$$

Determining the direction of pylon whirl thus reduces to simply establishing the sign of the quantity (bc - ad).

The whirl direction of the tip-path-plane <u>in space</u> requires the prior evaluation of a_1 and b_1 in space. This is established by first adding $\bar{a}_1$ to $\bar{\phi}_y$ and $\bar{b}_1$ to $\bar{\phi}_z$ and then using the relations in Eq. 3-156.

(c) Note on Solution of the Stability Determinant

The use of unsteady aerodynamics is generally a prerequisite for subsonic fixed-wing flutter analyses. Because unsteady aerodynamic formulations, such as follow from a kernel function or doublet-lattice approach, have a complicated dependence on reduced frequency they are, in practice, defined only for harmonic motion ($\lambda = i\beta$). This precludes the more general solution approach of searching for frequency solutions of the form $\lambda = \alpha + i\beta$ and the stability analysis is limited to locating the stability boundaries of the system, i.e., those conditions for which neutral stability ($\lambda = i\beta$) exists. Since flutter is concerned with the borderline case between exponentially damped and exponentially divergent oscillations, characterized by a self-sustained motion of constant amplitude (i.e., $\lambda = i\beta$), the specification of harmonic motion in the aerodynamics is adequate for establishing flutter boundaries.

Often, however, aeroelastic problems require more than just the determination of the flutter speed. In order to be able to predict the rate of approach to a flutter speed and the subsequent violence of the instability, the response on either side of the critical point must be known. Also, in establishing the degree of validity of a theory quite often only subcritical data from wind tunnel or flight tests are available for correlation.

In the customary V-g method of flutter analysis* the structural damping which must be artificially supplied to or withdrawn from the system to just maintain constant amplitude motion (i.e., the simple harmonic motion characteristic of neutral stability) in the mode in question is regarded as the unknown. The flutter point is established when the required (artificial) damping is equal to the actual damping in some mode. This approach is consistent with the fact that the aerodynamics have been defined only for harmonic motion. Damping solutions away from the flutter point have no direct relation to the true system damping and the slope of the g vs V curve can not, in general, be taken as an indication of the severity of flutter. Zisfein, Frueh, and Miller (Refs. 3-24 and 3-25) have shown that under certain simplifying assumptions the required damping calculated by the V-g analysis can be related to the true rate of decay as a function of airspeed.† A more recent

---

*See, for example, Ref. 3-1.

†Another procedure for establishing such a relationship has been given by Scanlan and Rosenbaum (Ref. 3-26).

development by Hassig (Ref. 3-27) provides for an approximate true damping solution by a determinant iteration scheme using the equations based on aerodynamics defined only for simple harmonic motion.

If quasi-steady aerodynamics are employed, such as in the formulation herein, the aerodynamics need not be restricted to motions which are harmonic and a true damping solution can be obtained from the calculated eigenvalues in accordance with Eqs. 3-152. The slopes of the resulting ζ versus V curves are now a direct measure of the sensitivity of the system modes to increases in airspeed. In the case in which unsteady effects are approximated by means of Theodorsen's circulation function, although the general frequency solution $\alpha + i\beta$ is obtained the results are strictly applicable only at the neutral stability condition since the circulation function was originally defined only for simple harmonic motion. It is also to be noted that for the case in which the reduced frequency is not zero the aerodynamic matrices are explicit and implicit functions of both reduced frequency and airspeed. This implies that the aerodynamics can not be specified simply by choosing the reduced frequency as in fixed-wing flutter formulations and a modified iterative approach must be used. A suggested procedure is described in Chapter 5.

CITED REFERENCES

3-1. Bisplinghoff, R. L., and H. Ashley: Principles of Aeroelasticity, John Wiley and Sons, Inc., New York, 1962.

3-2. Theodorsen, T., and I. E. Garrick: "Mechanism of Flutter—A Theoretical and Experimental Investigation of the Flutter Problem," NACA Report 685, 1940.

3-3. Hurty, W. C., and M. F. Rubinstein: Dynamics of Structures Prentice-Hall, Inc., Englewood Cliffs, New Jersey, 1964.

3-4. Milne, R. D.: "On the Estimation of Structural Damping From Aircraft Resonance Tests," Journal of the Aero/Space Sciences, Vol. 27, May 1960, pp. 339-342, 376.

3-5. Nissim, E.: "On a Simplified Technique for the Determination of the Dynamic Properties of a Linear System with Damping," Journal of the Royal Aeronautical Society, Vol. 71, February 1967, pp. 126-128.

3-6. Coleman, R. P.: "Damping Formulas and Experimental Values of Damping in Flutter Models," NACA TN 751, February 1940.

3-7. Richardson, J. R., and H. F. W. Naylor: "Whirl Flutter of Propellers with Hinged Blades," Report No. 24, Engineering Research Associates, Toronto, Canada, March 1962.

3-8. Gevarter, W. B.: "Physical Interpretation of Helicopter Chordwise Vibration," Proceedings of the 13th Annual National Forum of the American Helicopter Society, May 1957, pp. 60-71.

3-9. Young, M. I.: "A Simplified Theory of Hingeless Rotors with Application to Tandem Helicopters," Proceedings of the 18th National Forum of the American Helicopter Society, May 1962, pp. 38-45.

3-10. Gaffey, T. M.: "The Effect of Positive Pitch-Flap Coupling (Negative δ_3) on Rotor Blade Motion Stability and Flapping," Journal of the American Helicopter Society, Vol. 14, No. 2, April 1969.

3-11. Nara, H. R., ed.: Vector Mechanics for Engineers, Part II, John Wiley and Sons, Inc., New York, 1962.

3-12. Sissingh, G.: "Contribution to the Aerodynamics of Rotating-Wing Aircraft," NACA TM 921, December 1939.

3-13. Hall, W. E., Jr.: "Prop-Rotor Stability at High Advance Ratios," Journal of the American Helicopter Society, June 1966.

3-14. Houbolt, J. C., and W. H. Reed, III: "Propeller-Nacelle Whirl Flutter," Journal of the Aerospace Sciences, Vol. 29, March 1962.

3-15. Synge, J. L., and B. A. Griffith: Principles of Mechanics, McGraw-Hill Book Company, New York, 1959.

3-16. Ravera, R. J.: "Effects of Steady State Blade Angle of Attack on Propeller Whirl Flutter," Grumman Aircraft Engineering Corporation, Report No. ADR 06-01-63.1, July 1963.

3-17. Lord, Rayleigh: The Theory of Sound, Vol. I, Dover Publications, New York, 1945.

3-18. Caughey, T. K.: "Classical Normal Modes in Damped Linear Dynamic Systems," Journal of Applied Mechanics, Vol. 27, June 1960, pp. 269-271.

3-19. Frazer, R. A., W. J. Duncan, and A. R. Collar: Elementary Matrices, Cambridge University Press, New York, 1960.

3-20. Foss, K. A.: "Co-ordinates Which Uncouple the Equations of Motion of Damped Linear Dynamic Systems," Journal of Applied Mechanics, Vol. 25, September 1958, pp. 361-364.

3-21. Caughey, T. K., and M. E. J. O'Kelly: General Theory of Vibration of Damped Linear Dynamic Systems," Caltech Dynamics Laboratory Report, June 1963.

3-22. Halfman, R. L.: Dynamics, Vol. 2, Addison-Wesley Publ. Co., Reading, Mass., 1962.

3-23. Flax, A. H.: "Aeroelasticity and Flutter," Section C., Vol. VIII, of High Speed Aerodynamics and Jet Propulsion, Princeton University Press, Princeton, New Jersey, 1961.

3-24. Zisfein, M. B., and F. J. Frueh: "New Dynamic System Concepts and Their Application to Aeroelastic System Approximations," AIA/ONR Symposium Proceedings - Structural Dynamics of High Speed Flight, April 1961.

3-25. Frueh, F. J., and J. M. Miller: "Prediction of Dynamic Response from Flutter Analysis Solutions," AFOSR 65-0952, June 1965.

3-26. Scanlan, R. H., and R. Rosenbaum: Introduction to the Study of Aircraft Vibration and Flutter, Macmillan Company, New York, 1951, pp. 339-343.

3-27. Hassig, H. J.: "An Approximate True Damping Solution of the Flutter Equation by Determinant Iteration," Journal of Aircraft, Vol. 8, November 1971.

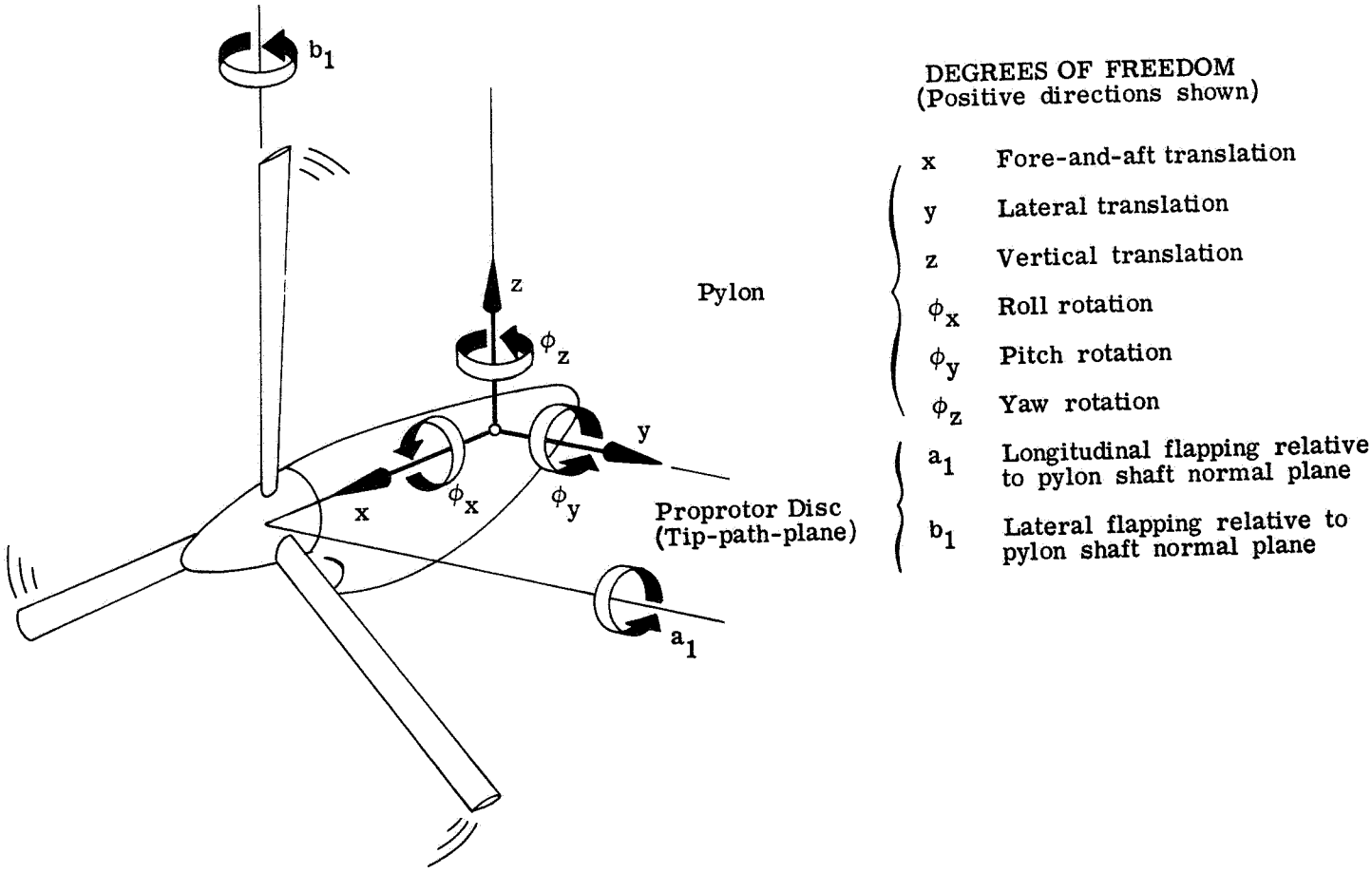

Figure 3-1.- Degrees of freedom employed in mathematical model of proprotor/pylon/wing system.

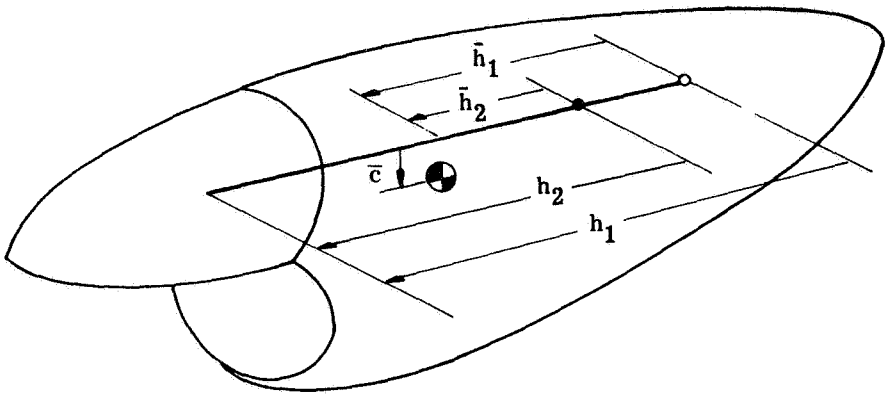

h_1 ~ Longitudinal distance from effective pylon pitch pivot to proprotor hub

h_2 ~ Longitudinal distance from effective pylon yaw pivot to proprotor hub

$\bar{h}_1$ ~ Longitudinal distance from effective pylon pitch pivot to pylon center-of-gravity

$\bar{h}_2$ ~ Longitudinal distance from effective pylon yaw pivot to pylon center-of-gravity

$\bar{c}$ ~ Vertical distance of pylon center-of-gravity from proprotor shaft axis

Figure 3-2.- Rigid body idealization employed for pylon showing non-coincident pitch and yaw pivot axes.

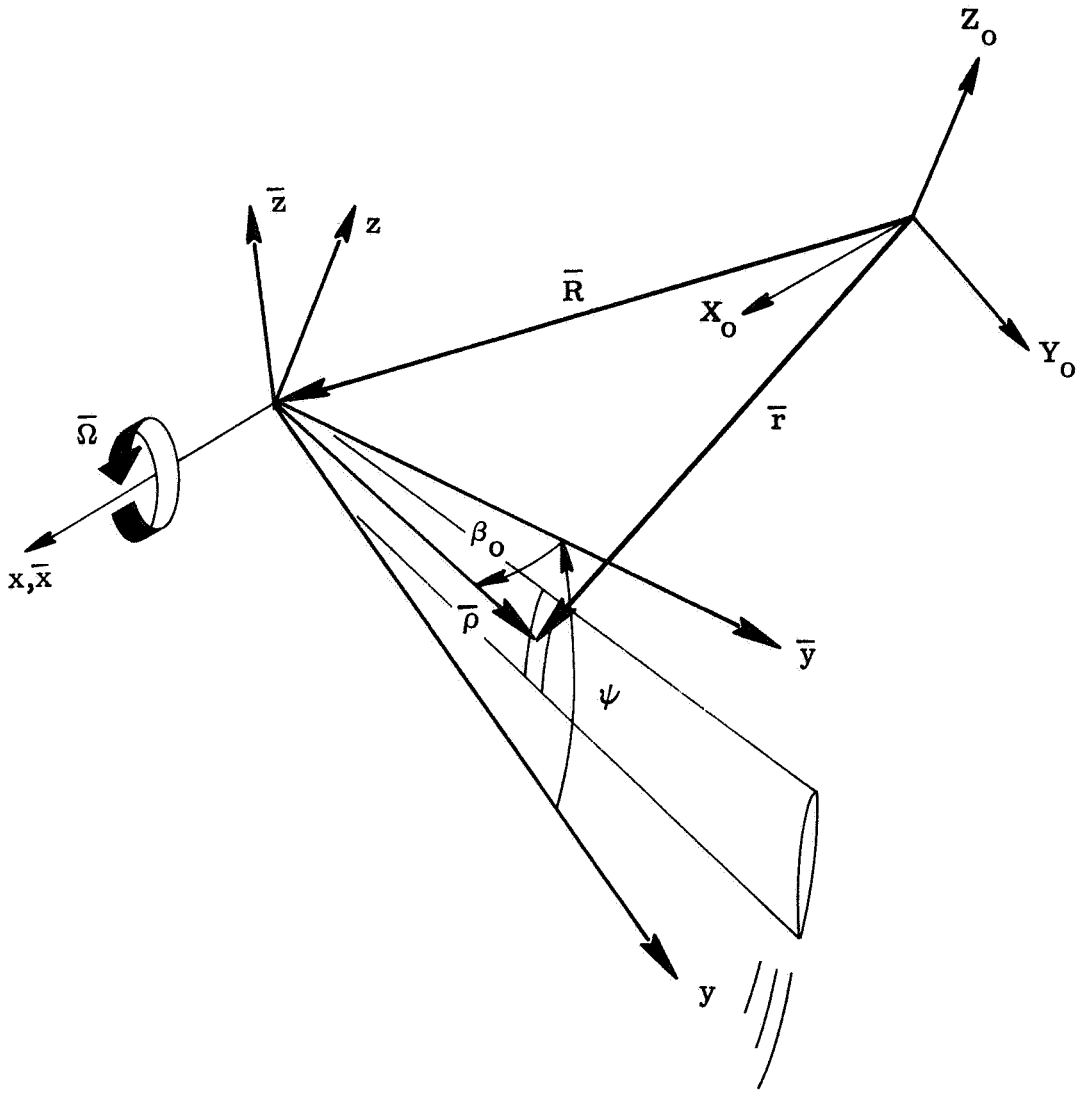

Figure 3-3.- Displacement vectors and auxiliary coordinate systems used in obtaining the absolute velocity of a blade element mass.

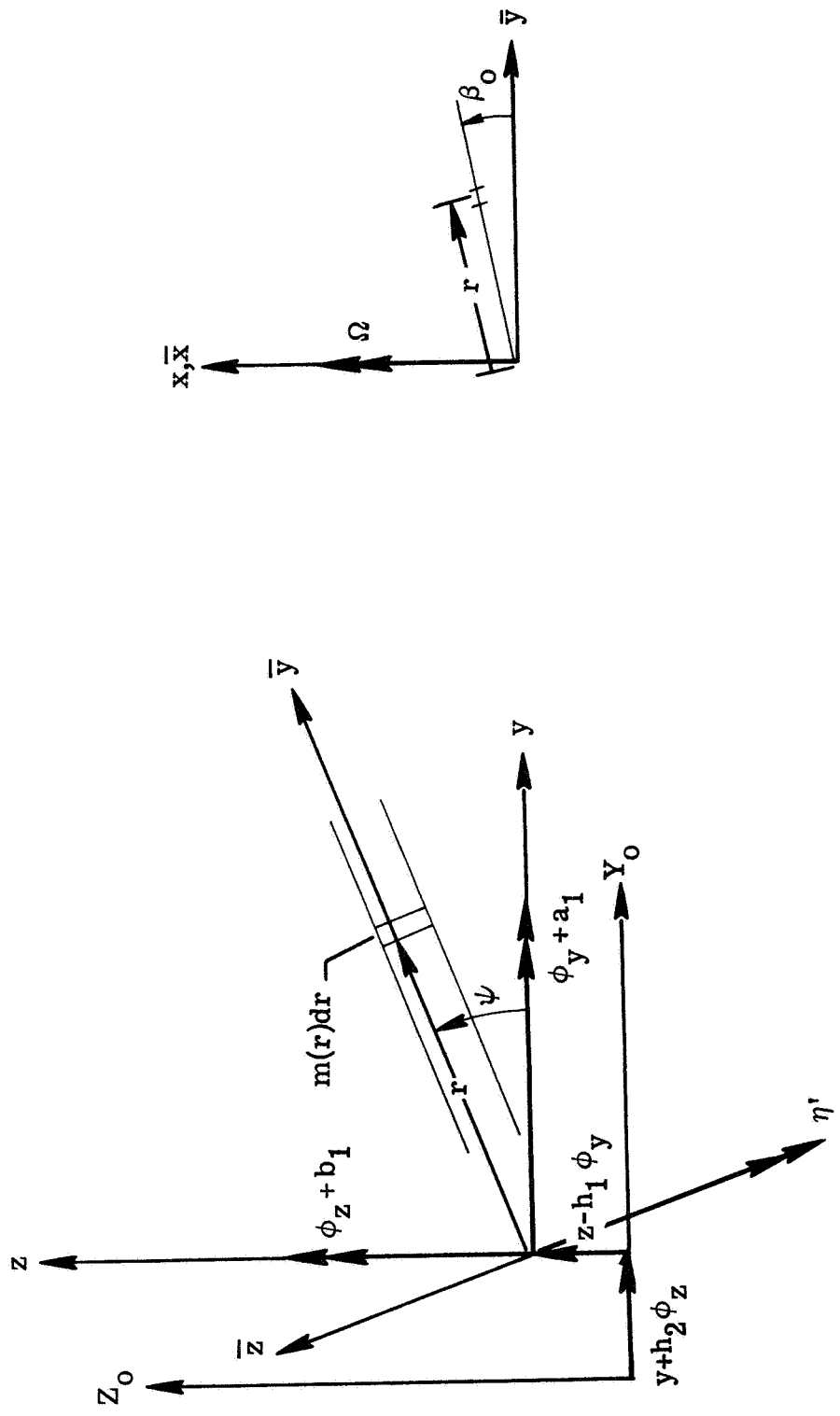

Figure 3-4.- Perturbation displacements and rotations of proprotor hub, tip-path-plane, and n^{th} blade as viewed from upstream.

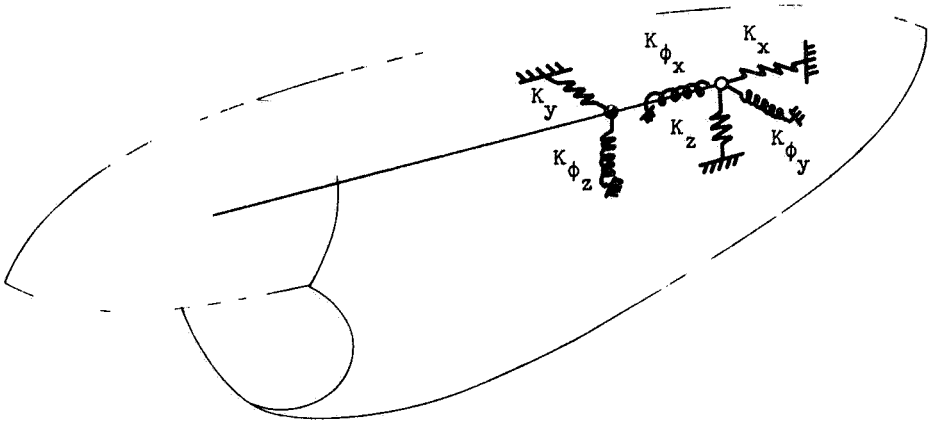

Figure 3-5.- Idealization employed to represent the pylon support stiffnesses.

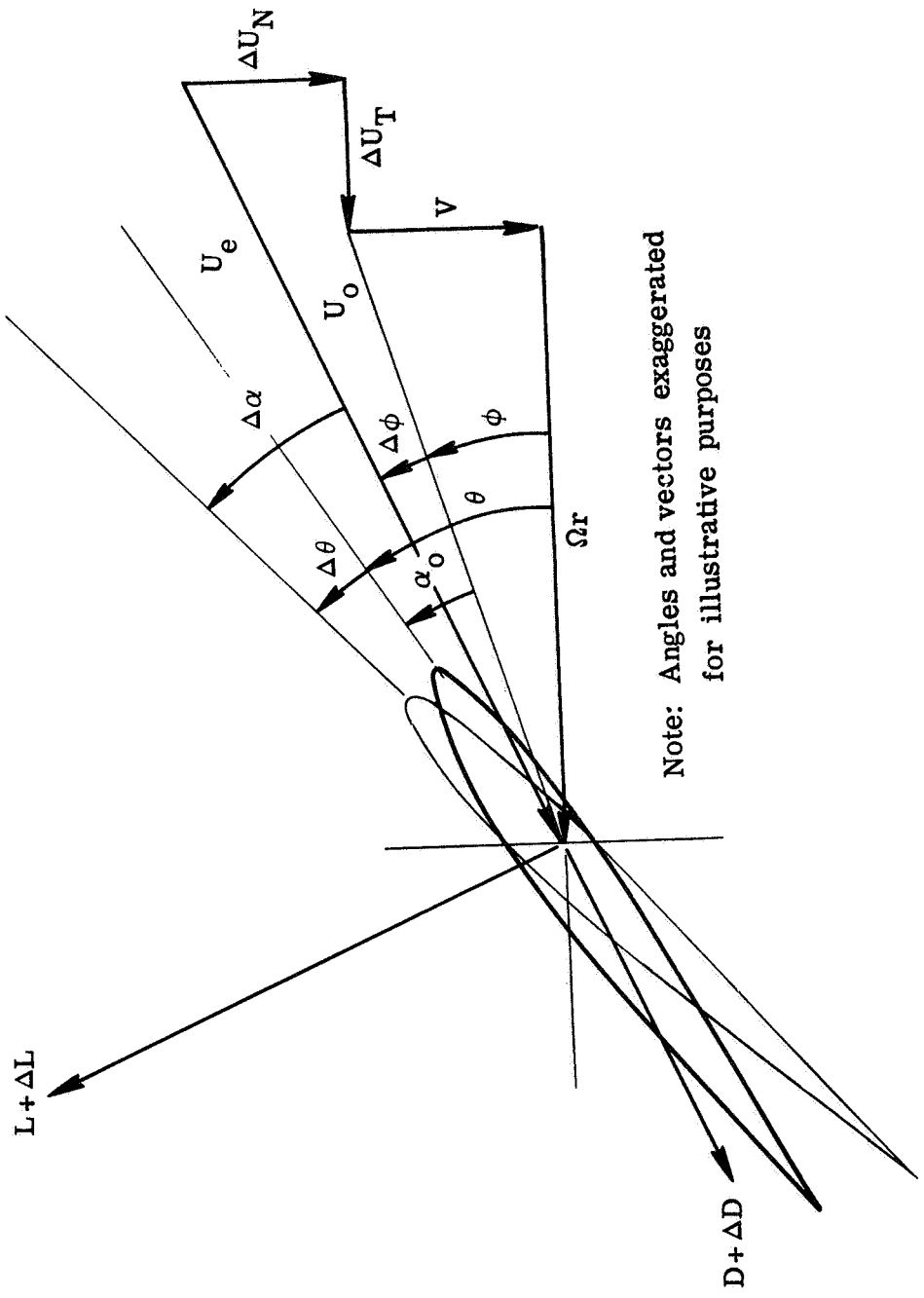

Figure 3-6.- Inflow geometry and aerodynamic loading associated with a typical blade element.

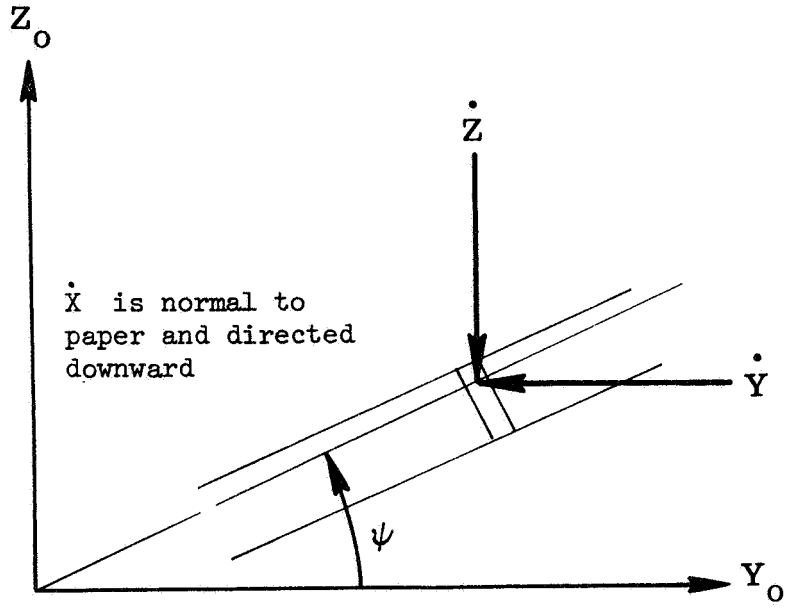

Figure 3-7.- Perturbation velocities at blade section.

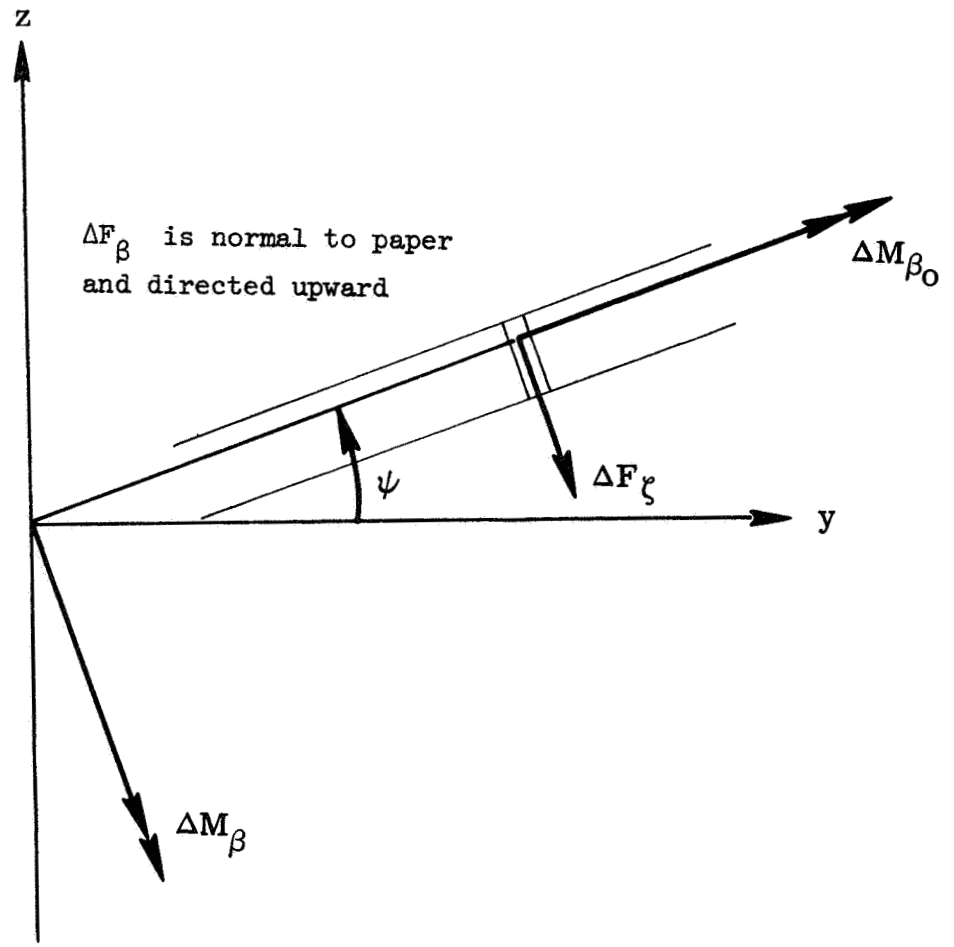

Figure 3-8.- Perturbation forces and moments acting on blade section.

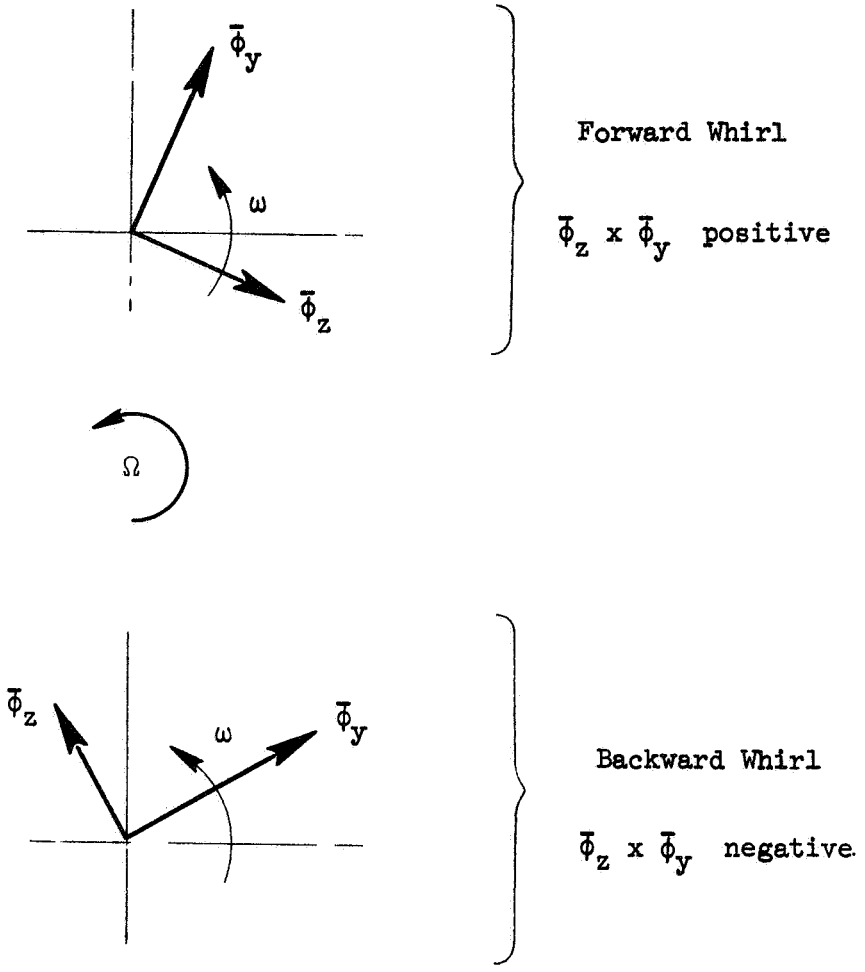

Figure 3-9.- Determination of pylon whirl direction.

CHAPTER 4

ANALYTICAL TREND STUDIES

Introduction

Proprotor/pylon instability, like propeller/nacelle whirl flutter, is an instability associated with the high advance ratios typically encountered in high-speed flight and, as in propeller whirl flutter, pylon/wing stiffness and damping have a major influence on stability. However, because of the blade flapping and pitch-change freedoms available to the proprotor, pylon support stiffness and damping are not the only parameters governing stability. Design parameters associated with the rotor configuration, such as proprotor type, pitch-flap coupling, and blade flapping restraint also assume a major role in determining the resultant stability or instability of the proprotor/pylon/wing system. Although the design values of these particular parameters are generally dictated by considerations other than stability their influence on the stability of the overall system must nevertheless be assessed. The additional freedoms in which a proprotor is able to respond can also give rise to a dynamic environment in which the proprotor/pylon/wing system can exhibit instabilities in modes other than the familiar propeller/nacelle precessional mode. In particular, depending on the characteristics of the system, instabilities associated with either the proprotor, pylon, or wing modes can occur. The possibility that two unstable

response modes can occur simultaneously, or nearly so, also exists.* This leads to so-called "bi-modal" instabilities in which the pylon responds in a steady or continuously changing Lissajous pattern. Other aircraft characteristics which explicitly depend upon the dynamic behavior of the proprotor must also be considered. These include steady-state flapping, transient flapping required to generate the airload moments to precess the proprotor in response to aircraft maneuvers, and the destabilizing shear forces which accompany any precessional motion of the proprotor. These shears can destabilize the aircraft short period and Dutch roll modes in the same manner as the proprotor/pylon/wing elastic system.

Based on the equations developed in Chapter 3 this chapter will present the principal findings of some generalized trend studies shedding additional light on the role of several system design parameters on proprotor/pylon stability, frequency response characteristics of the proprotor-generated shear forces and moments, and proprotor flapping. The specific configuration chosen to form the basis of these parametric studies is the Bell Model 266 tilt-proprotor design developed during the Army Composite Aircraft Program in 1966-1967. An artist's conception of the Model 266 in the high-speed proprotor cruise mode was shown earlier in Fig. 1-6. Attention herein is directed to considerations of the right-hand proprotor/pylon/wing system taken to be cantilevered at the wing root with the proprotor fully converted forward.

---

*See, for example, Refs. 4-1 and 4-2.

The chapter is divided into five sections. Some of the distinguishing design features of the Model 266 are presented first. Proprotor/pylon instability involves an intimate coupling between certain proprotor flapping modes and pylon motions. The nature of this coupling is briefly discussed in the next section. This is followed by fundamental considerations of proprotor/pylon instability as affected by pylon/wing stiffness and damping, pitch-flap coupling, blade flapping restraint, and blade flapping frequency. Sections presenting the frequency response characteristics of the proprotor shears and moments and blade flapping conclude the chapter.

The trend studies included in this chapter have been selected with a view toward delineating some of the salient dynamic response characteristics of a proprotor/pylon/wing system. The frequency response characteristics of the shear forces and moments and blade flapping will, where appropriate, be examined in light of their effects on proprotor/pylon stability, aircraft rigid-body stability, and flapping behavior. Some selected analytical studies extending and complementing the results of this chapter are also included in Chapter 5.

Some Characteristic Design Features of the Model 266

The Model 266 represents a design evolution of the XV-3 convertiplane. It has two, three-bladed, contra-rotating proprotors of semi-rigid, teetering, or seesaw type in which the blades are rigidly attached to the yoke spindles of a non-underslung hub/yoke assembly. The hub assembly is in turn gimbal-mounted to the drive

shaft (mast) to permit flapping or tilting of the tip-path-plane relative to the mast. Blade feathering motion is provided by pitch-change bearings housed in the blade grips. The blade centrifugal force is carried to the yoke by a retention strap inside the spindle bore. Three degrees of precone are built into the hub yoke spindles to minimize steady blade out-of-plane bending moments and reduce feathering bearing loads. The blades are relatively stiff inplane, the lowest frequency being above the rotor rotational speed for all operating ranges. In the airplane mode the first inplane frequency is about 1.5 cycles/rev. A non-symmetric hub-flapping restraint (which is equivalent to blade flapping restraint) located in the non-rotating system is employed to improve the aircraft control power and response characteristics in pitch while operating in the helicopter mode. Its location in the fixed system implies that pitching moments are produced directly as a result of tilting the proprotor disc, thereby augmenting control moments from tilting of the thrust vector.

Blade pitch control is effected through a conventional helicopter-type swashplate assembly. The pitch links are connected to pitch horns on the trailing edge of the blades so that when the blades flap up the blade pitch increases, that is, positive pitch-flap coupling (negative δ_3) is employed in contrast to the more conventional negative pitch-flap coupling (positive δ_3). Pitch-flap coupling is employed on proprotors to reduce first harmonic flapping. Although either positive or negative δ_3 will reduce one-per-rev flapping, considerations of blade flap-lag stability

(Ref. 4-3) dictate the use of negative δ_3 on the Model 266.

The propulsion system consists of a T64 free turbine engine and associated gearbox located in each of the wing tip mounted pylons. The effect of the opposing requirements of high blade twist and low solidity in cruise and low twist with high solidity in helicopter flight are minimized by reducing the rotor rpm in the airplane cruise mode, thereby increasing propulsive efficiency.

Some of the primary design parameters of the Model 266 are summarized in Table 4-1. The interested reader will find a more detailed account of the Model 266 design in the state-of-the-art paper by Wernicke (Ref. 4-4). Complete documentation of the design may be found in Ref. 4-5. The particular physical parameters employed in the analytical trend studies are given in Table 4-2.

The Rotor/Pylon Dynamic System

(a) Flapping Modes of a Gimbaled Proprotor

A three-bladed semi-rigid proprotor such as on the Model 266 has two uncoupled rigid body flapping modes. In the rotating coordinate system these two modes have the same frequency and damping but one involves precession in the direction of rotor rotation and the other precession opposite to the direction of rotor rotation. Their frequency and damping, as derived in Appendix B, are given by

$$\bar{\omega}_\beta \equiv \frac{\omega_\beta}{\Omega} = \left[1 + \frac{K_H}{I_R \Omega^2} + \frac{1}{2} \gamma B_3 \tan \delta_3\right]^{1/2} \qquad (4\text{-}1)$$

$$\zeta_\beta = \frac{\gamma A_5}{4\bar{\omega}_\beta} \qquad (4\text{-}2)$$

Note that in the absence of flapping restraint and pitch-flap coupling the natural frequency of these modes in the rotating system are one-per-rev (1/rev). Use of flapping restraint in conjunction with positive or negative pitch-flap coupling raises or lowers the natural frequency of these modes from 1/rev. It is of interest to examine these modes as they would appear to an observer in the non-rotating system. With reference to the sketch below the required transformation from rotating system tip-path-plane coordinates a_{1R}, b_{1R} to fixed system tip-path-plane coordinates

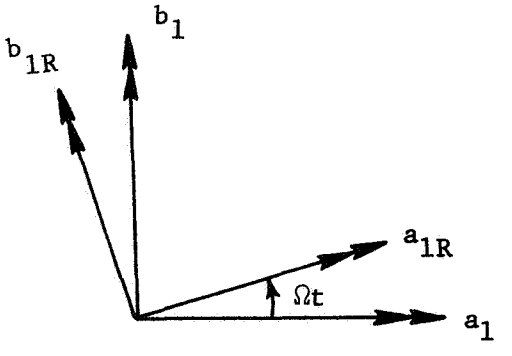

a_1, b_1 is given by

$$a_1 = a_{1R} \cos \Omega t - b_{1R} \sin \Omega t$$

$$b_1 = a_{1R} \sin \Omega t + b_{1R} \cos \Omega t \tag{4-3}$$

A forward whirl precessional motion of the tip-path-plane in the rotating system can be written as

$$a_{1R} = \bar{a} \cos \omega_\beta t$$

$$b_{1R} = \bar{a} \sin \omega_\beta t \tag{4-4}$$

where ω_β is the flapping natural frequency defined by Eq. 4-1 and $\bar{a}$ is the amplitude of whirl. Substituting Eqs. 4-4 into Eqs. 4-3 and making use of trigonometric identities,

$$a_1 = \frac{\bar{a}}{2} [\cos(\omega_\beta - \Omega)t + \cos (\omega_\beta + \Omega)t$$

$$- \cos(\omega_\beta - \Omega)t + \cos(\omega_\beta + \Omega)t]$$

$$b_1 = \frac{\bar{a}}{2} [\sin(\omega_\beta + \Omega)t - \sin(\omega_\beta - \Omega)t \tag{4-5}$$

$$+ \sin(\omega_\beta - \Omega)t + \sin(\omega_\beta + \Omega)t]$$

Eqs. 4-5 reduce to

$$a_1 = \bar{a} \cos(\omega_\beta + \Omega)t$$
$$b_1 = \bar{a} \sin(\omega_\beta + \Omega)t \qquad (4\text{-}6)$$

Eqs. 4-6 indicate that a forward whirl in the rotating system transforms to a forward whirl in the fixed system if ω_β is greater than, equal to, or less than Ω.

A backward whirl precessional motion of the tip-path-plane in the rotating system can be written as

$$a_{1R} = \bar{a} \cos \omega_\beta t$$
$$b_{1R} = -\bar{a} \sin \omega_\beta t \qquad (4\text{-}7)$$

Substituting Eqs. 4-7 into Eqs. 4-3 and proceeding as above yields

$$a_1 = \bar{a} \cos(\omega_\beta - \Omega)t$$
$$b_1 = -\bar{a} \sin(\omega_\beta - \Omega)t \qquad (4\text{-}8)$$

as the motion in the fixed system. Note that for the case of backward whirl in the rotating system the motion observed in the fixed system is a backward whirl if $\omega_\beta > \Omega$, a steady longitudinal tilt of the tip-path-plane if $\omega_\beta = \Omega$ and a forward whirl if $\omega_\beta < \Omega$.

The above considerations are also directly applicable to the blade inplane whirl modes which "appear" in the rotating system as a forward and backward whirl of the cg of the displaced blades.

In the fixed system, the flapping modes manifest themselves as a weaving or wobbling of the tip-path-plane in the forward or backward directions. For the particular combination of positive pitch-flap coupling and hub restraint employed on the Model 266 the flapping natural frequency in the rotating system at low airspeeds is .875 cycles/rev and decreases with increasing airspeed while the associated damping is about 30 percent of critical and also decreases with airspeed. In the fixed system these flapping modes constitute a low frequency forward precession of the tip-path-plane at .125 cycles/rev and a high frequency forward precession at 1.875 cycles/rev.

In the absence of precone(steady-state coning for the case of a rotor with offset flapping hinges)the flapping modes can not flutter by themselves. However, in the presence of precone these modes can be destabilized. In particular, positive precone has a destabilizing effect upon the high frequency flapping mode and negative precone is destabilizing upon the low frequency flapping mode. For rotor rpm typical of proprotor cruise operations the precone required for instability is much larger than that which exists in practice and these precone-induced flapping instabilities are mainly of academic interest.

For completeness, it should be pointed out that the rigid body flapping modes can also be destabilized by coupling with blade inplane elastic bending, the coupling in one such instability being associated with the sign of the pitch-flap coupling ratio and another

being caused by elastic coning in the presence of control system/ blade torsion flexibility. A comprehensive treatment of these types of instabilities is given in Refs. 4-3 and 4-6.

Before closing this discussion on flapping it should be noted that the flapping due to small mast angle of attack is a 1/rev forced response in which the blades flap with respect to the swash-plate so as to minimize the cyclic variation in blade section angle of attack around the azimuth. This flapping appears as a steady longitudinal and/or lateral tilt of the tip-path-plane in the fixed system. The flapping natural frequency, ω_β, is the frequency of the transient motion which would be observed in the rotating system if the tip-path-plane of steady 1/rev flapping were set into motion by "plucking".

(b) The Role of Pylon Freedoms

The rigid body flapping modes of a stiff inplane proprotor with zero precone can not flutter by themselves. When this proprotor is mounted on a pylon which has freedom of motion, both the pylon modes and the flapping modes can be destabilized. Since angular motions of the pylon represent angular motions of the control plane in space for a proprotor having the swashplate rigidly attached to the pylon, pylon motions and flapping motions are strongly coupled. In addition to the familiar pylon whirl instability associated with one of the pylon modes and occurring near a pylon-mode coupled natural frequency the shear forces can destabilize the flapping modes. A flapping mode instability appears

as a whirl of the tip-path-plane and pylon near a tip-path-plane coupled natural frequency with large flapping in space. (The XV-3 instability encountered in the Ames tunnel in 1962 was in a low-frequency, backward whirl flapping mode.) In general the low-frequency flapping mode can be destabilized for relatively low pylon support stiffnesses in combination with large values of flapping restraint or positive δ_3. The high-frequency flapping mode can be destabilized if the pylon support stiffnesses are such as to place the pylon mode frequencies close to the second flapping mode frequency.

Several aspects of rotor/pylon mode coupling will be brought out in the following sections.

Proprotor/Pylon Instability

Because of the additional flapping and feathering freedoms available to a proprotor and the many rotor design parameters which can influence stability the dynamic characteristics of the typical proprotor are such that various types of instabilities associated with the proprotor/pylon/wing system can occur. The influence of several structural and kinematic parameters on proprotor/pylon stability will be presented here in a manner which will hopefully provide useful design guidelines. The results are based on an idealized proprotor/pylon/wing system in accordance with the mathematical model developed in Chapter 3 and embodied in computer program PRSTAB6. Since the wing is taken as cantilevered at its root the results are, of course, not indicative of stability

in free-flight. These results do however, represent a lower bound on stability for the Model 266 since its free-flight stability is increased compared to that of the cantilevered wing. Wing elasticity is accounted for in terms of equivalent wing tip spring rates referenced to the pylon mast/conversion axis intersection. To insure a blade flapping frequency independent of azimuth a symmetric hub restraint was employed in the trend studies. Mach number effects, except in one case, are neglected.

(a) Pylon Support Stiffness

Proprotor/pylon combinations employing proprotors with more than two blades are generally rigidly mounted to the wing tips to take maximum advantage of the stiffness and damping inherent in the wing structure. The effective wing support conditions at the pylon/wing junction will then have a strong influence on stability. In such an arrangement the pylon freedoms are equivalent to certain wing freedoms: pylon pitch to wing torsion, pylon yaw to the rotational component of wing inplane bending, etc. The effects of several of these pylon support stiffnesses on proprotor/pylon stability will be established below in the manner of Ref. 4-7 by sequentially adding pylon degrees of freedom to the basic tip-path-plane pitch and yaw-degrees of freedom of the proprotor. These results generally extend those of Ref. 4-7 in that both flapping restraint and pitch-flap coupling are taken to be non-zero (representing a more realistic proprotor design condition), damping effects are indicated, and several additional features are included.

Pylon Pitch: The stability of the three degree-of-freedom system which includes the pylon pitch (wing torsion) degree of freedom is given in Fig. 4-1. The flutter speed is plotted as a function of the uncoupled pylon pitch static natural frequency* normalized on the proprotor speed at which the stability calculations were made. Instability occurs in the pylon pitch mode,† being driven by the destabilizing shear force component inphase with the pitch rate. This illustrates that a proprotor can be dynamically destabilized in a single plane, in contrast to a propeller/nacelle combination. At the higher pitch frequencies reflective of current design practice, pylon damping is seen to have a negligible stabilizing effect.

Pylon Yaw: The effects of adding the pylon yaw degree of freedom to the 3° of freedom system are indicated in Fig. 4-2 for the case of $\omega_{pitch}/\Omega = 0.80$. Here the flutter speed is given as a function of the ratio of uncoupled pylon yaw natural frequency to uncoupled pylon pitch natural frequency. The dramatically destabilizing effects of pylon isotropy are clearly evident in the extended region of instability along the line representing a stiffness ratio of unity. Pylon damping is seen to be quite effective in stabilizing the system under isotropic and near isotropic support conditions but has only a small effect for

*The uncoupled static natural frequency is taken to be that observed in the transient response resulting from statically displacing the system in the degree of freedom in question and releasing it, all other degrees of freedom being "locked out" with zero rotor rpm.

†Mode designations herein are based on the uncoupled mode motion which predominates in the coupled mode.

non-isotropic support conditions.

For pylon yaw-to-pitch frequency ratios below .75/rev flutter is in the pylon yaw mode, with the pylon and tip-path-plane precessing in the forward whirl direction near the pylon yaw coupled natural frequency. As the frequency ratio is increased beyond .75/rev the flutter mode initially changes to a backward whirl associated with the pylon pitch mode and then, at 1.4/rev, changes back to a forward whirl but remaining associated with the pylon pitch mode. Note that if the frequency ratio is greater than about 1.5 the effect of adding the yaw degree of freedom (i.e., the freedom in the stiffer direction) is negligible. This is further illustrated by including the stability boundary for the case of no pylon yaw freedom. For pylons which are rigidly attached to the wing tips the yaw-to-pitch frequency ratio will normally be about 2.0 to 3.0. For the Model 266 this ratio is 2.24.

As a sidelight, results based on the use of a representative section aerodynamic theory are also shown. This theory, as indicated in Chapter 3, lumps the aerodynamic loading at some "representative" blade radial station in a manner not unlike the so-called typical section approaches employed in early fixed-wing flutter analyses. The specific results shown indicate that the location of the "correct" representative section moves inboard on the blades as the flutter airspeed increases.

Wing Beam: The addition of the wing beam degree of freedom (≡ vertical translational component of wing vertical bending) to

a pylon which has freedom in pitch permits the wing beam freedom to couple with pylon pitch to create two pylon/wing modes of motion: a so-called inphase mode in which the pylon pitching motion and wing vertical displacement are in the same direction and an out-of-phase mode in which the pitching motion of the pylon is in a direction opposite to that of the wing vertical displacement. Each of these coupled modes is characterized by the predominance of an uncoupled mode: the former by wing vertical displacement and the latter by pylon pitching (wing torsion). For descriptive purposes the inphase coupled pylon/wing mode in which wing vertical bending predominates will be herein designated as the wing beam mode and the out-of-phase coupled pylon/wing mode in which pylon pitching (wing torsion) motion predominates will be designated as the pylon pitch (or wing torsion) mode. These designations are also prompted by frequency considerations: the inphase mode has a frequency near the uncoupled wing vertical bending natural frequency and the out-of-phase mode oscillates near the uncoupled pylon pitch (wing torsion) natural frequency. The wing beam mode is equivalent to a pure pitching motion about a node located aft of the pylon physical pivot; the pylon pitch mode is equivalent to a pure pitching motion about a node between the proprotor disc and the physical pivot.

The effect of adding the wing beam degree of freedom to the 4° of freedom system above can be stabilizing or destabilizing depending on its frequency ratio with respect to pylon pitch. This is illustrated in Fig. 4-3. At very low levels of wing beam frequency the pylon motion involves mainly vertical translation,

with very little precession of the proprotor in space. The precession-generated shears, which constitute the destabilizing forces, are thus initially dominated by the stabilizing damping contribution associated with hub translational motion. This does not represent a viable design solution however, since the corresponding wing stiffnesses would be too low to satisfy basic strength requirements. Flutter at these low stiffness levels occurs in the wing beam mode, the pylon/rotor combination executing a forward whirl precession. As the wing beam frequency is increased the stability initially decreases quite rapidly because the coupling between wing beam and pylon pitch increases, the coupling having the dual effect of moving the effective pivot forward toward the physical pivot, thereby reducing hub translational damping, and reducing the effective pylon pitch stiffness. The stability continues to decrease as wing beam frequency is further increased because the wing beam mode begins to couple with the low frequency ($\Omega - \omega_\beta$) flapping mode. In this region ($.10 < \omega_{beam}/\Omega < .40$) the instability is still in the wing beam mode with the pylon/rotor combination executing a forward precessional whirl motion. Because of the strong coupling with a flapping mode a considerable amount of flapping (in space) distinguishes the flutter mode in this region. If ω_β were equal to Ω the frequency of the low frequency flapping mode in the fixed system would be zero, there would be no coupling with this mode and the elongated region of instability shown in Fig. 4-3 about $\omega_{beam}/\Omega = .25$

would not occur*. As wing beam frequency is increased beyond .70/rev an abrupt reduction in stability occurs in a small range of frequency about .80/rev, the reduction being quite large for zero damping. For no damping the instability is in the pylon pitch mode (the out-of-phase coupled pylon/wing mode) with large flapping in space. When pitch is out of phase with wing beam motion the effective pylon pitch stiffness increases with increasing wing beam stiffness until the pylon pitch mode couples with the high frequency ($\Omega + \omega_\beta$) flapping mode. Unusual features of the flutter mode are the whirl direction: the pylon exhibits a backward precessional whirl while the tip-path-plane whirls in the forward direction relative to space. For nonzero damping only a slight reduction in stability occurs; flutter is in the wing beam mode with both the pylon and tip-path-plane whirling in the forward direction. For wing beam frequencies beyond .80/rev the flutter modes for both values of damping are identical, a forward whirl in the wing beam mode.

Wing Chord: The effects of adding the fore-and-aft translational component of wing inplane bending ($\equiv$ wing chord) to the 5° of freedom system are summarized in Fig. 4-4. As wing chord stiffness is increased the flutter mode changes from a forward whirl in the pylon yaw mode to a forward whirl in the wing beam mode. Because of this change in flutter mode, pylon damping has no effect upon stability beyond $\omega_{chord}/\Omega = .30$. Wing chord frequency ratios

*See Fig. 7c of Ref. 4-7.

beyond about .5/rev are seen to have a negligible influence upon stability.

The effects of Mach number upon stability are indicated for the region of chord frequencies greater than..3/rev. Both the Prandtl-Glauert and compressible flow aspect ratio corrections are reflected in the Mach-number-corrected results. As might be expected, stability is decreased.

(b) Pitch-Flap Coupling

Considerations of blade flapping while operating in the high-speed proprotor mode generally indicate that flapping amplitudes must be reduced. One means of effecting a reduction in flapping is through the use of pitch-flap coupling (δ_3). Either positive or negative pitch-flap coupling ($-\delta_3$ or $+\delta_3$) is effective in reducing flapping. The effects of δ_3 on the stability of the 4° of freedom proprotor/pylon system for the case of non-isotropic pylon supports for two values of hub restraint and two rotor rpm are displayed in Fig. 4-5. The destabilizing effects of large positive or negative δ_3 on proprotor/pylon stability are noteworthy and constitute the most significant feature of δ_3 as regards proprotor/pylon stability. It should be pointed out that the wide range of δ_3 values shown was chosen to better illustrate the effects of δ_3 on stability. The maximum values of positive or negative δ_3 are in practice dictated by considerations of blade flap-lag stability and static divergence (Ref. 4-3) and generally fall well within the extremes shown.

(c) Flapping Restraint

A summary of the results concerning the effect of flapping restraint (as reflected in the blade flapping natural frequency) on proprotor/pylon stability is given in Fig. 4-6 for both the four and five degree-of-freedom systems. δ_3 was set to zero so that the uncoupled flapping natural frequency would be independent of aerodynamic conditions. For the 4° of freedom case maximum stability occurs at a blade flapping natural frequency of about 1.12 cycles/rev. This is in agreement with the results of Young and Lytwyn (Ref. 4-1) who analytically demonstrated that the pylon support stiffness and/or damping requirements for prevention of whirl flutter are a minimum when the blade fundamental flapping natural frequency is 1.1 to 1.2 cycles/rev.* It is of interest to describe the change in flutter mode as flapping frequency is increased from 1/rev. This will be done with the aid of root loci showing the frequency and damping variation with airspeed for each of the modes of the system, arrows indicating the direction of root movement with increasing airspeed. The root designation selected for the root loci plots was suggested by the fact that each of the coupled modes of the system is characterized by the predominance of an uncoupled mode.

For frequencies below about 1.09 cycles/rev flutter is in the forward whirl pylon pitch mode. The root locus for the particular

*Ref. 4-1 established this optimum on the basis of considerations on a rotor having centrally hinged flapping blades restrained by springs. More recently, Ref. 4-8 demonstrated that this optimum also exists when the flapping restraint is achieved through a combination of hinge offset and spring restraint.

case of $\omega_\beta/\Omega = 1.0$ is given in Fig. 4-7. Flutter occurs in the low frequency ($\omega_\beta - \Omega$) flapping mode for $\omega_\beta/\Omega > 1.09$ (Fig. 4-8), the pylon/rotor combination precessing in the backward whirl direction. It is to be noted that these whirl directions are also in agreement with the findings of Ref. 4-1.

Fig. 4-6 also shows the effects of including the wing beam degree of freedom. Maximum stability occurs at about $\omega_\beta/\Omega = 1.14$, indicating that a "design optimum" in the sense of Ref. 4-1 also exists in the more general case which includes wing vertical bending. Note that wing beam freedom is slightly destabilizing at low values of ω_β/Ω and stabilizing at higher values of ω_β/Ω. This is associated with the flutter mode shape. At low blade flapping frequencies wing beam motion is inphase with pylon pitch thereby reducing the effective pitch stiffness relative to the case for no wing beam freedom. This is destabilizing on proprotor/pylon stability. At the higher flapping frequencies pylon pitch and wing beam are out of phase with each other, effectively stiffening the pylon in pitch, which is stabilizing.

The variation in flutter mode and direction of pylon whirl with increasing flapping frequency is of particular interest in this case, there being several such changes. Below $\omega_\beta/\Omega = 1.09$ flutter is in the wing beam mode with the pylon/rotor combination precessing in the forward whirl direction. For ω_β/Ω between 1.09 and 1.16 a backward whirl instability in the pylon pitch mode occurs. The high frequency ($\omega_\beta + \Omega$) flapping mode is unstable

for ω_β/Ω between 1.16 and 1.65, the whirl now being again in the forward direction. Beyond 1.65 flutter is in the low frequency $(\omega_\beta - \Omega)$ flapping mode, the whirl now occurring in the backward precessional direction. Root loci showing the root movement leading to each of these flutter modes are presented in Figs. 4-9 to 4-12.

The maximum value of flapping restraint which can be employed in practice is dictated by considerations of allowable blade loads.* This generally limits the maximum flapping frequency (for $\delta_3 = 0$) to values well below 1.5 cycles/rev, depending on the particular design. The results of Fig. 4-6 are thus for the most part mainly of academic interest.

(d) Effects of Pitch-Flap Coupling on Stability of the Five Degree-of-Freedom System

An indication of the effects of δ_3 on proprotor/pylon stability for the case in which wing beam freedom is included are displayed in Fig. 4-13. The sharp reduction in stability associated with large values of δ_3 arise from the coupling of the wing beam mode with the low-frequency flapping mode, the frequency of which in the fixed system is increased by positive or negative δ_3. In each case shown, flutter is in the wing beam mode with the direction of pylon whirl being determined by the flapping natural frequency as indicated. The flapping frequency at which stability is a

---

*See, for example, the "Review and Discussion" of Ref. 4-1 by Wernicke and Gaffey which forms an integral part of that reference.

maximum occurs in the range 1.02 to 1.05 cycles/rev for the range of parameters studied. This suggests that an optimum flapping frequency in the sense of Ref. 4-1 also exists for $\delta_3 \neq 0$ and for K_H/δ_3 combinations.†

Frequency Response Characteristics of Proprotor Shear Force and Moment Derivatives

It was shown in Chapter 2 that airload moments are required to precess a proprotor in response to pylon oscillatory motions. At high advance ratios these moments are accompanied by shear forces which are phased with the pylon motion such that they tend to increase its pitching or yawing velocity and hence constitute negative damping on the pylon motions. These shears are the primary forces which destabilize the proprotor/pylon/wing elastic system and the aircraft rigid body modes.

Disturbances occurring in flight can, depending on their frequency content, excite the elastic proprotor/pylon/wing system or the aircraft rigid body modes in an oscillatory manner. Any motions of this type effectively represent oscillatory motions of the proprotor mast (control axis) in space. Since the proprotor-generated forces and moments are a function of these oscillatory motions it is of interest to examine the dependency of the frequency response characteristics of these forces and moments on several system design parameters.

---

†Young and Lytwyn did not consider δ_3 effects.

Proprotor inplane shear forces are proportional to the tip-path-plane precessional rate in space. Now the relationship of the proprotor response in space to that of the control plane (swashplate)is quite complicated,depending on the proprotor inertial properties, airspeed, rpm, flapping restraint, pitch-flap coupling, and control feedbacks. Consequently both proprotor/pylon stability and aircraft rigid-body stability will be sensitive to those parameters which affect proprotor response. The effect of several such parameters on the frequency response characteristics of these forces and moments will be delineated below by examining their variation during sinusoidal pitching oscillations of the pylon.* Attention is directed to the pitch plane only since, neglecting flow asymmetries and assuming a symmetric hub restraint, the forces and moments generated by yawing oscillations follow directly from the pitch results by virtue of symmetry.

The majority of these studies are for a velocity of 350 knots and a rotor speed of 238 rpm. This represents a tip inflow ratio ($V/\Omega R$) of 1.23. Although this is somewhat larger than that consistent with maximum propulsive efficiency in the high-speed cruise mode of flight, it is a value which can be realized in an overspeed flight condition. Also, during wind-tunnel tests of scaled models (in which the full-scale $V/\Omega R$ is maintained) testing is done beyond scaled flight speeds to establish margins of safety. All results are based on the analysis developed in Appendix C.

*This is equivalent to control axis pitching motions if the swashplate is fixed to the mast.

The resultant shears and moments acting on a harmonically oscillating proprotor are algebraically complex quantities indicating that components proportional to both pitch angle and pitch rate contribute to their absolute value. To facilitate the interpretation of these forces and moments they will be separated into the above-mentioned components in the studies to be presented below. The separation of the normal force and pitching moment into components inphase with pitch angle and pitch rate is schematically illustrated in the sketch below. The components proportional to pitch angle are normalized by the maximum pitch amplitude α_m

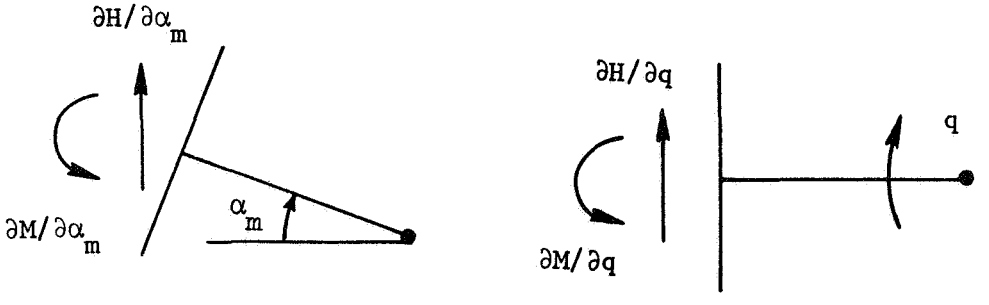

$$\alpha = \alpha_m \sin \omega_p t \qquad \dot{\alpha} = \alpha_m \omega_p \cos \omega_p t = q \cos \omega_p t$$

while the components proportional to pitch rate are normalized by the maximum pitch rate q $(= \alpha_m \omega_p)$. Normalized in this manner the forces and moments assume the form of derivatives. With reference to the H-force components, the $\partial H/\partial \alpha_m$ term is the portion of the total H-force which is inphase or 180° out-of-phase with the pylon pitch displacement. When it is inphase with the

pitch displacement it acts as a negative spring force tending to reduce the effective pylon pitch stiffness; when it is 180° out-of-phase with the pylon displacement it acts as a positive spring force, tending to increase the pylon pitch stiffness. $\partial H/\partial \alpha_m$ is a maximum at $\alpha = \alpha_m$ and zero when $\alpha = 0$. The $\partial H/\partial q$ term is the component of the total H-force which is inphase or 180° out-of-phase with the pylon pitch rate. It constitutes a negative (destabilizing) damping on the pylon pitching motion when it is inphase with the pitching velocity and positive damping when it is 180° out-of-phase with the pitching velocity. $\partial H/\partial q$ is a maximum when $\alpha = 0$ and zero when $\alpha = \alpha_m$. The sign convention which will be employed in the graphical results is given in Fig. 4-14.

(a) Proprotor Rotational Speed

The frequency response characteristics of the shear forces and moments for two values of rpm are shown in Fig. 4-15. Consider the variation of the normal force component. The proprotor contributes large negative damping to pylon motions of low frequency. If the pylon coupled natural frequency falls within this range (below 2.5 cps for $\Omega = 300$ rpm, for example) the negative damping from the H-force will at some forward speed exceed the inherent structural damping and any positive aerodynamic damping and instability will result. As frequency is increased the negative damping decreases and eventually becomes positive. Simultaneously, $\partial H/\partial \alpha_m$ increases in a manner to reduce the pylon natural frequency in pitch. Hence, even if the pylon coupled natural

frequency is sufficiently high to ensure a stabilizing contribution from $\partial H/\partial q$, the increasing negative spring effect of $\partial H/\partial \alpha_m$ with increasing airspeed (see Fig. 4-16a) will act so as to reduce the pylon coupled natural frequency until $\partial H/\partial q$ becomes destabilizing and the negative damping effect is finally able to overcome the combined positive damping. This is precisely the mechanism by which the pylon pitch mode was driven unstable in the results for the 3° of freedom system shown in Fig. 4-1.

The magnitude and phase of $\partial H/\partial \alpha_m$ and $\partial H/\partial q$ are seen to be strongly dependent on the pylon pitch frequency and hence on the magnitude and phase of the tip-path-plane response ($\dot{a}_1$) relative to the motion of the pylon mast ($\dot{\alpha}$). For a steady continuous pitching motion in which $\omega_p = 0$, $\dot{a}_1$ is zero and $\partial H/\partial q$ contributes a large negative damping force to pylon motions. When the pylon is oscillating $\dot{a}_1$ is not zero. The tip-path-plane response can be quite large if the pylon is excited at one of the fixed-system flapping natural frequencies. The crests and troughs apparent in the response curves are associated with the fixed system flapping modes. For the particular rotor parameters indicated, $\partial H/\partial \alpha_m$ and $\partial H/\partial q$ become more destabilizing at pylon frequencies near $\Omega - \omega_\beta$ while for pylon frequencies near $\Omega + \omega_\beta$ $\partial H/\partial \alpha_m$ becomes less destabilizing and $\partial H/\partial q$ becomes less stabilizing. This implies that parameters which alter the proprotor flapping natural frequency can significantly affect the stability of both the pylon modes and the flapping modes. The

results presented earlier in Figs. 4-6 to 4-12 are indicative of these effects for the case of flapping restraint.

At low pylon pitch frequencies the proprotor tip-path-plane is essentially inphase with the pylon angle ($a_1 \approx 0$) and the total H-force is predominantly inphase with the pitch rate. The damping component of the H-force then predominates at low pylon frequencies. As the pylon frequency is increased the proprotor disc begins to lag the pylon motion more and more until the tip-path-plane eventually assumes a fixed vertical orientation in space, being unable to respond fast enough to the high frequency pylon oscillations. The total H-force is then predominantly inphase with the pylon pitch displacement and the destabilizing forces act on the pylon primarily in the sense of a negative spring. Summarizing, the effect of the proprotor on pylon oscillations is to reduce both damping and frequency, the negative damping predominating at low pylon frequencies and a negative spring term predominating at higher pylon frequencies.

Note that as the proprotor rpm is increased the pitch frequency at which $\partial H/\partial q$ becomes stabilizing increases, implying that increased pylon stiffness and/or damping would be required to maintain the same level of stability as rpm increases.

Considerations similar to those above are generally applicable to the pitching moment response characteristics shown in Fig. 4-15c. Since proprotors usually have some type of flapping restraint (in the form of a spring, flex-hinge or offset flapping hinge)

these moments can be transferred to the pylon and, with reference to Fig. 4-15c, can contribute either a stabilizing or destabilizing influence on pylon motions. For the particular conditions indicated $\partial M/\partial q$ is destabilizing for pylon pitch frequencies located near the fixed system flapping mode frequencies; the opposite is true for $\partial M/\partial \alpha_m$. The corresponding side force and yawing moment response characteristics are presented in Figs. 4-15b and d.

Tilt-proprotor aircraft are generally designed to have contra-rotating rotors in order to minimize the coupling between longitudinal and lateral rigid body motions. With reference to Figs. 2-12a and 2-12b it is then seen that the side forces and yawing moments cancel out during aircraft pitching motions while the normal forces and pitching moments sum to zero during yawing motions.

(b) Airspeed

The effects of forward flight velocity on the frequency response of the normal force and pitching moment are shown in Fig. 4-16. Since the rotor rpm will remain fixed the pylon pitch frequency is normalized on the rpm, in accordance with customary practice in rotary-wing dynamics. The effect of increased airspeed is seen to be an increase in the magnitude of the forces and moments, as might have been expected. There is a negligible influence on the pylon pitch frequency at which $\partial H/\partial q$ contributes positive damping, in contrast to the case of increasing rotor rpm.

This suggests that the destabilizing effects of increasing airspeed are solely a result of the increasing magnitude of $\partial H/\partial \alpha_m$ and $\partial H/\partial q$.

(c) Pitch-Flap Coupling

The negative damping contributed by the proprotor is a function of the amplitude and phase of the tip-path-plane response relative to the motion of the control axis. Two factors which increase the rotor response rate are $+\delta_3$ and K_H since they both act to increase the flapping natural frequency. The effect of δ_3 on the frequency response of the normal force and pitching moment derivatives for the case of zero hub restraint are shown in Fig. 4-17. For $\delta_3 = 0$, $-22\text{-}1/2^\circ$, and $+22\text{-}1/2^\circ$, the corresponding flapping natural frequencies in the rotating system are 1.0, .74, and 1.2 cycles/rev, respectively. These modes occur at fixed system frequencies of $|\Omega \pm \omega_\beta|$ and lead to the crests and troughs seen in the response curves at those frequencies. There is no low-frequency peak for $\delta_3 = 0$ because this mode has zero frequency in the fixed system. Note that the use of δ_3 decreases the destabilizing $\partial H/\partial \alpha_m$ forces at low pylon frequencies but increases the $\partial H/\partial q$ forces. This indicates that δ_3 is destabilizing on the aircraft short period mode. At higher frequencies δ_3 can be stabilizing or destabilizing relative to the $\delta_3 = 0$ case depending on the pylon frequency.

The destabilizing effect of δ_3 on proprotor/pylon stability demonstrated earlier in Fig. 4-5 can be explained with

reference to Fig. 4-17b. As airspeed increases $\partial H/\partial \alpha_m$ decreases the pylon pitch stiffness more and more until $\partial H/\partial q$ becomes destabilizing. The magnitude of $\partial H/\partial q$ is larger for $\delta_3 \neq 0$ and hence can more quickly exceed the net positive damping in the system as pylon frequency continues to be reduced. Alternatively, this may be viewed as the pylon being destabilizing by coupling with the low-frequency flapping mode at a lower airspeed since increased δ_3 moves this frequency to the right.

The frequency of the second flapping mode either increases or decreases depending on whether δ_3 is positive or negative. The design consideration of separating the pylon modes from the flapping modes indicates that careful attention must be directed to the system coupled frequency spectrum when employing either positive or negative δ_3.

(d) Flapping Restraint

The increase in the proprotor response rate due to flapping restraint can be stabilizing or destabilizing depending on its value and the frequency of pylon oscillation. This is brought out in Fig. 4-18. Increased K_H is seen to lessen the destabilizing effect of $\partial H/\partial q$ at low frequencies ($\partial H/\partial q$ even becomes stabilizing for very large values of K_H) but decreases its stabilizing effect at intermediate pitch frequencies.

It is of interest to examine the variation of the zero pitch-frequency force and moment derivatives with flapping restraint and interpret the limiting conditions of infinite flapping restraint

in light of the results shown for a propeller in Fig. 2-14 which were obtained by simple physical considerations. These results are summarized in Fig. 4-19 for three values of δ_3. As K_H is increased to "infinity" the derivatives will be asymptotic to the propeller limits indicated. It is seen that, in agreement with the results of Fig. 2-14, $\partial Y/\partial\alpha_m$ and $\partial M/\partial\alpha_m$ go to zero while $\partial H/\partial\alpha_m$, $\partial H/\partial q$, $\partial Y/\partial q$, $\partial M/\partial q$, $\partial N/\partial\alpha_m$, and $\partial N/\partial q$ approach non-zero limits. The limiting directions are also in agreement with those shown in Fig. 2-14. Note that of all the non-zero limiting values all are small except $\partial H/\partial\alpha_m$ and $\partial N/\partial\alpha_m$. Hence of the forces and moments which can destabilize the backward whirl mode only $\partial N/\partial\alpha_m$ (and $\partial M/\partial\psi_m$) are of sufficient magnitude to do so. This then constitutes another "proof" that the cross-stiffness moments are the driving terms for backward whirl flutter of a propeller.

(e) Shaft Length

Fig. 4-20 illustrates the effect of shaft length on the normal force and pitching moment frequency response behavior of a proprotor and propeller. Since these results are for a forced response of the proprotor/pylon system the differences between the results for $h = 6.92$ and $h = 0$ are indicative of the aerodynamic damping associated with transverse velocities of the proprotor or propeller hub. Increasing the shaft length is stabilizing in the sense that hub translational damping is increased. This has already been shown analytically in Refs. 4-9 to 4-11 for the case of a propeller. If the changes in inertia which accompany increases in shaft length are accounted for, the

stabilizing effect due to increased hub translational damping is essentially negated by the destabilizing effect of a decrease in the effective pylon support stiffness in pitch and yaw so that the net stability of the system is basically unchanged.* It is to be noted that this conclusion is not in agreement with that of Ref. 4-11 which found that the net stability of the system was significantly increased even if the increase in system inertia was taken into account.

For the case of a proprotor the net effect of increased shaft length is highly destabilizing on whirl flutter. This is a consequence of the frequency response characteristics of the proprotor H-forces. With reference to Fig. 4-20a it is seen that for pylon pitch frequencies beyond about .5 cycles/rev increased shaft length is aerodynamically stabilizing. However, as airspeed increases the increasing negative spring effect of $\partial H/\partial \alpha_m$ reduces the pylon frequency until $\partial H/\partial q$ becomes destabilizing. In this range of pylon frequencies increases in shaft length are seen to have a negligible aerodynamic effect. Since the effective pylon pitch stiffness has been reduced the net effect of increased shaft length is destabilizing.

The propeller forces and moments are constant with frequency of excitation because, as pointed out in Chapter 2,there is no lag of the propeller disc relative to its shaft. This also causes

---

*These results are not shown herein.

$\partial H/\partial \alpha_m$ to be independent of shaft length. Recalling that $\partial M/\partial q$ is a function of the disc pitch rate in space shaft length has no effect on this derivative. $\partial M/\partial \alpha_m$ is of course identically zero for a propeller.

(f) Altitude

The manner in which the zero frequency normal force derivatives vary with altitude are given in Fig. 4-21. $\partial H/\partial q$ increases with altitude. This implies a destabilizing effect of the inplane shears on the aircraft short period and Dutch roll modes. Since the horizontal and vertical tail contributions to aircraft damping in pitch and yaw remain relatively constant with altitude the proprotor contribution to these aircraft motions becomes increasingly destabilizing with altitude. The decreasing magnitude of $\partial H/\partial \alpha_m$ with increasing altitude indicates that aircraft longitudinal and lateral static stability are increased with altitude.

(g) Proprotor Stabilization by Blade Pitch Control Feedback

Inplane shears generated by proprotor precession in response to pylon motion are the cause of instability. These forces are dependent on the motion of the tip-path-plane in space, or, what is equivalent, the motion of the tip-path-plane relative to the swashplate (control plane). The preceding results were based on the assumption that the centerline of the mast and the control axis were identical, since the swashplate was taken to be rigidly affixed to the shaft. When the shaft pitches the swashplate follows. This induces blade angle of attack changes, resulting in precessional airload moments which are accompanied by

destabilizing shear forces. If the proprotor could be uncoupled from the pylon or swashplate motions in a way which would minimize the angular motion of the proprotor control axis in space the destabilizing shears could be reduced. The direct approach of increasing pylon support stiffness is limited by weight considerations. Since it is the control plane and not the mast which determines proprotor behavior in space, various means for accomplishing this uncoupling based on the use of blade pitch control feedback are possible. A mechanical displacement uncoupling scheme, termed "swashplate/pylon coupling" will be employed here to illustrate the effectiveness of such a technique. Swashplate/pylon coupling (Refs. 4-2 and 4-12) is based on a mechanical arrangement whereby the swashplate angular displacement relative to the mast during oscillatory motions of the pylon is opposite to that of the pylon tilt.

Results indicative of the effectiveness of a blade pitch control feedback based on longitudinal swashplate/pylon coupling are shown in Fig. 4-22. For the coupling ratio used ($K_1 = +1.0$) the tip-path-plane remains essentially vertically oriented in space. These results are to be compared with the corresponding results in Fig. 4-20a for the case of no coupling. The significant stabilizing effects are readily apparent.

If $\delta_3 \neq 0$ (or, more generally, if $\omega_\beta/\Omega \neq 1$) the effective control axis is rotated and a swashplate command for a longitudinal tilt of the tip-path-plane will also cause the tip-path-plane to tilt laterally. Control phasing is incorporated into the

swashplate/pylon mechanism to phase the swashplate and tip-path-plane in a manner which will eliminate this cross-coupling between longitudinal and lateral tip-path-plane motions in a given flight condition. This phasing is accomplished by adjusting the control linkages such that the swashplate control inputs to the pitch horns appear on the blades at an azimuth position more retarded or advanced than the swashplate tilt, which is the source of the control deflection, depending on whether ω_β/Ω is greater than or less than one. The effectiveness of swashplate/pylon coupling is generally increased by the use of control phasing. Fig. 4-22 also shows the results of using a phasing equal to the δ_3 angle in conjunction with $K_1 = +1.0$.

(h) Zero Frequency Shear Force Characteristics During Proprotor Feathering

Whereas aircraft rigid body dynamic stability considerations dictate the tail requirements for tilt-rotor operation in the high-speed cruise mode, tail requirements for a folding proprotor are dictated by considerations of static stability. This is due to the nature of the response characteristics of the shear forces during the feathering sequence of transition. An indication of the magnitude of the H-forces during this period at an airspeed which is representative of the transition speed is given in Fig. 4-23. No transient effects are included. It is seen that as the rotors are stopped the flight condition of minimum static margin is encountered because angle-of-attack stability decreases by an increasing amount as $\partial H/\partial \alpha_m$ increases.

The corresponding results for a proprotor with infinite flapping restraint (ie., a propeller) are shown for comparison. At rpm typical of proprotor operation (200 to 400 rpm) $\partial H/\partial \alpha_m$ is small relative to that of a propeller because flapping reduces 1/rev airload moments and hence $\partial H/\partial \alpha_m$. $\partial H/\partial q$ on the other hand is large since airload moments are required to precess the proprotor. The situation for a propeller in the same range of rpm is reversed, $\partial H/\partial \alpha_m$ is large and $\partial H/\partial q$ is small. The corresponding limiting values of $\partial H/\partial \alpha_m$ and $\partial H/\partial q$ at $\Omega = 0$ for the proprotor and propeller are identical because with flapping identically zero at $\Omega = 0$ (see Fig. 4-29) the proprotor is effectively a propeller. Note that positive hub translational damping also exists for $\Omega = 0$. The peak in the curves for $\delta_3 = -22\text{-}1/2^\circ$ is related to the flapping associated with passing through the flapping natural frequency (see Fig. 4-29).

Proprotor Flapping Characteristics

Blade flapping is designed into rotor systems to relieve unbalanced moments across the rotor disc, to provide a means of controlling the aircraft longitudinally and laterally in hover and low-speed helicopter flight, and to relieve 1/rev blade-root bending moments in the airplane mode. During airplane mode operations a flapping proprotor will develop a flapping angle with respect to a plane normal to the shaft if the aircraft is pitched or yawed, as in a maneuver, or if operated at a steady angle of attack or sideslip, as in trimmed 1g flight. Flapping

during maneuvers performed at high advance ratios can lead to especially large flapping angles because at the large inflow angles associated with high advance ratios the perturbation forces contributing to the precessing moment (ΔF_β in Fig. 2-21) are reduced, and the proprotor must flap more to generate enough moment to precess the proprotor.

When the mast is given an angular displacement with respect to the freestream velocity, cyclic variations in blade section angle of attack are produced. The resulting 1/rev flapping moments cause the tip-path-plane to precess to a new steady-state position relative to the mast such that the aerodynamic moments are either balanced by the hub spring moments (if $K_H \neq 0$) or are zero (if $K_H = 0$).

The value of this steady-state tip-path-plane flapping angle can be written (Appendix D) as a function of ω_β/Ω in the form

$$\frac{\partial \beta}{\partial \alpha_m} = \frac{\lambda^2 A_3}{\left[A_5^2 + \frac{4}{\gamma^2}\left(\bar{\omega}_\beta^2 - 1\right)^2\right]^{1/2}} \tag{4-9}$$

where, using Eq. 4-1,

$$\bar{\omega}_\beta^2 - 1 = \frac{K_H}{I_R \Omega^2} + \frac{1}{2}\gamma B_3 \tan \delta_3 \tag{4-10}$$

Under oscillatory conditions the flapping derivatives, like the force and moment derivatives, are mathematically complex quantities having components proportional to both pitch angle and pitch rate.

Considerations other than flapping per se dictate that some means be employed to reduce the flapping amplitude during airplane mode operations. Several means for reducing flapping are available to the designer (Ref. 4-7). These include the use of flapping restraint, hinge offset, pitch-flap coupling, and blade pitch control feedback mechanisms. The first three reduce flapping by detuning the blade flapping natural frequency from 1/rev according to Eq. 4-9, thereby removing it from 1/rev resonance with the cyclic airloads due to shaft angle of attack. The influence of several of these methods will be presented below. Results were obtained using computer program ROTDER4 which is based on the analysis developed in Appendix D and are presented following the sign convention indicated in Fig. 4-14.

The variation of the total flapping derivative $\partial\beta/\partial\alpha_m$ with airspeed* and the effectiveness of δ_3 in reducing flapping are brought out in Fig. 4-24. If no δ_3 is employed the flapping derivative increases rapidly with airspeed. Positive δ_3 is seen to be somewhat more effective in reducing flapping than negative δ_3.

The effects of δ_3 on $\partial\beta/\partial\alpha_m$ for a fixed airspeed are illustrated in Fig. 4-25. For zero hub restraint the flapping curve is symmetric about $\delta_3 = 0$ and both positive and negative δ_3 are just as effective in reducing flapping. This can also be seen with reference to Eqs. 4-9 and 4-10. However, K_H in

*δ_3 was held fixed as airspeed was increased.

conjunction with negative δ_3 reduces the effectiveness of negative δ_3 while K_H in conjunction with positive δ_3 increases the effectiveness of positive δ_3.

The left result in Fig. 4-26 indicates that large values of flapping restraint are quite effective in reducing flapping. However, as pointed out earlier, blade loads generally limit the maximum flapping restraint which can be employed in practice. Pitch-flap coupling (δ_3) has a negligible effect on blade loads and can be equally effective in reducing flapping, as reference to the result in the right half of Fig. 4-26 will verify.

The tip-path-plane derivatives corresponding to Fig. 4-26 are given in Fig. 4-27 as a function of the flapping natural frequency. The sign of the longitudinal tip-path-plane derivative $\partial a_1/\partial \alpha_m$ is constant with ω_β/Ω such that the rotor disc is flapped aft at the top for a nose-up pitch attitude. A reversal in the sign of the lateral flapping derivative $\partial b_1/\partial \alpha_m$ occurs at a flapping frequency of 1/rev. As the sketches indicate, below 1/rev the tip-path-plane is flapped laterally outboard, away from the wing leading edge while for ω_β/Ω > 1/rev the tip-path-plane flaps laterally inboard toward the wing leading edge. Since 1g trimmed cruise flight will result in some positive mast angle of attack, wing/rotor 3/rev aerodynamic interference and attendant vibrations are minimized if the tip-path-plane flaps away from the wing leading edge (assuming cyclic pitch is not available for this purpose). On this basis, if $\omega_\beta/\Omega > 1$ the proprotors should turn inboard-down, and

if $\omega_\beta/\Omega < 1$, inboard-up. The effective dihedral is also increased if $\omega_\beta/\Omega < 1$ and the direction of rotation is inboard-up. Note that as ω_β/Ω is increased both $\partial a_1/\partial \alpha_m$ and $\partial b_1/\partial \alpha_m$ approach zero, as they should for the limiting case of a propeller.

The frequency response characteristics of the tip-path-plane flapping derivatives are illustrated in Fig. 4-28. As pylon pitch frequency is increased from zero the magnitude and phase of the derivatives vary considerably. The crests and troughs evident in the response curves occur at the fixed system flapping mode frequencies. At high pylon frequencies $\partial b_1/\partial \alpha_m$ approaches zero and $\partial a_1/\partial \alpha_m$ approaches the negative of the pylon pitch angle. As pointed out earlier this is a consequence of the pylon oscillating too fast for the rotor to respond and the tip-path-plane remains essentially fixed in space. Both $\partial a_1/\partial q$ and $\partial b_1/\partial q$ approach zero with increasing frequency.

The effect of employing a swashplate/pylon coupling ratio of +1.0 in conjunction with a control phasing equal to the δ_3 angle are included in Fig. 4-28 for the case of zero pylon pitch frequency. $\partial a_1/\partial \alpha_m$ is seen to be about equal to the negative of the pitch angle indicating that the tip-path-plane is vertically oriented in space. $\partial b_1/\partial \alpha_m$ is almost zero so there is little lateral flapping.

The flapping behavior of a proprotor at low rpm, such as that which might be experienced during the feathering sequence of transition for a folding proprotor aircraft, constitutes an impor-

tant design consideration. For $\omega_\beta/\Omega = 1.0$, Eq. 4-9 becomes

$$\frac{\partial \beta}{\partial \alpha_m} = \lambda^2 \frac{A_3}{A_5} = 1.8\ \lambda^2 \qquad (4\text{-}11)$$

As the proprotor slows down the inflow angle increases and flapping sensitivity to changes in shaft angle of attack increases rapidly in accordance with Eq. 4-11. Fig. 4-29 gives an indication of the flapping sensitivity to angle of attack as a function of rotor rpm for three values of δ_3. Steady-state values are given. The peaks in the response curves occur when the rotor rpm is in resonance with the blade flapping natural frequency, the maximum amplitudes being determined by the amount of flap damping.

CITED REFERENCES

4-1. Young, M. I., and R. T. Lytwyn: "The Influence of Blade Flapping Restraint on the Dynamic Stability of Low Disk Loading Propeller-Rotors", Journal of the American Helicopter Society, October 1967.

4-2. Hall, W. E.: "Prop-Rotor Stability at High Advance Ratio", Journal of the American Helicopter Society, June 1966.

4-3. Gaffey, T. M.: "The Effect of Positive Pitch-Flap Coupling (Negative δ_3) on Rotor Blade Motion Stability and Flapping", Journal of the American Helicopter Society, April 1969.

4-4. Wernicke, K. G.: "Tilt Proprotor Composite Aircraft, Design State of the Art", Journal of the American Helicopter Society, April 1969.

4-5. Exploratory Definition Final Report, Model 266 Composite Aircraft Program, Bell Helicopter Company, Report Nos. 266-099-201 through 223, July 1967.

4-6. Hohenemser, K. H.: "On a Type of Low-Advance-Ratio Blade Flapping Instability of Three-or-More Bladed Rotors Without Drag Hinges", Proc. of the 13th Annual National Forum of the American Helicopter Society, May 1957.

4-7. Gaffey, T. M., J. G. Yen, and R. G. Kvaternik: "Analysis and Model Tests of the Proprotor Dynamics of a Tilt-Proprotor VTOL Aircraft", Presented at the Air Force V/STOL Technology and Planning Conference, Las Vegas, Nevada, September 1969.

4-8. Rao, K. V. K., and D. Sundararajan: "Whirl Flutter of Flapped Blade Rotor Systems", NAL TN-18, October 1969.

4-9. Reed, W. H., III, and S. R. Bland: "An Analytical Treatment of Aircraft Propeller Precession Instability", NASA TND-659, 1961.

4-10. Houbolt, J. C., and W. H. Reed, III: "Propeller-Nacelle Whirl Flutter", Journal of the Aerospace Sciences, March 1962.

4-11. Sewall, J. L.: "An Analytical Trend Study of Propeller Whirl Instability", NASA TND-996, April 1962.

4-12. Edenborough, H. K.: "Investigation of Tilt-Rotor VTOL Aircraft Rotor-Pylon Stability", Journal of Aircraft, March-April, 1968.

TABLE 4-1

MODEL 266 DESIGN PARAMETERS

WEIGHTS	
Design Gross Weight	28000 lb
Payload	6600 lb
VTOL Overload Gross	35000 lb
STOL Overload Gross	40000 lb
PROPROTOR SYSTEM	
Direction of Rotation	Inboard Up
Diameter	38.5 ft
Chord	1.92 ft
Number Blades/Proprotor	3
Disc Loading (Hover, DGW)	12.0 lb/ft^2
Solidity	.095
RPM Schedule	
Helicopter Mode	387-408 rpm
Conversion Mode	298-382 rpm
Airplane Mode	238-298 rpm
Lock Number	4.54
Pitch-Flap Coupling (δ_3)	Max -22.5°
	Min -18°
Maximum Flapping Angle	± 9.5°
Blade Aerodynamic Twist	-43.5°
Longitudinal Hub Restraint	1500 ft-lb/deg
Lateral Hub Restraint	250 ft-lb/deg
WING SYSTEM	
Span	49.6 ft
Taper Ratio (c_r/c_t)	1.1
Airfoil Section	
Root Chord	NACA 64A223
Tip Chord	NACA 64A219
Wing Loading (DGW)	73.3 lb/ft
Aspect Ratio	6.43
Forward Sweep (1/4 chord)	6.2°
DESIGN FACTORS (DGW)	
Airspeed (knots)	V_C V_L
Helicopter	160 184
Conversion	200 230
Airplane	360 414
Limit Load Factor	
Helicopter	+2.5g,-.5g
Conversion	+2.5g,-.5g
Airplane	+4.0g,-1.0g

TABLE 4-2

PHYSICAL PARAMETERS EMPLOYED IN TREND STUDIES

	M_R	43.8 slugs
	M_P	87.5 slugs
	I_B	791 slug-ft^2
	I_{cg} (pylon)	580 slug-ft^2
	h	6.92 ft*
	$\bar{h}$	2.60 ft
	$\bar{c}$	1.10 ft
	R	19.25 ft
	β_o	0°
	c	1.92 ft
	ρ	.00238 slug-ft^3*
	a_o	5.73
	η_1	0.0
	η_2	1.0
	K_1	0.0*
	ε	0°*
	K_H	Varied
	δ_3	Varied
Pylon support stiffness and damping	K_{pitch}	Varied
	K_{yaw}	Varied
	K_{beam}	Varied
	K_{chord}	Varied
	g	Varied

*Unless noted otherwise

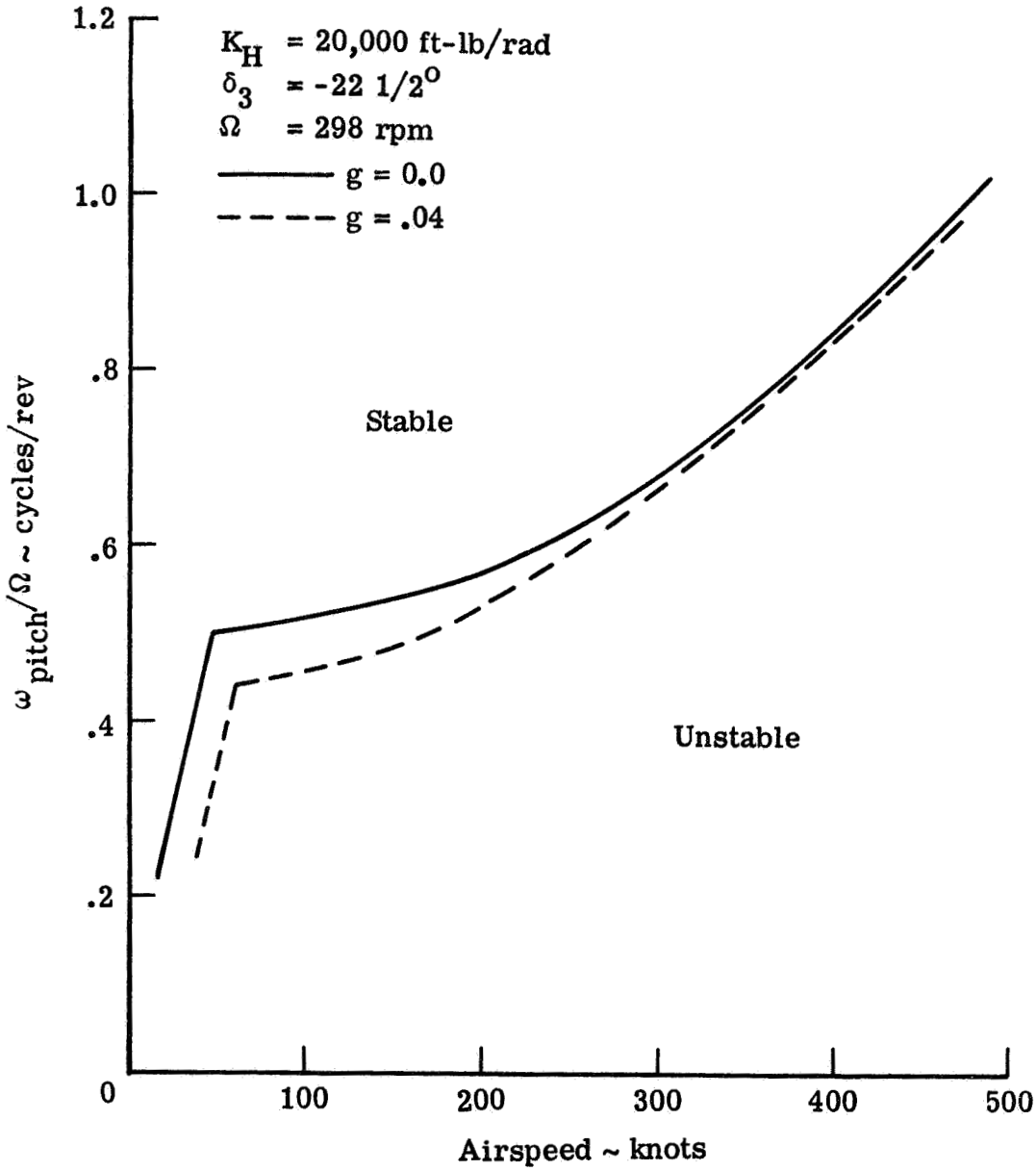

Figure 4-1.- Effect of pylon pitch stiffness on stability.

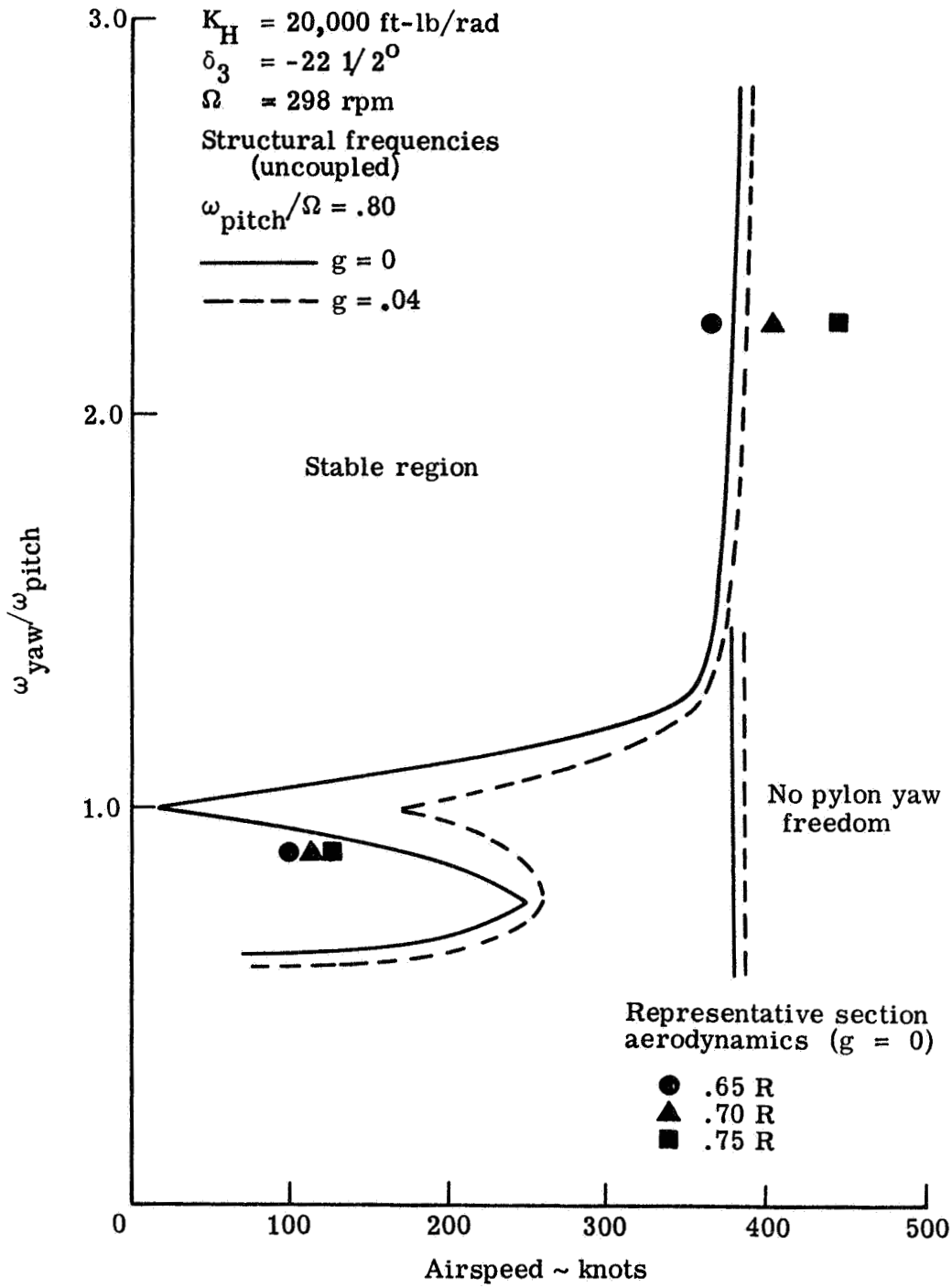

Figure 4-2.- Effect of pylon yaw stiffness on stability.

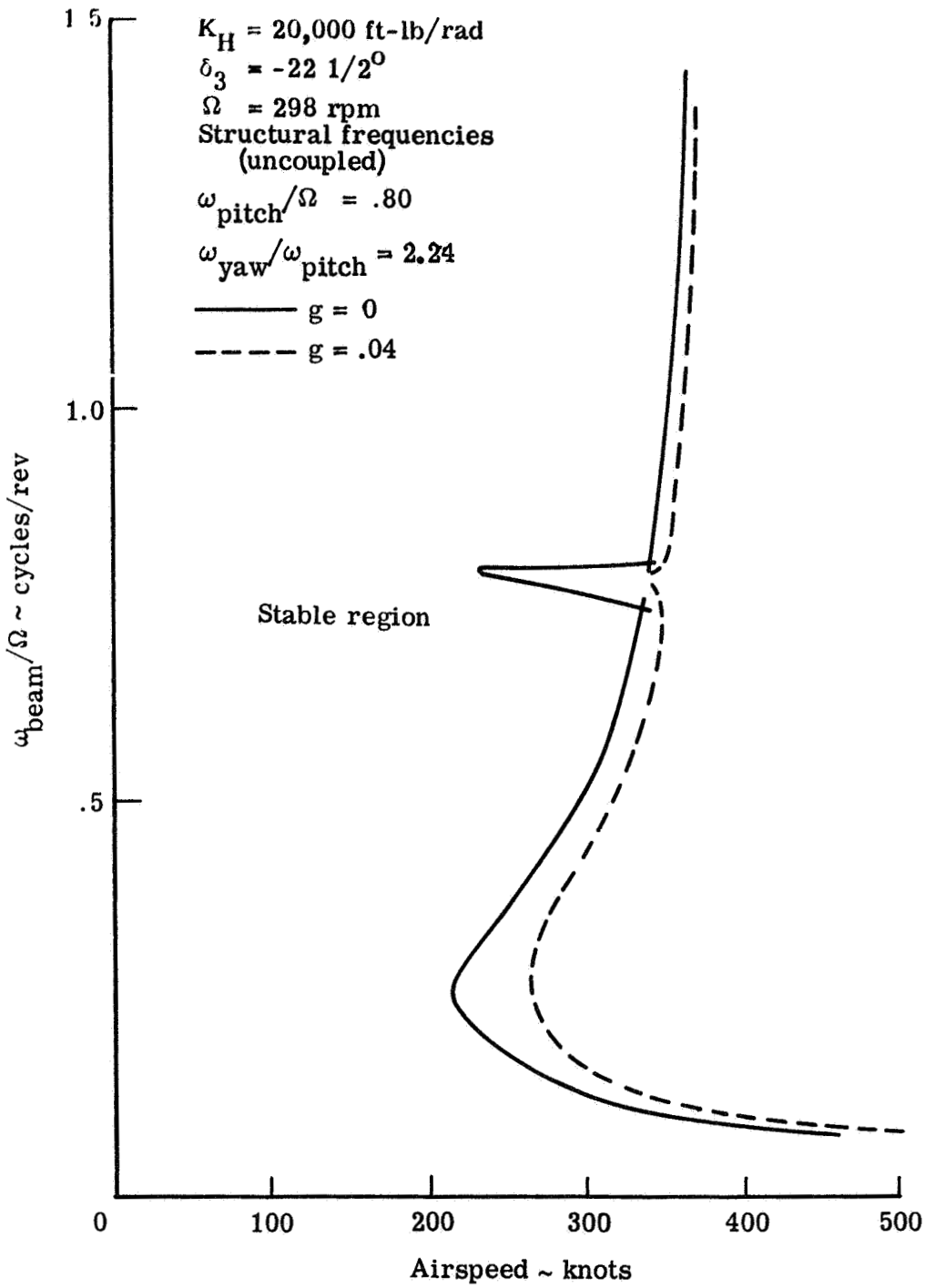

Figure 4-3.- Effect of wing vertical bending stiffness on stability.

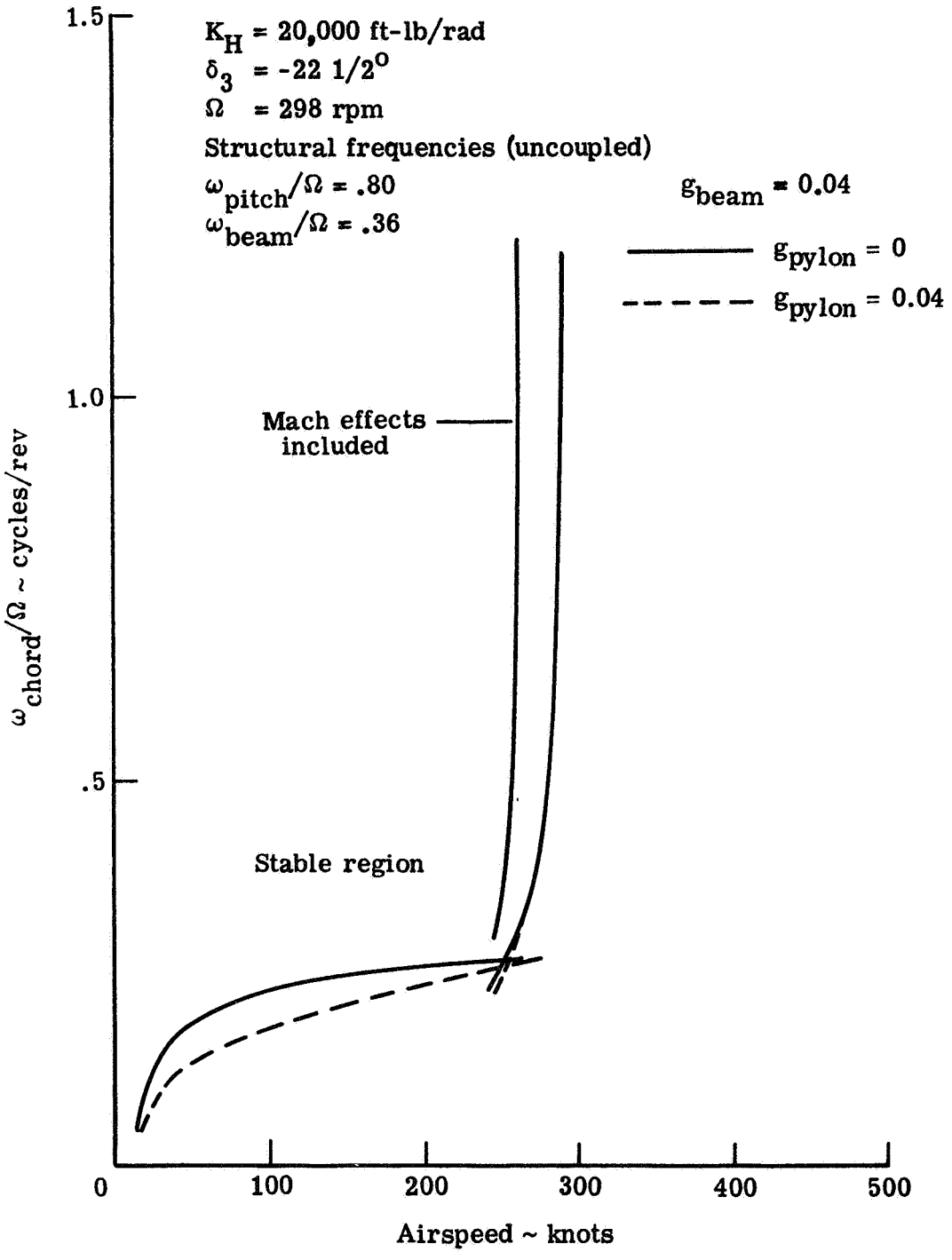

Figure 4-4.- Effect of wing chordwise stiffness on stability.

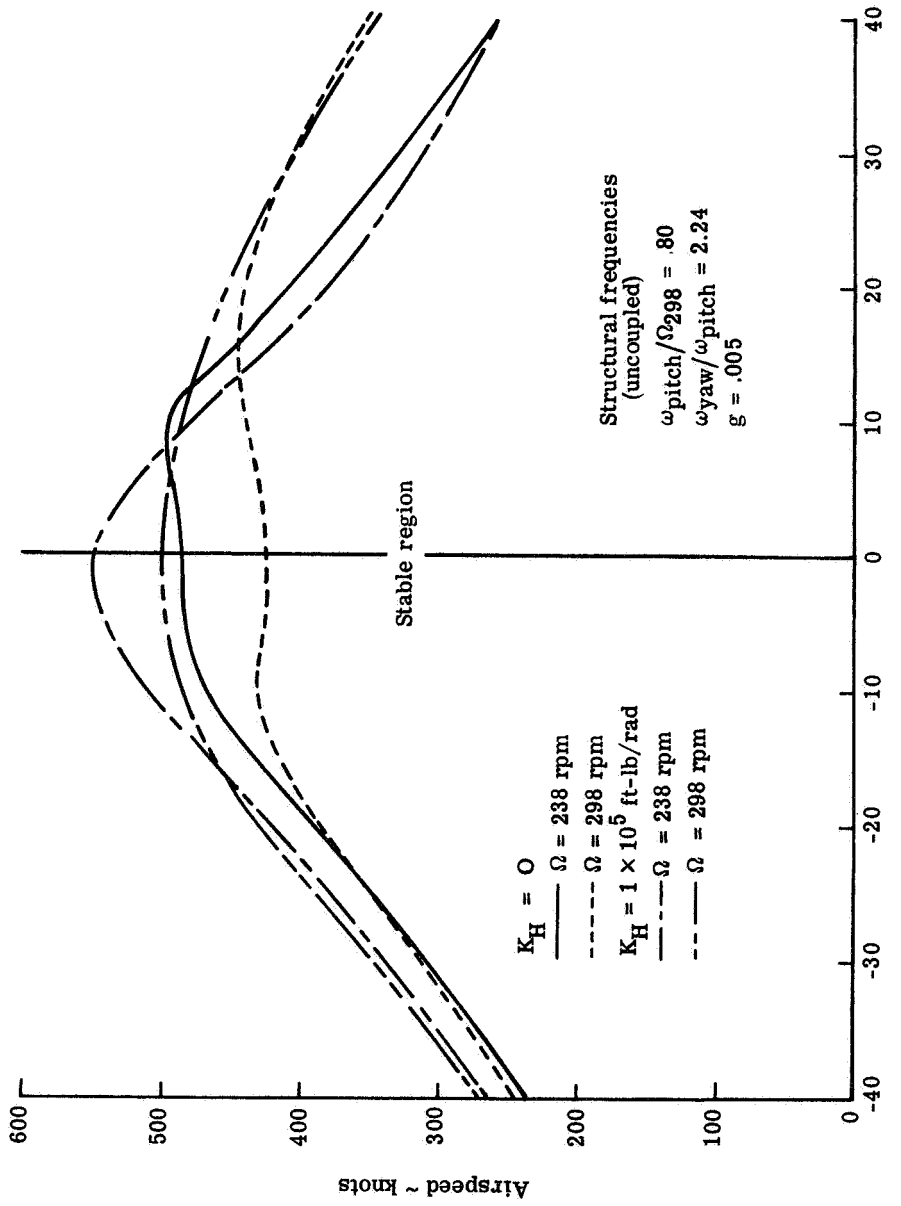

Figure 4-5.- Effect of δ_3 on stability of four degree-of-freedom system.

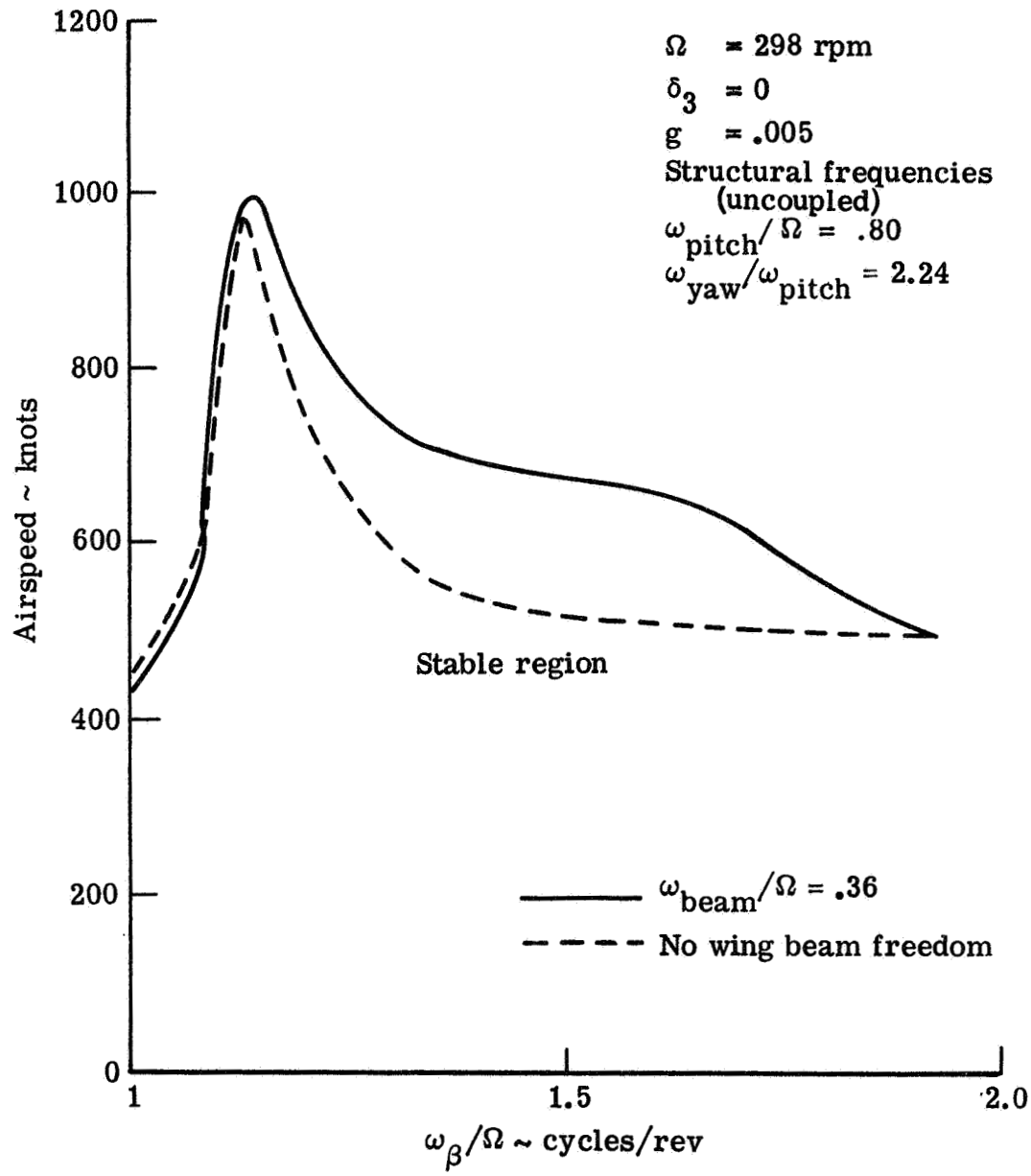

Figure 4-6.- Effect of blade flapping natural frequency on proprotor/pylon stability.

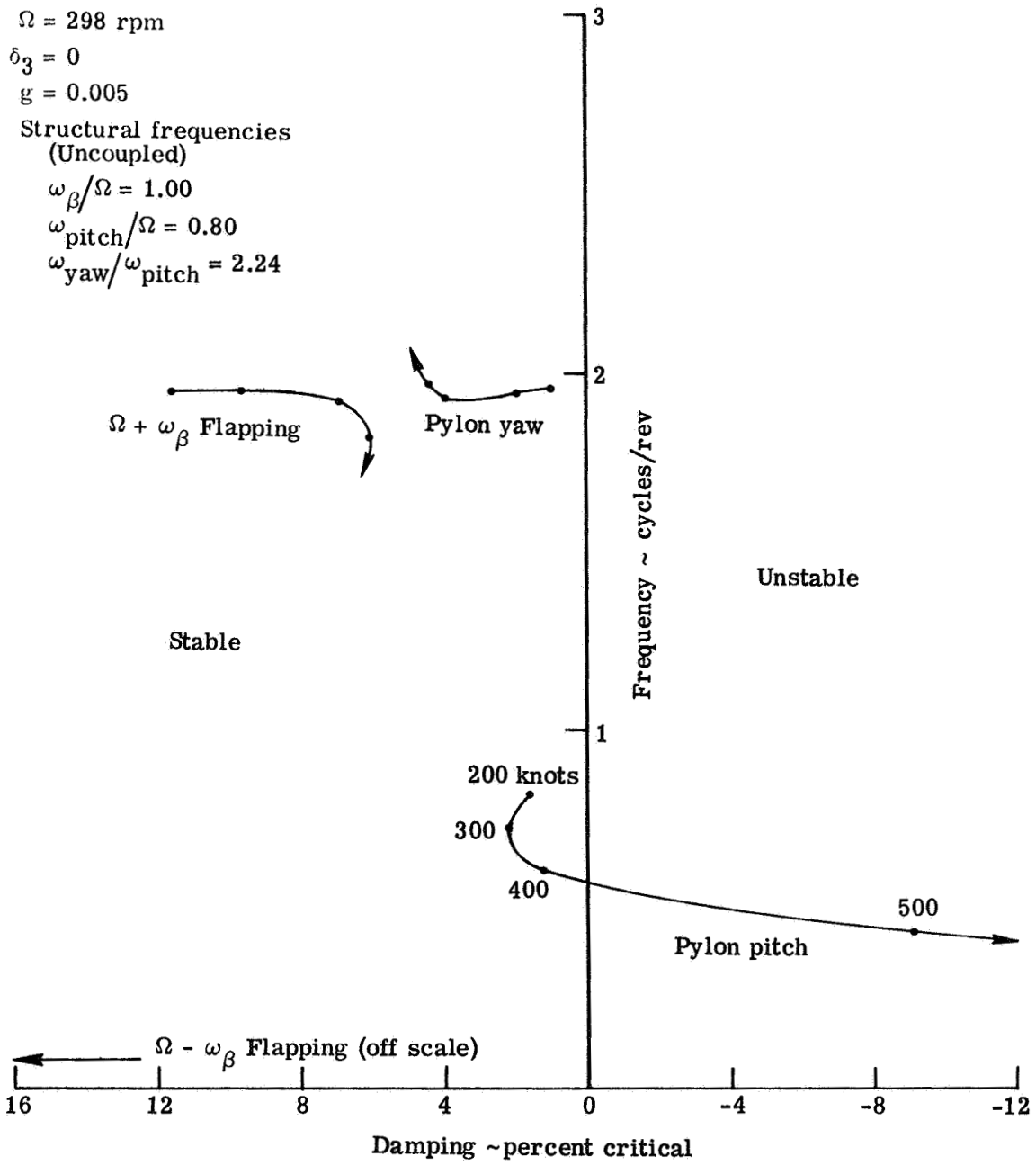

Figure 4-7.- Root locus for four degree-of-freedom proprotor/pylon system ($\omega_\beta/\Omega = 1.00$).

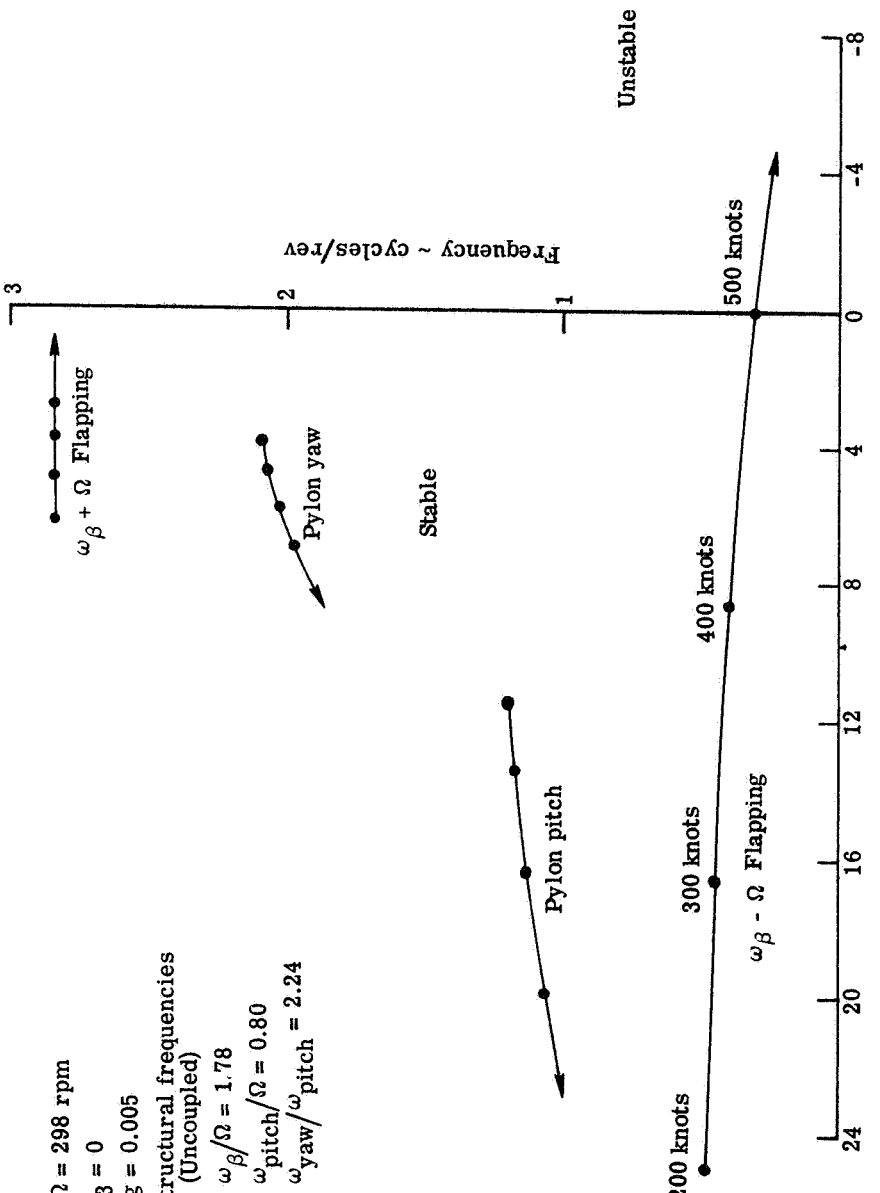

Figure 4-8.- Root locus for 4 degree-of-freedom proprotor/pylon system ($\omega_\beta/\Omega = 1.78$).

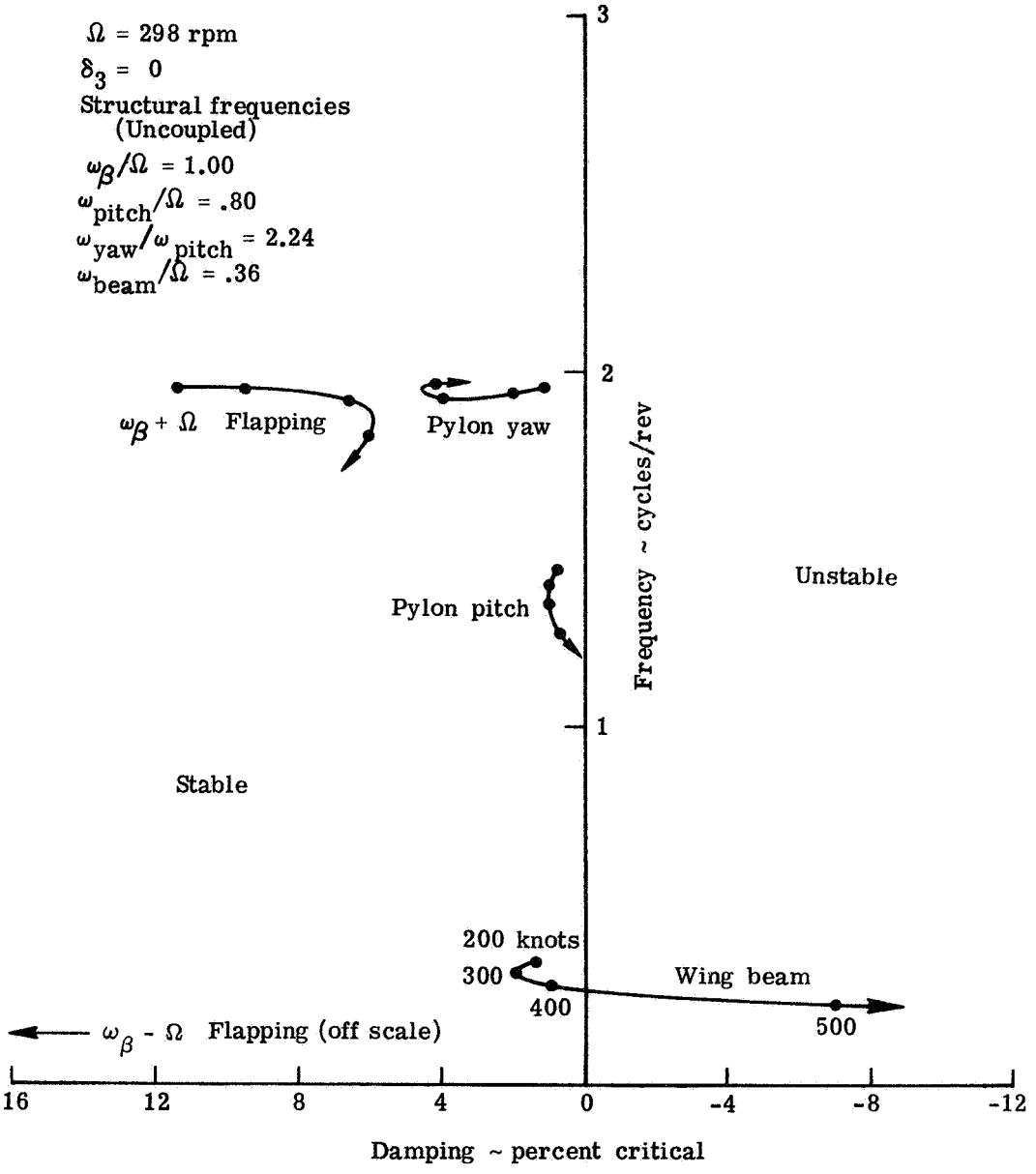

Figure 4-9.- Root locus for five degree-of-freedom proprotor/pylon system ($\omega_\beta/\Omega = 1.00$).

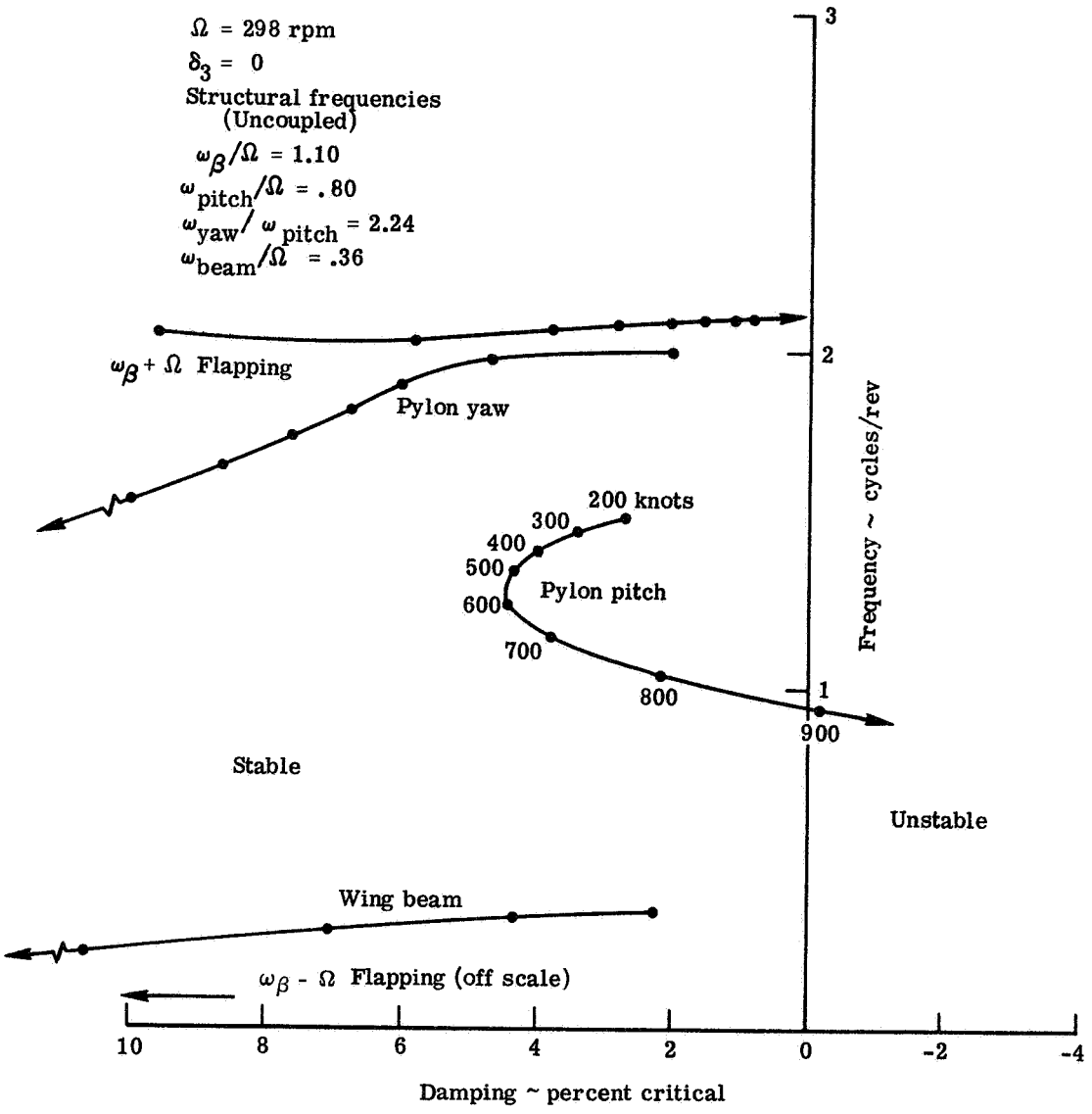

Figure 4-10.- Root locus for five degree-of-freedom proprotor/pylon system (ω_β/Ω = 1.10).

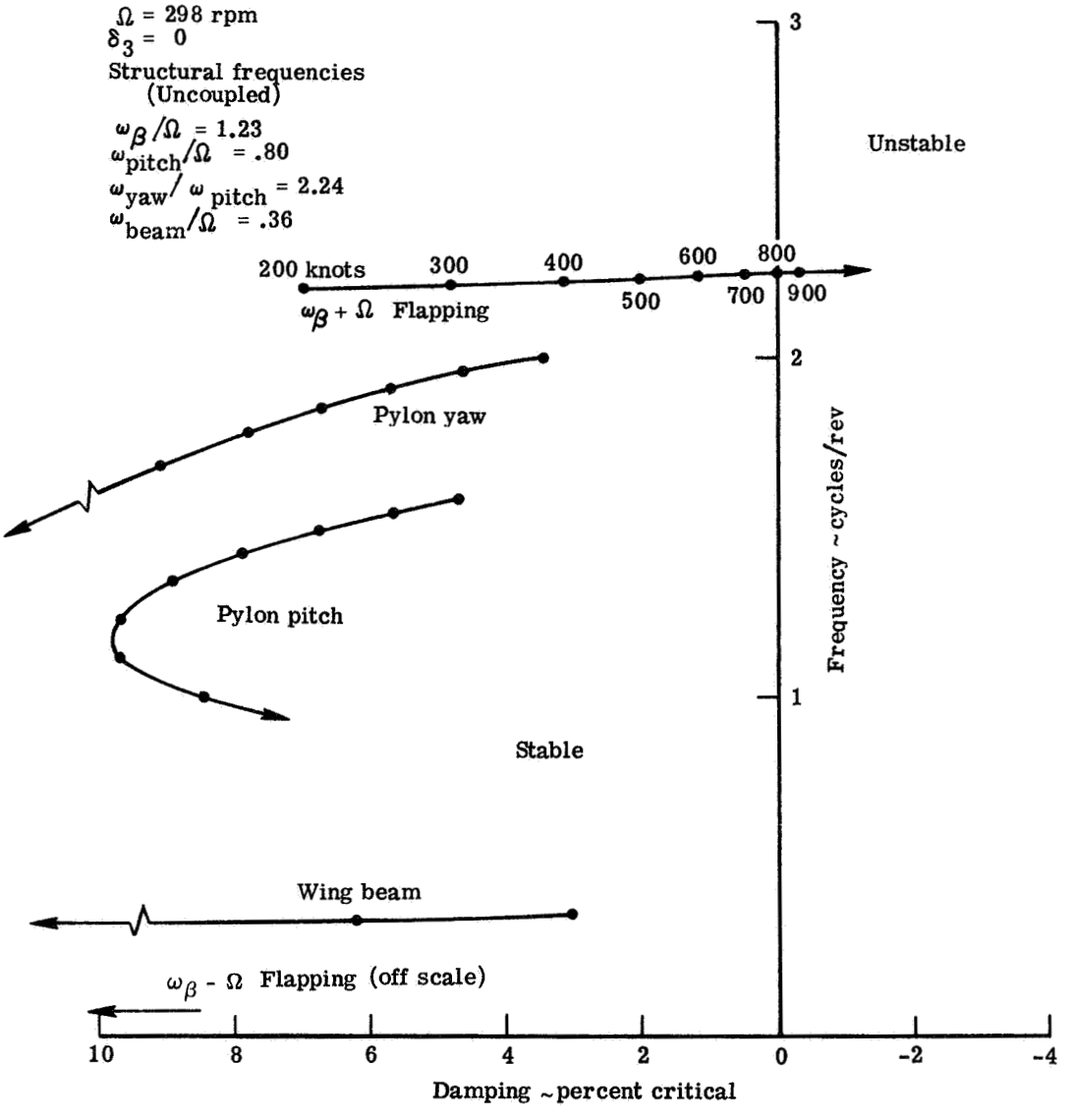

Figure 4-11.- Root locus for five degree-of-freedom proprotor/pylon system ($\omega_\beta/\Omega = 1.23$).

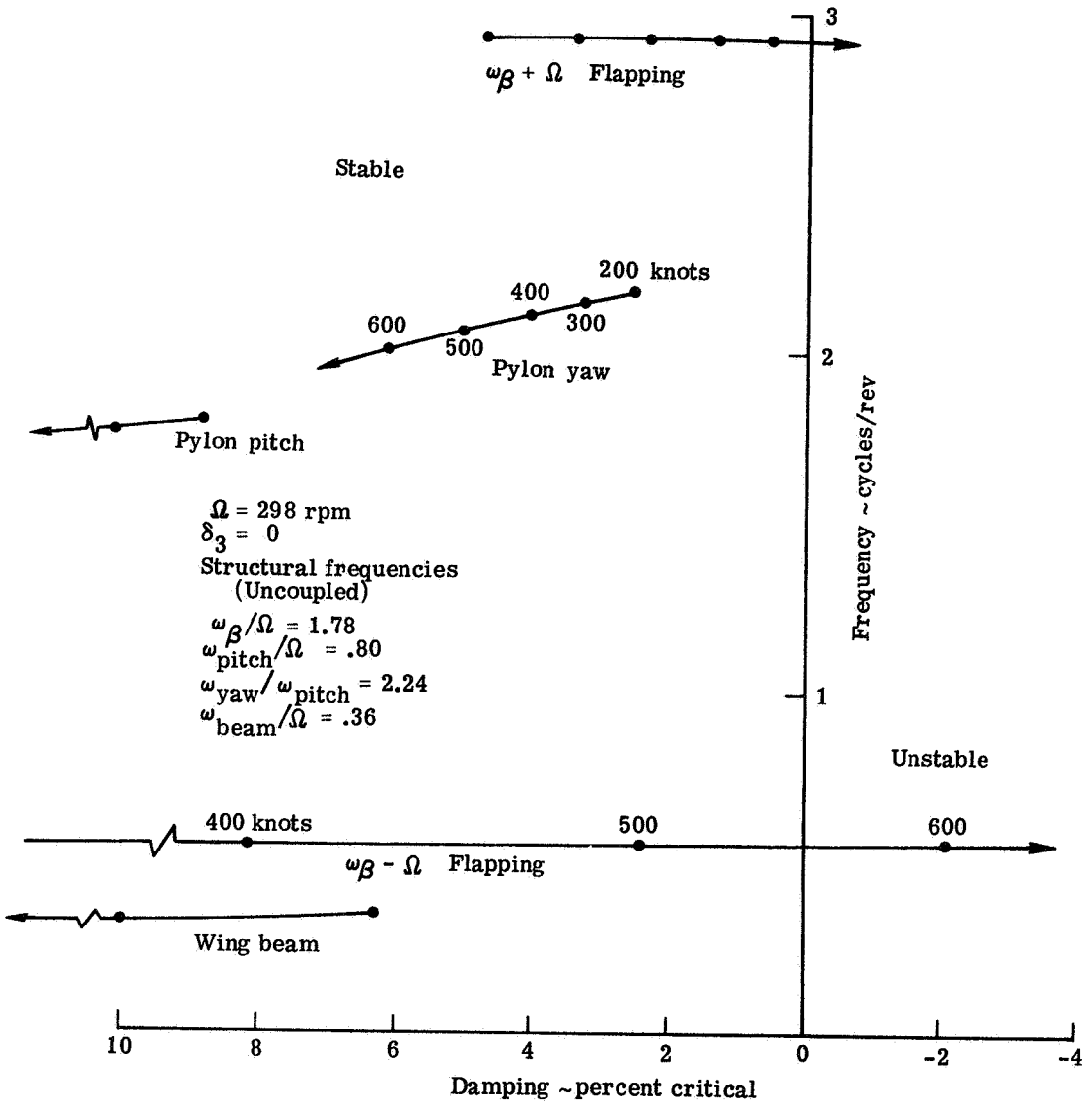

Figure 4-12.- Root locus for five degree-of-freedom proprotor/pylon system (ω_β/Ω = 1.78).

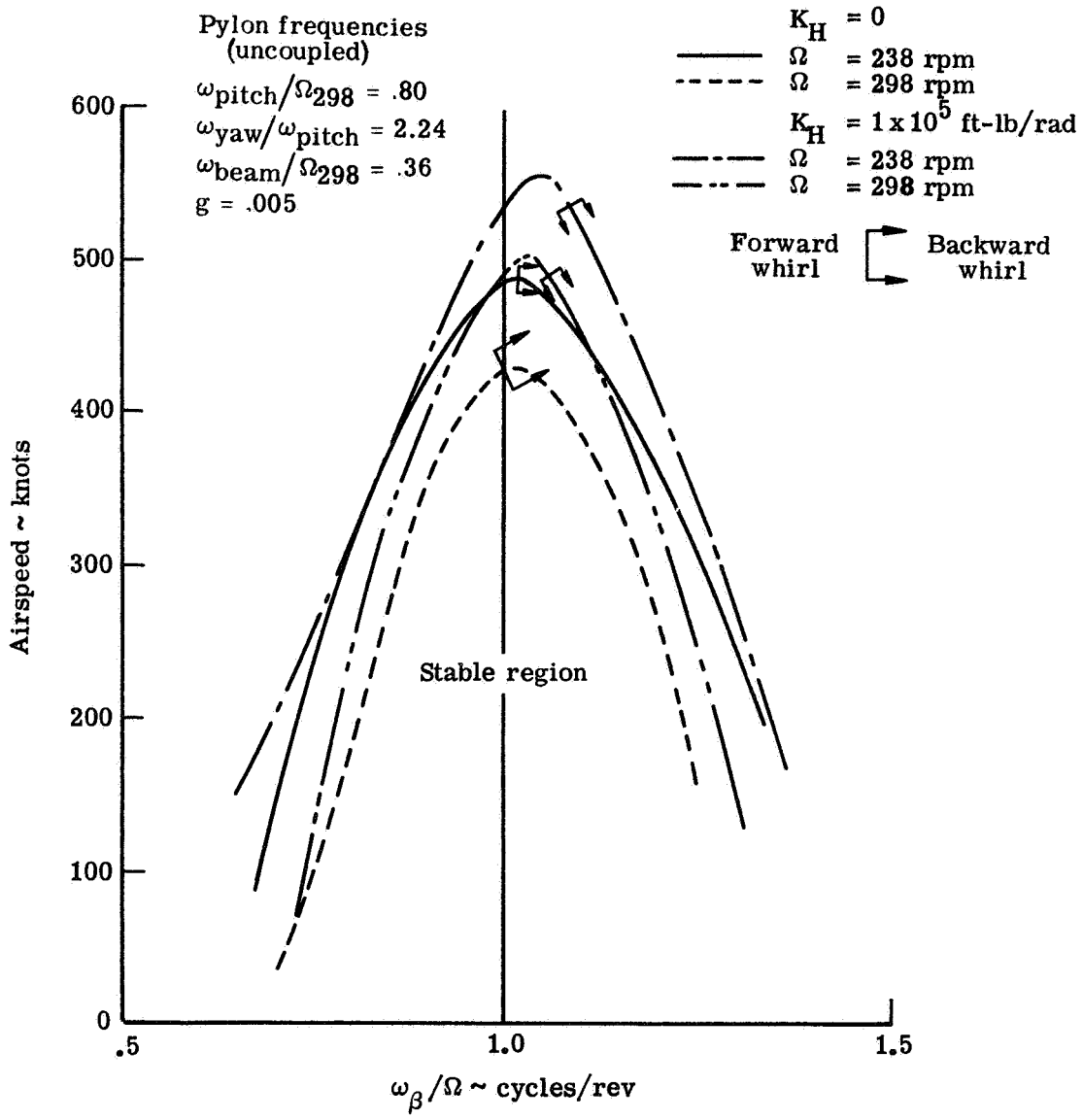

Figure 4-13.- Effect of flapping frequency on stability of five degree-of-freedom proprotor/pylon system.

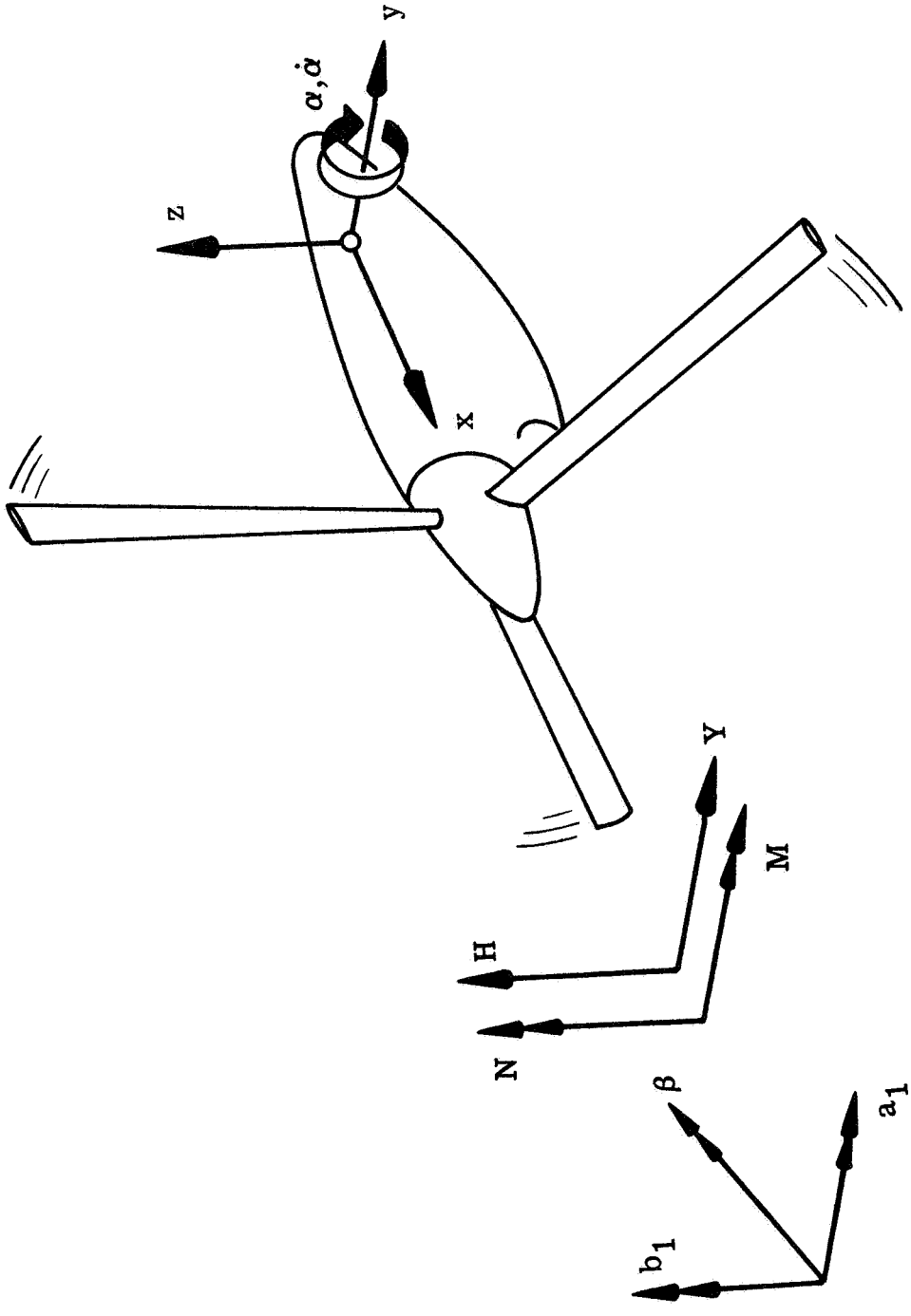

Figure 4-14.- Sign convention employed for presentation of proprotor force and moment derivatives and proprotor flapping derivatives.

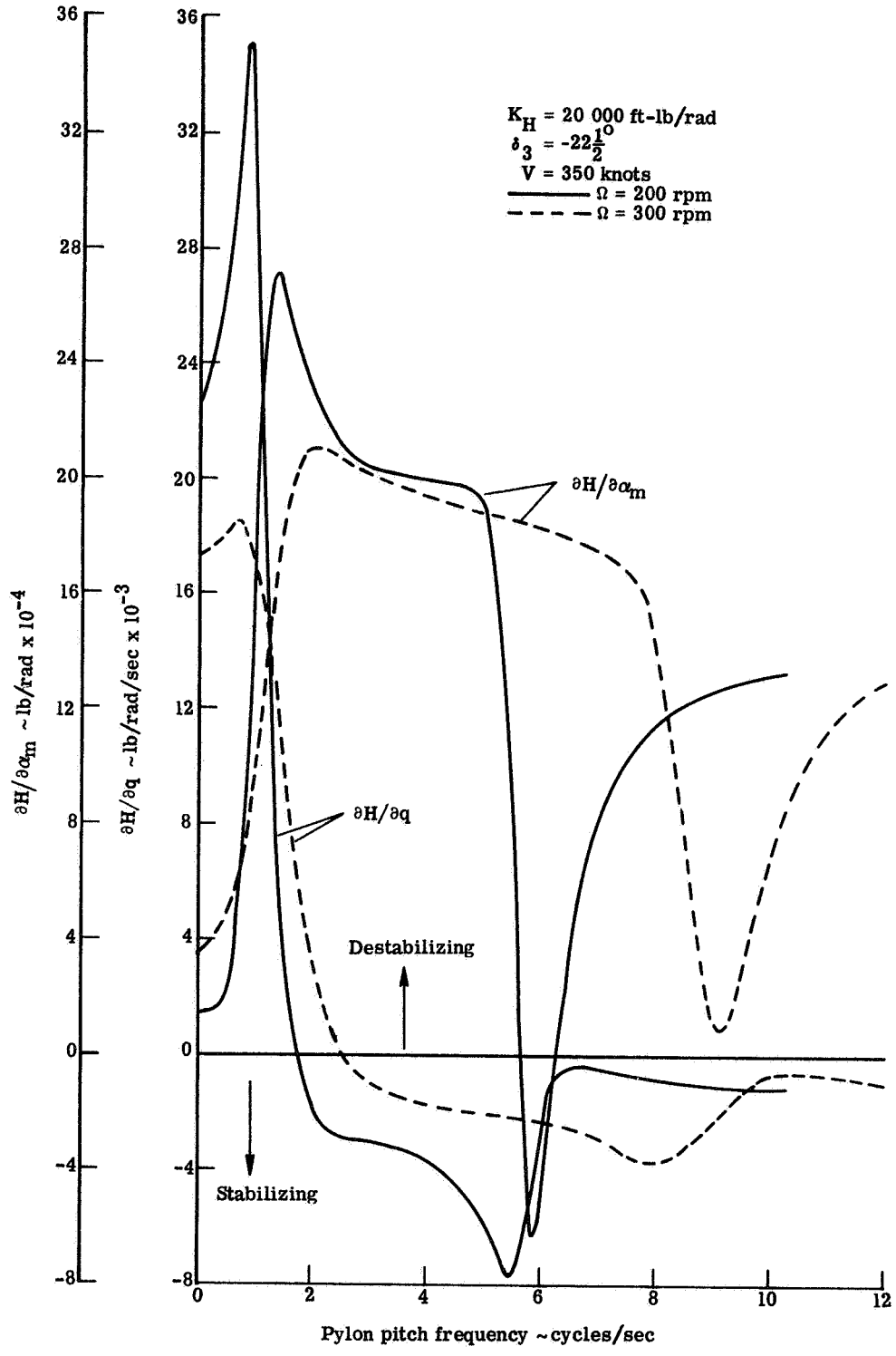

(a) Normal force

Figure 4-15.- Effect of proprotor rotational speed on frequency response of shear force and moment derivatives.

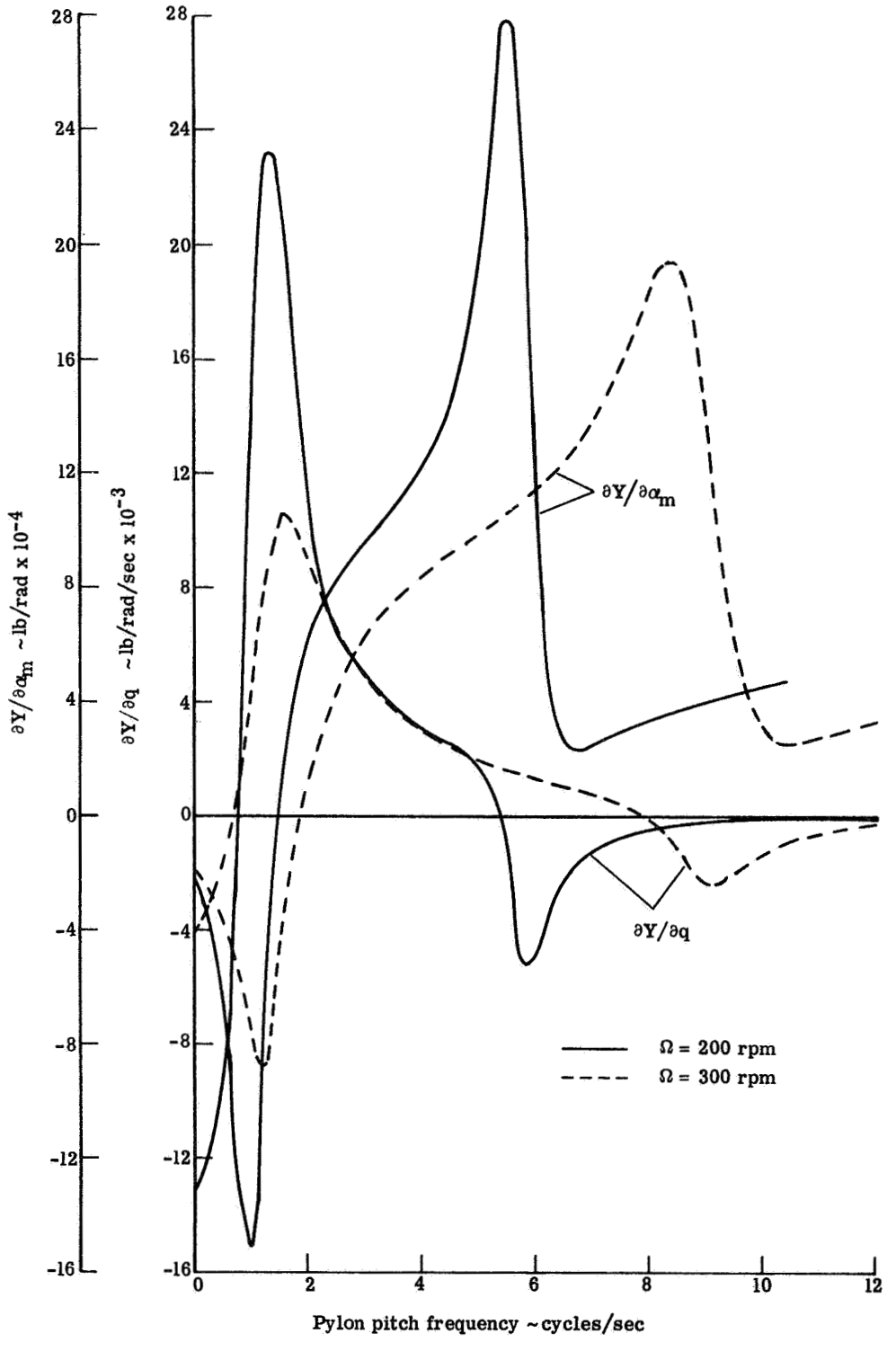

(b) Side force

Figure 4-15.- Continued.

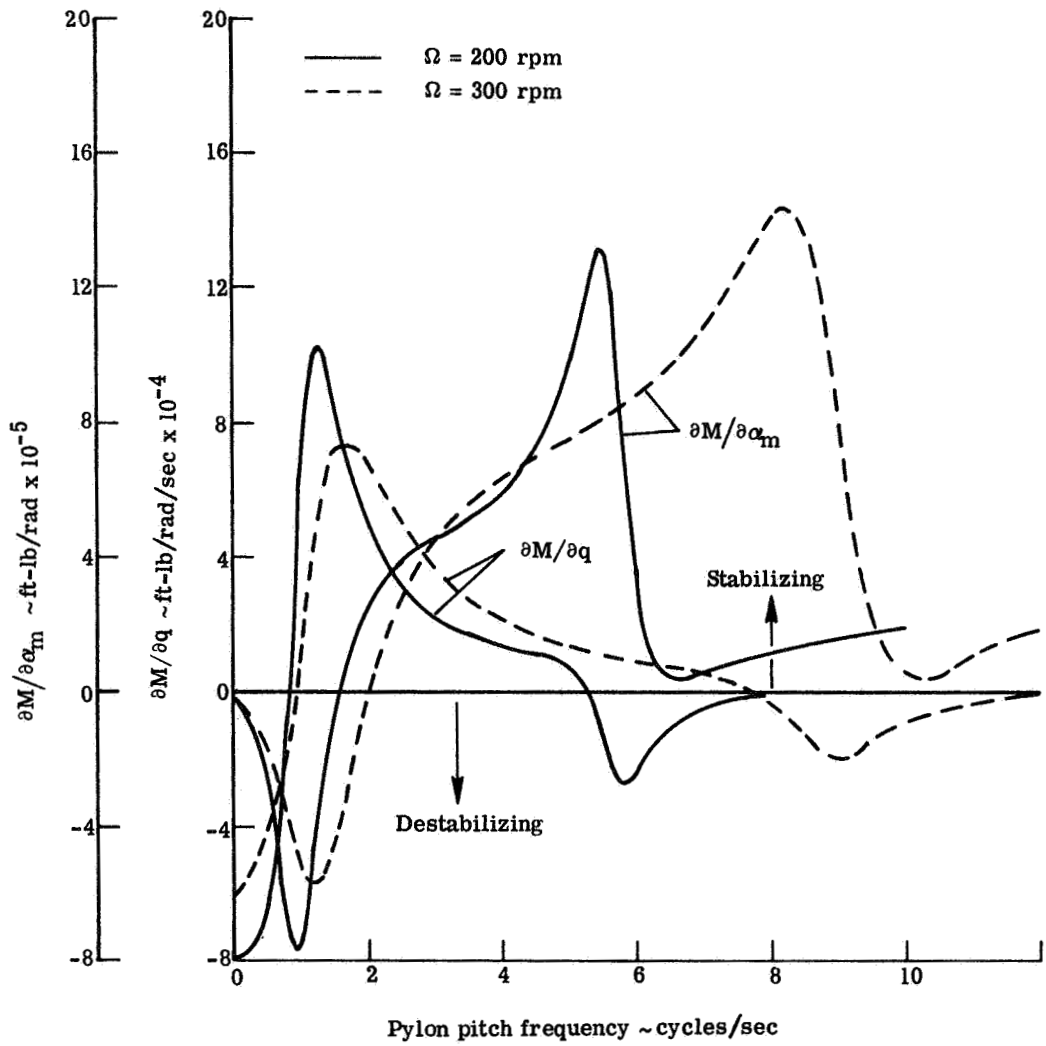

(c) Pitching moment

Figure 4-15.- Continued.

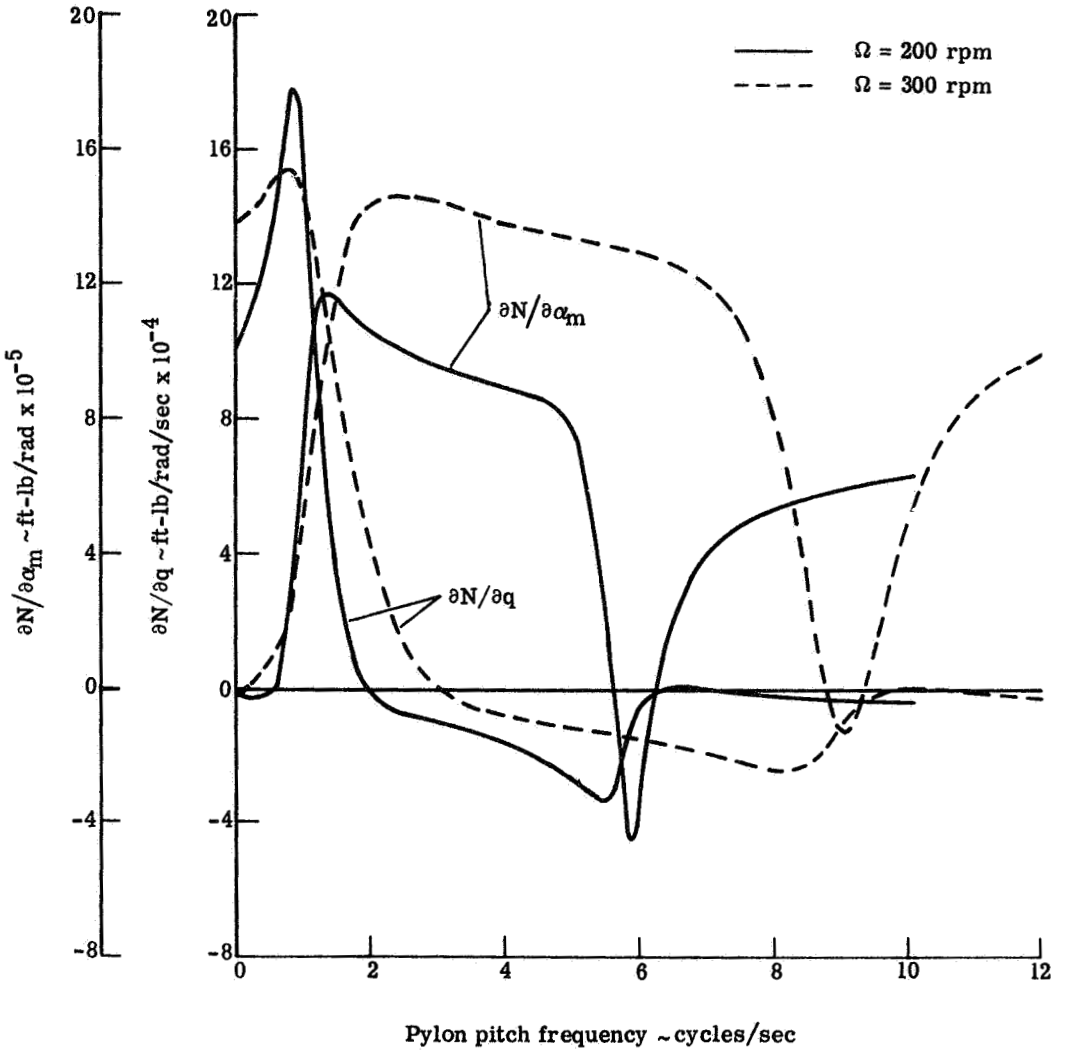

(d) Yawing moment

Figure 4-15.- Concluded.

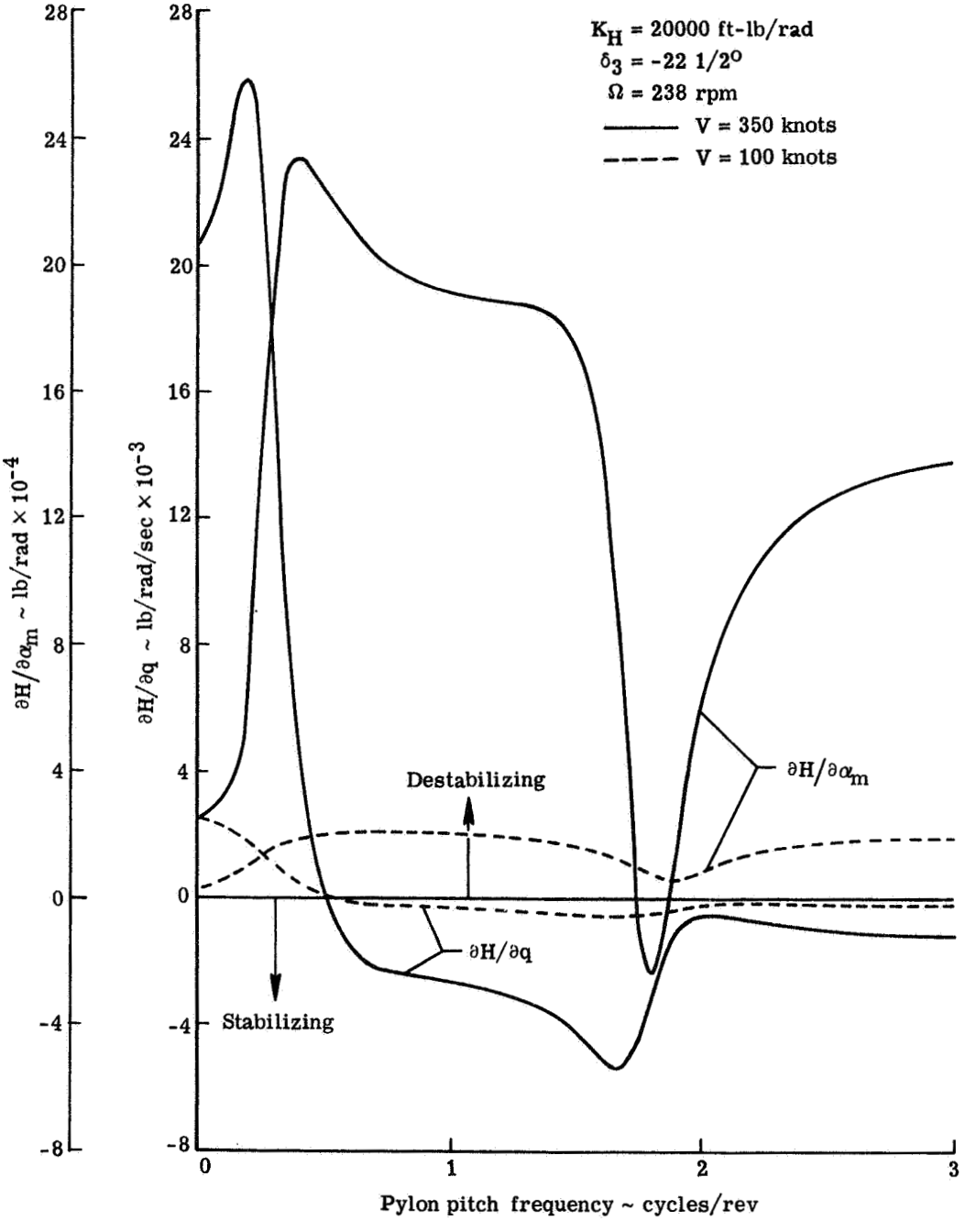

(a) Normal force

Figure 4-16.- Effect of airspeed on frequency response of shear force and moment derivatives.

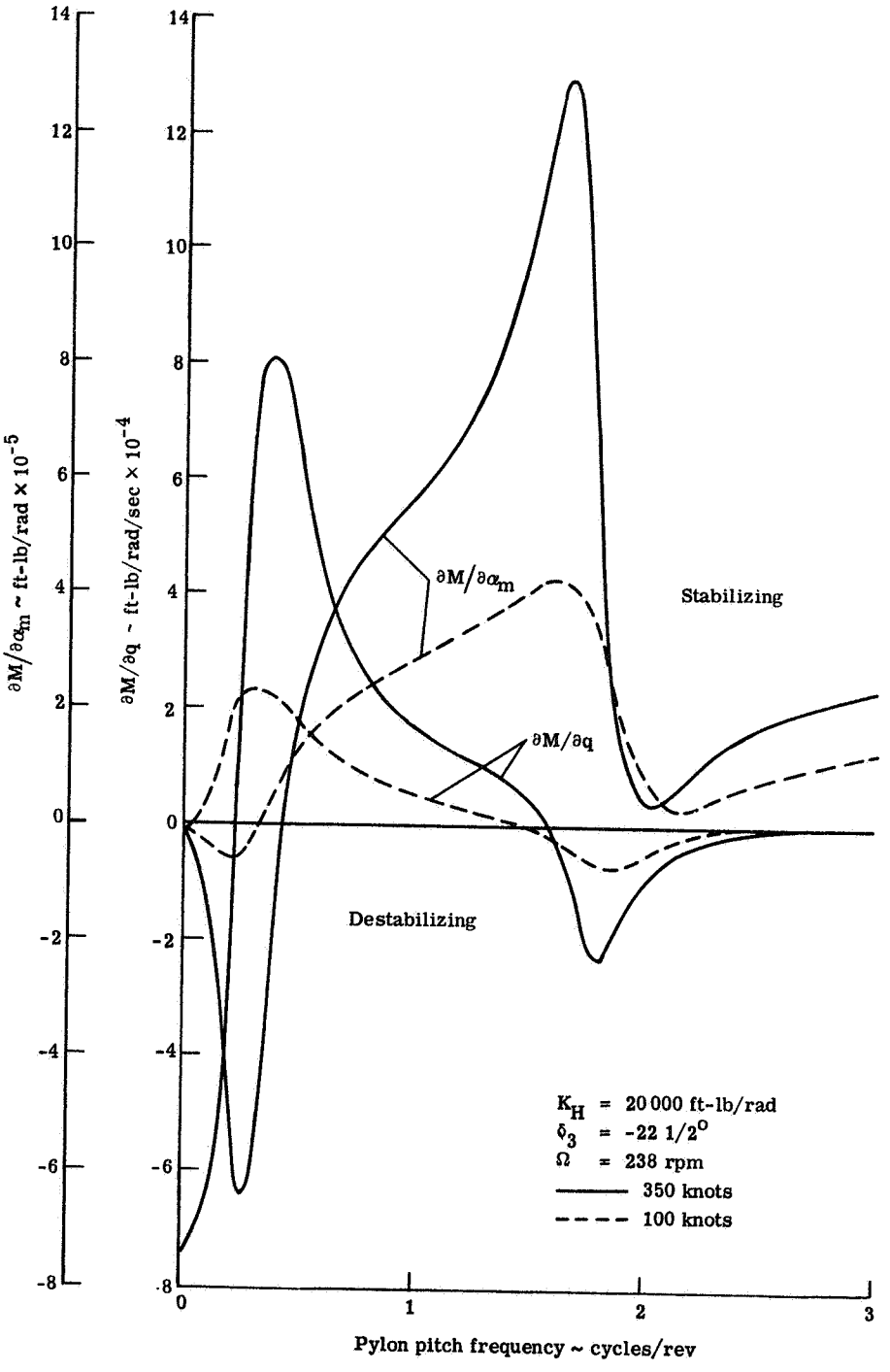

(b) Pitching moment

Figure 4-16.- Concluded.

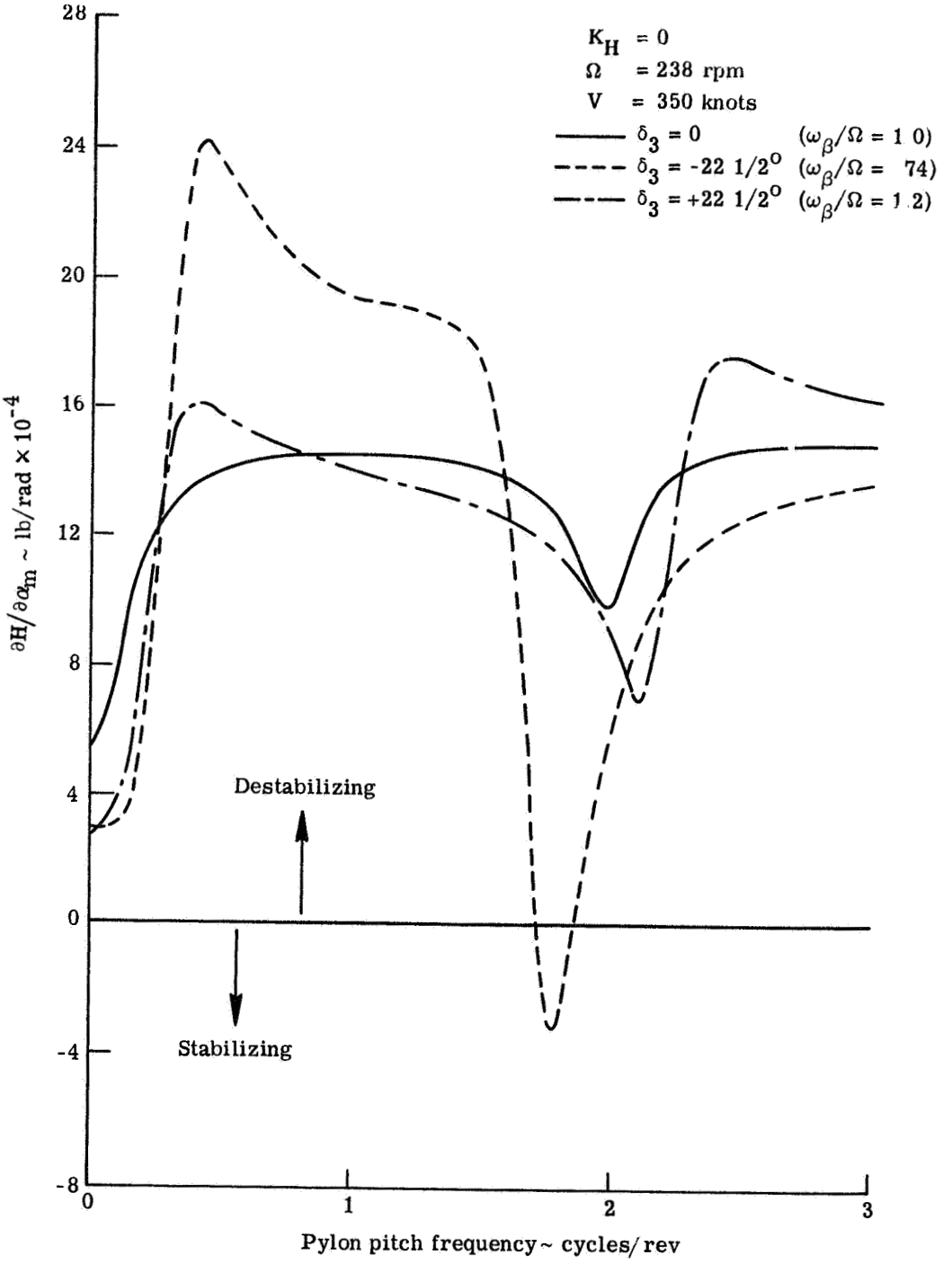

(a) Normal force due to pitch angle.

Figure 4-17.- Effect of δ_3 on frequency response of normal force and pitching moment derivatives.

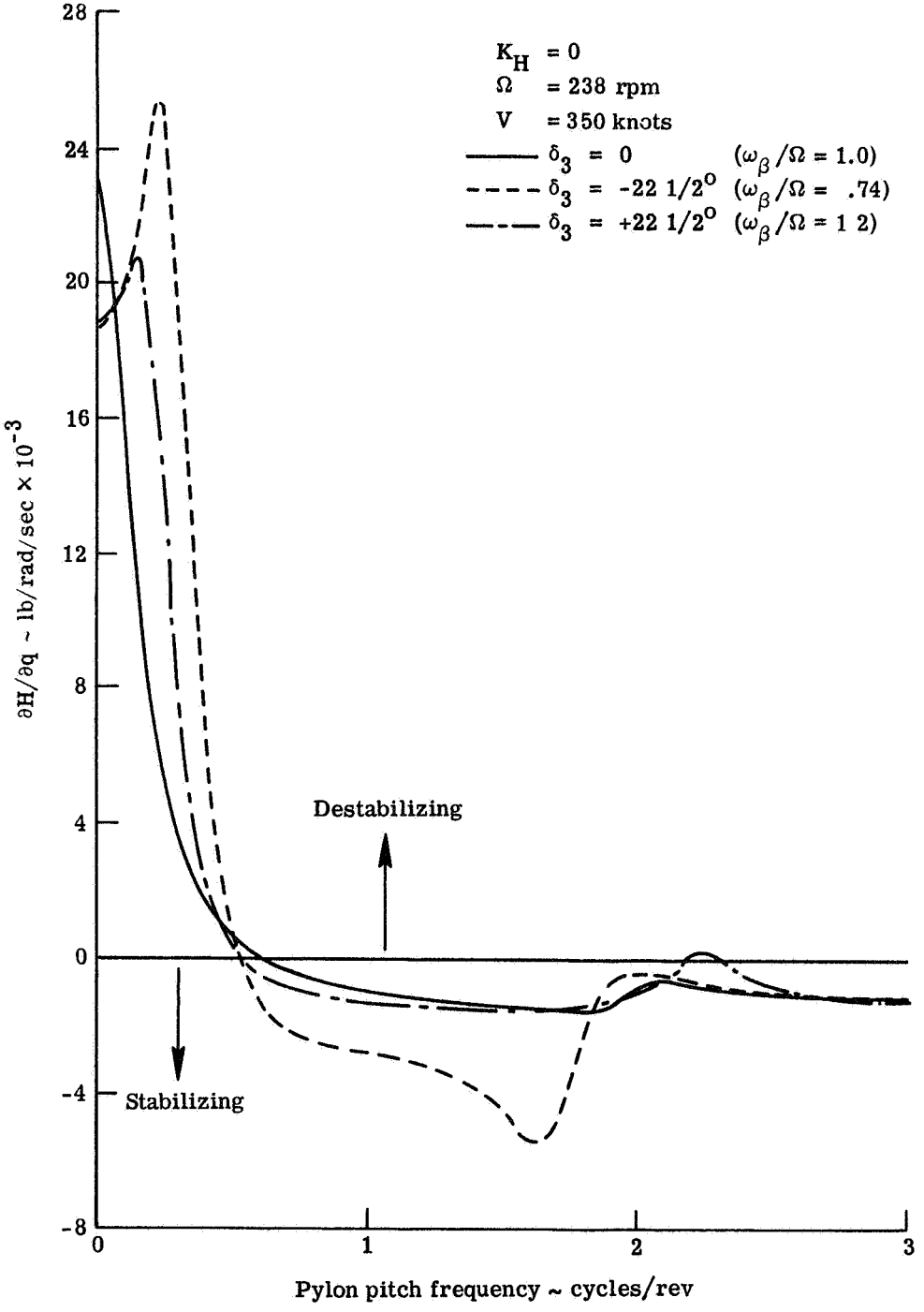

(b) Normal force due to pitch rate.

Figure 4-17.- Continued.

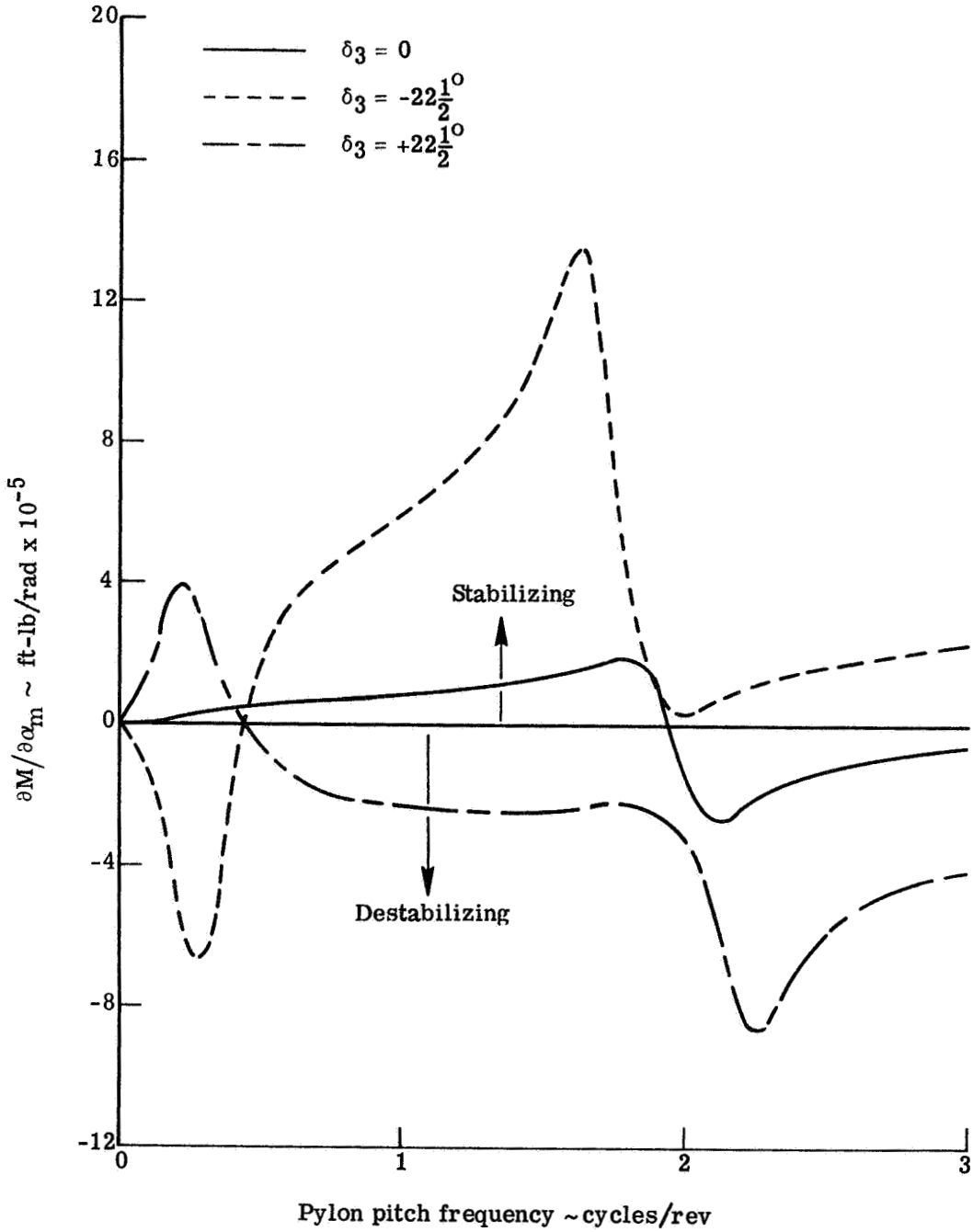

(c) Pitching moment due to pitch angle

Figure 4-17.- Continued.

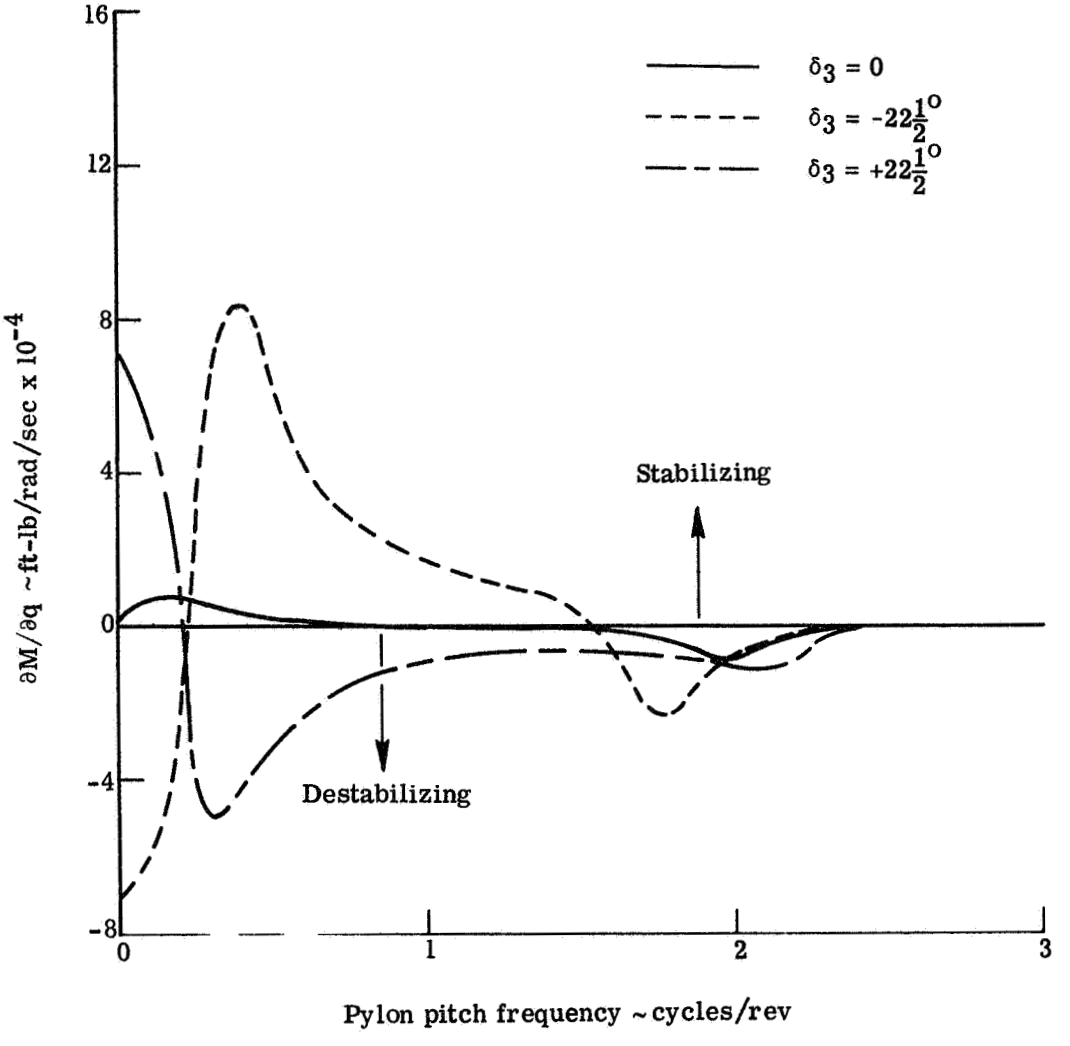

(d) Pitching moment due to pitch rate.

Figure 4-17.- Concluded.

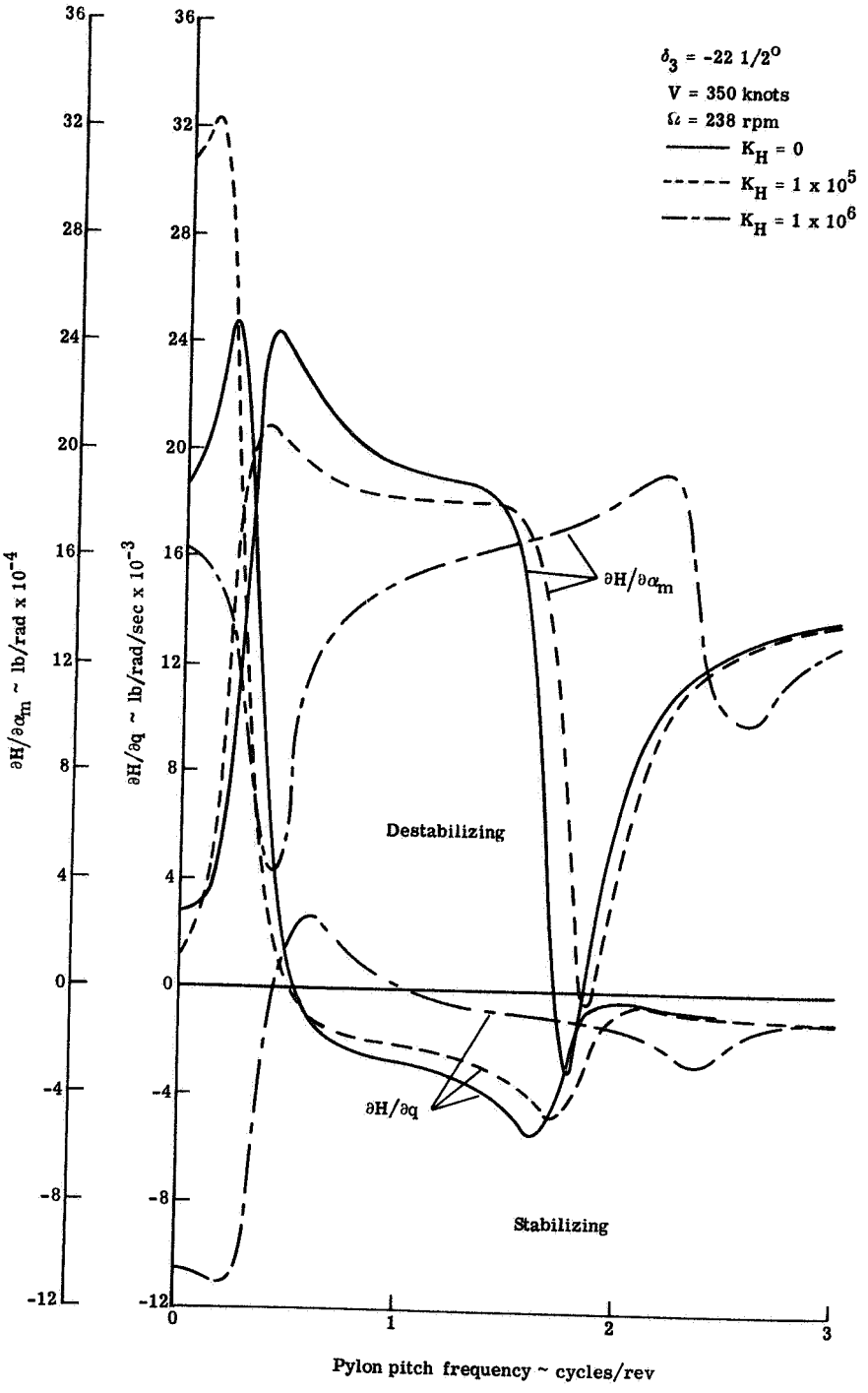

(a) Normal force

Figure 4-18.- Effect of hub restraint on normal force and pitching moment frequency response.

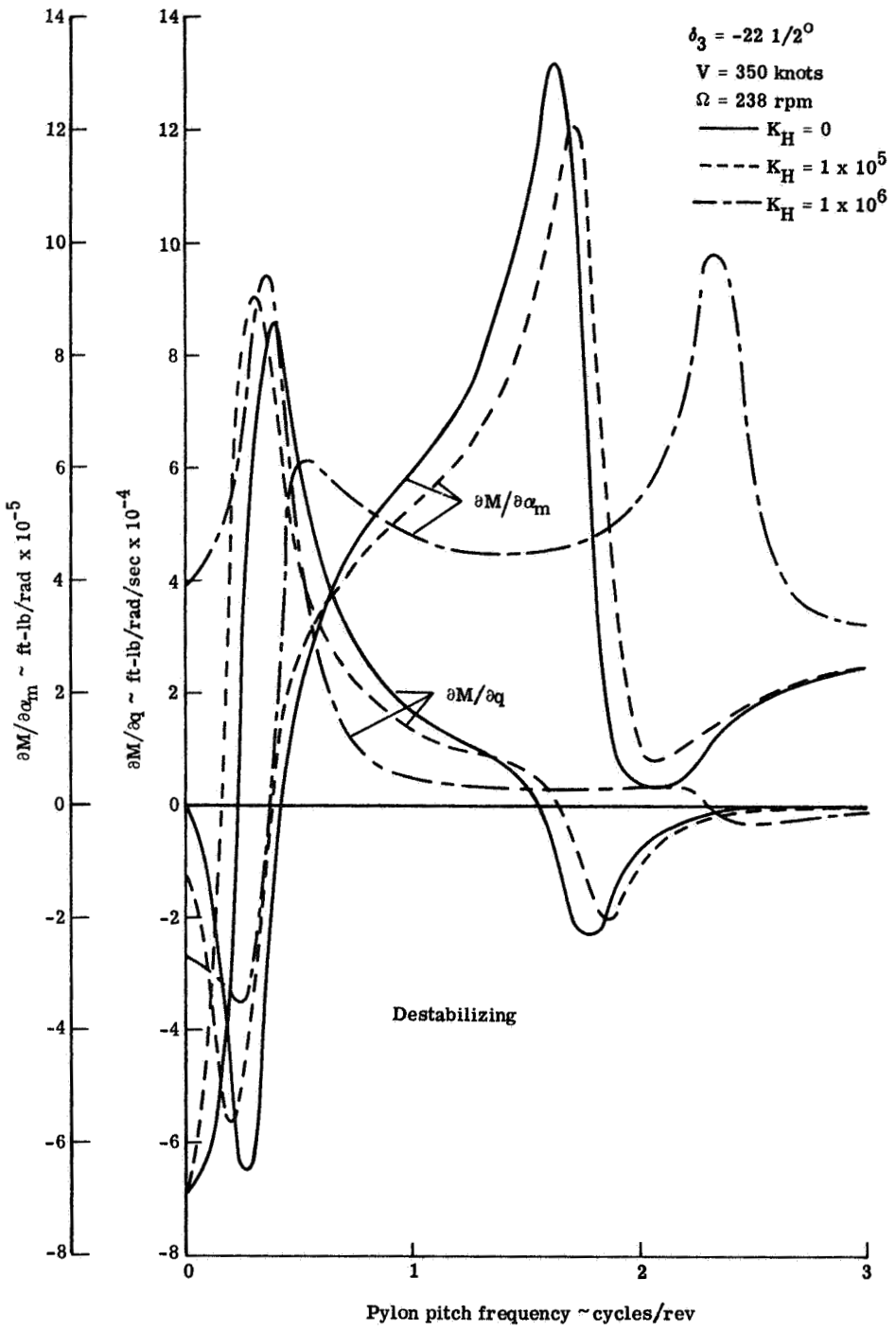

(b) Pitching moment

Figure 4-18.- Concluded.

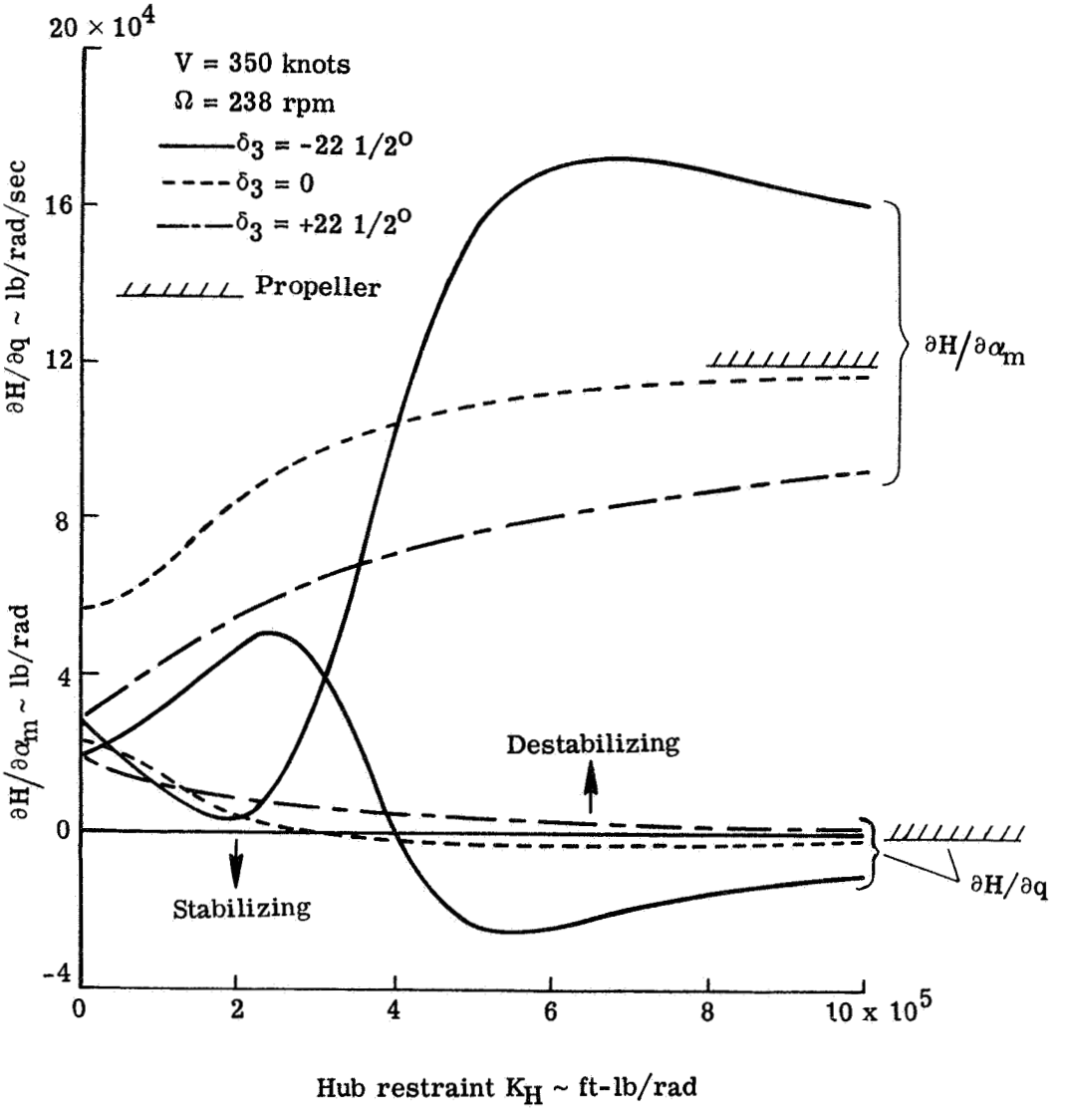

(a) Normal force

Figure 4-19.- Variation of zero frequency shear force and moment derivatives with hub restraint.

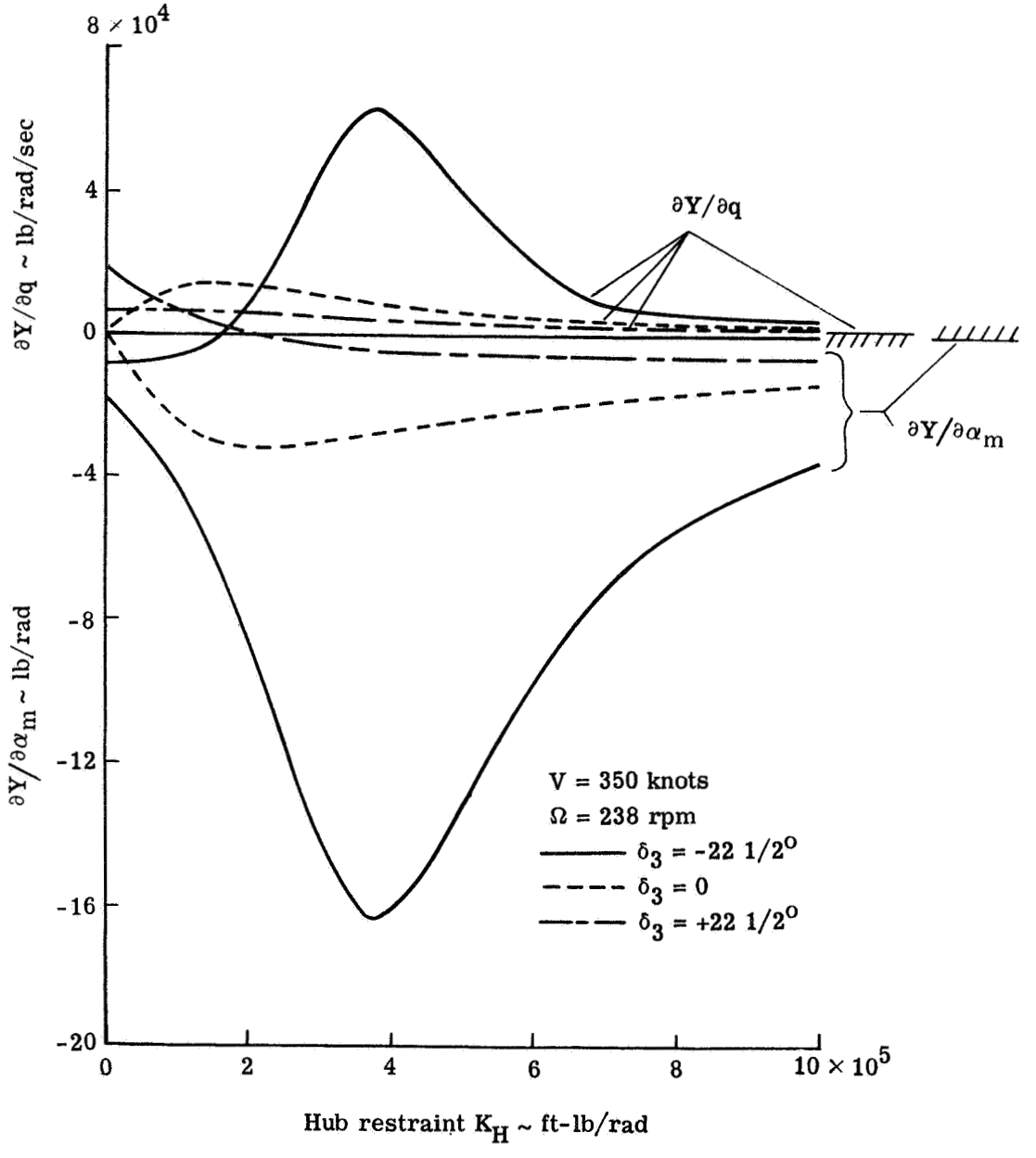

(b) Side force

Figure 4-19.- Continued.

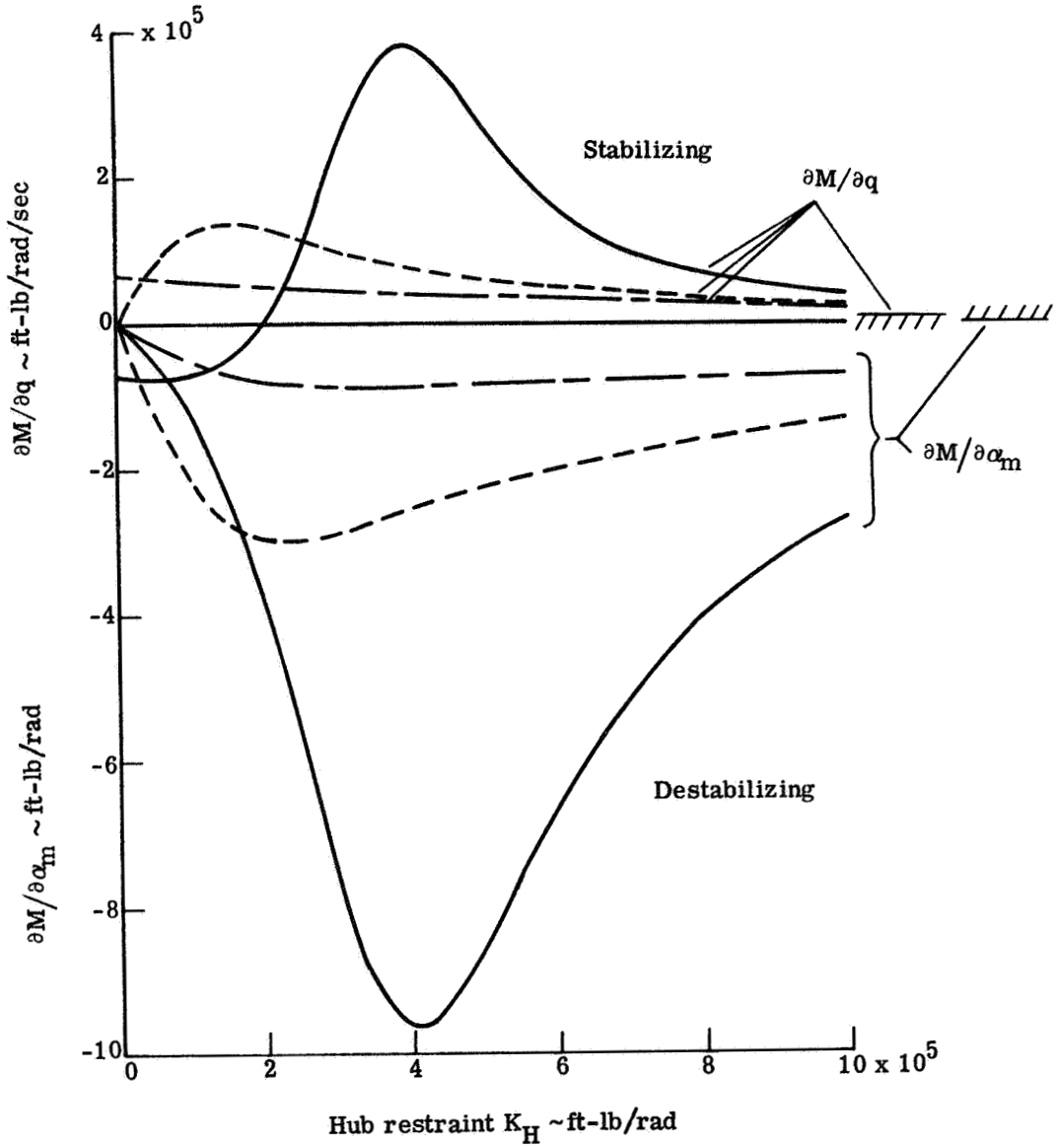

(c) Pitching moment

Figure 4-19.- Continued.

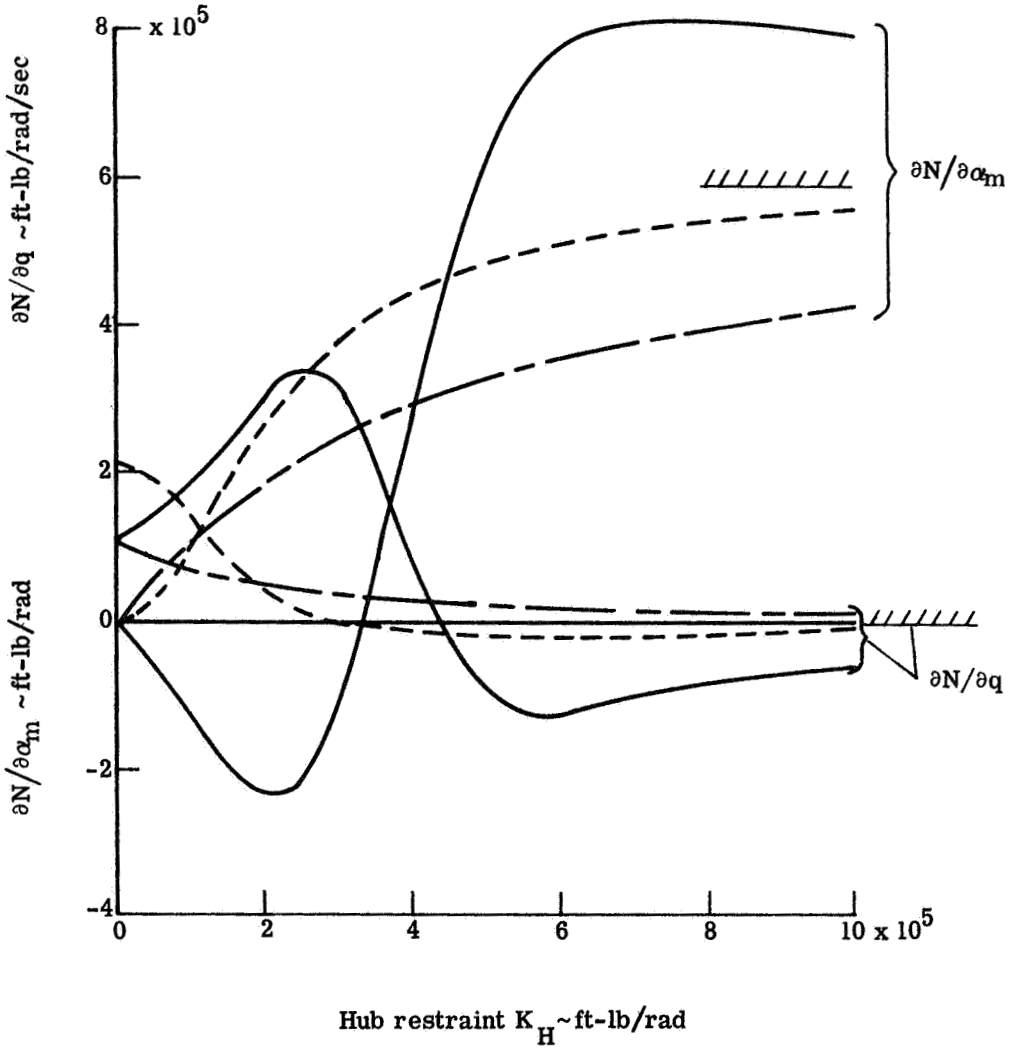

(d) Yawing moment

Figure 4-19.- Concluded.

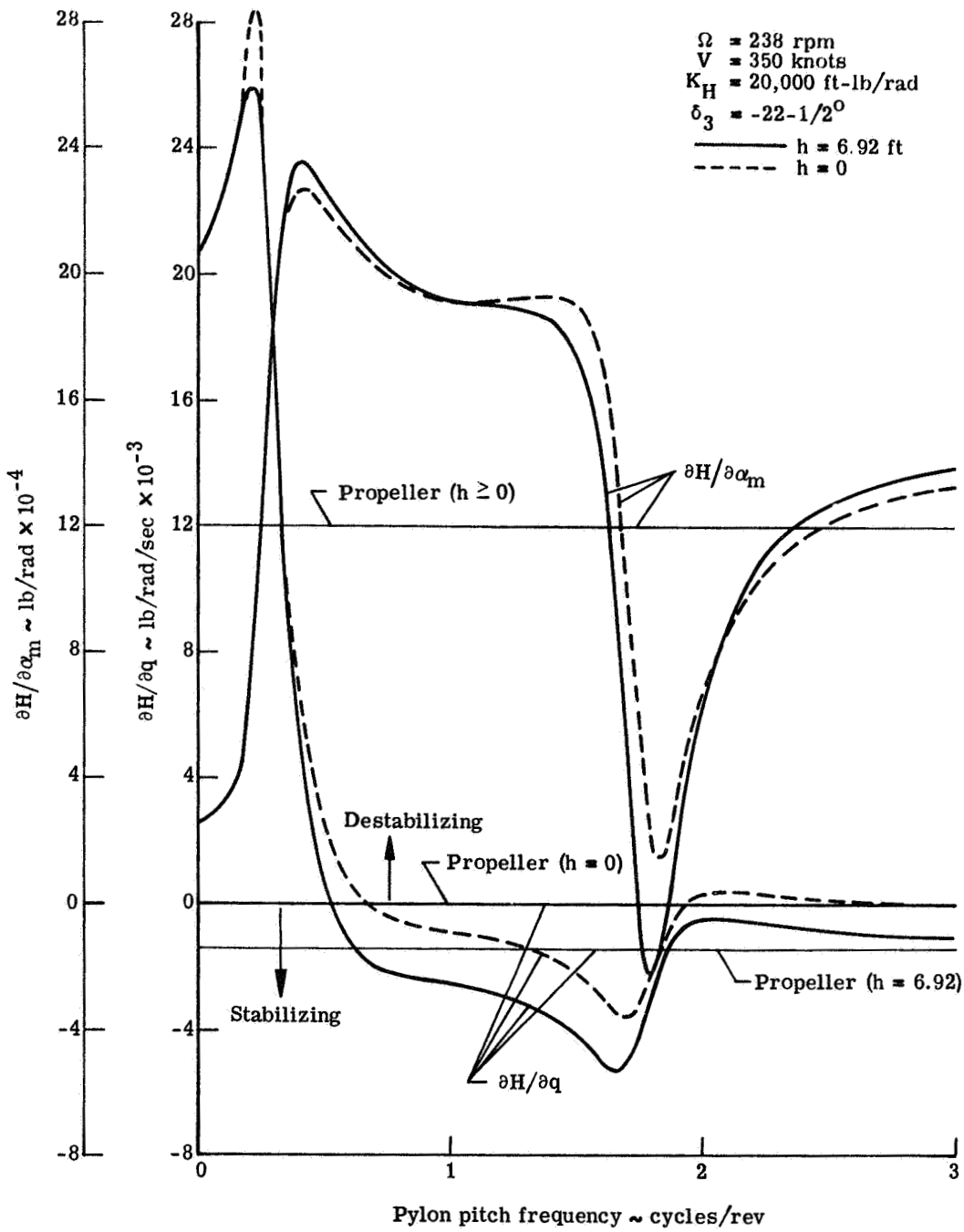

(a) Normal force

Figure 4-20.- Effect of shaft length on frequency response of proprotor and propeller force and moment derivatives.

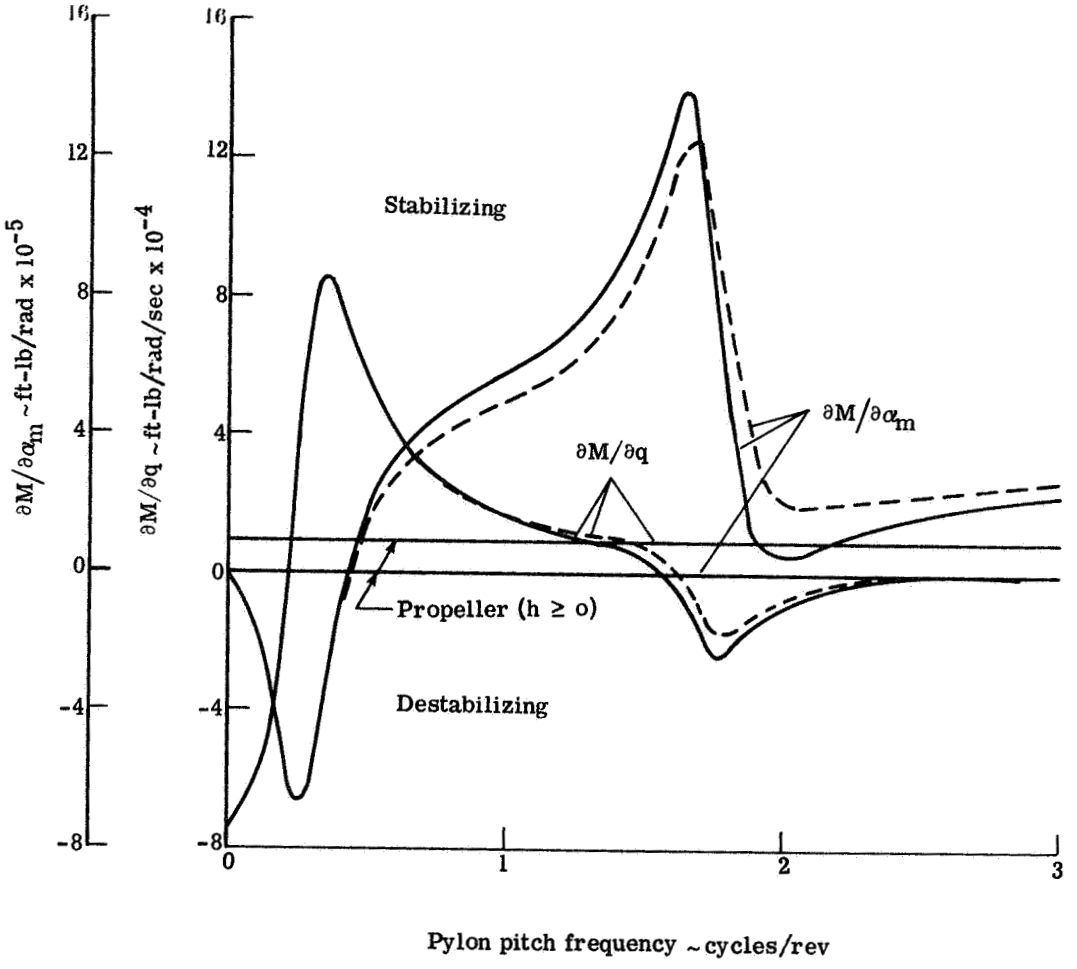

(b) Pitching moment

Figure 4-20.- Concluded.

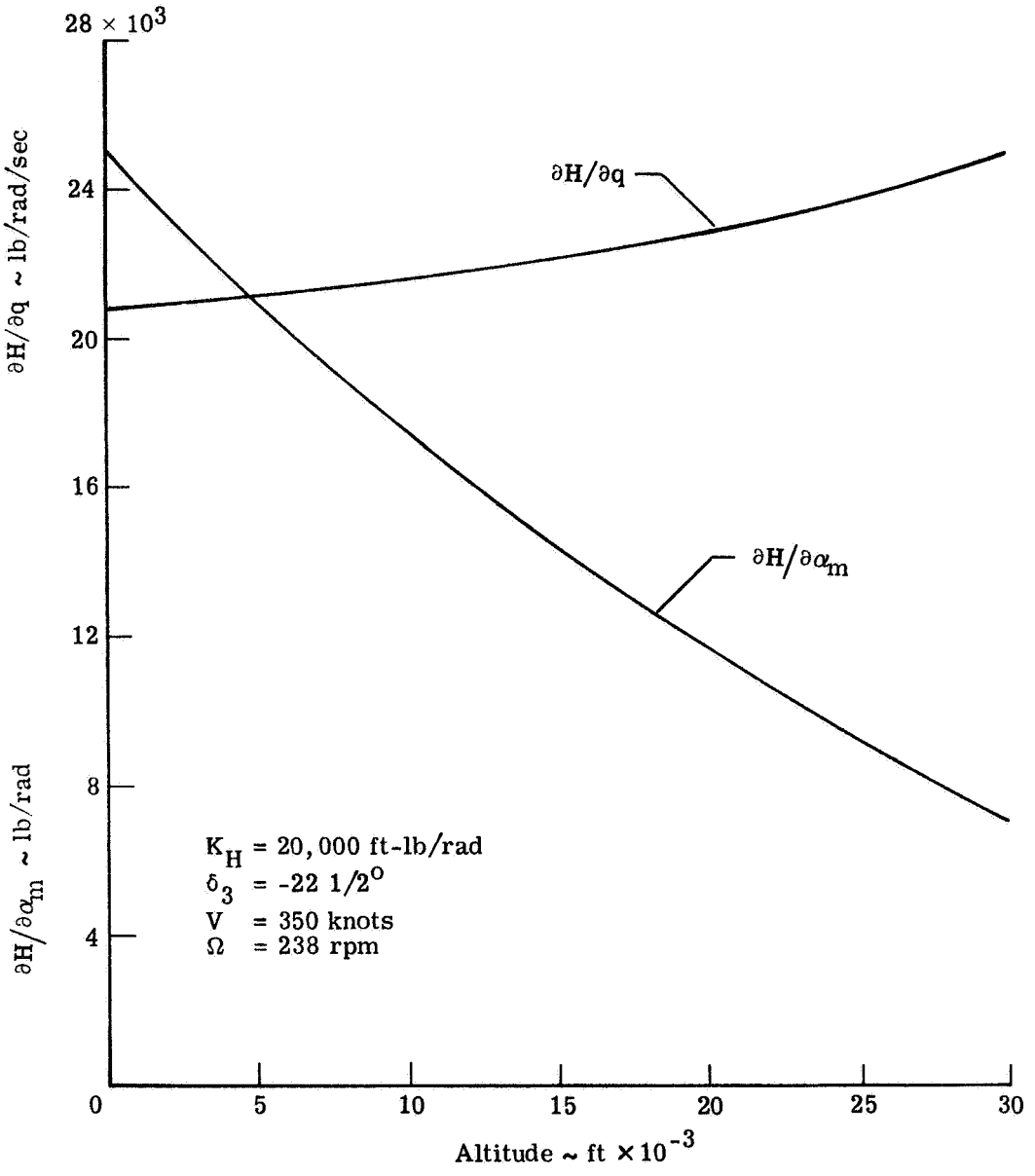

Figure 4-21.- Effect of altitude on zero frequency normal force derivatives.

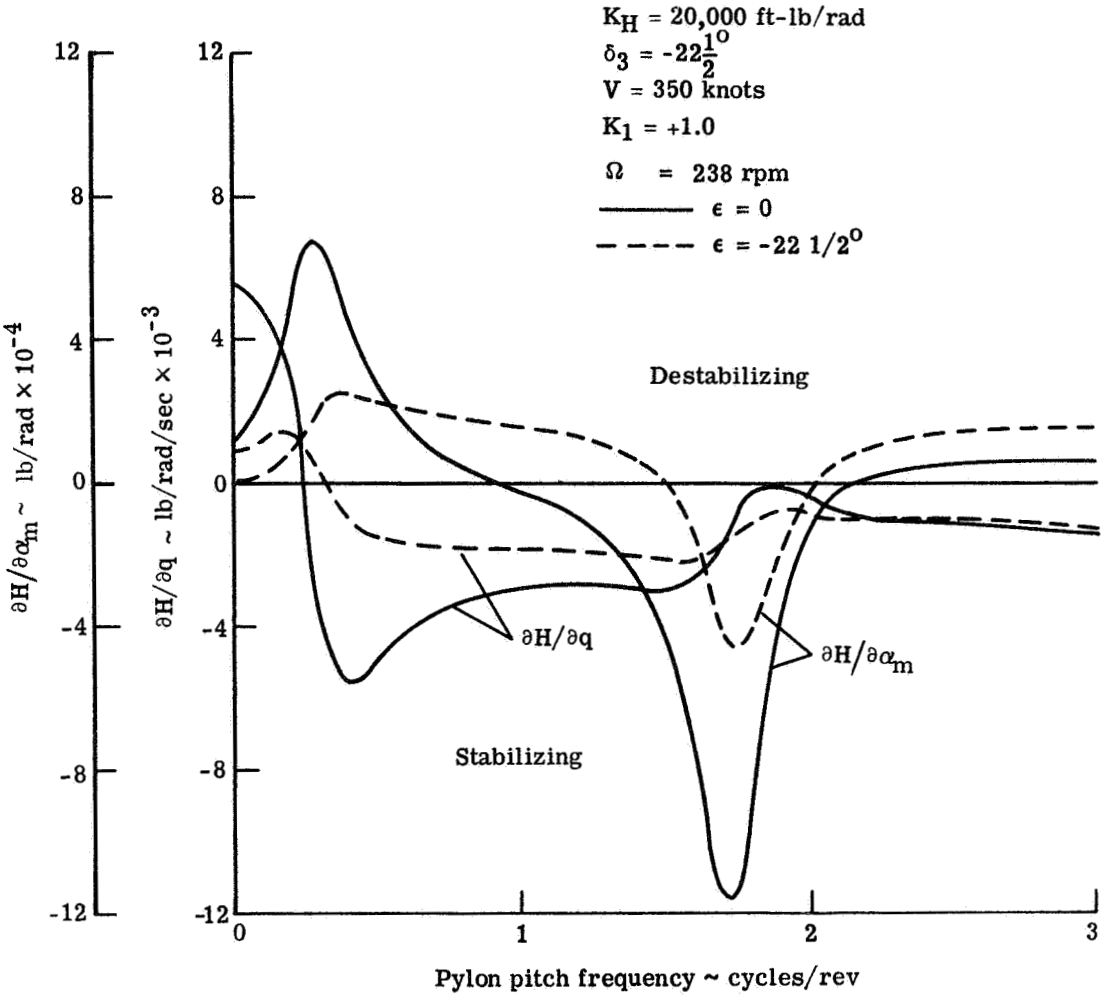

Figure 4-22.- Effect of swashplate/pylon coupling and control phasing on normal force frequency response.

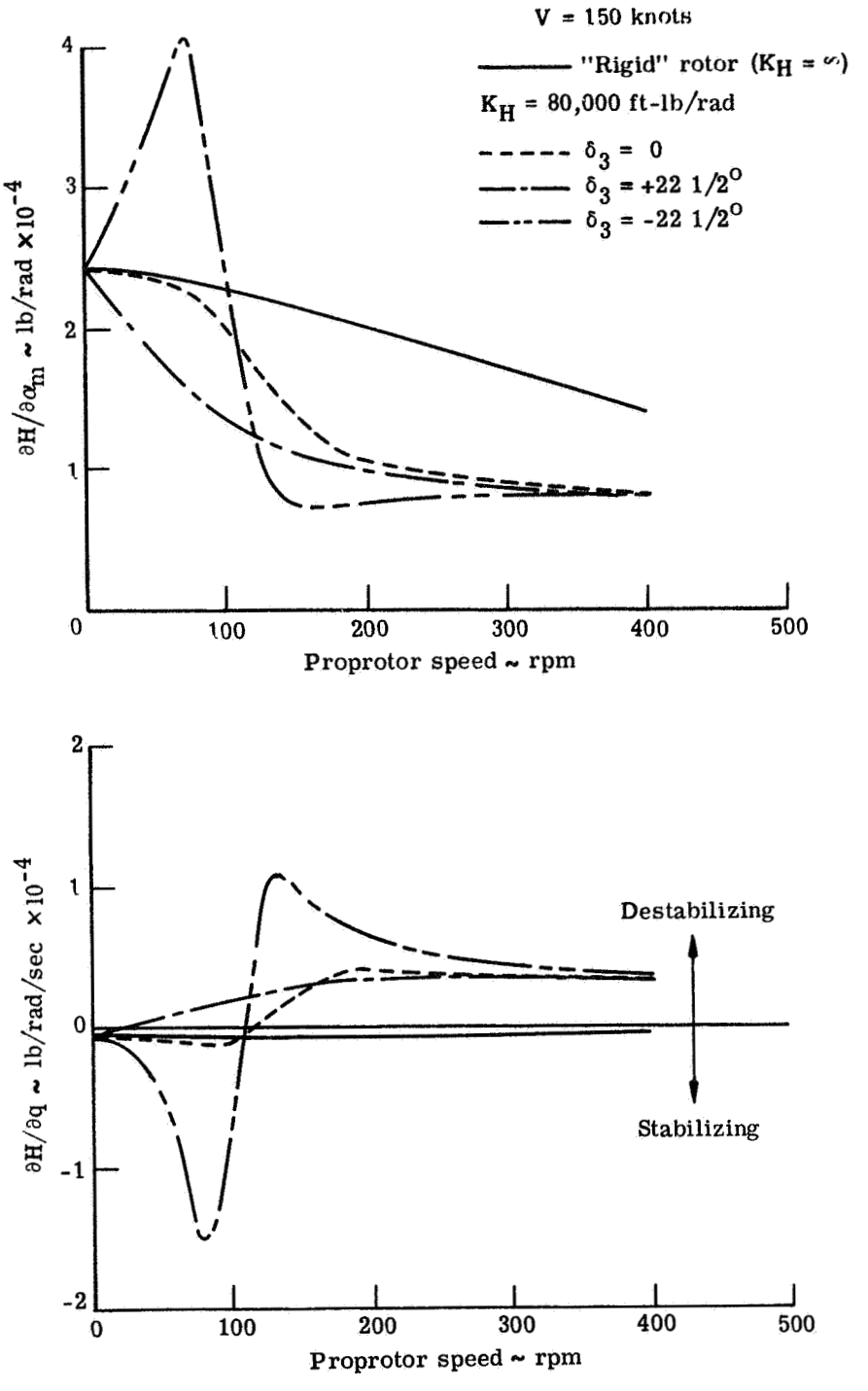

Figure 4-23.- Variation of zero frequency normal force derivative with rotor rpm.

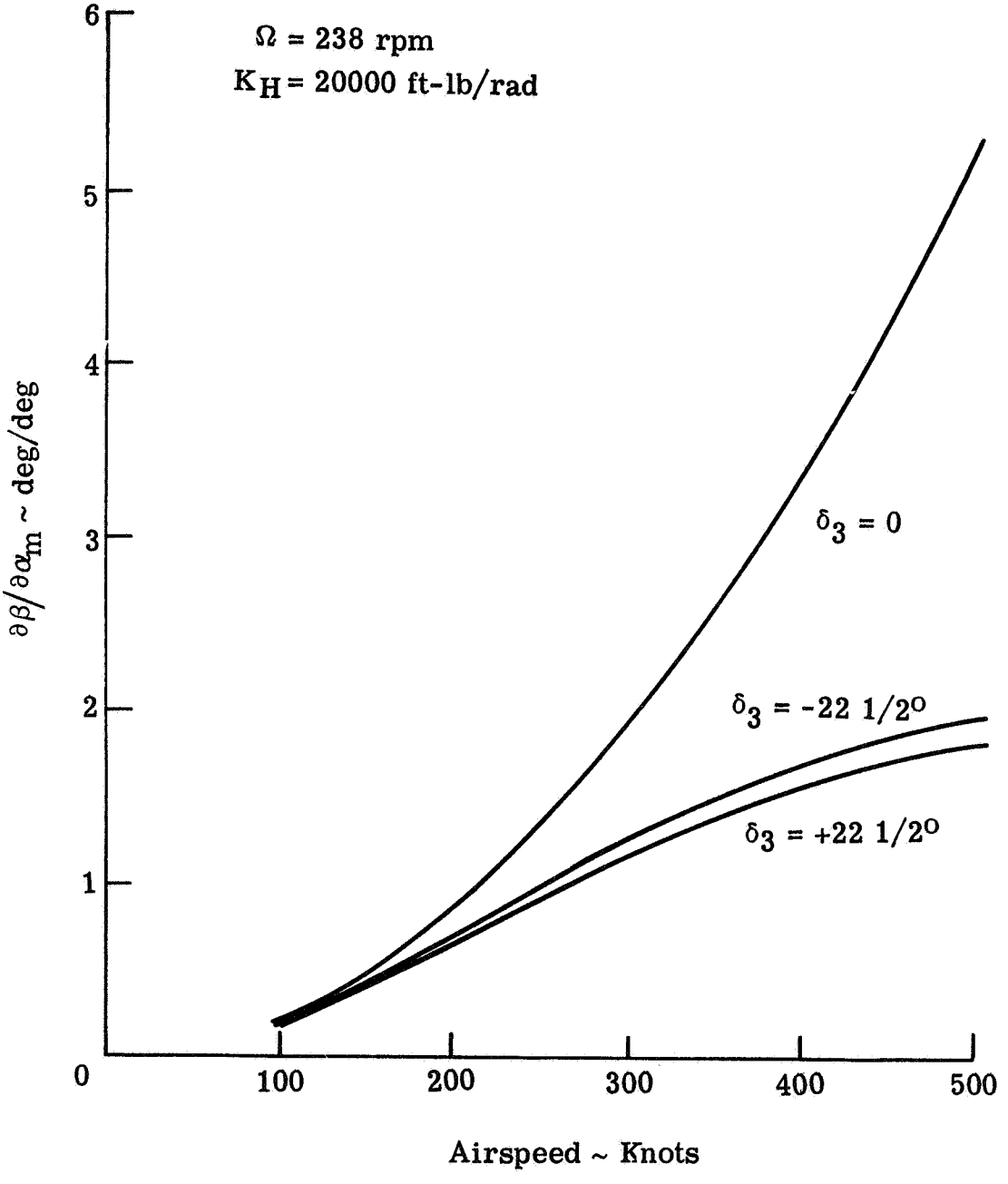

Figure 4-24.- Variation of total blade flapping derivative with airspeed.

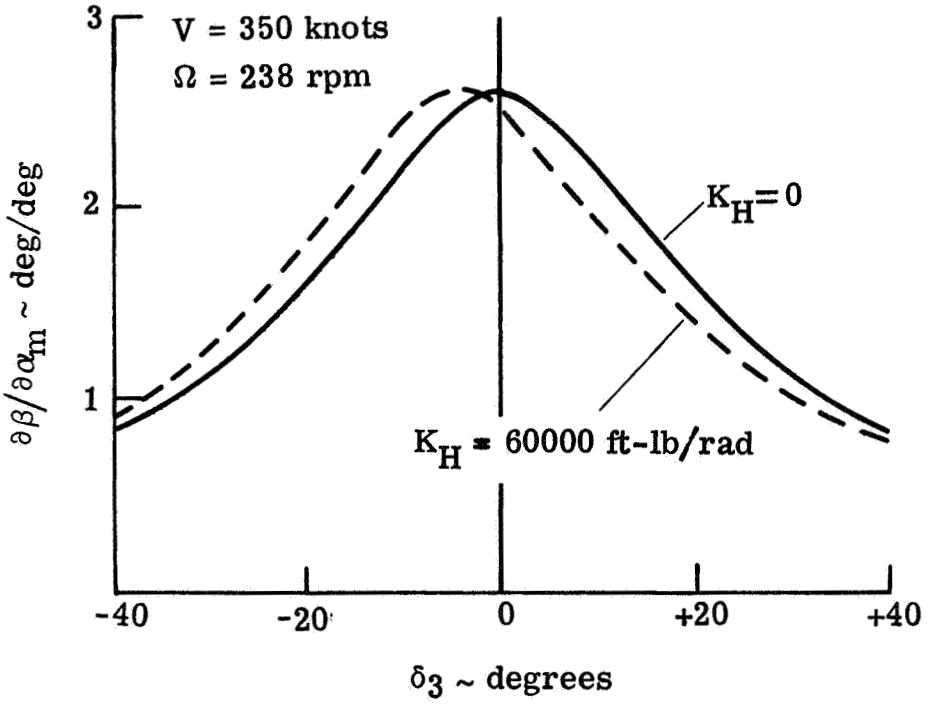

Figure 4-25.- Effect of δ_3 on blade flapping.

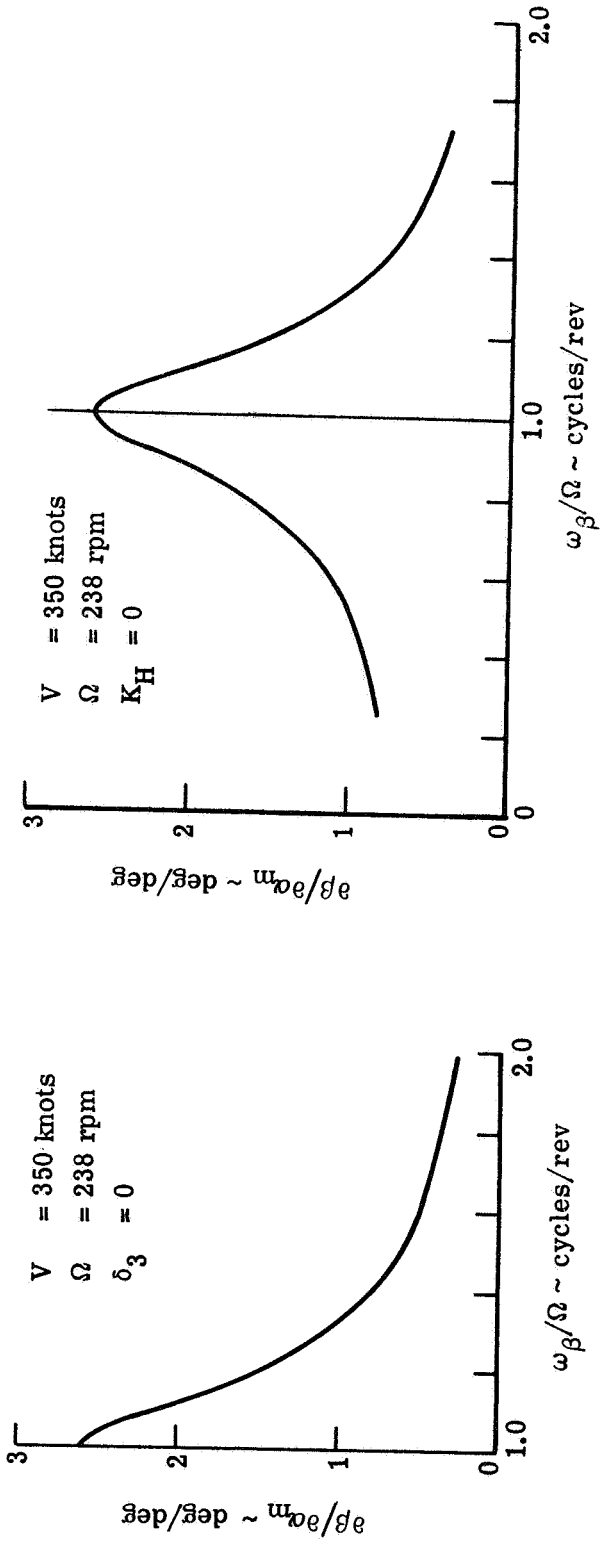

Figure 4-26.- Variation of blade flapping with flapping natural frequency.

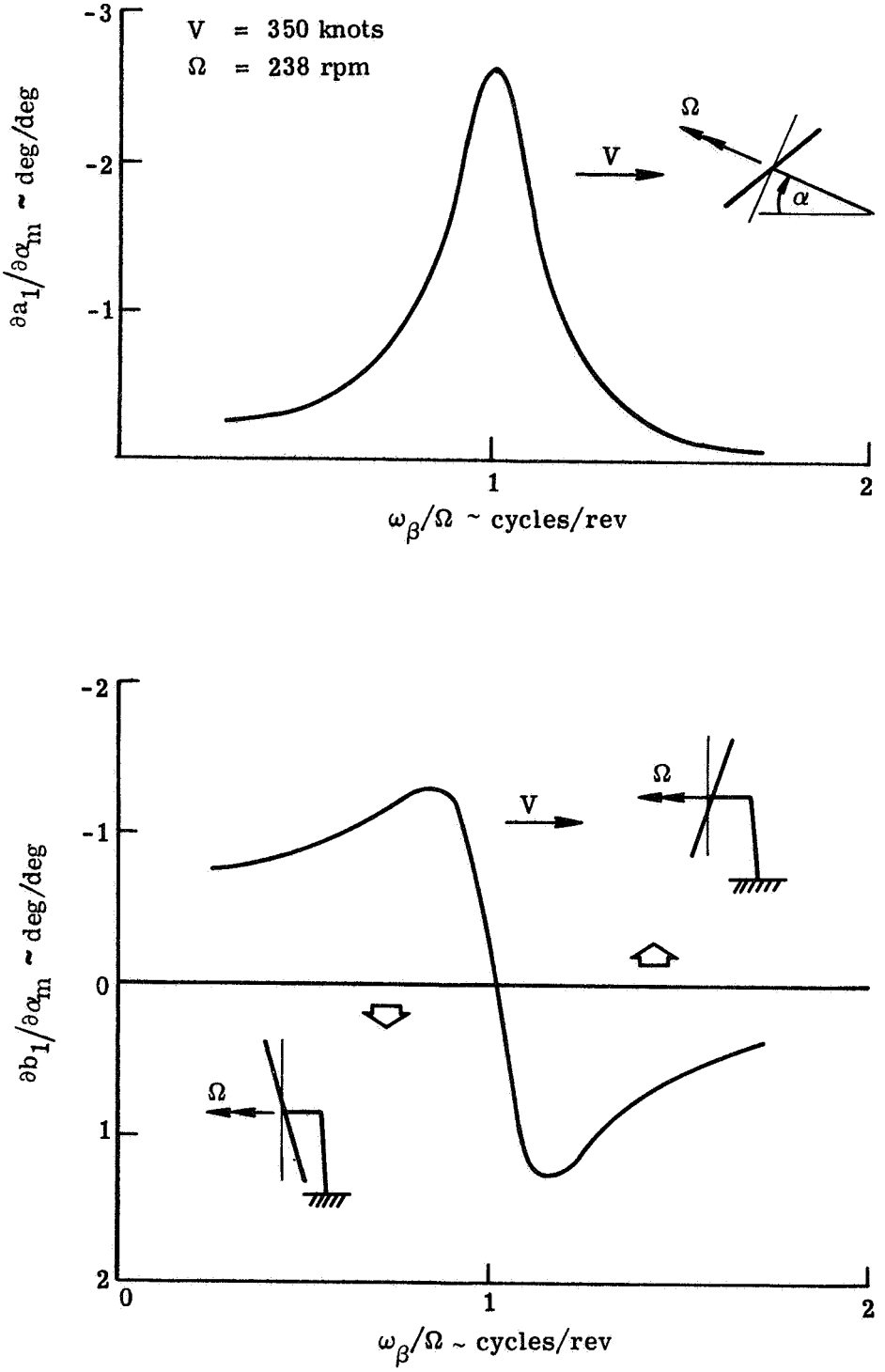

Figure 4-27.- Tip-path-plane flapping derivative variation with blade flapping frequency.

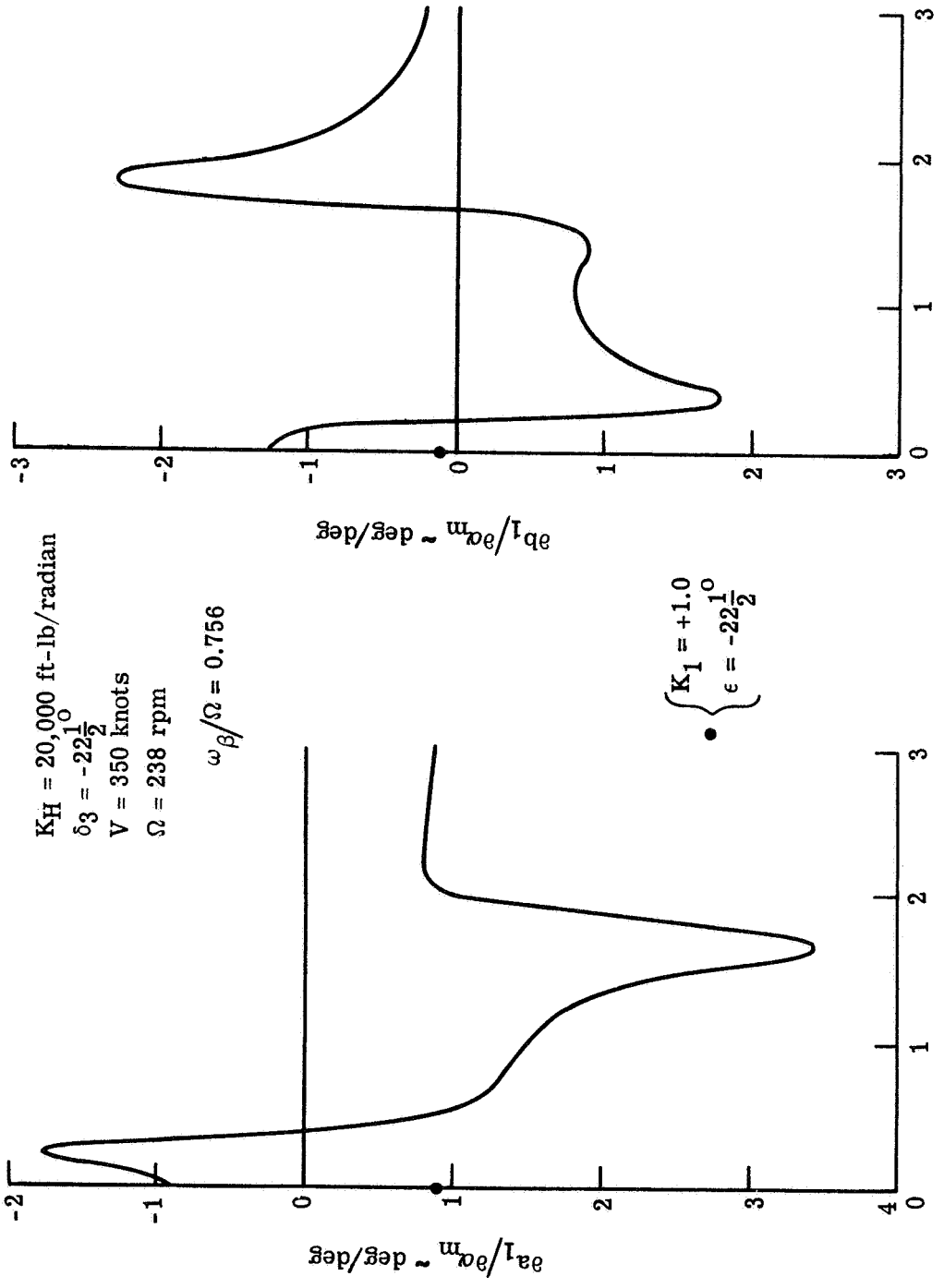

(a) Pitch angle components

Figure 4-28.- Frequency response of tip-path-plane flapping derivatives.

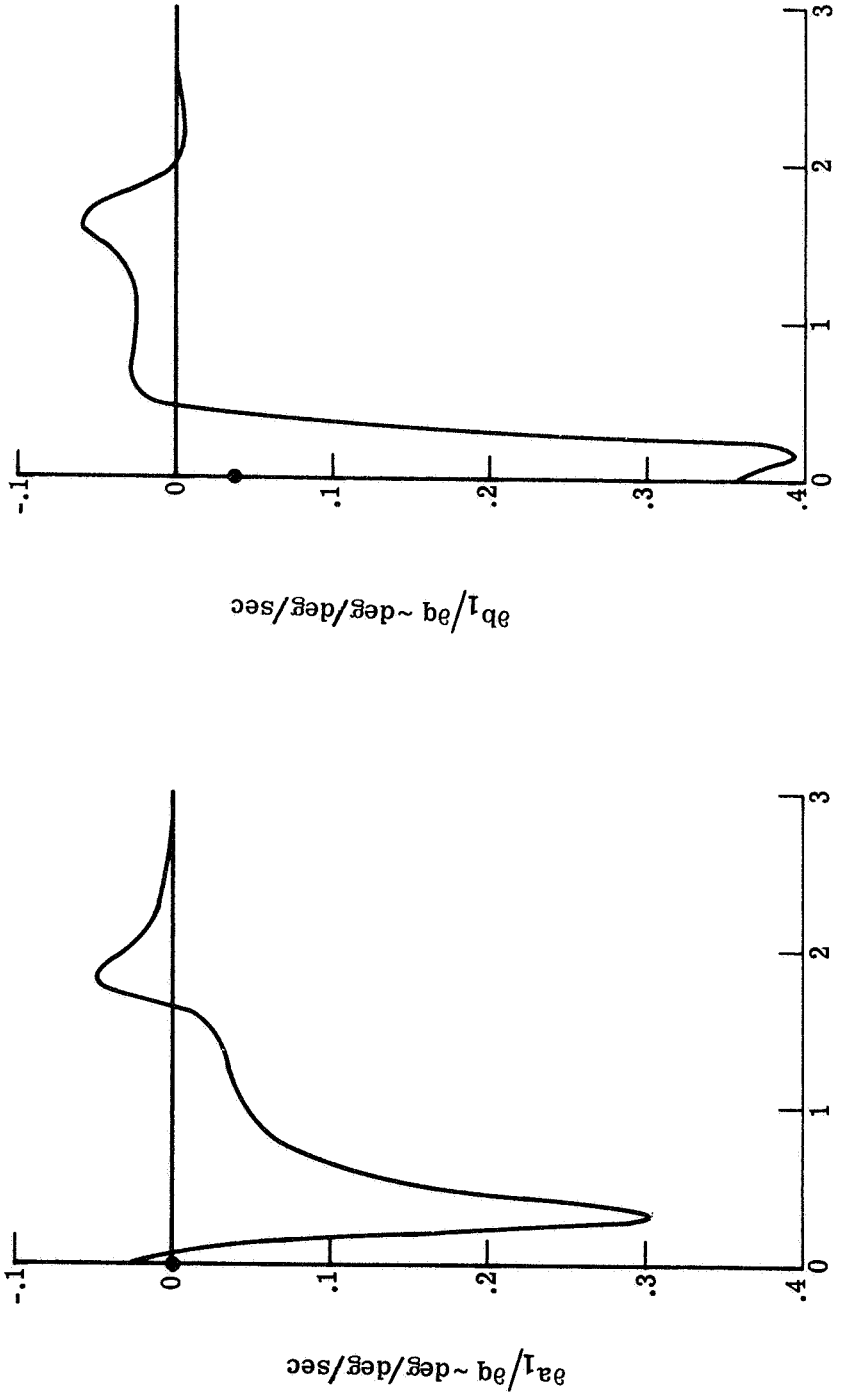

(b) Pitch rate components

Figure 4-28.- Concluded.

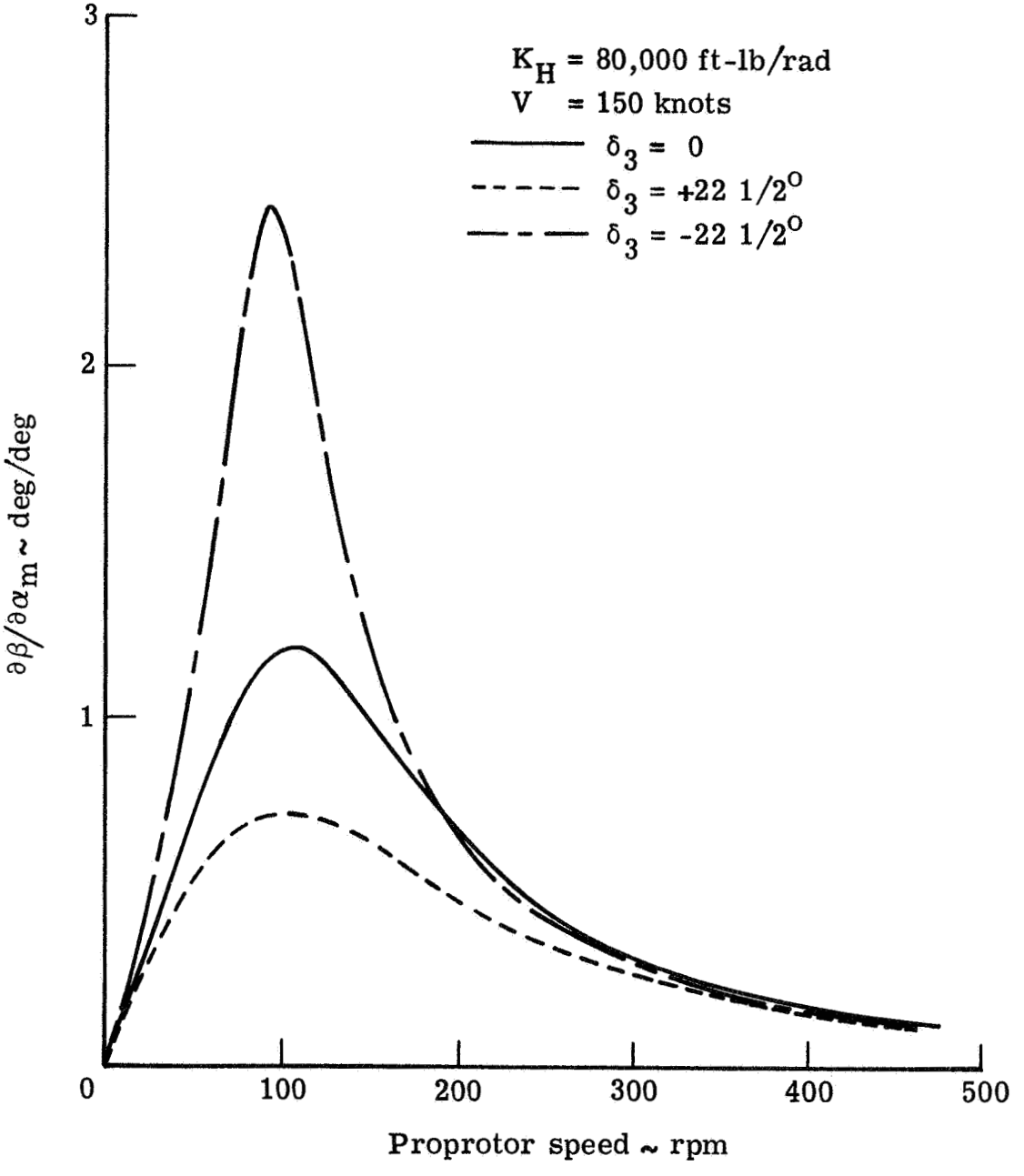

Figure 4-29.- Variation of steady-state flapping derivative with rotor rpm.

CHAPTER 5

MODEL TESTS AND CORRELATIONS

Introduction

The experimental portion of a generalized aeroelastic research program related to V/STOL dynamics was formally initiated in August 1968 when, in response to a request by NASA Langley Research Center, the U. S. Army Aviation Materials Laboratories (AVLABS) transferred to Langley a 0.1333-scale semi-span, dynamic aeroelastic model of the Bell Helicopter Company Model 266 tilt-rotor. This model was originally designed and built by Bell under Army contract in support of research pertaining to the exploratory definition phase of the Army Composite Aircraft Program. The availability of this model to Langley, its suitability for general aeroelastic research and the need for additional studies to further define the aeroelastic characteristics of proprotor-type aircraft subsequently led to a joint NASA/Bell test program in September 1968.

The model, as mounted in the Langley transonic dynamics tunnel for this investigation, is shown in Figs. 5-1 and 5-2. Although the model was not designed for extensive parametric variations, in that it represents a specific design, it did permit a fairly diversified test program. Objectives established for this program included the determination of the following items:

- The influence of hub restraint, pylon yaw support stiffness, rotor rpm, and wing degrees of freedom on proprotor/pylon stability
- Blade loads and motions in the helicopter, conversion, and

airplane modes of flight

- The effect of highly twisted blades on autorotational performance
- Thrust effects on wing mode damping
- Proprotor/pylon/wing frequency response characteristics during simulated vertical sinusoidal gust excitation
- Pylon static divergence
- Vibration levels in all flight modes
- Preliminary investigation of rotor inflight stopping and starting, simulating one phase of transition of a folding proprotor

The majority of the above objectives were met. Some of the principal results of this test program were initially presented at the Air Force V/STOL Technology and Planning Conference in September 1969 (Ref. 5-1).

Interest in the tilting-folding variant of the tilt-rotor concept led to a subsequent joint NASA/Bell test program in the Langley transonic dynamics tunnel to investigate any potential problem areas associated with aircraft of this type. This investigation, conducted in January 1970, utilized essentially the same model employed in the initial study but modified to incorporate a faster and more powerful collective drive motor to permit rapid feathering and unfeathering of the proprotor and a fold-hinge fitting between the blade grips and the yoke for the folding portion of the test. The main objectives of this test program were to investigate stability at low (including zero) rpm, during rotor stopping and starting, and during blade folding and to assess the effect of various rates of feathering and unfeathering on the

overall dynamic response of the system. Fig. 5-3 shows the model mounted in the transonic dynamics tunnel for the rotating portion of this study. The model is shown in two partially folded configurations in Figs. 5-4 and 5-5. Although the model was not scaled to any specific folding proprotor design its dynamic and aeroelastic characteristics were such that it was representative of a typical gimbaled folding proprotor design. All objectives of the test program were met. The experimental investigation identified an apparently new form of the flutter phenomenon involving the rotor at zero and low rpm. Because of its novel character the effect of various system parameters on this instability was established both experimentally and analytically.

The majority of the experimental results to be reported in this chapter were obtained during the aforementioned joint NASA/Bell studies of the 0.1333-scale semi-span model of the Bell Model 266 tilt-rotor in the Langley transonic dynamics tunnel. Although emphasis will be placed on proprotor/pylon stability selected results in the areas of gust response, thrust effects and blade flapping are also included.* At this point the author would like to acknowledge the test support contributed by Bell in these cooperative efforts. Specifically, this support included: measurement of model physical parameters, model build-up,

---

*The results of the January 1970 test pertaining to the dynamic response characteristics during feathering and unfeathering and stability during blade folding may be found in Ref. 5-2.

instrumentation hook-up, calibrations, and shake testing. The author, although only superficially involved in these aspects, assumes responsibility for the experimental results shown. To provide additional data for correlation, selected experimental results pertaining to the Bell Model 300 tilt-proprotor design are also included. Analytical-experimental correlation is shown where possible using the proprotor analyses developed in this dissertation. Selected analytical studies for several configurations not tested are additionally presented to isolate or point out the effect of various parameters on stability. Both these studies and the experimental results in essence constitute a continuation of the analytical studies of Chapter 4 since they complement and extend the results therein.

In each case, unless otherwise noted, both experimental and analytical results are for the pylon fully converted forward into the airplane mode of operation and the rotor in a windmilling (non-thrusting) condition. Equivalent full-scale values are given unless stated otherwise. It should be noted that the measured stability of the model can not be interpreted directly as representing the stability of the Model 266 design since compressibility was not scaled and free-flight effects were not present. The principal benefit of the model tests is to generate parametric data for correlation with analysis and to experimentally establish the effect of system parameters on stability and dynamic response.

For completeness, basic descriptive information pertaining to the 0.1333-scale model, the characteristic features of the wind-tunnel facility, and a brief account of the testing technique are given below before presenting the results of these investigations.

Description of Model

(a) Design and Construction

The 0.1333-scale model as mounted in the Langley transonic dynamics tunnel was shown previously in Fig. 5-1. Only the proprotor, pylon, and wing are aeroelastically and dynamically scaled, the fuselage maintaining only the scaled external aerodynamic shape. The model is attached at its wing root to a mount which is effectively rigid, its lowest frequency being well above any important elastic mode frequency of the model. Note that the mounting arrangement is not that normally employed for testing semi-span models in that the model, being mounted away from the tunnel wall, lacks a reflection plane through the vertical plane of symmetry of the fuselage. This arrangement was dictated mainly by the requirement of placing the rotor in the center of the tunnel. Nevertheless, for the proprotor-related dynamic phenomena of interest in these studies a mounting arrangement of this type has been established to be quite satisfactory*.

---

*This was experimentally substantiated during the January 1970 test program. Flutter speeds with and without a reflection plane (Fig. 5-6) were essentially the same.

Simulation of the distributed wing beamwise, chordwise, and torsional stiffness is provided by means of a hollow aluminum beam-type spar having chordwise flanges. The spar, which lies along the calculated elastic axis of the full-scale aircraft, has segmented, box-like, non-structural aerodynamic fairings which provide the spanwise distribution of airfoil contour. These segments consist of balsa end ribs and a covering of thin balsa planking and paper. Single point contact of these sections with the wing spar through an X-frame arrangement within the fairings ensure concentration of the wing elastic characteristics in the spar. To provide surface continuity, the space between these sections is filled by strips of foam rubber. The wing spar and aerodynamic fairings are ballasted to represent a 15-percent fuel wing weight distribution. Additional ballast in the form of lead weights can be distributed along the wing spar to simulate an increased fuel weight distribution or to maintain the weight distribution when testing is done with the wing fairings removed.

The pylon is attached to the wing spar with a tapered conversion spindle at the rear of the spar and locked to the wing tip in pitch at the front of the spar. An adjustable yaw flexibility was provided (September 1968 test) in the form of an assembly of helicoidal springs housed in a box-like structure ahead of the wing spar between the pylon and the wing tip. Items within the pylon assembly which were simulated include the proprotor mast and bearing assembly, pitch-flap coupling, and an adjustable hub (flapping) restraint. Some of the details of the pylon for the

model oriented as shown in Fig. 5-1 are illustrated in Fig. 5-7 which shows a close-up view of the pylon/hub area with its fairings removed. A portion of the beam spar construction and the adjustable yaw restraint assembly are visible. The pylon is not elastically scaled and can be taken to be effectively rigid. Its overall mass and inertia is however scaled.

Proprotor blade beamwise and chordwise stiffness distributions are scaled from the center of rotation to the blade tip. Blade torsional stiffness is only approximately scaled. However, since the blades are very stiff torsionally, small deviations from the design torsional stiffness distribution are taken to be of secondary importance.

The proprotor blades are of constant chord and consist of a negatively twisted (-27.7°) aluminum spar covered with fiberglass skin. Expanded foam is used to maintain the blade contour. Lead weights are bonded to the spar to obtain the proper weight and static unbalance. To tune the blade inplane frequency a lead weight was added near the tip of each blade. This biased the weight distribution toward the blade tips leading to blade flapping moments of inertia which were about 14-percent higher than the target scaled inertia. The blade pitch-change axis is preconed 3° and lies along the blade quarter-chord line. The blades are attached to a stainless steel yoke/spindle assembly which is in turn attached to the mast through a gimbal housed within the yoke. Blade feathering freedom about the spindle is provided by two

needle bearings located in the blade grip assembly. A wire wound strap passing through the blade grip and spindle carries the blade steady centrifugal force and feathering moment. Control system flexibility about the blade pitch change axis is not scaled but is sufficiently stiff so that the net blade pitch stiffness remains high enough to preclude any blade torsional oscillations of consequence, that is, blade pitch enters primarily as a kinematic freedom. Trailing edge pitch horns are linked by conventional pitch links to a plate located above the hub, which is translated parallel to the rotor shaft to change blade collective pitch. This control system, shown in Fig. 5-7, was used for all testing done in the airplane mode. A wide range of collective pitch was available by adjusting the mean of the collective pitch range by repositioning the pitch horns on the blade grips. For testing in the helicopter and conversion modes a different control system, having both collective and cyclic pitch capability, was used. This control system is shown in Fig. 5-8.

A 3 HP, variable frequency, constant speed, water cooled electric motor housed within the cavity of the fuselage fairing provided a relative wide range of scaled values for the proprotor thrust when operating in a powered configuration. Power is transferred to a reduction gear box in the pylon through a torsionally scaled driveshaft supported along the trailing edge of the wing spar by bearing hangers. A portion of this drive shaft at the coupling near the pylon may be seen in Fig. 5-7.

The model for the rotating portion of the January 1970 test differed somewhat from that described above for the September 1968 test. To provide for the large range of collective pitch required for remote feathering and unfeathering of the rotor, the walking beam arrangement shown in Fig. 5-9 was employed. The added weight and inertia contributed by this control system modification was compensated for by the removal of the simulated engine located below the transmission (Fig. 5-8). This adjustment maintained essentially the same pylon weight and inertia as in the original configuration. Another modification was the replacement of the variable yaw restraint assembly (Fig. 5-7) by the permanent yaw lock-out arrangement shown in Fig. 5-9.

Simulation of the mass and stiffness properties in the manner indicated above ensured that all important modes and frequencies of vibration on a per-rev basis of the full-scale proprotor/pylon/wing system would be preserved as nearly as possible. Shown in Table 5-1 are the target and actual natural frequencies for several of the lower modes of the model.

(b) Physical Properties

The basic pylon/wing configuration for the September 1968 test consisted of a simulated 100% fuel wing weight distribution with the wing aerodynamic fairings removed and the pylon yaw degree of freedom locked out.

Since the wing mass is distributed and small in comparison to the combined mass of the rotor and pylon, for analysis purposes

it is sufficient to account for the wing motions in the guise of wing tip displacements in the fundamental modes of motion, as discussed in Chapter 3. This allows the wing distributed mass and stiffness to be represented by equivalent concentrated masses, springs, and dampers. Wing tip measured spring rates were referenced to the pylon/conversion axis intersection which was taken to be the location of the effective pitch axis of the pylon A shake test with the blades replaced by an equivalent lead weight established the basic modes and frequencies of interest. Measured mass and inertia properties, in conjunction with the wing effective mass and inertia based on the fundamental wing modes and the known wing mass and inertia distributions, were used to calculate the coupled modes and frequencies of the system. The measured spring rates were then adjusted to bring the calculated frequencies into agreement with the measured shake test frequencies.

Damping corresponding to each of the fundamental modes was established by "plucking" the model in the beamwise, chordwise, torsional, and pylon yaw degrees of freedom and recording the subsequent decaying oscillation in each degree of freedom. The resulting time histories were used to determine the frequencies (as a check on the shake test results) and damping, the damping as a fraction of critical damping being obtained from the relation $\zeta = .11/N_{1/2}$, where $N_{1/2}$ is the number of cycles for decay to half amplitude. The frequencies established by "plucking" were essentially the same as those from the shake test. Hence, in

addition to determining the damping in each of the fundamental modes by "plucking", the modal frequencies were also taken to be those obtained by this means of excitation. The frequency and damping were checked several times for each series of runs on a given configuration. The damping values used in the analytical correlations actually represent an average of all the measured values in each degree of freedom. Since the damping values so measured are for a coupled motion it is believed that they are more representative of the actual damping in the system than if all degrees of freedom except the one in question were locked out and the resulting one degree-of-freedom damping measured.

The basic pylon/wing configuration for the January 1970 test consisted of a 15% fuel wing weight distribution with the wing aerodynamic fairings installed and the pylon yaw degree of freedom locked out. The pylon mass and inertia characteristics were essentially unchanged since the increased mass and inertia resulting from the control system modifications were fairly well accounted for by removing the simulated engine weight. For analysis purposes the differences were neglected.

A summary of the model physical characteristics employed in the correlation studies is given in Table 5-2. The new yaw restraint and the removal of the lead weights from along the wing spar are believed to be the cause for the reduced levels of damping in the January 1970 test. The significantly reduced value of wing effective mass in this test is a consequence of the reduced fuel weight distribution. With the simulated engine

removed the vertical offset of the pylon center of gravity from the wing chord plane is negligible and has been set to zero. For both fuel weight distributions, the wing effective masses and inertias in the wing degrees of freedom other than vertical bending are negligible compared to the pylon weight and inertia and hence have been neglected.

(c) Instrumentation

Instrumentation employed to record model response consisted of wire resistance strain gages, accelerometers, and position potentiometers. Wing beamwise and torsion strain gages were located at 15% span position and chordwise bending gages at 28% span. Blade beamwise and chordwise bending moments were measured at the 35% blade radius on one blade. Flapping relative to the mast was measured in the rotating system by means of a strain-gaged cantilever member mounted on the mast and connected by a spring to the hub gimbal ring. Mast torque was monitored by the output from strain gages on the mast and used for setting the rotor thrust levels when operating with power. Pitch link axial loads were monitored to provide an indication of blade root torsional bending moments. Pylon yaw motion (when unlocked) was sensed by a strain-gaged cantilever member. Pylon acceleration levels were recorded by five accelerometers mounted on the pylon: two oriented to give pylon forward and aft vertical acceleration, two to give pylon forward and aft lateral acceleration, and one to give fore and aft acceleration. Rotor rpm was indicated

directly on a tachometer driven by the signal from a magnetic pickup. Rotor rpm and the azimuth position of a reference blade were given by another magnetic pickup which pulsed every 90° of rotor rotation. This signal was recorded on the oscillographs. The pulse corresponding to a specific azimuth position of the reference blade was larger than the others. This feature was used mainly for blade balancing purposes. A flow direction transmitter (Fig. 5-2) which gave readings proportional to the angular rotation of the balsa vane was employed for measuring the gust-induced angle of attack.* Model angle of attack and pylon tilt angle were hand adjustable. Remote electrical or electromechanical controls were used to control collective and cyclic pitch remotely from the control room. Rotor torque (and hence thrust) levels were set by means of mast torque calibration curves. Collective and cyclic control positions and mast torque were indicated on the model operators control console.

A transient external excitation could be applied to the model by means of two lightweight cables attached to the model and routed to the control room. A vertical cable on the conversion axis near the pylon (Figs. 5-7 and 5-9) provided the means for wing beamwise (vertical) excitation while a horizontal cable oriented parallel with the airstream and downstream of the pylon (Fig. 5-6)

---

*The flow direction transmitter was mounted on an effectively rigid boom support. A lateral rod member was added to increase the lateral rigidity of the boom but was not installed at the time the picture (Fig. 5-2) was taken.

was used to provide chordwise (fore and aft) excitation. Both cables could be used to restrain the pylon motion in the event of an instability.

Data from the rotating system were brought out through the transmission by a slip-ring assembly. All data from the model were recorded on direct-readout oscillographs and on magnetic tape. A permanent photographic record was made of all flutter points and response phenomena of interest.

(d) Scaling Considerations

The current modeling state-of-the-art is such that the similarity parameters which must be simultaneously satisfied to maintain complete similitude (Ref. 5-3) can not all be satisfied in practice and the majority of the similitude requirements must be relaxed. Scaling was thus dictated by the minimum conditions imposed by the similarity laws which had to be satisfied to insure a proper dynamic and aeroelastic simulation of the important proprotor-related phenomena.* A brief summary of some of these considerations is given below.

Synonymous with the need for a dynamic and aeroelastic representation of the full-scale aircraft (ie., a flutter model) are the requirements for the maintenance of the full-scale geometric shape and mass, stiffness, and damping distributions. Additionally, the full-scale reduced frequency k and mass-density

---

*The reader may find the modeling and scaling considerations of Ref. 5-4 of interest in this regard.

ratio μ, or the combined parameter $V/b\,\omega_{ref}\sqrt{\mu}$, must be maintained. Only then can the model flutter behavior as determined in the wind tunnel be interpreted in terms of full-scale behavior. It is also desirable to preserve the full-scale Mach and Reynolds numbers. For low-speed flutter models compressibility effects can generally be neglected and the Mach number scaling requirement can be relaxed. The Reynolds number requirement was taken to be of secondary importance in this particular case and no attempt was made to achieve similitude in this parameter. This similitude is often neglected in flutter modeling since experience has demonstrated that Reynolds number effects generally have a negligible effect on the flutter characteristics of main lifting surfaces.

The need to maintain full-scale damping distributions in the various model modes of vibration was obviated by employing construction methods and materials which minimized the structural damping, thereby leading to values less than those which would be obtained on the full-scale aircraft. This insured that the model would exhibit conservative values of damping.

Specific considerations involved in the selection of the model length, time, and mass scaling are given below.

Length: Wind tunnel size and wall interference and blockage considerations led to the selection of a model length 0.1333 times the full-scale length.

Time: In low-speed testing, the velocity scale factor is generally established by requiring that the available tunnel speed represent one or more flight conditions of the full-scale aircraft. Although this consideration permits the selection of a velocity scaling of unity, the convenience realized by having the model strains and accelerations equal to those on the corresponding components of the full-scale aircraft suggested that the full-scale Froude number be maintained instead. This also insures that the static aeroelastic behavior is simulated, in particular the scale of aeroelastic deflections under steady gravity loads, which is important for the correct scaling of blade bending loads. Hence deflection similarity due to aerodynamic, inertial, and gravity loadings is maintained. The Froude number specification in conjunction with the previous requirement of mass-density ratio similitude implies that the model operates at the same lift coefficient as the full-scale aircraft. Assuming that the lift curve-slope characteristics are maintained this further implies that angles are preserved.

The velocity scale which preserves the Froude number, in combination with the selected length scale, then determines the time and frequency scale factors from the requirement that the full-scale reduced frequency* be maintained.

---

*The reduced frequency is equivalent to the reciprocal of the advance ratio .

Mass: Since various proprotor dynamic phenomena are a function of the ratio of blade aerodynamic forces to blade inertia forces (Lock number in the parlance of rotary-wing dynamicists) proper simulation of the full-scale aircraft required preservation of this quantity. Assuming the lift-curve-slope characteristics of the model and airplane are maintained, the foregoing requirement is equivalent to the preservation of the mass-density ratio. The maximum dynamic pressure at sea level was judged to be most critical from a proprotor stability point of view. This established the model design point. Since fluid density becomes a free parameter if the Reynolds number requirement is relaxed the fluid density ratio can be selected on the basis of the density at the altitude of the design point. Selecting sea-level wind-tunnel conditions implied a fluid density scale factor of unity which, in conjunction with Lock number similarity, set the mass scale factor.

Using the length, mass, and time scale factors established above, the required scale factors for stiffness, mass moment of inertia, spring rate, etc., were then easily evaluated. The pertinent scale factors are summarized in Table 5-3.

NASA-Langley Transonic Dynamics Tunnel

The majority of the experimental investigations to be reported herein were conducted in the NASA-Langley transonic dynamics tunnel (Fig. 5-10) which is a continuous flow, single-return, variable pressure, slotted-throat tunnel having a test section 16 feet square (with cropped corners). The control room and test

section walls are provided with large windows for close viewing of the model. Some of the general features of the structural arrangement of this tunnel are schematically depicted in Fig. 5-11.

Although most runs were conducted in air under near atmospheric conditions at Mach numbers less than 0.30, the tunnel is capable of operation at stagnation pressures from near vacuum to slightly above atmospheric and of Mach numbers up to 1.2. Either air or freon-12 can be used as a test medium. The results to be presented do include one reduced pressure stability run in air to simulate altitude and some flapping derivative data obtained at reduced pressures in freon through a Mach number of 0.62. The particular operating curves employed in flutter testing are shown in Fig. 5-12.

The Langley transonic dynamics tunnel has the capability for studying aircraft gust response by means of a unique airstream oscillator system. This system (Fig. 5-13) consists of two sets of biplane vanes located on the side walls of the tunnel entrance section. The vanes are driven by a hydraulic motor through linkages to produce a nominally sinusoidal vane oscillation about a mean angle of attack of zero. Fig. 5-13 shows the interior of the tunnel, looking downstream toward the test section from the entrance section, and schematically shows the general arrangement of the airstream oscillator system. The vanes can be oscillated inphase or 180° out of phase to produce nominally sinusoidal vertical or rolling gusts, respectively. The gusts are generated by the cross-stream flow components induced by the trailing vortices from

the vane tips. Some general descriptive information pertaining to the characteristics of this system may be found in Refs. 5-5 and 5-6.

Test Procedure

Flutter points were established in the following manner: For a given model configuration the windmilling rpm was set by remotely adjusting the collective pitch of the blades and held constant as the tunnel was brought up to a low speed. The model was transiently excited in the wing beamwise and chordwise directions using the cable system described earlier and the stability of the response observed visually and recorded on oscillographs. The airstream velocity was incrementally increased and the model again excited. This procedure was continued until a sustained, approximately constant amplitude oscillation (indicating neutral stability) was observed in some mode of motion. The tunnel conditions were then recorded as the condition for flutter. The tunnel velocity was reduced to a low value, the rotor rpm set to a new value and the above procedure repeated. Rotor speeds below 238 rpm (January 1970 test) were selected to avoid 1/rev and 3/rev resonance with the pylon/wing and blade natural frequencies. In addition to recording the subcritical wing beamwise and chordwise transient response, steady-state levels of loads, vibration, and blade flapping were recorded.

Thrust effects on wing beam and chord mode damping were established by holding the tunnel speed and rotor rpm constant

and incrementally changing the thrust by varying the blade collective pitch. At each thrust level, the model was excited in the beam and chord directions and the resulting transient response recorded.

The model gust frequency response characteristics were obtained by holding tunnel speed and rotor rpm constant and incrementally increasing the tunnel oscillating vane frequency from zero to the maximum allowable by the tunnel conditions by means of an electrical control system located in the tunnel control room. Steady-state system response data were taken at each increment of frequency.

Flapping derivatives were determined by evaluating the slope of the curve of flapping angle versus mast angle of attack for each combination of tunnel speed and rotor rpm.

Presentation of Results

Because of the differences in the basic configuration it was judged that a chronological presentation of the test results would be appropriate, beginning with the September 1968 test and followed by the results of the January 1970 test. Continuing in this chronological sequence, some additional results pertaining to the Bell Model 300 tilt-rotor conclude the presentation.

(a) September 1968 Test

Parametric Study of Proprotor Stability: Various system parameters affect proprotor stability; some are stabilizing while others are destabilizing. To provide an indication of the relative degree to which stability can be affected, and to provide a wide

range of configurations for correlation with analysis, several system parameters were varied either individually or in conjunction with other parameters and the level of stability established. These results are presented and discussed below.

A baseline stability boundary, based on a reference configuration, was established first to provide a basis for comparison of specific effects. An indication of the relative degree to which stability can be affected can then be ascertained by varying selected system parameters away from the baseline configuration. The reference configuration consisted of the basic Model 266 configuration with the pylon yaw degree of freedom locked out and the wing aerodynamic fairings removed, with lead weights distributed along the wing spar to simulate a 100% fuel wing weight distribution. The hub restraint was set to zero and the δ_3 angle nominally set to -22.5°. The stability boundary corresponding to this reference configuration as well as the changes in this boundary due to several parameter variations are shown in Fig. 5-14.

(1) Altitude - Altitude has a highly stabiliting effect on proprotor/pylon stability. This increased stability is a consequence of the fact that both $\partial H/\partial \alpha_m$ and $\partial H/\partial q$ decrease with altitude for pylon pitch frequencies near the wing elastic mode frequencies. This means that a given level of these destabilizing shears is attained at progressively higher airspeeds as altitude increases.

(2) Hub Restraint - The stabilizing influence of moderate flapping restraint was verified as shown in Fig. 5-14. A

non-isotropic hub restraint was employed* having the ratio of longitudinal to lateral hub flapping restraint equal to 6.0. The longitudinal restraint gave an uncoupled longitudinal tip-path-plane flapping frequency of 0.27 cycles/rev. Increasing the flapping restraint increases the flapping natural frequency, bringing it closer to the "optimum" flapping frequency in the sense of Young and Lytwyn (Ref. 5-7). This increases stability since the pylon support stiffness requirements are reduced. In Ref. 5-8 data are presented which show that hinge offset is also stabilizing. Since flapping restraint is equivalent to hinge offset as far as their effects on the blade flapping natural frequency, the results of Ref. 5-8 substantiate the trend obtained here.

(3) Pylon/Wing Freedom - Although the proprotor/pylon/wing system of a tilt-rotor aircraft can exhibit various forms of instability the instability encountered with the reference configuration was in the wing beam mode,** that is, the coupled pylon pitch/wing vertical bending mode in which the pylon is pitching inphase with the wing vertical motion at a frequency near the fundamental wing beam bending natural frequency. This motion

---

* Specifically, K_{a_1} = 86,000 ft-lb/rad and K_{b_1} = 14,325 ft-lb/rad.

** Recall the discussion in Chapter 4 regarding the descriptive designations adopted for the coupled pylon/wing modes.

was accompanied by a negligible amount of wing chordwise bending and very little rotor flapping relative to space. Because of the large ratio of pylon yaw to pylon pitch stiffness the pylon angular motion, although primarily pitch, did exhibit some yawing motion resulting in a highly elliptical forward precession whirl of the pylon/rotor combination. Figs. 5-15 and 5-16 show the measured and calculated damping and frequency variation with airspeed for the wing beam and chord modes for the reference stability boundary of Fig. 5-14. Results are shown through the flutter point. Damping of other modes was such that no other modes were excited by the beamwise and chordwise excitation. A root locus showing the behavior of the flapping modes and pylon/wing modes as a function of airspeed for Ω = 238 rpm is given in Fig. 5-17. The initial increase in stability of the wing beam mode before instability occurs is associated with the fact that $\partial H/\partial q$ initially becomes more stabilizing with increasing airspeed (Fig. 4-16a) until $\partial H/\partial \alpha_m$ becomes sufficiently large to lower the pitch frequency to a level where $\partial H/\partial q$ becomes increasingly destabilizing with increasing airspeed. The decrease in frequency of the pylon/wing modes with increasing airspeed is caused by the negative spring effect of $\partial H/\partial \alpha_m$. The computer output corresponding to the root locus of Fig. 5-17 for an airspeed of 380 knots (just beyond the flutter speed) is given in Table 5-4. A dramatic illustration of the damping contributed by the proprotor is given in Fig. 5-18 which shows the damping of the wing beam mode versus airspeed for

the cases in which the rotor is on and off.

When the pylon yaw stiffness was reduced by unlocking the pylon yaw degree of freedom and soft-mounting the pylon in yaw relative to the wing tip (K_{yaw} = 5 x 10^6 ft-lb/rad) the stability decreased slightly (Fig. 5-14). Flutter was still in the wing beam mode, the pylon/rotor combination executing a low-amplitude, elliptical forward whirl motion. The particular yaw flexibility employed in this variation effectively produced a more nearly isotropic arrangement of the pylon support spring rates. Since the region of instability in a plot of critical pylon yaw stiffness against critical pylon pitch stiffness is extended along the line representing a stiffness ratio of unity (see Fig. 4-2, for example) the configuration approaching isotropy in the pylon supports is more prone to experience an instability than one in which one of the stiffnesses is significantly less than the other. Sample traces of the model response at flutter for the case of the pylon yaw unlocked (diamond symbol in Fig. 5-14) are shown in Fig. 5-19. The computer output corresponding to this configuration for an airspeed of 320 knots is presented in Table 5-5.

Suppression of the wing beam and chord degrees of freedom* gave a significant increase in stability. This result might appear

---

*The manner in which the wing beam and chord degrees of freedom were locked out moved the effective pylon pitch pivot forward from the conversion axis to the wing elastic axis (so that h_1 = 5.86 ft and $\bar{h}_1$ = 1.33 ft). The effective pylon yaw pivot remained at the conversion axis location (h_2 = 6.92 ft and $\bar{h}_2$ = 2.39 ft).

to be at variance with the sometimes-invoked analogy in rigid propeller whirl flutter considerations which regard the effects of wing vertical bending as equivalent to an increase in the hub translational damping which is significantly stabilizing for a propeller. However, because of the blade flapping freedoms the frequency response characteristics of a proprotor are fundamentally different from those of a propeller (see Fig. 4-20a). In particular, $\partial H/\partial q$ for a propeller is always stabilizing irrespective of the mast pitching frequency while the sign of $\partial H/\partial q$ for a proprotor is highly dependent on the frequency of the mast pitching oscillation. For the proprotor, locking out the wing beam degree of freedom increases the pylon pitch frequency relative to its value in the coupled pylon/wing mode in which the pylon pitch and wing beam motions are inphase (as in the flutter mode). This increases the separation between the pylon pitch mode and the low frequency flapping mode which, as pointed out in Chapter 4, is stabilizing.* Some experimental results showing the stabilizing effect of increased wing torsional stiffness are presented in Ref. 5-8. If in addition to locking out the wing beam and chord freedoms, the pylon yaw degree of freedom is unlocked (K_{yaw} = 3.76×10^6 ft-lb/rad) a decrease in stability is realized, as indicated in Fig. 5-14. The particular combination of increased pylon pitch stiffness and reduced pylon yaw stiffness gave a

*The reader is also referred to the discussion associated with Fig. 4-15a in Chapter 4.

system which was more nearly isotropic in nature and hence, by the reasoning employed above, more likely to experience an instability.

With the wing beam and chord degrees of freedom suppressed and the pylon locked to the wing tip in yaw the instability was effectively a pure pylon pitch oscillation near the pylon pitch natural frequency. When the pylon yaw stiffness was adjusted to produce approximately the same uncoupled frequency as that in the pitch direction the instability manifested itself as a low-amplitude forward whirl of the pylon near the pylon pitch natural frequency. In both cases in which the wing freedoms were suppressed, rotor flapping in space was small but of somewhat larger magnitude than when the wing was unrestrained.

(4) Wing Aerodynamics - The stiffness of a strength-designed wing for tilt-rotor application is generally sufficiently high to relegate the flutter speed of the pylon/wing combination (with blades replaced by an equivalent weight) to speeds well beyond the proprotor mode flight envelope. This suggests that wing aerodynamics will contribute primarily to damping wing motions as far as proprotor/pylon stability is concerned. Credence is given to this contention in Fig. 5-14 which shows that stability is increased with the wing aerodynamic fairings installed.* This indicates that proprotor aerodynamic forces are predominant in the ultimate balance of forces at flutter and provides some justification, a posteriori, that in this flutter mode at least,

*Flutter was in the wing beam mode.

wing aerodynamics can be neglected as a first approximation.

The general trend of decreasing stability with increasing rotor rpm shown for the reference and 10,000 ft stability boundaries over the rpm range shown was found for all values of the adjustable parameters of the model. The predicted flutter mode and frequency was, in all cases, in agreement with the corresponding measured mode and frequency.

Damping Concept: The linear structural damping concept in which the damping force is proportional to the elastic restoring force but inphase with the velocity of motion is commonly employed in fixed-wing flutter analyses to account for energy dissipation, in contrast to the more familiar viscous model of damping in which the damping force is proportional to the velocity of motion. The analytical results shown in Figs. 5-14 through 5-17 were based on the use of the structural damping model. Since this model of damping is strictly valid only for nondecaying sinusoidal motions, such as at the neutral stability condition just prior to flutter, a rigorous mathematical justification for associating any physical interpretation to the predicted sub-critical response is lacking. The reasonable sub-critical correlation for $\Omega = 238$ rpm seen in Fig. 5-15 for the case of structural damping is even more remarkable with reference to the corresponding results for the case of viscous damping in Fig. 5-20 — the predicted sub-critical response is essentially the same for both types of damping for all three rpm. The author offers the following comments for consideration regarding this apparent anomaly.

Damping, either structural or viscous, is introduced into the equations of motion as an equivalent constant damping coefficient appropriate to each mode of vibration, the coefficients being established on the basis of matching the energy dissipation of the true damping mechanism at some critical frequency condition, such as at a resonance condition or at flutter. For frequencies other than that for which the damping coefficients were evaluated either model of damping will, generally speaking, predict the wrong damping force. Damping in the physical model was established from measured wind-off decay traces. With reference to Figs. 5-16 and 5-17, the coupled frequencies of the model (in particular the wing beam mode) vary relatively slightly with increasing airspeed through the flutter speed so that the frequency at which each of the damping coefficients was evaluated is not far removed from the flutter frequency. That the predicted sub-critical damping using structural damping is in general agreement with the levels predicted using viscous damping should therefore be no surprise. These thoughts are implicit in a recent note by Scanlan (Ref. 5-9) commenting on a paper by Crandall (Ref. 5-10).

Since the structural damping representation is mathematically correct at the neutral stability condition it is of interest to compare the stability boundaries resulting from the use of structural and viscous damping. This comparison is made in Fig. 5-21 for the case of the reference configuration. The use of viscous damping is seen to be analytically destabilizing

relative to the use of structural damping. Recalling* that structural and viscous damping dissipate the same amount of energy in a single-degree-of-freedom sinusoidal motion of frequency ω when $g = 2\zeta(\omega/\omega_n)$, if the flutter frequency is less than the frequency of the corresponding in-vacuum mode the quantity 2ζ must be greater than g to maintain the same energy dissipation. Since the approximation $g = 2\zeta$ was used in the calculations (as is commonly done) and the flutter frequency was such that $\omega/\omega_n < 1$, the use of viscous damping resulted in the reduced level of stability shown in Fig. 5-21. Similar effects have been demonstrated for propeller whirl flutter (Ref. 5-11).

Unsteady Aerodynamics: Vortex shedding from the rotor blades results in a lag in the blade element lift from its quasi-steady value based on the instantaneous angle of attack. A cursory study was made on the influence of this aerodynamic lag on the stability of the baseline configuration by introducing the effects of flow unsteadiness via Theodorsen's Circulation Function. These results are summarized in Fig. 5-22. The quasi-steady results correspond to a reduced frequency of zero so that the Circulation Function becomes identically equal to 1.0. Unsteady aerodynamics are seen to be analytically stabilizing on proprotor/pylon stability, a result already established for propellers in Ref. 5-12. It should be mentioned that this stabilizing influence is predicted even if Mach number effects are included.

* See, for example, W. T. Thomson: Vibration Theory and Applications, Prentice-Hall, 1965, pp. 72-73.

The unsteady boundaries are based on two ways of selecting the reduced frequency: in one case the wake frequency was assumed to be the rotor speed and the reduced frequency specified using that frequency; in the other case the wake frequency was taken to be equal to the coupled wing beam natural frequency (since flutter was known to occur in that mode). The second approach to the selection of reduced frequency yields a stability boundary more nearly in agreement with the quasi-steady result since the flutter frequency is near the coupled wing beam natural frequency and this known value was used to specify, in effect, the flutter reduced frequency.

The following procedure is suggested if Theodorsen unsteady aerodynamics are to be used to generate the proprotor aerodynamics:

1. Calculate the system coupled natural frequencies over the range of rotor rpm for which flutter calculations will be made.

2. Using the frequency of one of the system modes just calculated, say the lowest mode frequency, carry out a flutter solution. This establishes a flutter speed.

3. Choose another mode frequency and repeat step 2, etc.

4. The lowest flutter speed so calculated is taken to be the one of practical interest.

Pylon Static Divergence: For the model configuration in which the wing beam and chord degrees of freedom were locked out, the flapping freedom was additionally locked out and the pylon yaw restraint reduced to a level (K_{yaw} = 692,000 ft-lb/rad) conducive to precipitating a pylon static divergence before encountering a whirl instability. As the airspeed was incrementally increased the model pylon was plucked in yaw and the resulting frequency of

oscillation noted. The minimum rotor rpm consistent with the maximum permissible blade collective pitch was maintained as speed was increased in order to maximize the destabilizing shear force $\partial Y/\partial \psi_m$ (see Fig. 4-23) so that the divergence speed could be kept relatively low. Some points were repeated at higher rpm to give an indication of the effects of rotor rpm. These results, along with the calculated variation, are shown in Fig. 5-23. The data actually represent a composite of all data points irrespective of the rotor speed, which varied between 80 and 120 rpm. Analyses indicated that the experimental spread on rotor rpm had a relatively small effect on the predicted variation of frequency with airspeed. The average rotor speed (100 rpm) was used in the calculated results which are shown in the figure. Data could not be obtained through the divergence speed because the limited yaw freedom available (see Fig. 5-7) permitted the pylon to hit the yaw stops at speeds beyond about 280 knots. In the region where data was obtained, however, agreement with the calculated results is good.

Thrust Effects: Thrust has generally been found to have a stabilizing effect on both propeller and proprotor whirl stability. Data were obtained with the model operating in a powered configuration with wing fairings installed and zero hub restraint for several values of rotor rpm at flight speeds somewhat below the corresponding windmilling neutral stability airspeed.* Of

*The square symbol in Fig. 5-14.

particular interest is the effect of thrust on the damping of the wing beam mode. Some typical results are presented in Fig. 5-24, which shows the wing beam mode damping as a function of the proprotor thrust for two combinations of rotor rpm and airspeed. Positive values of thrust indicate a net propulsive force; negative values indicate that the proprotor thrust is acting in the drag sense (ie., aft). The cruise thrust range for the Model 266 is also indicated, the range shown including extremes which could be encountered in flight. Also shown is the measured value of damping for the corresponding windmilling condition. Note that thrust significantly increases the level of damping in the wing beam mode. A small portion of this increase is due to drive train mechanical damping. The important conclusion to be drawn from these results is that the damping levels are a minimum near the negative thrust level of the windmilling condition. This implies that the windmilling condition represents a minimum stability condition as far as proprotor stability is concerned, justifying the use of windmilling models in lieu of powered models. The same conclusion has been established by other investigators.

Data obtained at other rotor speeds and airspeeds gave results leading to the same conclusion as above.

Gust Response: Analytical methods for determining aircraft response to turbulence are more often than not based on power spectral analysis techniques which require the definition of the aircraft frequency response function, that is, the response to

sinusoidal gust excitation. A study to assess the feasibility of measuring the frequency response function utilizing aeroelastic models in a semi-free flight condition using the gust generated by the oscillating vane system of the transonic dynamics tunnel has been underway for several years. Some of the early findings of this investigation may be found in Refs. 5-5 and 5-13.

For two "flight" conditions well within the proprotor stability boundary (see Fig. 5-14) the system excitation was recorded for several model configurations. Although the model was not "free" the data so obtained do give an indication of the cantilevered frequency response characteristics and permit an evaluation of the effects of rotor and wing aerodynamics, rotor speed, and airspeed on system response.

A measure of the gust-induced angle of attack (or, simply, gust or stream angle) was provided by means of a small balsa vane flow direction transmitter, located approximately two rotor diameters upstream (Fig. 5-2) which gave readings proportional to the stream angle. The variation of the vertical component of the stream angle for an inphase (symmetric) oscillation of the biplane vanes is shown in Fig. 5-25. The curve shown is an average of data obtained from runs at several tunnel speeds. The amplitude of the stream angle has been normalized on the maximum amplitude of oscillation of the biplane vanes (6°) and plotted against the frequency parameter ω/V, where ω is the frequency of vane oscillation in rad/sec and V is the tunnel

velocity in ft/sec. This parameter is proportional to the reciprocal of the wavelength (spacing) between the vortices shed from the tips of the oscillating vanes. The result shown in Fig. 5-25 compares very well with measurements obtained by others (see, for example, Ref. 5-6) using hot wire anemometers and fast response pressure probes.

The results selected for presentation here, the wing root vertical bending moment amplitude response as a function of gust frequency, can be taken as one measure of the response of the system to vertical gust excitation. In order to ascertain the relative influence of the rotor and wing lifting surfaces, three model configurations were employed: wing only, with the rotor blades replaced by an equivalent lumped weight; rotor only, with the wing aerodynamic fairings removed; wing and rotor combined. These results are summarized in Figs. 5-26 to 5-28. In each of these figures the wing bending moment response has been normalized by the maximum amplitude of the gust angle using the curve of Fig. 5-25. The gust frequencies indicated are the equivalent full-scale values.

Comparison of the rotor-on and rotor-off response curves for the wing panels-on configuration of Fig. 5-26 illustrates two proprotor-related effects: first, the significant contribution of the rotor inplane H-force ($\partial H/\partial \varepsilon_g$) to wing bending loads, as indicated by the relative magnitudes of the bending moments; and second, the rotor contribution to wing beamwise

damping,* as indicated by the relative sharpness of the resonance peaks. The peak amplitudes occur when the gust frequency is in resonance with the wing beam frequency. This peak for the blades-off configuration is shifted to the higher frequency side of the rotor-on peak because the proprotor inplane shear force decreases the frequency of the wing beam mode. For the rotor-on case the bending moment is considerably larger than for the rotor-off case throughout the range of gust frequencies investigated. The wing chord mode frequency (about 2.8 cps) is within the gust frequency range but is absent from the response curves because the gust excitation is primarily vertical and there is very little coupling between the wing beam and wing chord modes. These results indicate that inplane shears generated by vertical gusts while in a cruise mode increase gust sensitivity.

Comparison of results with the rotor on for the cases in which the wing aerodynamic fairings are on and off (Fig. 5-27) shows that the bending moment response with the fairings on is somewhat larger at gust frequencies up to the wing beam frequency and thereafter remains about the same as for the fairings off. The resonance peaks are seen to occur at about the same frequency and have approximately the same width. This suggests that rotor damping predominates at wing beam resonance.

An indication of the effect of rotor rotational speed on the

---

*At this particular airspeed the proprotor contributes positive damping to the wing beam mode.

bending moment response may be obtained from Fig. 5-28 for the case of all wing fairings removed. The particular rpm shown represent the high and low cruise rpm for the Model 266. The bending moment is seen to be significantly increased when rpm is reduced, particularly in the region of resonance. For the Model 266 the design cruise rpm based on maximum propulsive efficiency is 238 rpm while the higher value is intended for turbulence penetration and during maneuvering because blade flapping is reduced. With reference to Fig. 5-28 increased rpm during turbulence penetration is also beneficial in reducing the wing bending loads.

Somewhat obscurred in the response curves of Fig. 5-28 is a heavily damped, low-amplitude resonance "peak" at a gust frequency of about 0.8 cps. This resonance is a manifestation of the low frequency flapping mode. The flapping frequency in the rotating system is about 0.8 cycles/rev. This gives a fixed system frequency of 0.2 cycles/rev for the $\Omega-\omega_\beta$ flapping mode. A rotor speed of 238 rpm is equal to 0.8 cps in the fixed system; for 298 rpm the fixed system frequency is 1.0 cps. The flapping modes are generally well damped for moderate or zero values of flapping restraint as pointed out in Chapter 4. These results constitute an experimental verification. The flapping at these frequencies was accompanied by visibly larger pylon pitching motions. The corresponding high frequency flapping mode frequencies (5 to 6 cps) were beyond the excitation capability of the oscillating vane

system.

The results shown in Figs. 5-26 to 5-28 indicate that "free-flight" rotary-wing models, in particular tilt-rotor models, could be used to measure the necessary frequency response functions for use in gust response analyses.

Blade Flapping: Some results showing the effects of non-symmetric hub restraint on the total flapping derivatives are given in Fig. 5-29. The data were obtained by Bell in the Ling-Temco-Vought 7 x 10-ft low-speed wind tunnel during the Composite Aircraft Program. Both $\partial\beta/\partial\alpha_m$ and $\partial\beta/\partial\psi_m$, the change in the maximum steady flapping per unit change in pitch and yaw angle respectively,are shown as a function of airspeed for both the high and low rpm design speeds of the Model 266. Because of pitch-flap coupling and the non-isotropic hub restraint a deflection of the mast in pitch or yaw results not only in longitudinal or lateral flapping but also some lateral and longitudinal flapping, respectively. β is the magnitude of the vector sum of these two flapping components. The results show that an increase in the flapping derivatives is associated with either an increase in airspeed or a reduction in rpm, as already demonstrated by the trend studies of Chapter 4. An indication of the effects of wing/rotor aerodynamic interference is provided for the high rpm condition where additional data is shown for the case of the wing aerodynamic fairings removed. Comparison of the panels-on and panels-off data indicates that the effect of the rotor/wing aerodynamic interference is to increase the flapping derivative

slightly relative to the case with the wing panels removed. The remaining difference between the pitch and yaw results are a consequence of the non-symmetric hub restraint. The data shown for $\partial\beta/\partial\alpha_m$ are slightly lower than those for $\partial\beta/\partial\psi_m$ because the larger flapping restraint is in the longitudinal direction. Also shown in Fig. 5-29 are the corresponding predicted derivatives based on the use of an aerodynamic loading distributed over the blade and an aerodynamic loading "lumped" at the 3/4-blade radius. Agreement between the measured and calculated values is good for both theories. Since the calculated results do not account for any rotor/wing aerodynamic interference the difference between the calculated pitch and yaw derivatives gives the complete effect due to the asymmetric hub restraint.

In the feathering sequence of transition, flapping sensitivity to a given mast angle of attack varies with rotor rpm. A typical variation of the steady-state flapping response is given in Fig. 5-30. The data were actually obtained during the January 1970 test and served to establish a steady-state flapping response baseline for evaluating the transient flapping response during feathering.The inclusion of these results here, however, seems appropriate. Since the proprotor mast was not affixed to a rigid structure the wind-on mast angle of attack α_m was not known (it was nominally 1°). The important conclusion following from Fig. 5-30 is that the trend is predicted correctly. It is also to be noted that the predicted results are in good agreement with the measured values even at very low rpm. The peak in the

flapping response occurs when the rotor speed is in resonance with the flapping natural frequency.

(b) January 1970 Test

Proprotor Stability: A reference configuration was again established. This consisted of the basic Model 266 configuration with the pylon yaw freedom locked out, a hub restraint of 86,800 ft-lb/rad*, $\delta_3 = -22.5^\circ$, and a simulated wing fuel weight distribution of 15% with the wing aerodynamic fairings installed. Fig. 5-31 shows the flutter boundary for this configuration as a function of rotor rpm from a value representing an overspeed condition down to zero rpm, the low rpm regime being important for stability considerations related to the feathering sequence of transition for a folding proprotor aircraft. The annotation accompanying the calculated results indicates that the proprotor/pylon/wing system would experience a wide variety of modes of flutter across the range of rotor rpm shown. At the two extremes of rotor rpm the experimentally determined flutter speeds agree reasonably well with the predicted values. Excessive vibration or oscillatory loads resulting from operation near resonances with the pylon/wing or blade modal frequencies often limited the maximum airspeed which could be reached. These points are indicated by the solid symbols.

---

*This gave an uncoupled flapping natural frequency of 1.28 cps.

The calculated stability boundaries in Fig. 5-31 represent the first or lowest flutter airspeed. Calculations were, however, carried out through 700 knots (with no Mach correction) in order to establish the character of the higher flutter modes. Needless to say the precise definition of the boundary required fine increments in rotor rpm. Fig. 5-32 compares the measured and calculated flutter frequencies, the calculated frequencies representing an airspeed sweep through 700 knots. The predicted flutter modes and frequencies were in agreement with the experimental results in all cases but that at Ω = 215 rpm. A wing torsion instability having a frequency of 6.9 cps was predicted whereas the measured instability involved a coupled wing beam/rotor flapping motion at 1.6 cps, near the wing beam natural frequency. Although significant wing torsion activity was visually observed in the 175 to 220 rpm range the flutter observed at 215 rpm was clearly in the wing beam mode and not torsion. To investigate the possibility that the wing torsion instability was "masked" in some manner various system parameters were analytically varied to assess the sensitivity of the wing torsion instability to these parameters. However, before presenting the results of these parametric studies it will be illuminating to discuss the nature of the flutter modes occurring through the rpm spectrum.

The flutter mode for $\Omega \gtrsim 240$ rpm was in the wing beam mode, that is, in the coupled pylon/wing mode in which pylon pitching (wing torsion) is inphase with wing beamwise bending. These

flutter modes are the same as those obtained for the baseline stability boundary in the September 1968 test and all have a root behavior similar to the one shown in Fig. 5-17.

Between Ω = 240 rpm and Ω = 220 rpm and again between 120 rpm and 165 rpm flutter is predicted to be in a coupled wing beamwise bending/rotor rigid-body flapping mode. Root loci showing the root behavior in these rpm ranges are given in Figs. 5-33 and 5-34. These show that instability is associated with the low frequency flapping root.

A wing torsion mode instability is predicted in the rpm range between 165 and 220. Recall that the wing torsion mode is characterized by an out of phase coupled wing beam and torsion motion with torsion being the predominant motion and somewhat more flapping in space than for the wing beam mode. An indication of the root behavior in this regime may be obtained from Fig. 5-35.

Below 120 rpm flutter is predicted to be in the high frequency ($\Omega + \omega_\beta$) flapping mode. Root loci plots corresponding to several rotor rpm in this range, including zero rpm, are presented in Figs. 5-36 to 5-39. The point labeled "no flutter" at 79 rpm was limited by blade loads as a consequence of excessive wobbling of the tip-path-plane, indicative of the approach to some type of flapping instability. A small region of increased stability is evident in the region of 50 rpm. This is due to flapping coupling with the wing beam mode as implied by Fig. 5-38.

The zero rpm (ie., stopped rotor) instability is associated with the $\Omega + \omega_\beta$ flapping mode (Fig. 5-39) and is characterized by predominantly large amplitude flapping oscillations of the tip-path-plane near the uncoupled tip-path-plane flapping natural frequency on the hub springs (1.28 cps), which was well below the lowest wing structural frequency. Although the rotor was not turning, the tip-path-plane flapping motion observed visually had a forward wobbling motion as though a travelling wave was moving in the forward whirl direction. There was negligible wing beam, chord, and torsion motion accompanying the flapping. Fig. 5-40 shows the variation in flap damping with airspeed. A hub damping of $\zeta_R = .015$ was used in obtaining the stability boundary in Fig. 5-31. The results in Fig. 5-40 indicate that the rotor hub structural damping is closer to $\zeta_R = .025$. It is to be noted, however, that the correct trend is predicted over the range in which data was obtained. A sample of the computer output corresponding to this flutter point is given in Table 5-6. Sample traces of the zero rpm instability are shown in Fig. 5-41 for a time about 7 seconds after a wing chord excitation. At this particular time the flapping is actually diverging, having a negative damping equal to 1.16% of critical. The instability is quite mild with a relatively long buildup time after chordwise excitation.

The low rpm flutter mode was similar in character to the zero rpm flutter mode: a predominantly large amplitude flapping motion near the $\Omega + \omega_\beta$ flapping mode frequency, the tip-path-plane exhibiting a wobbling motion in the forward whirl direction, but with slightly less flapping.

In the low rpm range where flutter data were obtained the predicted flutter characteristics are in agreement with the measured ones. This is pleasantly surprising in light of the simplicity of the mathematical model, particularly as regards blade stall effects. At these low rpm a significant portion of the inboard section of the blade is stalled and a portion of the outboard end. These effects were approximately accounted for by estimating the distribution of blade section windmilling angle of attack at the low values of rpm and using blade root cutout and tip cutoff to eliminate the regions developing negligible lift (ie., the stalled portions). Trend studies (not presented here) have shown that this has a stabilizing effect on the low rpm flapping instability.

The zero and low rpm instabilities were not anticipated prior to the test, as reference to the comments in the test log at the time the zero rpm instability was encountered would indicate. Since the instability was not understood at the time of the test, in order to gain insight into the nature of the instability and to assess the influence of system parameters, two adjustable parameters were varied (K_H and δ_3) and analytical trend studies on the effect of system degrees of freedom, precone, and structural damping were additionally carried out. The results of these

parametric studies will be presented below after summarizing the results of the wing torsion instability sensitivity study.

Wing Torsion Instability: The particular effects of wing torsion structural damping and proprotor precone on the wing torsion instability are brought out in Fig. 5-42. A reduction in wing torsion structural damping is destabilizing, as might have been anticipated. Precone is also seen to be destabilizing.

For rotor rpm in the range indicated the steady centrifugal forces and airload drag acting on the blades tend to bend the blades aft in a direction to "wash out" part of the built-in precone angle. The actual coning angle in this range of rpm is probably closer to one or two degrees, and this would have the effect of slightly reducing the size of the torsion instability region.

The effect of wing aerodynamics was established earlier to be primarily in damping the wing beam motion for the coupled mode in which the wing beam motion is inphase with the wing torsion motion. Now the wing torsion instability involves the out-of-phase coupled wing/pylon mode which is characterized as mainly a pitching motion of the pylon about an effective pivot just aft of the rotor. Since this position is located ahead of the wing aerodynamic center the wing loading acts as a positive spring on pylon pitching motions as well as contributing to increased damping in this mode. Wing aerodynamics are not included in the analysis so the effect of wing aerodynamic damping on the torsion instability

was assessed indirectly by increasing the wing torsion structural damping. The combined effect of reduced precone and increased damping ($\beta_0 = 2^\circ$, $g_t = .06$) to "account" for wing aerodynamic damping is seen to shift the torsion instability boundary to airspeeds beyond those associated with the coupled wing beam/rotor rigid-body flapping instability. This result suggests that the torsion instability can be masked, at least to the extent that it was not encountered experimentally.

Fig. 5-43 summarizes the results of the analytical study for assessing the influence of the rotor hub (gimbal) structural damping on the wing torsion mode instability. The predicted increase in stability with increasing damping might have been anticipated since the flutter mode involves significant flapping of the tip-path-plane relative to the mast making damping quite effective. The results of Fig. 5-40 indicate that ζ_R might be closer to .025 than .015 which is in a direction to minimize the region of torsion instability. Rotor hub structural damping was found to have no noticeable effect on the calculated stability for rpm greater than about 240 rpm since the motion at flutter is predominantly beamwise.

Low Rpm Flapping Instability: To gain some insight into the degrees of freedom important in the flutter mechanism at low rpm the pylon/wing degrees of freedom were sequentially suppressed analytically and the stability boundary evaluated. These results are summarized in Fig. 5-44. The chordwise freedom was established to have no effect on stability below 120 rpm and thus the 5° of

freedom result is identical to that in Fig. 5-31. This boundary is included here for reference. Deleting the wing beam degree of freedom gives a boundary which correctly predicts the flutter airspeed, mode, and frequency through 30 rpm. Beyond 30 rpm, although the flutter airspeed is not predicted correctly the flutter mode and frequency are. This indicates that the flapping instability is not caused by flapping coupling with the wing vertical bending motion, that is, any flapping moments arising from the vertical translation of the hub due to wing beam bending are not the cause of the instability even though the flap damping is very small at the high inflow angles associated with low rpm. Note that there is now no region of increased stability near Ω = 50 rpm, implying that wing beam freedom is indeed stabilizing on the flapping mode in this region (refer again to the root locus of Fig. 5-38).

In the 3° of freedom case having the pylon pitch and yaw freedoms suppressed the shape of the stability boundary through about 80 rpm is predicted rather well, although the flutter speeds agree with the reference values only below about 40 rpm and above about 80 rpm.

The 2° of freedom case, retaining just the tip-path-plane pitch and yaw freedoms, surprisingly enough predicts the general

average shape of the boundary through 100 knots, with excellent results below 30 rpm.

In all cases the flutter speed, mode, and frequency were predicted reasonably well at very low (including zero) rpm where data was available for correlation. This suggests that in this low rpm range at least, parameters other than the pylon support conditions dictate the stability of the flapping modes, in particular the rotor design parameters. Some of these were systematically varied to establish their influence on stability. Results of these parameter variations are given below.

(1) Proprotor Precone - The effects of precone on the stability of the 5° of freedom system are shown in Fig. 5-45, other parameters being fixed at their reference configuration values. Decreasing precone is seen to be highly stabilizing. No instability was predicted for $\beta_0 = 0^{\circ}$ through 500 knots. Based on the results of the low rpm trend studies presented thus far, it can be concluded that precone is the cause of the flapping instability at low (and zero) rpm. In Chapter 4 it was pointed out that large values of precone destabilize this same mode at high rpm. It appears that at low rpm any precone, however small, can destabilize the flapping mode.

(2) Rotor Hub Structural Damping - Since the flapping instability involves mainly tip-path-plane flapping it might be surmized that hub structural damping would have a beneficial influence on stability. This was already demonstrated in Fig. 5-40 for the case of zero rpm. Its effects on stability through

a rotor speed of 100 rpm are shown in Fig. 5-46 and indicate an overall stabilizing influence. The pylon/wing damping was also varied for a fixed ζ_R with negligible effect on the predicted stability. Hence, the only structural damping important at low rpm is that arising from the hub gimbal.

(3) Hub Restraint - A rotor design parameter which was both experimentally and analytically varied was the hub flapping restraint. The zero rpm stability was found to be highly dependent on K_H (Figs. 5-47 and 5-48), an increase or a decrease from the nominal value employed in the reference configuration leading to substantially higher flutter speeds. Some calculated results showing the effect of hub restraint on stability through a rotor speed of 80 rpm are given in Fig. 5-49 for the 5° of freedom system.

(4) Pitch-Flap Coupling - For $\delta_3 = -32^\circ$ the stability boundary from high to zero rpm was again established both experimentally and analytically. These results, given in Fig. 5-50, indicate that increased negative δ_3 is destabilizing throughout the rpm range investigated. The points denoted as "no flutter" were again limited by vibration or loads at the airspeeds shown. The corresponding measured and calculated flutter frequencies are given in Fig. 5-51, the calculated results again representing an airspeed sweep through 700 knots. For rpm greater than about 240 flutter, as in the case of $\delta_3 = -22.5$, was in the wing beam mode with the pylon executing a low-amplitude, highly elliptical

forward whirl. Rotor flapping in space was again small. The low rpm flutter had the same general characteristics as that for $\delta_3 = -22.5^\circ$ except that the flapping amplitudes were significantly larger and the flutter frequency was reduced slightly. The flutter mode and frequency agreed with the measured ones in all cases but that at $\Omega = 218$ rpm, where flutter was predicted in the wing torsion mode but occurred in a coupled wing beam/rotor flapping mode near the wing beam coupled natural frequency. This discrepancy is immediately evident in Fig. 5-51. However, the earlier comments relating to the suppression of the wing torsion instability are also applicable here.

The flutter point experimentally determined at $\Omega = 172$ rpm was in the predicted mode. The sub-critical response, shown in Fig. 5-52, illustrates an interesting modal response behavior similar to that found by Hall (Ref. 5-14). Besides the measured wing beam damping and frequency variation, Fig. 5-52 includes the calculated values for both the wing beam and low-frequency flapping modes. This behavior may be related to the associated root locus shown in Fig. 5-53. Note that as airpseed is increased the wing beam mode becomes more stable while the low-frequency flapping mode becomes less stable. This indicates a transition or switch from a dominant wing beam mode to a dominant flapping mode with an accompanying change in frequency. This movement can be interpreted in terms of the measured model behavior in Fig. 5-52. The wing beam mode, being least stable at low speeds,

is at first dominant. As airspeed increases, however, its damping continually increases. The damping of the $\Omega - \omega_\beta$ flapping mode meanwhile is continually decreasing. A mode switch occurs analytically at 280 knots at a damping 17% of critical. Beyond 280 knots the $\Omega - \omega_\beta$ flapping mode is the dominant mode and very abruptly becomes unstable as velocity is increased to about 320 knots. Since the flapping mode frequency is only slightly less than the wing beam frequency in the vicinity of flutter there is only a gradual, albeit distinct, transition in frequency of the beam mode as the flapping mode begins to predominate over the wing beam mode.* This same situation existed at $\Omega = 218$ rpm for $\delta_3 = -22.5^\circ$ (Fig. 5-33) but the response traces below flutter were such that reliable damping and frequency could not be determined from them. Table 5-7 gives the computer output corresponding to Fig. 5-53 for an airspeed of 320 knots. Examination of the $\Omega - \omega_\beta$ flapping mode (#12) indicates that a larger amount of wing beam motion is associated with this mode than in the wing beam mode (#9). This implies that the flutter mode is not necessarily determined by the root which goes unstable as airspeed is increased but the frequency at which a root (either pylon/wing or rotor flapping) goes unstable. It is also to be noted that the coupling between the wing beam and $\Omega - \omega_\beta$ flapping modes is implied by the frequency behavior shown in Fig. 5-52.

---

* The mode switch reported by Hall (Ref. 5-14) was from a high frequency pylon mode to the low frequency flapping mode so his results show an abrupt drop-off in frequency.

A summary of the effects of δ_3 on the zero rpm flutter speed is presented in Fig. 5-54. Flutter points were also obtained for two δ_3 with the wing aerodynamic fairings removed. These results imply that wing/blade aerodynamic interference is not a precipitating factor in the flapping mode instability.

As a point of interest Fig. 5-55 shows the calculated flutter boundaries in the rpm range representative of cruise flight for three values of δ_3. As already shown in Chapter 4 large positive or negative δ_3 is destabilizing on proprotor/pylon stability. These results demonstrate that negative δ_3 is slightly more destabilizing than positive δ_3. Whirl is in the forward direction at flutter for $\delta_3 = 0$ and -32° and in the backward direction for $\delta_3 = +32^\circ$.

In closing this discussion on the low rpm flapping instability it should be mentioned that the necessity of limiting the flapping amplitude during the feathering sequence of transition indicates that significantly increased values of hub restraint are needed as rpm approaches zero. This suggests that the low rpm instability may be only of academic interest, at least for the design configuration investigated. However, since it was a new phenomenon attention was directed to it and the related studies did permit exercising the analytical procedures by providing data for correlation.

Blade Flapping Degree of Freedom: With flapping completely locked out the stability increased but blade loads limited the maximum speed attainable. Although no flutter points could be

obtained, stability was demonstrated over the same rpm range as the reference configuration through 300 knots for $\Omega > 0$ and through 365 knots for $\Omega = 0$. Fig. 5-56 compares the wing beam mode damping versus airspeed for $\Omega = 300$ rpm for flapping locked and unlocked. The significant increase in the level of damping with flapping locked out is notable.

(c) Some Results Applicable to the Bell Model 300 Tilt-Proprotor

Several companies are actively engaged in proprotor research directed at the advancement of proprotor technology. As part of its effort, Bell Helicopter Company, in 1969, designed and built a 25-foot flight-worthy proprotor for full-scale verification of technology developed since the XV-3 and Transcendental Convertiplanes. Subsequently, Bell contracted with NASA-Ames and the Army Aeronautical Laboratories (Ames Directorate) for tests of the 25-foot proprotor in the Ames full-scale wind tunnel and for design studies of a proof-of-concept tilt-rotor aircraft. The Bell design resulting from that study has been designated the Model 300.

The two NASA-Ames/Bell test programs employing the 25-foot proprotor were conducted in the Ames tunnel: a dynamic test in July 1970 and a performance test in November 1970. Figs. 5-57 and 5-58, respectively, show the proprotor mounted in the Ames full-scale tunnel for these tests. In addition to establishing stability and performance characteristics* steady-state flapping

*Some of these results are presented in Ref. 5-15.

in the airplane mode was measured for several combinations of rotor rpm and tunnel speed during the dynamic stability test. One combination was repeated during the powered test to obtain an indication of the influence of wing/rotor aerodynamic interference on steady-state blade flapping. These results, expressed in derivative form, are tabulated in Table 5-8. Both the component and total flapping derivatives are given. The predicted results agree well with the measured values except for the lateral derivatives $\partial b_1/\partial \alpha_m$,where the calculated values are about half of the measured values. As indicated by a comparison of the 185 knot, 500 rpm data, wing/rotor aerodynamic interference has a negligible influence on the longitudinal flapping response but increases the lateral flapping response by about a factor of two over that for the case of no wing interference. This accounts for the discrepancy noted above since the analysis does not include any interference effects. This is demonstrated by the fact that the predicted value of $\partial b_1/\partial \alpha_m$ agrees with the measured value in the case of no wing interference.

Several scale models have also been built by Bell in support of their effort. Two of these are shown in Figs. 5-59 and 5-60. An experimental investigation conducted by Bell in the LTV low-speed wind tunnel with the model proprotor mounted on a strain-gage balance was directed at measuring the static normal- and side-force derivatives as a function of tunnel speed and rotor rpm. Some of their data are shown in Figs. 5-61 and 5-62 along with the predicted results using the analysis developed in Appendix C.

Model values are presented. The measured trends are predicted but the calculated values are larger in magnitude in all the cases. However, blade root conditions (such as effective root cutout and spinner effects on the flow field) are known to have a strong influence on the static forces and are probably the reason for the lack of quantitative agreement.

A recent joint NASA/Bell test program (August 1971) in the Langley transonic dynamics tunnel (Fig. 5-60), directed at determining the static stability and control characteristics of tilt-rotors operating in the airplane mode at high Mach and Reynolds numbers, provided the opportunity to measure the blade flapping characteristics at high Mach numbers since the model and sting to which it was attached were effectively rigid and the pitch sweeps were restricted to angles below stall. These results are believed to be the first which provide an experimental indication of the effect of high subsonic Mach number on proprotor flapping in the airplane mode of flight. Flapping was measured in both air and freon for several values of tunnel speed over a range of pitch angles. The resultant derivatives, obtained by evaluating the slopes of the flapping amplitude versus pitch angles curves, are shown in Fig. 5-63. Since the range of inflow ratios over which the derivatives were measured was the same in air and freon, and the test medium densities were about the same, an indication of the Mach number (ie., compressibility) effects on the flapping derivatives can be gotten by comparing the air and freon results. The speed of sound in freon is approximately half that in air so that

for a given tunnel speed (or inflow ratio) the Mach number in freon is about twice that in air. The calculated results for air had no Mach number correction applied to them but did account for the change in δ_3 with airspeed. Although the calculated results for freon included a Mach correction to the lift curve slope in addition to the δ_3 variation with airspeed, the measured dropoff in the flapping derivative at high Mach numbers could not be predicted until blade drag was included. Since the flapping derivative analysis does not include blade drag its effects were approximated by multiplying the perturbation change in blade section angle of attack by a constant representative of the "average" blade drag coefficient in the drag rise Mach number region. The drag rise associated with operation at high Mach numbers is seen to reduce the flapping as Mach number is increased and suggests that calculations based on the neglect of drag will predict conservative values of flapping at Mach numbers where drag is influential.

Additional Application of Stability Analysis

The results presented in this Chapter demonstrate that the analytical predictions are in general agreement with experimental data and thus provide validation of the proprotor stability and response analyses developed in this dissertation. Although the analyses have been developed for a proprotor of the semi-rigid (or gimbaled) type characteristic of Bell designs and are thus strictly applicable only to designs of that type, the analyses have a somewhat broader range of applicability. Specifically, the

stability analysis derived in Chapter 3 has also been applied (Ref. 5-16) to a large bulk of whirl flutter data obtained during a joint NASA/Grumman test program (March 1971) in the transonic dynamics tunnel employing a research configuration of a semi-span model of the Grumman "Helicat" tilt-rotor (Fig. 5-64). This tilt-rotor design is characterized by a proprotor having blades with offset flapping hinges. The objective of this particular investigation was the extensive parametric study of forward and backward whirl flutter, with emphasis on forward whirl, varying such parameters as pylon pitch and yaw stiffness and damping, hinge offset, and pitch-flap coupling.

For analysis purposes the restoring centrifugal force moment from the offset flapping hinge was represented by introducing an equivalent hub spring in the manner outlined in Appendix B. Analysis based on the equivalent gimbaled proprotor generally predicted the flutter speed, mode, and frequency of the whirl instability in each case. Some flutter data were obtained in which both the forward and backward whirl modes were very lightly damped (or one mode had zero damping while the other had a very small amount of positive damping). The analysis also predicted these "bi-modal" instabilities. Although results based on an equivalent system are not always satisfactory, the degree of correlation in this instance was extremely encouraging. These findings are being prepared as a NASA publication (Ref. 5-16).

CITED REFERENCES

5-1. Gaffey, T. M., J. G. Yen, and R. G. Kvaternik: "Analysis and Model Tests of the Proprotor Dynamics of a Tilt-Proprotor VTOL Aircraft", Presented at the Air Force V/STOL Technology and Planning Conference, Las Vegas, Nevada, September 1969.

5-2. Yen, J. G., G. E. Weber, and T. M. Gaffey: "A Study of Folding Proprotor VTOL Aircraft Dynamics", AFFDL-TR-71-7 (Vol. I), September 1971.

5-3. Molyneux, W. G.: "Aeroelastic Modeling", RAE TN-Structures 353, March 1964.

5-4. Kuntz, W. H., L. S. Wasserman, and H. R. Alexander: "Dynamically Similar Model Tests of Rotary Wing and Propeller Types of VTOL Aircraft", Presented at the Air Force V/STOL Technology and Planning Conference, Las Vegas, Nevada, September 23-25, 1969.

5-5. Gilman, J., Jr., and R. M. Bennett: "A Wind-Tunnel Technique for Measuring Frequency Response Functions for Gust Load Analysis", Journal of Aircraft, Vol. 3, Nov.-Dec. 1966.

5-6. Abbott, F. T., Jr.: "Brief Description of the Characteristics of the Langley Transonic Dynamics Tunnel Airstream Oscillator", Langley Meeting on Aircraft Response to Turbulence, Langley Research Center, Hampton, Virginia, September 24-25, 1968.

5-7. Young, M. I., and R. T. Lytwyn: "The Influence of Blade Flapping Restraint on the Dynamic Stability of Low Disk Loading Propeller-Rotors", Journal of the American Helicopter Society, October 1967.

5-8. Brandt, D. E.: "Aeroelastic Problems of Flexible V/STOL Rotors", Presented at the AGARD 34th Flight Mechanics Panel Meeting(AGARD Conference Proceedings No. 46: Aeroelastic Effects from a Flight Mechanics Standpoint), Marseilles, France, April 1969.

5-9. Scanlan, R. H.: "Linear Damping Models and Causality in Vibrations", Journal of Sound and Vibration, Vol. 13, 1970, pp. 499-503.

5-10. Crandall, S. H.: "The Role of Damping in Vibration Theory", Journal of Sound and Vibration, Vol. 11, 1970, pp. 3-18.

5-11. Reed, W. H., III, and S. R. Bland: "An Analytical Treatment of Aircraft Propeller Precession Instability", NASA TN D-659, 1961.

5-12. Houbolt, J. C., and W. H. Reed, III: "Propeller-Nacelle Whirl Flutter", Journal of the Aerospace Sciences, Vol. 29, March 1962.

5-13. Gilman, J., Jr.: "A Progress Report with Preliminary Results on a B-52 Wind-Tunnel Model Program Using the Airstream Oscillator", Langley Meeting on Aircraft Response to Turbulence, Langley Research Center, Hampton, Virginia, September 1968.

5-14. Hall, W. E., Jr.: "Prop-Rotor Stability at High Advance Ratios", Journal of the American Helicopter Society, Vol. 11, June 1966.

5-15. Wernicke, K. G., and H. K. Edenborough: "Full-Scale Proprotor Development", Presented at the 27th Annual National Forum of the American Helicopter Society, May 1971.

5-16. Kohn, J. S., and R. G. Kvaternik: "An Experimental and Analytical Investigation of Whirl Flutter for a Stiff-Inplane, Offset Flapping-Hinge Proprotor", proposed NASA Technical Note.

TABLE 5-1

SUMMARY OF NATURAL FREQUENCIES FOR 0.1333-SCALE SEMI-SPAN DYNAMIC AEROELASTIC MODEL

MODE	FULL SCALE* (CPS)	MODEL TARGET* (CPS)	MODEL ACTUAL (CPS)	
BLADE (Ω = 0; 60° Root Collective)				
1st Collective	5.5	15.2	14.2	
2nd Collective	17.1	46.8	43.0	
1st Cyclic	5.3	14.6	13.5	
2nd Cyclic	15.6	42.7	39.2	
3rd Cyclic	36.3	99.4	88.6	
WING (Coupled Cantilever Modes)			100% FUEL	15% FUEL
1st Beamwise	1.8	4.9	5.4	5.8
2nd Beamwise	27.0	73.9	66.0	74.0
1st Chordwise	3.1	8.5	8.4	9.0
1st Torsion	7.3	20.0	18.4	17.8
PYLON YAW				
Soft-Mounted	6.0	16.4	16.5	----
Locked	---	----	33.5	36.5

*100% fuel wing weight distribution

TABLE 5-2

MODEL 266 PHYSICAL PARAMETERS USED IN CORRELATIONS*

M_R	45.0	slugs
M_P	84.2	slugs
I_B	900	slug-ft^2
$I_{cg\ (pylon)}$	845	slug-ft^2
h	6.92	ft
$\bar{h}$	2.39	ft
R	19.25	ft
a_o	5.85	
η_1	.12	
η_2	1.00	
K_{pitch}	2.3×10^6	ft-lbs/rad
K_{yaw}	12.5×10^6	ft-lbs/rad
K_{beam}	25200	lbs/ft
K_{chord}	42300	lbs/ft
ζ_R	.015	

	September 1968 Test		January 1970 Test	
ζ_{pitch}	.0130		.0075	
ζ_{yaw}	.0130		.0100	
ζ_{beam}	.0130		.0050	
ζ_{chord}	.0130		.0075	
$\bar{c}$	1.1	ft	0.0	ft
ρ	.00222	slugs/ft^3	.00238	slugs/ft^3
WEM_{beam}	5.37	slugs	.81	slugs

*Values given are for the baseline configuration. Variations from these values are indicated in the text.

TABLE 5-3

SCALE FACTORS FOR 0.1333-SCALE SEMI-SPAN
DYNAMIC AEROELASTIC MODEL

Parameter	Scale factor (model/airplane)
Length	0.1333
Reduced frequency (advance ratio)	1.00 (1.00)
Mass-density ratio (Lock number)	1.00 (1.00)
Froude number	1.00
Velocity	0.365
Time	0.365
Mass	0.00237
Mach number	0.365
Rotor solidity	1.00
Reynolds number	0.0487
Frequency	2.738
Mass moment of inertia	4.2095×10^{-5}
Torsional spring rate	3.157×10^{-4}
Linear spring rate	1.777×10^{-2}
Stiffness (EI, GJ)	4.2095×10^{-5}
Force	2.369×10^{-3}
Bending moment	3.157×10^{-4}

TABLE 5-4

COMPUTER OUTPUT FOR PROPROTOR STABILITY ANALYSIS OF REFERENCE CONFIGURATION (SEPTEMBER 1968 TEST; Ω = 238 rpm, V = 380 kts)

PROPROTOR STABILITY CORRELATION LANGLEY TDT TEST 139 - RUN NO.1 BASELINE STABILITY BOUNDARY (238 RPM)

ROTOR RPM	VELOCITY FT/SEC	VELOCITY KNOTS	VELOCITY KEAS	ADVANCE RATIO MU	LOCK NUMBER	INFLOW ANGLE PHI
2.38000000E+02	6.41891892E+02	3.80000000E+02	3.80000000E+02	4.20315546E+00	3.79975079E+00	6.0725989[illegible]E+01

**** BLADE FLAPPING FREQUENCY(CYCLES/REV) = .772 **** BLADE DAMPING(PERCENT CRITICAL) = 15.600

SYSTEM EIGENVALUES REAL	SYSTEM EIGENVALUES IMAGINARY	FREQUENCY CPS	FREQUENCY CYCLES/REV	DAMPING PERCENT CRITICAL	
1.24025350E-01	-6.79366697E+01	1.08124250E+01	-2.72582142E+00	1.82560782E-01	
1.73761452E+00	6.78474300E+01	1.08062116E+01	2.72425503E+00	2.55917569E+00	
-1.04420538E+00	4.42161575E+01	7.10088838E+00	1.79013993E+00	-2.34041769E+00	
-8.04979738E-01	-4.44049933E+01	7.06727418E+00	-1.78166576E+00	-1.81281356E+00	
1.32379635E+00	-3.68804804E+01	5.85697836E+00	-1.47654917E+00	-3.59722573E+00	
-2.29728154E+00	3.66143332E+01	5.82735212E+00	1.46908037E+00	-6.27426841E+00	
-5.16052234E-01	1.80144113E+01	2.86708261E+00	7.22793935E-01	-2.86466332E+00	
-4.79532047E-02	-1.80143836E+01	-2.86707820E+00	-7.22792823E-01	-2.66193980E-01	
5.21586245E+00	9.00247283E+00	1.43278805E+00	3.61207072E-01	-5.79381082E+01	
-5.23779236E+00	-8.74154631E+00	-1.39221523E+00	-3.50978631E-01	5.98772750E+01	
4.01389076E-01	-9.58240438E+00	-1.52508702E+00	-3.84475720E-01	4.18881379E+00	
6.68666690E-02	9.34143277E+00	1.48673520E+00	3.74807194E-01	7.15807421E-01	◁ Flutter mode

SYSTEM EIGENVECTORS

ROW	COL	1 REAL	1 IMAGINARY	2 REAL	2 IMAGINARY	3 REAL	3 IMAGINARY	4 REAL	4 IMAGINARY
1		2.17566478E+00	1.9776273E-01	2.16819594E+00	2.2063000E-01	3.5352683E-01	1.5984074E-02	3.4644198E-01	3.7246557E-02
2		1.0000000E+00	0.	1.0000000E+00	0.	1.0000000E+00	0.	1.0000000E+00	0.
3		5.71166450E-04	-2.5136C775E-03	9.1732592E-04	2.4768924E-03	-3.6097594E-04	-1.5423740E-02	-2.8211204E-04	1.9562110E-02
4		1.4638461E-03	-1.0016173E-02	2.1957440E-03	9.8329652E-03	-1.2809784E-02	3.7077170E-03	-1.2783841E-02	3.4446044E-03
5		4.1236778E-05	-2.3768942E-04	5.0974835E-05	2.2540668E-04	-2.2094314E-03	2.5103755E-03	-1.9473936E-03	-2.1395992E-03
6		1.8769014E-05	1.0280967E-02	2.6605226E-04	-1.0396014E-02	-5.2734891E-04	-7.1398519E-04	-4.4417735E-04	7.6809767E-04
7		-1.2439804E-02	-2.0917520E-03	-1.2106766E-02	2.2761838E-03	-9.3143241E-02	-8.7911404E-02	-1.0296927E-01	7.6550678E-02
8		5.5837296E-03	-1.4686900E-C3	-5.4208413E-03	1.6014162E-03	-2.7415138E-01	-2.3627442E-01	-3.1730582E-01	1.8684732E-01
9		-1.7065403E-01	-3.9107783E-02	-1.6976659E-01	5.7980188E-02	6.8852556E-01	0.	6.9126249E-01	0.
10		-6.8021986E-01	-1.3465903E-01	-6.7144843E-01	1.3199947E-01	-1.5204819E-01	-5.7539546F-01	-1.4266691E-01	5.7043923E-01
11		-1.6101904E-02	-2.8368862E-03	-1.5664699E-02	3.0624399E-03	-1.0969631E-01	-1.0119778E-01	-1.2008427E-01	8.8679322E-02
12		6.9845494E-01	0.	7.0632491E-01	0.	3.2405965E-02	-2.2782756E-02	3.4664926E-02	1.9105389E-02

ROW	COL	5 REAL	5 IMAGINARY	6 REAL	6 IMAGINARY	7 REAL	7 IMAGINARY	8 REAL	8 IMAGINARY
1		2.0371693E-01	-3.0774547E-02	2.0173839E-01	3.0845343E-02	-4.9365818E+00	5.1877815E-01	-4.9597543E+00	-6.6138929E-01
2		1.0000000E+00	0.	1.0000000E+00	0.	1.0000000E+00	0.	1.0000000E+00	0.
3		-6.7376004E-03	-6.9439293E-03	-6.7459632E-03	6.2805?5CE-03	7.6988394E-04	-5.0825726E-04	7.6734112E-04	4.7957424E-04
4		2.8005088E-03	-6.8555399E-03	2.0616733E-03	6.9543816E-03	-6.2238613E-05	-4.9157183E-04	-4.4333894E-05	4.8893739E-04
5		6.1219260E-04	4.8943394E-03	4.9486334E-04	-4.9226224E-03	-1.7405595E-05	6.6831346E-04	-3.2164804E-05	-6.6734681E-04
6		-3.6481260E-04	-4.3885642E-04	-3.6128486E-04	4.3081585E-04	2.6172430E-05	-1.8617741E-05	2.6899095E-05	1.6142891E-05
7		1.6960378E-01	-2.5621237E-02	1.6992565E-01	2.5981247E-02	9.7855557E-01	0.	9.7886065E-01	0.
8		8.3256636E-01	0.	8.4230696E-01	0.	-1.9604458E-01	-2.0600369E-02	-1.9391246E-01	2.5858463E-02
9		-2.4397313E-01	3.3074024E-01	-2.0588177E-01	-3.3465678E-01	8.7586550E-03	1.4131293E-02	8.6024379E-03	1.3846174E-02
10		-2.5599387E-01	-9.3968171E-02	-2.5936629E-01	5.9510622E-02	8.8874954E-03	-8.6751531E-04	8.8100316E-03	7.7519248E-04
11		1.7930362E-01	-2.9068090E-02	1.7910170E-01	2.9427741E-02	-1.2030294E-02	-6.5834613E-04	-1.2020299E-02	6.1143053E-04
12		-1.5667189E-02	1.4006236E-02	-1.4944064E-02	-1.4217916E-02	3.2188131E-04	4.8108865E-04	2.8951433E-04	-4.8534471E-04

ROW	COL	9 REAL	9 IMAGINARY	10 REAL	10 IMAGINARY	11 REAL	11 IMAGINARY	12 REAL	12 IMAGINARY ◁ Flutter mode	
1		7.5876829E-03	1.3804545E-02	6.1706173E-03	-1.3724982E-02	1.3661654E-02	1.1728748E-03	1.2930038E-02	-8.4909377E-04	x
2		1.0000000E+00	0.	1.0000000E+00	0.	1.0000000E+00	0.	1.0000000E+00	0.	z
3		-2.5027919E-03	-2.3492342E-02	-3.4146592E-03	2.5463774E-02	1.1588243E-02	1.6413133E-03	1.2805448E-02	-1.8901960E-03	a_1
4		-1.6726458E-02	2.6307393E-C3	-1.8434471E-02	-3.5766831E-03	1.8163748E-03	8.1686061E-03	1.8307022E-03	-9.2632146E-03	b_1
5		3.7218860E-03	3.6486564E-03	3.8567062E-03	-3.7628069E-03	-3.0143583E-04	-5.0248033E-03	-9.9072516E-05	5.2373433E-03	ϕ_y
6		2.7666090E-05	-7.9735831E-04	6.0751212E-05	8.6591747E-04	3.4031582E-04	5.4236254E-07	3.7722340E-04	-1.9393653E-05	ϕ_z
7		7.1831957E-03	1.3066647E-02	5.7946516E-03	-1.2888741E-02	1.3439074E-02	1.1537660E-03	1.2693185E-02	-8.3354007E-04	
8		9.4669161E-01	0.	9.3907163E-01	0.	9.8370768E-01	0.	9.8168199E-01	0.	
9		2.2454339E-01	1.0000151E-01	2.4063082E-01	-1.0350407E-01	2.0379121E-02	-1.1038442E-01	1.8513397E-02	1.1949484E-01	
10		6.3466070E-02	-1.6413938E-01	6.5289684E-02	1.8002531E-01	7.9003960E-02	-1.4126449E-02	8.6654104E-02	1.6481981E-02	
11		-5.2220135E-02	1.4475079E-02	-5.3325465E-02	-1.4377817E-02	-4.8270690E-02	8.7157888E-04	-4.8930915E-02	-5.7527554E-04	
12		7.0338940E-03	4.4075745E-03	7.2564509E-03	-5.0669199E-03	1.4179619E-04	-3.2608261E-03	2.0638818E-04	3.5225102E-03	

TABLE 5-5

COMPUTER OUTPUT FOR PROPROTOR STABILITY ANALYSIS OF PYLON YAW UNLOCKED CONFIGURATION (SEPTEMBER 1968 TEST; Ω = 298 rpm, V = 320 kts)

PROPROTOR STABILITY CORRELATION - LANGLEY TDT TEST 139 RUN NO.3 PYLON YAW UNLOCKED (298 RPM)

ROTOR RPM	VELOCITY FT/SEC	VELOCITY KNOTS	VELOCITY KEAS	ADVANCE RATIO J	LOCK NUMBER	INFLOW ANGLE PHI
2.98000000E+02	5.40540541E+02	3.20000000E+02	3.09056575E+02	2.82684846E+00	3.80443786E+00	5.01885988E+01

**** BLADE FLAPPING FREQUENCY(CYCLES/REV) = 831 **** BLADE DAMPING(PERCENT CRITICAL) = 18.704

SYSTEM EIGENVALUE REAL	SYSTEM EIGENVALUE IMAGINARY	FREQUENCY CPS	FREQUENCY CYCLES/REV	DAMPING PERCENT CRITICAL	
-3.0470145[illegible]E+00	5.6768174[illegible]E+01	9.03493559[illegible]E+00	1.81911454E+00	-5.36747033E+00	
-3.03050789E+00	5.67118196E+01	9.02596578E+00	1.81730855E+00	-5.34369746E+00	
4.39875964E-01	3.59626955E+01	-6.23655956E+00	-1.26776367E+00	1.11185217E+00	
-7.09524915E-01	3.94562416E+01	6.28602208E+00	1.26564203E+00	-1.78377609E+00	
-2.65880228E+00	3.44886040E+01	5.48900311E+00	1.10516781E+00	-7.70926429E+00	
-1.54756096E+00	3.45610454E+01	5.49101256E+00	1.10557300E+00	-4.48554749E+00	
-7.00691914E-01	1.80245366E+01	2.86869410E+00	5.77589416E-01	-3.88721180E+00	
-2.32171259E-01	1.80244940E+01	2.86868732E+00	-5.77588050E-01	-1.28808753E+00	
-6.69361629E+00	6.32427325E+00	1.32484924E+00	2.66748168E-01	-7.98101659E+01	
-6.73646953E+00	-6.17950534E+00	-1.30140871E+00	-2.62109136E-01	-8.23579086E+01	
4.30337519E-01	1.01630116E+01	1.60807156E+00	3.23772797E-01	4.25916017E+00	
7.81015835E-02	9.98149584E+00	1.58860443E+00	3.19853235E-01	7.82463718E-01	◁ Flutter mode

SYSTEM EIGENVECTORS

ROW	COL	1 REAL	1 IMAGINARY	2 REAL	2 IMAGINARY	3 REAL	3 IMAGINARY	4 REAL	4 IMAGINARY
1		3.7472283E-01	3.6028587E-02	3.7183339E-01	-5.5993186E-02	1.7668011E-01	-5.8004952E-03	1.7618620E-01	6.9444451[illegible]-03
2		1.0000000E+00	0.	1.0000000E+00	0.	1.0000000E+00	0.	1.0000000E+00	0.
3		6.6113219E-04	1.2317387E-02	6.5904410E-04	1.2336466E-02	3.1766241E-03	-4.3795976E-03	3.1911557E-03	4.3314[illegible]-03
4		1.2212337E-02	6.9351669E-04	1.2225667E-02	6.7253867E-04	-1.3333745E-03	-3.5863054E-03	-1.4125787E-03	3.6819[illegible]-03
5		9.1793849E-04	7.0599560E-04	9.2265518E-04	-9.2265518E-04	5.6731573E-05	4.5875080E-03	-2.9067665E-05	4.5755495-01
6		7.4861625E-04	4.9264963E-04	8.0383902E-04	-4.0471054E-04	1.1708137E-03	1.4436350E-03	1.1477576E-03	1.5066644[illegible]-01
7		3.9545256E-02	2.6046318E-02	4.0511713E-02	2.3749699E-02	1.6434277E-01	-5.3954543E-04	1.6389468E-01	6.4599702[illegible]-01
8		1.1128846E-01	5.8570596E-02	1.1595503E-01	4.5409033E-02	9.3017132E-01	0.	9.3023943E-01	0.
9		7.0126501E-01	0.	7.3148353E-01	0.	1.7466493E-01	1.2374855E-01	1.6884427E-01	1.2667775[illegible]-01
10		2.1563494E-03	6.9535559E-01	1.0917702E-03	6.9537913E-01	-1.4247043E-01	5.1253156E-02	-1.4442602E-01	5.8[illegible]-02
11		4.9859723E-02	3.2162859E-02	5.0889088E-02	2.9557987E-02	1.8152241E-01	-6.2213004E-04	1.8074302E-01	2.0775577[illegible]-01
12		3.0381715E-02	4.3278652E-02	2.8926446E-02	4.4171637E-02	5.7628749E-02	-4.5685241E-02	5.8698762E-02	4.6[illegible]-02

ROW	COL	5 REAL	5 IMAGINARY	6 REAL	6 IMAGINARY	7 REAL	7 IMAGINARY	8 REAL	8 IMAGINARY
1		1.2932166E-01	2.4197968E-02	1.2892557E-01	-2.2276698E-02	-6.1253657E+00	4.7659873E-01	-6.1449357E+00	-5.9566707E-01
2		1.0000000E+00	0.	1.0000000E+00	0.	1.0000000E+00	0.	1.0000000E+00	0.
3		7.4855965E-03	5.0858867E-04	7.5678657E-03	-5.4280838E-04	5.5019642E-04	-4.4252506E-04	5.4945397E-04	4.1834336E-04
4		2.0911693E-03	1.0553923E-02	2.2416728E-03	-1.0569673E-02	-1.1364020E-04	-3.1364020E-04	-1.1936041E-04	3.1834654E-04
5		3.2367711E-04	-2.7222619E-03	3.5639709E-04	2.0837441E-03	-2.9683055E-05	5.5518829E-04	-4.0861233E-05	-5.5353434E-04
6		-5.7743487E-03	7.0730237E-03	-5.8648031E-03	7.9794768E-03	6.4864046E-05	-4.7312611E-05	6.6864161E-05	4.0288825E-05
7		9.1962958E-02	1.7211352E-02	9.0972526E-02	-1.5720306E-02	9.8534849E-01	0.	9.8547333E-01	0.
8		7.1127263E-01	0.	7.0562051E-01	0.	-1.5989561E-01	-1.2441060E-02	-1.5887870E-01	1.5401107E-02
9		2.3638975E-03	-2.5956021E-01	-7.0157251E-03	2.6193934E-01	7.5908130E-03	1.0227091E-02	7.4128936E-03	-1.0000938E-02
10		-5.9148530E-01	3.0806045E-02	-5.4364275E-01	-5.3110320E-02	5.7491968E-03	-2.2493055E-03	5.7657474E-03	2.0775301E-03
11		9.3025877E-02	1.8491063E-02	9.2040443E-02	1.6449331E-02	-9.9862143E-03	-9.2401704E-04	-9.9676896E-03	8.6501782E-04
12		2.8677795E-01	1.7823014E-01	2.8437626E-01	1.8999314E-01	8.0734332E-04	1.2022284E-03	7.1070354E-04	-1.2113022E-03

ROW	COL	9 REAL	9 IMAGINARY	10 REAL	10 IMAGINARY	11 REAL	11 IMAGINARY	12 REAL	12 IMAGINARY ◁ Flutter mode
1		3.4706591E-03	1.8890919E-02	1.9019079E-03	-1.8822541E-02	1.8660116E-02	2.0657196E-03	1.8150301E-02	-1.6182582E-03 x
2		1.0002000E+00	0.	1.0000000E+00	0.	1.0000000E+00	0.	1.0000000E+00	0. z
3		-1.1636306E-02	-2.9808377E-02	-1.3440565E-02	3.0674785E-02	9.3137294E-03	9.2431752E-03	9.9146926E-33	-2.5904056E-03 a_1
4		-2.4350562E-02	1.5033987E-02	-2.5227644E-02	-1.4790153E-02	1.0071395E-03	6.2230989E-03	8.2498718E-04	-6.7957117E-03 b_1
5		4.9272051E-03	3.5985073E-03	5.0397575E-03	-3.5923419E-03	-3.4308565E-04	-5.6379087E-03	-1.1644641E-04	5.7593756E-33 ϕ_y
6		9.9272979E-05	-3.1257655E-03	1.8787300E-04	3.2563099E-03	7.2376662E-04	-2.2862263E-06	7.7847225E-04	-4.7893866E-05 ϕ_z
7		3.0787578E-03	1.6734459E-02	1.6617965E-03	1.6446239E-02	1.8408435E-02	2.0378580E-03	1.7887414E-02	-1.5948195E-03
8		8.8499065E-01	0.	8.7375233E-01	0.	9.8651238E-01	0.	9.8551611E-01	0.
9		3.2544023E-01	1.0111703E-01	3.4144652E-01	-9.6702584E-02	2.6672666E-02	-9.3138845E-02	2.6630476E-02	9.8761148E-02
10		9.2978801E-02	-2.8891950E-01	4.8969150E-02	3.0598310E-01	6.3310429E-02	-7.4979146E-03	6.7895801E-02	7.7038503E-03
11		-6.2668941E-02	1.7166300E-02	-6.3533753E-02	-1.7023021E-02	-5.7112010E-02	1.0402691E-03	-5.7493283E-02	-7.1251941E-04
12		2.5393492E-02	2.1619336E-02	2.5369404E-02	-2.3472741E-02	2.8836433E-04	-7.3137854E-03	5.3885234E-04	7.7665770E-03

TABLE 5-6

COMPUTER OUTPUT FOR ZERO RPM STABILITY ANALYSIS OF REFERENCE CONFIGURATION (JANUARY 1970 TEST; V = 160 kts)

PROPROTOR STABILITY CORRELATION LANGLEY TDT TEST 164 RUN NO.1 - 1 RPM

ROTOR RPM	VELOCITY FT/SEC	VELOCITY KNOTS	VELOCITY KEAS	ADVANCE RATIO J	LOCK NUMBER	INFLOW ANGLE PHI
1.0000000E+00	2.7027027E+02	1.6000000E+02	1.6000000E+02	4.2120042IE+02	4.0736315BE+00	8.9679490BE+01

SYSTEM EIGENVALUES REAL	SYSTEM EIGENVALUES IMAGINARY	FREQUENCY CPS	FREQUENCY CYCLES/REV	DAMPING PERCENT CRITICAL	
-1.3342815E+00	7.0343286BE+01	1.1195418E+01	6.7172809E+02	-1.8968143AE+00	
7.6743396ZE-01	-7.0343194ZE+01	1.1195467IE+01	6.7172802SE+02	1.0939853BE+00	
-8.2674015IE-01	4.2917415ZE+01	6.8305187ZE+00	4.0983112BE+02	-1.9263512ZE+00	
4.2237163JE-01	-4.2916945OE+01	-6.8304439AE+00	-4.0982663BE+02	9.8416045ZE-01	
-2.7138498IE-01	1.8096215JE+01	2.8801022IE+00	1.7280613ZE+02	-1.4997050BE+00	
2.7137451IE-01	-1.8096215YE+01	-2.8801022IE+00	-1.7280613ZE+02	1.4996202IE+00	
-3.4111691JE-01	1.3215585AE+01	2.1033257AE+00	1.2619954AE+02	-2.5811714ZE+00	
5.4644808BE-02	-1.3215663IE+01	-2.1033331IE+00	-1.2620028IE+02	4.1348518BE-01	
1.7345081UE-02	-8.0053137SE+00	-1.2740852SE+00	-7.6445115BE+01	2.1666959IE-01	
1.1026467AE-02	8.0050618BE+00	1.2740431GE+00	7.6442709BE+01	1.3774368IE-01	◊ Flutter mode
-2.5431128JE-01	7.7778151IE+00	1.2378778BE+00	7.4272672BE+01	-3.2637033BE+00	
-2.4536626ZE-01	7.7780492OE+00	-1.2379149BE+00	-7.4274898IE+01	-3.1545989BE+00	

SYSTEM EIGENVECTORS

ROW	COL	1 REAL	1 IMAGINARY	2 REAL	2 IMAGINARY	3 REAL	3 IMAGINARY	4 REAL	4 IMAGINARY
1		-4.3629801GE-02	-1.7654496E-01	2.0935746E-02	6.9003472E-01	5.5974071E-34	6.8102827E-35	-5.2614409E-34	-1.9973540E-34
2		5.2584468JE-07	-9.1540952E-06	3.5155292E-07	9.1652158E-06	-4.0857804E-04	-2.1209945E-02	2.0880837E-04	2.1216703E-02
3		1.1849716E-06	-1.8554110E-05	-5.1153443E-07	-1.8603304E-05	6.5737584E-05	7.0750967E-03	-1.5299157E-04	-7.0729199E-03
4		1.9626062E-04	-1.0343997E-02	1.1287584E-04	1.0340228E-02	7.4926617E-07	-2.9369980E-05	3.4608716E-06	2.9143255E-05
5		1.1479080E-06	-2.2307760E-05	8.2656094E-07	2.2321667E-05	-8.2562583E-05	-6.5055741E-03	1.0401431E-04	6.5052955E-03
6		2.0031645E-04	-9.7418309E-03	-8.2611856E-05	-9.7450147E-03	8.7647691E-07	1.8164945E-05	-7.3155702E-07	-1.8173574E-05
7		7.8703614E-01	-1.8490923E-01	3.0656339E-01	1.9872283E-01	-5.5847402E-34	4.2039215E-33	1.9844571E-33	3.9256870E-33
8		6.4463077E-04	-2.4775514E-05	6.4498035E-04	-1.7695657E-05	9.1361301E-01	0.	9.1065286E-01	0.
9		1.3067362E-03	5.8578387E-05	1.3990084E-03	2.1706159E-05	-3.0369921E-01	-3.0279794E-03	-3.0361273E-01	-3.5785402E-03
10		7.2789256E-01	0.	7.2787337E-01	0.	1.2598642E-03	5.6437909E-05	1.2593596E-03	-1.3621231E-04
11		1.5704339E-03	-5.3775054E-05	1.5708117E-03	-4.1012532E-05	2.7927068E-01	1.8350466E-03	2.7921531E-01	-1.7163244E-03
12		-6.8555896E-01	1.0929720E-03	-6.8555886E-01	-1.6674734E-03	-7.8031712E-04	2.2598434E-05	-7.8015565E-04	2.5867305E-05

ROW	COL	5 REAL	5 IMAGINARY	6 REAL	6 IMAGINARY	7 REAL	7 IMAGINARY	8 REAL	8 IMAGINARY
1		-8.2729136E-04	-5.5153603E-02	8.2724456E-04	5.5163604E-02	4.6803348E-31	7.3908036E-31	-7.0622902E-31	-5.0513386E-31
2		-9.4620917E-31	-1.0998339E-28	2.7690030E-42	3.2772959E-40	-1.9418173E-03	-7.5230077E-02	3.1126278E-04	7.5277857E-02
3		-9.1013026E-32	2.1952059E-29	-1.6603902E-42	-6.5043090E-41	-3.7994751E-04	-4.3733357E-03	-1.1652593E-04	4.3971780E-03
4		3.7615072E-31	-2.7186539E-30	1.0760897E-43	-2.7780143E-43	-1.0043511E-05	1.0698852E-04	-2.5822154E-05	-1.0223188E-04
5		-1.7226199E-32	1.5470220E-30	-3.2805592E-43	4.3327566E-42	1.0599622E-04	2.5860071E-03	4.4065595E-05	-2.5897830E-03
6		2.6246212E-32	-3.3229330E-31	-8.5253952E-45	6.7311459E-44	-1.0064374E-06	-6.5820601E-06	-2.7681821E-07	6.7068149E-06
7		9.9847699E-01	0.	9.9847699E-01	0.	-1.8385567E-29	1.1537380E-29	-1.2985391E-29	1.7198589E-29
8		1.9142469E-27	1.4924716E-29	5.7722045E-39	4.1456926E-41	9.9487190E-01	0.	9.9486380E-01	0.
9		3.4910188E-28	-4.8847436E-30	-1.0587755E-39	1.3723231E-41	5.7925798E-32	-3.5294100E-03	5.8105255E-02	1.7802511E-03
10		1.0212136E-28	3.3744129E-30	-4.4437512E-41	-4.1509503E-42	-1.4104900E-03	-1.6922648E-04	-1.3524731E-03	3.3567345E-04
11		2.0016112E-28	6.6680429E-31	7.9486734E-40	1.0278160E-41	-3.4211755E-02	5.1867132E-04	-3.4223292E-02	-7.2387422E-04
12		-8.6433555E-29	3.6580714E-30	4.7793135E-41	4.6095533E-43	8.7323090E-05	-1.1055407E-05	8.8619880E-05	4.0248287E-06

ROW	COL	9 REAL	9 IMAGINARY	10 REAL	10 IMAGINARY ◊ Flutter mode	11 REAL	11 IMAGINARY	12 REAL	12 IMAGINARY	
1		1.4580638E-39	-4.3068271E-40	1.0664244E-38	-8.4487708E-39	2.3175445E-39	-1.2063061F-38	-3.8092460E-41	1.9534281E-39	x
2		-8.9137829E-03	1.7283220E-02	1.0257302E-02	-1.6389801E-02	1.5865999E-02	6.7293463E-33	1.4778345E-02	-7.7101157E-03	z
3		7.0902126E-02	3.5751897E-02	6.9928891E-02	-3.4635508E-02	-3.3674416E-03	1.0298930E-01	3.2318598E-03	1.0244915E-01	a_1
4		2.0174258E-04	9.3110702E-32	1.2987995E-04	-9.4291039E-02	6.9353157E-32	-2.2357318E-02	6.9725543E-32	2.4074398E-02	b_1
5		3.2671646E-03	2.6033533E-04	3.2156654E-03	-4.2644679E-04	1.0004603E-03	-4.2812967E-03	-7.0486918E-04	4.3076234E-03	ϕ_y
6		1.6168744E-04	7.4445103E-04	1.1392603E-04	-7.5968014E-04	4.9916049E-34	-3.3592517E-04	5.2242233E-04	3.1649356E-04	ϕ_z
7		-1.5998147E-38	-6.0272120E-38	3.3268468E-37	4.4806194E-37	5.0927365E-37	9.6370712E-38	8.2171567E-38	6.6706385E-39	
8		1.3820299E-01	7.1657408E-02	1.3108827E-01	-8.2291062E-02	-5.6376521E-02	1.2169147E-01	-6.3595693E-02	-1.1305256E-01	
9		2.8743496E-01	-5.6697364E-01	2.7803045E-01	5.5940319E-01	8.0188823E-01	0.	7.9764751E-01	0.	
10		7.4538389E-01	0.	7.9480703E-01	0.	1.5625382E-01	5.4510182E-01	1.7014353E-01	-5.4823653E-01	
11		2.1434806E-03	-2.6133163E-02	3.4491904E-03	2.5736899E-02	3.3553567E-02	-6.6926145E-03	3.3676322E-02	4.4255108E-03	
12		5.9623686E-03	-1.2814461E-03	6.0825427E-03	9.0360834E-04	2.4858221E-03	3.9678081E-03	2.3335176E-03	-4.1410834E-03	

TABLE 5-7

COMPUTER OUTPUT FOR PROPROTOR STABILITY ANALYSIS OF CONFIGURATION WITH $\delta_3 = -32°$ (JANUARY 1970 TEST; Ω = 172 rpm, V = 320 kts)

CORRELATION STUDIES TDT TEST 164 DELTA 3 = -32 DEGREES

PROP RPM	VELOCITY FT/SEC	VELOCITY KNOTS	KEAS	ADVANCE RATIO J	LOCK NUMBER	INFLOW ANGLE PHI
1.72000000E+02	5.40540541E+02	3.20000000E+02	3.20000000E+02	4.89767931E+00	4.07863158E+00	6.43085434E+01

**** BLADE FLAPPING FREQUENCY(CYCLES/REV) = .679 **** BLADE DAMPING(PERCENT CRITICAL) = 16.975

SYSTEM EIGENVALUES REAL	SYSTEM EIGENVALUES IMAGINARY	FREQUENCY CPS	FREQUENCY CYCLES/REV	DAMPING PERCENT CRITICAL	
-1.73927562E+00	6.86555805E+01	1.09268750E+01	3.81170058E+00	-2.53333466E+00	
-3.09304653E-01	-6.86668806E+01	-1.09286735E+01	-3.81232796E+00	-4.50442265E-01	
6.03007645E-01	-4.13951200E+01	-6.58823797E+00	-2.29822555E+00	1.45671191E+00	
3.73462351E-02	4.13522184E+01	6.5814099 7E+00	2.29584069E+00	9.03125310E-02	
-2.53028924E+00	2.86208267E+01	4.55514604E+00	1.58900443E+00	-8.84072731E+00	
-2.44337476E+00	-2.85559450E+01	-4.54481980E+00	-1.58540225E+00	-8.55644862E+00	
-3.34229946E-01	1.80936008E+01	2.87968600E+00	1.00454163E+00	-1.84722737E+00	
-6.28085310E-02	-1.80936008E+01	-2.87968600E+00	-1.00454163E+00	-3.47131186E-01	
-3.99019333E+00	1.10055440E+01	1.75158673E+00	6.11018627E-01	-3.62562116E+01	
-3.92292700E+00	-1.08587986E+01	-1.72823147E+00	-6.02871443E-01	-3.61267130E+01	
2.55578964E-01	-8.14320864E+00	-1.29603191E+00	-4.52104154E-01	3.13855355E+00	
2.00322205E-01	7.98578318E+00	1.27097687E+00	4.43364024E-01	2.50848540E+00	◁ First flutter mode

SYSTEM EIGENVECTORS

ROW	COL 1 REAL	1 IMAGINARY	2 REAL	2 IMAGINARY	3 REAL	3 IMAGINARY	4 REAL	4 IMAGINARY
1	3.35503111E-42	3.65650976E-41	1.24119446E-42	-1.17267866E-41	-4.66059026E-40	-7.71396976E-41	-5.21106336E-39	5.65204776E-39
2	2.97757856E-06	1.05368466E-04	-6.07732546E-06	-1.05092206E-04	3.23110166E-04	2.21807866E-02	2.00941176E-05	-2.22495346E-02
3	6.22188106E-04	7.93005766E-04	5.53250356E-04	-8.76211876E-04	7.61336276E-03	-5.78396166E-03	2.69979606E-03	5.57539886E-03
4	8.48483476E-04	1.21034006E-02	6.63974016E-04	-1.01433866E-02	-3.29771246E-04	3.56752646E-03	-5.76867736E-04	-3.56580796E-03
5	2.04509496E-05	3.61254616E-04	1.58323326E-07	-3.62149156E-04	1.86272086E-05	6.15231296E-03	-6.35473086E-05	-6.15899476E-03
6	-2.63205646E-04	1.03896916E-02	-4.67183306E-05	1.03716586E-02	1.30381166E-04	-1.94595886E-04	1.37279716E-04	1.76158896E-04
7	1.66815916E-40	1.62653726E-41	5.36369266E-41	-6.50491546E-42	-5.68022416E-40	3.64247856E-39	-4.30870776E-38	-4.18598386E-38
8	7.27931146E-03	2.11625906E-05	7.21467376E-03	6.49816496E-04	9.18371156E-01	0.	9.20068336E-01	0.
9	5.55264136E-02	4.13368816E-02	5.69945156E-02	3.77344256E-02	-2.37851916E-01	-1.11668266E-01	-2.30454586E-01	1.11850776E-01
10	-6.95130546E-01	4.06805286E-02	-6.96770036E-01	-4.24521946E-02	1.47479336E-01	1.58021666E-02	1.47432536E-01	-2.39879096E-02
11	2.48377156E-02	7.75750446E-04	-2.48675426E-02	1.36619366E-04	2.54686966E-01	2.93881676E-03	2.54685726E-01	-2.85783746E-03
12	7.13768046E-01	0.	7.12703836E-01	0.	-7.97669896E-03	-5.51448666E-03	-7.27943396E-03	5.68339956E-03

ROW	COL 5 REAL	5 IMAGINARY	6 REAL	6 IMAGINARY	7 REAL	7 IMAGINARY	8 REAL	8 IMAGINARY
1	5.77033796-34	-.9985010E-31	1.11995886-33	3.74844156-34	-1.01902576-03	-5.51651466-02	-1.91558376-04	5.51832786-02
2	-2.29526026-03	-2.59623456-02	-2.22154496-03	2.59633996-02	-1.02602576-40	-1.21346096-40	-3.07599236-40	4.38009756-40
3	-1.56482626-02	3.98065246-03	-1.58805866-02	3.65923026-03	6.39377566-42	3.09080546-41	1.40200166-41	-1.04707186-40
4	-5.35047226-03	1.53302036-02	-4.97941506-03	-1.55086096-02	1.29525586-41	-6.90999056-42	4.48472206-41	1.98042506-41
5	-1.25873496-04	-2.35819406-03	-4.10522776-05	2.32826606-03	1.09800486-42	1.12800836-42	2.96215426-42	-4.33986506-42
6	-7.66639096-06	9.77203066-05	-7.72094956-04	-7.55904366-05	5.28945336-43	1.07653706-42	1.35130206-42	-3.75092946-42
7	-2.26501746-30	1.43719986-31	5.37127566-33	-1.23274556-32	9.98476726-01	0.	9.98476226-01	0.
8	7.48871466-01	0.	7.46837466-01	0.	2.28131936-39	-1.81296656-39	8.11562956-39	5.51932436-39
9	1.53524196-01	-4.37793996-01	1.43295006-01	4.44544266-01	-5.72887976-40	1.04922766-40	-1.93382256-39	-2.43990866-40
10	-4.25224856-01	-1.91924796-01	-4.30680996-01	1.80083926-01	4.08108326-41	2.17680936-40	9.15781176-41	-7.37728216-40
11	6.78119596-02	2.36430986-03	6.65861436-02	-4.51653996-03	3.71600546-40	-1.22999666-40	1.26560696-39	3.37008736-40
12	-8.57017286-04	-2.21891056-02	-2.72039006-04	2.22325976-02	-2.24497636-41	4.85195216-41	-8.29898746-41	-1.54903936-40

ROW	COL 9 REAL	9 IMAGINARY	10 REAL	10 IMAGINARY	11 REAL	11 IMAGINARY	12 REAL ◁ First flutter mode	12 IMAGINARY	
1	-1.65197416-32	5.01727296-33	1.95350106-32	-1.50012666-32	-1.86588586-35	3.00961316-35	-1.61236656-32	1.15420896-32	x
2	-2.82882096-02	-7.80230706-02	-2.85433706-02	7.90090426-02	3.71430506-03	1.18344486-01	3.02185666-03	-1.20465386-01	z
3	3.49828836-04	-1.51575726-02	6.46486666-04	1.57813686-02	2.13374786-02	1.47331416-03	2.23785776-02	-1.04163146-03	a_1
4	-1.05853296-02	-5.93017726-04	-1.11264236-02	8.21080236-04	3.17274446-03	1.77205036-02	3.74146966-03	-1.86763166-02	b_1
5	2.48598466-03	2.74024036-03	2.51850926-03	-2.84563056-03	5.18392926-04	-6.34492016-03	6.49933226-04	6.50312066-03	ϕ_y
6	-4.84113186-05	-5.45028196-04	-1.58008986-05	5.68491946-04	7.27167486-04	1.17559416-04	7.58199806-04	-1.37217886-04	ϕ_z
7	-2.74750016-31	-4.04869236-31	-2.26150566-31	-6.70791706-31	1.25541696-33	6.69477176-34	-4.11996616-31	-7.00611676-31	
8	9.71561756-01	0.	9.69916836-01	0.	9.64653116-01	0.	9.62615796-01	0.	
9	1.65421646-01	6.43316996-02	1.68830586-01	-6.89255206-02	1.74309156-02	-1.73378996-01	1.28011686-02	1.78501806-01	
10	4.87639946-02	-1.14131056-01	5.25640886-02	1.17598546-01	1.45112646-01	-2.13073326-02	1.49894516-01	2.61372846-02	
11	-4.00773956-02	1.64255246-02	-4.07800576-02	-1.61847836-02	-5.15355186-02	-5.84300986-03	-5.18023156-02	6.49294526-03	
12	6.19150236-03	1.64197506-03	6.23512526-03	-2.05857376-03	1.14315956-03	-5.89143086-03	1.24767656-03	6.02733156-03	

TABLE 5-8

COMPARISON OF MEASURED AND CALCULATED FLAPPING DERIVATIVES
FOR BELL 25-FOOT PROPROTOR

Velocity	Proprotor Speed	Total Derivative $\partial\beta/\partial\alpha_m$		Component Derivatives			
				Longitudinal $(\partial a_1/\partial\alpha_m)$		Lateral $(\partial b_1/\partial\alpha_m)$	
Knots	RPM	Measured†	Calculated	Measured†	Calculated	Measured†	Calculated
100	425	.182	.168	.187	.165	.096	.034
140	425	.320	.321	.328	.312	.171	.075
140	458	.300	.277	.357	.269	.171	.066
185	500	.415	.396	.398	.380	.219	.111
100	422	.179	.171	.181	.167	.078	.034
92.5	250	.475	.413	.440	.412	.120	.014
132.5	229	.970	.978	.960	.977	.30	.046
185*	500	.408	.396	.390	.380	.125	.111

* Powered test

† Measured by Bell in NASA-Ames full-scale tunnel

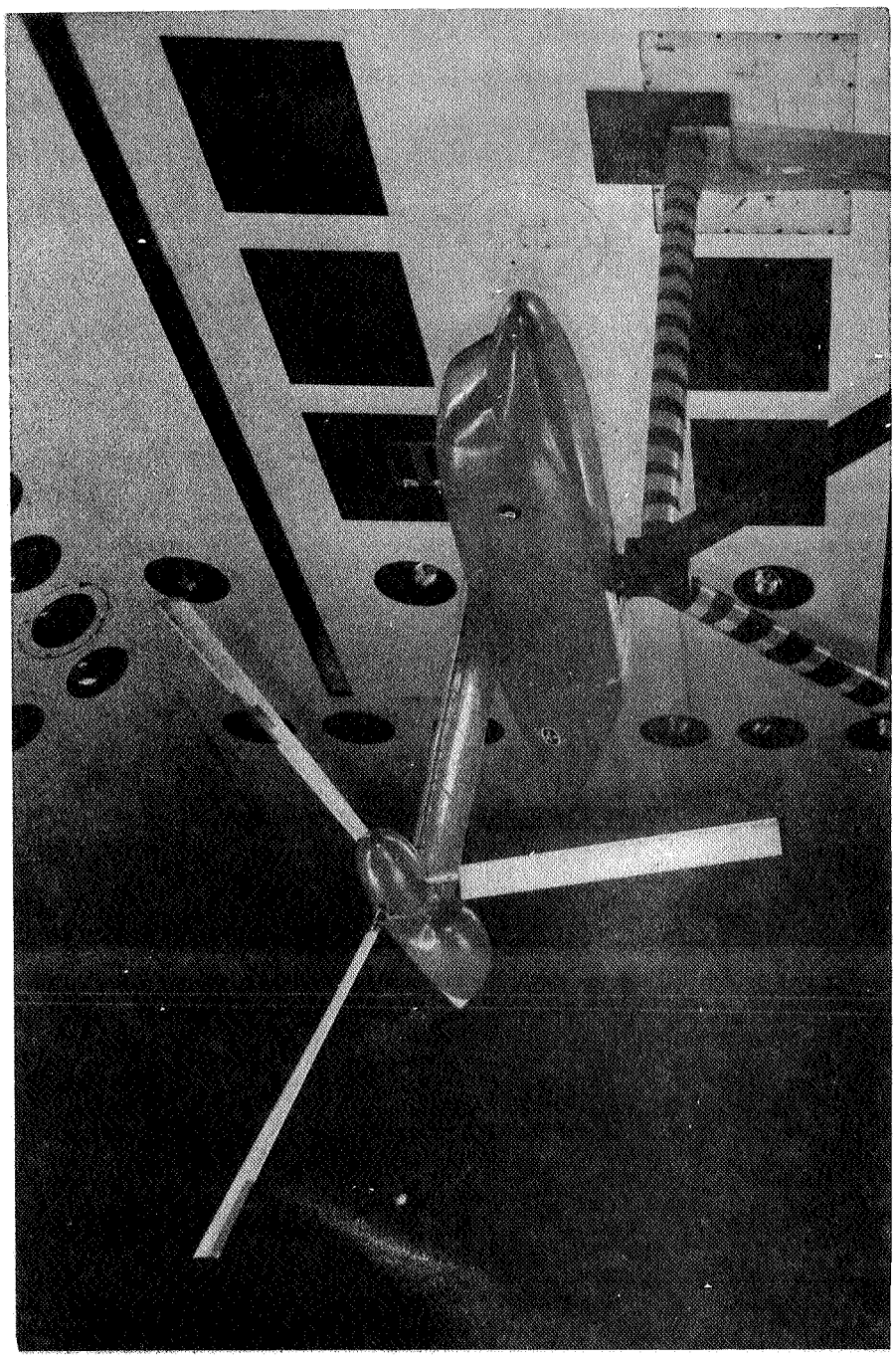

Figure 5-1.- Bell Model 266 0.1333-scale semi-span dynamic aeroelastic tilt-rotor model in Langley transonic dynamics tunnel (September 1968).

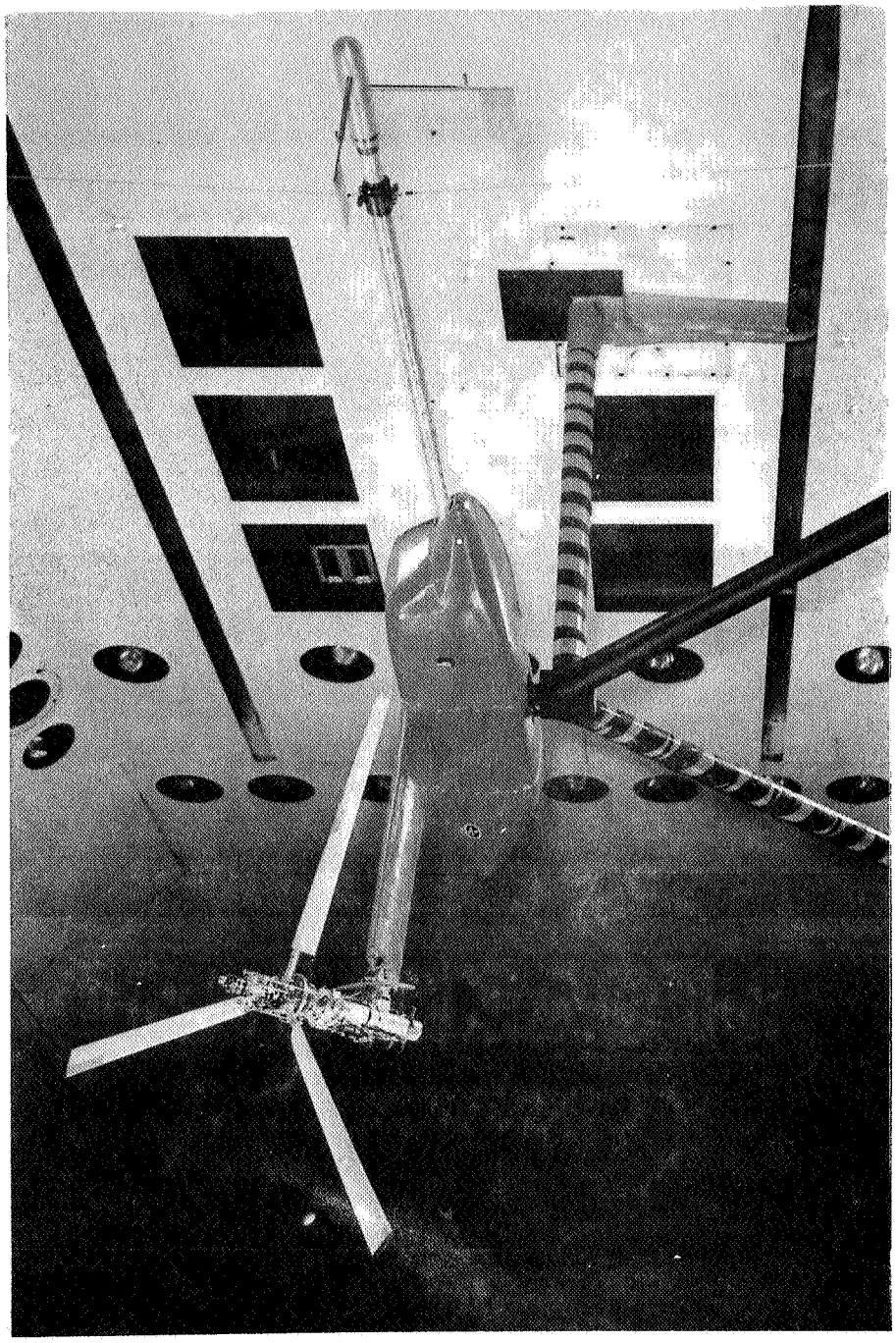

Figure 5-2.- 0.1333-scale semi-span tilt-rotor model in simulated conversion mode (September 1968).

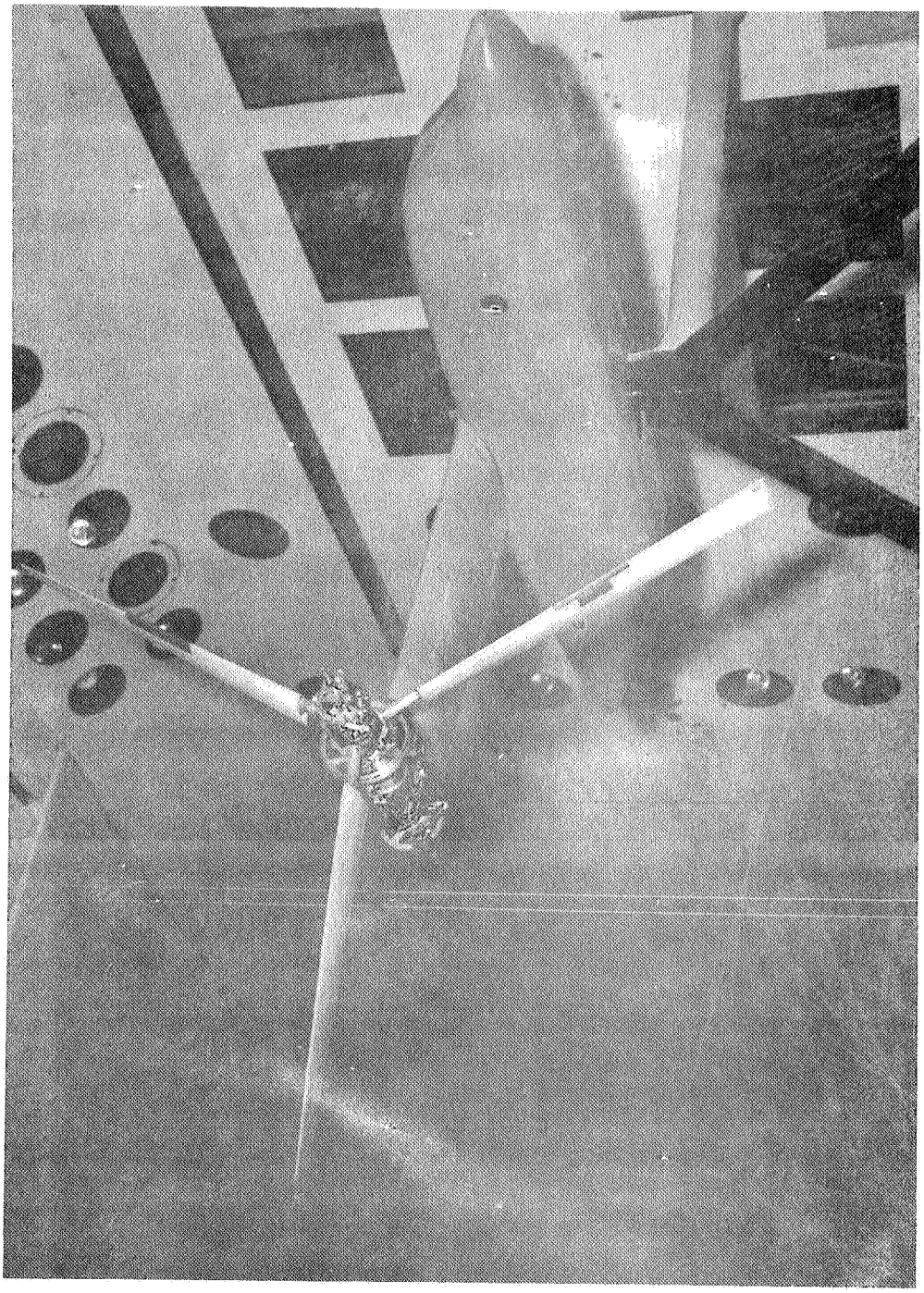

Figure 5-3.- Reference configuration for rotating portion of January 1970 test.

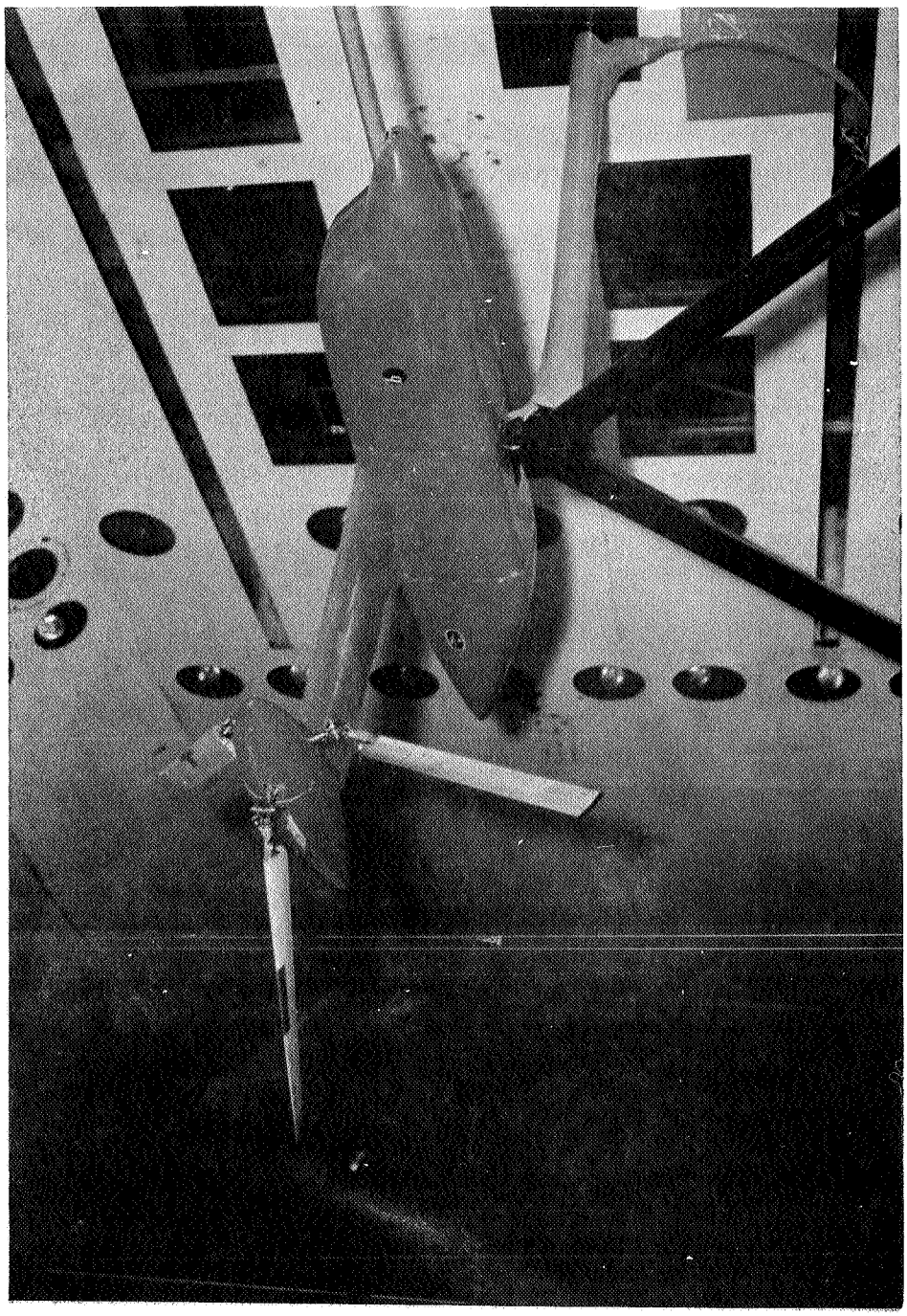

Figure 5-4.- Folding proprotor configuration employed to simulate the blade folding sequence of transition.

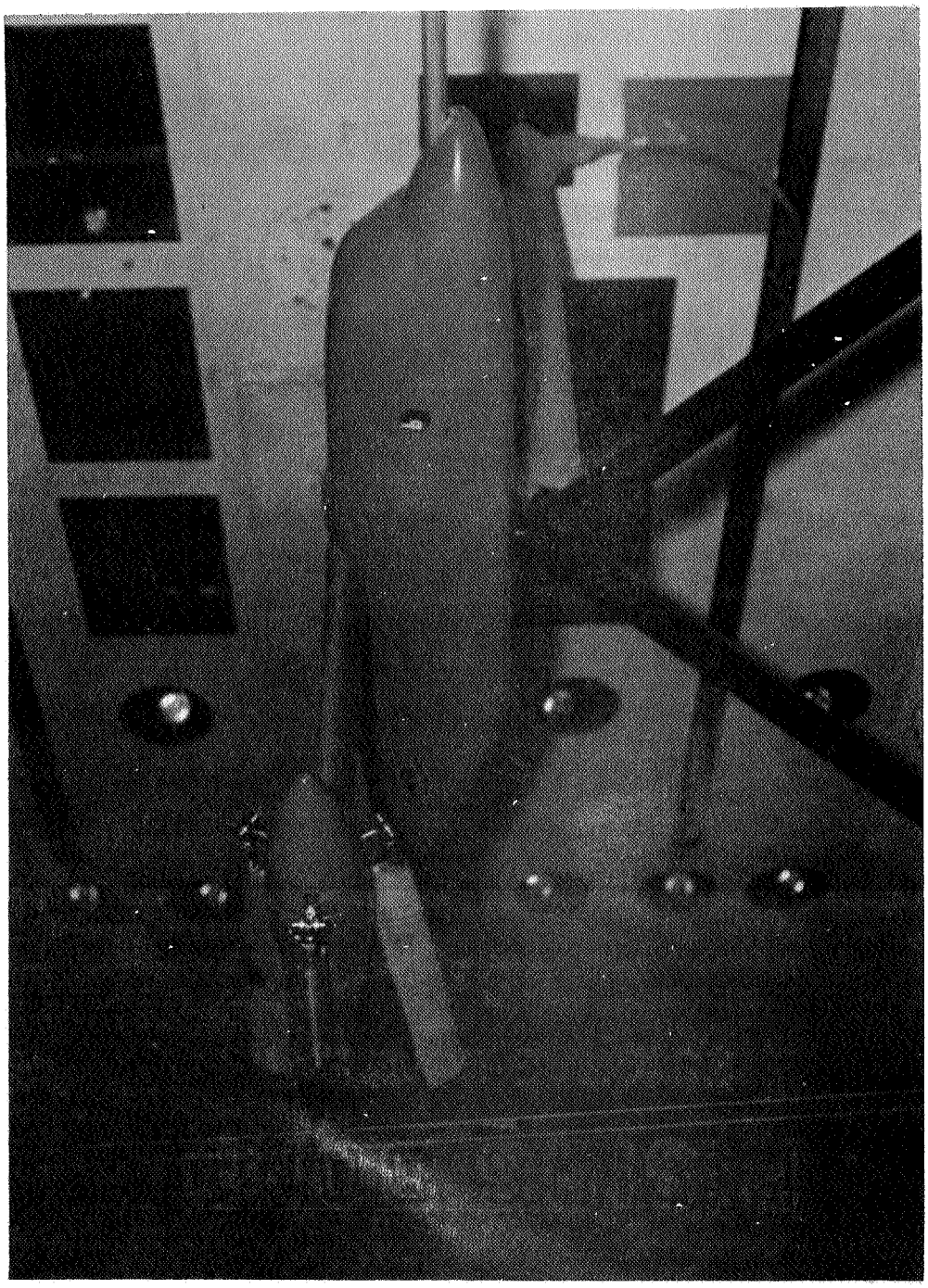

Figure 5-5.- Folding proprotor model with blades nearly fully folded.

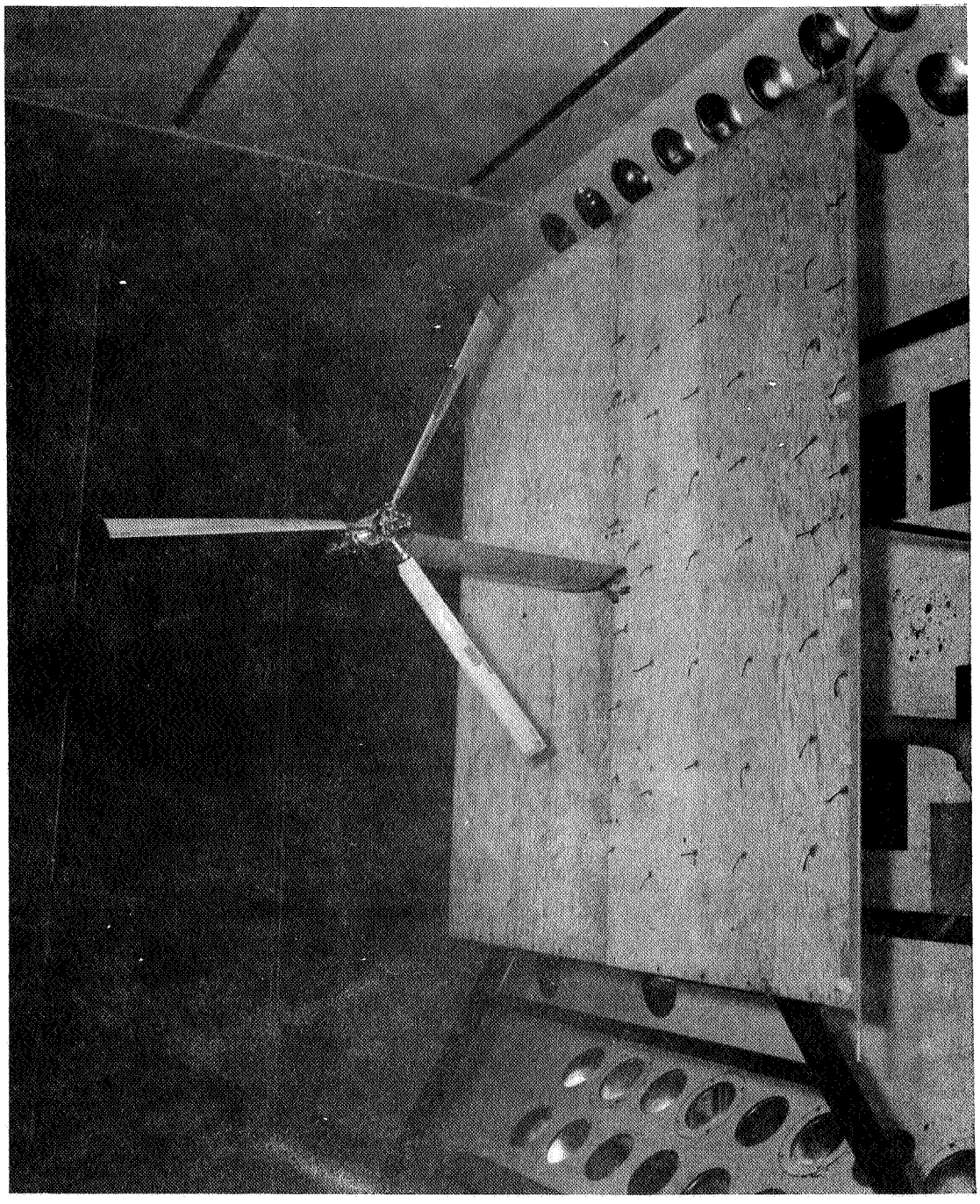

Figure 5-6.- Temporary reflection plane setup used to verify that proprotor-related dynamic phenomena were not affected by the unconventional mounting arrangement.

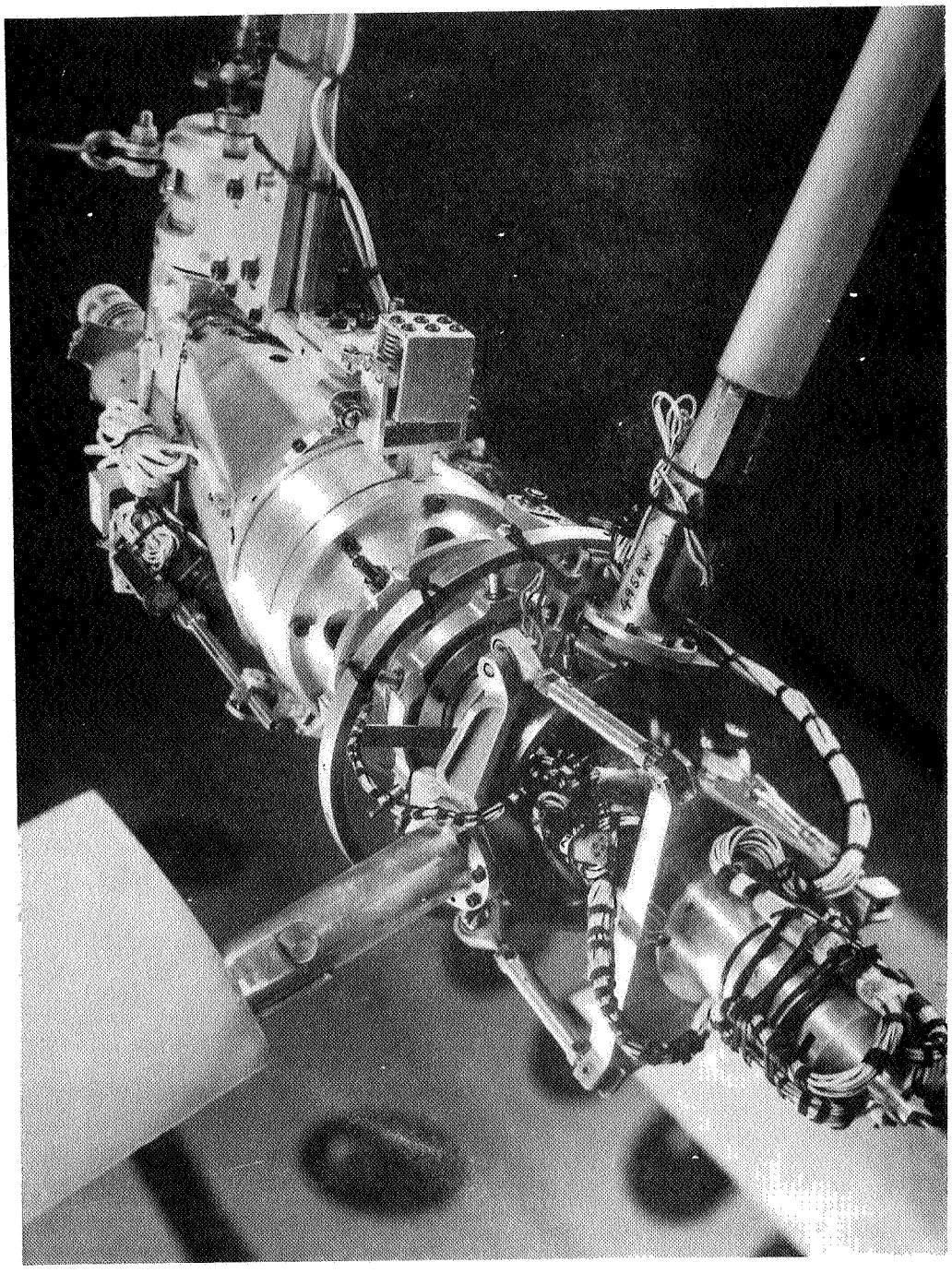

Figure 5-7.- Details of model pylon showing control system employed for testing in the airplane mode of flight (September 1968 test).

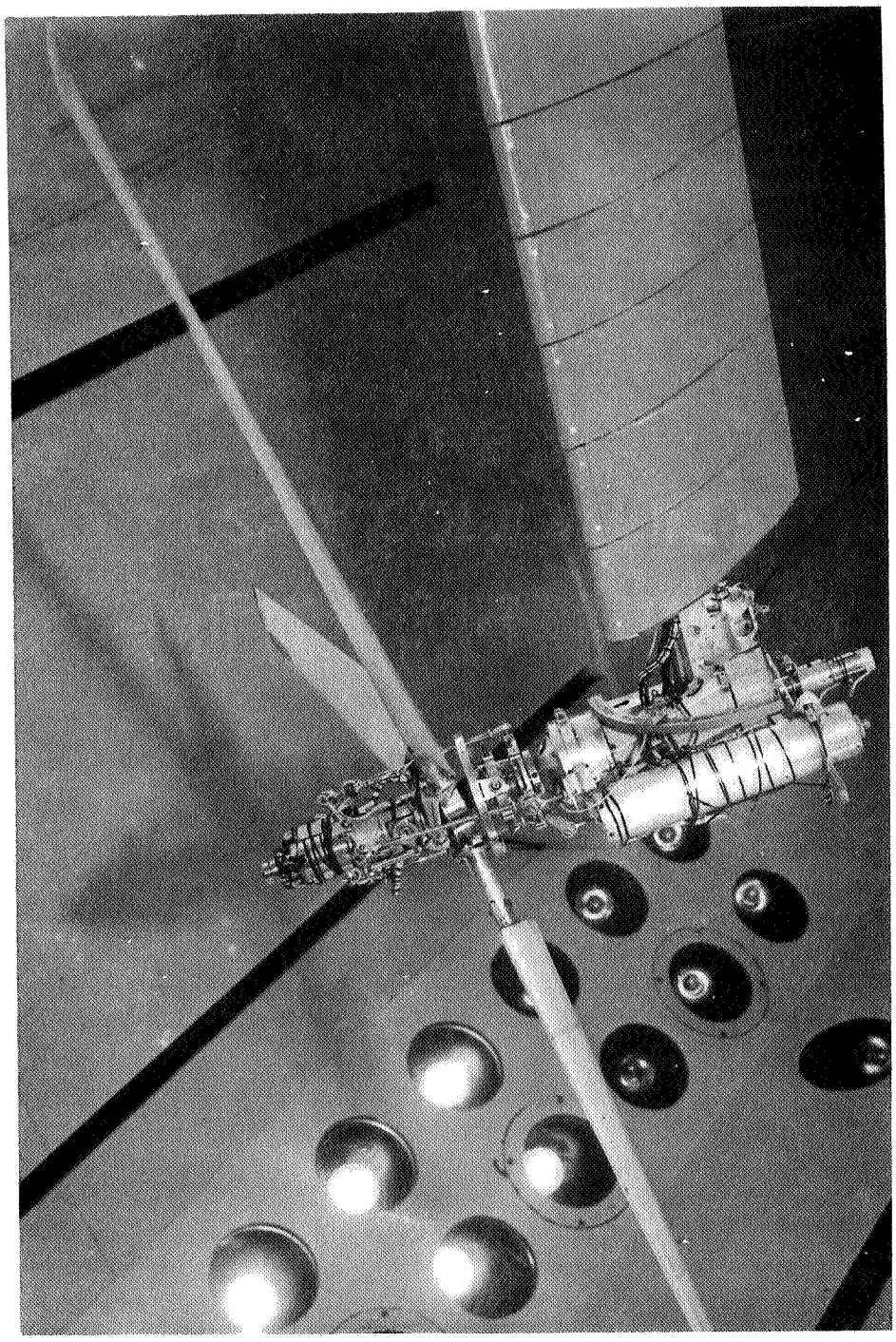

Figure 5-8.- Control system employed for testing in the helicopter and conversion mode of flight (September 1968 test).

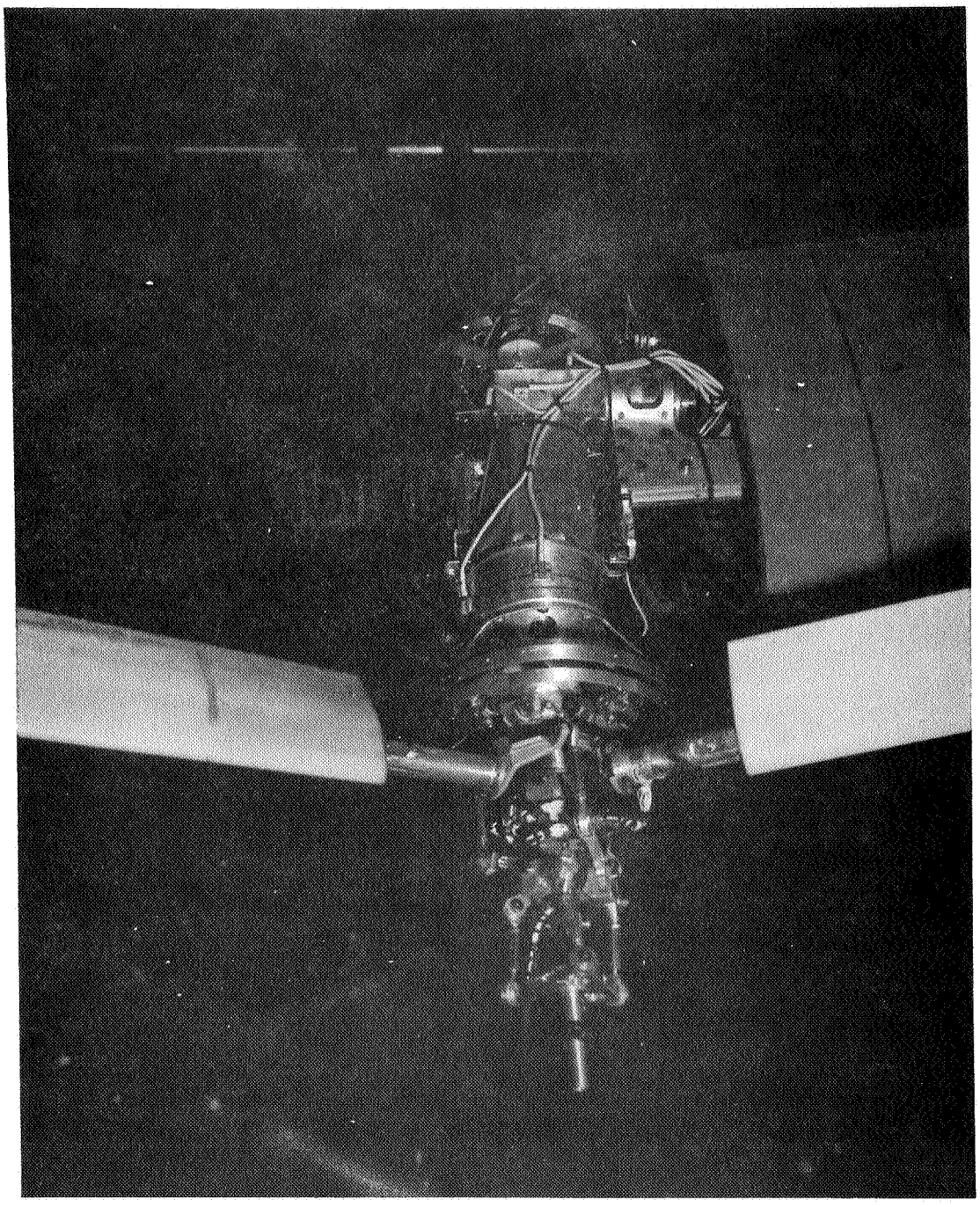

Figure 5-9.- Model pylon details for January 1970 test.

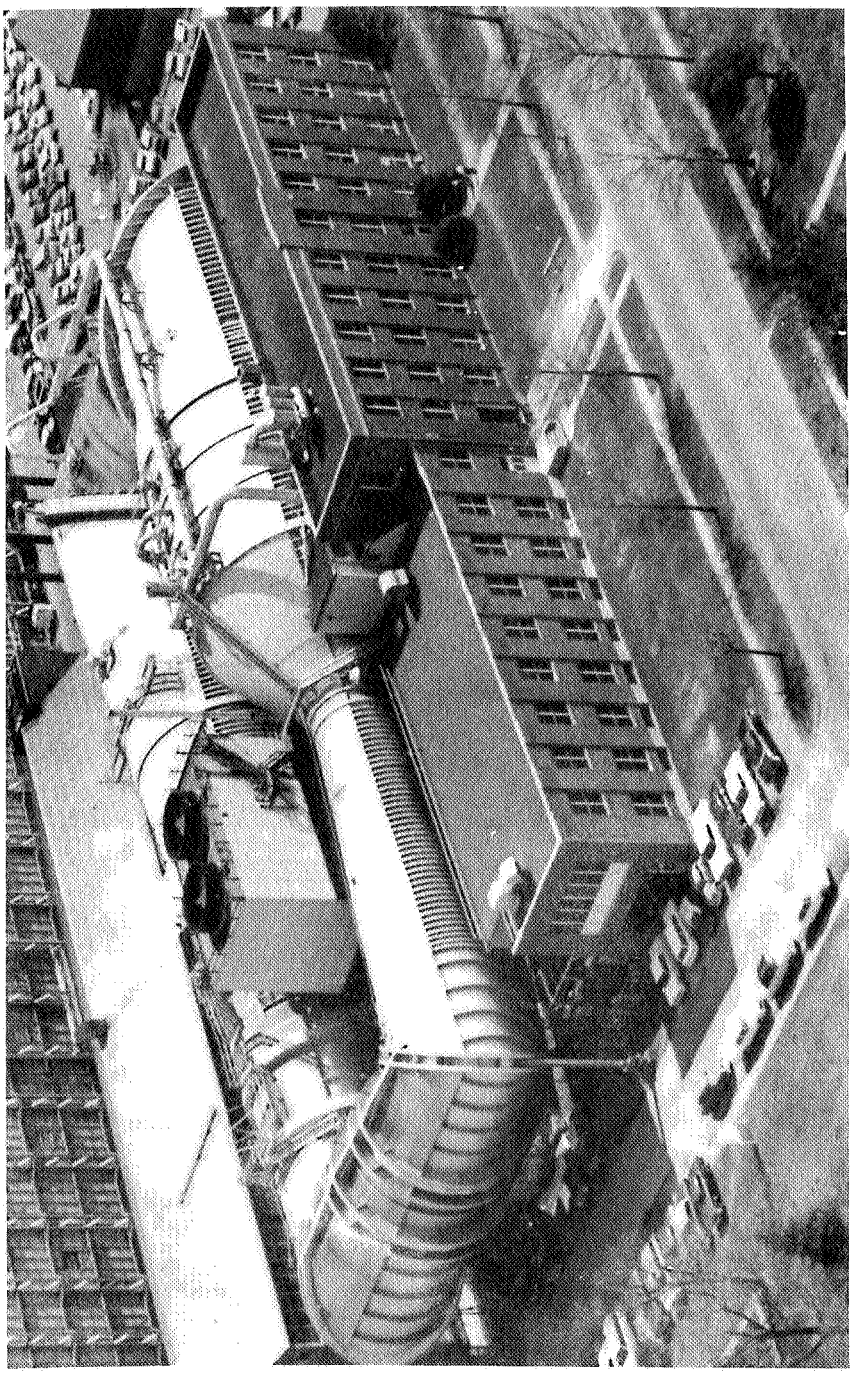

Figure 5-10.- NASA-Langley transonic dynamics tunnel.

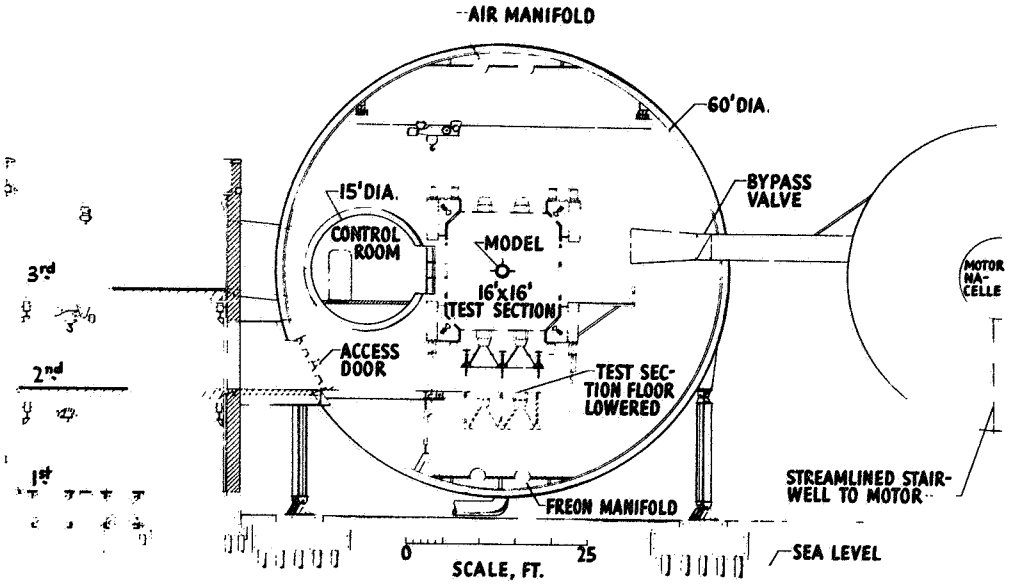

(a) Cross-section through test section

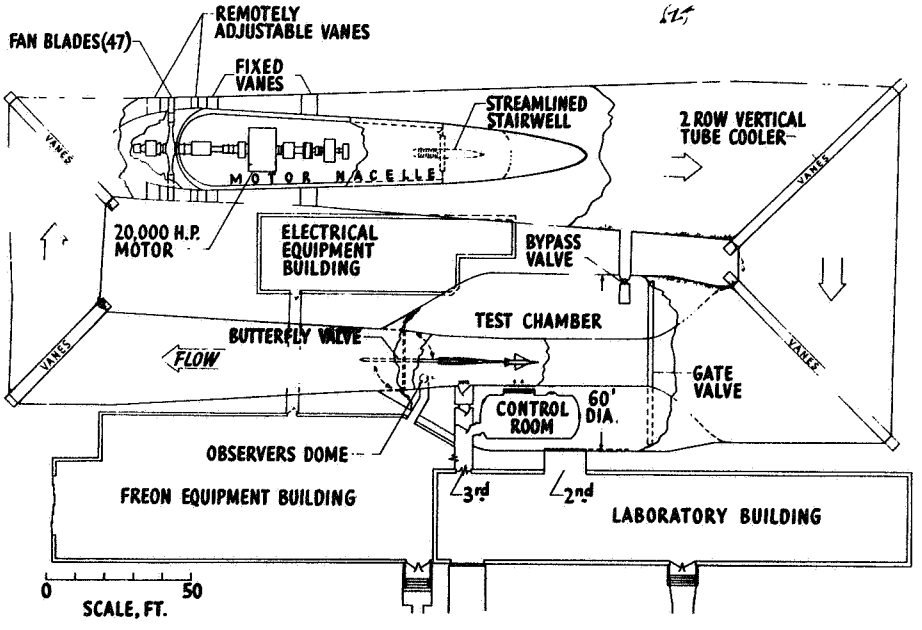

(b) Plan view

Figure 5-11.- General arrangement of the Langley transonic dynamics tunnel.

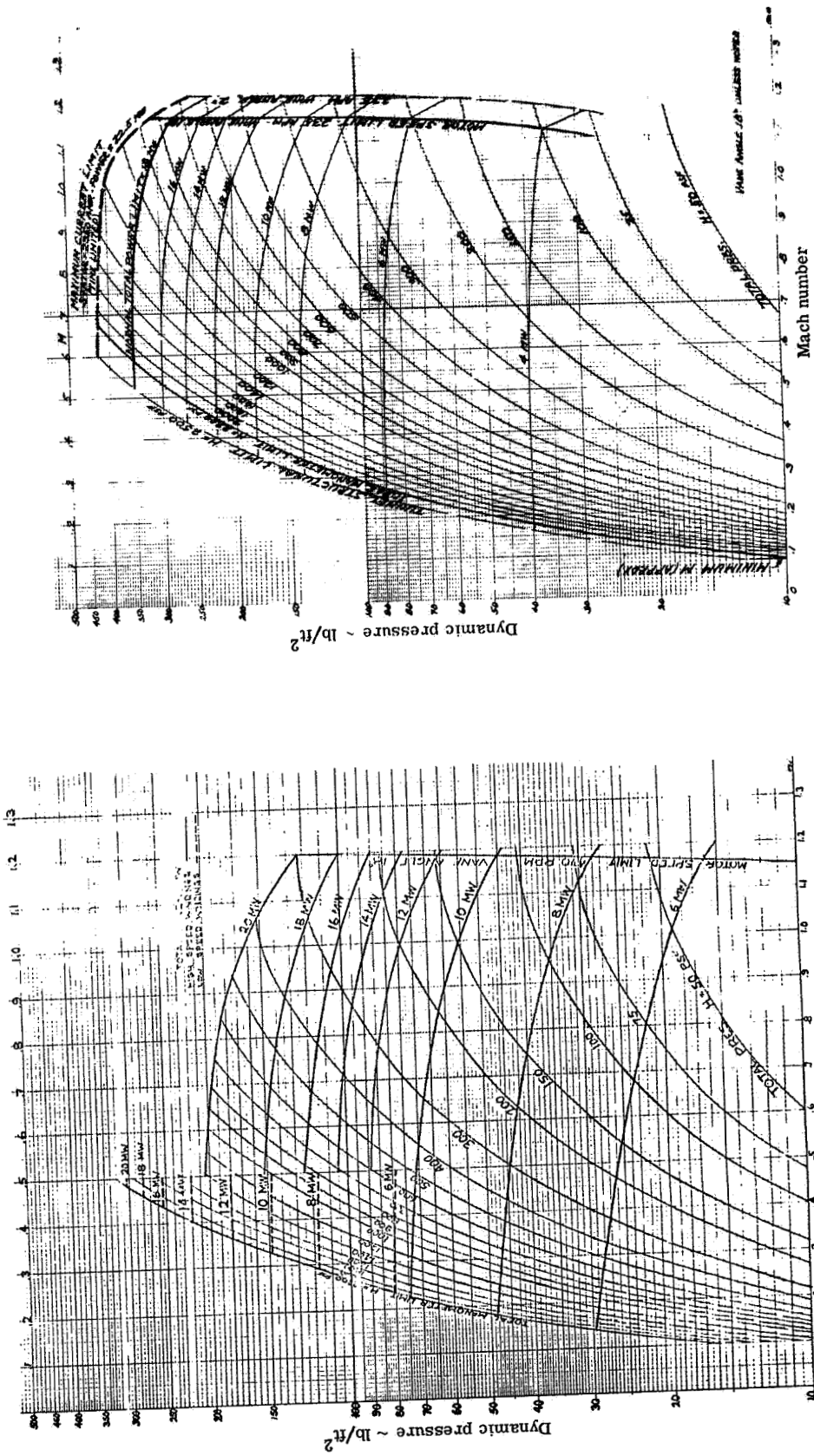

(a) Operation with air

(b) Operation with freon

Figure 5-12.- Operating curves for the Langley transonic dynamics tunnel.

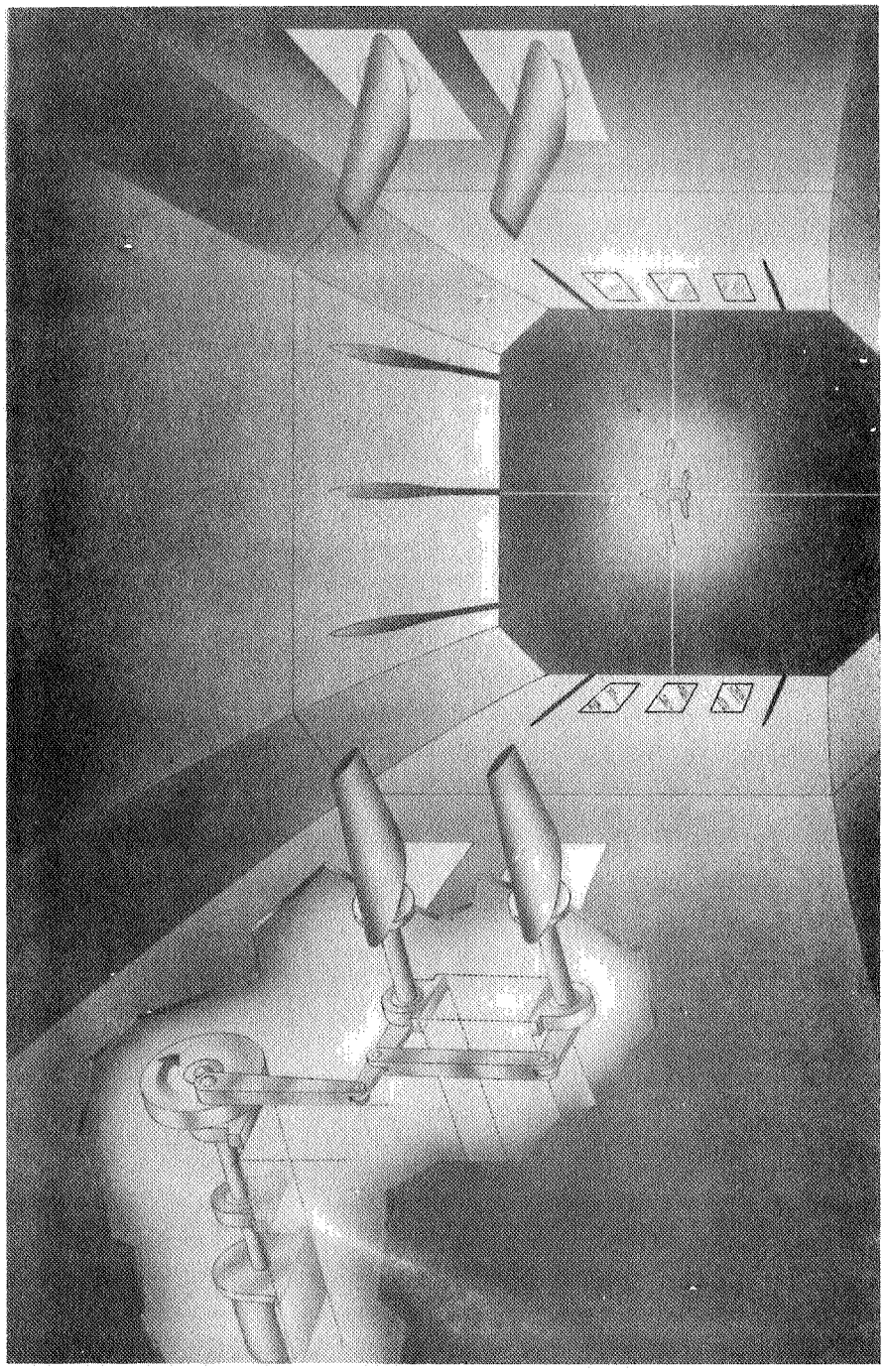

Figure 5-13.- Langley transonic dynamics tunnel airstream oscillator showing cutaway of driving mechanism.

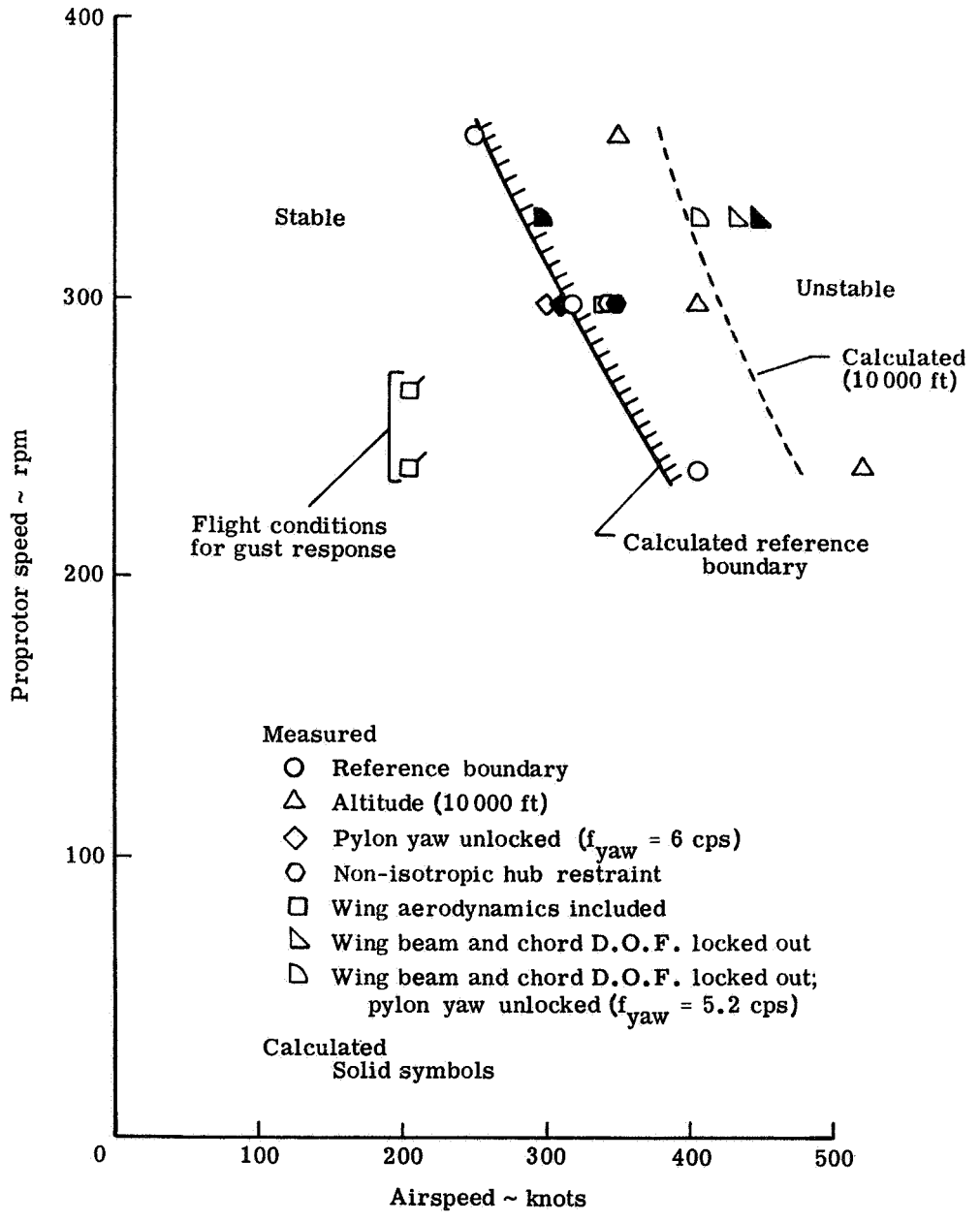

Figure 5-14.- Effect of several system parameters on proprotor/pylon stability.

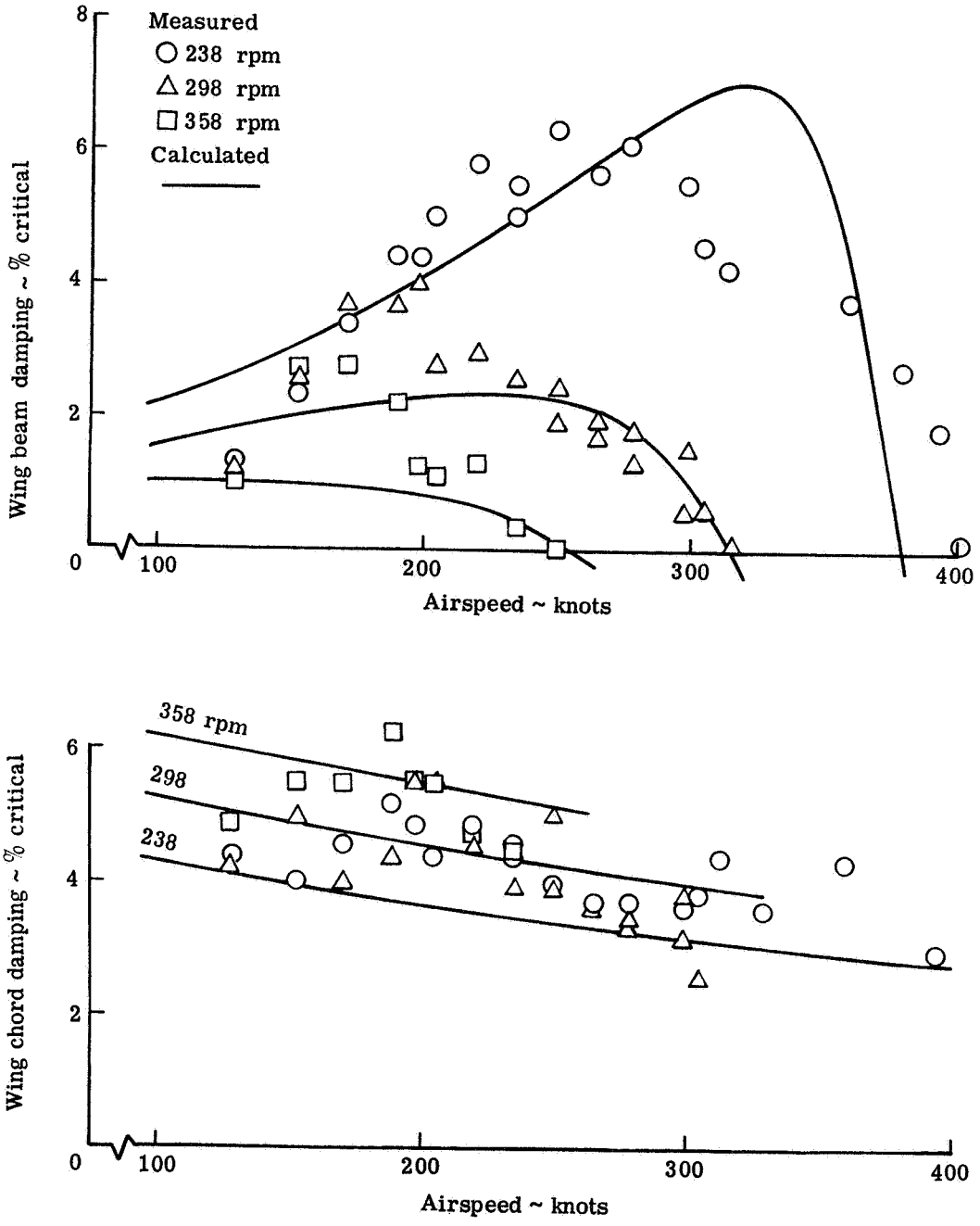

Figure 5-15.- Comparison of measured and calculated wing beam and chord mode damping versus airspeed for reference stability boundary (structural description of damping).

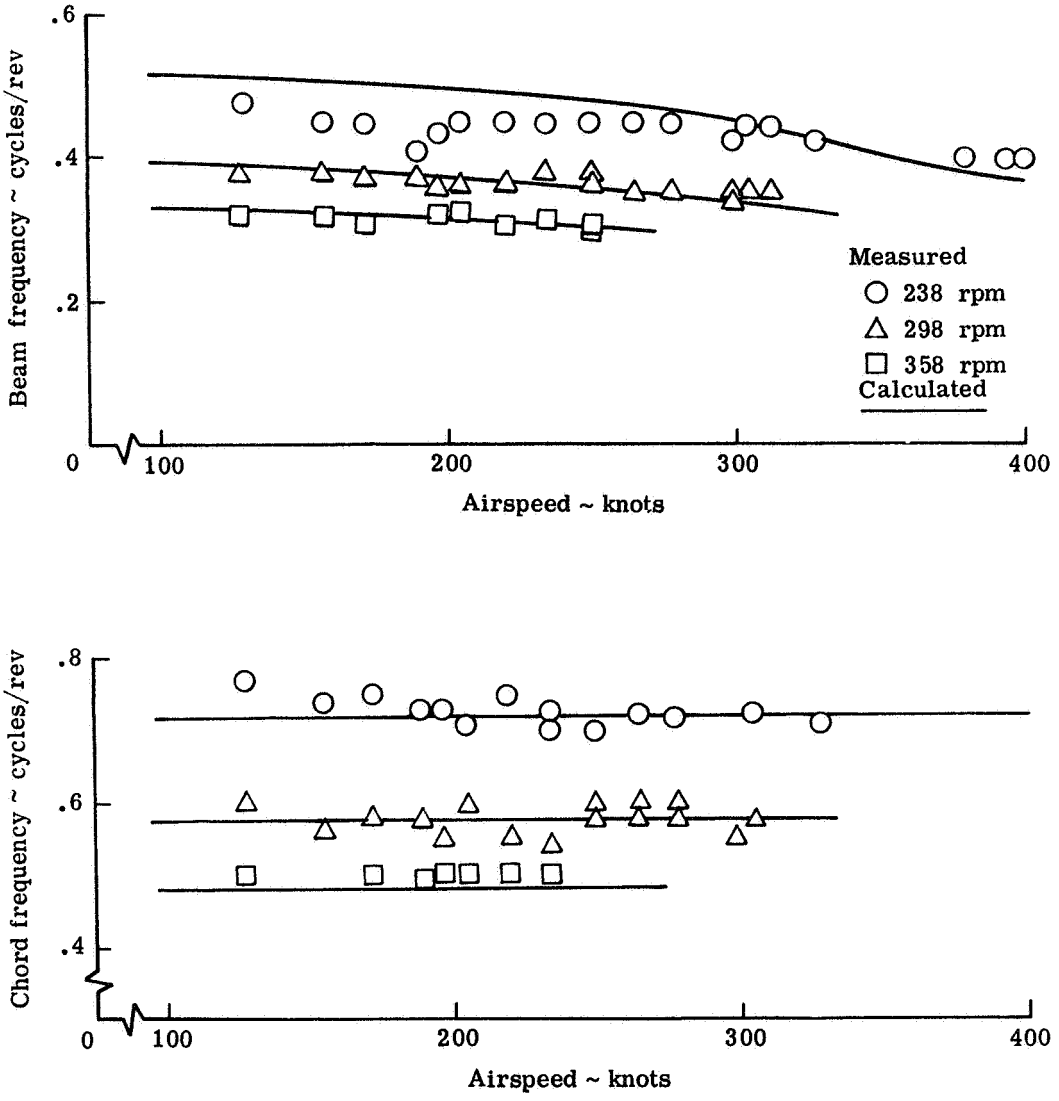

Figure 5-16.- Comparison of measured and calculated wing beam and chord mode frequency versus airspeed for reference stability boundary (structural description of damping).

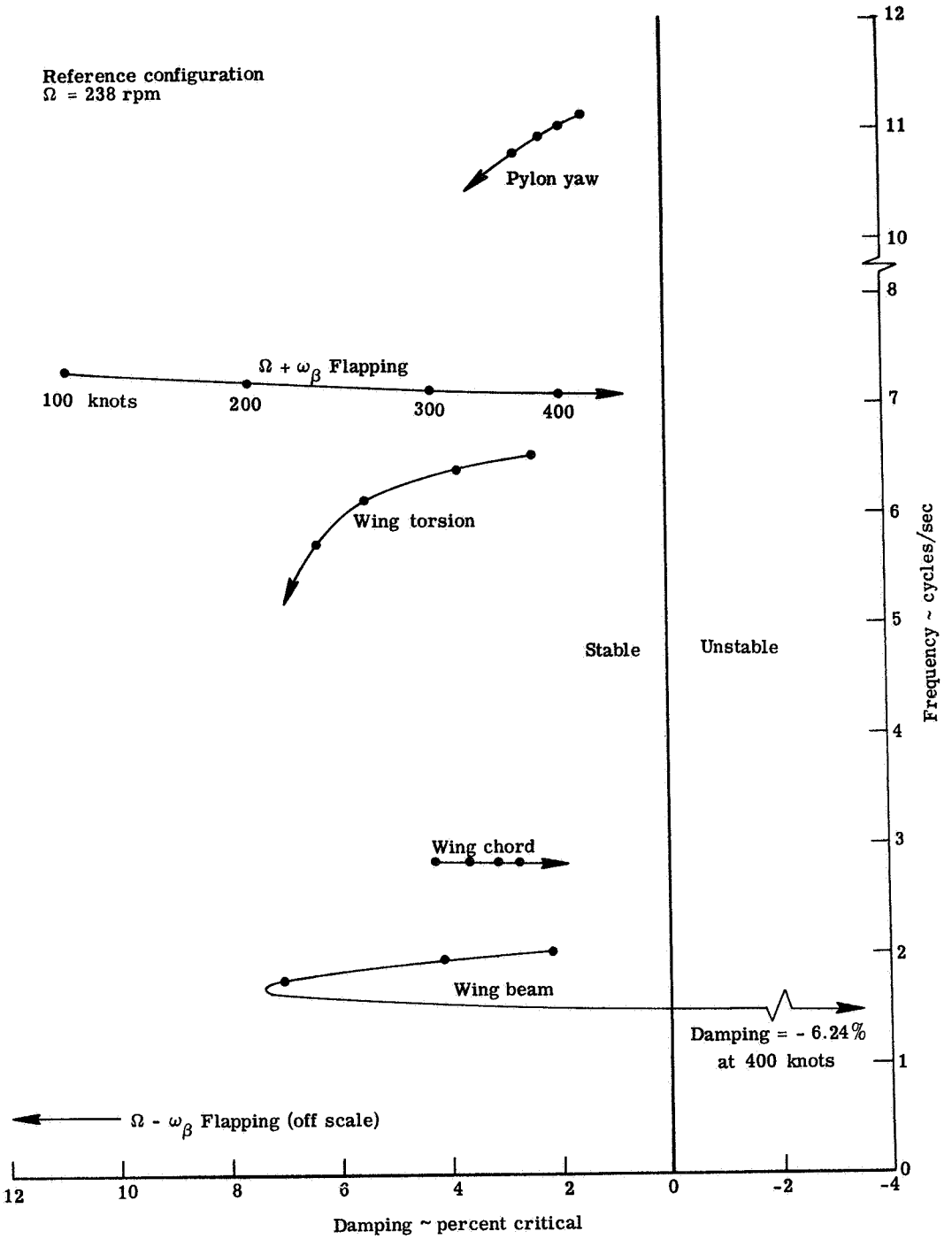

Figure 5-17.- Root locus for reference stability boundary (Ω = 238 rpm).

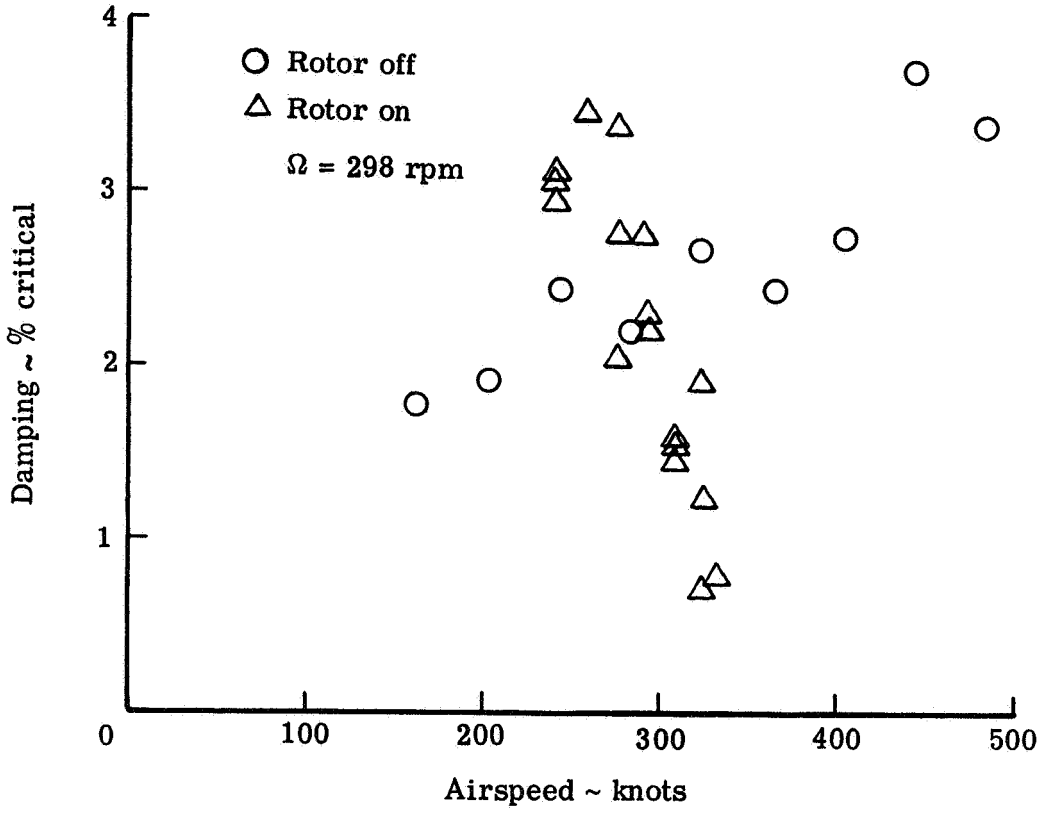

Figure 5-18.- Measured effect of proprotor on wing beam mode damping (wing fairings on).

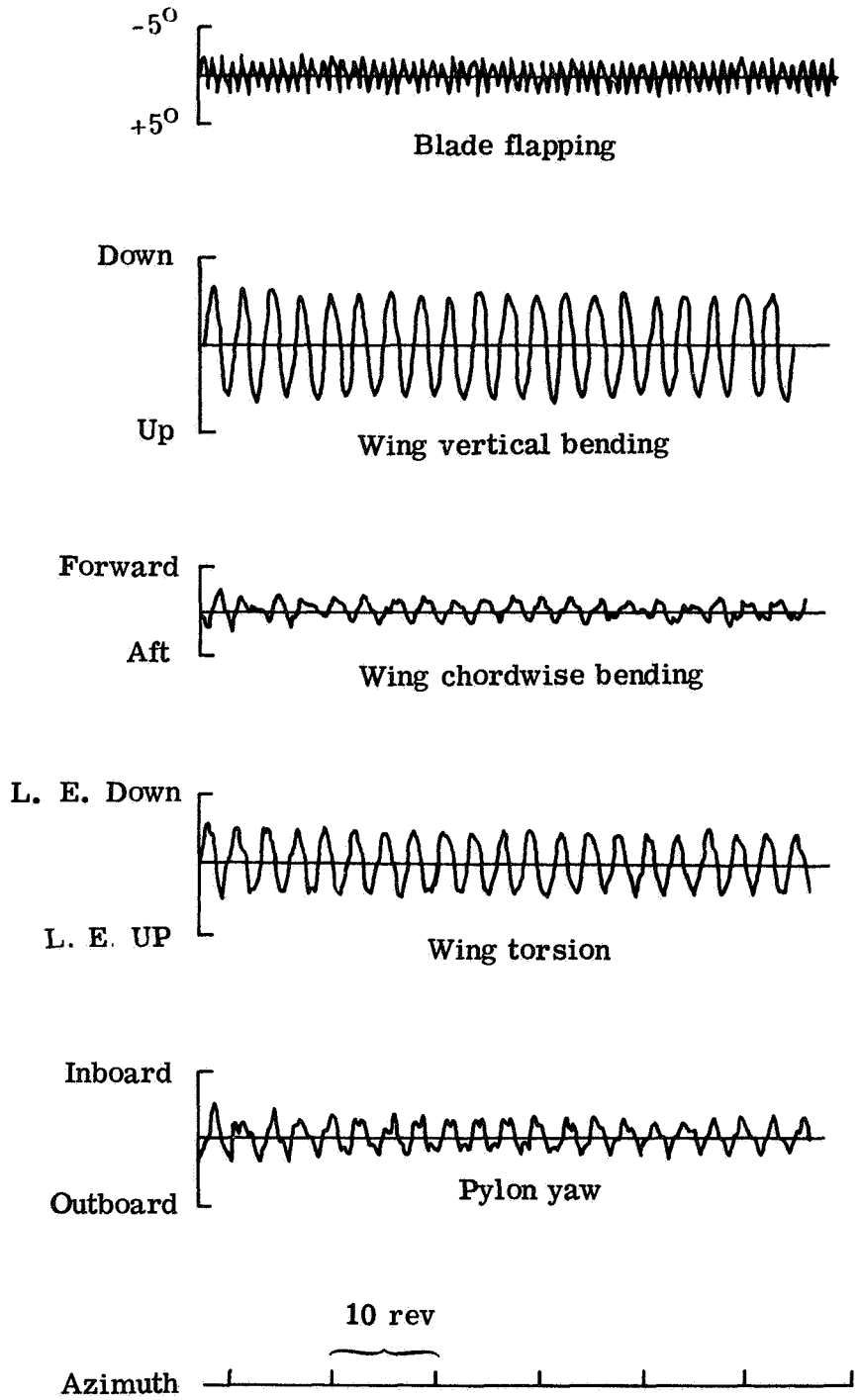

Figure 5-19.- Traces of model response at flutter for case of pylon yaw unlocked (diamond symbol in Fig. 5-14).

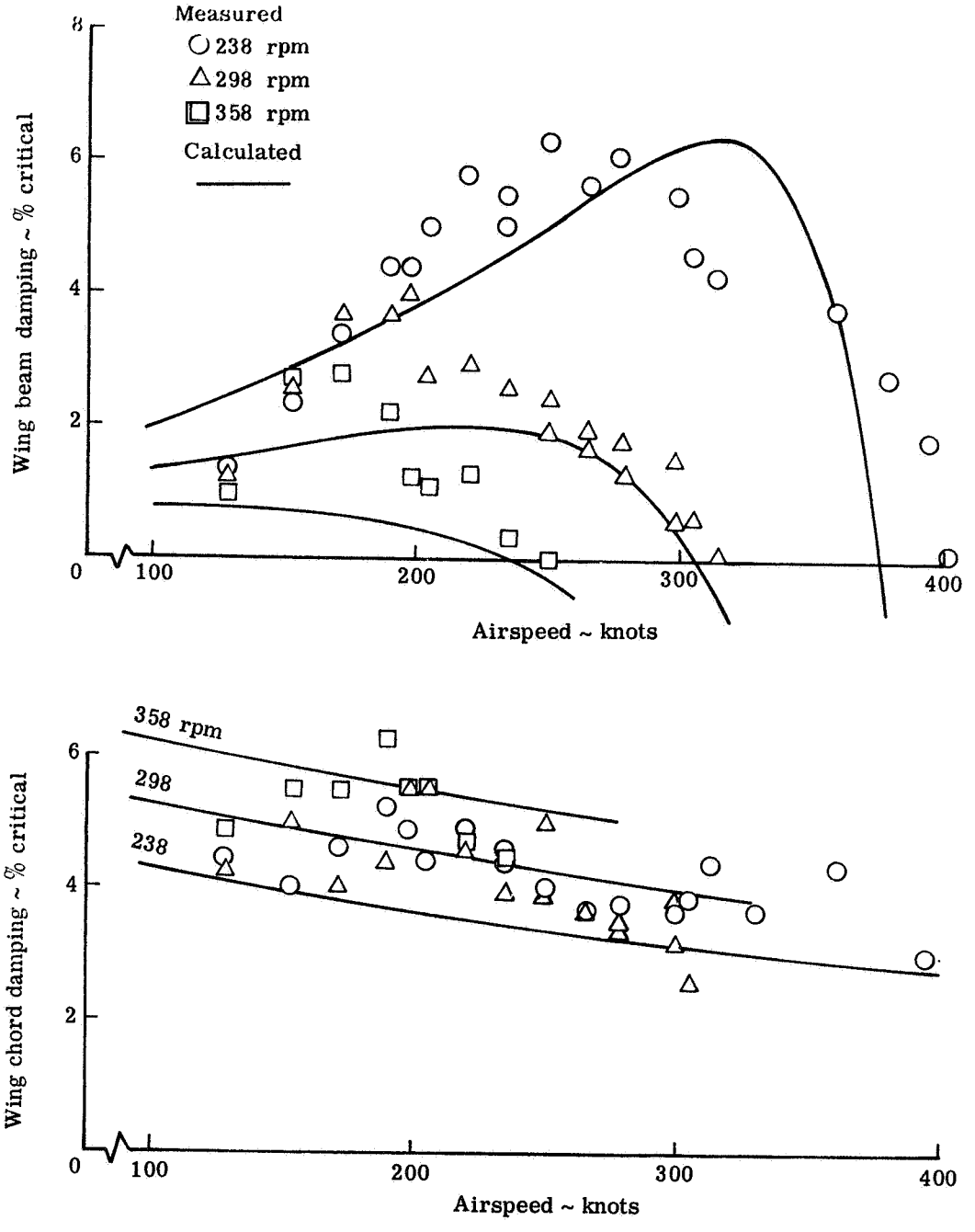

Figure 5-20.- Comparison of measured and calculated variation of wing beam and chord mode damping with airspeed (viscous description of damping).

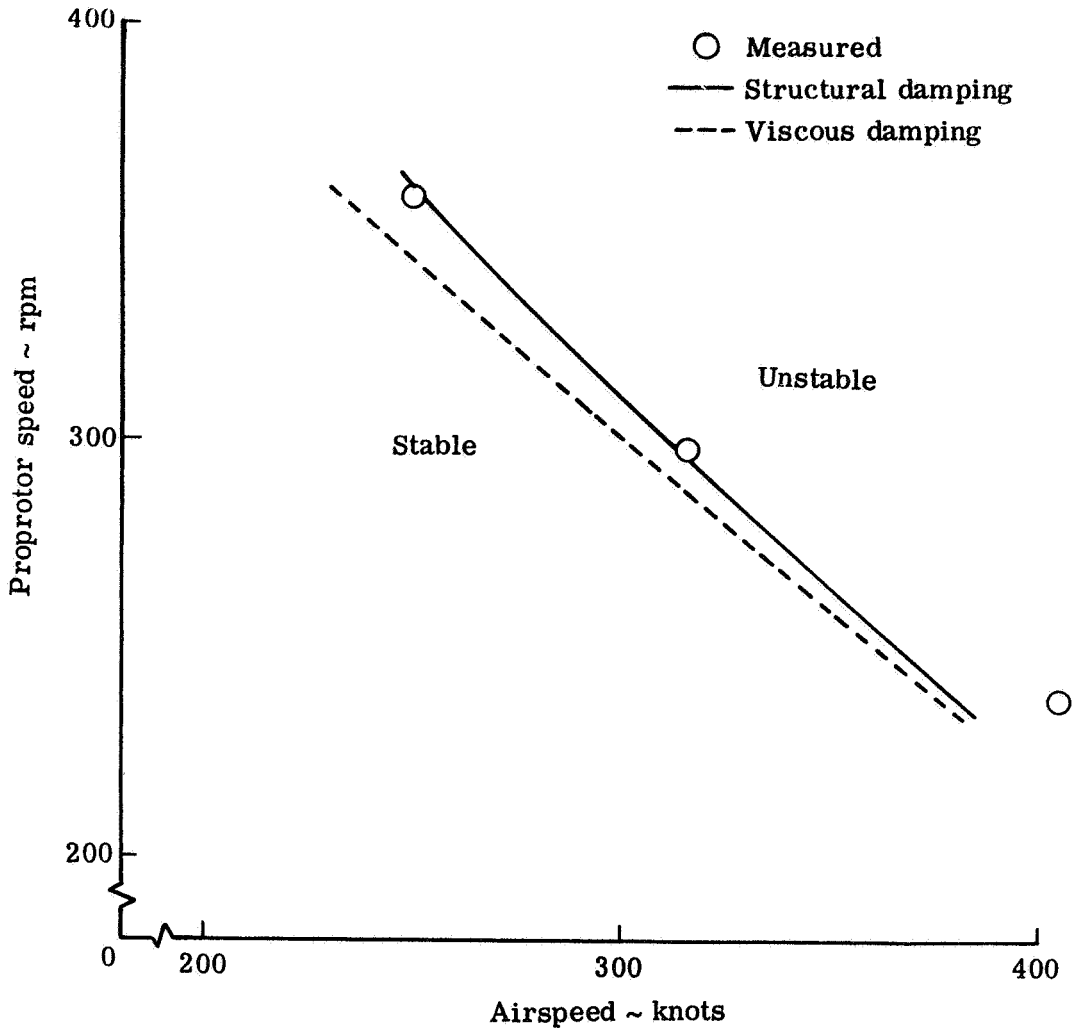

Figure 5-21.- Comparison of stability boundaries for structural and viscous damping (reference configuration).

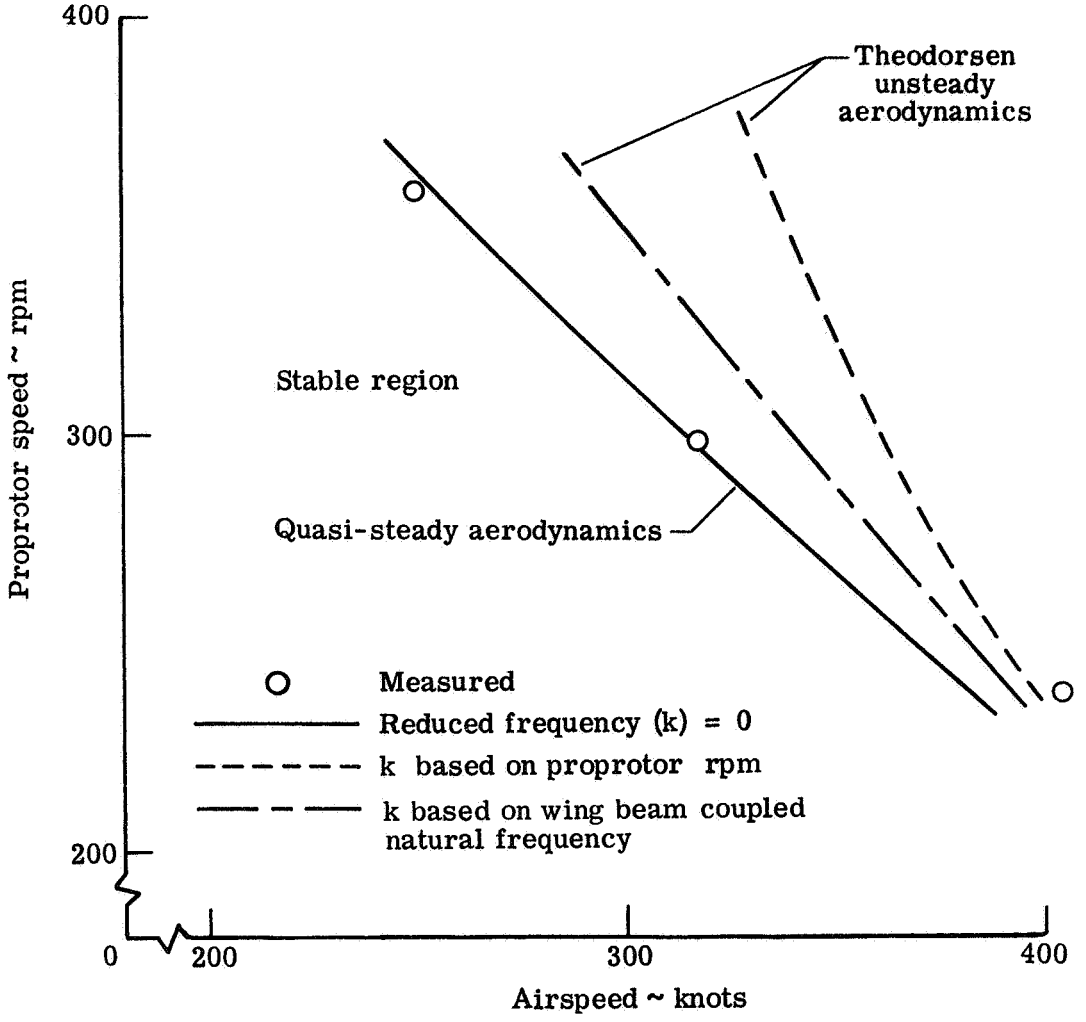

Figure 5-22.- Comparison of stability boundaries for quasi-steady and unsteady aerodynamics (reference configuration).

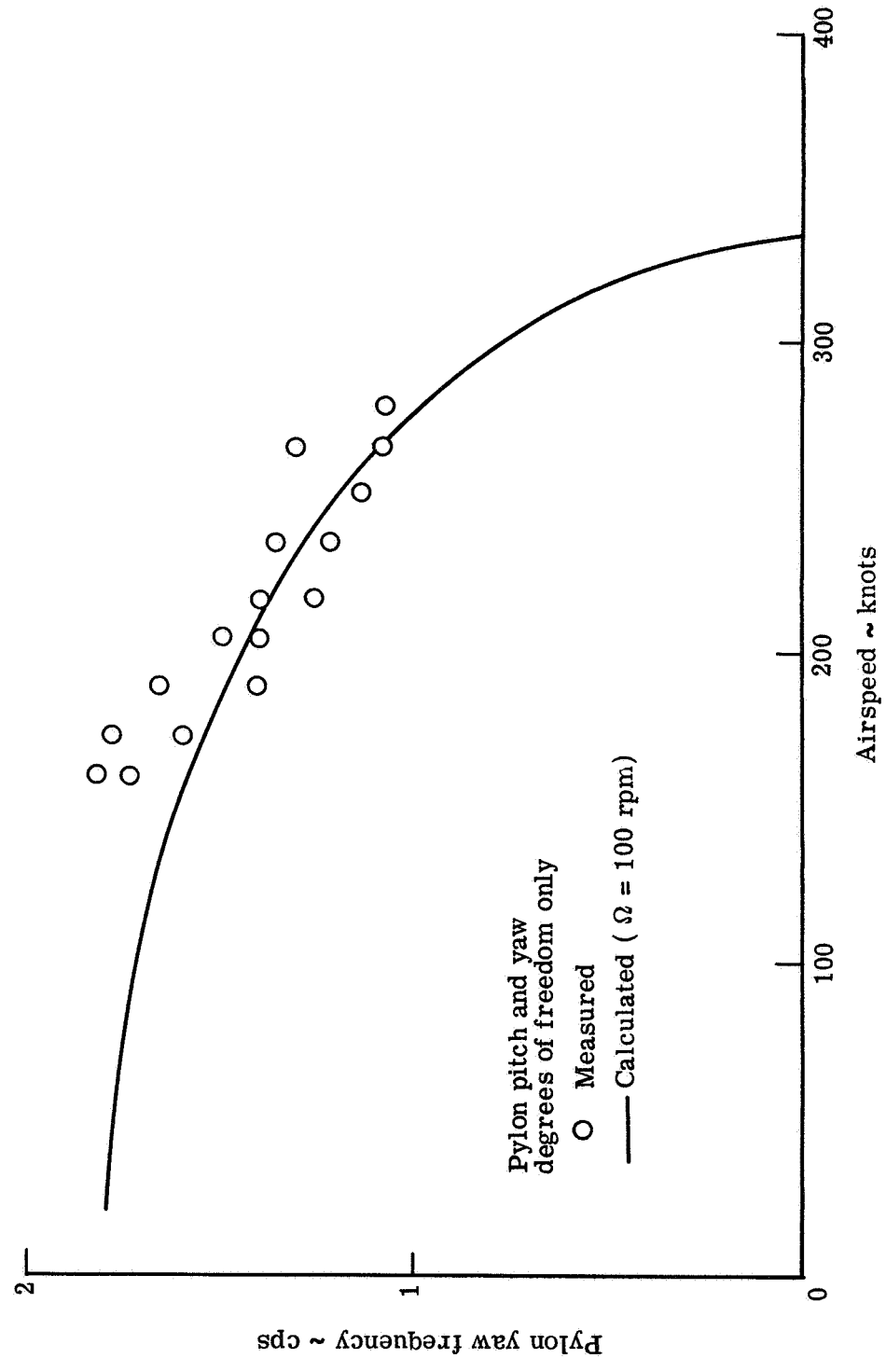

Figure 5-23.- Variation of pylon yaw frequency with airspeed for configuration having only pylon pitch and yaw degrees of freedom and very softly restrained in yaw.

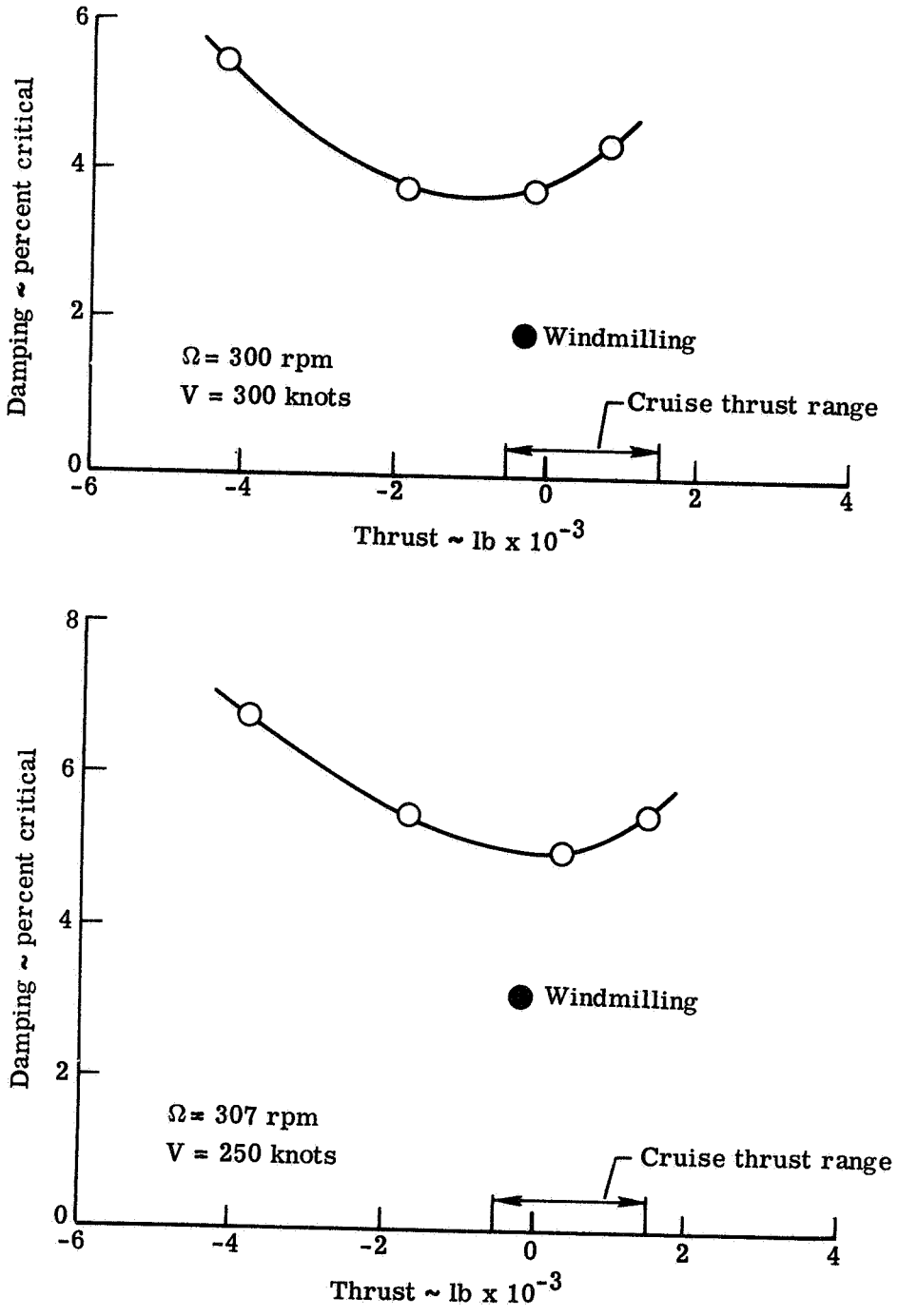

Figure 5-24.- Measured effect of thrust on wing beam mode damping.

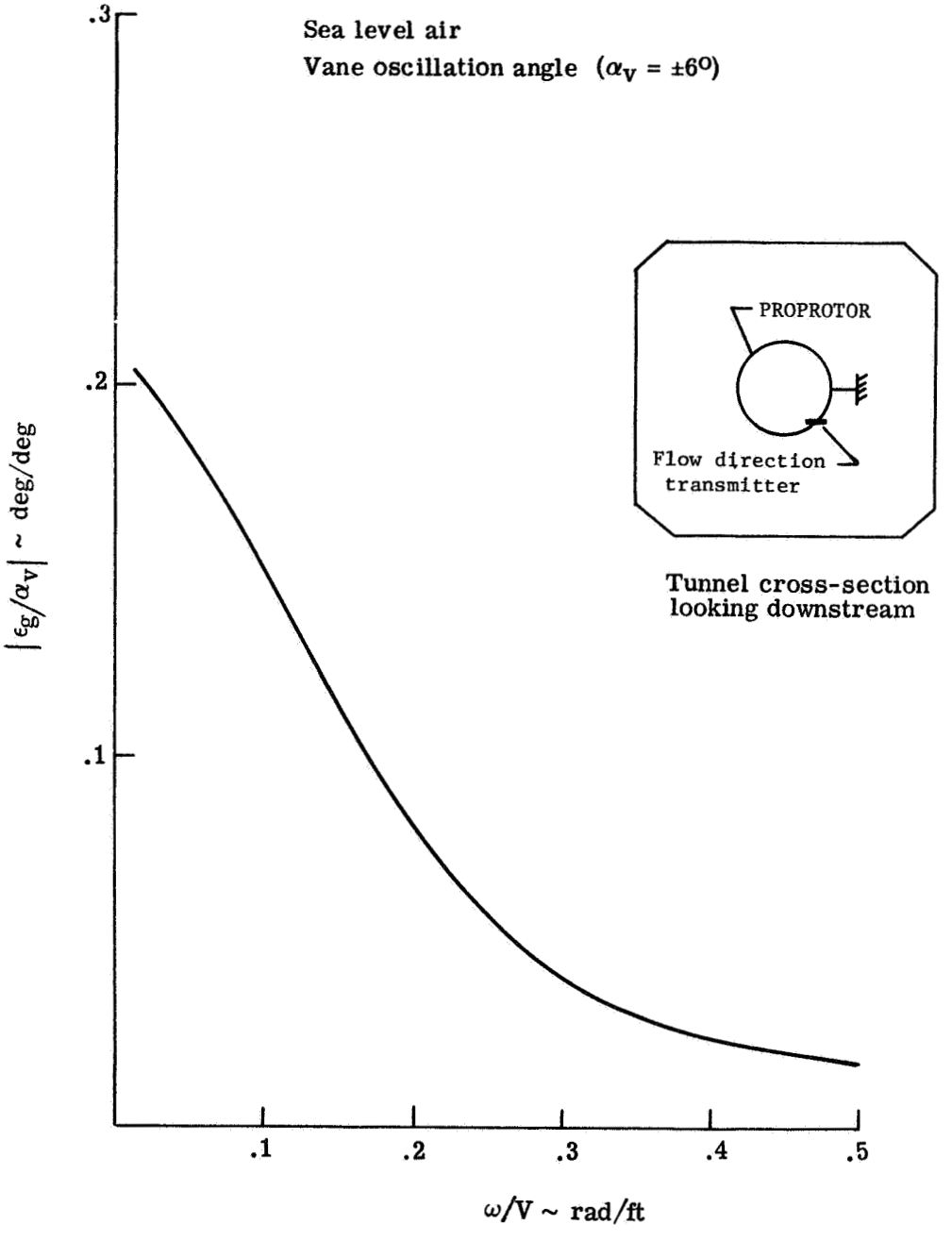

Figure 5-25.- Measured variation of vertical component of gust angle with frequency parameter for vanes oscillating inphase.

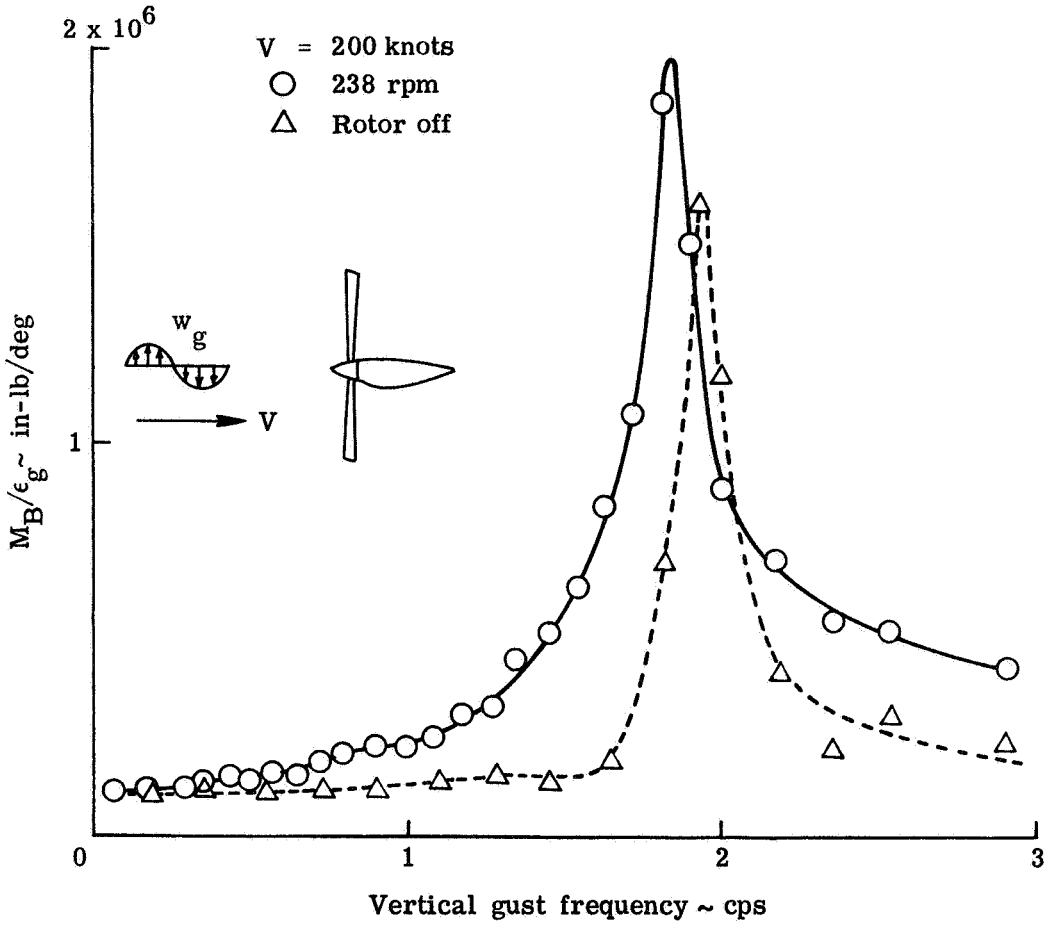

Figure 5-26.- Measured effect of proprotor on wing root bending moment amplitude response function.

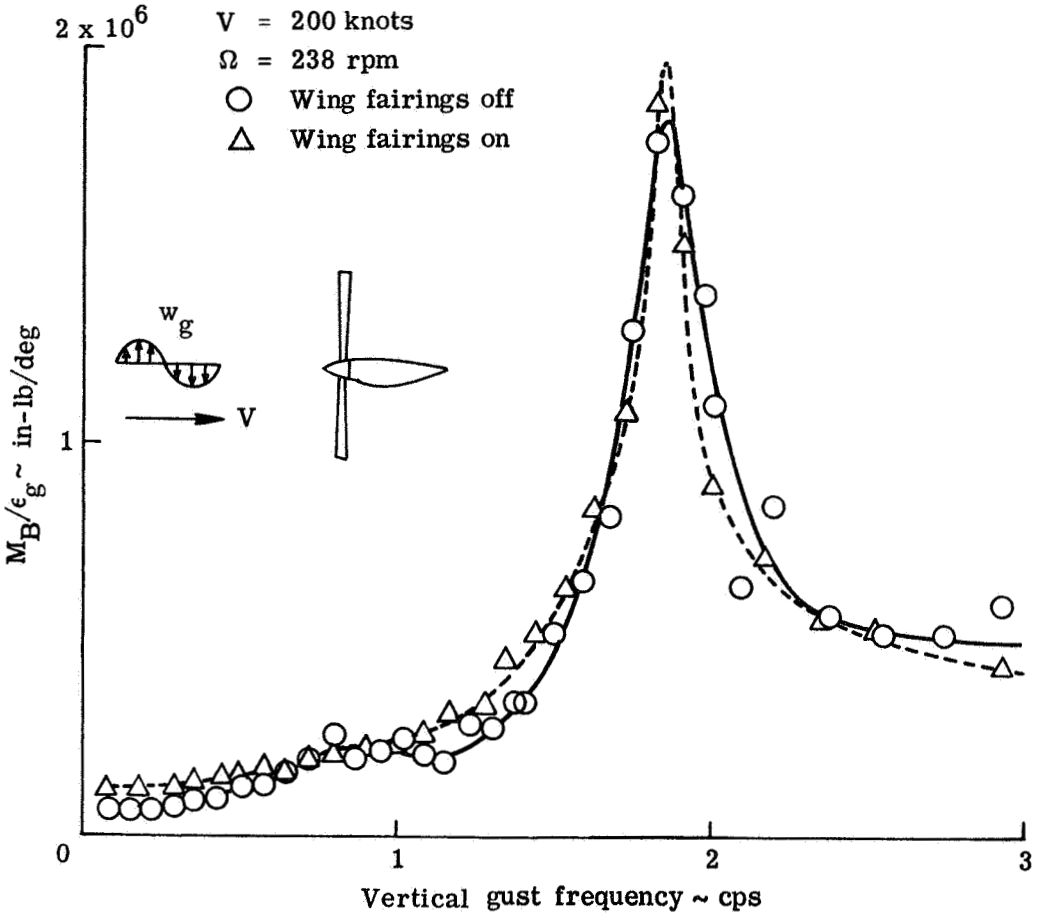

Figure 5-27.- Measured effect of wing aerodynamics on wing root bending moment amplitude response function.

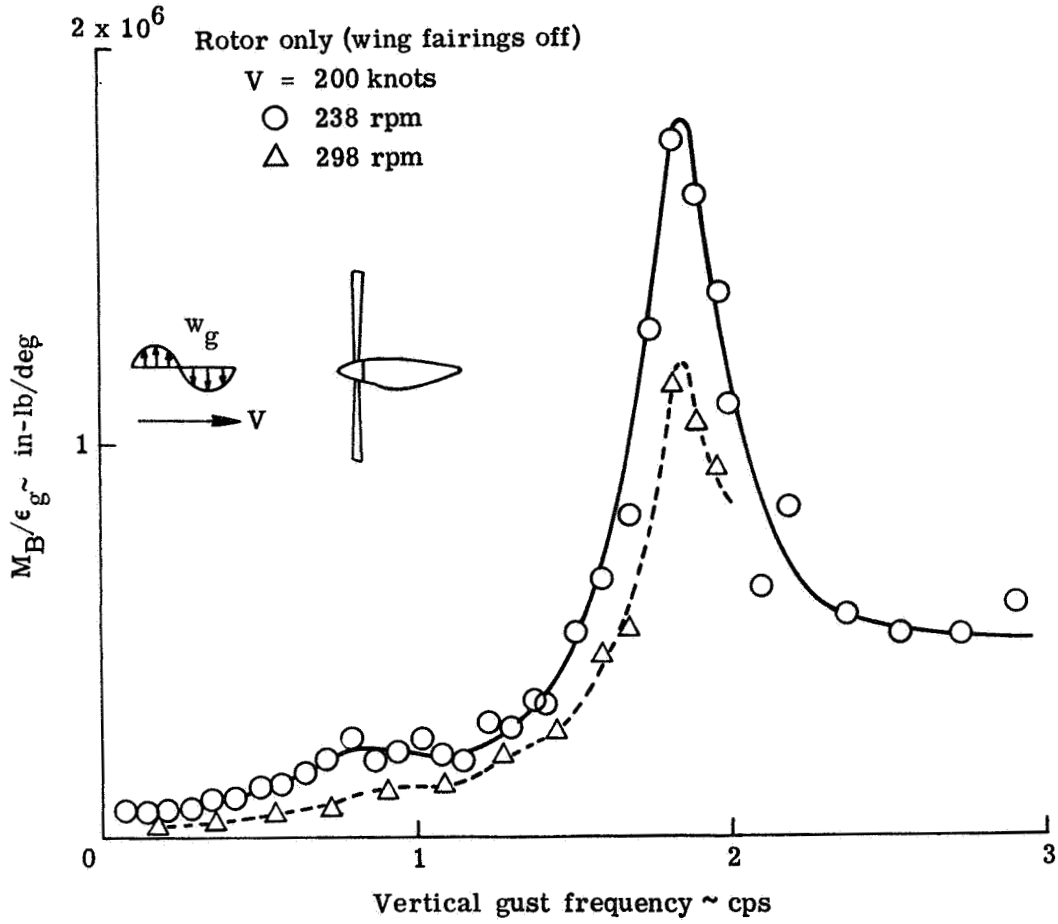

Figure 5-28.- Measured effect of proprotor rpm on wing root bending moment amplitude response function.

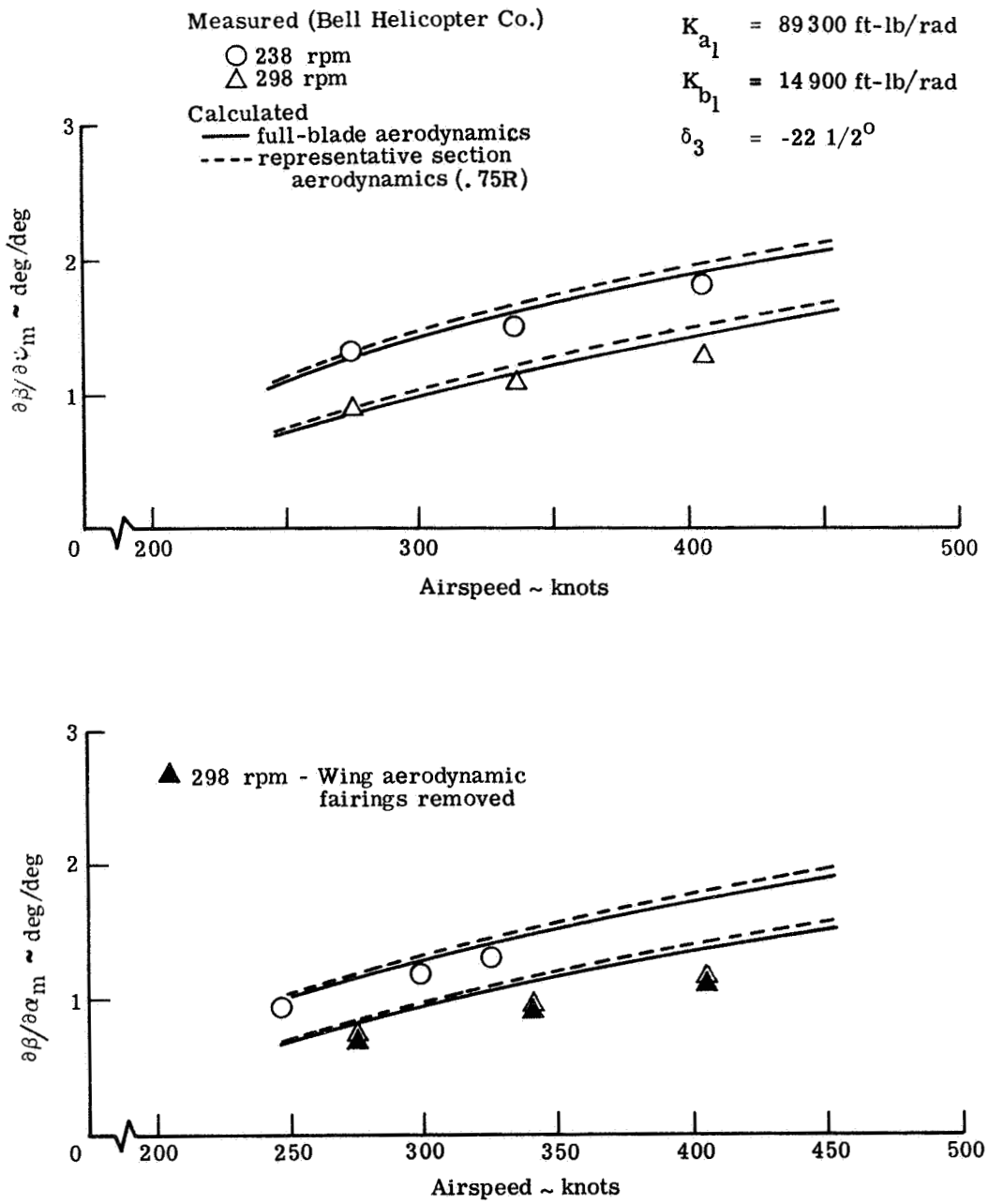

Figure 5-29.- Comparison of measured and calculated variation of blade flapping derivatives with airspeed.

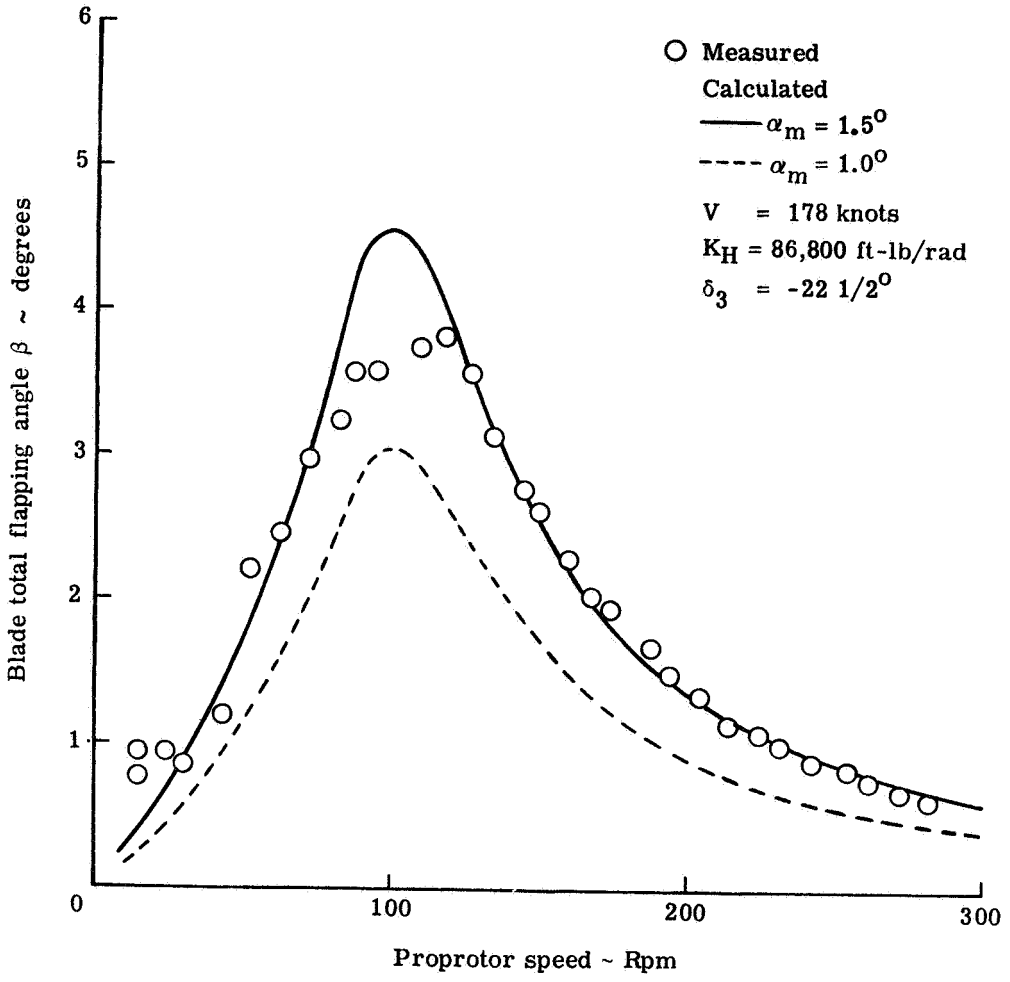

Figure 5-30.- Variation of steady-state blade flapping with proprotor rpm.

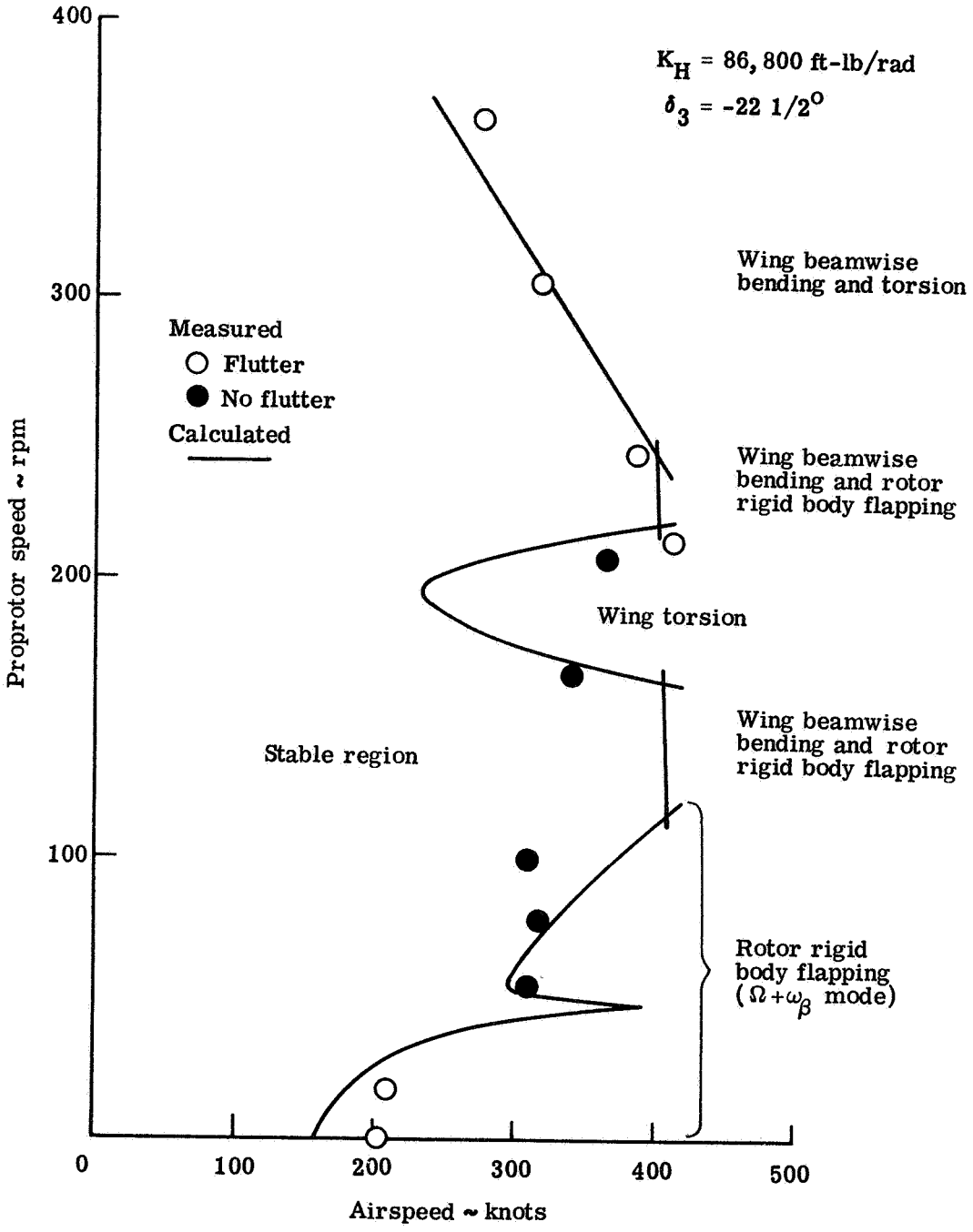

Figure 5-31.- Reference stability boundary for January 1970 test showing variation in character of flutter mode as rpm is reduced to zero.

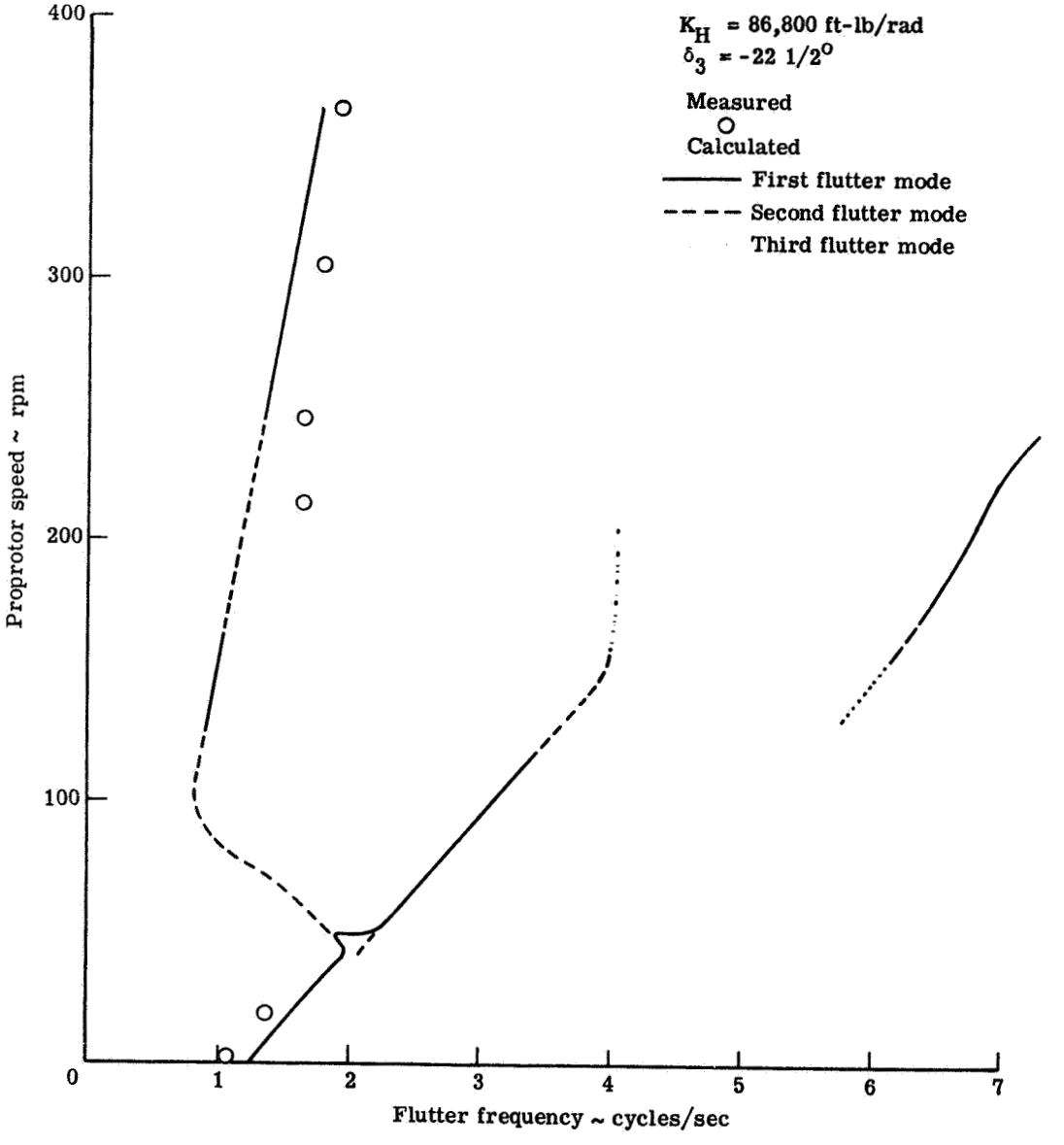

Figure 5-32.- Comparison of measured and calculated flutter frequencies.

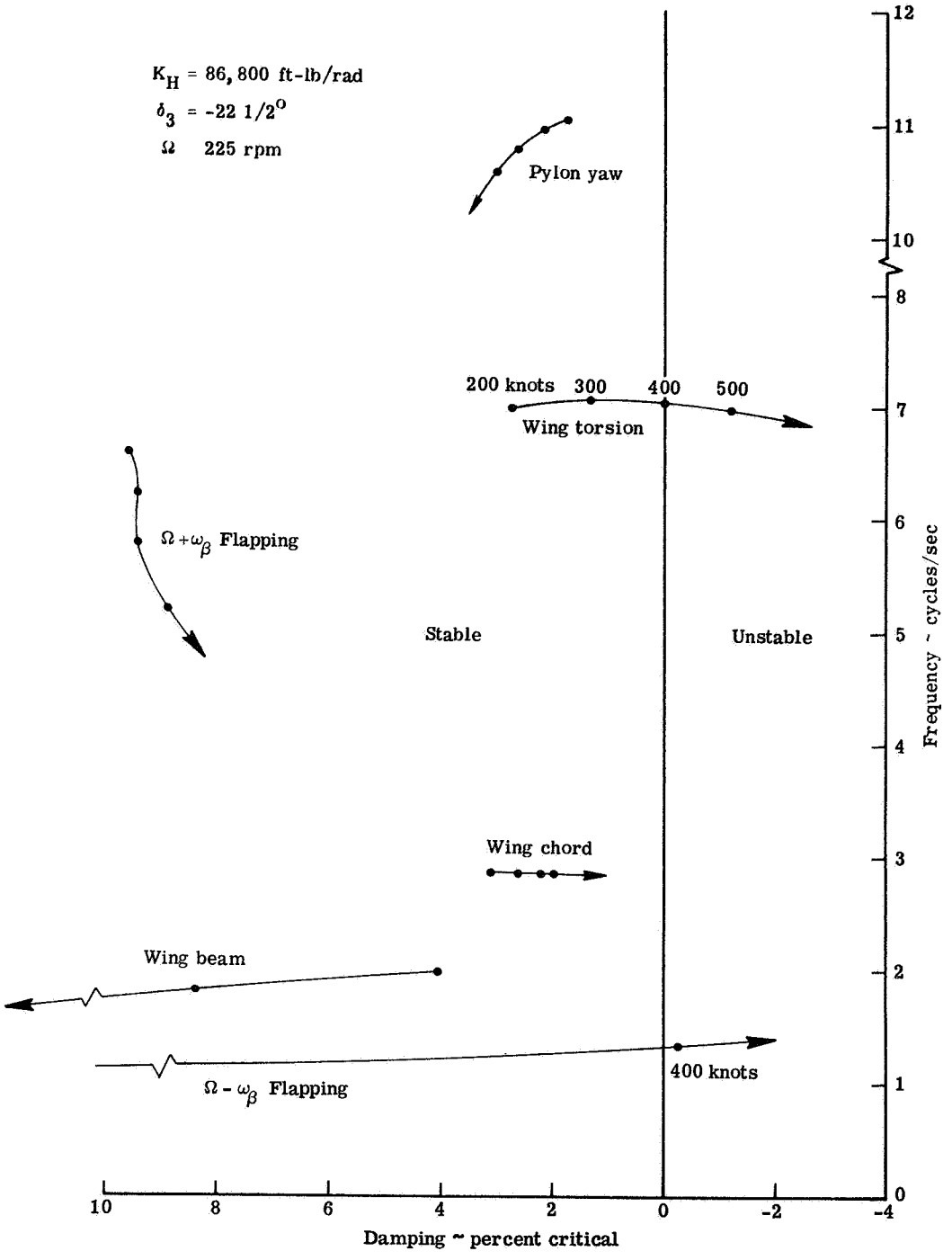

Figure 5-33.- Root locus for Ω = 225 rpm (reference configuration).

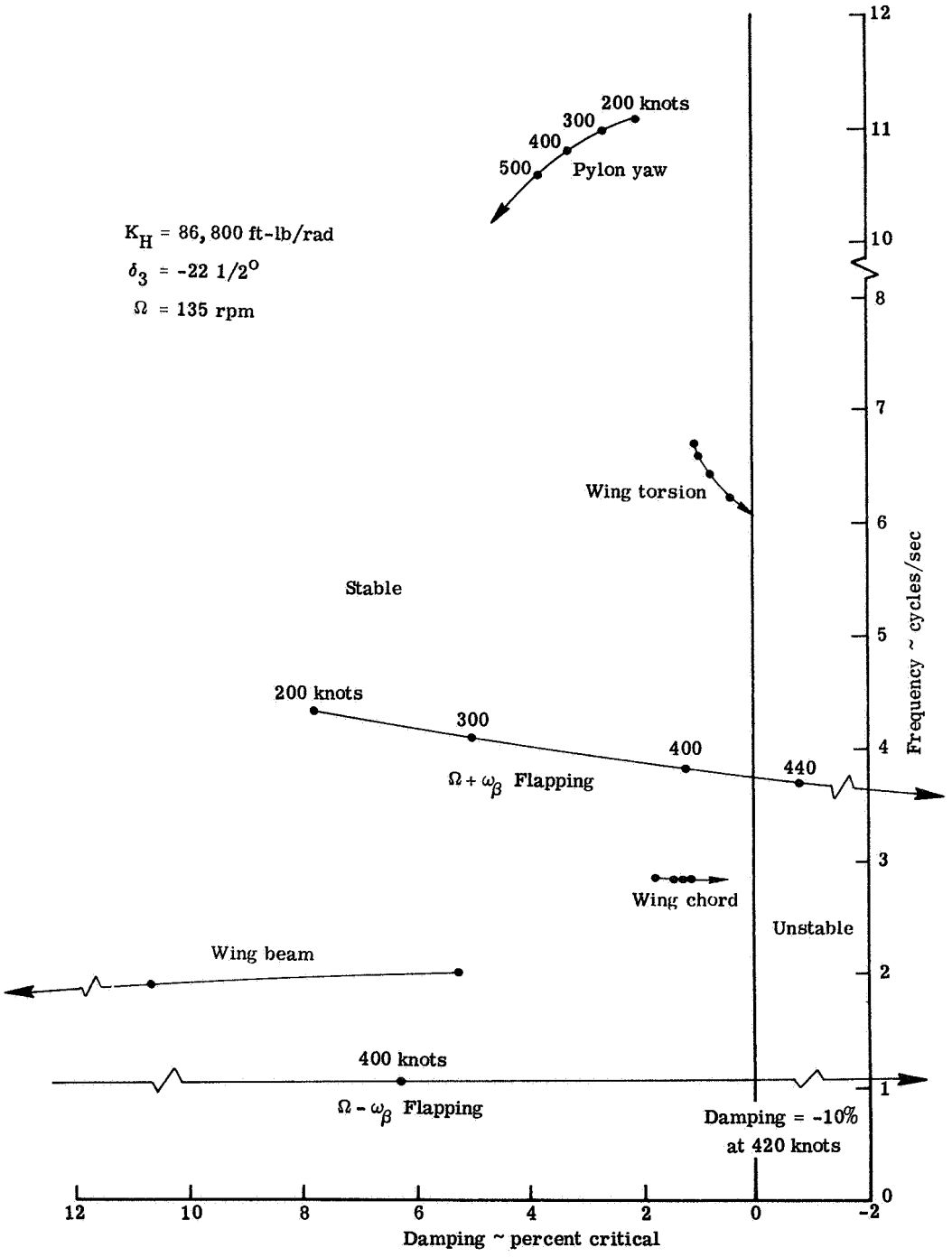

Figure 5-34.- Root locus for Ω = 135 rpm (reference configuration).

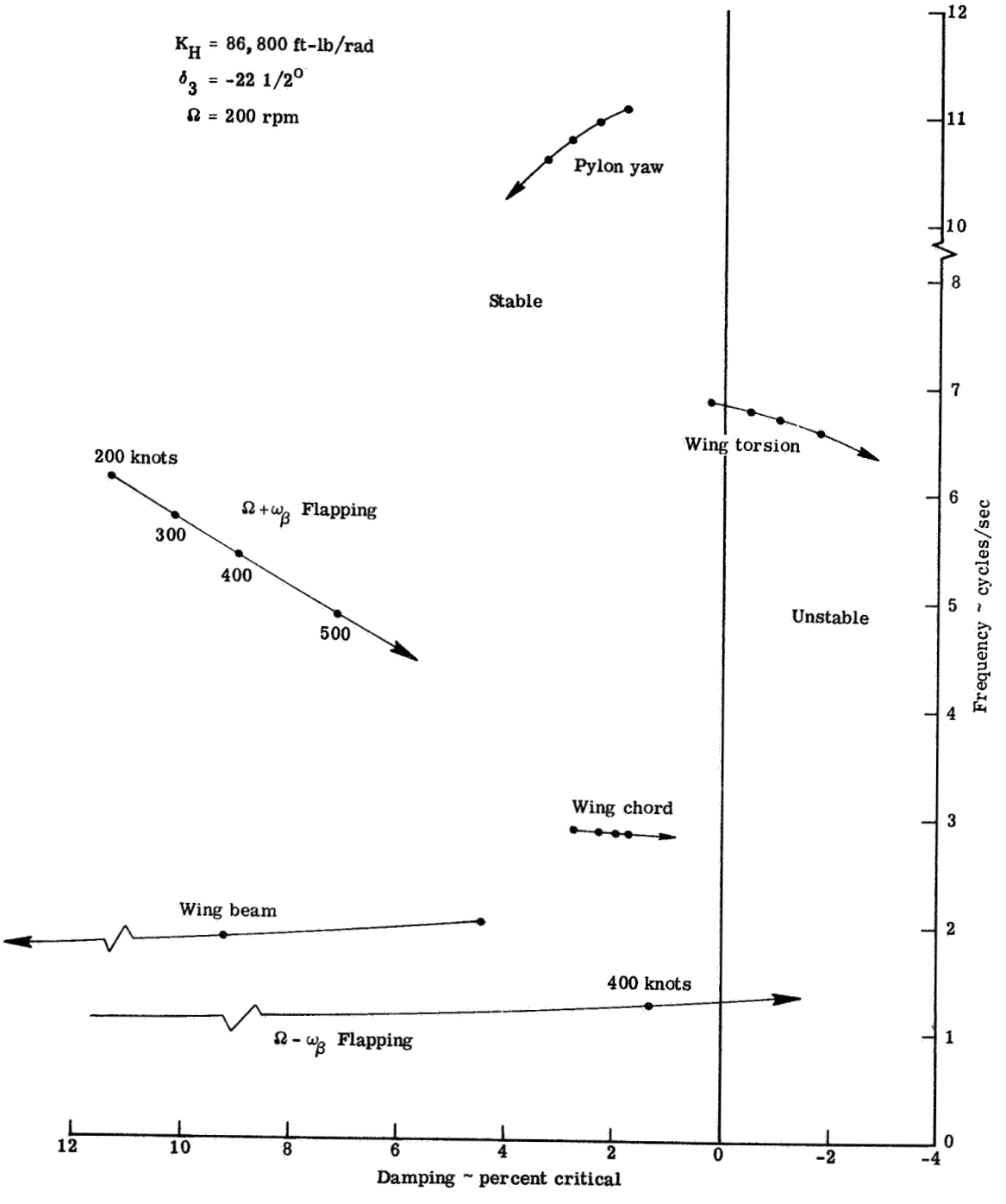

Figure 5-35.- Root locus for Ω = 200 rpm (reference configuration).

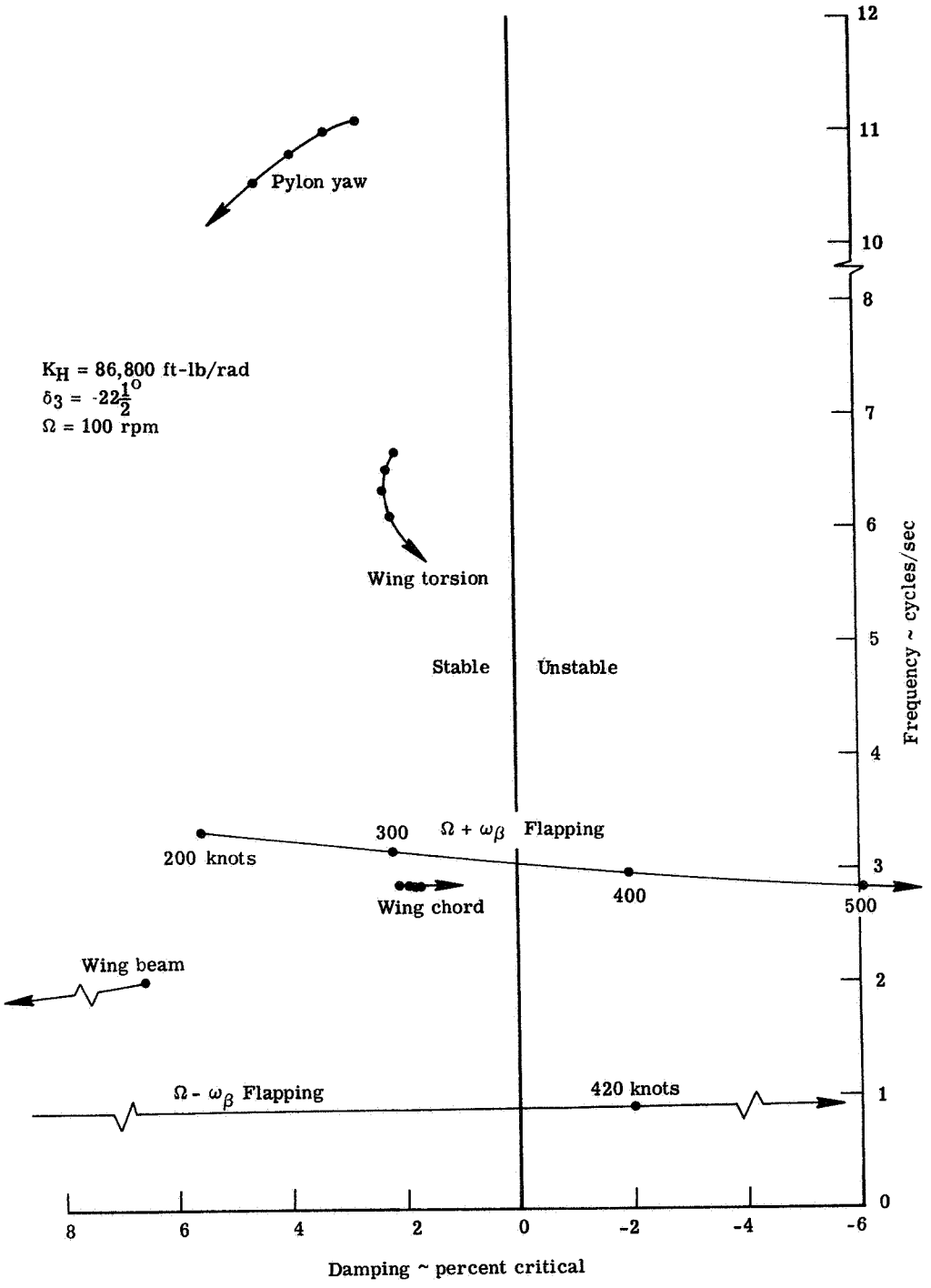

Figure 5-36.- Root locus for Ω = 100 rpm (reference configuration).

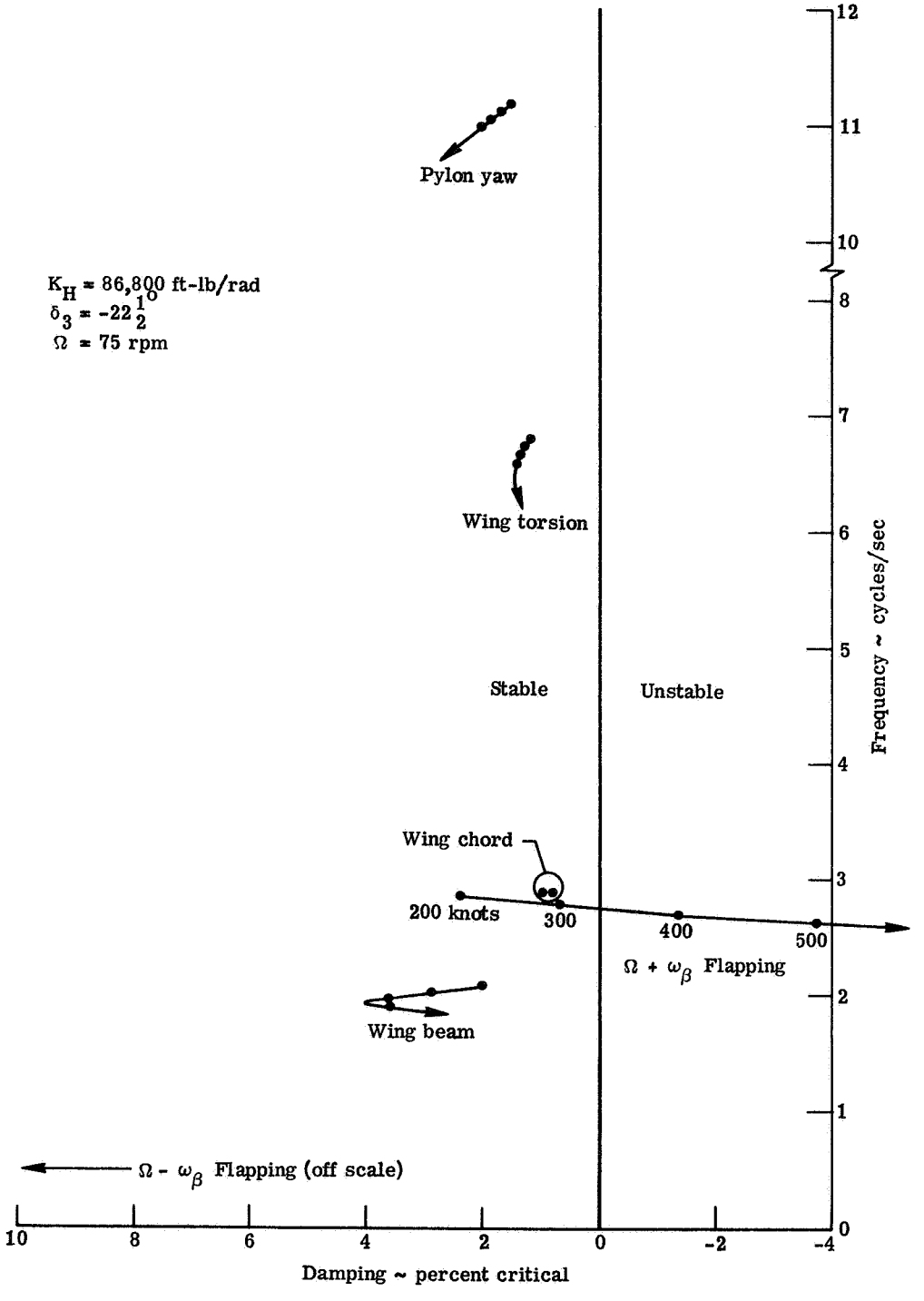

Figure 5-37.- Root locus for Ω = 75 rpm (reference configuration).

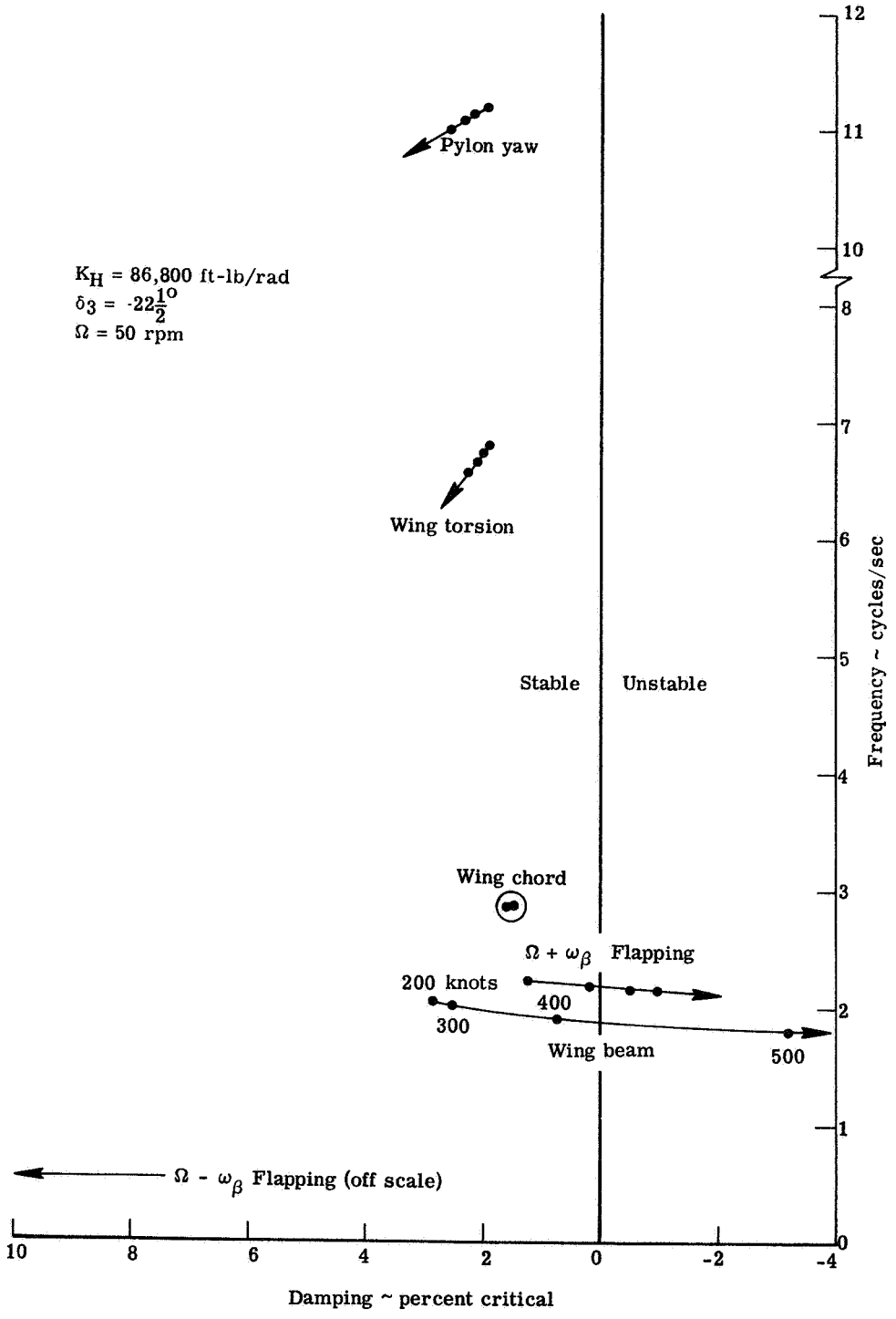

Figure 5-38.- Root locus for Ω = 50 rpm (reference configuration).

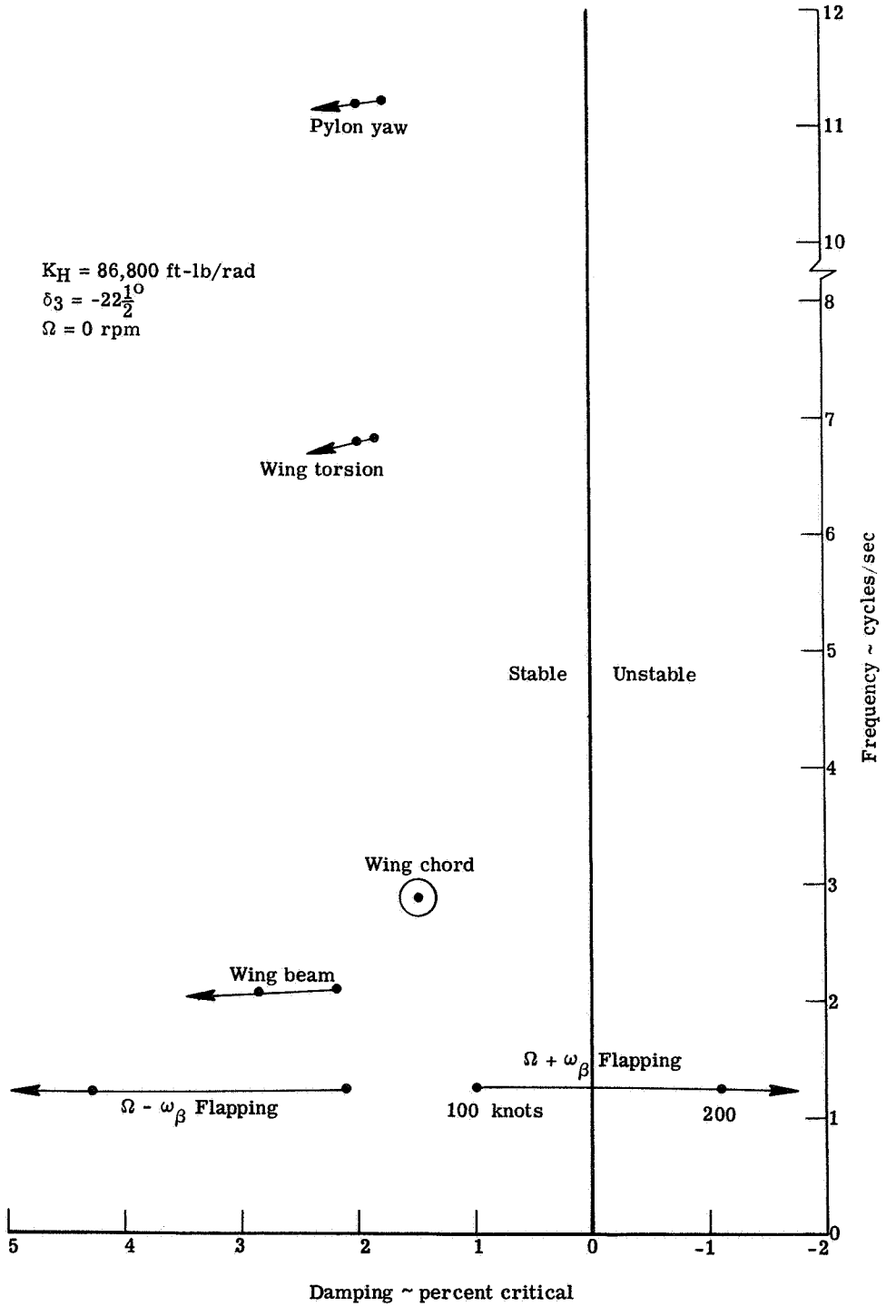

Figure 5-39.- Root locus for Ω = 0 rpm (reference configuration).

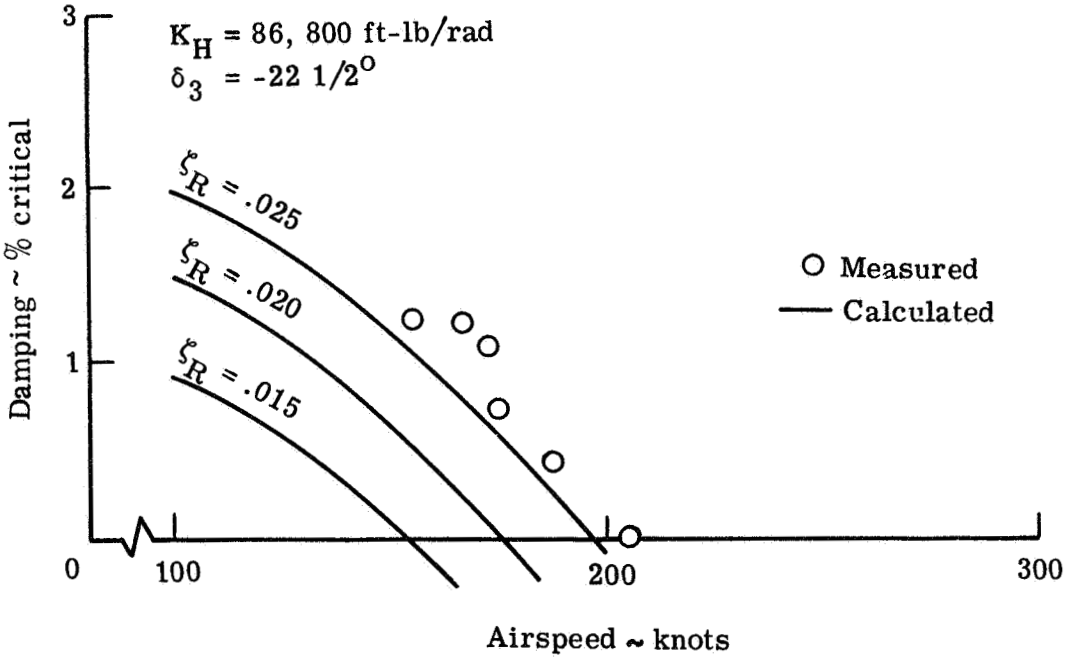

Figure 5-40.- Variation of $\Omega + \omega_\beta$ flapping mode damping with airspeed for $\Omega = 0$ rpm.

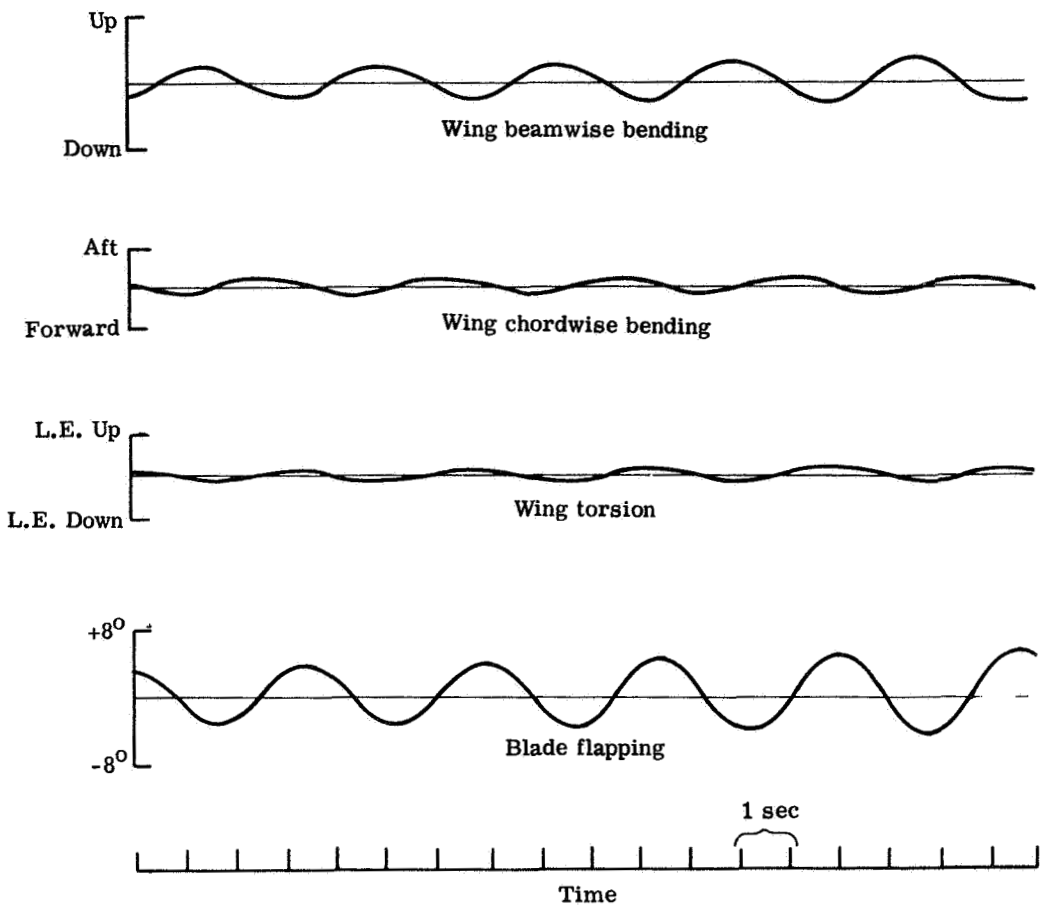

Figure 5-41.- Typical traces showing model response at flutter for zero rpm (flapping response is slowly diverging here).

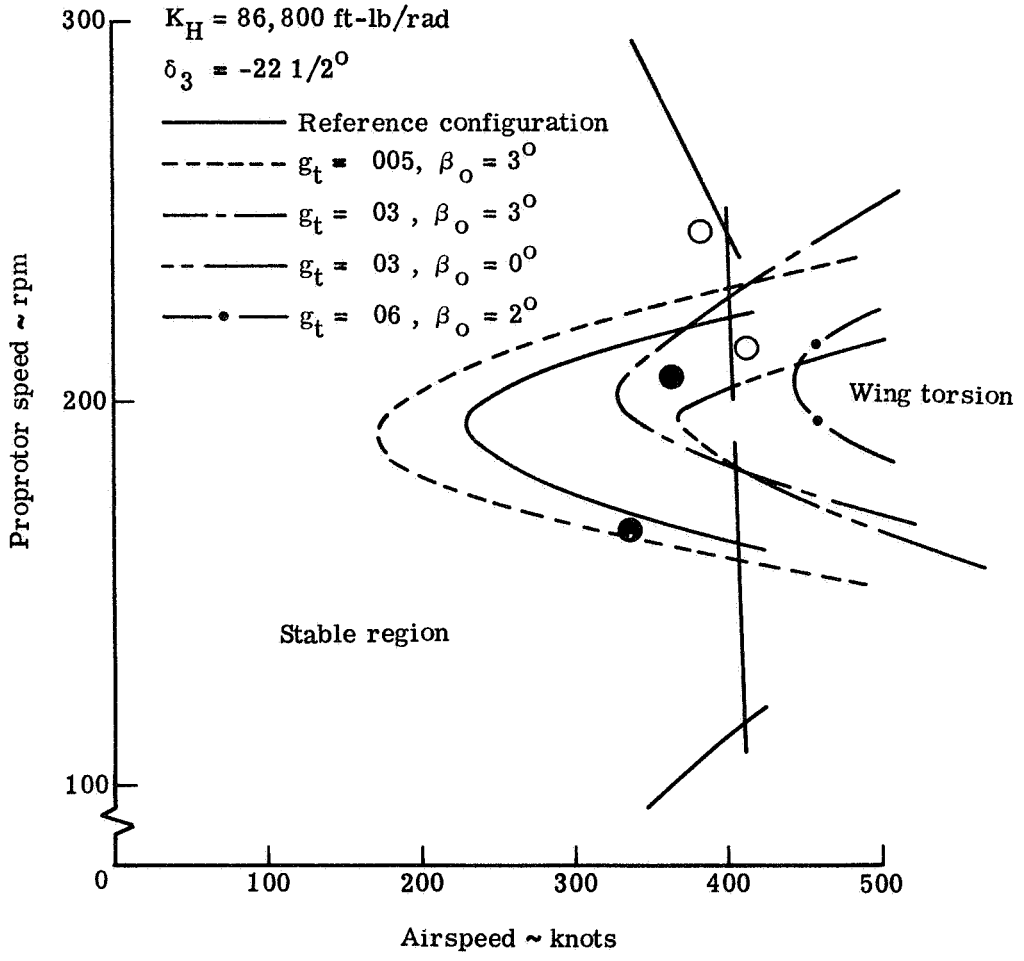

Figure 5-42.- Calculated effect of wing torsion structural damping and proprotor precone on wing torsion mode instability.

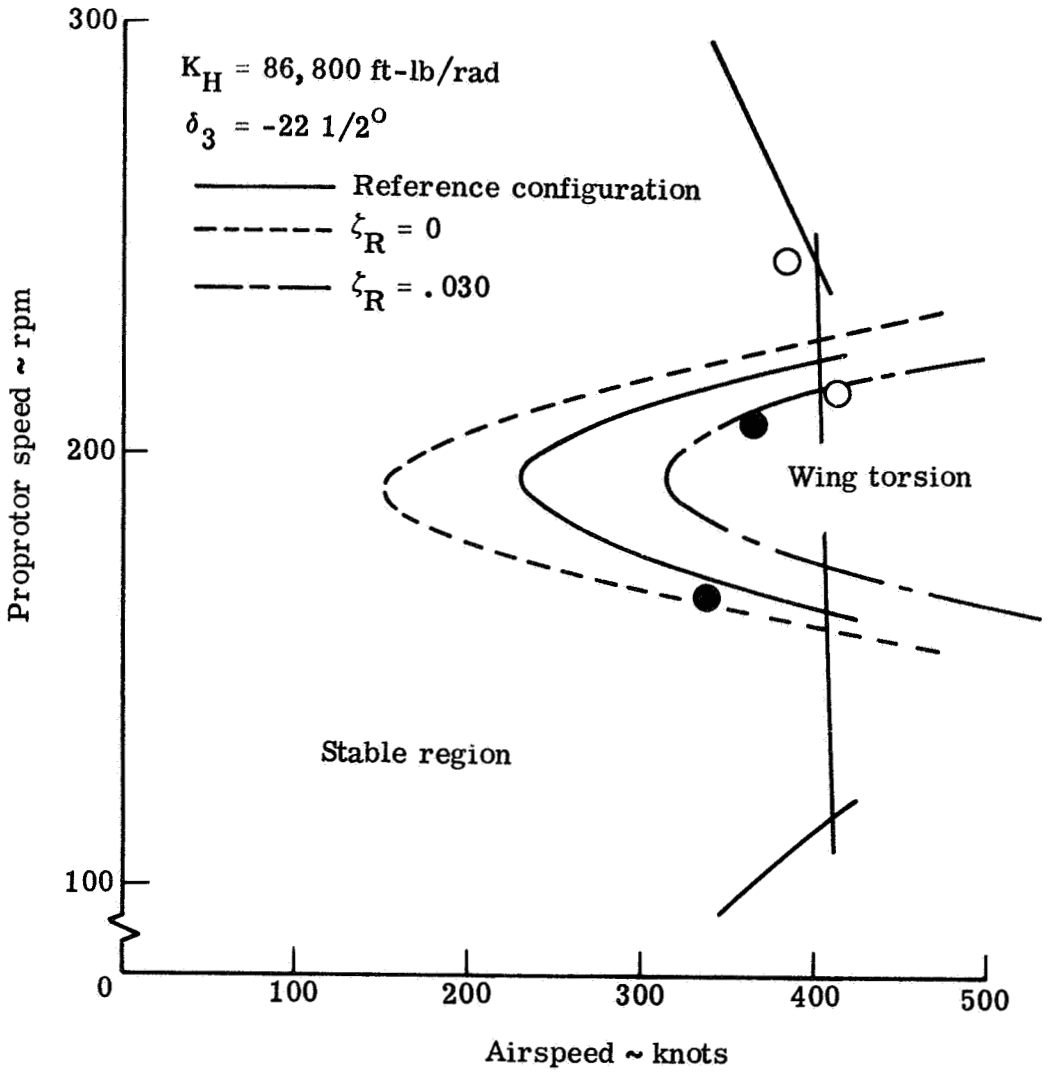

Figure 5-43.- Calculated effect of proprotor hub structural damping on wing torsion mode instability.

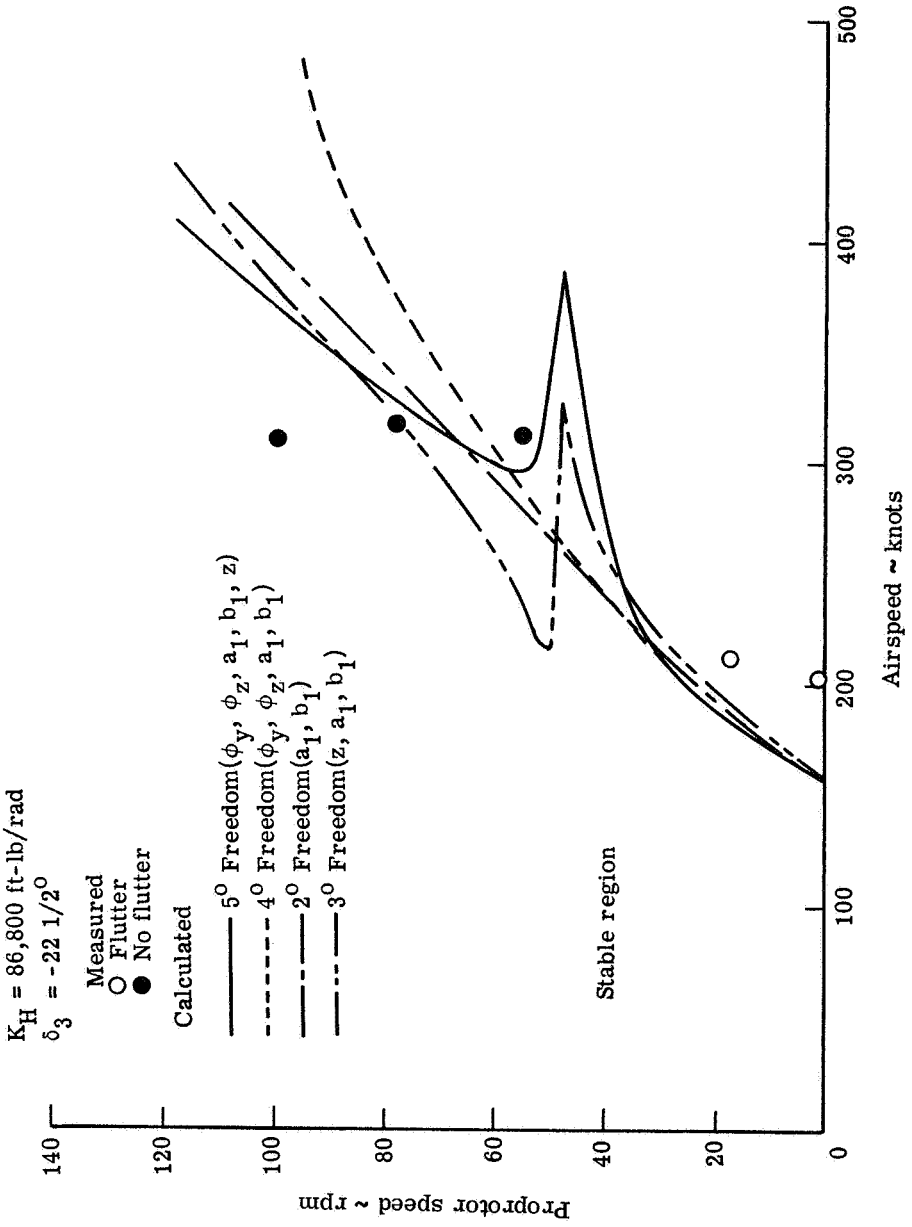

Figure 5-44.- Calculated effect of pylon/wing degrees of freedom on flapping stability at low rpm.

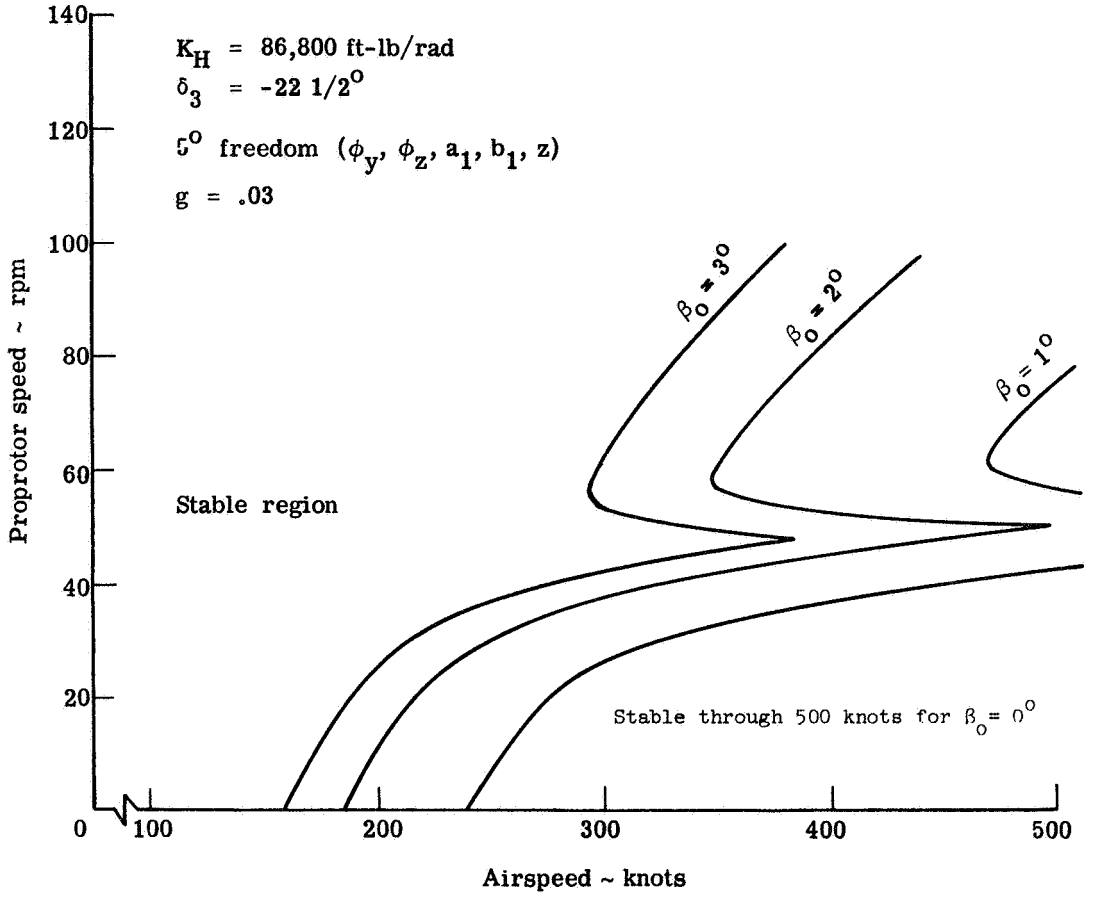

Figure 5-45.- Calculated effect of precone on flapping mode stability for 5° of freedom system.

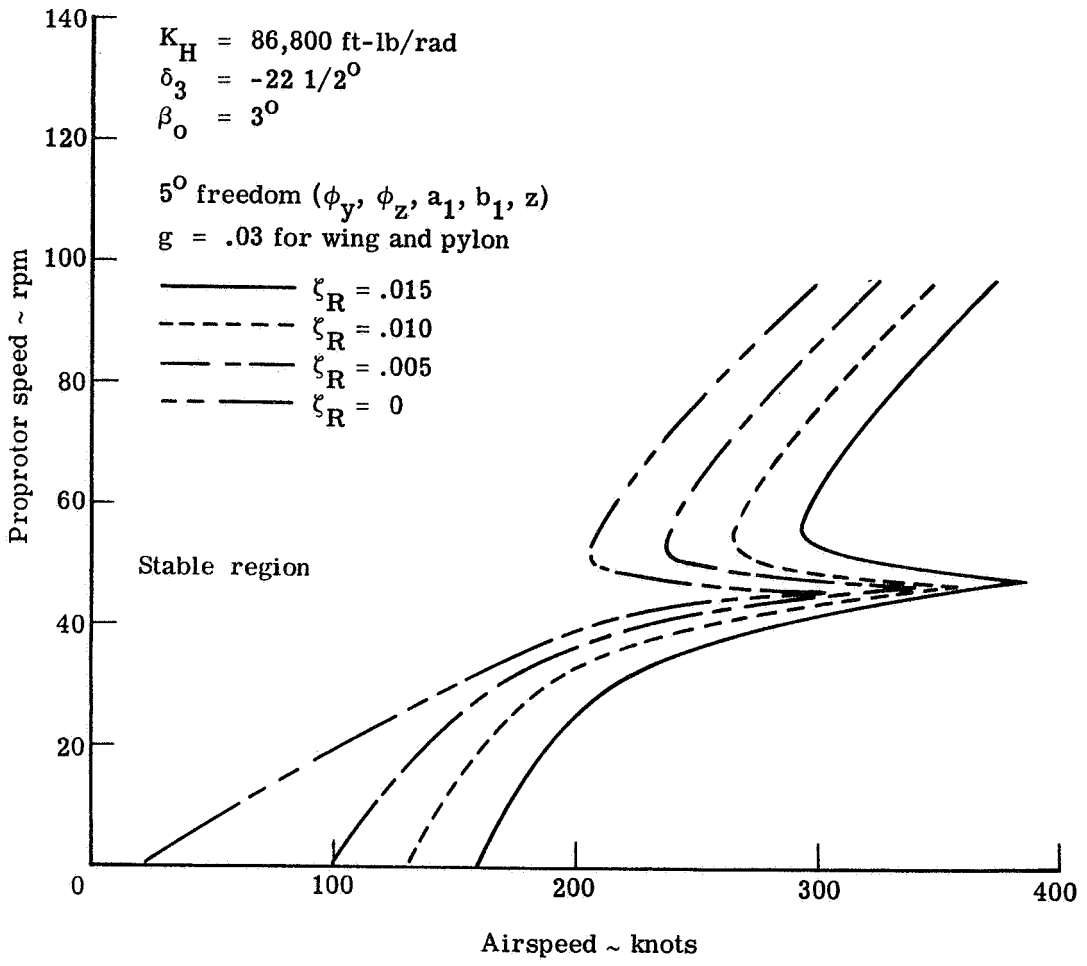

Figure 5-46.- Calculated effect of proprotor structural damping on flapping mode stability at low rpm for 5° of freedom system.

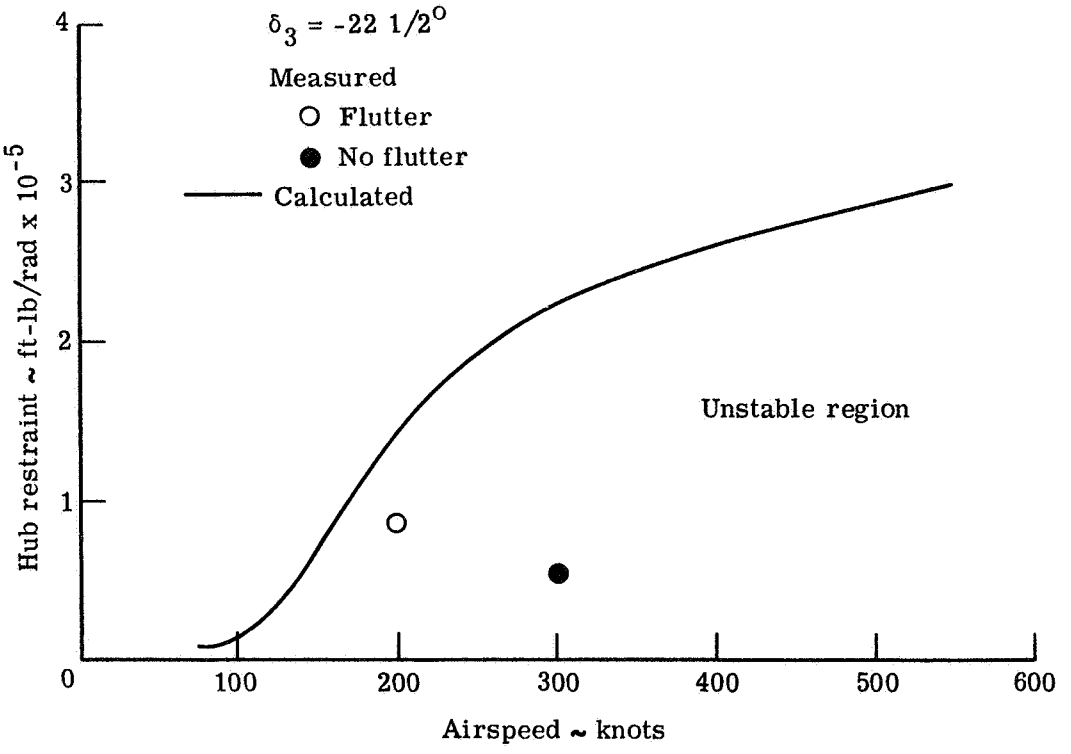

Figure 5-47.- Effect of hub restraint on flapping mode stability at zero rpm (δ_3 = -22.5°).

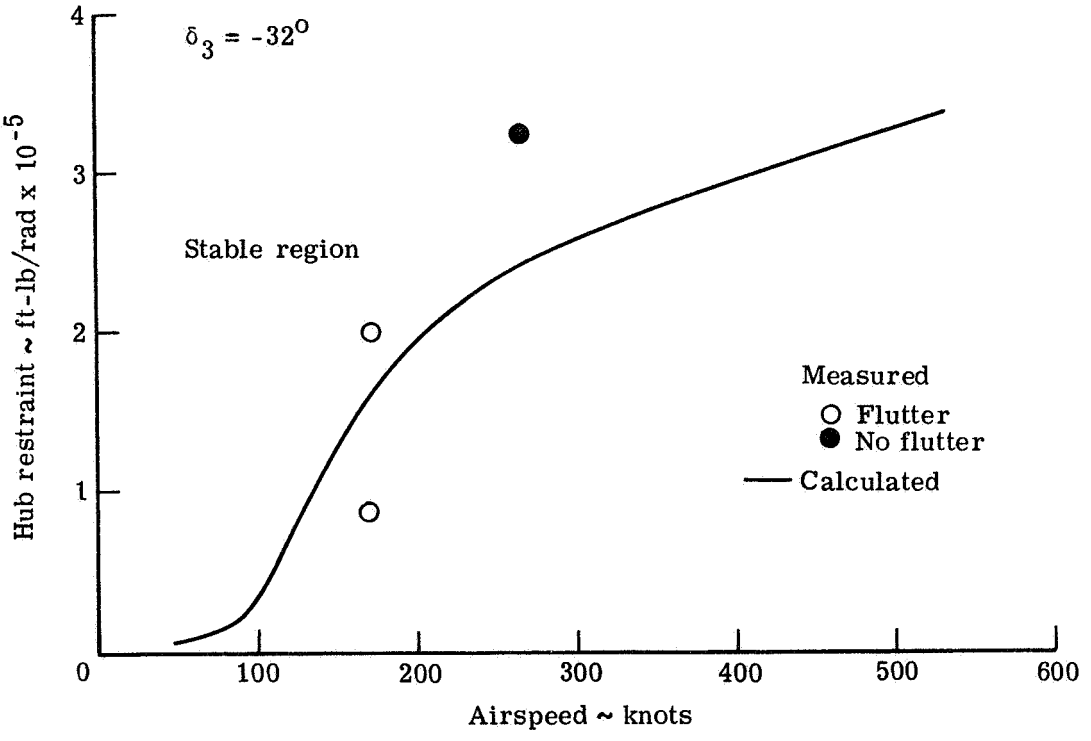

Figure 5-48.- Effect of hub restraint on flapping mode stability at zero rpm ($\delta_3 = -32^o$).

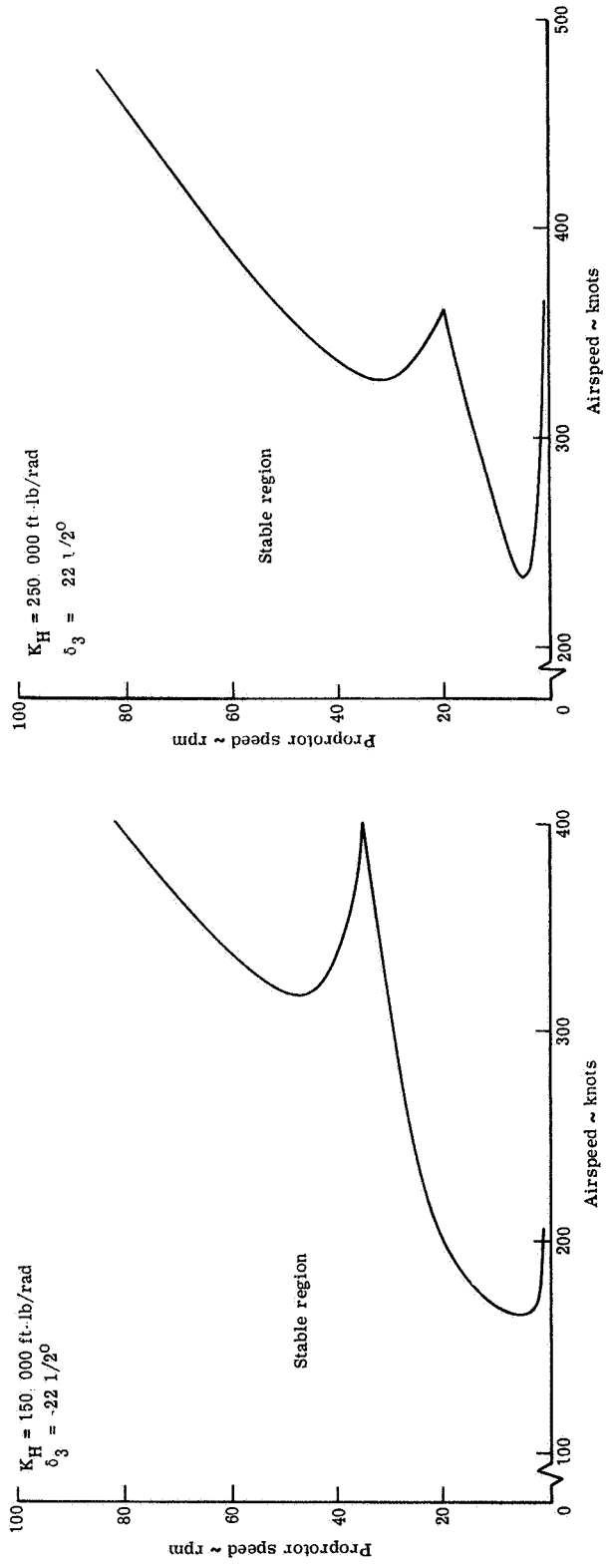

Figure 5-49.- Calculated effect of hub restraint on flapping mode stability at low rpm.

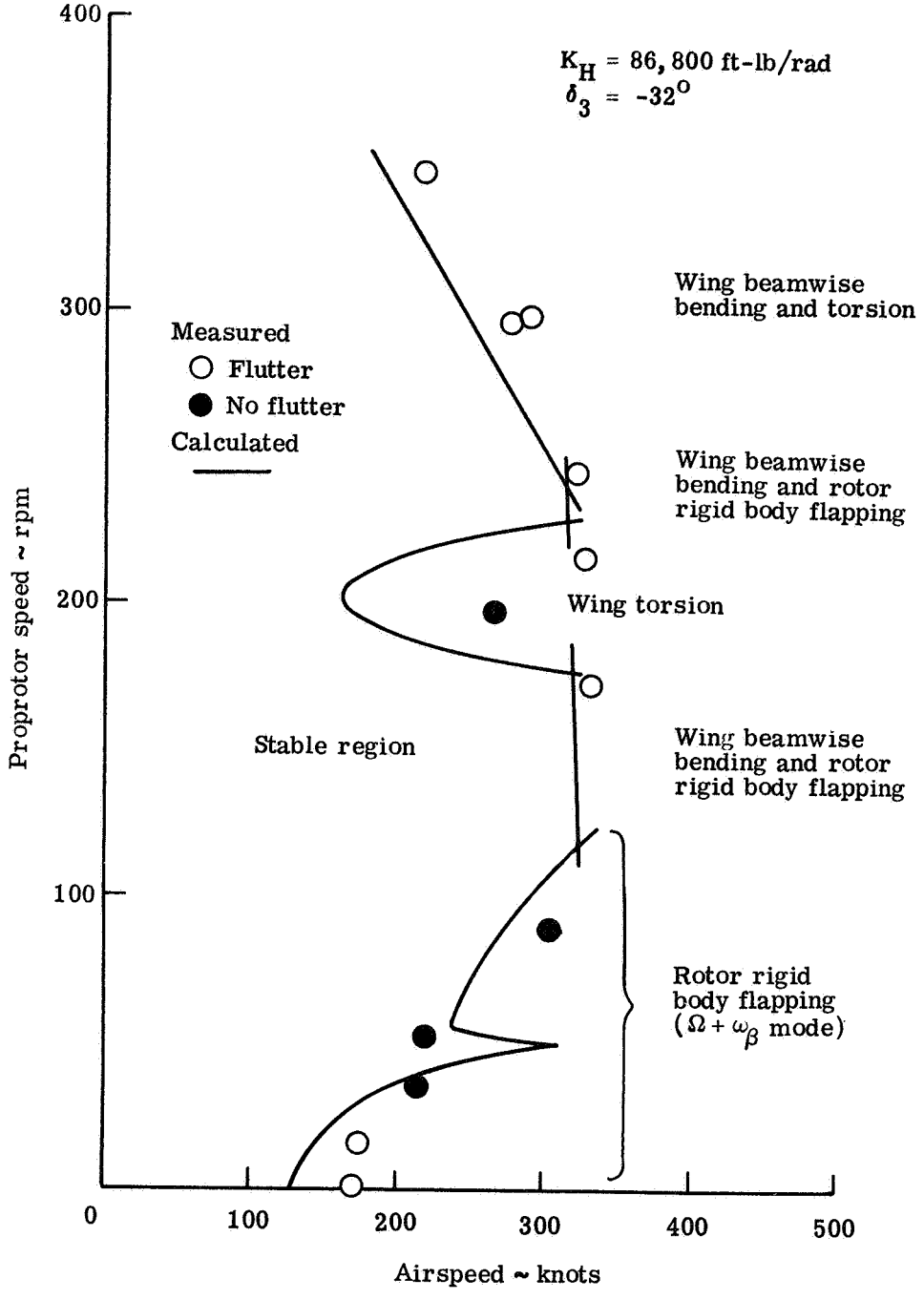

Figure 5-50.- Effect of increased negative δ_3 on stability of reference configuration ($\delta_3 = -32°$).

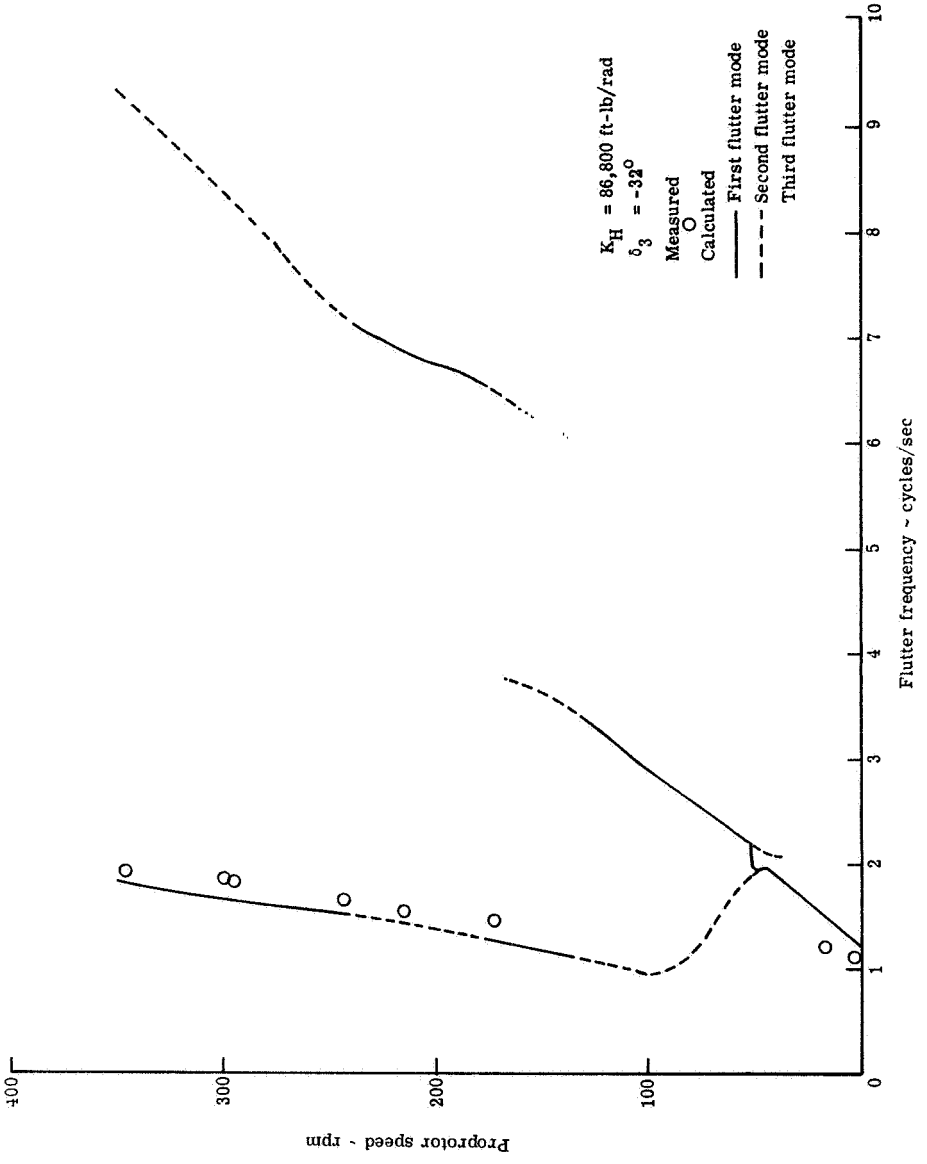

Figure 5-51.- Comparison of measured and calculated flutter frequencies ($\delta_3 = -32^\circ$).

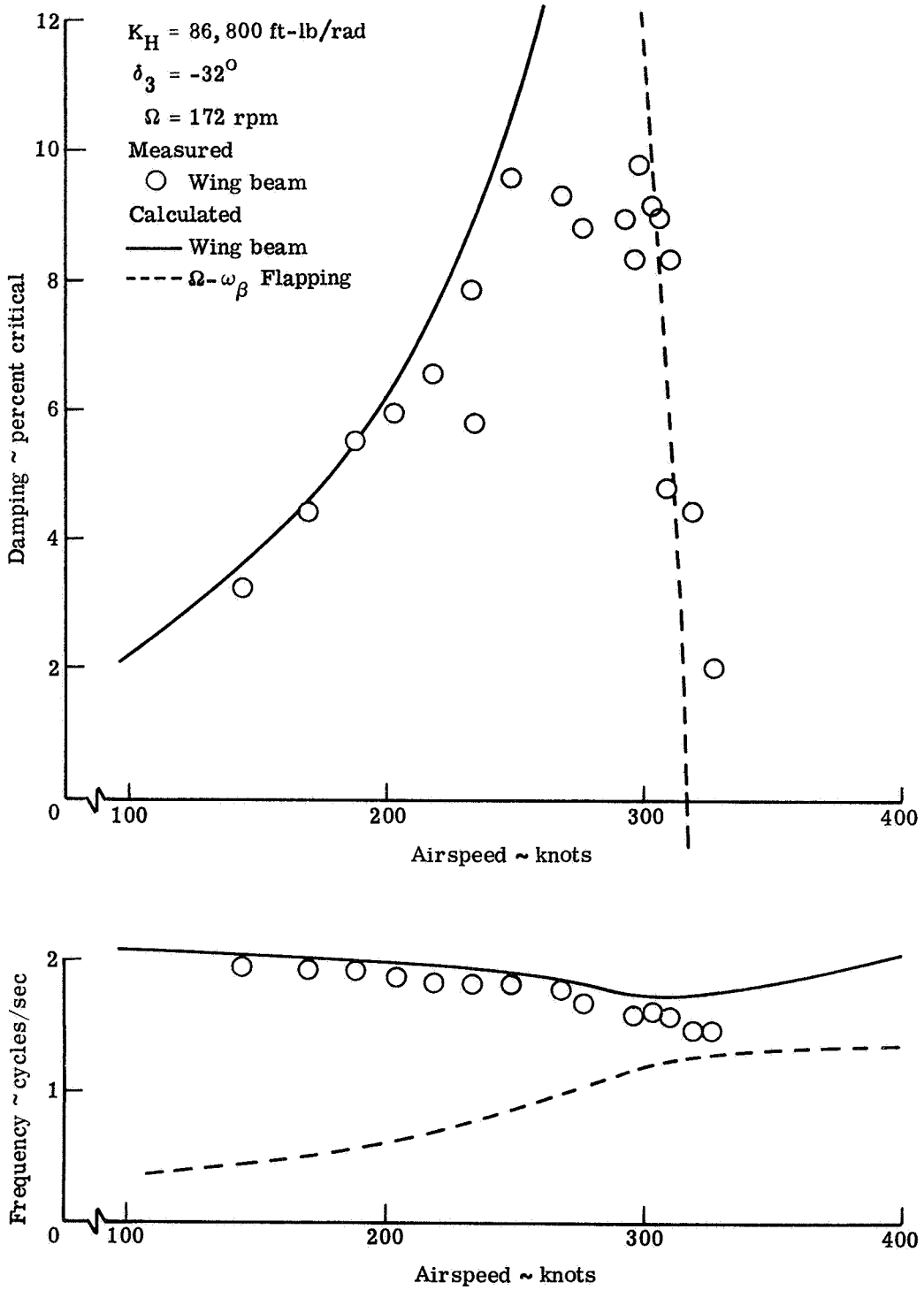

Figure 5-52.- System response characteristics for flutter at Ω = 172 rpm.

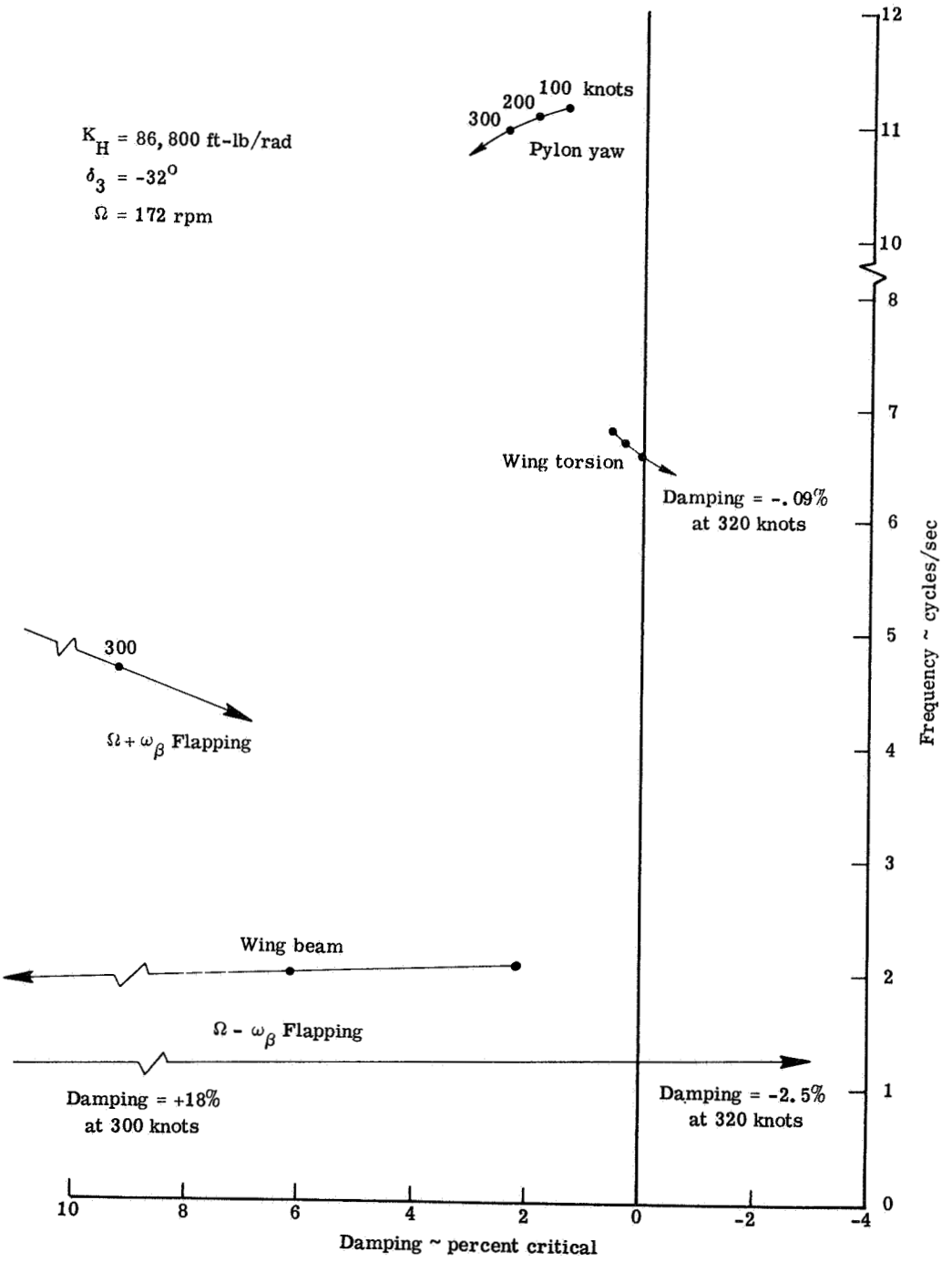

Figure 5-53.- Root locus for Ω = 172 rpm.

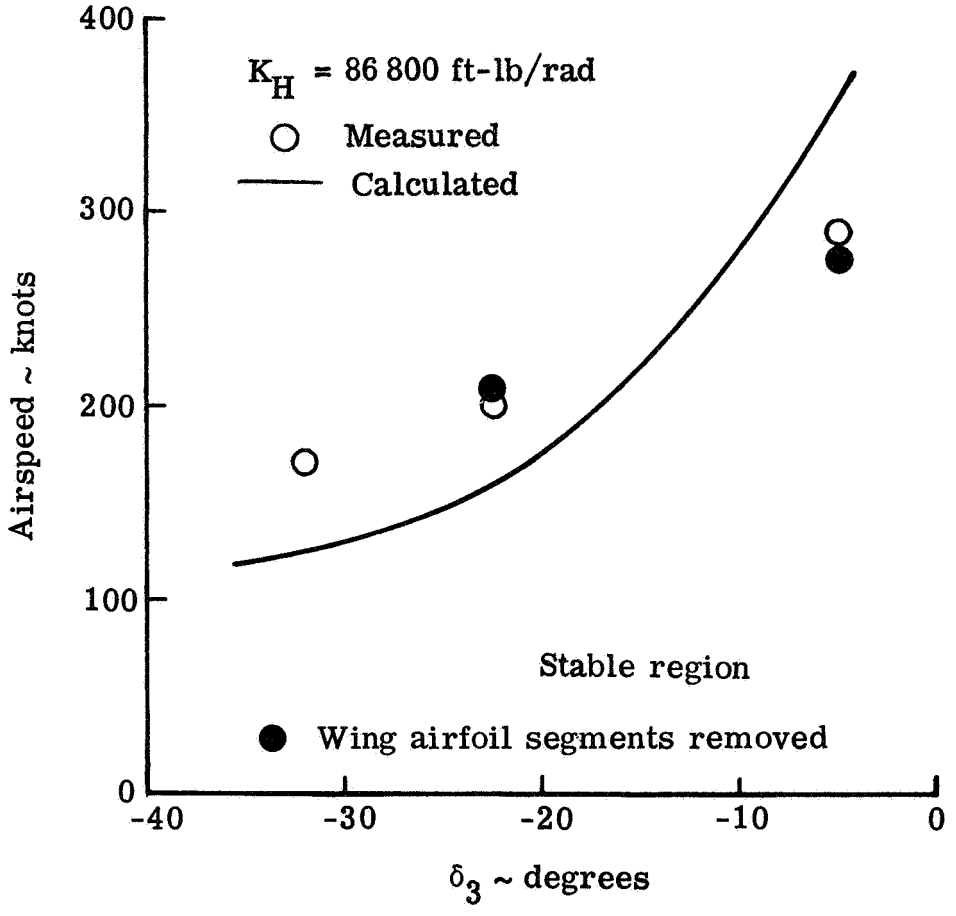

Figure 5-54.- Variation of zero rpm flutter speed with δ_3.

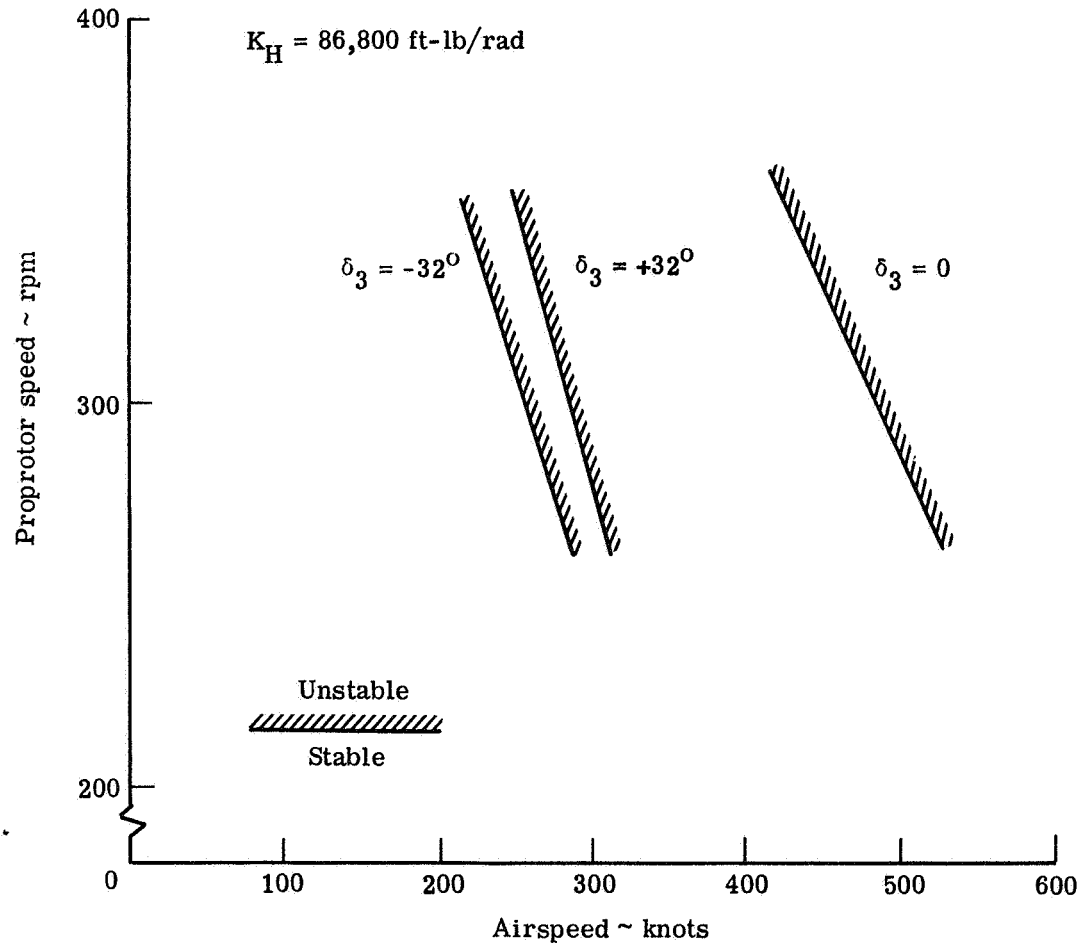

Figure 5-55.- Calculated effect of δ_3 on proprotor/pylon stability at high rpm.

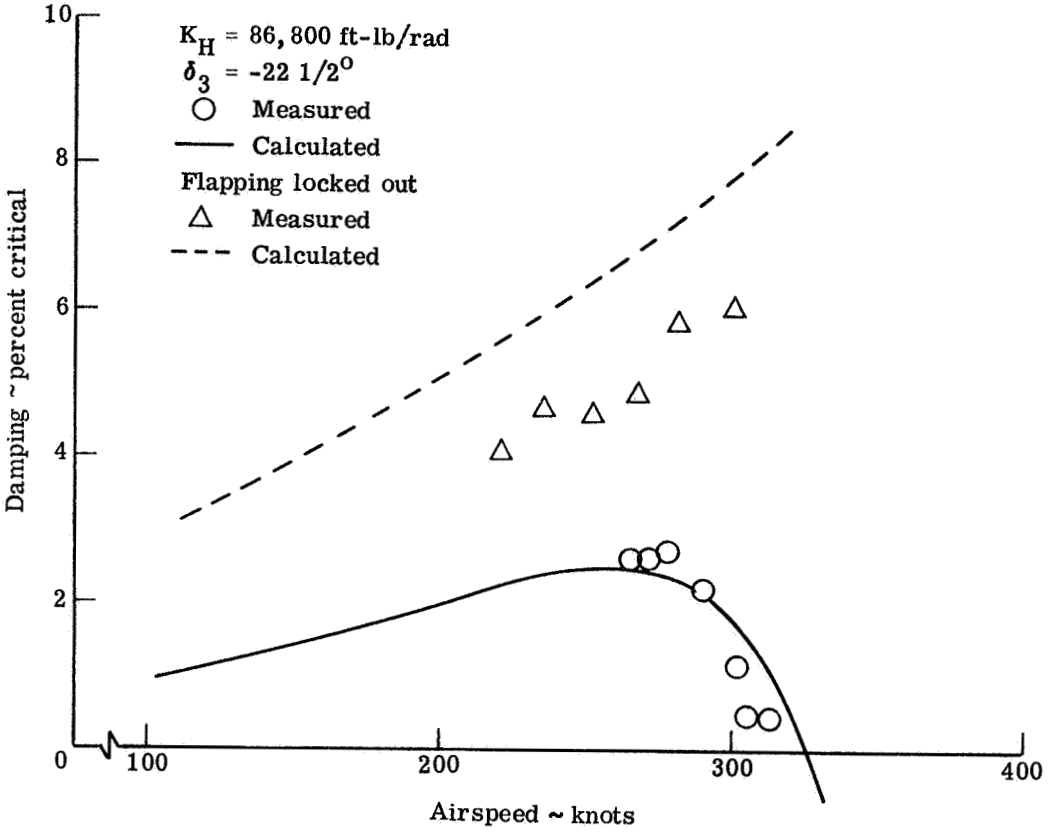

Figure 5-56.- Effect of blade flapping degree of freedom on wing beam mode damping (Ω = 300 rpm).

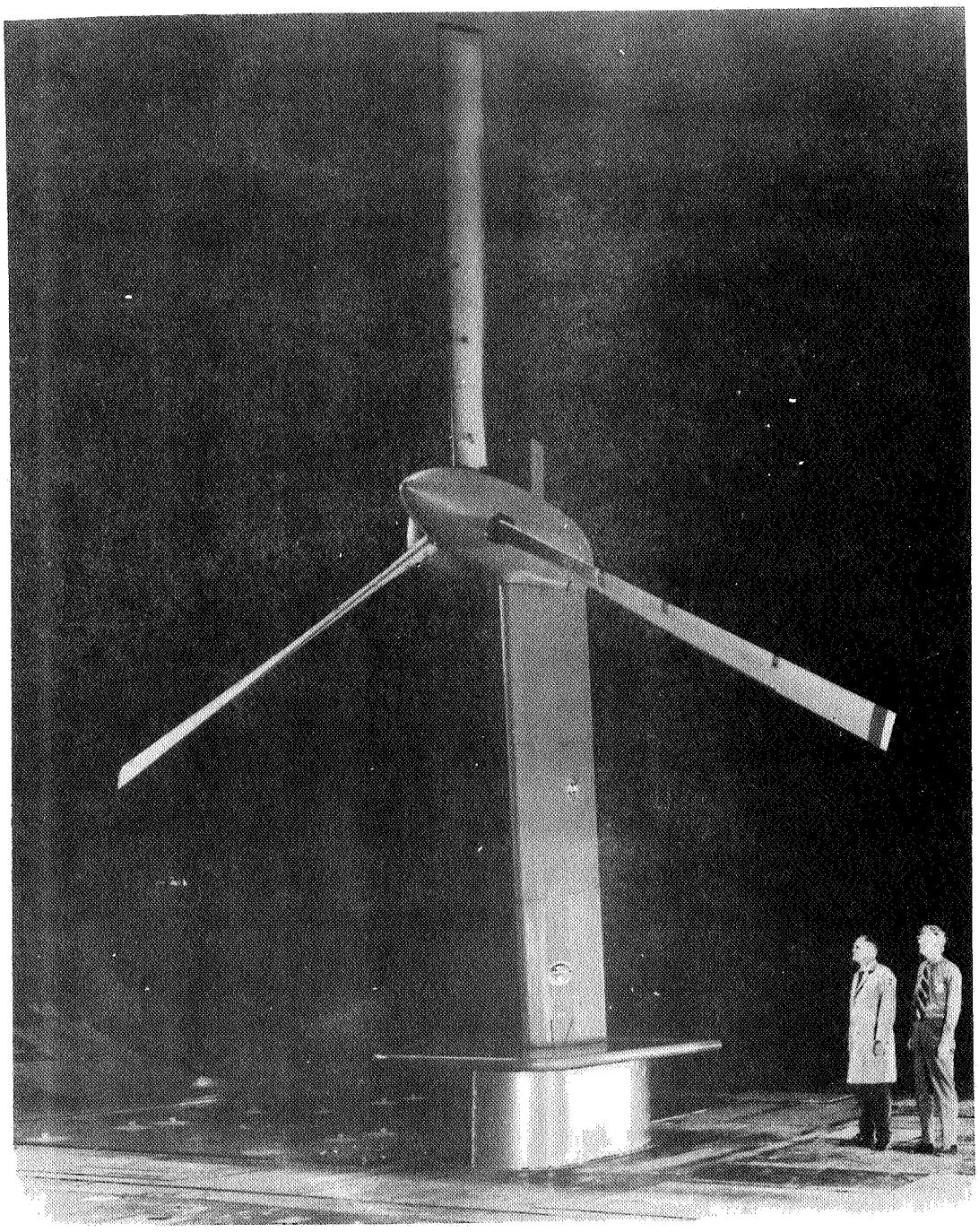

Figure 5-57.- Bell 25-foot flight-worthy proprotor in NASA-Ames full-scale tunnel for dynamic testing.

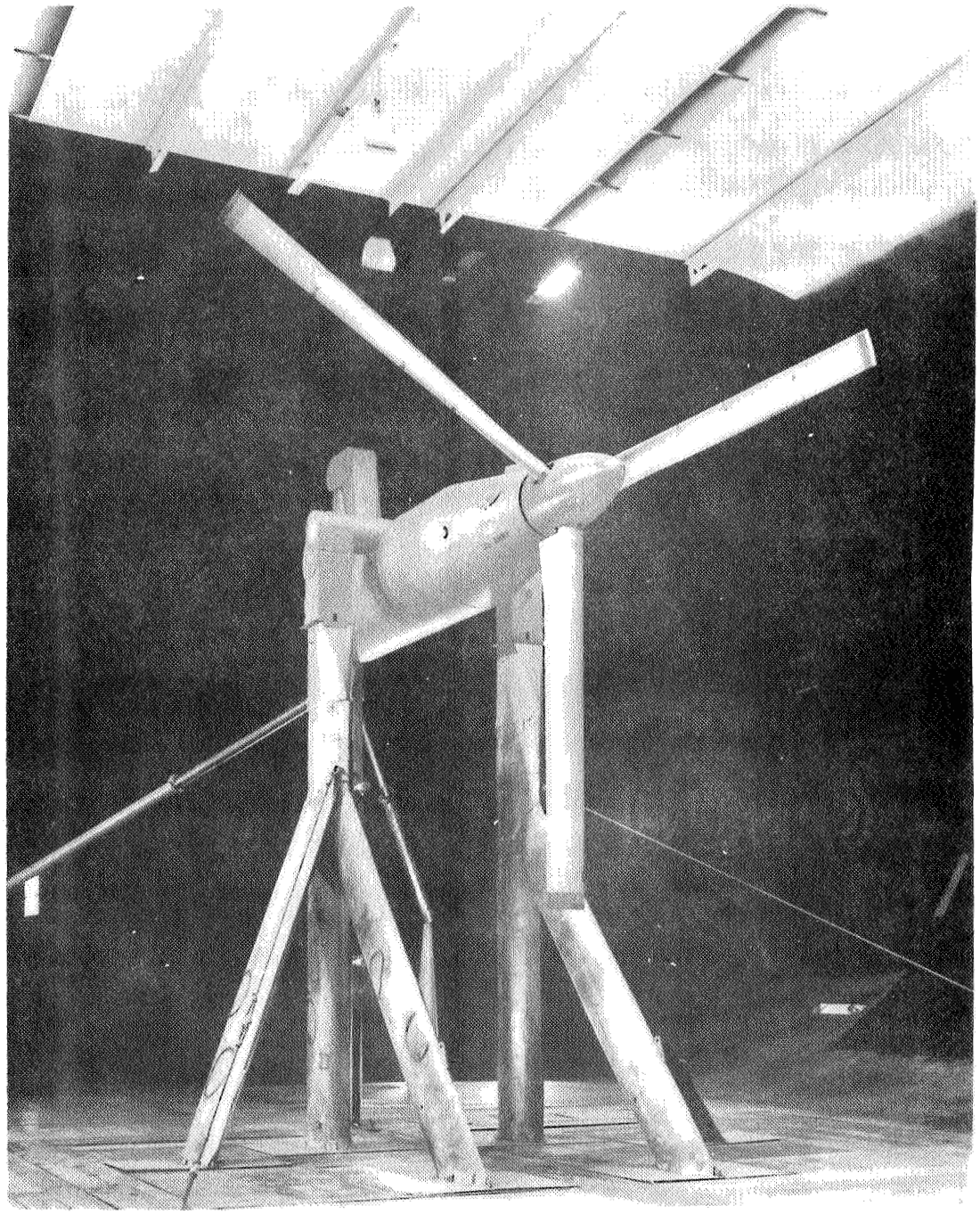

Figure 5-58.- Bell 25-foot flight-worthy proprotor in NASA-Ames full-scale tunnel for performance testing.

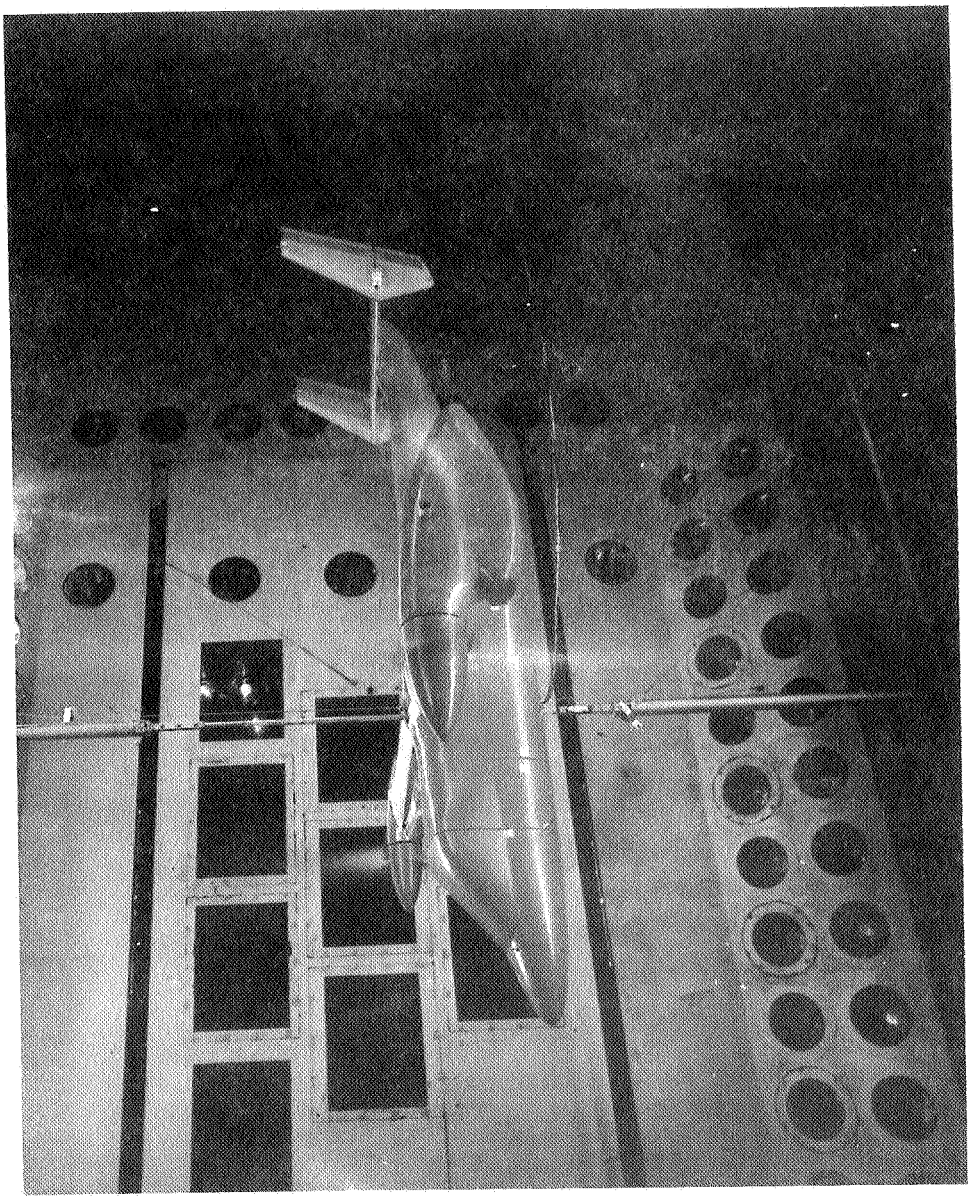

Figure 5-59.- 1/5-scale "free-flight" dynamic aeroelastic model of the Bell Model 300 tilt-proprotor in the Langley transonic dynamics tunnel.

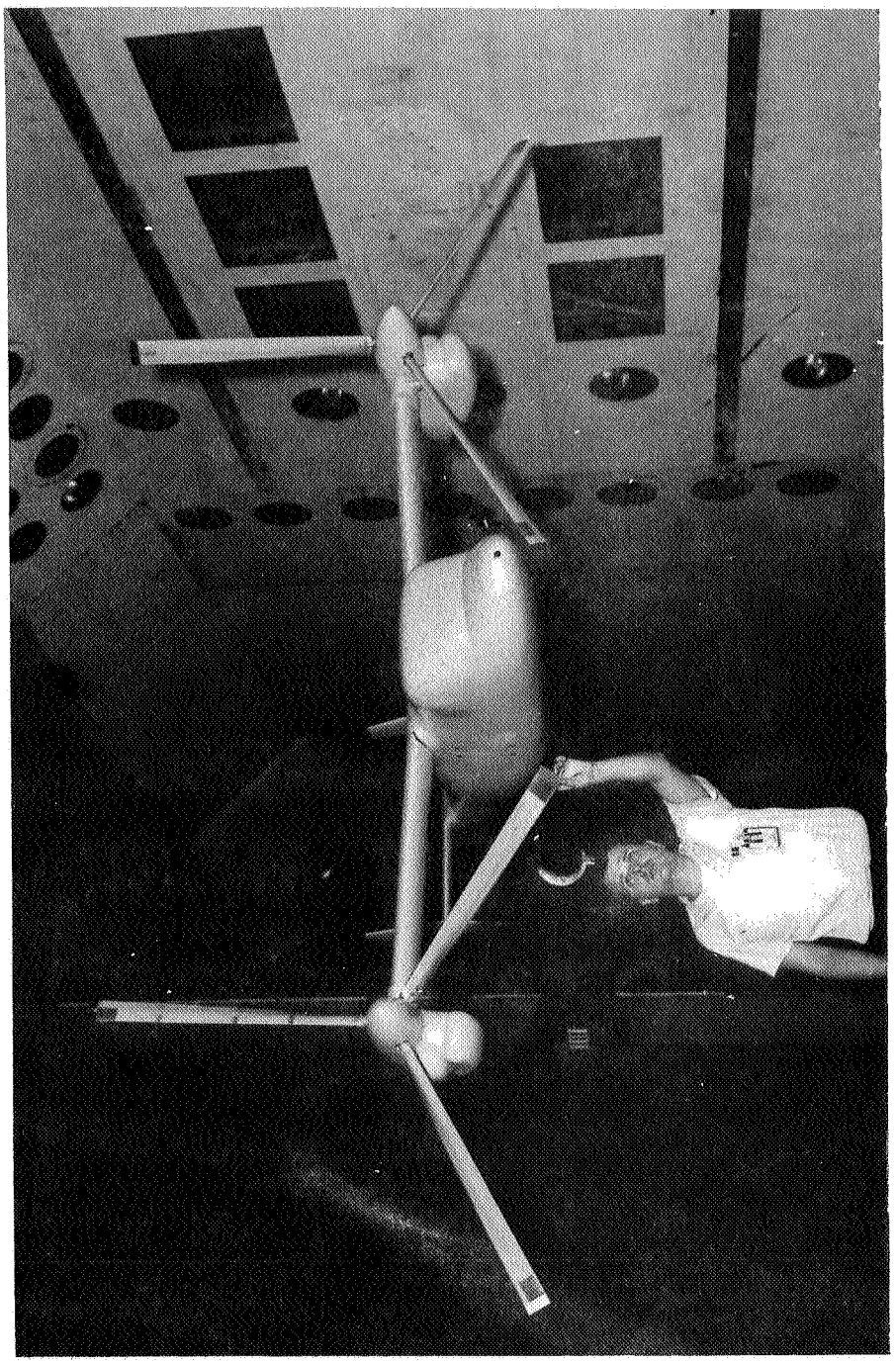

Figure 5-60.- 1/5-scale rigid force and moment model of Bell Model 300 tilt-proprotor (with dynamically and aeroelastically scaled rotors) in Langley transonic dynamics tunnel.

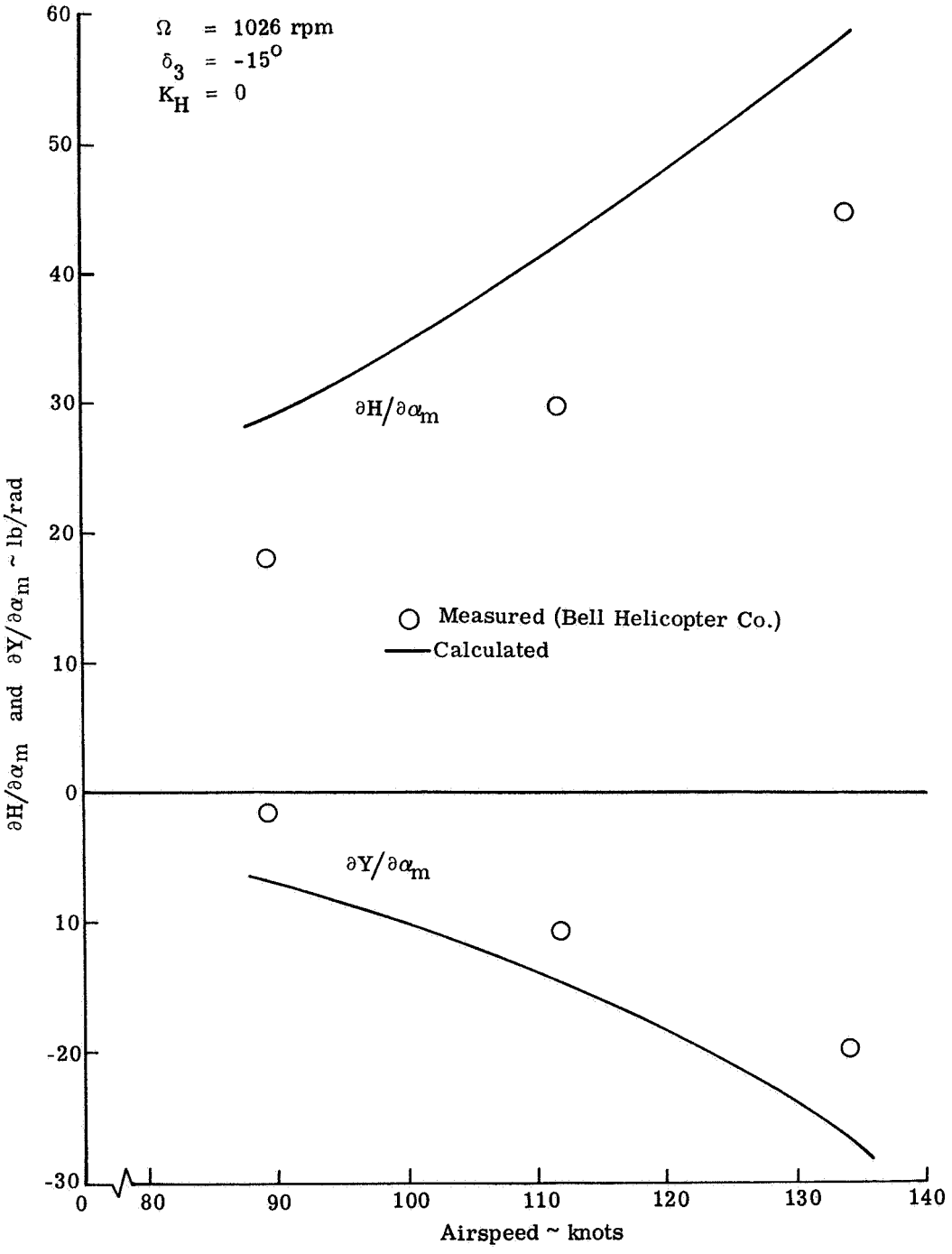

Figure 5-61.- Variation of zero frequency normal- and side-force derivatives with airspeed (model values).

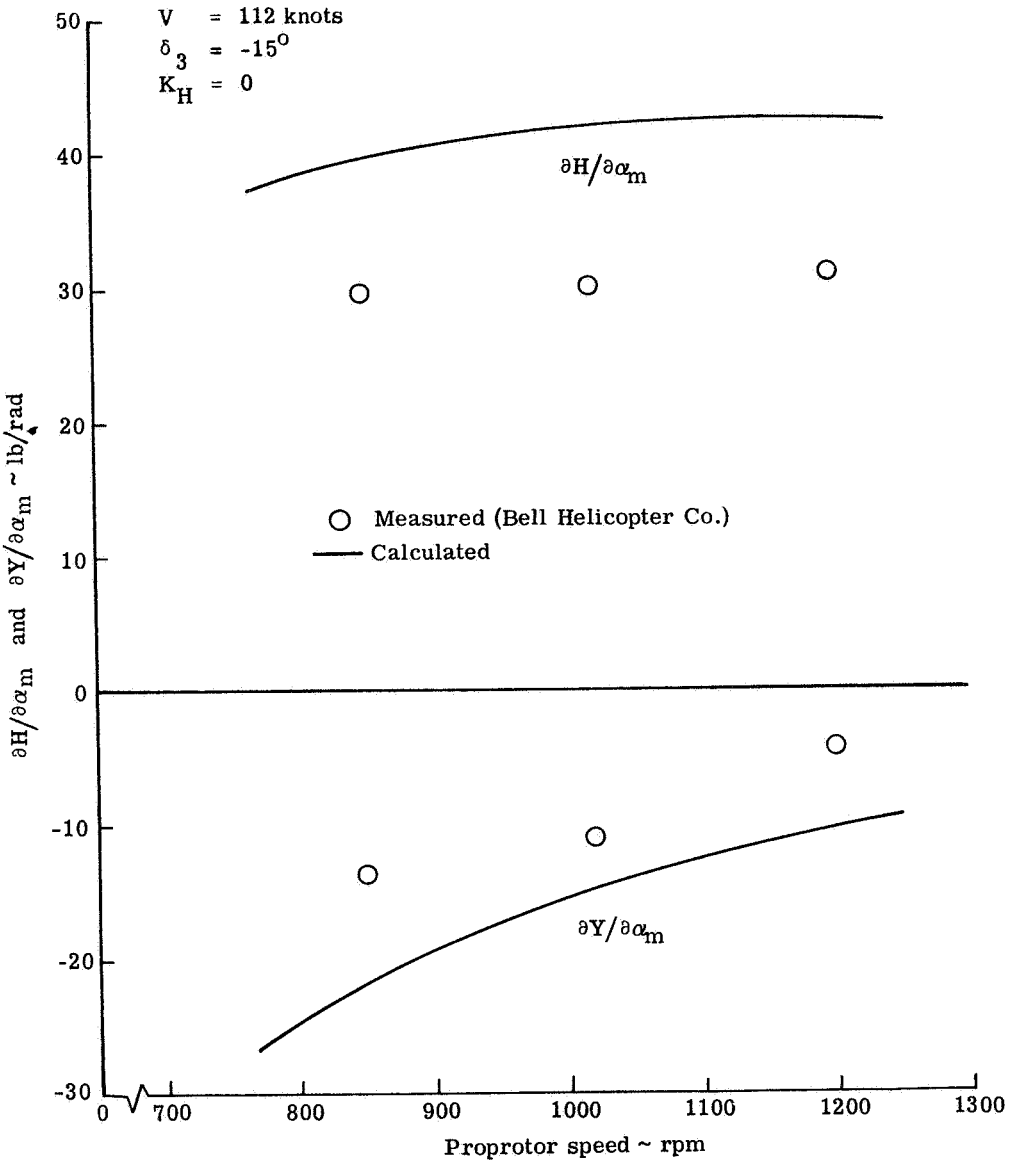

Figure 5-62.- Variation of zero frequency normal- and side-force derivatives with proprotor rpm (model values).

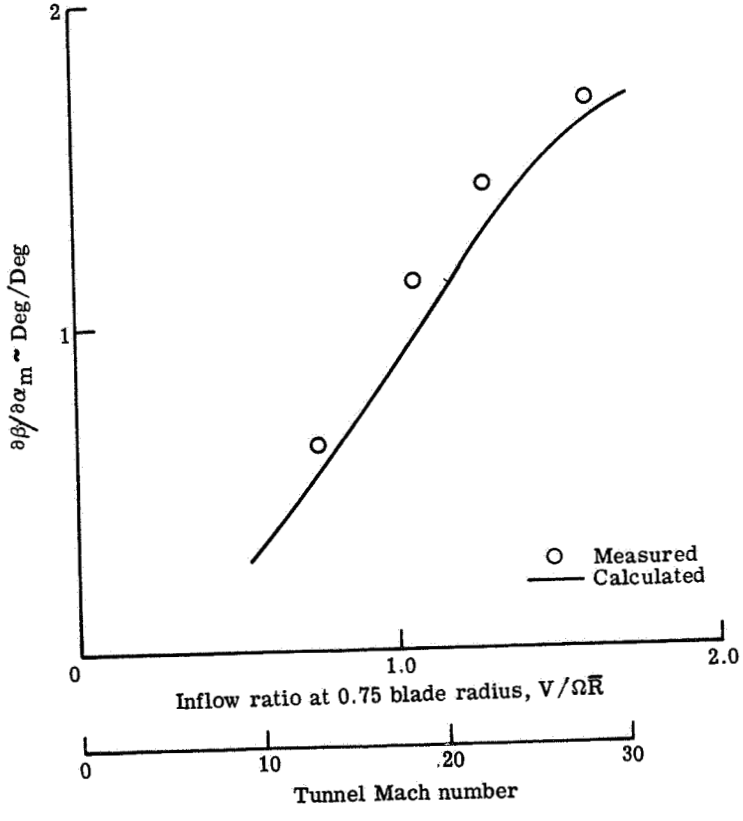

(a) Air test medium

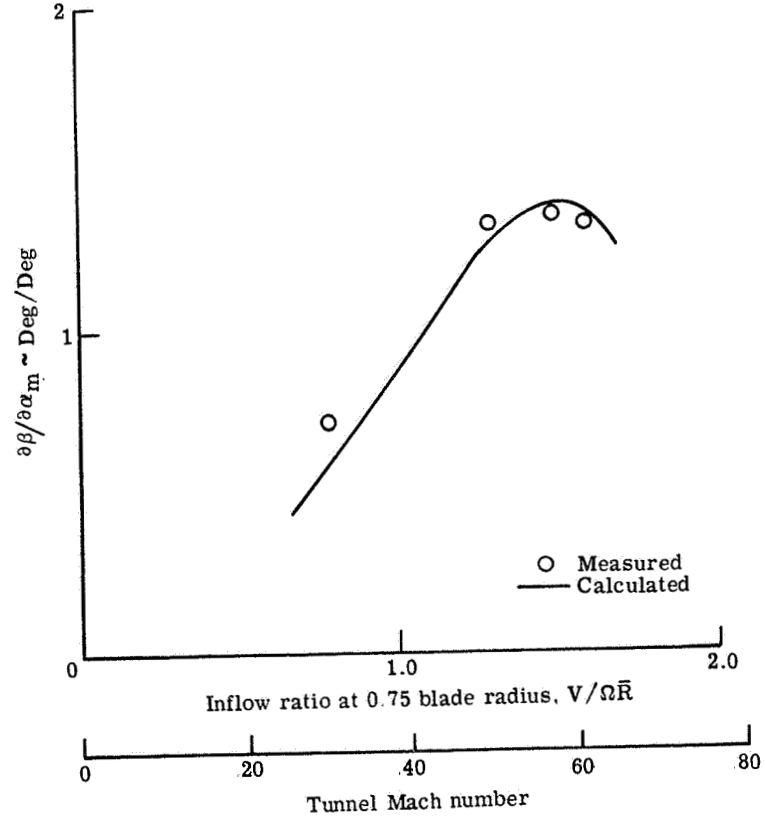

(b) Freon test medium

Figure 5-63.- Effect of Mach number on proprotor flapping derivative.

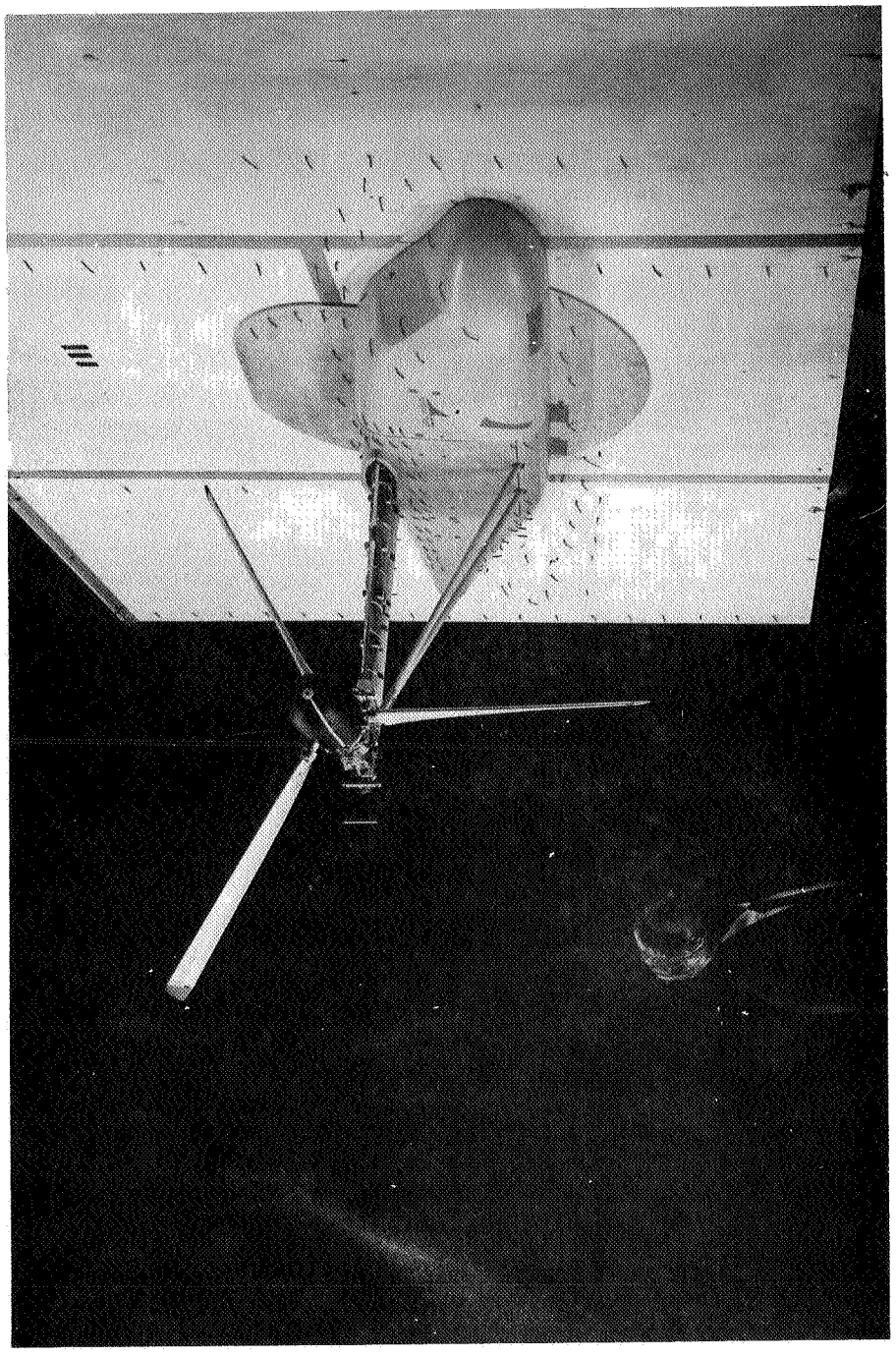

Figure 5-64.- Semi-span model of Grumman "Helicat" tilt-rotor in whirl flutter research configuration.